Fatigue Analysis of Welded Joints Using Local Reference Stress

by

Badr Bedairi

A thesis

presented to the University of Waterloo

in fulfillment of the

thesis requirement for the degree of

Doctor of Philosophy

in

Mechanical and Mechatronics Engineering

Waterloo, Ontario, Canada, 2017

Examining Committee Membership

The following served on the Examining Committee for this thesis. The decision of the Examining Committee is by majority vote.

External Examiner	Nabil Bassim Professor
Supervisor(s)	Grzegorz Glinka Professor
Internal Member	Marianna Polak Professor
Internal-external Member	Adrian Gerlich Professor
Other Member(s)	Hyock Ju Kwon Professor

AUTHOR'S DECLARATION

I hereby declare that I am the sole author of this thesis. This is a true copy of the thesis, including any required final revisions, as accepted by my examiners.

I understand that my thesis may be made electronically available to the public.

Abstract

Of the many parts of a machine, welded joints are the most susceptible to fatigue loading. The unusually complex geometry of a welded joint combined with the heating process during welding produces a high amount of stress that can result in fatigue cracks and failure. In welded joints, fatigue cracks usually emanate from critical locations such as a weld toe, where the stress is highly elevated. It is important to design welded structures based on the fatigue failure criterion in tandem with the usual design requirements. There is also a need to accurately assess the fatigue damage of welded joints for maintenance purposes because existing welds may contain defects or fatigue cracks. Therefore, accurate estimates of the fatigue life of welded joints are thus essential components of structural design and maintenance.

The three most common methods of estimating fatigue life, and the ones selected for consideration in this work, are the nominal stress-life (S-N) method, the local strain-life (ε-N) method, and the Linear Elastic Fracture Mechanics (LEFM) method. Challenges arise from the fact that each method requires different and precise information concerning critical stresses that affect the fatigue life of welded joints. For each method, different stresses defined at the critical locations of a welded joint must also be obtained. The S-N method requires a determination of the nominal stress σn, the ε-N method requires an estimate of the peak stress σpeak, and the LEFM method requires the calculation of the stress distribution in the prospective crack plane σ(y). The complex geometry and loading that characterize welded joints make these critical stresses difficult to determine, so that variations in the definition of stress constitute the primary current source of inconsistencies in weldment fatigue analysis.

The goal of the study presented in this thesis was to develop one universal weldment stress analysis method that can supply accurate and consistent stress information for all contemporary fatigue analysis methods. A determination of accurate and consistent stress data at weld-critical zones requires that the stresses in that area be reviewed and related to a reference stress that must be located at the most critical weld zone and must also be related to the actual stresses there. The work conducted for this thesis involved the development of this kind of reference stress, which has been termed “local reference stress.”

A number of issues complicate the determination of stress in the most critical areas of a welded joint, including the weld toe or weld throat, such as residual stress generated by the heating process during welding and elevated stress due to an abrupt change in geometry. Reliance on the well-known nominal stress that is dependent only on the cross-sectional area and ignores other geometric factors associated with the weld is therefore insufficient. Peak stress is also difficult to determine even with the use of a three-dimensional (3D) finite element (FE) method because the magnitude of the stress on the surface of the weld toe can be captured only by a fine mesh. The through-thickness stress distribution in the critical cross-section of a weldment is even more challenging to establish using conventional FE packages because of the steep stress gradient associated with the prospective crack plane. The methodology presented in this thesis offers a convenient means of evaluating the critical stresses that affect the fatigue life of welded joints. The new method is based on an FE technique, which was used effectively for generating well-defined reference stress values at critical areas in a weld.

The local reference stress on the weld toe line and the associated linear through-thickness stress distribution constituted the basis for determining the necessary stress data required as input for each of the three fatigue-analysis methods. The objective was to analyze an entire welded structure using a shell FE model that involves a relatively small number of elements. Subsequent post-processing of the local reference stress produced the required stress data, such as the peak stress or the through-thickness stress distribution. While the stress data are based on a simple shell FE model and the local reference stress concept, they yet were able to supply accurate and detailed stress information for any of the fatigue life estimation methods.

The developed method is based on a unique reference stress related to the actual critical non-linear stress across the weld toe. Determining weldment fatigue life using the local reference stress and the associated stresses resulting from the post-processing enable the inclusion of the weld macro; micro-geometrical features; and other factors that affect the fatigue life of welded joints, such as the stress concentration and residual stress.

The shell FE modelling method also has the advantage of simulating a full structure in a relatively short time, thus requiring substantially less computational time and resources than 3D FE models. The tests also revealed that, with the new method, the thickness of the shell element that simulates the weld is very important because it affects joint stiffness. For this reason, the thickness of the weld shell

element should be equal to the thinner of the welded plates. The stress data obtained based on the shell FE local reference stress were validated against detailed 3D FE models. These data were then applied for the prediction of fatigue life using the strain-life and the LEFM methods. Five case studies were modelled and analyzed in order to compare the fatigue life predictions produced using the developed methodology against experimental fatigue life data.

The proposed shell FE local reference stress proved able to simulate the stress fields in a variety of welded joints, such as T-joints (fillet joints), and square or circular tube on a plate. The shell FE local reference stress data were compared to the results obtained using detailed fine mesh 3D FE models. The accuracy of the stress data based on the shell FE models was under 15 % in all the joints except for the gusset, which was around 20 %. The difference between the peak stress resulting from the shell FE local reference stress and the peak stress resulting from the 3D FE modelling is within 10 % for all the case studies, with the exception of the first case, which was within 20 %. With respect to the number of elements, the difference between the shell and the 3D FE models was very large. The data produced by the proposed shell FE model matched that produced by the 3D fine mesh elements with respect to accuracy, but required nine to 204 times fewer elements. As a result, the proposed shell FE modelling method offers the advantage of simulating a full structure in a relatively short time and with fewer computational resources, as was particularly proven in the last case study involving a complex tubular joint. Such accurate stress data then enables fatigue life to be evaluated using the post-processed shell FE local reference stress data.

Acknowledgements

First, I would like to thank my supervisor Professor Grzegorz Glinka for his patience, guidance, and support.

I would like to thank my sponsor Taibah University for their trust and long term support throughout my scholarship.

I would like also to acknowledge the John Deere Company laboratory and their staff for providing the experimental data. I would like to extend my acknowledgement to the people who have taken part in the development of the current method, especially Ramtin Kahvaie-Zad and Malik Shahid.

My special thanks to my mother, Nafisa Ashoor, for her endless prayers and kind support. To my eldest brother and role model Engineer Tarik Bedairi, thank you for being greatest support through my life. I am also deeply thankful to my wife, Arwa Khushaim, for her great support and comfort through every step in my studies.

Last but not least, I would like to thank my friends Dr. Bassam Gholam, Dr. Semyon Mikheevskiy, Dr. Amin Eshraqi, and Dr. Sergey Bodanov for their continuous support and gentle criticism.

Dedication

To my mother, my wife, and my sons (Yosef and Rayyan) and all those who believed in me.

Table of Contents

List of Figures

List of Tables

Nomenclature

2D	2-Dimensional
3D	3-Dimensional
a	Crack size
a_i	Initial crack size
a_f	Final crack size
b	Fatigue strength exponent
c	Fatigue ductility exponent
2c	Crack length on the surface
a/c	Crack aspect ratio
C, p, m, γ	Material constants in the Fracture Mechanics equations
E	Young's Modulus
ESED	Equivalent strain energy density
F	External force
FEM	Finite Element Method
FAT	Fatigue design class
I	Moment of Inertia
K	Stress intensity factor
K_A	Stress intensity factor at the deepest point A of a semi-elliptical crack
K_B	Stress intensity factor at the surface point B of a semi-elliptical crack
K′	Cyclic strength coefficient
K_t,	Stress concentration factor
K_{th}	Threshold stress intensity factor
$K^m_{t,hs}$	Membrane hot spot stress concentration factor
$K^b_{t,hs}$	Bending hot spot stress concentration factor
K_{max}	Maximum stress intensity factor
K_{min}	Minimum stress intensity factor
L	Length
h, hp	Weld leg lengths of the weld's base and attachment plate, respectively
m	Slope of S-N curve
$m_A(x,a)$	Weight function at the deepest point A of a semi-elliptical crack

$m_B(x,a)$	Weight function at the surface point B of a semi-elliptical crack
M, M_b, M_c	Bending moment
N	Number of cycles
n'	Cyclic strain hardening exponent
N_f	Total fatigue life
N_{blck}	Number of blocks (stress history repetitions)
N_i	Fatigue crack initiation life
N_p	Fatigue crack propagation life
P, V, H	Axial applied load
SCF	Stress concentration factor
R	Stress ratio (ratio of minimum stress to maximum stress)
S, σ	Stress
S-N	Stress-life curves
SIF	Stress intensity factor
SWT	Smith-Watson-Topper fatigue damage parameter
t, t_p	Thickness of the base and attachment plate, respectively
x, y	Through-thickness distance from the weld toe
Y	Geometry factor
ε	Strain
ε_f'	Fatigue ductility coefficient
ε-N	Strain-life curves
ν	Poisson's Ratio
σ_b	Bending stress
σ_f'	Fatigue strength coefficient
σ_{hs}	Hot spot stress
σ_{hs}^m	Hot spot membrane stress
σ_{hs}^b	Hot spot bending stress
σ_m	Membrane stress
σ_n	Nominal stress
σ_{peak}	Peak stress or maximum elastic notch stress
σ_r	Residual stress
σ_{sH}	Structural hot spot stress by Haibach

$\sigma(y)$	Stress distribution through the thickness in the Y-axis (normal to weld toe) or actual through-thickness stress distribution based on 3D FE modelling
$\sigma(y_i)$	Nodal stress value at distance yi from the weld toe surface
$\sigma_{xx}(y)$	Stress distribution through the thickness in the Y-axis (normal to weld toe) or Monahan through-thickness stress distribution based on shell FE modelling
σ_{ys}	Monotonic yield strength
ρ, r	Actual notch radius or weld toe radius
θ	Weld toe angle
τ_{xy}, τ_{yz}, τ_{zx}	Shear stress components
δ_{el}	Finite element size
ΔK	Stress intensity factor range
Δy_i	Distance between two adjacent nodes of the FE model
$\Delta\varepsilon^a$	Actual elastic plastic strain range
$\Delta\sigma_{hs}$	Hot spot stress range
θ	Weld toe angle

Chapter 1
Introduction

1.1 Challenges in fatigue analysis of welded joints

Machine components and structures are typically welded together, as welding is one of the most-used joining methods. Welded joints in vehicles of all types, mechanical engineering tools, and pipes are examples of components which are subjected to repeated cyclic loads. This type of loading, which is more damaging than static loading, causes fatigue damage to machine components such as welded joints, leading to mechanical failure. Moreover, welded joints have micro geometrical features (e.g., weld angle θ and weld toe radius ρ), macro geometrical features (e.g., weld shape and size) and residual stress, which result in complex stress states. Fatigue loading of a component will produce small cracks that will eventually propagate through the critical cross-section. In the case of welded joints, fatigue cracks usually emanate from critical locations such as a weld toe, where the stress is highly elevated. Hence, it is important to design welded structures based on the fatigue failure criterion in tandem with the usual design requirements. Furthermore, because existing welds may contain defects or fatigue cracks, there is a need to accurately assess the fatigue damage for maintenance purposes. Therefore, accurate fatigue life estimation of welded joints is essential for structure design and maintenance.

There are currently a few methods used to estimate the fatigue life of welded joints, but only the three most common methods are discussed in this thesis. Each method requires precise information concerning critical stresses affecting the fatigue life of welded joints. Critical stresses are not easy to determine, as welded joints have complex geometry and loadings. One of the best techniques to determine the critical stresses of components is finite element analysis (FEA) or FEM finite element method. The FEA is used by industry for virtual design purposes, and has been adopted as a productive modelling technique which minimizes the amount of time required for designing components (e.g., using virtual modelling instead of making physical prototypes) or improving existing ones (e.g., testing virtual design instead of physical destructive tests). However, using the FEA method for the fatigue stress analysis of welded joints is challenging because of the geometrical and loading complexity of welds, due to stress concentration and residual stresses.

Due to the number of challenges posed by estimating the fatigue life of welds, it is important to have a general understanding of various discontinuities and stresses welds are subjected to. The high

level of stress concentration produced by weld joint's micro geometrical features significantly reduces the fatigue life. Welded joints are often known to contain discontinuities, and welding codes to some extent allow for certain discontinuities such as notches, porosity, misalignment, undercut, etc. The allowable tolerance of discontinuities ranges are specified so that any weld containing discontinuities beyond the specified range will be considered defective or in need of repair. However, the problem is that welding codes do not specifically account for the effect of these micro geometrical features. This is probably because these features may have been accounted for already in the design stage of the codes. The number of combinations of micro geometrical features may be another reason that welding design codes do not account for the resultant different stress concentrations. The FEA can be used to model welds, but it requires a considerable number of elements resulting in a very fine mesh to capture the effect of the stress concentration. Moreover, the mechanical material properties of welded joints may be changed due to the welding process, which alters the chemical composition and microstructure of the joint. The heat input during the welding process, associated with various thermal cycles, also produces residual stress around the weld line. The fatigue lives of weldments suffer from residual stress created during the welding process, and welding design codes have to take this stress into account. Since these codes are based on welded specimens, it is fair to assume that the effect is included within the codes. As a result, it can be concluded that estimating the fatigue life of welded joints has a considerable number of challenges, and in order to overcome these challenges, the various fatigue life estimation methods are reviewed.

Fatigue life is generally predicted using one of three methods: the nominal stress-life (S-N) method, the local strain-life (ε-N) method, and the Linear Elastic Fracture Mechanics (LEFM) method. Nevertheless, there are six modules necessary for any of the above fatigue analysis method, as illustrated in Figure 1-1.

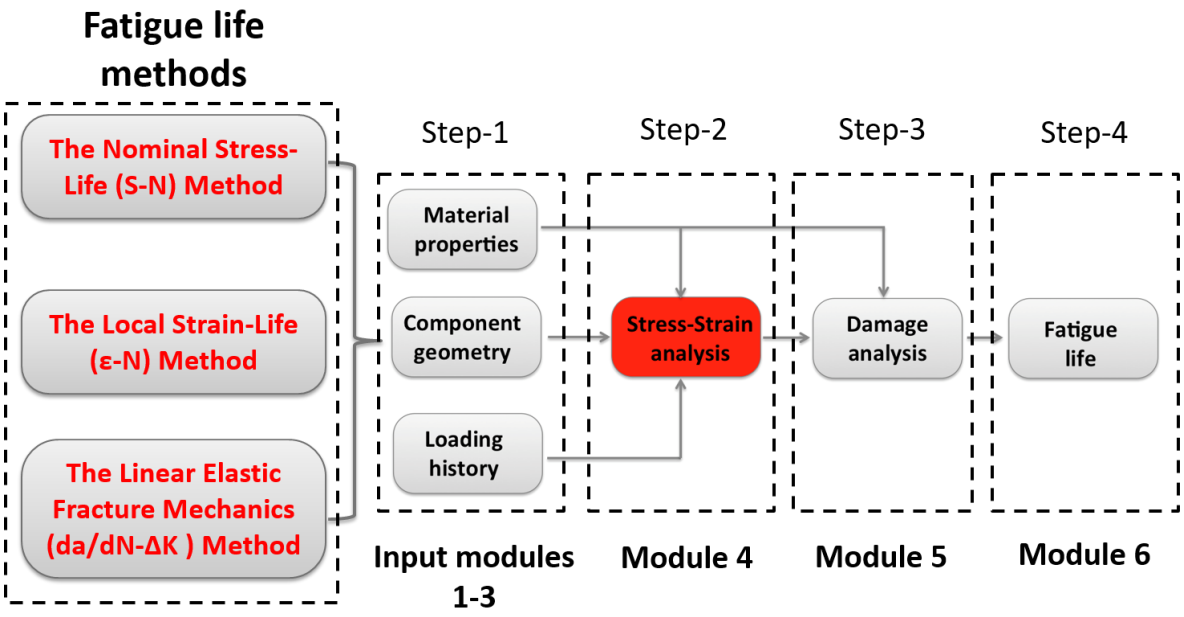

Figure 1-1: General steps for fatigue analysis

The first step in fatigue analysis is dealt with the input modules, which are: the material properties, the component geometry, and the loading history. The second step is the stress analysis module, while the third and fourth steps are evaluating the fatigue damage and the fatigue life. The material properties module is the most well-established one, but the stress analysis module requires more investigation because of the complexity of weld geometry and loading history. The format of the loading history is the same in each of the three contemporary fatigue analysis methods, but the definition of material properties and the stress parameters change depending on the method chosen for the fatigue life estimation.

The stress definition in fatigue analysis varies considerably based on the method used. The variation of the stress definition is currently the main source of inconsistencies when carrying out fatigue analyses of weldments. Therefore, it is important to briefly discuss the most popular fatigue analysis methods, including the input stresses to the stress analysis module (stress-strain analysis; see Figure 1-1). Some of the advantages and disadvantages of these methods are also stated in order to highlight the overall research objectives of this thesis.

The S-N method was the first one used for evaluating the fatigue life of machines. This method is based on stress-life or S-N curves, which can be found in various handbooks and standards such as

the ASTM E739-10 [1]. S-N curves are fitted as a result of testing several cylindrical smooth specimens subjected to fatigue/cyclic loading. S-N curves are expressed as the nominal stress amplitude, σ_a or nominal stress range, $\Delta\sigma_a$, versus the fatigue life in load cycles, N. Therefore, the required stress input to the stress analysis module (see step 2 in Figure 1-1) of the stress-life method is the nominal stress. Determining the nominal stress is rather difficult in welded joints due to the effect of the geometrical features of the welds, as will be shown later in Section (2.1). Even though the S-N method is relatively easy to use, it is not reliable when applied to weldments [2] because of the micro geometrical features, microstructural changes, and complex loading accompanying welded joints. For example, an infinite number of material S-N curves are needed to cover all types of welded joints encountered in practice because each welded joint has different geometrical features, resulting in an infinite number of stress concentration factors. Beyond this, the S-N method cannot account for the residual stress or the variation of load sequences. Therefore, the strain-life (ε-N) method was introduced to address some of these shortcomings.

The ε-N method has gained more attention recently because it is capable of evaluating both high- and low-cycle fatigue applications. For welded joints, the strain-life method can account for the effect of the stress concentration and the residual stress among other loading factors such as the mean stress. It is also sensitive to the sequence of loading, and can be used to estimate fatigue crack initiation life if the material fatigue properties, as well as the detailed stress information (peak stress) at the critical location (e.g., weld toe), are known. Detailed stress information may be acquired by conducting a three-dimensional finite element analysis (3D FEA) with a very large number of elements and a fine mesh around high stress areas, which also results in a very long computational time. However, even when using detailed 3D FE modelling, it is difficult to capture the proper peak stress at a weld toe because the result is sensitive to the mesh size, not to mention that the ε-N method provides the fatigue life only up to crack initiation. The total fatigue life of a joint or machine may be considered right up to the fracture point rather than just the crack initiation, because sometimes when a crack occurs in an in-service component, it takes time for the crack to grow to the point of failure. Therefore, the Linear Elastic Fracture Mechanics (LEFM) method was implemented.

The LEFM method predicts fatigue-crack-growth life based on the stress intensity factor parameter (SIF), which describes local stresses and strains in the vicinity of a growing crack. This method can estimate the fatigue-crack-growth life but it requires knowledge of stress intensity factors

(SIFs), which are available in handbooks. Unfortunately, these handbooks SIFs are not readily available for welded joints subjected to fatigue loading. One possible and efficient solution to this problem is by determining the stress intensity factor by using the weight function technique. To find the stress intensity factor, the proper weight function and the through-thickness stress distribution in the prospective crack plane must be known. The through-thickness stress distribution may be determined by using the FEA technique, but unfortunately, using FEA to determine the stress distribution in a weldment critical cross-section is very difficult because of the high stress gradient through the weld toe thickness. While the LEFM method can account for the effect of the stress concentration, residual stress, and the mean stress, the method demands an estimation of the initial crack size.

Thus, it can be concluded that the main key to fatigue life evaluation of welded joints relies on the ability to provide the required stress input. The input stress used for the fatigue life estimation must include several factors. The complex stress deriving the fatigue life of weldments is affected by the weld's micro and macro geometrical features in addition to the residual stress produced by the welding itself. For instance, the micro geometrical features of the weld create stress concentration, while the welding process produces residual stress. Both factors are detrimental to fatigue life. As a result, providing accurate stress information for the fatigue life estimation becomes very difficult. Figure 1-2 shows a typical welded T-joint subjected to multiple loads resulting in various stress distributions through the welded joint's critical section.

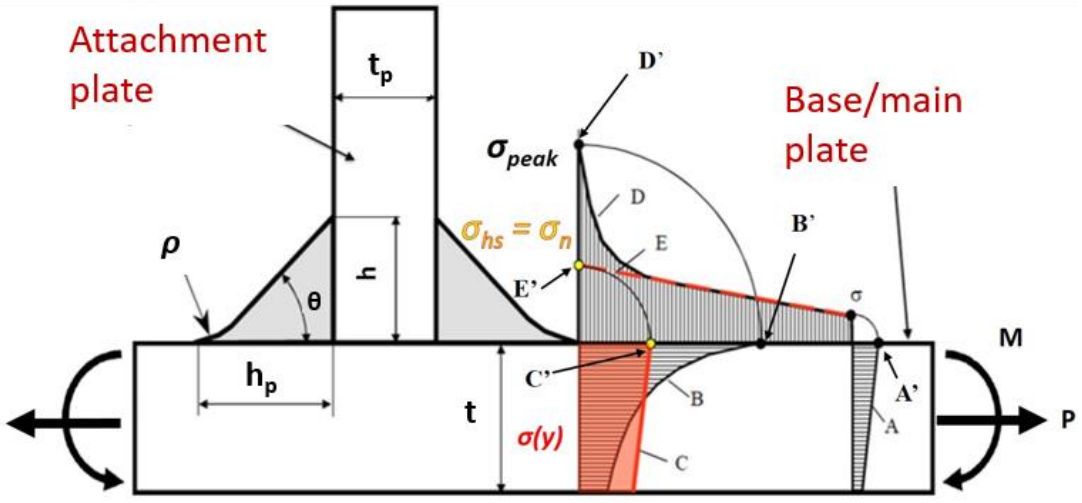

Figure 1-2: Various stresses and stress distributions in a welded T-joint subjected to various external loads [3]

Figure 1-2 includes various stress distributions in a typical T-joint resulting from remotely applied bending and tensile forces M and P. These distributions, shown in Figure 1-2, A, B, C, D, and E, are stresses in the direction normal to the weld toe line. In Figure 1-2, points A', B', C', D', and E', located on the base plate surface in the direction normal to the weld toe line, represent the maximum magnitudes of each stress distribution. The following list explains the stress distributions shown in Figure 1-2:

A) The remote nominal stress distribution, away from the weld's micro geometrical effect.
B) The non-linear through-thickness stress distribution $\sigma(y)$ is the actual stress distribution across the weld toe critical cross-section. This stress distribution is the needed stress data for the LEFM or (da/dN-ΔK) method, and can be determined by using the FEA method or the simplified analytical method presented in the thesis.
C) The nominal stress distribution is based on the most well-known stress index/quantity, which can be calculated mathematically to estimate an equivalent linearized stress distribution across the weld cross-section across the weld cross-section.
D) The non-linear stress distribution along the surface of the base plate.
E) The linearized stress distribution along the base plate surface, results from a linear extrapolation of two surface stress points away from the weld toe.

The following list explains the various stresses along the plate surface, as shown in Figure 1-2:

A') The maximum remote nominal stress on the plate surface away from the weld toe
B') The peak stress σ_{peak} is the actual maximum stress at the weld toe. This is the needed stress for the (ε-N) method. The peak stress can be determined by using the FEA method or the method presented in the thesis.
C') The nominal stress σ_n is the maximum stress of the nominal/linear stress distribution (Figure 1-2, C). This is the required stress for the S-N method.
D') The maximum stress magnitude of the distribution D. B' and D' are the same stress acting at the same point.
E') The hot spot stress σ_{hs} has the same magnitude as the nominal stress σ_n determined by the simple tensile and bending stress formula. The hot spot stress/structural stress can be determined either experimentally (as represented in Figure 1-2, E) or by using FE, as will be discussed later in Section 2.1.1.

Note that points E, and D in Figure 1-2 are showing stress distributions based on surface stress values whereas, E', and D' are the maximum values of these distributions. The nominal stress shown

in Figure 1-2C', is one value resulting from the classical method to determine the nominal stress. The through thickness nominal stress distribution in Figure 1-2C, can be found by integrating the classical nominal stress equation across the main plate thickness. The actual non-linear through-thickness stress distribution σ(y) shown in Figure 1-2B, can be found by using the FEA. In some cases (weld shapes) the nominal stress and the hot spot stresses have the same stress magnitudes.

In summary, various stress values must be known, depending on the fatigue analysis method. The following are the stress inputs for each of the fatigue methods mentioned above:

a') For the nominal S-N method, the nominal stress σn (see Figure 1-2, C' and E')
b') For the local ε-N method, the linear elastic peak stress σpeak (see Figure 1-2, B' and D')
c') For the LEFM, the linear elastic through-thickness stress distribution σ(y) (see Figure 1-2, B)

Each of the above stresses is not easy to determine for welded joints. Determining the nominal stress is not easy because it is not clearly defined. The nominal stress depends on the critical welded plate cross-section area which ignores the effect of the weld's shape on the actual critical stress distribution. Determining the peak stress is difficult because of its high magnitude which cannot be easily captured when using the FEA method. Determining the through-thickness stress distribution σ(y) is difficult as well because of its very high gradient, starting from the weld toe surface and across the weld critical cross-section.

The peak stress and the through-thickness stress distribution can be determined by using three-dimensional finite elements (3D FE) such as brick or tetrahedral elements. One challenge when modelling a welded structure is capturing the high level of surface stress (σ_{peak} in Figure 1-2, B' and D') and its associated non-linear through-thickness stress distribution gradient (σ(y) in Figure 1-2, B), which requires a very fine mesh in order to find accurate stress data. Modelling a real welded component will take a large number of elements which will result in very long computational time. However, there are different types of elements that can be used in order to reduce the computational time, such as the shell element or (shell FE). As for determining the hot spot stress, few studies have been conducted using the shell FE formulation, but there are no specific rules on how to model welded joints, nor are there details on how to determine the peak stress.

1.2 Objectives

Designing machine components for required fatigue life is not an easy task, especially when considering the difficulties in determining the fatigue life of welded joints. The available fatigue life analysis methods are also not easy to apply to welded joints due to the complexity of weld geometry and loading. Thus, appropriate and accurate stress analysis is needed for the fatigue life estimation of weldments. There are two main challenges when determining the fatigue life of weldments. The first is how to find the stresses necessary for each fatigue analysis method, and the second challenge is associated with limitations of the fatigue analysis methods when applied to weldments.

The stress input data for each fatigue life method is not easily found, and this is especially true for welded joints. The nominal stress in the weld toe region has no physical representation that can be measured experimentally, but it is rather a mathematical linearization estimation of the stress across the weld toe critical section. The peak stress and the stress distribution may be found using the FEA however, to capture the peak stress, which has a very high stress level, requires a very fine mesh and a considerable number of elements. As a result, long computational times and resources are needed for even a small part, let alone a full/complete structure. The same can be said for determining the stress distribution that has high gradient through the thickness of the weldment critical area.

To sum up, the nature of the stress required for each fatigue analysis method is different and they are difficult to find, especially for welded joints. ***Thus, the goal of the current study is to develop one universal weldment stress analysis method that can supply accurate and consistent stress information for all contemporary fatigue analysis methods.*** In order to have an accurate and consistent stress data at the weld critical zones, the stresses in that area must be reviewed and related to a reference stress. This reference stress, has to be located at the most critical weld zone and related to the actual stresses there. Thus, the proposed stress is referred to by the author as “Local reference stress”. The FE coarse mesh technique with shell elements is investigated and used to produce the required local reference stress with less computational cost and time in comparison with. Some special rules must be set for where and how to find the reference stress. The reference stress is next post-processed to determine the stress data required for each of the fatigue life estimation method. The stress data resulted from the coarse mesh shell FE modellings, have to be validated against 3D FE detailed models for verification. The last step is to use the stress data based on the proposed methodology for predicting the fatigue life of several welded joints to test its accuracy and efficiency.

The objectives and proposed procedures can thus be set as follows:

- Review the stress data of available welded joints.
- Establish one universal stress analysis method that can supply the stresses required by all of the three fatigue life estimation methods.
  - Find a unique stress quantity that can be related to the nominal stress, the peak stress and the through-thickness stress gradient, at weldment critical stress zones.
  - Establish a FE procedure to simulate welded joints using relatively large shell element in order to save time and model full structures in the future.
  - Provide details concerning the determination of the required local reference stress.
  - Create a post-processing method of the local reference stress to determine the stress data necessary for each of the contemporary fatigue life estimation methods.
- Validate the stress data acquired based on the coarse shell FE model against the stress data determined from a detailed 3D FE model.
- Predict the fatigue life of several types of welded joints using the strain-life and LEFM method, based on the local reference stress.
  - Investigate the effect of adding the residual stress to the fatigue life calculation of welded joints.
- Validate the fatigue life predictions against experimental fatigue life data.
- Investigate an area of research that could improve the proposed work.
  - Investigate/enrich the stress concentration factor equations of fillet welds.
  - Investigate/enrich the stress intensity factor for edge and central cracks in plates with variable thicknesses.

1.3 Thesis outline

Chapter 2 includes the literature review, the contemporary fatigue life analysis methods, and the discussion of difficulties concerning fatigue analysis of welded joints. Chapter 3 includes the methodology, detailing: 1) how to model a welded joint using the coarse shell element and produce information necessary for the determination of required stress data; 2) how to find the local reference stress; and 3) how to use the local reference stress to determine the necessary stress information for all three of the fatigue analysis methods. Chapter 4 includes verification of the shell FE stress data by modelling the same welded joints using detailed 3D FE models. Chapter 5 provides two case studies that illustrate the methodology, while another three case studies are presented in Appendix A. The conclusion and recommendations are summarized in Chapter 6 in addition to some future work including some data in areas that will improve the proposed methodology.

The five case studies are modelled based on the experimentally tested welded components provided by the John Deere (JD) laboratory. The proposed methodology was applied to JD welded

joints and the fatigue lives were predicted for each case and then compared to the experimental fatigue life data sets. Based on the proposed stress analysis method, the ε-N method was used to estimate the fatigue crack initiation life, while the LEFM method was used to evaluate the fatigue crack propagation life. The total fatigue life can be evaluated as the sum of cycles to crack initiation and crack propagation.

Chapter 2
Review and discussion of the fatigue life estimation methods for welded joints

In general terms, machines are designed to meet certain life goals. It is necessary to use welding technique to join machine parts which are subjected to fatigue loading. Fatigue loading is one of the major reasons that machines fail. Failure occurs in machines' welded areas because weldments are the weakest links in resisting fatigue loading. Cracks initiate in the weld area and then propagate through the cross-section, causing machine failure. For this reason, designers have to consider the effect of fatigue when setting the life goals of mechanical structures. A considerable amount of research has been carried out on fatigue life evaluation methods, including those of welded joints. The common fatigue life estimation methods mentioned in Chapter 1 are discussed in this section for components in general, and for welded joints in detail. Welded joints bring with them factors affecting fatigue life estimation; therefore, the advantages and disadvantages of each method are stated as well. The review focus is toward the stress analysis module of each method when predicting the fatigue life of welded structures. Procedures for applying the contemporary fatigue life estimation methods (S-N, ε-N, and LEFM) to welded joints are stated, along with the associated challenges in finding the stress required stress for each method in order to find areas where further development is needed. The last section reviews the history of using the FEA to assess for the fatigue stress analysis of welded joints. The aim of this Chapter 2 is to highlight the necessity and benefits resulting from of the proposed methodology, as will be discussed in Chapter 3.

2.1 Fatigue life prediction of weldments using the stress-life (S-N) method

The stress-life method uses fatigue S-N curves which is the result of multiple fatigue tests carried out under fully reversed loading, alternating around a zero applied mean stress with constant nominal stress ranges $\Delta\sigma_n$ or nominal stress amplitudes σ_a. The fatigue life N_f is defined by the number of load cycles to specimen failure, where each cycle is equal to two load reversals, $2N_f$. The S-N curves are experimentally derived for a variety of characteristic geometrical configurations. This method requires the knowledge of the nominal stress to estimate the fatigue life.

From 1850 to 1860, Wohler [4] performed laboratory fatigue tests, using repeated bending stresses, on railway axles. This was the first known systematic investigation of the fatigue phenomenon. Wohler also used the stress amplitude versus the number of cycles and showed that fatigue life increases with the decrease of the stress amplitude to the point where if the stress amplitude is further decreased to a low enough level, components will not fail at all. As a result, Wohler established the concept of the S-N diagram and the fatigue limit; he also noted the importance in a fatigue analysis of the stress amplitude over the maximum stress. In 1910, Goodman [5] contribution included a model that was developed to account for the mean stress effect on fatigue life of metals. Basquin [6] provided an empirical equation to mathematically describe the fatigue S-N curves of metals using the linear log-log relationship in the finite life region as shown in Figure 2-2. Fatigue damage accumulation models were developed during 1920s and 1930s. Palmgren [7] introduced a model for fatigue damage accumulation in that period. Miner [8] popularized Palmgren linear damage-accumulation which is known as Palmgren-Miner linear damage hypothesis. Matsuishi and Endo [9] introduced the rainflow cycle counting method.

The general procedure for fatigue life estimation using the S-N method is shown in Figure 2-1 while Figure 2-2 shows a typical fatigue S-N curve.

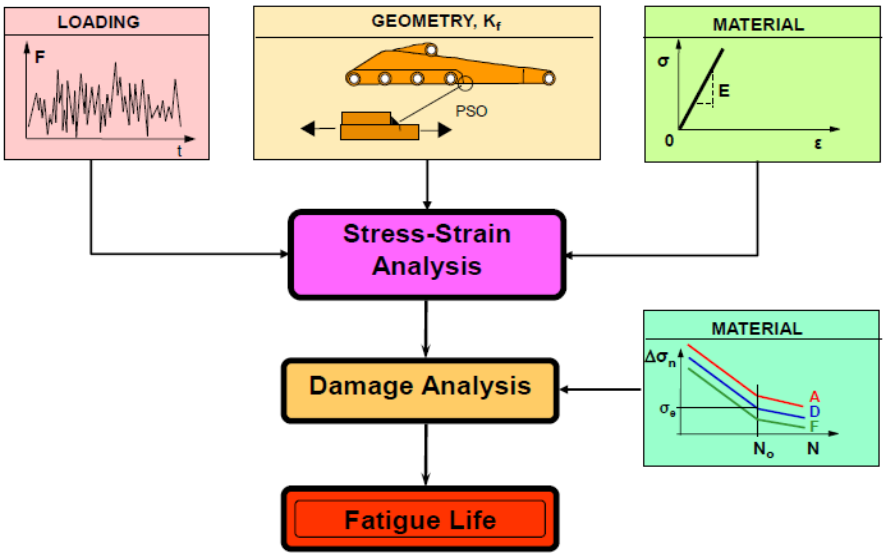

Figure 2-1: Fatigue life estimation procedure based on the nominal S-N method [3]

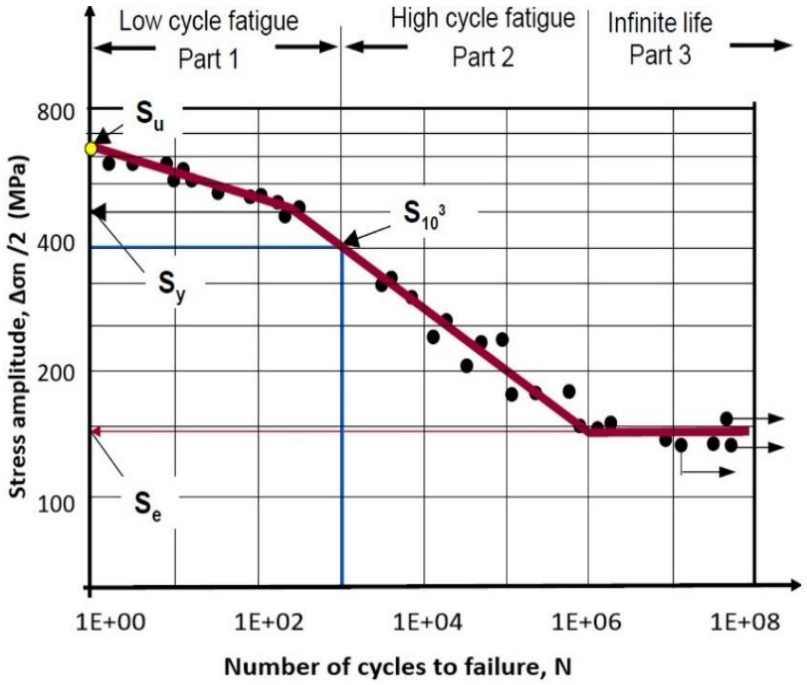

Figure 2-2: Illustration of a typical S-N curve [3]

The loading, geometry, and material properties are required as inputs in order to select the fatigue S-N curve for the specified component (see Figure 2-1). Since S-N curves are based on the nominal stress, an appropriate nominal stress must be determined to evaluate the fatigue life. After selecting an appropriate S-N curve for the analyzed component, the nominal stress acting in the component's critical cross section is used to evaluate the fatigue damage, after which the fatigue life can be evaluated. The procedure for estimating the fatigue life of welded joints using the S-N method is illustrated in Figure 2-3 and is also summarized as follow:

1) Define the external loads that represent the fatigue loading applied to the structure (Figure 2-3a).
2) Determine and analyze the internal loads acting in the critical or chosen component's cross-section (nominal stress at weld toe or root) (Figure 2-3b and c).
3) Select a proper S-N curve (from ready-made family of welded joints S-N curves) based on the specified material and the type of welded joint (Figure 2-3d and e).
4) Identify the stress parameter used for the determination of the S-N curve (nominal or reference stress)
5) Determine the analogous stress parameter for the chosen cross-section of the structure

6) Identify the appropriate stress history of the selected welded joint (Figure 2-3f)
7) Extract the stress cycles from the fatigue loading history by using the rainflow [9] method (Figure 2-3g)
8) Evaluate the fatigue damage associated with each load cycle and sum them up by using the Minar-Palgren hypothesis (Figure 2-3h and i).
9) Determine the fatigue life in terms of number of cycles to failure N, or number of stress history repetitions, N_{blck}, (No. of blocks) (Figure 2-3j).
10) Note that the procedure has to be repeated several times in case multiple stress concentrations or several critical locations are found in the chosen component of the analyzed structure.

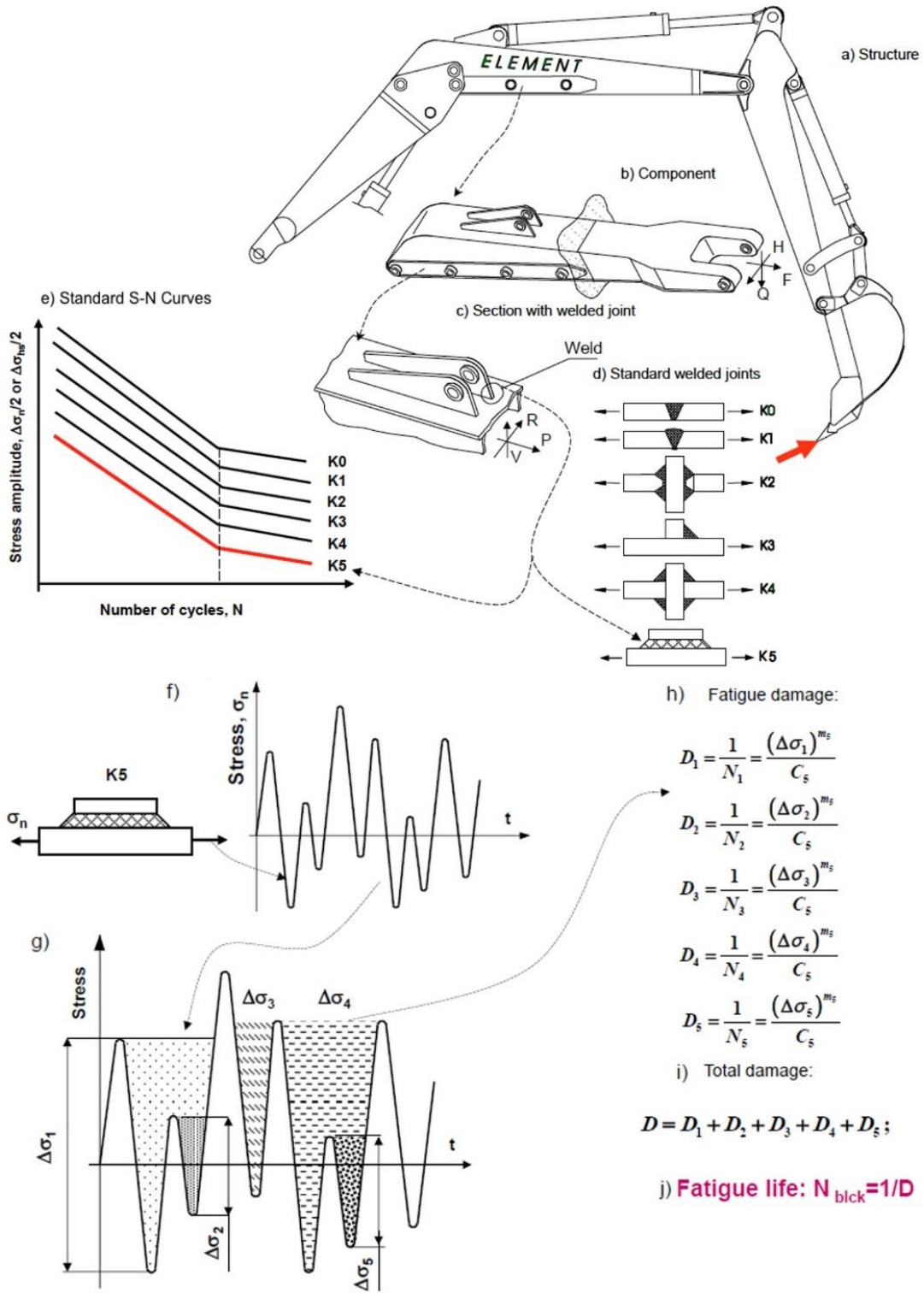

Figure 2-3: Steps for determining the fatigue life of weldments using the S-N method [3]

The S-N method accounts for the global geometry of welded joints but does not account for any of the welded joint local effects such as the macro geometrical features (weld shape and size) and the micro geometrical features (weld toe angle and radius). Application of this method requires fatigue S-N curves, which are generated through fatigue testing of small specimens or near-full-scale structures. S-N curves are available for general types of welded joints. The local effects of welded joints are included into the S-N curves obtained experimentally. Therefore, to apply this method to welded joints, the nominal stress range $\Delta\sigma_n$ should be clearly defined and the structural discontinuity of the analyzed welded element should be comparable with one of the standard specimens used to generate the selected S-N fatigue curves (see Figure 2-3d and e).

The strength of the S-N method is based on the simplicity of the nominal stress idea. It works well in the case of long fatigue life components or in the case of components subjected to constant amplitude loadings. However, the highly empirical nature of this method is its weakness. As shown in Figure 2-3d and e, the standard geometrical configurations used to generate S-N curves are not in practice closely similar to the welded joints being analyzed. Another important disadvantage is that the S-N method ignores local plastic strains, which are critical for short-life fatigue situations. The effect of the residual stress was also included to Wohler S-N curves based on experimental studies [10] yet this is still empirical which does not help in accounting for the actual residual stress in welded joints [10].

To summarize, the S-N method cannot account for the local plasticity, the residual stress, or the loading sequence effect. This method determines only the service life represents the final fracture which does not differentiate between crack initiation or propagation life. Despite the fact that the ready-made S-N curves for weldments include different factors associated with the weldment such as the residual stress, and the weld shape, the main problem remain is that this method requires determining the nominal stress in the critical cross-section. The nominal stress by definition depends on the critical cross-section area despite the welded joint's macro and micro geometrical features. In other words, two different welded joints (i.e. different weld shapes) of the same material, the same applied load to the same critical cross-section area, will result in the same nominal stress and consequently same fatigue life which is not correct. As a result, a sufficiently rich S-N database must be generated with multiple S-N curves to cover a wide variety of welded joint geometries, which in practice is difficult and expensive.

Defining the classical nominal stress, is rather difficult in the case of geometrically complex welded structures subjected to multiple simultaneously applied loads. One solution is to use hot spot stress, σhs. The hot spot stress (as will be explained in Section 2.1.1) can be determined experimentally and used for the fatigue life estimation of welded joints based on S-N curve and the hot spot stress.

2.1.1 The hot spot stress method

This section reviews the hot spot stress concept, and also reviews some studies that have used FEM to determine the hot-spot stress. The traditional nominal stress concept can be used for simple welded joints, but it is not practical to determine the nominal stress and then select one of the design S-N curves for a complex welded joint. The hot spot stress concept was first introduced in the design guidelines for tubular welded offshore structures [11]. The hot spot stress is also called structural hot spot or geometric stress. Since it was difficult to experimentally determine the hot spot stress of large size tubular joints, FEM is often used. The main idea of the hot spot stress method is to assess the stress for the S-N fatigue life estimation method by replacing the nominal stress. The advantages and disadvantages of this method are summarized at the end of this section.

The conventional method to estimate the hot spot stress is to use strain gauges located at distance 0.4T and 1T from the weld toe and extrapolate linearly the stress line to the weld toe location, as shown in Figure 2-4 (where T is the base plate thickness). The locations of the strain gauges are recommended by IIW [12]. The practical method of determining the hot spot stress is illustrate in Figure 2-4.

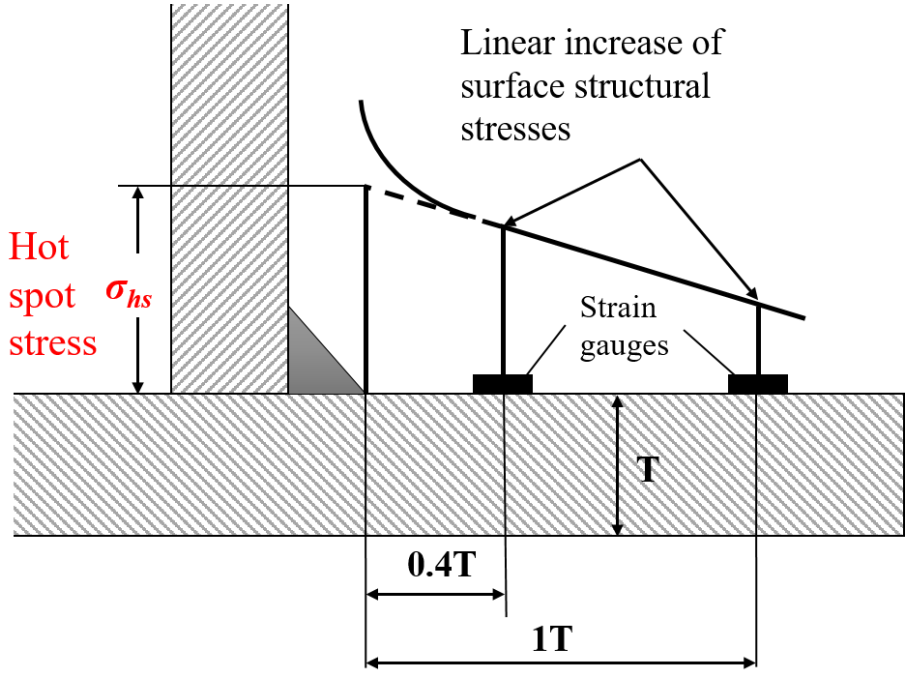

Figure 2-4: Experimental method of determining the hot spot stress in welded joints

Large size tubular joints in the offshore industry made it difficult to determine the fatigue life experimentally. Therefore, the FEM and the structural stress variant, which was developed for tubular connections in steel construction, led to the hot spot structural stress concept. This concept became a codified procedure for the fatigue assessment of large tubular components [13]. The fatigue strength of this method is mainly affected by stresses normal to the weld length dimension. Unfortunately, the FE stress analysis is dependent on the mesh size, which will affect the hot spot stress accuracy. However, Huther [14] and Fricke [15] provided recommendations concerned with the FEA meshing needed for the evaluation of the hot spot stress for various welded structures. Some procedures for evaluating the hot spot stress were also developed by Niemi, Tanskanen [16] as well as Fricke and Bogdan [17]. By measuring the stress or strain at certain distances from the weld toe, Radaj et. al.[18] proposed a method to estimate the range of the structural stress ($\Delta\sigma_{hs}$). According to [19], Haibach used the linear extrapolation method on strains extracted from the FE model at a distance of 1 to 2 mm from the weld toe to obtain the structural hot spot stress (σ_{sH}), as shown in Figure 2-5.

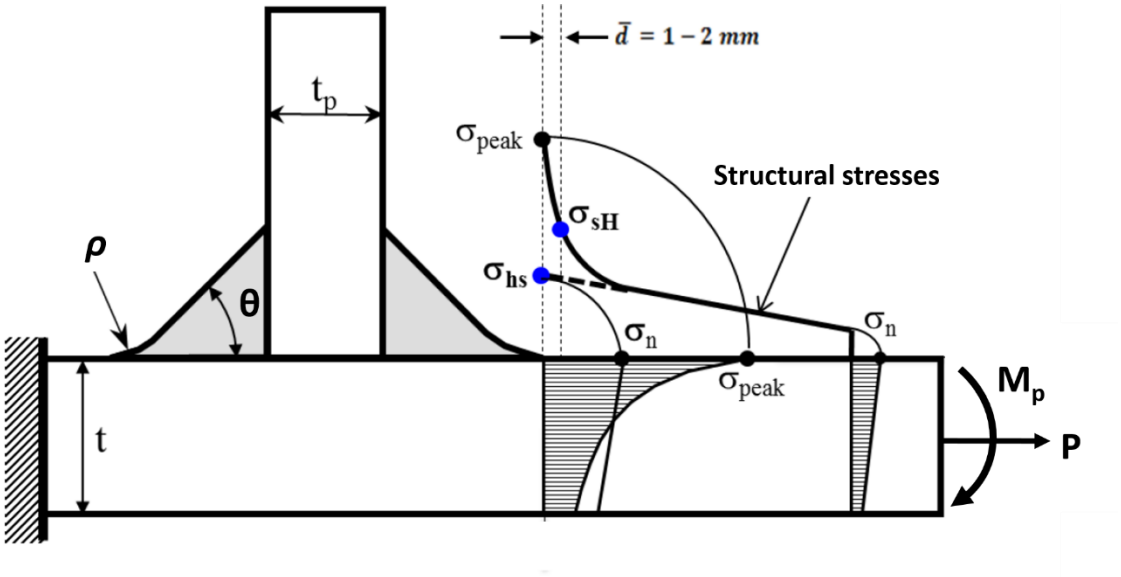

Figure 2-5: Haibach's structural hot spot stress and codified hot spot linear extrapolation procedure [18]

Maddox [20],[21] and Niemi [22] provided detailed case studies and recommendations to estimate the hot spot stress. Radaj's [23] structural stress definition was utilized by Dong [24] to find hot spot stress at the weld toe from the FE model using principles of elementary structural mechanics. Dong's work was demonstrated on several examples of simple 2D welded joints, and claimed to be mesh insensitive [25]. However, one limitation in Dong's work is that the misalignment effect on the structural stress was not included but rather presented in test specimens used for the master S-N curve. Estimation of the stress using this method does not include the effect of the residual stress, and fails in the case of welded edge gussets because it is difficult to define the points where the plate thickness is no longer relevant [26]. Xiao and Yamada [27] estimated the hot spot stress as the stress at 1mm under the weld toe surface (i.e., the expected crack path). In this way, the effect of thickness or size is included within the fatigue parameter. Noh et al. [28] plotted fatigue lives of the S-N curve versus the hot spot stress from the stress at a depth of 1mm, which happened to meet the lower bound of the design S-N curve in the Japanese design code JSSC-D, which also corresponds to the FAT 100 curve in the IIW recommendations.

The hot spot stress is believed to be close to the weld toe in a way that includes the effect of the stress concentration, but not the micro geometrical or local notch effect (weld toe radius ρ effect). However, since this method is used in conjunction with the master S-N curves, the local notch effect is included in the designed S-N curves. Using the hot spot stress instead of the nominal stress is very

useful when the nominal stress cannot be defined easily and the structural discontinuity cannot be compared with any classified S-N curve. However, using the hot spot stress method has a major challenge namely it requires determination of S-N curves based on the same hot spot stress definition.

The geometrical nature of weldments include geometrical discontinuity (stress concentration) which rise the actual stress field through the weld toe critical plate. Consequently, the actual through-thickness stress distribution $\sigma(y)$ becomes non-linear, with the maximum stress at the weld toe surface (peak stress, σ_{peak}) as shown in Figure 1-2. Therefore, determining the nominal stress based on the net cross-sectional area of the loaded plate, regardless of any associated geometrical discontinuity, making it a non-unique parameter which underestimates the critical stress in the case of welded joints. The hot spot stress, on the other hand, is based on a clear stress definition that is unique and can be determined by using FEM for any cross-section in the welded structure or for any component. The hot spot stress is an estimation based on surface stresses close to the weld toe, and it is considered equal to the nominal stress. The advantage of the hot spot stress concept is that it accounts for the effect of the overall geometry but not the micro-geometrical effects.

Therefore, the peak stress based on the hot spot stress concept can be expressed as follows:

$$\sigma_{peak} = \sigma_{hs} K_t \qquad (2.1)$$

Where σ_{hs} is the hot-spot stress and K_t is the SCF. Note that the SCF depends on the stress used, and has to be determined in the same way (e.g., by determining K_t using FE when using the hot spot stress is based on FE). The stress concentration factors in the handbooks to date are obtained for weldments under simple tension or bending loading as shown in Figure 2-6 which illustrate a T-joint subjected to a pure tensile load, P.

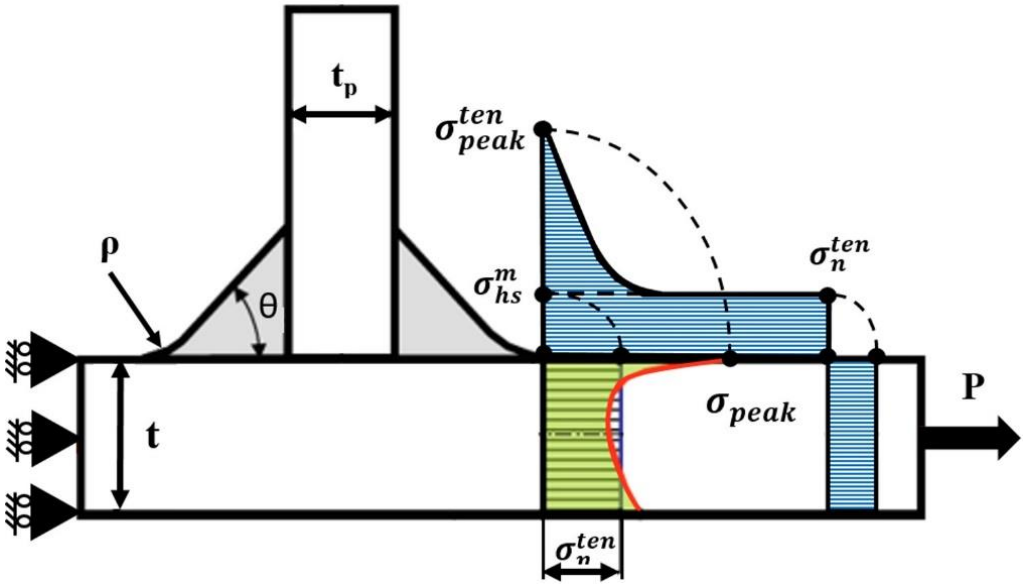

Figure 2-6 Typical T-joint subjected to pure axial tensile loading [3]

In the T-joint shown in Figure 2-6, the membrane hot spot stress equals to the nominal tensile stress:

$$\sigma_{hs} = \sigma_{hs}^{m} = \sigma_{n}^{ten} \tag{2.2}$$

The same can be said for a T-joint subjected to pure bending loading. Thus, the peaks stress based on the hot spot stress concept, in the case of pure tensile or pure bending loading conditions, can be expressed as follows:

$$\begin{aligned} \sigma_{peak}^{ten} &= \sigma_{hs}^{m} K_t^{ten} \quad \text{(For pure tensile loading)} \\ \sigma_{peak}^{ben} &= \sigma_{hs}^{b} K_t^{ben} \quad \text{(For pure bending loading)} \end{aligned} \tag{2.3}$$

In conclusion, neither of the stresses σ_n, and σ_{hs} represent the actual peak stress at the weld joint critical areas, nor do they provide any stress data through the thickness of the weld toe. Thus, neither of the stresses can be used for the strain-life method or the LEFM.

2.2 Fatigue life prediction of weldments using the strain-life (ε-N) method

The ε-N method or the local strain-life method is based on the concept that if the local notch tip strain history (or the weld toe stress history) and the strain history in the test specimen are the same, then

the fatigue response in the notch tip region and the specimen will also be the same and therefore their fatigue lives will be the same as well. Therefore the fatigue strain-life curve obtained from simple smooth material specimens can be used for the evaluation of fatigue lives of notched components. This method was developed for the non-welded components and was then extended to assess welded components fatigue lives which may experience local plasticity at the weld toe. The strain-life fatigue estimation method uses elasto-plastic strain range as an estimation parameter. The stress-strain analysis module (see Figure 1-1) of this method requires the knowledge of the linear-elastic peak stress in the critical area of the component in order to estimate the fatigue life.

Langer [29] studied the variable amplitude loading effect in fatigue analysis and divided the crack life phases into initiation and propagation, suggesting a damage sum of 1.0 for both phases. The notch effect on the monotonic and cyclic deformation of engineering materials was discussed by Neuber [30], who discovered that the importance of using the average stress over a small material volume ahead of a notch tip is more important than the peak stress at the notch tip. Coffin [31] and Manson [32] formulated the idea that plastic strain was responsible for fatigue damage. It should be mentioned that the empirical relationship between the number of stress reversals to fatigue failure and the plastic strain was proposed independently by both Coffin and Manson. For the current local ε-N fatigue analysis method, Topper [33] and Morrow [34] promoted Coffin [31] and Manson's [32] work, along with Neuber's rule [35].

The general procedure for estimating the fatigue life of a component by using the ε-N method is illustrated in Figure 2-7. The general procedure begins by determining the material properties, geometry, and loading of the component to be analyzed, after which the fatigue damage accumulated at the critical location can be calculated. Finally, the fatigue crack initiation life can be calculated.

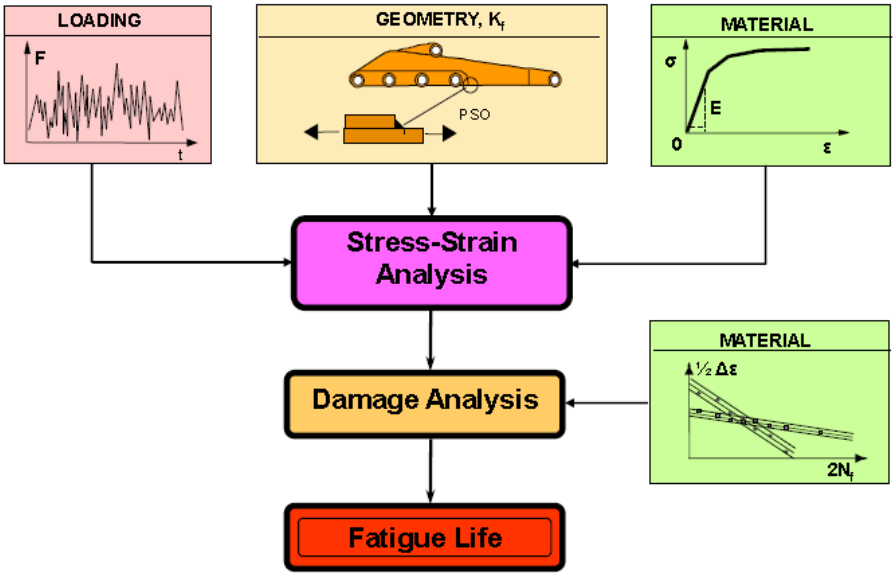

Figure 2-7: Fatigue life estimation procedure based on the local strain-life method [3]

The loading history required for the S-N fatigue method is the nominal stress. The nominal stress history must be taken for the critical cross-section of the analyzed component. The material properties of the strain-life method can be obtained by testing smooth specimens according to the ASTM standard [36]. In order to determine the fatigue parameters of the material's Ramberg-Osgood cyclic stress-strain curve and the Manson-Coffin curve (i.e. the cyclic strength coefficient, K´ and the fatigue ductility exponent, n´), the fatigue test data must be used to plot the Ramberg-Osgood cyclic stress-strain curve (Figure 2-8a) from the stabilized hysteresis loops [37]. In addition, the stress amplitude versus the plastic strains of the cyclic Ramberg-Osgood curve should be plotted as shown in Figure 2-8b. Then the elastic strain amplitude and the plastic strain amplitude are to be plotted separately versus the number of reversals obtained from the fatigue test data (Figure 2-8c and d).

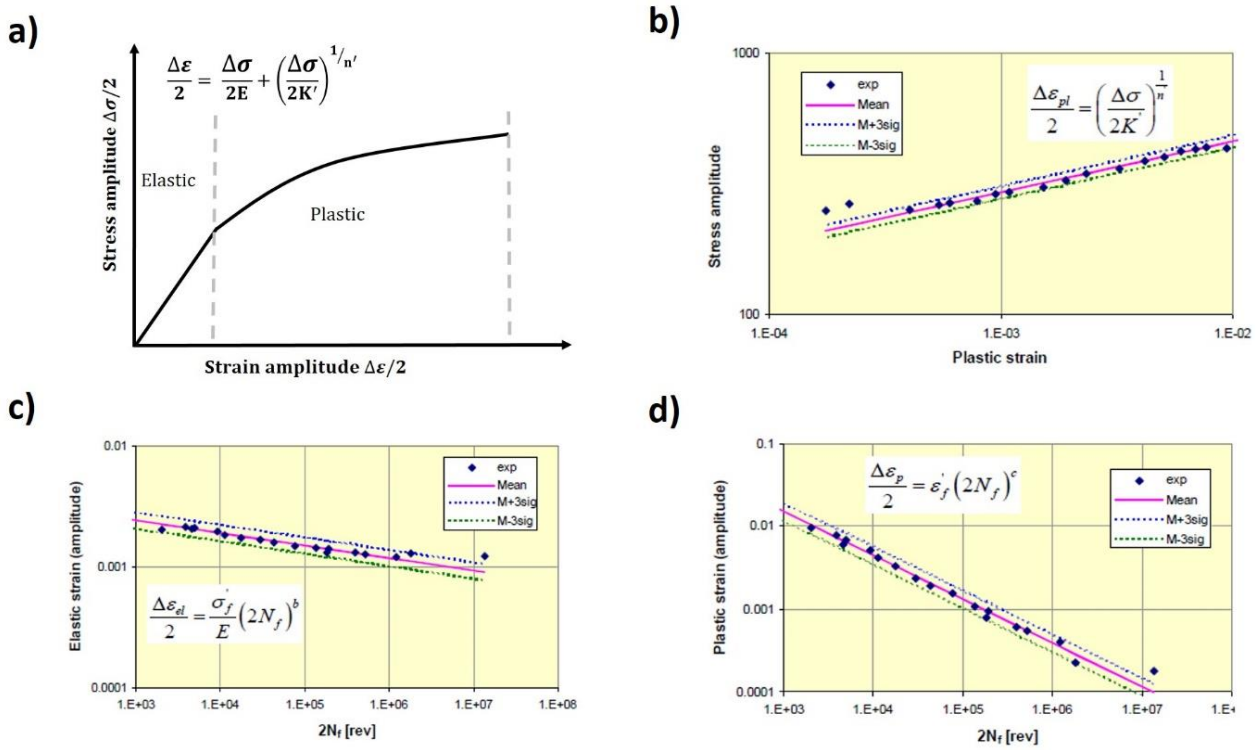

Figure 2-8: Material fatigue curves, a) Ramberg-Osgood cyclic stress-strain curve, b) The stress-plastic strain fatigue curve, c) The elastic strain amplitude-life ($\Delta\varepsilon_e/2$ - N_f) fatigue curve, d) The plastic strain amplitude-life ($\Delta\varepsilon_p/2$ - N_f) fatigue curve [3]

The most popular expression relating the strain range to the number of cycles, called the Manson-Coffin curve [31],[32] is given in terms of the total strain range $\Delta\varepsilon$:

$$\frac{\Delta\varepsilon}{2} = \frac{\sigma'_f}{E}(2N_f)^b + \varepsilon'_f(2N_f)^c \qquad (2.4)$$

The total strain-life curve (Manson-Coffin curve) is the summation of the two curves shown in (Figure 2-8c and d). Equation (2.4) allow determining the fatigue damage for crack initiation estimation. The elastic plastic strain-life curves shown in Figure 2-8c and d (in term of strain amplitudes) are summand in Figure 2-9 which represent the Manson-Coffin strain-life curve (red curve).

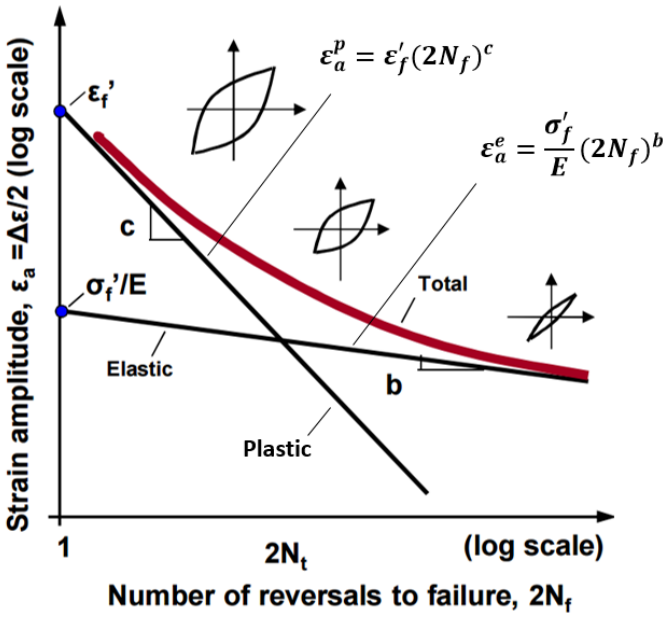

Figure 2-9: Typical fatigue strain-life curve [3]

The stress state is multi-axial in weldments. However, the multi-axial stress at the surface reduces to two normal stresses and one shear component. The stress normal to the weld toe line generates most of the fatigue damage due to the effect of the stress concentration. The peak stress is the stress value defined as the product of the stress concentration factors SCF, K_t, and the nominal stress, σ_n as follows (it can also by directly obtained from FE analysis when possible):

$$\sigma_{peak} = K_t \sigma_n \tag{2.5}$$

The rise in the local stress due to the stress concentration generally affects the local elastic stress to exceed the yield limit, which result in local plastic deformation. The notch effect is one of the micro geometrical factors of welded joints that affect critical stress and the fatigue life accordingly. For example, Figure 2-10 illustrate the notch effect on the critical stress of a T-joint where the stress is concentrated at the weld toe.

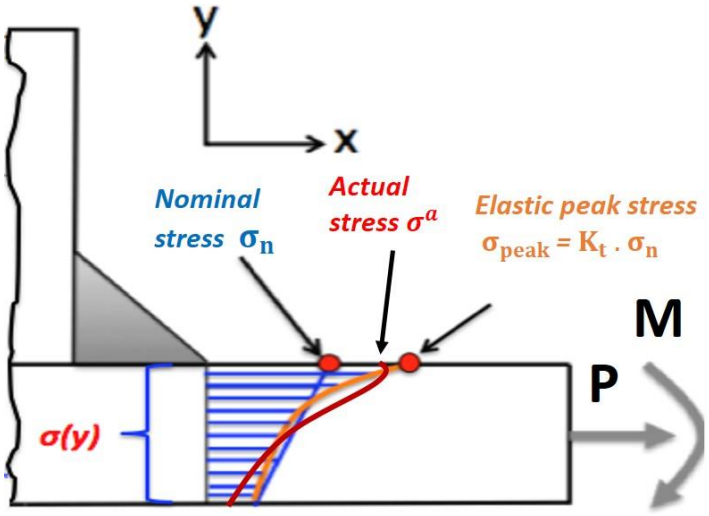

Figure 2-10: Illustration of elastic and plastic stresses at notch tip or T-joint weld toe

In order to determine the elastic-plastic strains and stresses at the notch tip (weld toe), when the pseudo-linear elastic stress exceeds the material yield limit, the Neuber rule [35] is used. The actual local notch tip or weld toe elastic-plastic strain and the stress responses ($\sigma^a_{max}.\varepsilon^a_{max}$) are calculated as follows according to Neuber rule [35]:

$$\frac{(K_t \cdot \sigma_n)^2}{E} = \sigma^a_{max}.\varepsilon^a_{max} \quad \text{or} \quad \frac{(\sigma_{peak})^2}{E} = \sigma^a_{max}.\varepsilon^a_{max} \tag{2.6}$$

Where the left hand side represents the applied load and the right hand side represents the notch tip elastic-plastic response. The above equation has two unknowns, namely the Neuber stress σ^a_{max} and strain ε^a_{max}, and therefore another equation is required. The well-known Ramberg-Osgood equation 2.7, which represents the material cyclic stress-strain curve, is used simultaneously with equation 2.6 to relate the linear elastic stress and strains to the actual elastic-plastic stresses and strains at the notch. The cyclic stress-strain curve and the Neuber rule are illustrated in Figure 2-11.

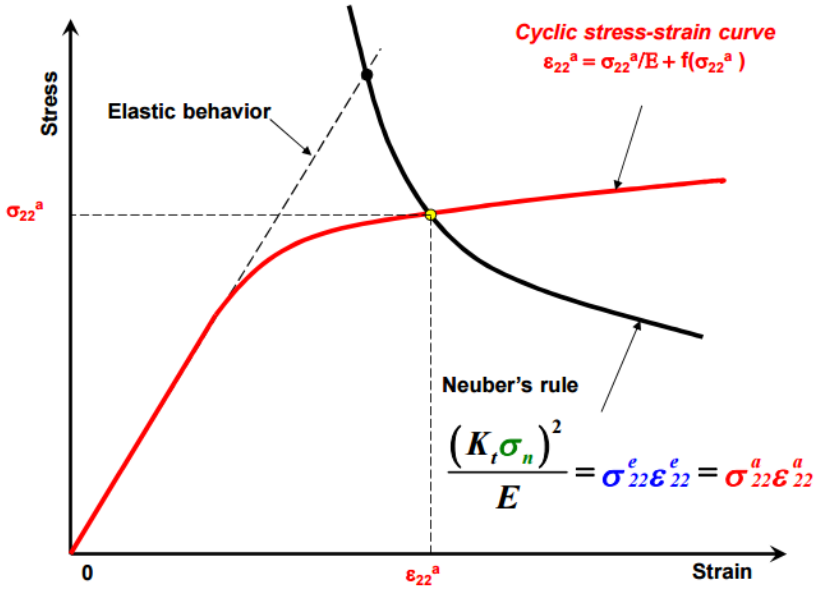

Figure 2-11: Illustration of the Neuber rule and the stress-strain curve [3]

The intersection point of the cyclic stress-strain curve and Neuber's hyperbola in Figure 2-11 denotes the solution to the system of the two equations, i.e. provides the actual values for the elasto-plastic strain and stress at the notch tip or at the weld toe. Therefore, in order to account for the notch effect, the actual elastic-plastic stresses and strain response must be determined for each fatigue loading cycle. Thus, the loading segment in the cyclic loading history (i.e., the tensile part of the first cycle) can be determined by using simultaneously the Ramberg-Osgood cyclic stress-strain equation and the Neuber rule, as:

$$\varepsilon_{max}^a = \frac{\sigma_{max}^a}{E} + \left(\frac{\sigma_{max}^a}{K'}\right)^{1/n'} \quad \text{and} \quad \frac{(\sigma_{peak})^2}{E} = \sigma_{max}^a . \varepsilon_{max}^a \tag{2.7}$$

For the unloading segment of the cyclic loading, the cyclic stress-strain curve is expanded by a factor of 2 (see red curve in Figure 2-12), and then the elasto-plastic strain range and the associated stress range are calculated:

$$\frac{(\Delta\sigma_{peak})^2}{E} = \Delta\sigma^a . \Delta\varepsilon^a \quad \text{and} \quad \Delta\varepsilon^a = \frac{\Delta\sigma^a}{E} + 2\left(\frac{\Delta\sigma^a}{2K'}\right)^{1/n'} \tag{2.8}$$

The Neuber rule procedure for determining the actual stress-strain response at the notch tip is shown in Figure 2-12, where S represent the applied loading stress or the nominal stress.

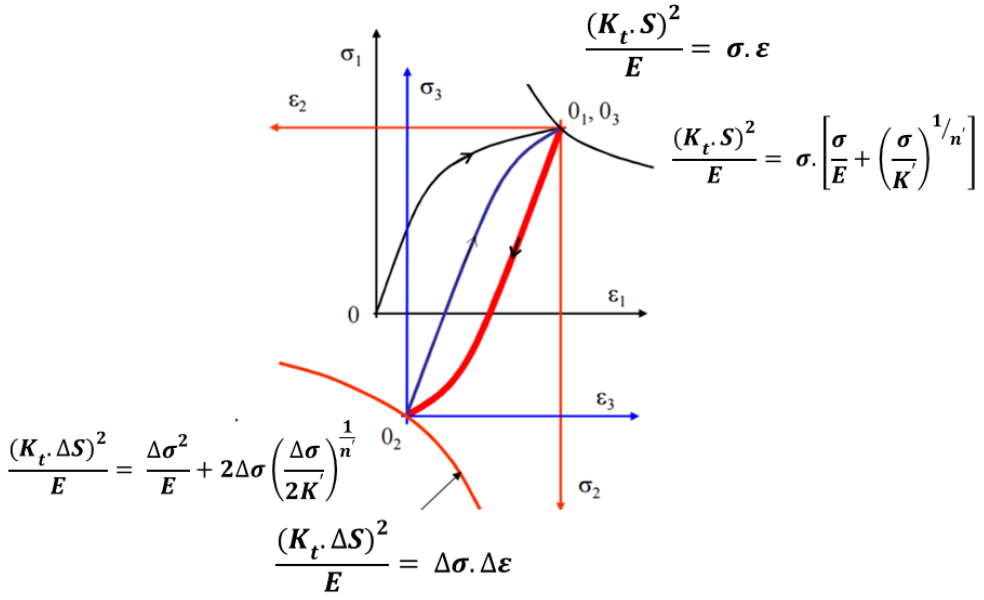

Figure 2-12: Notch tip stress-strain response (Neuber rule) [3]

The loading part (black curve) from point 0 to 0_1 shown in Figure 2-12, illustrates the determination of the actual values for the elasto-plastic strain and stress at the notch tip or the weld toe by using the system of the two equations (equation 2.7). The unloading part (red curve) from point 0_1 to 0_2 shown in Figure 2-12, illustrates the determination of the actual values for the elasto-plastic strain range and the associated stress range at the notch tip or the weld toe by using the system of the two equations (equation 2.8).

Material strain-life curves are generated based on test specimens subjected to constant strain amplitude around zero mean stress, whereas machine components in practice are often subjected to cyclic loading histories with non-zero mean stresses. Therefore, the mean stress effect in the ε-N method needs to be accounted for. Many models have been introduced to modify the ε-N equation to account for the non-zero mean stress effect. Morrow [38] introduced a strain-life equation that accounts for the mean stress σ_m effect by adding it to the elastic term of the Manson-Coffin curve [31],[32]. Another model, introduced by Smith, Watson, and Topper (SWT) [33], suggested that the Mason-Coffin equation could be written in a form involving the maximum stress of a given cycle or the stress corresponding to the tip of the hysteresis loop as follows (SWT equation):

$$\sigma_{max}\frac{\Delta\varepsilon^{a}}{2}=\frac{(\sigma_{f}')^{2}}{E}(2N_{f})^{2b}+\sigma_{f}'\,\varepsilon_{f}'\,(2N_{f})^{b+c} \tag{2.9}$$

However, it should be noted that the SWT is more conservative than Morrow's version. Note that the N_f in equation (2.9) is considered the number of cycles to failure assuming the life ends when the crack initiates. Thus, it could be written as N_i.

The well-known linear damage accumulation rule, by Palmgren [7] and Miner [8] (Palmgren-Miner linear damage hypothesis), is subsequently used to assess the fatigue damage (or SWT equation 2.9) induced by a variable amplitude cyclic stress history and it is given in the form of expression (2.10). The total fatigue damage given by the Miner rule or Palmgren-Miner linear hypothesis can be calculated as follow:

$$D=\sum_{i=1}^{k}\frac{n_i}{N_i} \tag{2.10}$$

Where D is the fatigue damage induced by stress ranges, n_i is the number of cycle of each stress ranges, and N_i is the number of cycles to failure at each stress range. The SWT equation 2.9 can be used to find the damaging cycles. Therefore, the total number of cycles to failure (fatigue life) is found as follow:

$$N_{blck}=\frac{1}{D} \tag{2.11}$$

Note that equation (2.11) determines the total number of cycles to crack initiation N_i.

The specific steps for using the ε-N method to estimate the fatigue life of welded joints (Figure 2-13) are as follows:

1) Find the external loads representing the fatigue loading applied to the structure and the specified component (welded connections) (Figure 2-13a).
2) Analyze the internal loads acting in the critical or chosen component's cross-section (weld toe or root) (Figure 2-13b and c).
3) Calculate the maximum elastic local stress (peak stress) acting at the critical point, such as a point on the weld toe line (Figure 2-13d).

4) Assemble the local stress history from the cyclic peaks and valleys of the loading sequences (Figure 2-13e and f).
5) Determine the elasto-plastic stress-strain response at the critical location (Figure 2-13g) using the Neuber rule's [35] procedure shown in Figure 2-11.
6) Obtain the stress-strain hysteresis loops or cycles (Figure 2-13h).
7) Determine the fatigue damage (N_f) induced by each cycle (Figure 2-13i and j) by using SWT equation (2.9) with the proper material constants according to ASTM standard [36] or by using the Ramberg-Osgood and the Manson-Coffin curves [31],[32](see Figure 2-9).
8) Summon the linear damage by using Palmgren-Miner linear hypothesis rule [8] (equations 2.10) (see Figure 2-13k)
9) Determine fatigue life to crack initiation by using equation 2.11 as shown in Figure 2-13.

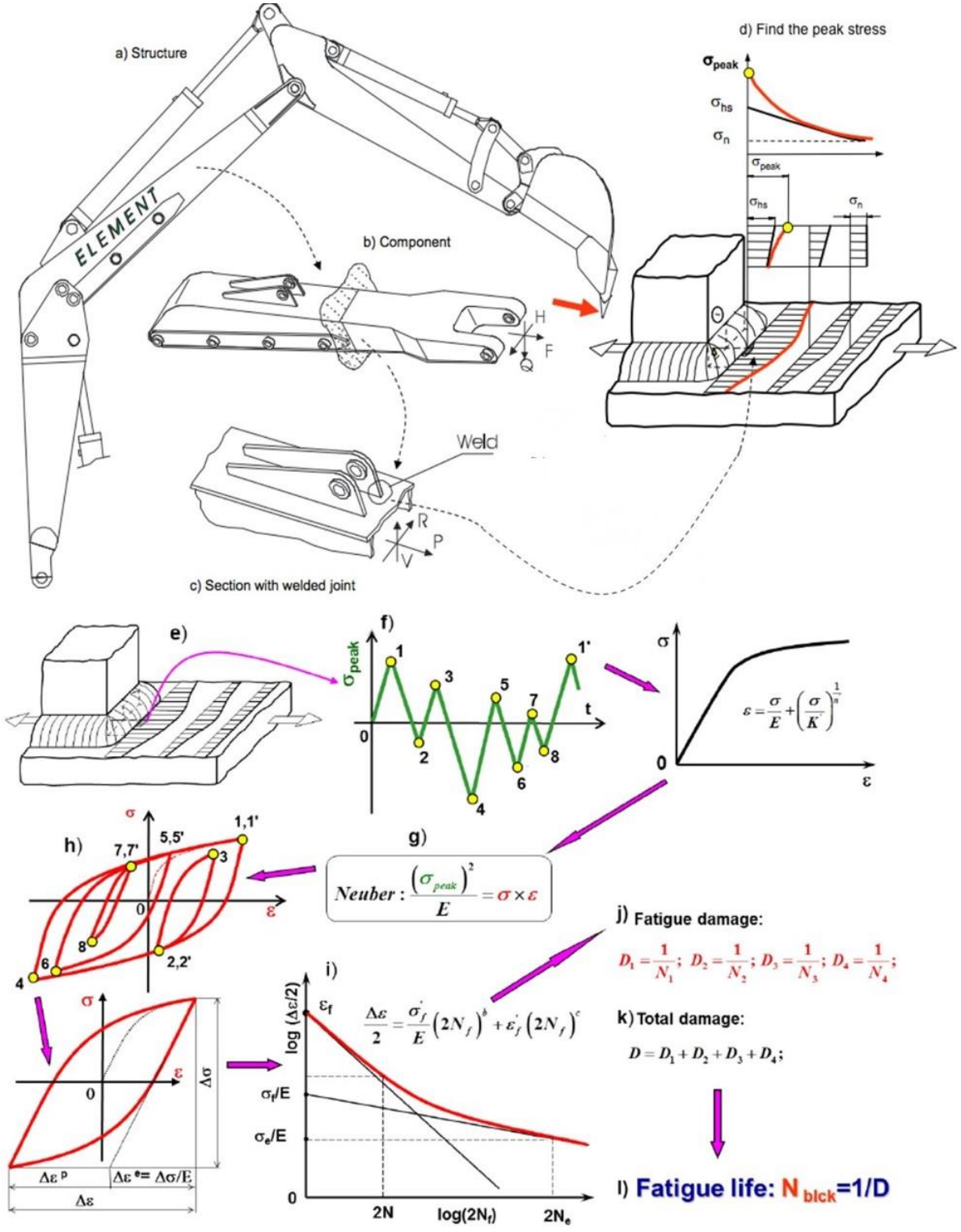

Figure 2-13: Steps in determining the fatigue life of weldments using the ε-N method [3]

The strain-life method is capable of accounting for the macro and micro geometrical features of welded joints. Unlike the S-N or hot spot methods, which estimate the fatigue life to final fracture, the ε-N method estimates the fatigue life to crack initiation only. The total fatigue life of a component is expressed as numbers of load cycles which include the technical crack initiation life and the subsequent crack propagation life to final fracture. The fatigue life up to a technical crack comprises the microstructural crack initiation life and the short-crack propagation life. In the case of un-notched components, most of the total fatigue life may be consumed in the initiation of the crack, whereas in sharply notched components the crack initiation life may be very short.

When using the strain-life method for welded joint fatigue life estimations, there are some factors that affect the fatigue life estimation. These factors, such as stress concentration, notch effect, and residual stress, are discussed in the following sub-sections.

2.2.1 Welded joint residual stress effect on the ε-N method

One factor that must be accounted for when using the strain-life method to estimate the fatigue life of welded joints is the residual stress. Residual stresses, also called internal stresses, occur in a structure or a component due to external forces or heating process like the case of welding, and subsequently remain after all external forces are removed. Residual stresses can occur at any stage of a component's service life. Usually, they are produced in a component after being subjected to high temperatures where the metal micro-structure changes. For example, the heating and cooling during and after welding can cause expansions and then contractions within the base metal and the heat affected zone (HAZ), all of which results in the generation of residual stresses at the weld and its surrounding areas. In case of a welded T-joint shown in Figure 2-14, the heating and cooling from the welding operation will form tensile residual stress in the area adjacent to the weld, and compressive residual stress in areas away from the weld.

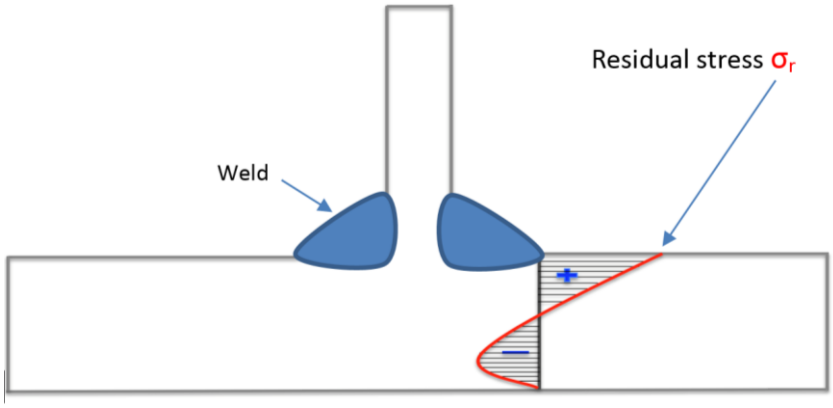

Figure 2-14: Illustration of the residual stress distribution in the heat affected zone (HAZ)

The maximum residual stresses are usually equal to one-half of the yield strength of the base material [39]. The residual stress affects the fatigue life of machine components largely because it interacts with the imposed cyclic stresses induced during operations. Unfortunately, the residual stress σ_r cannot be added linearly to the actual stresses at the notch tip. However, the residual stress can be combined with the pseudo-elastic stress in the Neuber rule (see Figure 2-15), as follows:

$$\frac{(K_t . S + \sigma_r)^2}{E} = \sigma . \varepsilon \qquad (2.12)$$

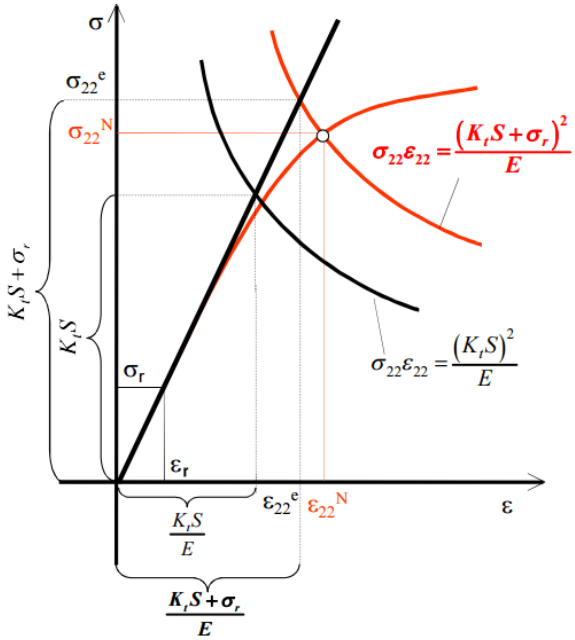

Figure 2-15: Adding the residual stress effect to the Neuber rule [3]

The red hyperbola curve shows the stress-strain response with the residual stress effect, while the black one shows the response without the residual stress effect. The notch stress-strain response must lie on the cyclic stress-strain curve and Neuber's hyperbola. As a result, the intersection point of the two curves should represent the actual values of the stresses and strains. Due to the presence of the residual stress, the actual stresses and strains will increase in the first reversal or the set-up cycle. The intersection point of the Neuber hyperbola and the cyclic stress-strain curve will shift according to the residual stress (compressive or tensile), as shown in Figure 2-16.

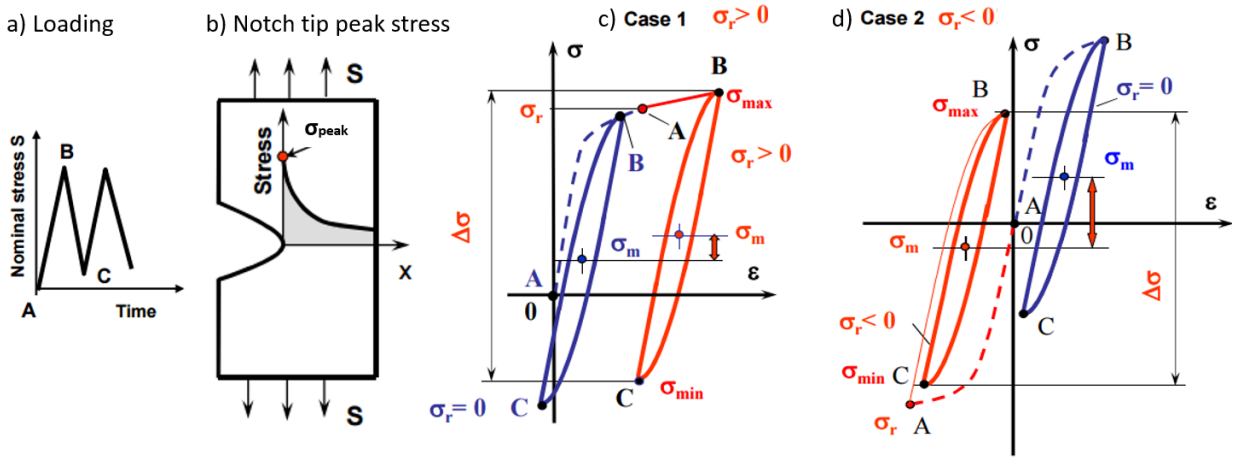

Figure 2-16: Residual stress effect on the notch tip stress-strain response: a) Loading history, b) Notched specimen, c) Tensile residual stress response, d) Compressive residual stress response [3]

Unlike the S-N method, the ε-N method takes the actual stress-strain response of the material into account. The ε-N fatigue method is preferred in cases of local plasticity (weld toe or notch tip) because the S-N fatigue method cannot correctly account for the plasticity at the notch tip. The ε-N method is also preferred when the load sequence effect and the residual stress are of importance. Nevertheless, the ε-N method requires certain special techniques to determine the peak stress. Those newly developed techniques are discussed later.

It should be noted that the local strain-life fatigue method enables evaluation of the fatigue life to initiate a relatively small crack. The remaining part of the fatigue life, which might be a significant part of the total life, is usually predicted by using the Linear Elastic Fracture Mechanics Method. The total fatigue life can be determined as the sum of the fatigue crack initiation and propagation lives.

2.3 Fatigue life prediction of weldments using the Linear Elastic Fracture Mechanics (LEFM) method

The concept of the Linear Elastic Fracture mechanics (LEFM) method is based on the analysis of fatigue crack propagation life. The LEFM approach can be used to evaluate or predict the crack growth or crack propagation life stage, assuming that the initial crack is already present. Irwin [40] has introduced the meaning of the stress intensity factor (SIF), denoted as K, and its importance in determining the static strength of cracked bodies. Irwin stated that instant fracture occurs, when the SIF reaches certain critical magnitude called the fractures toughness K_{IC} which is a material property.

Fracture mechanics based on fatigue crack growth analysis was then introduced by Paris [41], who used the stress intensity range ΔK to describe the fatigue crack growth rate da/dN. Although Paris's equation does not account for the mean stress effect, it is still being used today. The importance of crack tip closure in fatigue crack growth was later introduced by Elber [42], who developed a model showing that effective stress intensity factor controls fatigue crack growth, rather than the applied stress intensity factor range. In 1970, Paris [43],[44] established the threshold stress intensity factor concept, which is considered the fatigue limit below which fatigue crack growth cannot occur.

Paris [41] pointed out that the fatigue crack growth rate (da/dN) can also be described by using the SIF range, ΔK. For monotonic loading, the load/stress and the geometry combined are represented as K. For cyclic loading, the range of the stress intensity factor, ΔK, is the most important parameter governing fatigue crack growth rate. The fatigue crack growth material properties are given in the form of a da/dN versus ΔK curve, relating the fatigue crack growth rate to the SIF range ΔK. Note that the LEFM method will be used to predict the fatigue crack propagation life all case studies presented in Chapter 4. Therefore, this method is explained in detail below.

The general procedure for estimating the fatigue crack propagation life of a component using the LEFM method is shown in Figure 2-17. The procedure begins with determining the material properties, geometry, and loading of the analyzed component, after which the fatigue crack growth in a component can be determined. Finally, the fatigue crack propagation life can be estimated.

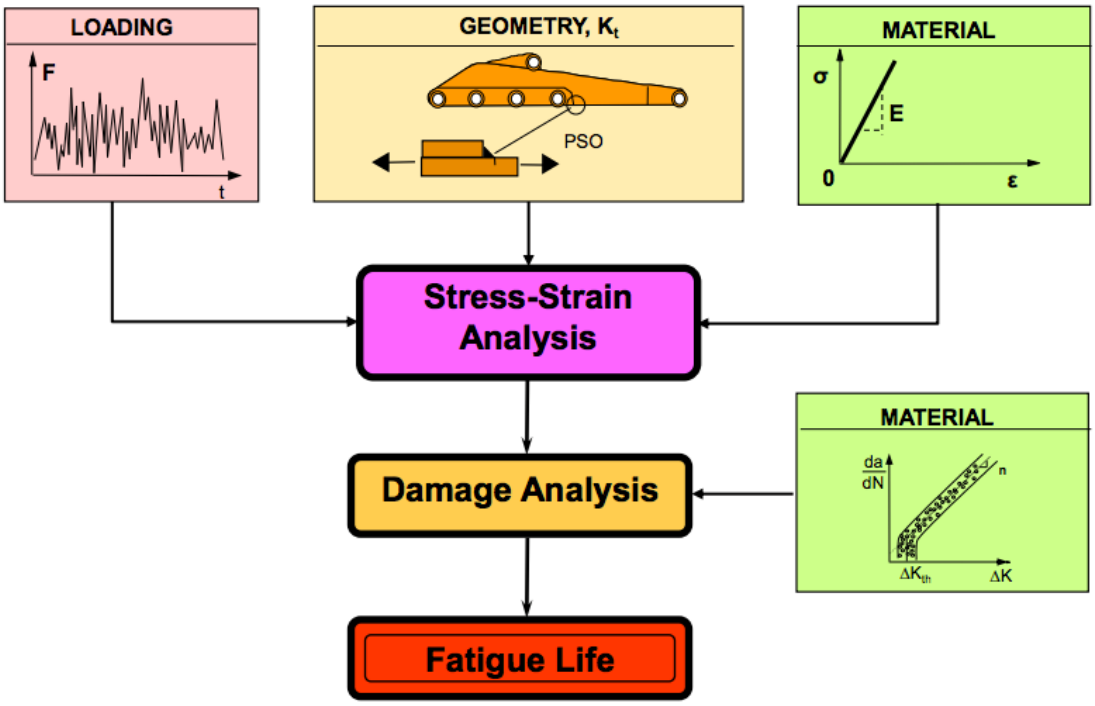

Figure 2-17: General steps of the fatigue life estimation using the LEFM method [3]

For the loading history shown in Figure 2-17, the stress intensity factor range must be determined for the critical cross-section of the analyzed component assuming an initial crack. The geometry of the selected component (Figure 2-17) is important in order to estimate the initial crack size, and shape. The critical cross-section of the analyzed component is important for determining the initial and final or critical crack size. The fracture mechanics method assumes the crack is already initiated as an initial crack size a_i that increases up to a critical crack size a_f. One problem is that there is no general rule as to what should be the initial crack size because the assumption may depend on inspection capabilities, material properties, and loading conditions. The critical crack size is the crack length where the final brittle fracture may occur. The mechanical properties of the analyzed component required for the LEFM method shown in Figure 2-17, can be found in handbooks or tested. For the stress analysis step in determining the fatigue crack propagation life using the LEFM method, the Paris law material constants (C, and m) must be determined along with the stress intensity factor. The SIFs can be found in handbooks. However, the SIF can also be determined using the FEM or weight function. The weight function requires the knowledge of the stress distribution

across the prospective crack plane as will be discussed in details later. In order to evaluate the fatigue crack growth life, the fatigue crack growth curve must be determined.

The fatigue crack growth curve has three regions, as shown in Figure 2-18. The first region (I) includes the threshold stress intensity range, ΔK_{th}, which is the limit below which cracks are not able to propagate [43], [44]. Cracks usually grow in the second region (II) until they reach the third region. The third region (III) includes the critical stress intensity factor K_c or the fracture toughness, K_{IC} [40].

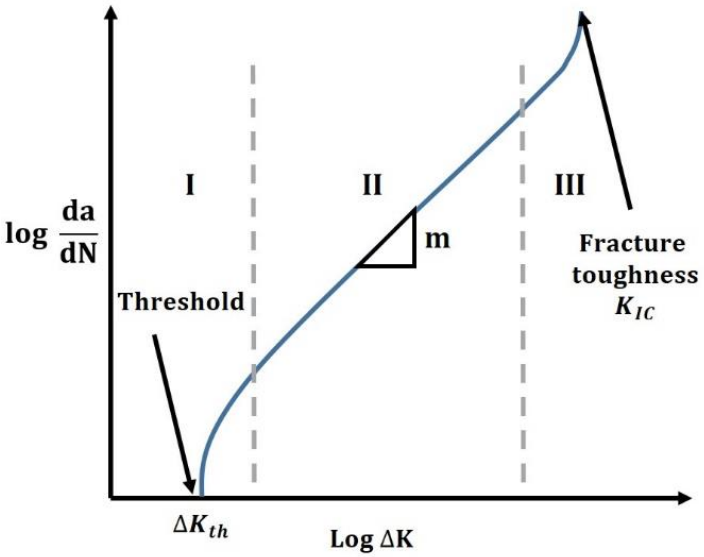

Figure 2-18: Typical fatigue crack growth curve

The Paris equation [45] is the most widely accepted expression for evaluating fatigue crack growth, and the Paris equation is applicable in Region II where the logarithmic response of (da/dN to ΔK) is linear (Figure 2-18). Paris equation also known as Paris law:

$$\frac{da}{dN} = C(\Delta K)^m \tag{2.13}$$

Two material constants C and m are required to evaluate the fatigue crack growth life within the LEFM method and they are determined experimentally according to the ASTM [46] standard procedure. As an alternative to the experimental method, Noroozi et al. [47],[48] proposed an analytical model to estimate the material constants required for fatigue crack growth, including the effect of the mean stress or the stress ratio R. This model is based on the analysis of the crack tip elastic-plastic stress-strain history and the strain-life material fatigue properties, i.e. Manson-Coffin

curve [31][32]. The analytical model to estimate the material constants required for fatigue crack growth [47],[48] is given as follows:

$$\frac{da}{dN} = C\,[(K_{max})^p\,(\Delta K)^{1-p}]^\gamma \tag{2.14}$$

Where: C, p, m, and γ are material constants; whereas the range of the stress intensity factor ΔK are determined as follows:

$$\Delta K = K_{max} - K_{min} \tag{2.15}$$

Where: K_{max} represents the maximum SIF However, it is better to rewrite Paris equation (2.13) and present it in a more compact form similar to the Paris equation as shown below:

$$\frac{da}{dN} = C(\Delta\kappa)^\gamma \tag{2.16}$$

Where: $\Delta\kappa = (K_{max})^p\,(\Delta K)^{1-p}$

Once the material constants C and m are known, the integration of the Paris equation can provide the crack growth life from initial crack size a_i to final crack size a_f. The crack growth life is presented in terms of the number of cycles to failure, N_p i.e.:

$$N_p = \int_{a_i}^{a_f} \frac{da}{C(\Delta K)^m} \text{ or } N_p = \int_{a_i}^{a_f} \frac{da}{C[(K_{max})^p\,(\Delta K)^{1-p}]^\gamma} \tag{2.17}$$

The stress intensity factor expressions can be found in handbooks [49] but not for welded structures that have complex geometry and loading mode at the critical areas such as the weld toe. However, there are other methods to determine the stress intensity factor which are the FEM and the weight function. The finite element method (FEM), however, is time-consuming for cracked bodies. The weight function technique [50], on the other hand, can be used to determine the SIF. The weight function method was found to be a more efficient solution in the case of welded joints.

The weight function method for calculating the stress intensity factor is based on the proven assumption that the stress intensity factor for any loading, S (Figure 2-19a) is equal to the stress

intensity factor obtained by applying to the cracked faces (Figure 2-19c) the stresses that used to be there when there was no crack (Figure 2-19b) [3].

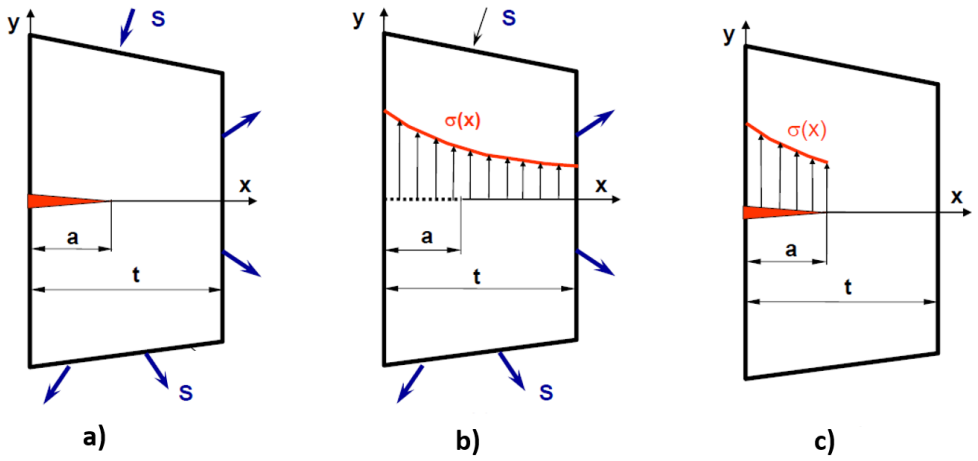

Figure 2-19: a) Body with a crack subjected to various loading; b) Uncracked body; c) Cracked body [3]

The weight function depends only on the geometry of the cracked body. In other words, the stress intensity factor in (Figure 2-19a) K_a equal to the SIF K_b of (Figure 2-19c). As a result, the stress intensity factor can be found for any crack geometry if the weight function for given configuration is known. The calculation of the stress intensity factor requires [49] integration of the product of the stress distribution σ(x) and the weight function m(x,a) over the crack area or the crack size in the case of one-dimensional cracks (Figure 2-20).

$$K = \int_0^a \sigma(x).\, m(x,,a).\, dy \tag{2.18}$$

Where a, is the crack length and m (x,a) is the weight function dependent on the crack geometry. This is the reason why the through-thickness stress distribution is required for the LEFM method. A family of universal weight functions for one-dimensional cracks was derived by Glinka and Shen [51],[52], in the following generalized form:

$$m(x,a) = \frac{2}{\sqrt{2\pi(a-x)}}\left\{1 + M_1\left(1-\frac{x}{a}\right)^{1/2} + M_2\left(1-\frac{x}{a}\right) + M_3\left(1-\frac{x}{a}\right)^{3/2} \ldots.\right\} \tag{2.19}$$

Where M_1, M_2, and M_3 given in references [51],[52] depend on the geometry of the crack.

Finding the stress intensity factor by using the weight function requires the application of the superposition method. The following steps summarize how to determine the stress intensity factor by using the weight function:

1) Calculate the through-thickness stress distribution $\sigma(y)$ in the prospective crack plane of the uncracked body (Figure 2-20).
2) Apply the stress from Step 1 to the crack surface.
3) Integrate the product of the stress distribution $\sigma(y)$ and the weight function m(y, a/t) over the crack surface area (Figure 2-20).

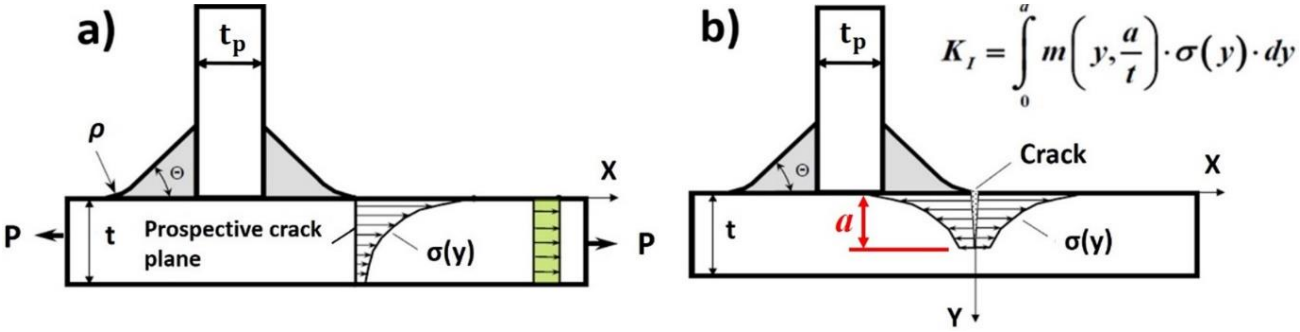

Figure 2-20: Superposition principle for calculating the stress intensity factor using the weight function method. a) Uncracked T-joint and the stress distribution in the prospective crack plane; b) Cracked T-joint with the "uncracked stress field" applied to the crack surface [3]

When the stress intensity range ΔK exceeds the threshold ΔK_{th}, the crack starts growing. Calculation of crack increments on a cycle-by-cycle basis is one way to estimate the fatigue crack growth life. The crack increment, Δa_i, is normally calculated for each cycle from the Paris equation for each cycle or the modified form of Paris equation (2.16) that include the effect of the mean stress or the stress ratio R. The sum of subsequent crack increments determine the instantaneous crack length. The crack increments can be calculated as follows:

$$\Delta a_i = C(\Delta K_i)^m \, \Delta N_i \quad \text{and} \quad a_f = a_o + \sum_{i=1}^{N} \Delta a_i \tag{2.20}$$

Numerical integration of Paris equation results in determining the fatigue life, as follows:

$$N = \sum_{i=1}^{n} \Delta N_i = \sum_{i=1}^{n} \frac{\Delta a_i}{C(\Delta K)^m} \tag{2.21}$$

The criterion for failure in the LEFM method is determined by two limits. The first is when the crack size reaches the assumed critical crack size $a_i \geq a_f$. The second is when the fracture toughness limit K_c is reached (i.e. when $K_{max} \geq K_c$).

The procedure for estimating the fatigue crack propagation life of welded joints by using the LEFM method is shown in Figure 2-21 and summarized as follows:

1) Determine the external loads and boundary conditions of the structure (Figure 2-21a),
2) Identify the internal loads in the selected component (Figure 2-21b and c),
3) Identify the proper nominal or appropriate reference stress (Figure 2-21d),
4) Extract the stress cycles by using rainflow counting method [9] (Figure 2-21e),
5) Determine the stress intensity factor either by the weight function or by using ready-made solution or the FE method (Figure 2-21f and g),
6) Determine the crack growth increments for each cycle (Figure 2-21h),
7) Calculate the associated fatigue life by determining the number of cycles, N that is required to grow the crack from the initial size, a_i to the final crack size a_f, (Figure 2-21i).

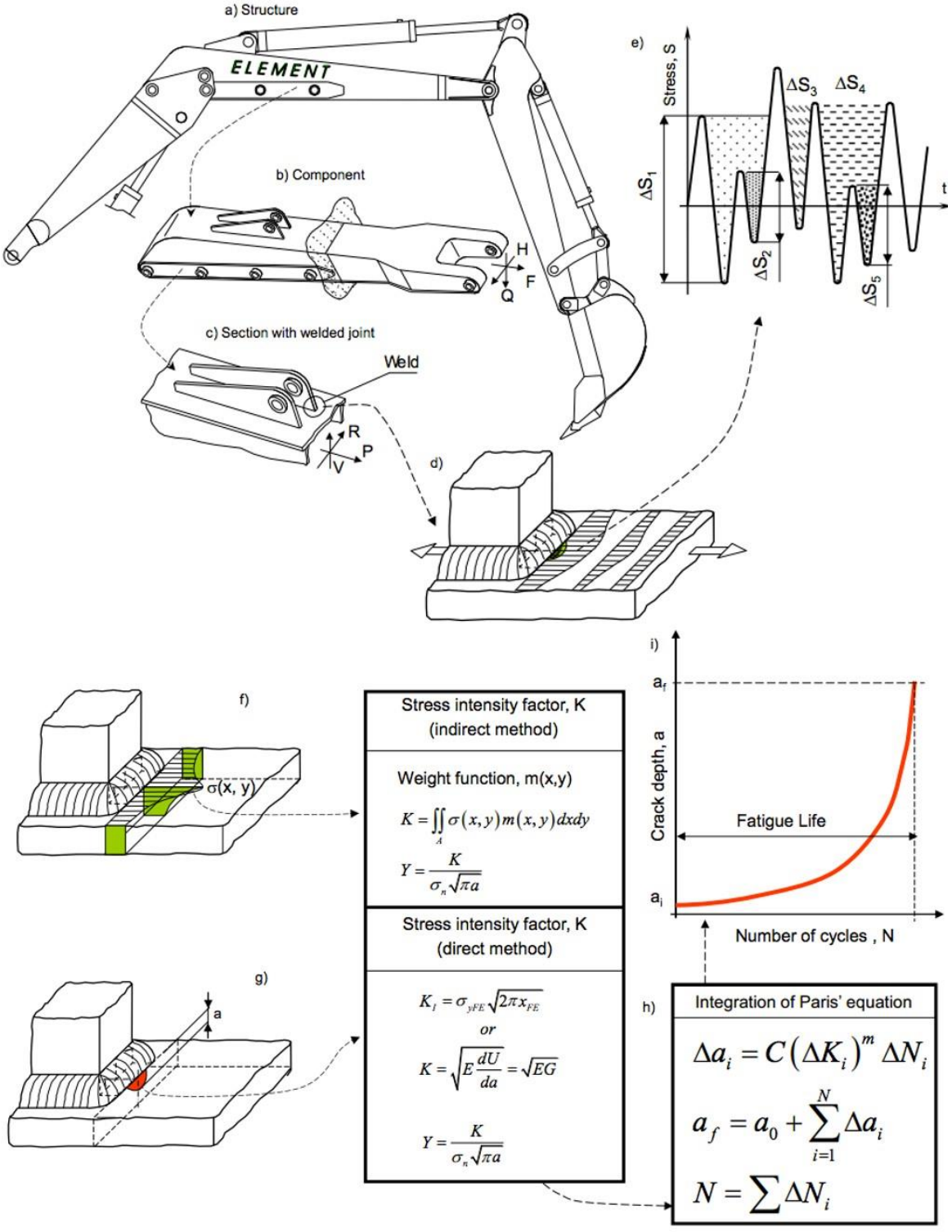

Figure 2-21: Fatigue life prediction steps based on the fracture mechanics method [3]

To sum up, the LEFM method is suitable for estimating the fatigue crack propagation life of welded joints because it is capable of including the various factors associated with weldments, such as the residual stress, mean stress effect, and stress ratio. However, this method relies on the stress intensity factor, which is not available for weldments or welded joints with variable plate thicknesses. In addition, this method depends on the initial crack size assumption and the distribution of the stress through the critical cross-section of weldments. For the initial crack size, there is no specific assumption method because the initial crack size varies with the material properties, so the assumption is empirical. The through-thickness stress distribution, which is very important, is not easy to determine even with the help of FEM because of the high peak stress, which results in a high stress gradient through the critical cross-section of the weldment. As mentioned earlier, using 3D FE modelling to find the peak stress and the associated through-thickness stress distribution is difficult for complex welded joints, not to mention full structures. Finding the actual peak stress and the through-thickness stress distribution for a single welded component requires a high number of 3D elements with a very fine mesh at the critical areas, which will take a long time and consume considerable computational resources. Regardless, many studies have been done to ease the use of FEM by using the shell FE, which requires a fewer number of elements in order to determine the peak stress, but none has extended the stress analysis to include the through-thickness stress distribution itself in order to use the LEFM method. Regardless, in the case of welded joints, the resultant through-thickness stress distribution $\sigma(y)$ (see Figure 1-2) is affected by the residual stress. Therefore, the residual stress effect on the fatigue crack growth must be accounted for when estimating the fatigue crack propagation life as will be discussed in Chapter 3. The through-thickness stress distribution in the prospective crack plane required for the LEFM method can be found using the FEM or some other analytical equations such as Monahan which will also be discussed in Chapter 3.

The following section reviews some of those studies in order to develop a stress analysis method that can determine the peak stress and the through-thickness stress distribution of a welded structure, regardless of the mesh sensitivity and computational time and resources.

2.4 Review of the stress analysis of welded joints using FEM

Due to complex geometry and loading configurations of welded structures and joints they require using sophisticated stress analysis method. Several methods proposed in the past are being briefly

reviewed below. Niemi [53] presented several methods to model simple welded joints using FE shell elements. Resembling some of Niemi's modelling ideas, Fricke and Von Stelle [54], provided useful suggestions regarding the modelling of diagonal and transverse welded members by using 3D and shell FE models. Their work resemble some of Niemi's ideas [53] included using shell element, solid element, and rigid bar in order to simulate the stiffness of the weld itself.

The French automotive industry [55] developed another shell FE modelling method for welded joints based on the hot spot stress concept. Their shell FE model suggests that the hot spot stress must be determined at the center of gravity of the first element adjacent to the weld toe. They also recommended that the welded plates should be modelled using standard shell element where the weld should be modelled with a series of rigid bar elements attached to the plates at specific locations. Fayard [55] validated the French model by modelling three different welded structures, with each structure being tested experimentally by using infra-red thermo-elasticity showing that the fatigue cracks initiated at the weld toe where the maximum hot spot stress was found at the weld toe in each test. The structural hot spot stress measured in [55] was evaluated by way of the extrapolation of experimentally measured stresses at certain reference points on the plate surface (or edge). Using shell FE modelling, Fayard also evaluated the hot spot stress by the linearization of stresses in the through-thickness direction (i.e., along the cross section of the crack plate). Doerk and Fricke [26] reviewed and applied three different methods on four different welded components for the determination of hot spot stress using shell and 3D FE modelling, and their results showed good agreements, but unfortunately no rules for the shell FE modelling were defined.

The shell and 3D FE models reviewed in this section provide stresses/strains which are determined away from the weld toe. Some of the reviewed models determined the hot-spot stress based on the extrapolation method, which is not consistent. All the stresses determined according to the reviewed FE models are meant to assist the S-N method.

To sum up this chapter, the main source of the scatter in the estimation of the fatigue life methods is that each fatigue method uses a different stress quantity. This is because many of the factors affecting the fatigue life of welded structures, such as macro and micro geometrical factors associated with the weld and the microstructural changes, are due to the welding process. All of these factors, which result in complex stresses at critical areas in addition to the complex and widely varying weldment geometries, affect the stress analysis step of the fatigue life estimation process. Hence, the

determination of stress data required for the fatigue life estimation of welded joints is a very difficult task.

The proposed methodology in this thesis uses shell FE to find stress data at the weld toe. The stress determined by using shell FE modelling is referred to in this study as “the local reference stress” in order to distinguish it from the previously mentioned hot spot stress or the nominal stress definition. The local reference stress can be uniquely related to any of the stress required for fatigue analyses regardless which method out of the three methods mentioned above is to be used.

Chapter 3
Methodology

3.1 Introduction

The first step in any of the fatigue life estimation methods (S-N, ε-N, and LEFM) involves three input modules, which are: the material properties, the component geometry, and the applied loading module (see Figure 1-1). The second step in the procedure is the stress analysis module. Once the stress analysis step is completed, the fatigue damage and fatigue life can be estimated. The stress analysis module, however, has proven to be in need of many improvements when determining the fatigue life of welded joints.

Welded joints have complex stress distributions due to many geometrical factors that affect stresses in the weld region as shown previously in Figure 1-2. Stresses at a weld's critical locations (toe or root) are affected by the stress concentration and the residual stress. The peak stress, which is the maximum stress at the weld toe of welded joints, is required for the ε-N method. The peak stress can be determined if the hot spot stress and the corresponding stress concentration factor are known (see equation 2.1), but unfortunately, the stress concentration factor (SCF) depends on the weld geometry and loading mode. Weldments have multiple loading modes and various geometrical features; hence, it is not easy to find the peak stress using appropriate stress concentration factor and the hot spot or the nominal stress (see equation 2.5). Another way to find the peak stress is by using the FE technique, but as mentioned before, 3D FE modelling with a large number of elements and very fine mesh is required at the weld toe to accurately capture the correct peak stress, which demands large computational resources and time for a complete full scale structure.

The through-thickness stress distribution in the prospective crack plane of welded joints is required for fatigue life estimation using the LEFM method. 3D FE modelling can be used to determine the actual non-linear through-thickness stress distribution (see distribution-B in Figure 1-2); however, the through-thickness stress distribution has a high stress gradient starting from the weld toe surface (including the peak stress point B' in Figure 1-2) to the other side of the welded plate thickness, which also requires a large number of elements and fine mesh.

Since the variation in the stress definitions is currently the main source of inconsistency when carrying out fatigue life estimation of welded joints, the proposed methodology concentrates on the fatigue stress analysis module. The specific goal of the methodology is to define a reference stress parameter that is related to the actual critical stress of welded joints and is capable of supplying the required stress data for all contemporary fatigue analysis methods using a coarse mesh shell FE model.

This chapter includes description of the procedure for the determination of the required stress data for each of the fatigue life evaluation methods. The analysis was done in order to clearly define the proposed reference stress parameter. A new shell FE model with a special set of rules to simulate welded joints is proposed to determine the new reference stress parameter. Then, a post-processing procedure is explained in order to relate the proposed reference stress parameter, extracted from the shell FE model, to the nominal stress, the peak stress, and the through-thickness stress distribution.

The proposed shell FE model is constructed to simulate welded joints according to a specific set of rules. The objective of the shell FE model rules is to provide a uniquely defined stress at the weld's critical area based on a simple FE model that requires relatively small number of elements capable of correctly including the weld stiffness. The shell FE model provides a linearized stress distribution through the thickness of the critical plate weld toe or at any other point of interest along the weld toe line in the structure. The linearized stress distribution obtained from the shell FE model is referred to by this author as "the local reference stress". The shell FE linearized stress field or the local reference stress includes two characteristic stress magnitudes, i.e. those at the surface and bottom node of the shell FE mesh simulating the welded joint plate. These local reference stresses are then post-processed to determine, when needed, the nominal stress field, the peak stress, and/or the nonlinear through-thickness stress distribution. The post-processed stresses are believed to include the weldment macro and micro geometrical features regardless of any variety of applied loading modes which result in better stress analysis for the fatigue life estimation of any complex welded structure.

3.2 Stress analysis of welded joints for fatigue evaluations

Welded joints contain complex geometry which results in complex stresses at the critical weld toe, as shown previously in Figure 1-2. The maximum stress at the weld toe and the through-thickness distribution is the main cause of fatigue damage and crack initiation and propagation. The stress

normal to the weld toe line has a maximum magnitude at the surface (the peak stress) and a non-linear through-thickness distribution. Therefore, stress data in that direction is the focus of this section. The stress state at the weld toe is multi-axial in nature; however, it is reduced to one shear and two in-plane normal stress components due to the free surfaces at the plate surface, as shown in Figure 3-1.

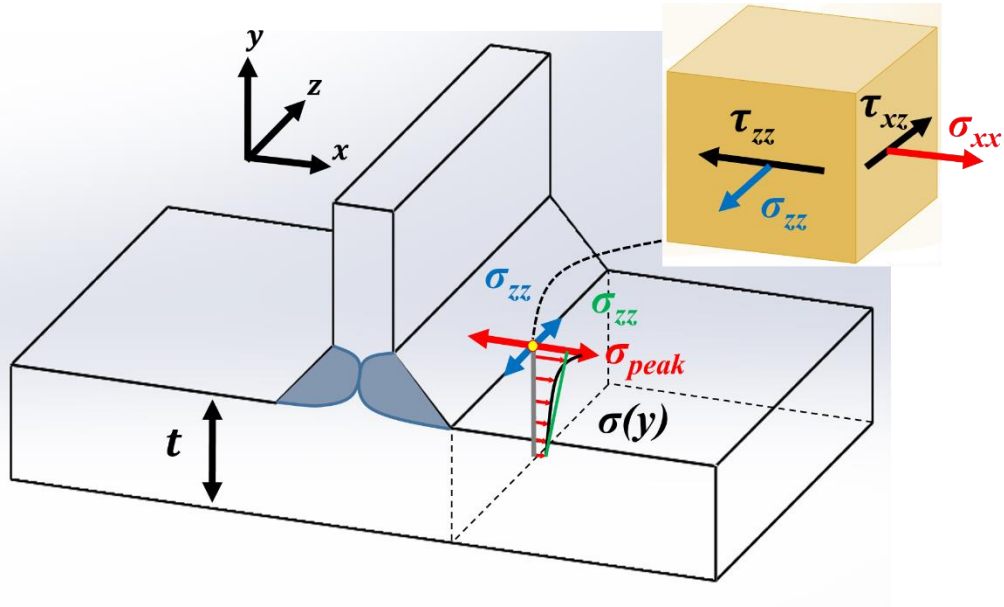

Figure 3-1: Stress state in the plate surface near the weld toe

The stress component that is normal to the weld toe line is the largest in magnitude because of the stress concentration. The main focus of the stress analysis should be the determination of the stress component that is normal to the weld toe line, because it is predominantly responsible for the fatigue damage in the critical area, as illustrated by σ_{xx} in Figure 3-1.

The nominal stress is required for the S-N method in order to determine the fatigue life of a given welded joint by using the proper S-N curve. The problem is that determining the nominal stress for a welded joint based on the classical method may overestimate or under estimate the fatigue life depending on the used S-N curve. That is because the classical method of determining the nominal stress depends on the critical plate cross-sectional area regardless of any discontinuity effect at the weld toe radius in case of weldment. The following figure shows two geometrically different structural components with the same plate cross-sectional area subjected to the same loading.

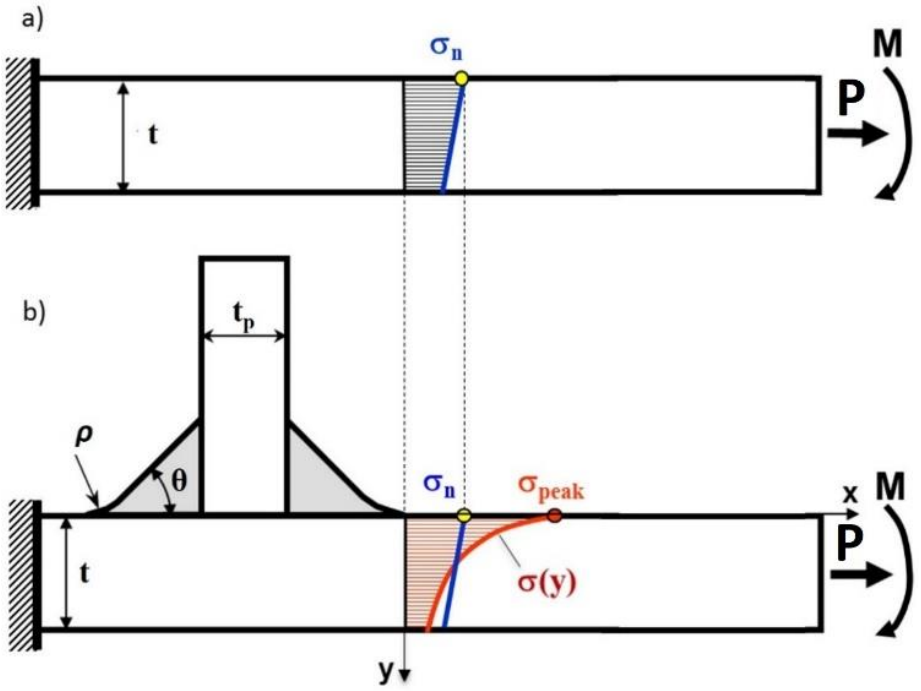

Figure 3-2: Various stress quantities: a) Loaded plate and b) Loaded weldment [3]

The classical method of determining the nominal stress is by using the simple tensile and bending stress equations, as follows:

$$\sigma_n^{ten} = \frac{P}{tL} \tag{3.1}$$

$$\sigma_n^{ben} = \frac{Mt}{2I} \tag{3.2}$$

Where P and M are the axial and bending forces, t is the main plate thickness, L is the plate width, and I is the cross-section moment of inertia. The nominal stress, based on the classical definition, can be calculated as the sum of the tensile and bending nominal stresses, as follows:

$$\sigma_n = \frac{P}{tL} + \frac{Mt}{2I} \tag{3.3}$$

The two structural components shown in Figure 3-2 are subjected to the same axial and bending loads, P and M. The classical method of determining the nominal stress works fine for components such as the first plate (Figure 3-2a). However, the second component (Figure 3-2b) has an abrupt

change in geometry due to the attached plate, which produces a stress concentration at the weld toe. The SCF elevates the nominal stress to the so-called peak stress and produces a non-linear through-thickness stress distribution. The peak stress can be determined by magnifying the nominal stress by the SCF, as mentioned earlier in equation (2.5). The through-thickness stress distribution can be determined by the following equation:

$$\sigma(y) = \sigma_n f(y) \tag{3.4}$$

The peak stresses at weld toes can be determined by using stress concentration factors available in the literature and any appropriate reference stresses (i.e. equation 2.1 and 2.5). However, the stress concentration factors SCFs are unique for specific geometry and loading modes which works fine when determining the peak stress for simple joints under specific loading mode (i.e. T-joint subjected to pure tensile loading) but not for complex structures subjected to multiple loading modes such as weldments. Therefore, the use of classical SCFs is limited to simple cases with simple configurations of geometry and loading which they were derived for. The nominal stress, σ_n, which is based on the cross-section area of the loaded component, regardless of any associated geometrical discontinuity such as the notch, is not a unique stress parameter in case of weldment. Determining a meaningful nominal stress in complex structures is often difficult and non-unique as shown in Figure 3-3 which illustrate two welded joints with the same cross-sectional area and subjected to the same loading, but the weld shapes are different.

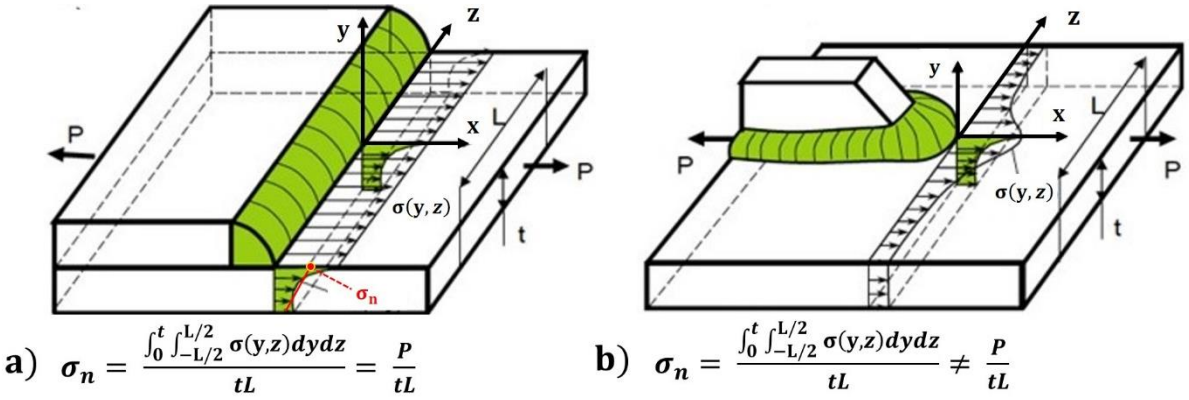

a) $\sigma_n = \frac{\int_0^t \int_{-L/2}^{L/2} \sigma(y,z)\,dydz}{tL} = \frac{P}{tL}$

b) $\sigma_n = \frac{\int_0^t \int_{-L/2}^{L/2} \sigma(y,z)\,dydz}{tL} \neq \frac{P}{tL}$

Figure 3-3: Two welded joints with the same net cross-sectional area and applied load, but different weld geometries require different S-N curves because of different local stress distributions [3]

The nominal stress in Figure 3-3 can be determined by the following equation:

$$\sigma_n = \frac{\int_0^t \int_{-L/2}^{L/2} \sigma(y,z)\,dy\,dz}{tL} = \frac{P}{tL} \tag{3.5}$$

The linearized nominal stresses through the critical plate thickness of both welded joints in Figure 3-3a, and b, will be the same leading to the same fatigue lives which is not correct because equation (3.5) depends on L. According to the definition of the nominal stress in equation (3.1), both cases (Figure 3-3a, and b) must have the same nominal stress because they have the same applied axial load, P, and the same cross-sectional area. This is not true, however, because in the case Figure 3-3a, the nominal or average stress does not depend on dimension L while in the case of Figure 3-3b, it does. Therefore the value of the nominal stress will be the same if the simple definition (equation 3.3) is used but it will be different if the integrals were to be used (equation 3.5). As a result, a sufficiently rich S-N database must be generated with multiple S-N curves to cover a wide variety of welded joint geometries, which in practice is difficult and expensive. Alternatively, the hot spot stress, explained in section (2.1.1), in conjunction with ready-made master S-N curves is often used to determine the fatigue life of weldments. The hot spot stress is based on the extrapolation of surface stresses away from the weld. The actual non-linear through-thickness stress distribution σ(y), in the weld toe, can be replaced in the initial analysis by the statically equivalent linearized stress as shown in Figure 3-4.

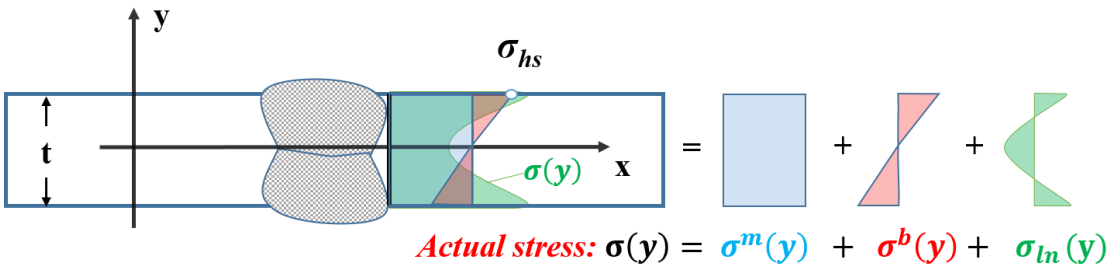

Figure 3-4: Actual stress field through the weld toe critical cross-section and the statically equivalent linear stress field

$$\sigma(y) = \sigma^m(y) + \sigma^b(y) + \sigma_{ln}(y) \tag{3.6}$$

The membrane and the bending stress parts (σ^m and σ^b) are distributed linearly through the plate thickness, while the remaining non-linear part σ_{ln}, caused by the local notch effect, is canceled out when integrating through the thickness because of a self-equilibrium condition [56]. Assuming a

linear statically equivalent stress distribution with the mid-plane thickness as the neutral point, the structural stress (hot spot stress) may be determine as the sum of the membrane and the bending stress parts [10]. According to [57] , the hot spot stress σ_{hs} can be defined mathematically as the algebraic sum of the uniform membrane hot spot stress σ_{hs}^{m} and the bending hot spot stress, σ_{hs}^{b}, as shown in Figure 3-5.

$$\sigma_{hs} = \sigma_{hs}^{m} + \sigma_{hs}^{b} \tag{3.7}$$

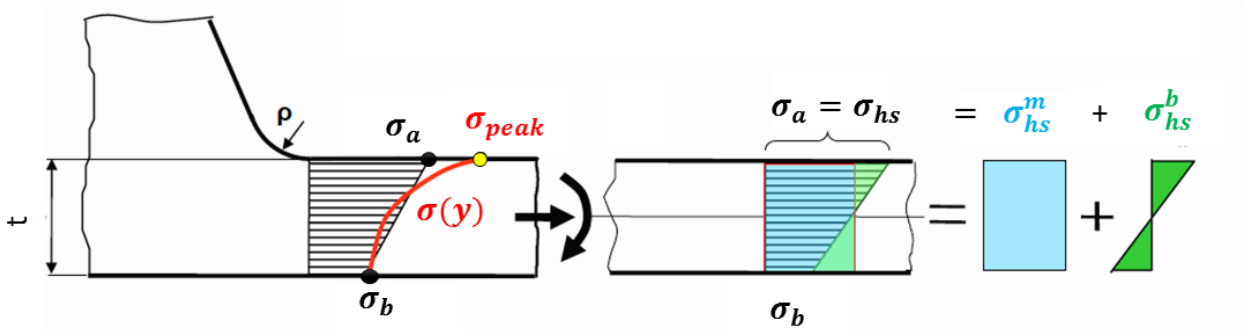

Figure 3-5: Illustration of the statically equavilant hot spot stress at the weld toe

The linearization of the actual non-linear stress distribution σ(y) is considered statically equivalent to the hot spot stress according to equation 3.7. Therefore, the hot spot and the associated membrane and bending hot spot stresses in equation 3.7 are different from the hot spot stress mentioned earlier in the literature review. This one may be called the statically equivalent hot spot stress because it is based on linearization of the actual non-linear through-thickness stress distribution. Accordingly, the peak stress can be determined based on the hot spot or the nominal stress with appropriate SCF (see equations 2.1 or 2.5). However, these two equations (equations 2.1 or 2.5) cannot always be used to determine the peak stress correctly because the stress applied to a welded joint in practice is usually a combination of tensile and bending loading, and the SCFs was found to be dependent not only on the weld geometry but also on the mode of loading. The membrane to bending stress ratio $\sigma_{hs}^{m}/\sigma_{hs}^{b}$ affects the stress concentration. In other words, two welded joints with the same geometrical configuration but different membrane to bending stress ratios would result in different stress concentration factors, which results in different peak stresses, as shown in Figure 3-6. Therefore, using the nominal stress or the hot spot stress as a reference stress (in equations 2.1 and 2.5) is not sufficient for the determination of peak stress.

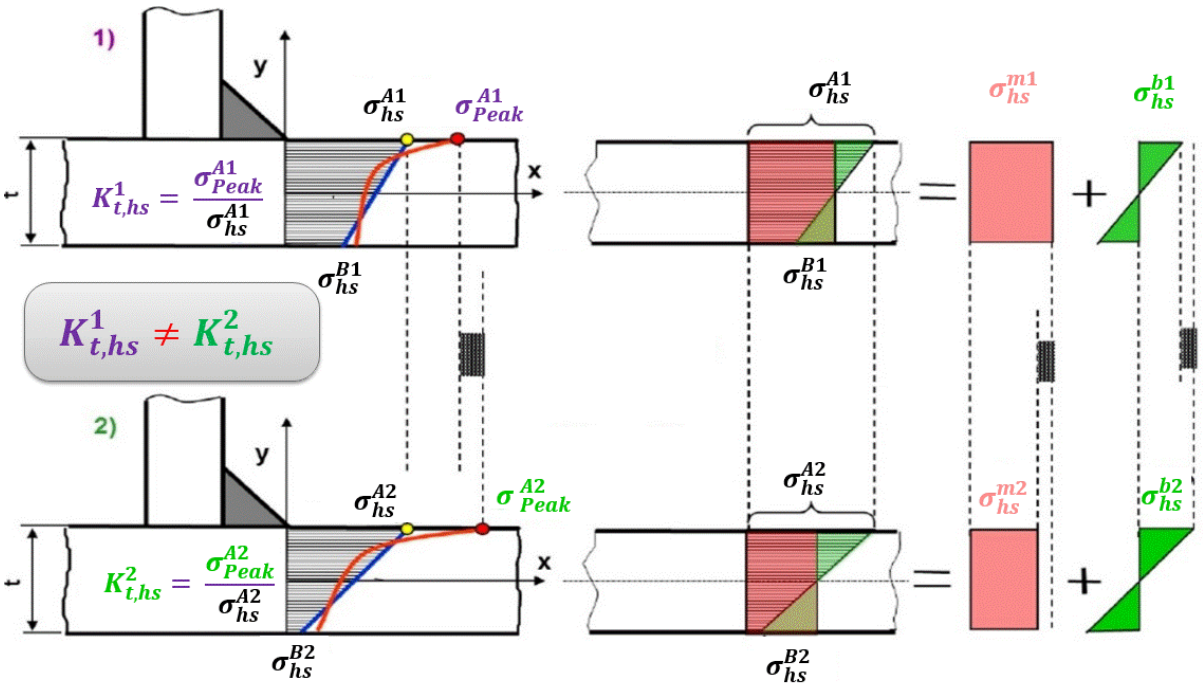

Figure 3-6: Two T-joints with the same geometry and various combinations of loading modes resulting in various local peak stresses and various through-thickness stress distributions

Since the peak stress at the weld toe depends on the membrane to bending stress ratio the stress concentration factor is not unique for a given geometry. Therefore it requires deriving very large number (theoretically infinite number) of K_t factors. In order to avoid such a situation the method described below has been developed.

3.3 The local reference stress concept

The local reference stress is defined as a linearized stress distribution of the actual non-linear stress distribution through the thickness of weld's critical plate or at any other point of interest along the weld toe line in the structure. The linearized local reference stress is a unique stress quantity because it is based on clear definition and can be used as a reference stress sufficient to determine the nominal, the peak stress and the actual non-linear stress distribution. Using the local reference stress to determine the other stress quantities required by the contemporary fatigue life estimation methods is clearly explained and justified by the proposed post-process procedure following this section. Therefore, using the local reference stress to determine the required stresses for the fatigue life analysis of welded joints is believed to include the weldment macro and micro geometrical features

regardless of any variety of applied loading modes. Unlike the nominal stress, which is based only on the cross-section area of the critical welded plate despite any discontinuity, the local reference stress is based on the linearization of the actual non-linear through-thickness stress distribution across the critical weld toe. The local reference stress accounts for the weld's macro geometrical features such as the weld shape and size which is not applicable by the definition of the classical nominal stress. Unlike the hot spot stress which is determined based on surface stresses away from the weld toe, the local reference stress is found at the weld toe line. Using the hot spot stress or the nominal stress as a reference stress to determine the peak stress (equations 2.1 and 2.5) fails due the membrane to bending stress ratio (see Figure 3-6). The membrane and bending hot spot stresses determined by the post-processing of the new local reference stresses allow for determining the peak stress, and the non-linear through-thickness stress distribution regardless of the membrane to bending stress ratio. According to equation (3.7), the summation of the membrane and bending hot spot stresses equal to total hot spot stress at the weld toe which is also believed to be equal to the nominal stress (Figure 1-2 and Figure 2-6). Determining the nominal stress from the membrane and bending hot spot stresses is different than the classical method because it is based on the local reference stress that is related to the actual non-linear through-thickness stress distribution.

3.4 Determining the peak stress of welded joints using the local reference stress

The peak stress is required to determine the fatigue crack initiation life using the ε-N method. Equations 2.1 and 2.5 can be used to determine the peak stress; however, determining the peak stress using these equations is not unique because of the SCF, which depends on the loading ratio (see Figure 3-6). Therefore, it is proposed to use two separate stress concentration factors for the membrane and bending. The local reference stress is a linear stress distribution through the thickness of the welded joint plate that has the maximum critical stress. By definition, the hot spot stress is the sum of the statically equivalent linearized membrane σ^m and bending σ^b hot spot stresses resulting from linearizing the actual stress distribution (Figure 3-5). Thus, to determine the peak stress at welded joints by modifying equation (2.1) to decompose the stress concentration factor and to summing the multiplication of the membrane hot spot stress σ_{hs}^{m} by the tensile concentration factor,

K_t^m, and the bending hot spot stress σ_{hs}^b by the bending concentration factor K_t^b. Hence, the peak stress is expressed as:

$$\sigma_{peak} = \sigma_{hs}^m K_t^m + \sigma_{hs}^b K_t^b \quad (3.8)$$

This was done to overcome the SCF dependency on the loading ratio so that the new equation would be applicable for any welding geometry and loading ratio. In order to use equation 3.8, the hot spot membrane σ_{hs}^m and the bending σ_{hs}^b stresses are required. These stresses are determined by post-processing the local reference stresses extracted from the shell FE, as will be shown in section (3.8). The required stress concentration factors can be found in the literature. As a result, equation 3.8 can be used to determine the peak stress required for the strain-life fatigue analysis method if the four factors (Membrane and bending hot spot stresses (based on the local reference stress) and the associated stress concentration factors) are known. These four factors can also be used to determine the through-thickness stress distribution, as will be proposed in the following section.

3.5 Determining the through-thickness stress distribution of welded joints using the local reference stress

When applied to weldment structures, the key aspect of the da/dN-ΔK method is the determination of the stress distribution σ(y) (see Figure 1-2) in the critical cross-section, as well as the subsequent calculation of stress intensity factors. The through-thickness stress distribution σ(y) can be found by using the FE method. In the case of the FE method, a detailed three-dimensional (3D) model must be conducted using a fine mesh at the weld toe. Unfortunately finding the through-thickness stress distribution using 3D FE modelling is very expensive computationally. Therefore, the use of the FE method is a less favorable choice for simple components, not to mention the difficulty involved in modelling a full structure. There is another way to determine the stress distribution in the weld toe cross-section worked out within the proposed methodology. The method is based on Monahan [58] generalized expressions derived for describing stress distributions in weldments. Monahan's expressions were was formulated for T-joints and tubular joints subjected to tension and/or a bending load. The dimensions of the joint used in Monahan expression are shown in Figure 3-7.

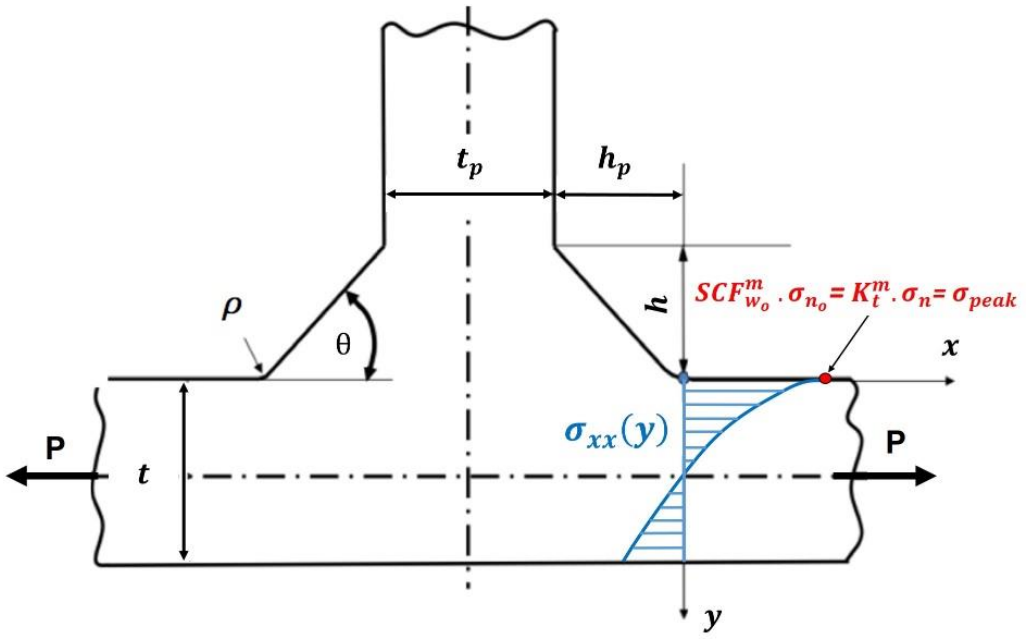

Figure 3-7: T-joint subjected to pure bending loading and the through-thickness stress distribution in x direction that is normal to the weld toe line (Monahan equation parameters)

The Monahan through-thickness stress distribution induced by pure axial loading is as follows [58]:

$$\sigma_w^m = \frac{SCF_{w_o}^m \, \sigma_{n_o}}{2\sqrt{2}} \left[\left(\frac{y}{\rho} + \frac{1}{2} \right)^{-0.5} + \frac{1}{2} \left(\frac{y}{\rho} + \frac{1}{2} \right)^{-1.5} \right] \frac{1}{G_m} \tag{3.9}$$

Where: σ_w^m, is the membrane through-thickness stress distribution, $SCF_{w_o}^m$, represents the membrane stress concentration factor or K_t^m, and σ_{n_o}, is the nominal stress normal to the weld to line. The exponents associated with the individual correction functions are determined using regression analysis, as follows:

$$G_m = 1 \qquad \text{for } \frac{y}{\rho} \leq 0.3$$

$$G_m = 0.06 + \frac{0.94 * e^{-E_m T_m}}{1 + E_m^3 T_m^{0.8} * e^{-E_m T_m^{1.1}}} \qquad \text{for } \frac{y}{\rho} > 0.3$$

$$E_m = 1.05 * \theta^{0.18} \left(\frac{\rho}{t} \right)^q$$

$$q = -0.12 \, \theta^{-0.62}$$

$$T_m = \frac{y}{t} - 0.3\ \frac{\rho}{t}$$

The through-thickness stress distribution induced by pure bending load is as follows [58] :

$$\sigma_w^b = \frac{SCF_{w_o}^b\ \sigma_{n_o}}{2\sqrt{2}} \left[\left(\frac{y}{\rho} + \frac{1}{2}\right)^{-0.5} + \frac{1}{2}\left(\frac{y}{\rho} + \frac{1}{2}\right)^{-1.5}\right]\left[\frac{\left(1 - 2\left(\frac{y}{t}\right)^{0.89}\right)}{G_b}\right] \tag{3.10}$$

Where: σ_w^b, is the membrane through-thickness stress distribution, $SCF_{w_o}^b$, represents the membrane stress concentration factor or K_t^b, and σ_{n_o}, is the nominal stress normal to the weld to line.

$$G_b = 1 \qquad \text{for } \frac{y}{\rho} \leq 0.4$$

$$G_b = 0.07 + \frac{0.93 * e^{-E_b T_b}}{1 + E_b^3 T_b^{0.6} * e^{-E_b T_b^{1.2}}} \qquad \text{for } \frac{y}{\rho} > 0.4$$

$$E_b = 0.9\ *\ \left(\frac{\rho}{t}\right)^{-\left(0.0026 + \frac{0.0825}{\theta}\right)}$$

$$T_b = \frac{y}{t} - 0.4\ \frac{\rho}{t}$$

Equations 3.9 and 3.10 are valid for weld angles within the range of ($\pi/6 \leq \theta \leq \pi/3$) and weld toe radii within the range of ($1/50 \leq \rho/t \leq 1/15$). In the case of a cruciform joints (symmetric welded joint), these equations can also be applied over the half of the plate thickness ($0 \leq y \leq t/2$) and the other part of the stress distribution is determined by using the symmetry properties.

The through-thickness stress distribution required for the LEFM method can be determined using the Monahan equations when replacing the stress concentration factors ($SCF_{w_o}^m$ and $SCF_{w_o}^b$) and the applied stresses (σ_{n_o}) in equations 3.9 and 3.10 with the stress concentration factors K_t^m and K_t^b and the membrane and the bending hot spot stresses σ_{hs}^m and σ_{hs}^b, respectively. Since welded joints are usually subjected to tensile and bending loading at the same time, it is proposed that one may add the Monahan equations by the method of superposition. Thus, the through-thickness stress distribution can be obtained by the following equation for the case of combined membrane and bending loading [59].

$$\sigma_{xx}(y) = \sigma_w^m(y) + \sigma_w^b(y) = \sigma_{hs}^m(y) + \sigma_{hs}^b(y)$$

$$\sigma_{xx}(y) = \left[\frac{K_t^m \sigma_{hs}^m}{2\sqrt{2}} \times \frac{1}{G_m}\right] + \left[\frac{K_t^b \sigma_{hs}^b}{2\sqrt{2}} \times \frac{1 - 2\left(\frac{y}{t}\right)}{G_b}\right] \left[\left(\frac{y}{\rho} + \frac{1}{2}\right)^{-1/2} + \frac{1}{2}\left(\frac{y}{\rho} + \frac{1}{2}\right)^{-3/2}\right] \quad (3.11)$$

The above equation (i.e., Monahan equation) can be used to determine the through-thickness stress distribution $\sigma_{xx}(y)$ based on membrane and bending hot spot stresses which resulted from post-processing of the local reference stresses as will be discussed in the following section. Determining the through-thickness stress distribution based on the local reference stresses is more reliable because it is related to the actual through-thickness stress distribution of the welded joint.

3.6 Determining the local reference stresses using special shell FE rules

The local reference stress can be obtained by using FEM (3D or shell elements). The shell FE is to be used because it directly provides a linearized stress distribution through the thickness of the modelled critical welded plate. With proper post-processing procedure (described in section 3.8), the local reference stress can be used to determine the membrane and bending hot spot stresses as shown in Figure 3-8. The local reference stress is found using a shell FE model with specific rules. The most realistic location for determining the actual weld joint critical stress is exactly at the weld toe location. Thus, the proposed shell FE model simulates welded joints with special rules to ensure that the stress data is extracted from the location that coincides exactly with the physical weld toe line of the actual welded joint. Since the stress distribution through shell elements is linear, according to the definition of shell element theory, the resulting stress distribution across the weld toe is linear, with two surface stresses. Both of the shell element surface stresses (maximum and minimum) are referred to by the author as the local reference stresses σ_a and σ_b, as shown in Figure 3-8. The proposed shell FE local reference stress at the weld toe, along with the actual stress field, the peak stress, and the associated membrane and bending hot spot stresses, are demonstrated in Figure 3-8.

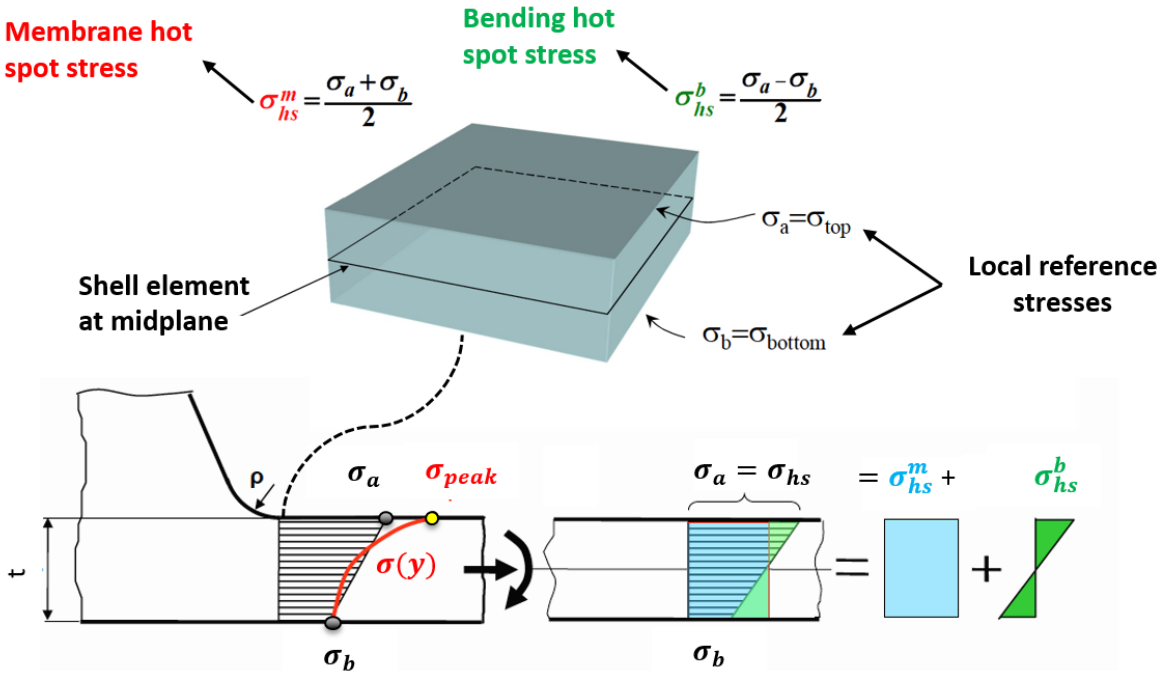

Figure 3-8: Illustration of the shell FE local reference stress concept, a) Shell finite element at the weld toe, b) Actual peak stress, non-linear through-thickness stress distribution, and the local reference stresses σ_a and σ_b; c) Statically equivalent linear through-thickness hot spot stress distribution, d) Linear membrane and bending hot spot stresses

A section of the shell element at the weld toe is shown in Figure 3-8a, whereas Figure 3-8b illustrate various stresses across the critical welded plate. The actual non-linearly distributed stress field is represented by the blue curve with the maximum peak stress at the weld toe surface. The linearized local reference stress distribution is represented by the linear line through the plate thickness which include the two surface stresses or the local reference stresses σ_a and σ_b (Figure 3-8b). The statically equivalent hot spot stress and its relation to the local reference stresses is shown in Figure 3-8c. The decomposition of the hot spot stress into membrane and bending hot spot stresses is shown in Figure 3-8d. Therefore, the local reference stress obtained from the shell FE can be used to determine the membrane and bending hot spot stresses by decomposition of the linear through-thickness stress field. As long as the shell FE linear stress field is obtained correctly, the membrane hot spot stress can be expressed as the average of the local reference stresses, while the bending hot spot stress is one-half the difference Figure 3-8a.

$$\sigma_{hs}^{m} = \frac{1}{2}\left[\sigma_a + \sigma_b\right] \tag{3.12}$$

$$\sigma_{hs}^{b} = \frac{1}{2}\left[\sigma_a - \sigma_b\right] \tag{3.13}$$

Equations 3.12 and 3.13 can determine the membrane and bending hot spot stresses while the summation of both equal to the total hot spot stress (equation 3.7). *It is very important to note that the hot spot stress in equation 3.7 is to be determined by equations 3.12 and 3.13, which are based on the shell FE local reference stresses* σ_a *and* σ_b*. Therefore, it must be distinguished from the originally defined hot spot stress concept in section 2.1.1, which was based on the extrapolation method (see Figure 2-4).*

The top local reference stress σ_a can be used as the nominal stress σ_n to supply the nominal stress needed for the S-N method. Determining the nominal stress based on the local reference stress is based on a clear relation to the actual welded joint critical stress distribution. Using the nominal stress based on the proposed methodology is more reliable when used to evaluate the fatigue life. Note that the current work is concerned with the peak and through-thickness stress distribution to obtain only the strain-life and the LEFM.

Various shell FE meshes/models were analyzed to establish some general rules for the consistent modelling of welded joints. Many shell FE research projects have been completed, but these projects have only evaluated hot spot stress and have been mostly focused on assessing the S-N method. The reviewed research regarding shell and 3D FE modelling of welded joints provides stress data that has been measured away from the weld toe. As a result, the effect of the welds' micro-geometrical features has not been accounted for. Modelling welded structures using the 3D FE technique requires a very fine mesh, which results in a large number of elements. The number of elements is considerable because the number of elements is multiplied by the elements' degrees of freedom. As a result, it requires much time and a considerable amount of computer resources to be solved. Nevertheless, a fine mesh is necessary when conducting 3D FE modelling of welded joints in order to capture the peak stress and its through-thickness stress gradient caused by the weldments' micro-geometrical features. Using 3D FE to model simple joints is possible; however, it is impractical to model a complete structure using 3D FE. Therefore, modelling welded joints using the shell FE technique is proposed to eliminate problems associated with 3D FE modelling, such as the large number of elements, the fine mesh, and the required computational resources. Another reason for selecting the shell FE was that shell FE provides linear stress distribution through the thickness.

The shell FE models reviewed in the literature do not provide consistent rules to model welded joints, nor provide detailed information on where to determine the required stresses. The problem is that when modelling a welded joint using shell FE, it is not clear where the stress of interest is located. For example, Figure 3-9a, and b show a simple T-joint subjected only to tensile loading P, yet the location of the required stress (e.g., hot spot stress) in the shell FE model remains unknown. Another inconsistency found in the literature is in the modelling of the weld itself, as the weld stiffness is often not accounted for. It is important to model the weld stiffness because the stresses in the weld toe region depend strongly on the local stiffness in the joint. For example, the model shown in Figure 3-9b was found to be insufficient because it does not include the stiffness of the weld. Therefore, it is necessary to set rules for constructing a new shell FE model that is able to find the stress data exactly at a welded joint's critical areas, such as the weld toe if possible. In addition, the stress at the weld toe must be related to the stresses required by the fatigue life analysis methods.

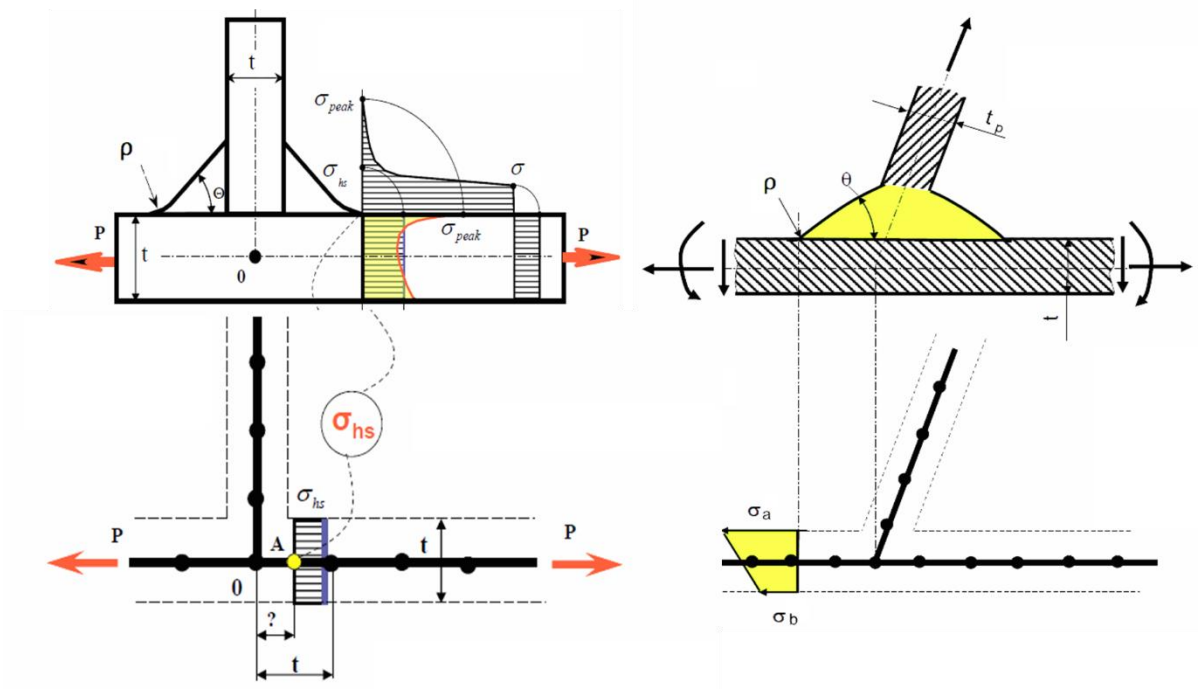

Figure 3-9: a) Simple T-joint weldment subjected to pure tensile loading P; b) Shell FE model of a T-joint; c) Inclined T-joint with complex loading modes; d) Shell FE modelling of the weld stiffness

Welded joints generally have complex geometry and loading, which makes it more complicated to model the weld stiffness and to find the location of the critical stress, such as the case in Figure 3-9c

and d. Thus, the first challenge was to find how to model the weld itself in order to correctly include the stiffness of the weld. The second challenge was to determine the location of the critical stresses. After an extensive number of shell FE modelling trials, the weld stiffness was modelled using the shell element with the thickness of the thinner welded plates. In addition, it is only logical to determine the stresses exactly at the weld toe (the physical location of the real weld toe).

In this proposed work, a set of rules was formulated for modelling welded joints using a shell FE technique that is consistent and unique for the determination of stresses at the weld toe's exact physical location. Modelling welded joints using the shell element requires two important points: (1) accurate simulation of the local weld's stiffness, and (2) accurate positioning of the reference points where the actual weld toe's stress is located in order to extract the local reference stresses σ_a and σ_b. These two points are included in the proposed shell FE model. The shell FE meshing rules are illustrated on a T-joint in Figure 3-10.

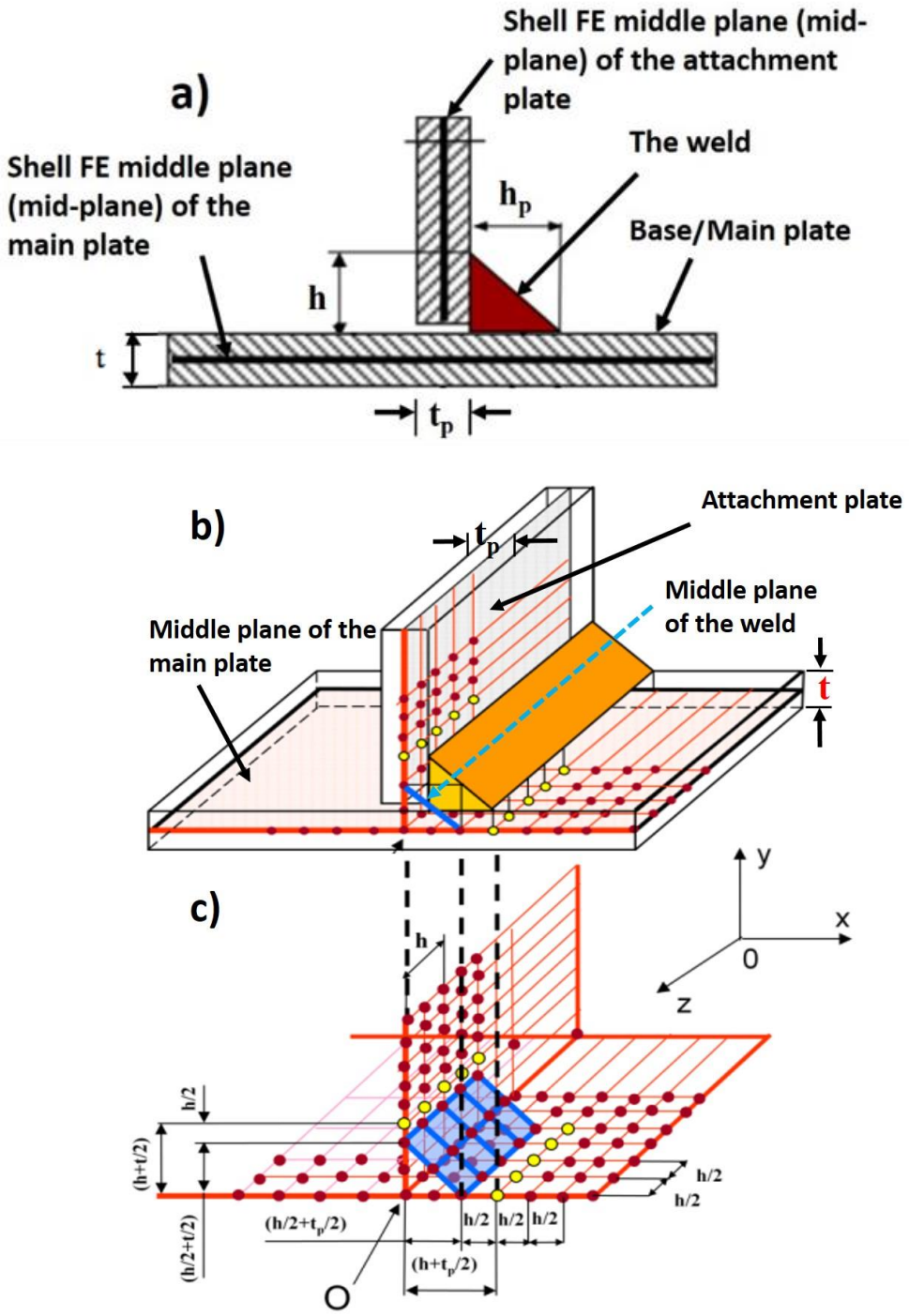

Figure 3-10: Shell finite element model of single fillet weld without penetration

The general rules proposed for modelling welded joints using shell FE are:

- Create two shell FE plans with the actual thicknesses of the welded plates (as mid-thickness) and then connect them at point O with an additional incline mid-thickness shell FE plans to represent the weld (i.e., main plate, attachment plate, and weld plate; see Figure 3-10a and b,).
- For the main plate shell elements, the size of (tp+hp) /4 in the x-direction should be given to the first and second rows of elements adjacent to the theoretical intersection line O, as shown in Figure 3-10b,
- For the attachment plate elements, the size of (t+h)/4 in the y-direction should be given to the first and second rows of elements adjacent to the theoretical intersection line O, as shown in Figure 3-10b,
- The weld must be simulated as an inclined shell plane attached to each plate and spanning the first two rows of elements in each plate (Figure 3-10b); note that when simulating the weld, the thickness of the shell element should be equal to the thinner plate of the weldment (e.g., either the main plate t or the attachment plate thickness tp),
- The size of the third row of elements on the main plate should be half the weld's leg length h/2 in the x and z directions,
- The size of the third row of elements of the attachment plate should be half the weld's leg length h/2 in the y and z directions,
- The previous two points are important to locate the reference points that should represent the physical location of the weld toe and throat. This makes it easy to extract the nodal stresses at the weld toe physical location, and no interpolation is necessary,
- The size of the weld leg h/2 or less should be given to all remaining shell elements in the weld region.

Finally, after applying the boundary conditions, local reference stresses σ_a and σ_b are extracted from the reference points (see yellow nodes shown in Figure 3-10c) that include the critical stresses. The next step is to post-process the local reference stress data in order to determine the stress data required for the fatigue life analysis. Modelling welded joints with shell FE resolves the fine mesh problem associated with 3D FE modelling. The shell FE technique can also allow for the modelling of a complete welded structure with a shorter time frame and less effort compared to 3D FE modelling. Modelling welded joints with shell FE requires a relatively small number of elements. The proposed shell FE modelling does not directly provide the stresses required for fatigue life analysis (σ_n, σ_{peak},

and σ(y)), but rather provides a linear stress distribution or (local reference stresses σ_a and σ_b) exactly through the critical cross-section of a welded joint, as shown Figure 3-8. Thus, the post-processing method must be performed for the shell FE's local hot spot stresses (σ_a and σ_b) in order to determine the membrane and bending hot spot stresses (σ_{hs}^{m} and σ_{hs}^{b}). According to equation 3.8, the SCFs are required in order to determine the peak stress. This will ensure that the peak stress, based on the proposed local reference stress concept and the corresponding membrane and bending hot-spot stresses, is independent of the geometry and loading mode of the welded joint.

3.7 Determining the stress concentration factors

Stresses arise where a geometrical or micro-structural discontinuity is found. This rise in the stress is called the stress concentration, and its effect is quantified by the "stress concentration factor K_t". Stress concentration factors elevate the local stress in welded joints of machine components. The geometrical features of welded joints create areas where stress concentrations occur, and the stress concentration factor depends solely on the geometry and the mode of loading. There are several handbooks that provide the stress concentration factors but non for welded joints.

The stress concentration factor K_t is defined as the ratio of the maximum or peak stress to the nominal stress.

$$K_t = \frac{\sigma_{peak}}{\sigma_n} \tag{3.14}$$

Welded joints in practice have complex geometries that cannot be compared to SCFs geometrical configurations available in handbooks. However, the finite element method (FEM) has proven to be an effective method for the evaluation of SCFs, regardless of how complex the weld geometry is. Researchers such as Niu and Glinka [60] and Monahan [58] who have used FEM to determine the SCFs for a variety of weld geometries, and their work has resulted in very useful yet empirical SCF equations. However, all of the available stress concentration factors for weldments have limited range of applications. The stress concentration factors can be used to determine the peak stress, but the loading ratio is found to have an influence on the results (see equation 3.8). Thus, it is proposed that one can use two separate stress concentration factors which are independent of the weld loading but unique for a given weld geometry (see equation 3.13). As introduced in [61] the SCFs can be

determined analytically by using the weld geometry. The SCF equations in this section are derived by using the FEM, and the welded joints' geometrical configurations are classed as either symmetric or non-symmetric. If welds are located on both sides of the plate, then it is considered symmetric, and a non-symmetric weldment has a weld on just one side of the plate.

3.7.1 Stress concentration factor of symmetric fillet welds in a T-joint attachment subjected to pure tensile and pure bending load

The symmetric fillet welds in a T-joint attachment is shown in Figure 3-11, where Figure 3-11A is subjected to pure tensile loading and Figure 3-11B is subjected to pure bending loading. The SCF at point A in Figure 3-11 is considered symmetric for a T-joint subjected to pure tensile and pure bending loading.

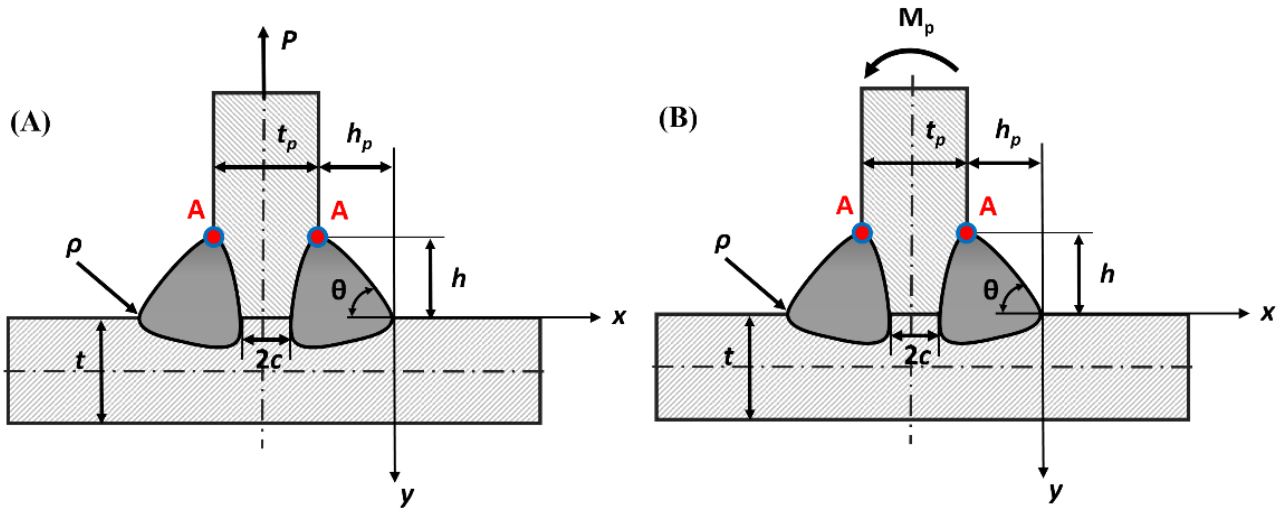

Figure 3-11: Terminology of a symmetric fillet weld in a T-joint attachment subjected to: A) Pure tension, and B) Pure bending loading [61]

The SCF for a symmetric fillet weld on a T-joint attachment subjected to pure tensile loading (Figure 3-11A) is as follows [61]:

$$K_t^m = \left[1 + \frac{1 - \exp\left(-0.9\left(\frac{\pi}{2} + \theta\right)\sqrt{\frac{W}{2h_p}}\right)}{1 - \exp\left(-0.45\pi\sqrt{\frac{W}{2h_p}}\right)} \times 2.2\left[\frac{h_p}{\rho} \times \frac{1}{2.8\left(W/t_p\right) - 2}\right]^{0.65}\right] \times \left[1 + 0.64\,\frac{\left(\frac{2c}{t_p}\right)^2}{\frac{2h}{t_p}} - 0.12\,\frac{\left(\frac{2c}{t_p}\right)^4}{\left(\frac{2h}{t_p}\right)^2}\right] \tag{3.15}$$

The SCF for a symmetric fillet weld of a T-joint attachment weld subjected to pure bending (Figure 3-11B) loading is [61]:

$$K_t^b = \left[1 + \frac{1 - \exp\left(-0.9\,\left(\frac{\pi}{2} + \theta\right)\sqrt{\frac{W}{2h_p}}\right)}{1 - \exp\left(-0.45\pi\sqrt{\frac{W}{2h_p}}\right)} \times \sqrt{\tanh\left(\frac{2t}{t_p + 2h_p} + \frac{2\rho}{t_p}\right)}\right] \times \left[\tanh\left(\frac{\left(\frac{2h_p}{t_p}\right)^{0.25}}{1 - \frac{\rho}{t_p}}\right)\right] \times \left(\frac{0.13 + 0.65\left(1 - \frac{\rho}{t_p}\right)^4}{\left(\frac{\rho}{t_p}\right)^{\frac{1}{3}}}\right) \times \left[1 + 0.64\,\frac{\left(\frac{2c}{t_p}\right)^2}{\frac{2h}{t_p}} - 0.12\,\frac{\left(\frac{2c}{t_p}\right)^4}{\left(\frac{2h}{t_p}\right)^2}\right] \tag{3.16}$$

$$\text{For both cases: } W = \left(t_p + 4h_p\right) + 0.3(t + 2h) \tag{3.17}$$

The above equations are validated for the weld parameter ranges of:

$(0.025 \le \rho/t_p \le 0.35)$, $(0.5 \le h_p/t_p \le 1.0)$, and $(20° \le \theta \le 50°)$

3.7.2 Stress concentration factor of non-symmetric fillet weld in a base plate of a T-joint subjected to pure tensile and pure bending load

A non-symmetric fillet weld on the base plate of a T-joint is shown in Figure 3-12, where Figure 3-12-A, is subjected to pure tensile loading and Figure 3-12-B is subjected to pure bending loading. The SCF at point B in Figure 3-12 is considered non-symmetric for a T-joint subjected to pure tensile and pure bending loading.

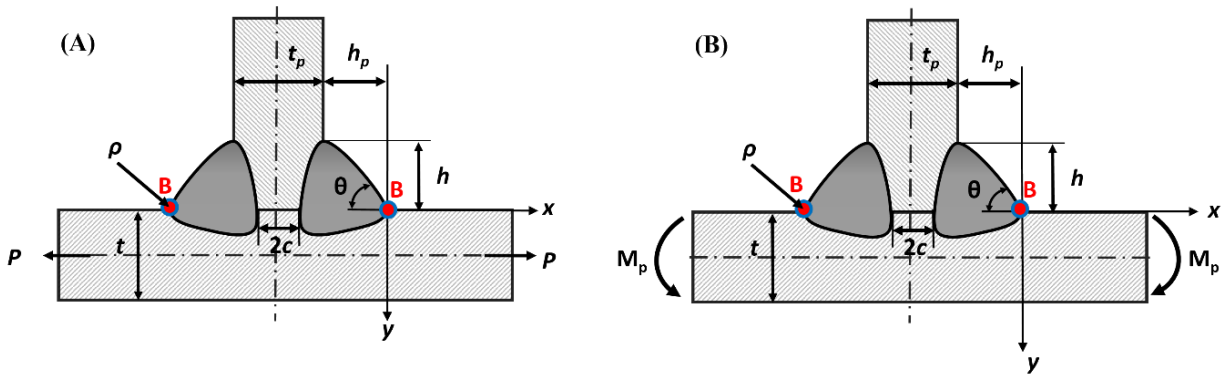

Figure 3-12: Terminology for a non-symmetric fillet weld on the base plate of a T-joint weld subjected to: A) Pure tension, and B) Pure bending loading [61]

The SCF for a non-symmetric fillet weld on a base plate of a T-joint weld subjected to pure tensile loading is as follows [61]:

$$K_t^m = \left[1 + \frac{1 - \exp\left(-0.9\theta\sqrt{\frac{W}{2h}}\right)}{1 - \exp\left(-0.45\pi\sqrt{\frac{W}{2h}}\right)} \times \left\{\frac{h}{\rho} \times \frac{1}{2.8\left(W/t\right) - 2}\right\}^{0.65}\right] \tag{3.18}$$

The SCF for a non-symmetric fillet weld on a base plate of a T-joint weld subjected to pure bending loading is [61]:

$$K_t^b = \left[1 + \frac{1 - \exp\left(-0.9\theta\sqrt{\frac{W}{2h}}\right)}{1 - \exp\left(-0.45\pi\sqrt{\frac{W}{2h}}\right)} \times 1.9\sqrt{\tan\left(\frac{2t_p}{t + 2h} + \frac{2\rho}{t}\right)}\right] \times \tanh\left[\left(\frac{\left(\frac{2h}{t}\right)^{0.25}}{1 - \frac{\rho}{t}}\right)\right] \times \left(\frac{0.13 + 0.65\left(1 - \frac{\rho}{t}\right)^4}{\left(\frac{\rho}{t}\right)^{1/3}}\right) \tag{3.19}$$

$$\text{Where: } W = (t + 2h) + 0.3\left(t_p + 2h_p\right) \tag{3.20}$$

The above equations are validated for the weld parameter ranges of:

$(0.025 \leq \rho/t_p \leq 0.35)$, $(0.5 \leq h_p/t_p \leq 1.0)$, and $(20° \leq \theta \leq 50°)$.

3.8 Post-processing of the local reference stress data

The membrane and bending hot spot stresses, based on the shell FE model, can be used to determine the nominal stress σ_n and the hot spot stress. Note that theses stresses are not determined using the classical method for the nominal stress not the extrapolation method for the hot-spot stress but rather based on the local reference stresses which is related to the actual critical stresses of the welded joint. Hence, with a proper S-N curve, the fatigue life of a welded joint can be predicted using either the stress-life or the hot spot fatigue life method. Regardless, the objective of the proposed method is to extend the use of local reference stresses to determine the peak and through-thickness stresses to help in predicting the fatigue life of welded joints using the strain-life and LEFM methods.

The objective of the post-processing procedure is to determine the peak stress and the through-thickness stress distribution of the modelled weld joint. After modelling a welded joint, the local reference stresses (σ_a and σ_b) are extracted as explained in Section 3.6. The post-processing procedures are as follows:

1) Determine the membrane and bending hot-spot stresses σ_{hs}^{m}, and σ_{hs}^{b} according to equations 3.12 and 3.13.
2) Based on the weld shape, mode of loading, and critical weld toe (symmetric or non-symmetric), determine the membrane and bending stress concentration factors K_t^m and K_t^b according to equations 3.15 - 3.17 or 3.18 - 3.20, respectively.
3) Determine the peak stress, σ_{peak} according to equation 3.13.
4) Determine the through-thickness stress distribution $\sigma_{xx}(y)$ using the Monahan equation (3.11).

The idea of the decomposing equation 3.8 in Section 3.4 could be achieved by using shell FE modelling even when analyzing an entire structure subjected to all service loading modes. It must be ensured that the shell FE model is realistically simulated, including the overall geometry, boundary conditions, and loads.

Determining the peak stress is important in order to evaluate the fatigue crack initiation life of welded joints using the strain-life method. This method of determining the peak stress makes it unique because it is independent of the loading mode, as it is based on load-separated stress concentration factors. Thus, the peak stress based on the presented method can be used for any membrane and bending load combination when applied to a welded joint, regardless of the stress

ratio. Another advantage of the proposed method is that it is based on reference stresses (i.e., statically equivalent hot spot stresses) located exactly at the weld toe, in contrast to the hot spot stress evaluation methods outlined in the literature.

Determining the non-linear through-thickness stress distribution is important in order to evaluate fatigue crack growth in welded joints using the LEFM method. According to the shell element theory, the distribution of the stress through the thickness is linear; i.e., the local reference stresses are linearly distributed through the shell element thickness from σ_a to σ_b. The local reference stress data were successfully related to the hot spot stresses in section 3.8, so they can be related to the through-thickness stress distribution, since the hot spot stress is nothing but a linearization of the actual non-linear through-thickness stress distribution (see equations 3.7 and 3.8, and Figure 3-4 and). It is important to note that the Monahan equation 3.11 for the through-thickness stress distribution was derived for a non-symmetric T-joint using a set of FE stress data. Therefore, within the mentioned geometric ranges, equation 3.11 is valid only for non-symmetric welded joints; however, in the case of symmetric welded joints, it is valid only over half of the plate thickness ($0 \leq y \leq t/2$).

Equation 3.8 can provide through-thickness stress distributions regardless of the overall geometry and the applied loading. This is because it is based on two separate hot spot stresses which are independent of the loading ratio effect. The non-linear through-thickness distribution based on the local reference stresses is considered fast and economical from a computational point of view.

Note that the resulting stress data (i.e., nominal, peak, and non-linear through-thickness distribution) from the post-processing will be validated against the stresses from the 3D FE model. The peak stress based on the local reference stress will be input to the stress analysis module of the strain-life method in order to predict the fatigue crack initiation life of welded joints. For the remaining fatigue crack propagation life, the LEFM method will be used. The through-thickness stress distribution, based on the local reference stresses and the appropriate weight function, will be used for the analysis. The weight function can be found in the literature, while the through-thickness stress distribution will be obtained by using the stress data obtained from the shell FE model. Lastly, the stresses will be used to predict the fatigue life of several welded joints. These welded joints were tested for fatigue life at the John Deere laboratory. Both the experimental and predicted fatigue life were shown in order to prove the worth of the proposed methodology.

3.9 Evaluation of the SIF effect within the LEFM method

Equation 2.18 can be used for one-dimensional cracks such as edge cracks. However, there are some crack models where the stress intensity factor needs to be evaluated for two critical points (two-dimensional crack models). Two-dimensional cracks are usually considered to be semi-elliptical in shape, and that assumption is based on the observation of planar cracks initiated from a surface. Semi-elliptical cracks (widely found in welded joints) have two critical points, which are the depth and the surface, as shown in Figure 3-13. Point A in Figure 3-13 is the depth point where the crack may grow through the component thickness, whereas Point B is the surface point where the crack may extend along the component width/surface. The crack size in the depth of a semi-elliptical crack is referred to as "a", while the surface crack length or crack width is referred to as "2C" (respectively, points A and B in Figure 3-13).

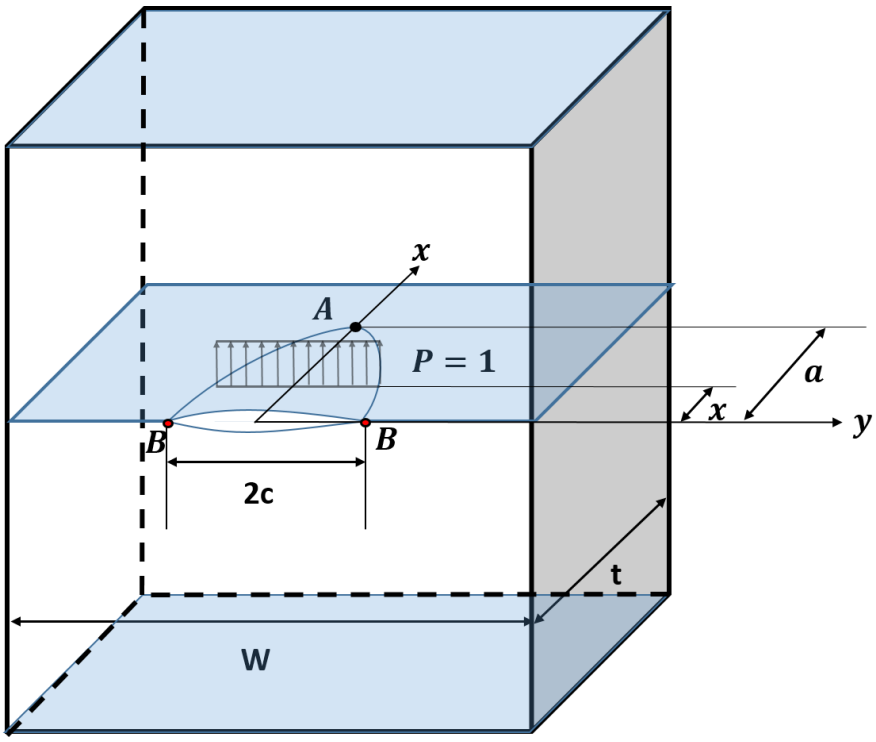

Figure 3-13: Semi-elliptical crack shape and geometry parameter

According to [51], points A and B in Figure 3-13 have different weight functions even though the through-thickness stress distribution σ(y) is the same. Thus, two integrals are needed to calculate the stress intensity factor at the deepest point and the surface point (points A and B in Figure 3-13).

$$K_A = \int_0^a \sigma(x).\, m_A(x,a).\, dx \quad \text{at point A} \tag{3.21}$$

$$K_B = \int_0^a \sigma(x).\, m_B(x,a).\, dx \quad \text{at point B} \tag{3.22}$$

The weight functions for the deepest point A and the surface point B are as follow:

$$m_A(x,a) = \frac{2F}{\sqrt{2\pi(a-x)}}\left\{1 + M_{1A}\left(1-\frac{x}{a}\right)^{1/2} + M_{2A}\left(1-\frac{x}{a}\right) + M_{3A}\left(1-\frac{x}{a}\right)^{3/2}\right\} \tag{3.23}$$

$$m_B(x,a) = \frac{2F}{\sqrt{2\pi}}\left\{1 + M_{1B}\left(\frac{x}{a}\right)^{1/2} + M_{2B}\left(\frac{x}{a}\right) + M_{3B}\left(\frac{x}{a}\right)^{3/2}\right\} \tag{3.24}$$

The M_{iA} and M_{iB} parameters can be found in [51],[52].

Semi-elliptical cracks tends to morph into edge cracks because the crack growth in the surface direction is faster than in the depth direction if sufficient time is given for crack growth [62]. Accordingly, the crack shape changes in every load cycle as well as the crack growth ratio (a/c) in both directions (points A and B in Figure 3-13). Consequently, the ratio a/c is an important geometrical characterization that should be accounted for when evaluating fatigue life using LEFM.

Since the LEFM method is based on the assumption of existing crack, it is important to have a good estimation of the initial crack size. However, there is no general accepted estimation of the crack initial crack size. The shape of the crack is also an important factor that will affect the fatigue life. The initial crack size a_i may be estimated based on the experimental observation of strain-life specimens according to ASTM standard [46]. In this standard, the specimens are subjected to strain controlled cyclic loading in order to obtain the cyclic stress-strain curve. One of the criterion to consider the failure of the test specimen is the shape deformation of the stabilized hysteresis loop [46]. It was found that the shape of the stabilized hysteresis loop changes at some point (a_i = 0.5 mm) due to crack nucleation/initiation. This phenomenon can be used to estimate the initial crack size needed for the LEFM analysis.

3.10 Evaluation of the residual stress effect within the LEFM method

The residual stress is usually distributed from tensile to compressive (see Figure 2-14) through the plate's thicknesses that are connected by the weld [39]. For that reason, the residual stress affects not only the peak stress magnitude, but also the through-thickness stress distribution. The residual stress and the load induced stress fields get superposed in practice. Due to nonlinearity of residual stress fields the standard handbook solutions for stress intensity factors cannot be used. Therefore the weight function technique is being used for the determination of stress intensity factors in the methodology being discussed. Since the stress intensity factor obtained using the product of the through-thickness stress distribution σ(y) and the weight function m (y,a) (see equation 2.18), the residual stress must be accounted for when using the LEFM method. Thus the residual stress intensity factor can be determined as:

$$K^{res} = \int_0^a \sigma_{res}(y) \cdot m(x,y) \cdot dy \tag{3.25}$$

The residual stress effect is accounted for by adding the residual stress intensity factor to the applied stress intensity factor resulting in the so-called effective stress intensity factor K_{eff}:

$$K^{eff} = K^{apl} + K^{res} \tag{3.26}$$

The effective maximum and minimum stress intensity factors can be calculated as follows:

$$K^{eff}_{max} = K^{apl}_{max} + K^{res} \tag{3.27}$$

$$K^{eff}_{min} = K^{apl}_{min} + K^{res} \tag{3.28}$$

Thus, the stress intensity range, ΔK can be expressed as:

$$\Delta K = K^{eff}_{max} - K^{eff}_{min} = K^{apl}_{max} - K^{apl}_{min} \tag{3.29}$$

Accordingly, the effective stress ratio, R^{eff} is calculated as follows:

$$R^{eff} = \frac{K_{min}^{eff}}{K_{max}^{eff}} = \frac{K_{min}^{apl} + K^{res}}{K_{max}^{apl} + K^{res}} \tag{3.30}$$

It can be noted that the residual stress field does not change the range of the stress intensity factor ΔK but it changes only the stress ratio R.

The most often used model to determine the effective stress intensity factor range, ΔK^{eff} is the crack closure model. The fatigue crack growth rate tends to increase with the increase of the stress ratio. Kurihara [63] proposed the simplest variation of the crack tip closure model using the crack opening ratio U, which increases with the increase in the stress ratio until it become constant (U=1 for R > 0.5). Kurihara's expression [63] is based on the crack tip closure model showing that the effective stress intensity range is:

$$\Delta K^{eff} = U\Delta K = U\,(K_{max}^{apl} - K_{min}^{apl}) \tag{3.31}$$

Where:

$$U = \frac{1}{1.5 - R^{eff}} \quad \text{for} \quad -5 \leq R^{eff} \leq 0.5$$
$$U = 1 \quad \text{for} \quad R^{eff} > 0.5 \tag{3.32}$$

Thus, using the appropriate weight function and knowing the residual stress with the associated through-thickness stress distribution induce by the applied load in the prospective crack plane, the minimum and maximum effective stress intensity factors K_{max}^{eff} and K_{min}^{eff} can be calculated. Using the effective stress intensity range with the Paris equation (2.13), the effect of the residual stress and the stress ratio are accounted for in the fatigue crack growth analysis.

To sum up, the LEFM method is suitable for estimating the fatigue crack propagation life of welded joints because it is capable of including the various factors associated with weldments, such as the residual stress, mean stress effect, and stress ratio. However, this method relies on the stress intensity factor, which is not available for weldments or welded joints with variable plate thicknesses. In addition, this method depends on the initial crack size assumption and the distribution of the stress through the critical cross-section of weldments. For the initial crack size, there is no specific assumption method because the initial crack size varies with the material properties, so the assumption is empirical. The through-thickness stress distribution, which is very important, is not

easy to determine even with the help of FEM because of the high peak stress, which results in a high stress gradient through the critical cross-section of the weldment. As mentioned earlier, using 3D FE modelling to find the peak stress and the associated through-thickness stress distribution is difficult for complex welded joints, not to mention full structures. Finding the actual peak stress and the through-thickness stress distribution for a single welded component requires a high number of 3D elements with a very fine mesh at the critical areas, which will take a long time and consume considerable computational resources. Regardless, many studies have been done to ease the use of FEM by using the shell FE, which requires a fewer number of elements in order to determine the peak stress, but none has extended the stress analysis to include the through-thickness stress distribution itself in order to use the LEFM method. The following section reviews some of those studies in order to develop a stress analysis method that can determine the peak stress and the through-thickness stress distribution of a welded structure, regardless of the mesh sensitivity and computational time and resources.

Chapter 4
Validation of the shell FE local reference stress data using 3D FE modelling

The stress data based on the shell FE model must be validated against the same stress data extracted from the detailed 3D FE model. The shell FE local reference stress data (σ_a and σ_b) were used to determine the hot spot stresses, then, with the SCFs, the peak stress and the through-thickness stress distribution were determined. The 3D FE modelling of a welded joint can determine the actual stress data, which are the peak stress σ_{peak} and the non-linear through-thickness stress distribution $\sigma(y)$. The peak stress from the 3D FE model can be directly compared to the one based on the shell FE local reference stress data or equation 3.8. The actual non-linear through-thickness stress distribution $\sigma(y)$ from the 3D FE model can also be compared to the through-thickness stress distribution $\sigma_{xx}(y)$ from the shell FE local reference stresses and Monahan equation 3.11. The shell FE local reference stress is a linearized stress distribution in the critical weld toe through-thickness. This linearized shell FE stress data can be compared to the actual stresses from the 3D FE by linearizing the actual non-linear through-thickness stress distribution. In other words, the linearization of the 3D FE actual non-linear through-thickness stress distribution $\sigma(y)$ can be used to determine the membrane and bending hot spot stresses, which are comparable to the membrane and bending hot spot stresses from post-processing the shell FE model (σ_a and σ_b). Figure 4-1 illustrates the compared stress data. This validation is based on the definition of the statically equivalent hot spot stress σ_{hs}, which is equal to the sum of the membrane and bending stresses (see equation 3.7). Consequently, there is a direct and unique relationship between the 3D FE actual non-linear through-thickness stress distributions of the critical weld toe and the linear stress field obtained from the shell FE model.

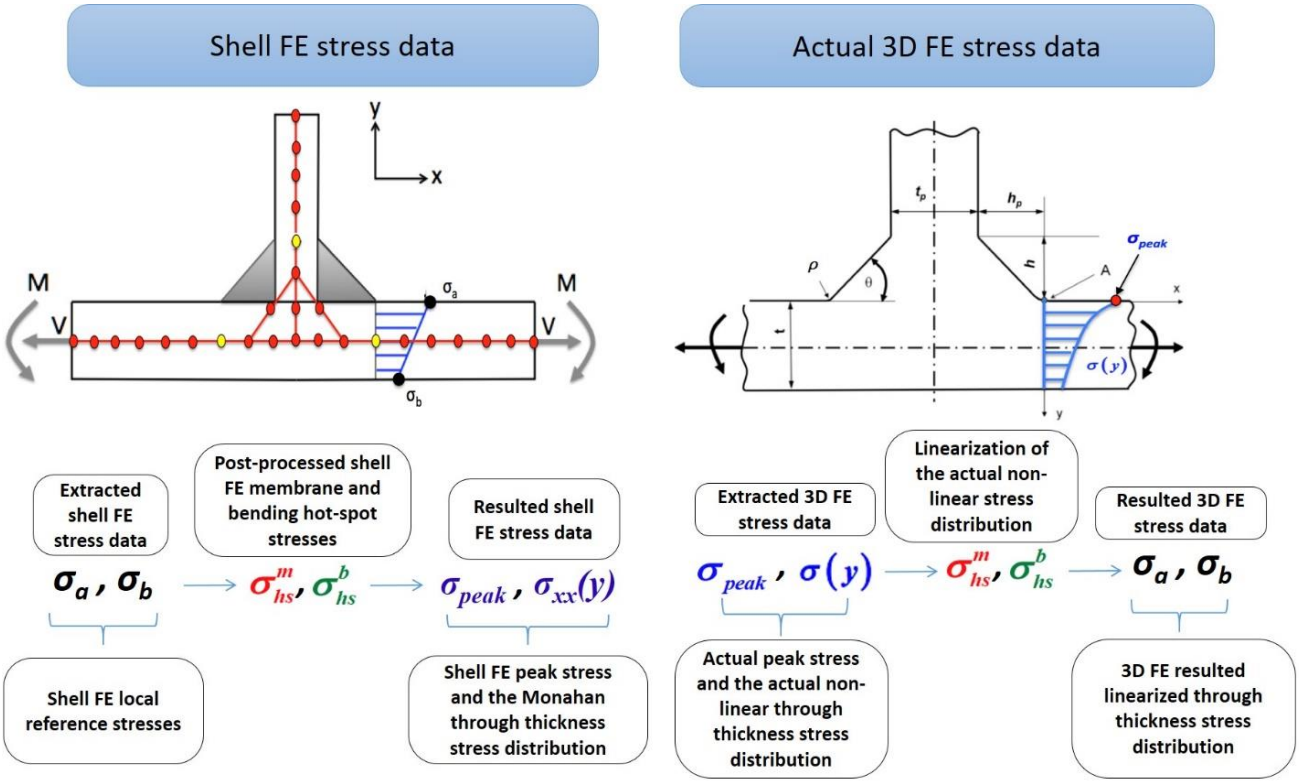

Figure 4-1: Stress data comparison between the shell and the 3D FE models

4.1 3D FE modelling

The recent improvements in computer power make it feasible to use 3D FE modelling for large structures. This can be achieved by using 3D brick or tetrahedral elements. Welded structures, on the other hand, are more complicated when modelled using 3D FE. One challenge when modelling a welded structure is capturing the high level of surface stress and its associated non-linear through-thickness distribution. Another challenge when using 3D FE modelling for welded joints is that the stresses around the weld toe are sensitive to the weld's micro-geometrical features (weld angle and weld toe radius), hence accurate modelling of the actual welded joint is required.

Modelling a welded joint using 3D FE with a sufficient amount of fine mesh elements at critical areas can directly produce actual stress data, which are the actual peak stress σ_{peak} and the actual non-linear through-thickness stress distribution $\sigma(y)$. A very fine mesh at the weld toe area is required to capture the magnitude of the maximum surface stress normal to the weld line and the associated non-linear through-thickness stress distribution. The smallest element at the weld toe line should be one-

quarter the weld toe radius ($\delta_{el} \leq \rho/4$) [64]. The magnitude of the peak stress is extracted from one element at the weld toe surface, whereas the stress values forming actual non-linear through-thickness stress distribution σ(y) are extracted through the main plate thickness under the weld toe. Note that both welded joint FE models (shell and 3D) must have the same material properties, geometrical features, and loading modes. Additionally, the stress data from both models must be extracted at the same location (weld toe area).

The previous paragraph shows the general guidelines to determine the actual peak stress σ_{peak} and the actual non-linear through-thickness stress distribution σ(y) using 3D FE modelling. As a result, the peak and through-thickness distribution based on the shell FE model can be validated when compared to the stress data from 3D FE modelling. For hot spot stress validation, a linearization of the actual non-linear stress distribution σ(y) is needed in order to find the membrane and bending hot spot stresses.

The goal is to extract the axial force P and the bending moment M from the 3D FE actual non-linear through-thickness stress distribution σ(y) at the weld toe. The axial force and the bending moment in at the critical weld toe cross-section can be used to determine the membrane and bending stresses (σ_{hs}^{m} and σ_{hs}^{b}). The 3D FE actual non-linear through-thickness stress distribution σ(y) shown in Figure 4-2 can be integrated to calculate the axial force and bending moment.

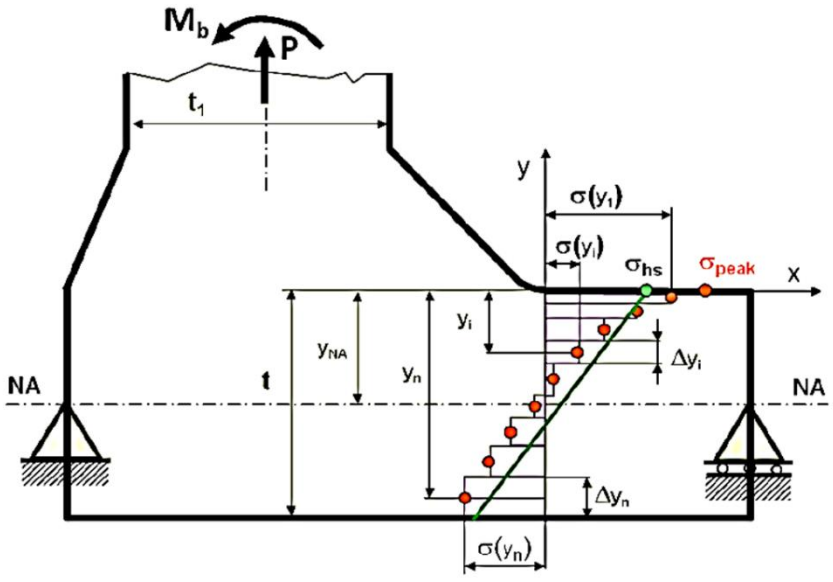

Figure 4-2: Example of a T-joint weld toe through-thickness stress distribution conducted using 3D FE, and the notation used in the linearization process

Assuming an imaginary area t x 1, the axial force P can be obtained by integrating the stress field along the line x = 0 and over the entire plate thickness:

$$P = \int_0^t \sigma(y)dy \tag{4.1}$$

Subsequently, the membrane hot spot stress is the average axial stress along the vertical line x = 0. When calculating the hot spot membrane stress, a unit of 1 is assumed in the z direction:

$$\sigma_{hs}^{m} = \frac{P}{1 \times t} \tag{4.2}$$

Substituting the last two expressions gives the hot spot membrane stress relation, as follows:

$$\sigma_{hs}^{m} = \frac{\int_0^t \sigma(y).1.dy}{1 \times t} = \frac{\int_0^t \sigma(y).dy}{t} \tag{4.3}$$

Using the same method, the internal bending moment M acting over an imaginary area 1 x t along the line x = 0 can be calculated:

$$M = \int_0^t \sigma(y)\, y\, dy \tag{4.4}$$

Using a simple bending formula, the corresponding shell bending stress can be obtained as follows:

$$\sigma_{hs}^{b} = \frac{M \times C}{I} = \frac{\int_0^t \sigma(y).1.y.dy \times \frac{t}{2}}{\frac{1 \times t^3}{12}} = \frac{6\int_0^t \sigma(y).y.dy}{t^2} \tag{4.5}$$

Where: $I = \frac{1 \times t^3}{12}$

The 3D FE analysis usually provides stress data in terms of stress magnitudes at a selected number of Gaussian points, nodal points, or centers of gravity of individual elements of the FE mesh. To obtain the membrane σ_{hs}^{m} and the shell bending stress σ_{hs}^{b} from such a discrete non-linear stress field,

a numerical integration procedure is required, and the analytical integration should be replaced with a summation of discrete increments. The surface stress σ_a is calculated as follows:

$$\sigma_{hs} = \sigma_a = \sigma_{hs}^{m} + \sigma_{hs}^{b} = \frac{\int_0^t \sigma(y).\,dy}{t} + \frac{6\int_0^t \sigma(y).\,y.\,dy}{t^2} = \frac{\sum_1^n \sigma(y_i).\,\Delta y_i}{t} + \frac{6\sum_1^n \sigma(y_i).\,y_i.\,\Delta y_i}{t^2} \quad (4.6)$$

The stress at the bottom side of the shell model can be calculated as follows:

$$\sigma_b = \sigma_{hs}^{m} - \sigma_{hs}^{b} = \frac{\int_0^t \sigma(y).\,dy}{t} - \frac{6\int_0^t \sigma(y).\,y.\,dy}{t^2} = \frac{\sum_1^n \sigma(y_i).\,\Delta y_i}{t} - \frac{6\sum_1^n \sigma(y_i).\,y_i.\,\Delta y_i}{t^2} \quad (4.7)$$

The local reference stresses found using the shell FE technique (σ_a and σ_b) can be compared to the linearized stress resulting from equations (4.6 and 4.7). Note that equations (4.6 and 4.7) resulted from processing the 3D FE stress data. The peak stress and the non-linear through thickness stress distribution resulting from processing the shell FE local reference stresses equations (3.8 and 3.11) can be compared to the 3D FE stress data (The actual peak stress and the actual non-linear through thickness stress distribution) see Figure 4-2.

Chapter 5
Case studies on the fatigue life prediction of welded joints using the local reference stress

5.1 Predicting the fatigue life of welded joints using strain-life and LEFM methods

The strain-life and LEFM methods are utilized in this work to determine the total fatigue life of welded joints. The strain-life method can determine the fatigue crack initiation life, N_i, while the LEFM method can estimate the fatigue crack propagation life N_p. The total fatigue life to failure, N_f is the sum of the fatigue life to crack initiation N_i and propagation N_p.

$$N_f = N_i + N_p \tag{5.1}$$

The maximum elastic local stress (peak stress) acting at the critical point of a welded joint based on the shell FE local reference stress can be calculated using equation 3.12 and 3.13. Assuming constant amplitude loading, the elastic peak stress can be related to the actual elastic-plastic stress at the notch tip using the Neuber rule [35] as per equation (2.6). The Ramberg-Osgood equation (2.7) is then used to calculate the corresponding elastic-plastic strain (actual strain) for the loading part. For the unloading part, the procedure is similar but with an expansion of the fatigue stress-strain curve by a factor of 2 as per equation 2.8. Accordingly, the elastic-plastic stress response can be determined and the corresponding elastic-plastic strain ranges can be determined using the SWT equation (2.9). The procedures are shown previously in Figure 2-12.

The final step is to evaluate the number of cycles to crack initiation N_i. The elastic-plastic or actual strain ranges resulting from the previous steps can be input to the Manson-Coffin [31],[32] equation (2.4) to determine the fatigue crack initiation life at the weld toe. SWT [33] equation (2.9) can be used instead in order to account for the mean stress effect on the fatigue crack initiation life. Note that the residual stress effect can be added to the applied elastic peak stress term in the Neuber rule [35] as per equation (2.12).

The LEFM method is mainly based on the Paris law (equation 2.13). The Paris law requires the stress intensity factor and material constants C and m. The stress intensity factor can be found in

handbooks, but in case of welded structures it can be evaluated using the weight function. This method of evaluating the stress intensity factor requires the proper weight function and the through-thickness stress distribution of the uncracked body in the weld toe prospective crack plane. The through-thickness stress distribution based on the shell FE local reference stress data and the Monahan expression (3.11) can be used for determining the stress intensity factor mentioned in equations (2.18 and 2.19) if the proper weight function m (y, a) are known. To evaluate the fatigue crack growth life of a welded joint, several factors like the stress ratio and the residual stress must be accounted for in the Paris law as per equation (3.22).

The fracture mechanics method assumes the crack is already initiated as an initial crack size a_i that increases up to a critical crack size a_f. The critical crack size is the crack length where the final brittle fracture may occur. As recommended by the IIW, the initial crack size can be assumed as (a_i = 0.15 mm), which is suitable for conservative fatigue life estimation. Other publications suggest (a_i = 0.5 mm) for some mechanical engineering applications. However, there is no general rule as to what should be the initial crack size because the assumption may depend on inspection capabilities, material properties, and loading conditions. The crack shape, such as circular or semielliptical, has to be assumed as well because it affect the stress intensity factor or the weight function.

In the present work the initial crack size a_i at depth or point A in Figure 3-13 was assumed to be 0.5 mm, while the crack shape was assumed to be semielliptical. The observed crack length from experiments showed an average surface crack of (c_i = 3.5 mm), which results in an initial aspect ratio of (a/c = 0.286). The Paris law material constants (C, and m) were determined based on equation (2.16). Equations (3.21 and 3.22) were used to determine the stress intensity factors for the initial crack size. The through-thickness stress distribution, based on the shell FE local reference stress data and the Monahan expression (3.11) was input to determine the stress intensity factors at two points, which were the surface and the depth point (Figure 3-13). Another input to determine the stress intensity factor was done to find the proper weight functions for cracks with semielliptical shape. Two weight functions are required in the case of semielliptical cracks (3.21 and 3.22). Then, the new propagated crack size caused by the stress cycles is determined by using equation (2.20). Equation (3.26 to 3.32) show how to account for the stress ratio and the residual stress effects. The previous procedures are repeated and the results are updated for each crack size increment at both the depth and surface points (A and B, Figure 3-13). The calculation must be carried on until the critical crack

size is achieved. The critical crack size can be assumed as 80% of the wall thickness for the deepest point. That is ($a_f = 0.8t$). Equation (2.21) can be used to calculate the fatigue crack growth life N_p. Finally, the total fatigue life can be calculated using equation (5.1).

The following figure illustrates the stress analysis steps:

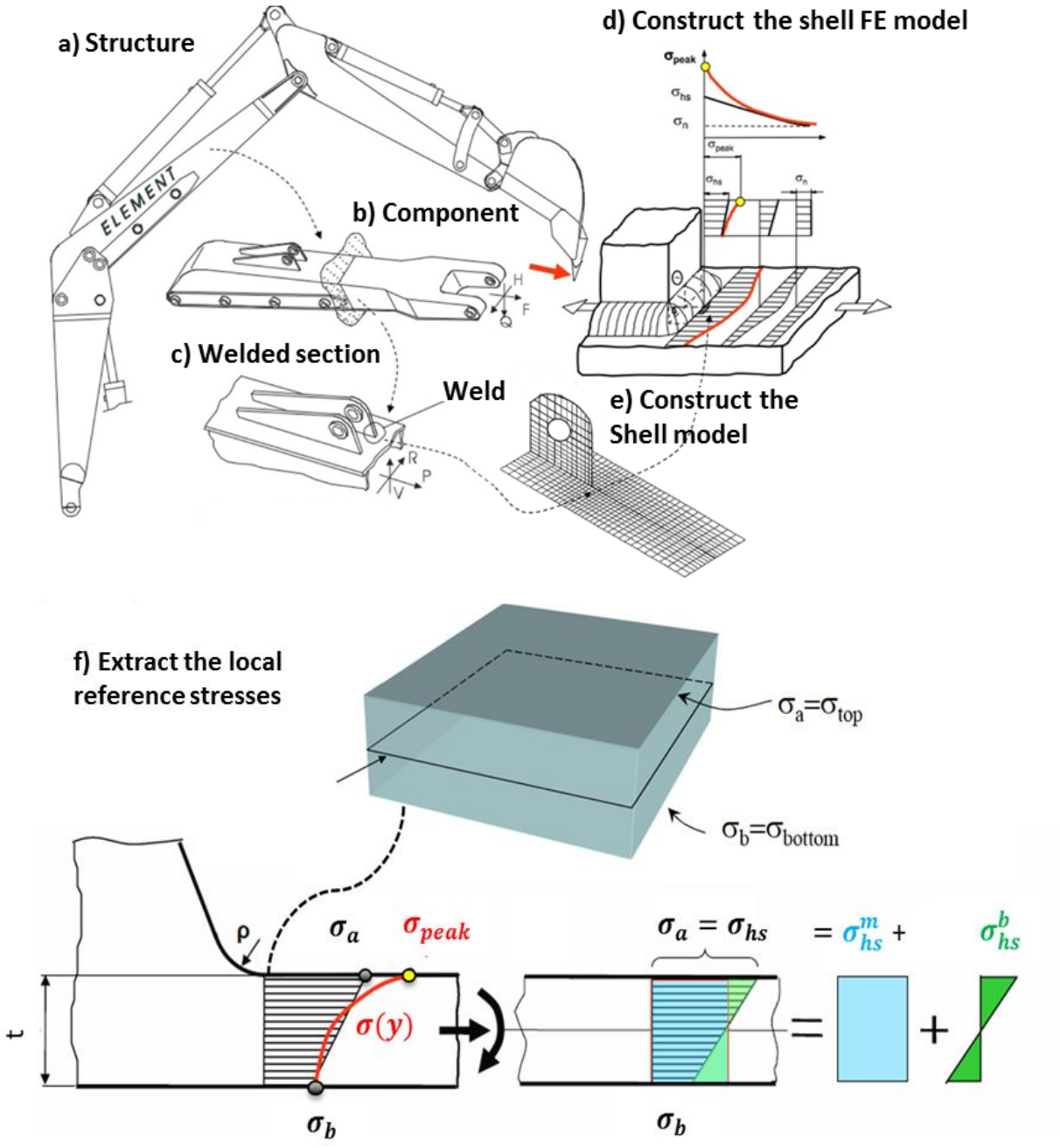

g) Determine the required stress data (Post-processing procedure)

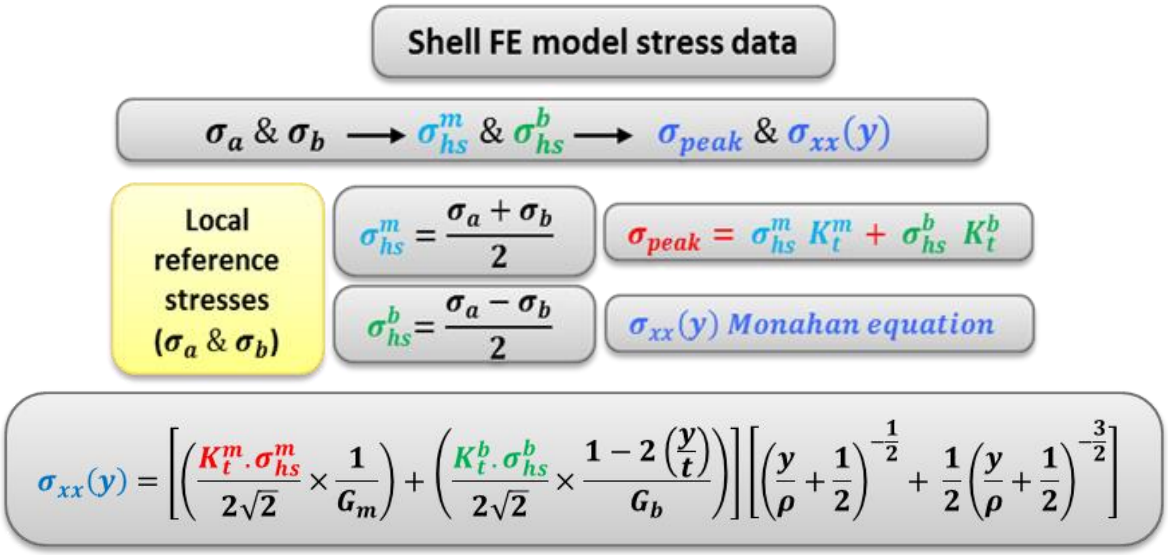

h) Validate the stress data

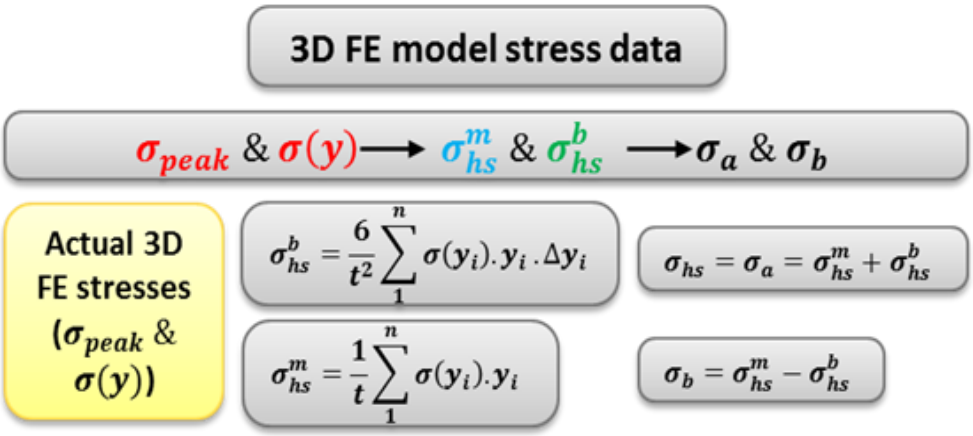

Figure 5-1: Summary of the methodology

5.2 Experimental data (case studies)

A significant amount of experimental data has been provided by the John Deere (JD) Company laboratories. These experiments evaluated the fatigue life of welded joints subjected to different loading modes. The presented methodology is demonstrated in this chapter to validate its capability of predicting the fatigue life of actual welded joints. These experimental welded joints or case studies are selected because they include different welded joints with different geometrical features and loading modes. Two case studies are presented here while three more case studies are added in the appendix. The case studies involve two different T-joints, tube-on-plate, square-tube-on-plate, and a complex welded joint. One of the T-joints and the tube-on-plate welded joint are presented here while the rest can be found in the appendix. These case studies are based on actual welded joints subjected to different fatigue loading to predict the fatigue lives. The experimental welded specimens were then modelled using the proposed shell FE and 3D FE models. The shell FE models were conducted to provide stress data in the weldment's critical areas, such as the weld toe. The stress data was validated for each case against stress data from detailed fine-meshed 3D FE models. Based on the shell FE modelling, the stress data (local reference stresses) were used to predict the fatigue life for each case. The ε-N and LEFM method were used for the fatigue life predictions. Finally, the fatigue life of each case study was compared to the experimental fatigue life data.

Note that all shell and 3D FE modelling was conducted using the ABAQUS FE software. The shell FE modelling was done according to Section 3.6, while the 3D FE modelling was conducted according to Section 4.1. The shell FE stress data (local reference stresses) was extracted from the weld's critical locations and then post-processed as per Section 3.8 in order to find the peak stress and the through-thickness stress distribution to evaluate the fatigue life of the experimental welded components. The strain-life method was used to predict the fatigue crack initiation life, whereas the LEFM method was used to predict the fatigue crack propagation life. For that, the in-house fatigue life prediction programs FALIN and FALPR were used to calculate the fatigue crack initiation life and the fatigue crack propagation life, respectively. The total fatigue life was calculated as the sum of both lives (the crack initiation life and the crack propagation life). The effect of the residual stress on the fatigue life calculation was individually included to study the significant of the difference.

The steps used to study each case were as follows:

1) Gather geometrical data about the welded joint (experimental specimen).
2) Gather information about the applied loads.
3) Gather material information for each welded joint to determine the material fatigue properties and other constants.
4) Conduct the shell FE modelling according to the proposed rules in the methodology chapter as per Section (3.6).
5) Extract the local reference stress data and perform the post-processing method to determine the required stress data for the fatigue analysis as per Section (3.8).
6) Conduct a detailed and fine-meshed 3D FE model of each experimental specimen to validate the stress data (membrane, bending, peak, and through-thickness stresses) acquired using shell FE modelling, as mentioned in Section (4.1).
7) Use the validated shell FE local reference stress data to predict the fatigue life of each welded joint, as per the strain-life and the LEFM methods.
8) Compare the predicted fatigue lives based on the proposed local reference stress data against the experimental fatigue lives.

The fatigue life evaluation steps according to Figure 1-1 were used in order to test the proposed fatigue stress analysis method in two case studies in this chapter, whereas the appendix contains an additional three case studies. Step one concerns providing the data required for the geometrical module. The second step is to supply the loading module, and the third step is to supply the material properties module. Steps four through six include using the proposed methodology to supply the stress analysis module for the fatigue analysis. The seventh step uses two of the well-known fatigue life methods to calculate the damage and fatigue lives of the experimental welded joints (damage and fatigue life modules). Step number eight involves the comparison of the predicted fatigue lives based on the proposed methodology and the actual experimental data in order to emphasize the efficiency and worth of the proposed fatigue stress analysis method.

5.3 Fatigue analysis of a T-joint subjected to in-plane cyclic loading

Eight samples of welded T-joints were tested by the JD laboratories. The T-joints were subjected to fully reverse cyclic loading of a lateral force in the gusset plate plane direction, as shown Figure 5-2. The base plate or main plate dimensions were $500 \times 500 \times 4$ mm, and the dimensions of the

vertical attachment plate (gusset plate), located at the center of the main plate, were $50 \times 100 \times 4$ mm. The material for the tested samples was 1008 steel. The welding was done using the Flux Core Arc Welding method. The dimensions of the weld were t = 4 mm, t_p = 4 mm, h = 4 mm, h_p = 4 mm, θ = 45°, and ρ = 0.55 mm.

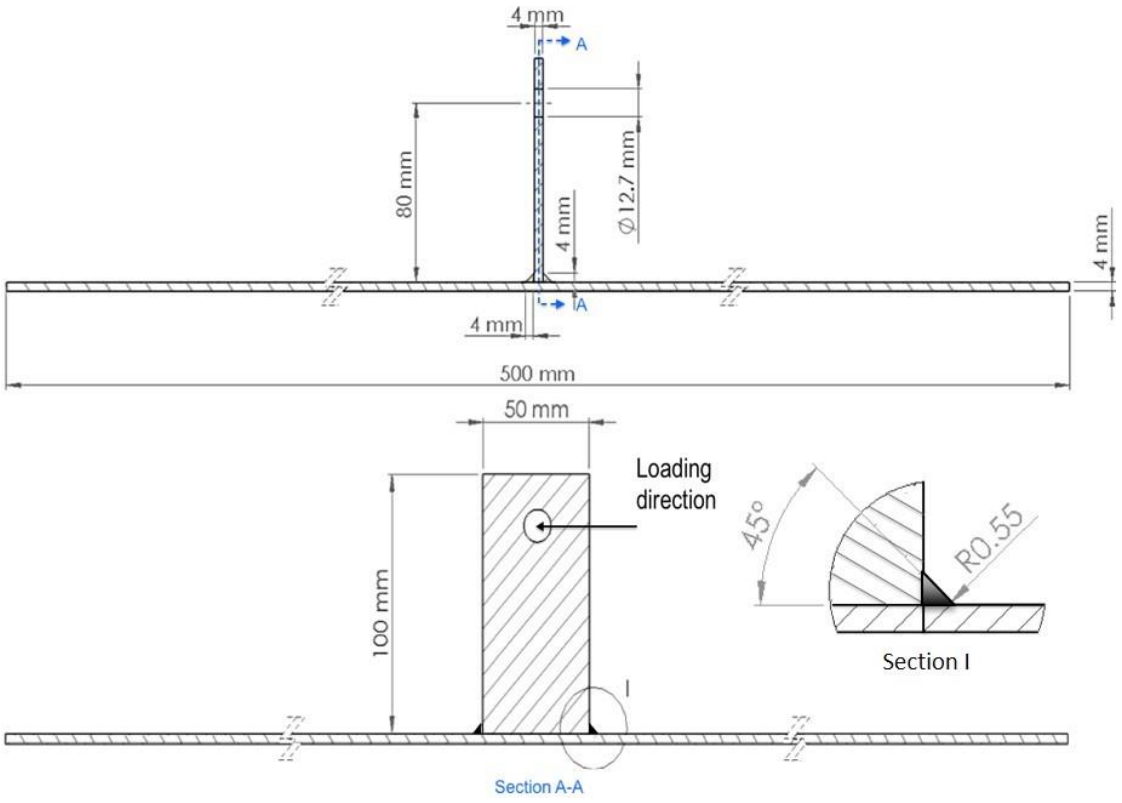

Figure 5-2: Geometries of the T-joint specimen subjected to in-plane cyclic loading

Six of the tested specimens were subjected to a load of F = ± 1320 N, while the rest of the test specimens were subjected to a load of F = ± 2000 N. The base plate of each specimen was fixed at all corners of the base plate by clamps with dimensions of 40 × 80 mm, whereas the pinhole of the gusset/attachment plate was subjected to lateral cyclic loading as shown in Figure 5-2. The expected critical stress area, where the crack is to initiate and grow, is one of the gusset weld toes for one of the experimental T-joint specimens, as shown in Figure 5-3. Therefore, the local reference stresses (σ_a and σ_b) are determined for that same region (weld toes of the attachment plate further sides).

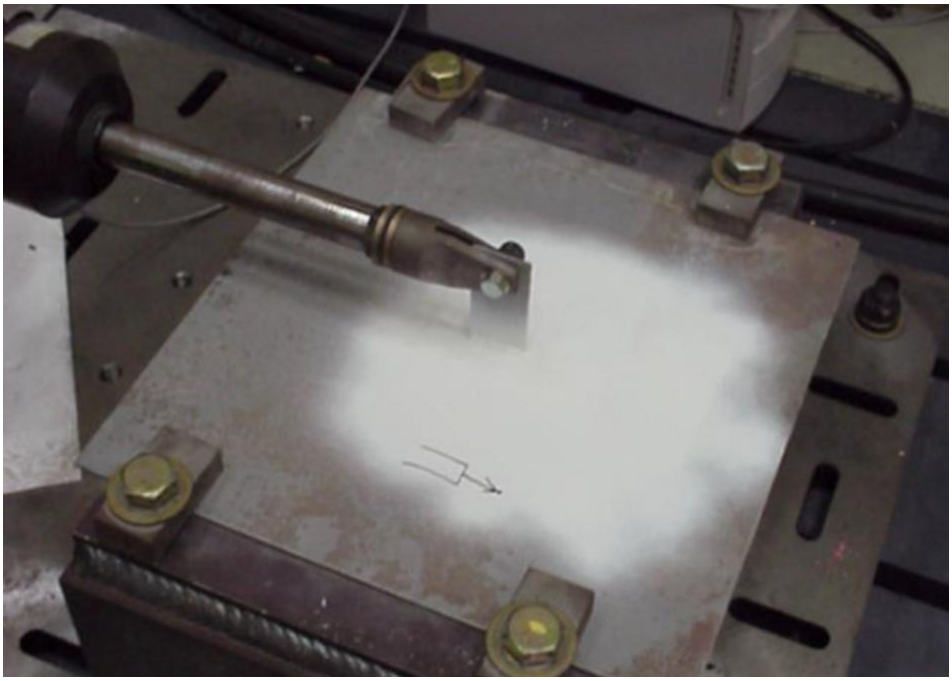

Figure 5-3: Test sample of the T-joint subjected to in-plane cyclic loading (JD)

5.3.1 Material properties

The material properties of the welded joint under investigation (1008 steel) were provided by the JD laboratories. The chemical composition and mechanical properties are shown in Table 5-1 and Table 5-2, respectively. The fatigue test data of 1008 steel are shown in Table 5-3.

Table 5-1: Chemical composition of 1008 steel (weight %)

C	Si	P	S	Mn	Ni	Cr	Mo	B	Al
107	40	5	15	330	9	19	22	.219	67.4

Table 5-2: Mechanical properties of 1008 steel

Ultimate strength (Su)	Yield strength (Sy)	Elastic modulus (E)
351.0 (MPa)	198.0 (MPa)	207447 (MPa)

Using the row experimental data obtained for a set of smooth specimens tested according to ASTM standard [1], the material fatigue properties of 1008 steel were determined at the University of Waterloo (UW). The fatigue parameters were determined using the Ramberg-Osgood and Manson-Coffin curves.

Table 5-3: Fatigue test results for 1008 steel (JD fatigue test data [66])

Experimental Total Strain Amp.	Stress Amp. (MPa)	Elastic Strain Amp.	Plastic Strain Amp.	Life (Rev.)
0.007	299.7	0.001444706	0.00418336	5428
0.006	286.8	0.001382522	0.003648938	6784
0.005	294.7	0.001420604	0.003970332	12452
0.004	269.5	0.001299127	0.003007642	19396
0.0035	258.4	0.001245619	0.002639253	29940
0.003	241.5	0.001164153	0.002139069	39994
0.00275	223.7	0.001078348	0.001686275	58892
0.0025	223.1	0.001075455	0.001672264	87502
0.00225	204.8	0.00098724	0.001281844	113448
0.00213	200.2	0.000965066	0.001194501	129826
0.002	193.2	0.000931322	0.00106947	184204
0.00175	179.3	0.000864317	0.000848072	239038
0.00163	173.3	0.000835394	0.000762979	341056
0.0015	165.5	0.000797794	0.000661271	401720
0.0014	160.9	0.00077562	0.000605828	566090
0.00132	158.9	0.000765979	0.000582739	801822
0.00125	153.1	0.00073802	0.000519167	1706230
0.00125	149.6	0.000721148	0.000483177	2111956

Figure 5-4 shows the Ramberg-Osgood fatigue stress-strain curve based on the experimental data in Table 5-3 . Manson-Coffin equation (2.4) was used to determine the fatigue curves, as shown in Figure 5-5 to Figure 5-7.

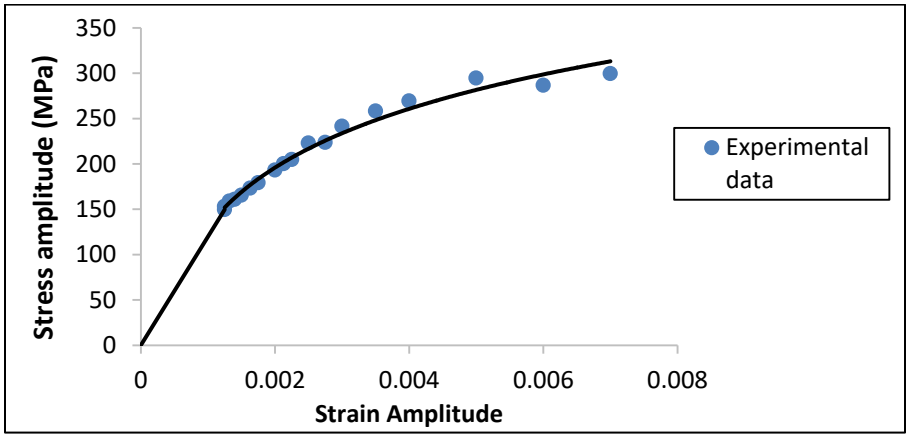

Figure 5-4: Stress-strain curve of the 1008 steel

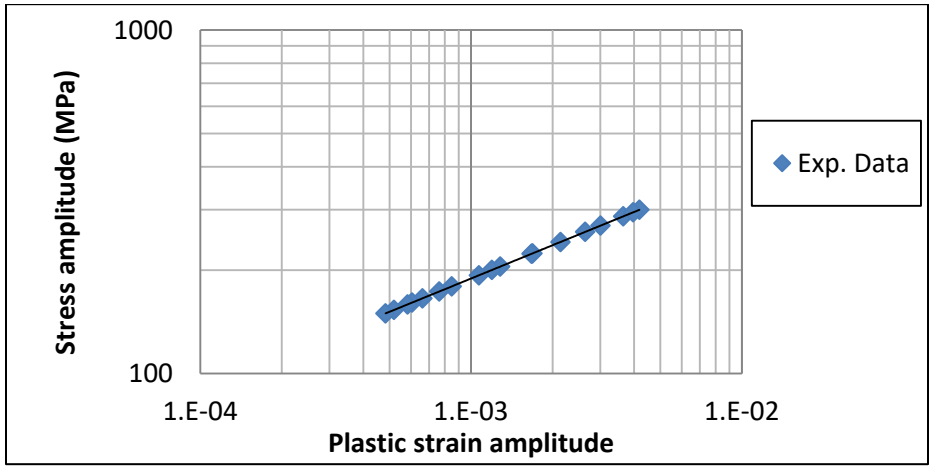

Figure 5-5: Stress-plastic strain fatigue curve for 1008 steel

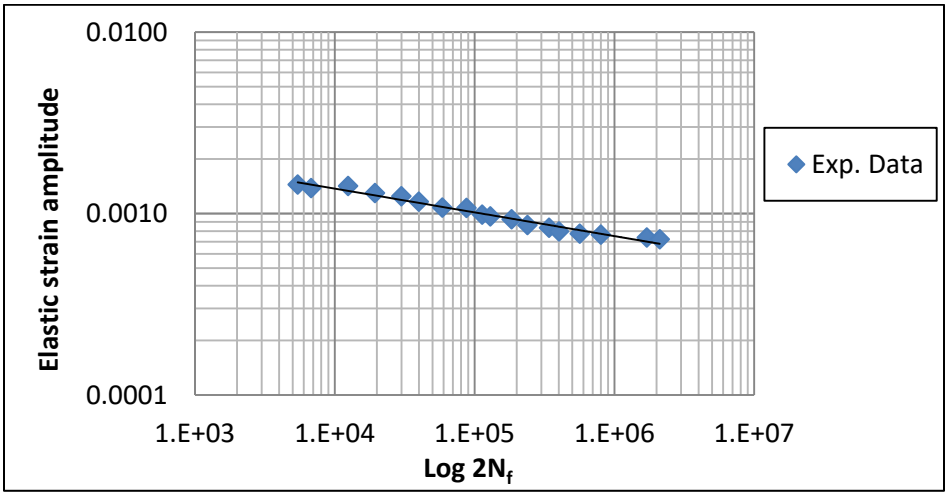

Figure 5-6: Elastic strain amplitude-life curve for 1008 steel

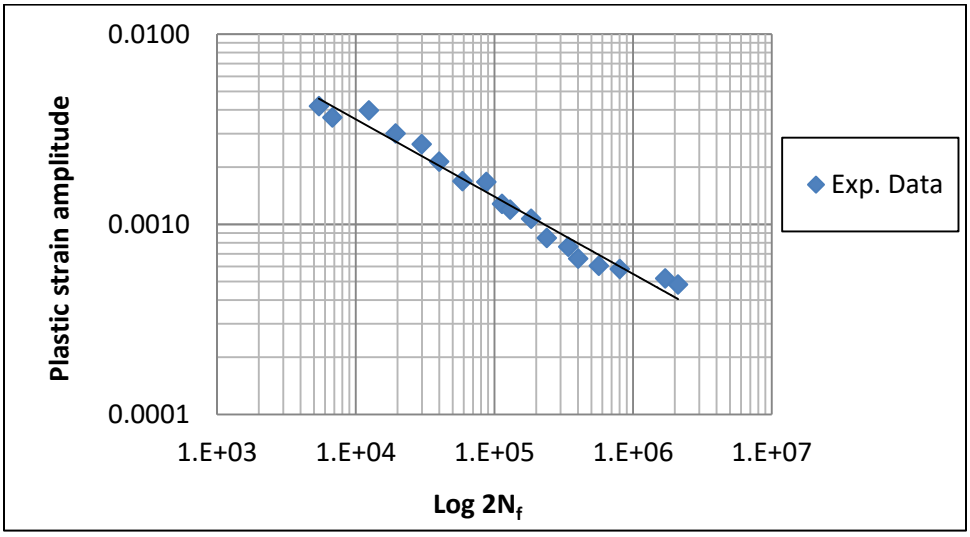

Figure 5-7: Plastic strain amplitude-life curve for 1008 steel

The UW analysis (curve fitting) results in the fatigue parameters shown in Table 5-4 for 1008 steel.

Table 5-4: Fatigue parameters of 1008 steel (UW)

Fatigue strength coefficient (σ_f')	**950.68 (MPa)**
Fatigue strength exponent (b)	**-0.1309**
Fatigue ductility coefficient (ε_f')	**0.151**
Fatigue ductility exponent (c)	**-0.4067**
Cyclic strength coefficient (K′)	**1747.1 (MPa)**
Cyclic strain hardening exponent (n′)	**0.3219**

5.3.2 Shell FE modelling of a T-joint subjected to in-plane cyclic loading

The aim of this shell FE model is to determine the local reference stresses (σ_a and σ_b) and perform the post-processing stress data in order to supply the required stresses for all of the contemporary fatigue life evaluation. The membrane and bending stresses (σ_{hs}^{m} and σ_{hs}^{b}) are determined by using equations (3.12 and 3.13). Based on the geometrical features of the welded joints, the membrane and bending SCFs (K_t^m and K_t^b) can be determined by using equations (3.15 and 3.20) in Section 3.7. According to equation (3.11), this is the required stress information that will determine the peak stress σ_{peak} based on the shell local stresses. The same stress data with proper SCFs (K_t^m, and K_t^b) can be used to determine the through-thickness stress distribution $\sigma_{xx}(y)$, as per the Monahan expression (3.11).

The shell FE model should have the same geometry as the experimental specimens, whereas the local reference stress must be extracted from a specific location (exactly at the weld toe having the

maximum stress normal to the weld toe line). In the present case, the weld's critical location or the location of the expected crack initiation is the lower weld toe of the gusset edge, as shown in Figure 5-3.

Note that the attachment plate and the main/base plate are modelled as middle-planes shell elements, and they are referred to as the attachment plate mid-plane and the main plate mid-plane. Both plates are modelled with the actual experimental welded T-joint thicknesses. The weld itself was also modelled as a middle-plane with a thickness equal to the thinner plate (i.e., thickness of attachment or base). Following the meshing rules described in section (3.6), the meshing of the shell FE model for the case under investigation is shown in Figure 5-10 to Figure 5-10.

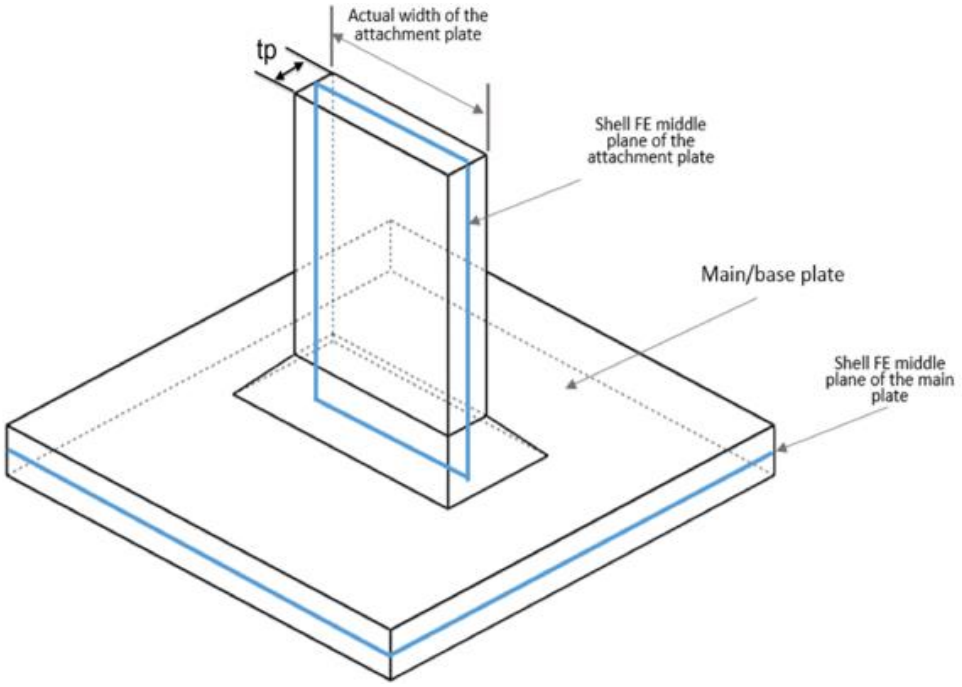

Figure 5-8: Shell FE modelling mid-planes for the T-joint subjected to in-plane bending load

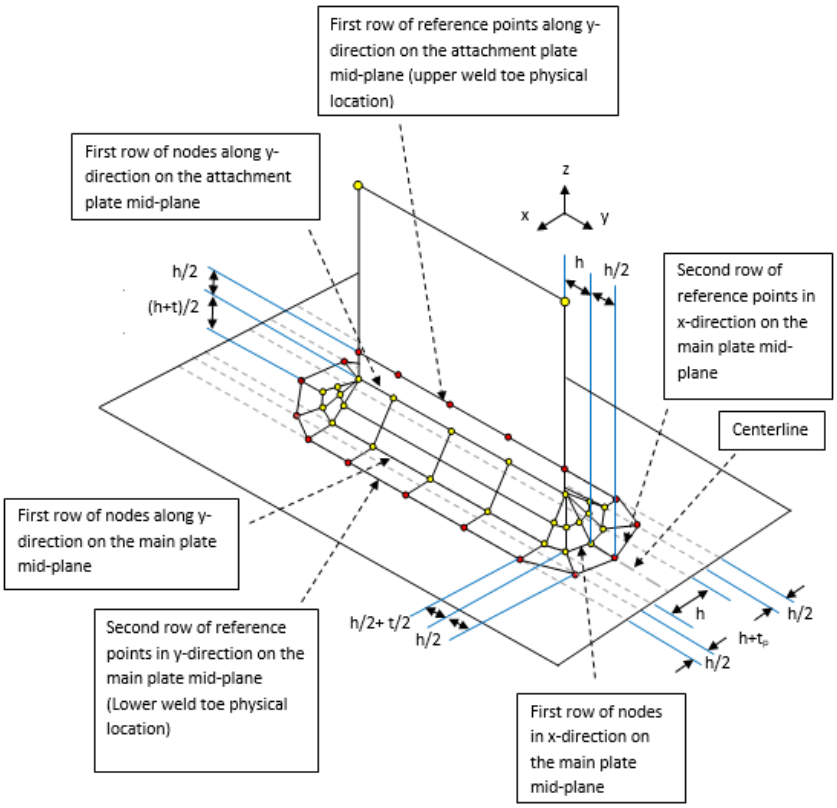

Figure 5-9: Shell FE modelling meshing rules for the T-joint subjected to in-plane bending load

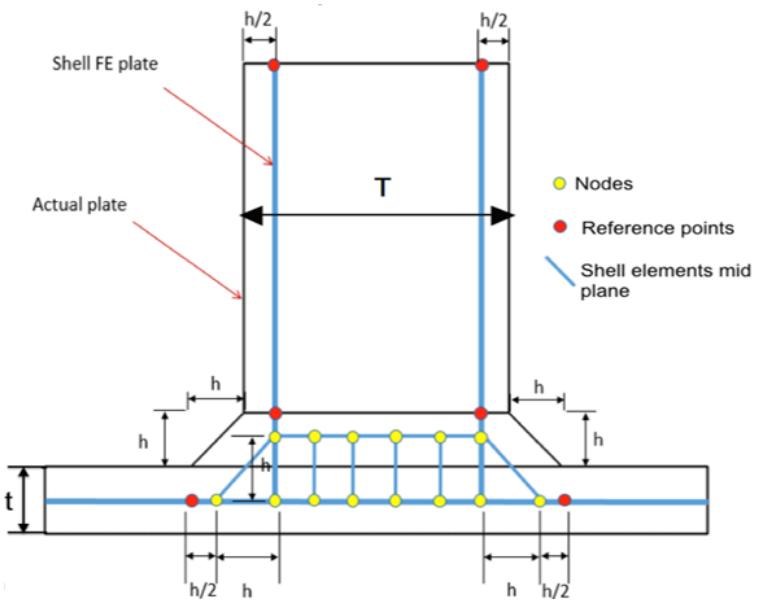

Figure 5-10: Shell FE modelling rules for the T-joint subjected to in-plane bending load

The meshing rules of the case under investigation were applied as follows:

- Meshing rules for the attachment plate mid-plane shell element:
- The width of the attachment plate mid-plane must be reduced by h/2 from the sides because of the gusset edges.
- The distance of the first row of nodes along y-direction on the attachment plate mid-plane should be at a distance of (h/2) + (t/2) from the main plate mid-plane.
- The second row of nodes including reference points on the attachment plate mid-plane along the y-direction should be at a distance of h + (t/2) from main plate mid-plane.
- The size of each element measured in the main plate mid-plane should be (h/2) in the z-direction.
- Meshing rules for the main plate mid-plane shell element:
- The distance of the first row of nodes along the y-direction on the main plate mid-plane should be at a distance of $(h+t_p)/2$ from the center line.
- The second row of the reference points on the main plate mid-plane along the y-direction should be h+ $(t_p/2)$ from the center line.
- Meshing rules for the weld edge shell element:
- The gusset mid-plane edge (curved end) should be created with at least two nodes with the size of (h/2).
- The first row of nodes of the gusset mid-plane must be on the main plate mid-plane with a distance of (h) from the attachment plate mid-plane edge along the x-direction.
- The second row of reference points of the gusset mid-plane must be on the main plate mid-plane with a distance of (h/2) from the first row of nodes along the x-direction (previous point).
- The thickness of the weld shell element must be equal to the thickness of the thinner plate.

The boundary conditions of the T-joint shell FE model under investigation are shown in Figure 5-11. The bottom plate corners were constrained for all displacement, while a lateral force of 1000 N was applied to the attachment plate pinhole.

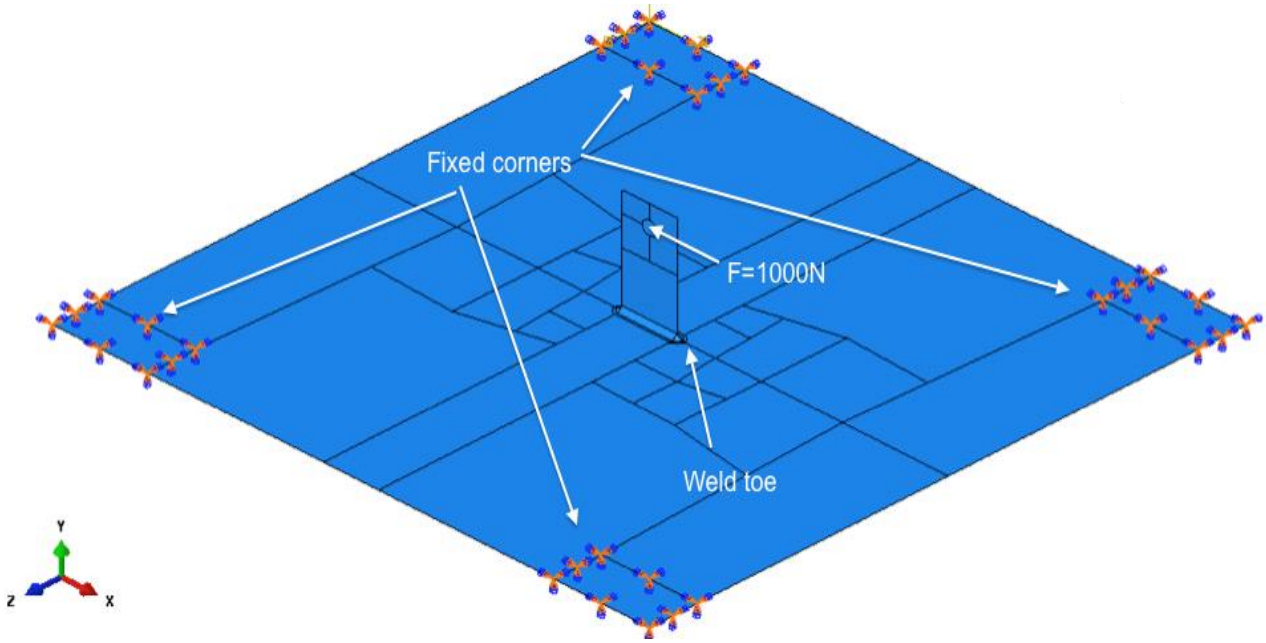

Figure 5-11: Shell FE model with boundary conditions for the T-joint subjected to in-plane cyclic loading (F = 1000 N)

According to the experiments, the maximum stress was expected to be at the weld toe of the gusset edge. Note that the reference points must coincide with the actual location of the weld toe of the experimental specimen.

Figure 5-12 indicates that the maximum stress is located at the weld toe, as expected. However, the required shell FE local reference stresses are to be extracted from a specific reference point and not at the maximum contour node. The distance between the attachment side and the weld toe reference point of the shell model was h+h/2 = 6 mm. At that specific reference point (at the critical location [weld toe]), the local reference stresses σ_a and σ_b were extracted on the opposite surface sides of the main plate (top and bottom).

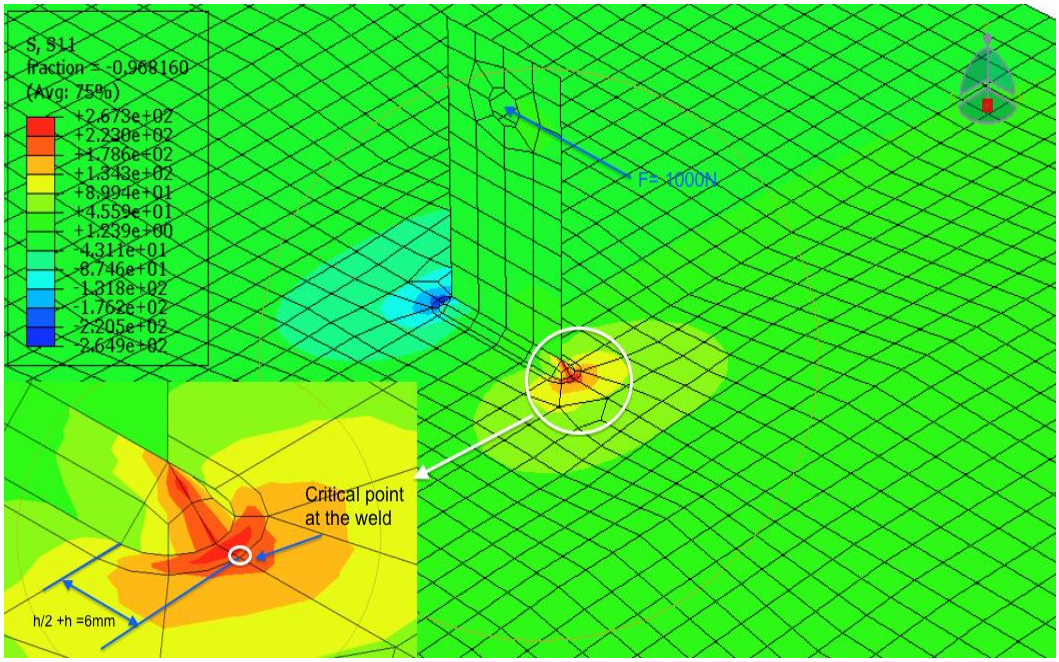

Figure 5-12: Shell FE stress contours of the maximum stress normal to the weld toe line; T-joint subjected to in-plane loading (F = 1000 N)

The local reference stresses σ_a and σ_b are obtained from a reference point located at the upper weld toe of the attachment plate as shown in Figure 5-13. The reference point contains the local reference stresses, which represent the surface and bottom stresses through the plate thickness. These stresses are used to determine the membrane and bending hot spot stresses that will be multiplied by the proper SCFs (see Section 3.7) to calculate the peak stress at the weld toe.

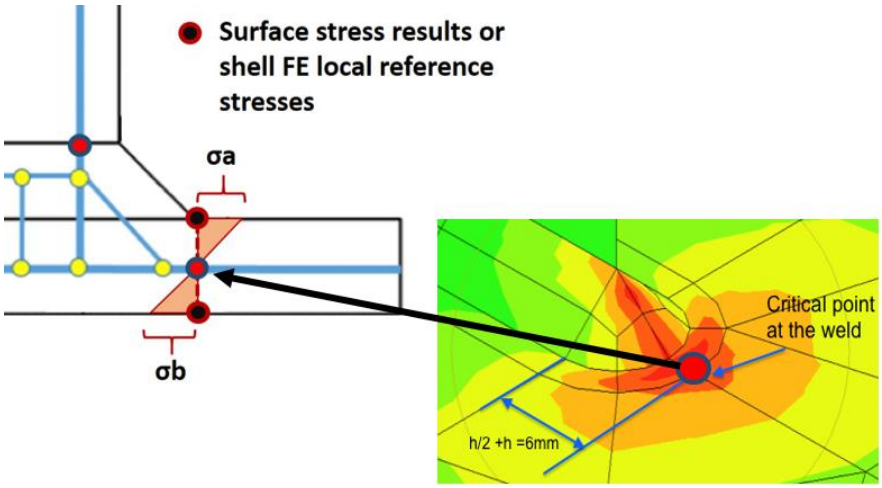

Figure 5-13: Shell FE local reference stresses σ_a and σ_b; T-joint subjected to in-plane loading

The local reference stresses through the base plate (σ_a and σ_b) were recorded as follows:

σ_a = 202.82 MPa

σ_b = -168.43 MPa

Therefore, the hot spot membrane and bending stresses σ_{hs}^{m} and σ_{hs}^{b}, per equations (3.12 and 3.13, respectively) were:

$$\sigma_{hs}^{m} = \frac{\sigma_a + \sigma_b}{2} = 17.19 \text{ MPa}$$

$$\sigma_{hs}^{b} = \frac{\sigma_a - \sigma_b}{2} = 185.63 \text{ MPa}$$

Using the weld geometrical features of the current case, the SCFs were calculated. However, because the attachment plate has a large thickness, the attachment plate thickness parameter, t_p was multiplied by a factor of 3 as an assumption for the SCFs at the edge of the gusset. According to available 3D FE data, the t_p parameter in equations (3.15–3.16) cannot be greater than 3t. Therefore, the assumption of $3t_p$ was used based on the fact that the effect of the edge disappears at distances greater than 3t, and the SCF equations are not valid for large values of t_p:

$K_t^m = 1.591$

$K_t^b = 2.166$

As per equation (3.8), the peak stress at the weld toe induced by the applied load was:

$$\sigma_{peak} = \sigma_{hs}^{m}.K_t^m + \sigma_{hs}^{b}.K_t^b = 429.25 \text{ MPa}$$

Figure 5-14 shows two stress distributions through the base plate thickness in the direction normal to the weld toe. The linear stress distribution (hashed line) represents the local reference stresses (σ_a and σ_b). The non-linear stress distribution (solid curve) represents Monahan equation $\sigma_{xx}(y)$ (equation 3.11).

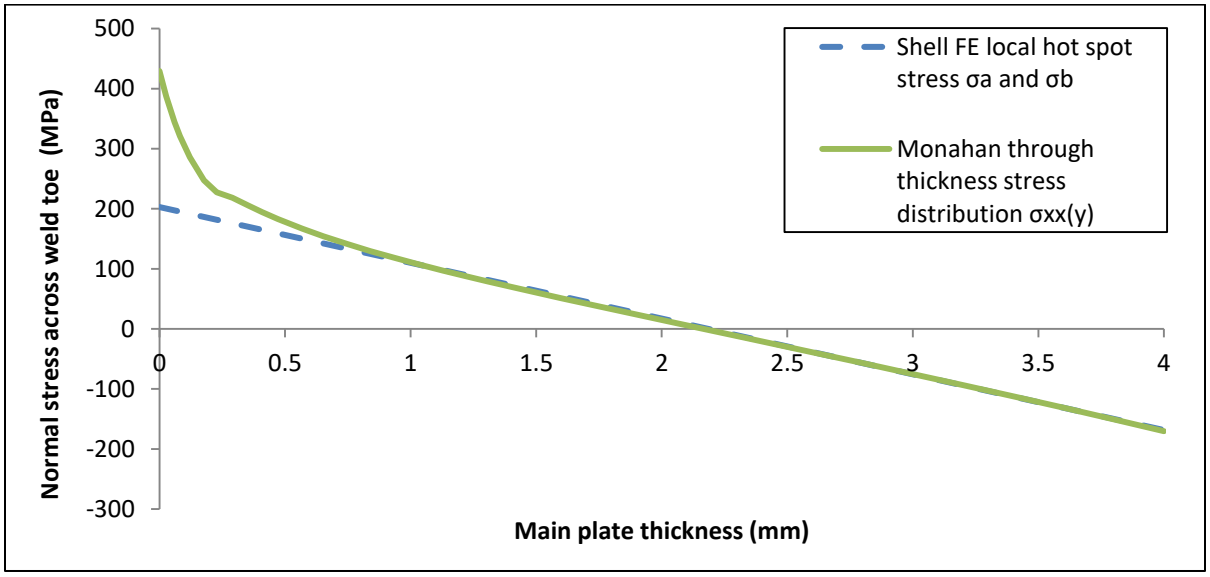

Figure 5-14: The shell FE local reference stress data at the weld toe cross section of the T-joint under in-plane bending; linear distribution of the local reference stresses (σ_a and σ_b); and the Monahan non-linear through-thickness stress distribution

Figure 5-14 provides the stress data (σ_a, σ_b, $\sigma_{peak,}$ and $\sigma_{xx}(y)$) required for the fatigue analysis of the case under investigation. The stress data in Figure 5-14 are obtained from a shell FE model and was validated against a detailed 3D FE model before proceeding with the fatigue analysis. A 3D FE model with the same geometry as the experiment is modelled in the following section to validate the shell FE local reference stress data.

5.3.3 Finite element 3D modelling of a T-joint subjected to in-plane cyclic loading

This section shows how to model welded joints by using the 3D FE method. The objective of 3D FE modelling is to validate the stress data obtained from the shell FE modelling. The validation includes the shell FE local reference stresses (σa and σb), the peak stress σpeak, and the through-thickness stress distribution $\sigma_{xx}(y)$ resulting from the post-processing method. The actual peak stress magnitude at the weld toe surface, in addition to the actual non-linear through-thickness distribution under the weld toe, can be extracted directly from the 3D FE model. The membrane and bending hot spot stresses can be determined by linearizing the 3D FE actual non-linear through-thickness stress distribution, according to Section (4.1). The linearization of the actual non-linear stress distribution results in determining the membrane and bending stresses that will be used to determine the stress quantities that are believed to be comparable to the local reference stresses (σa and σb).The stress

data must be extracted from the weld's critical location in the same way as the shell FE model. For the case under investigation, the critical locations are expected at one of the gusset edges (see Figure 5-3). According to the shell FE model, the maximum stress occurs at the lower weld toe on the compressive side. Therefore, it is expected the 3D FE model would have the peak stress at the same location. Figure 5-15 shows the 3D model boundary conditions. Due to the symmetry of the problem, only half of the component was modelled to reduce the computational time. The model was subjected to an in-plane bending stress generated by 1000 N. Just like the experiment and the shell FE model, the bottom corners of the base plate were constrained for all displacements in the 3D FE model, and the model elements were approximated by eight brick elements.

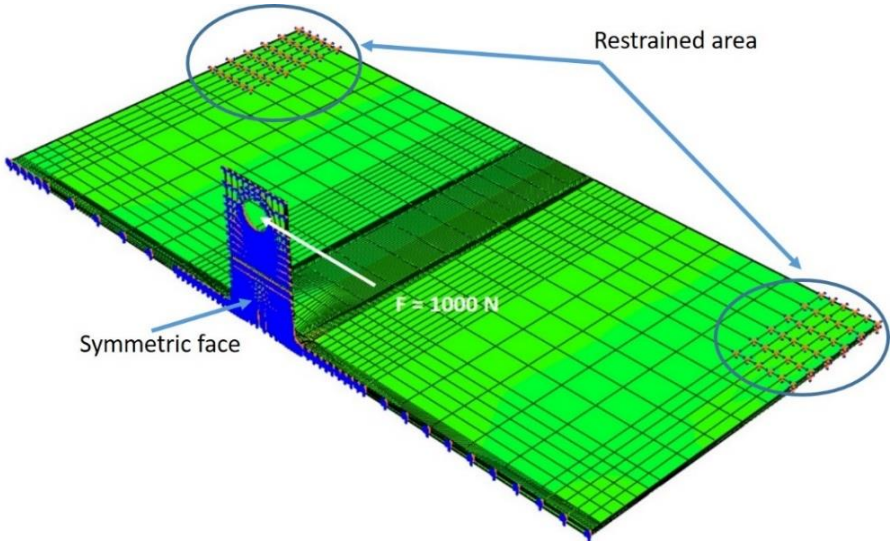

Figure 5-15: Boundary conditions of the 3D FE simulated T-joint subjected to in-plane bending load

The meshing was intensive at the critical area (weld toe of the gusset edges). This area was expected to have the peak stress normal to the weld toe. The element size at the weld toe should be small enough to find a converged stress. The recommended element size is at least equal to quarter of the weld toe radius [64]. The meshing of the weld toe is shown in Figure 5-16.

The maximum stress (peak stress) normal to the weld toe line in the 3D model was found at the expected location. Figure 5-16 shows the critical location of the 3D FE model where the stress data (the actual peak stress and the actual through-thickness stress distribution) are extracted.

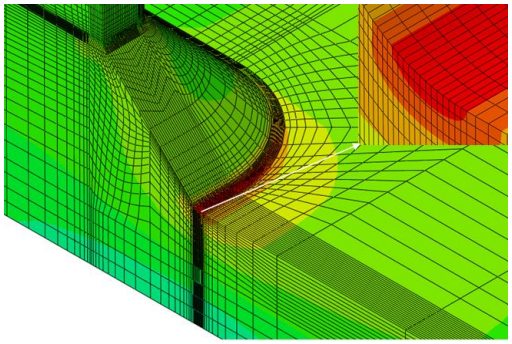

Figure 5-16: Fine mesh at the weld toe of the T-joint subjected to in-plane cyclic loading (3D FE model)

Based on the 3D FE modelling, the actual peak stress obtained at the weld toe was 358.39 MPa, and the actual non-linear through-thickness stress distribution is shown in Figure 5-17. The actual stress distribution was processed according to section (4.1), while the membrane and bending hot spot stresses were found by linearization, as mentioned in equations (4.3 and 4.5):

$\sigma_{hs}^{m} = 4.49$ MPa

$\sigma_{hs}^{b} = 215.31$ MPa

Equations (4.6 and 4.7) were then used to find the linearized surface stresses as:

$\sigma_a = \sigma_{hs}^{m} + \sigma_{hs}^{b} = 220.26$ MPa

$\sigma_b = \sigma_{hs}^{m} - \sigma_{hs}^{b} = -210.37$ MPa

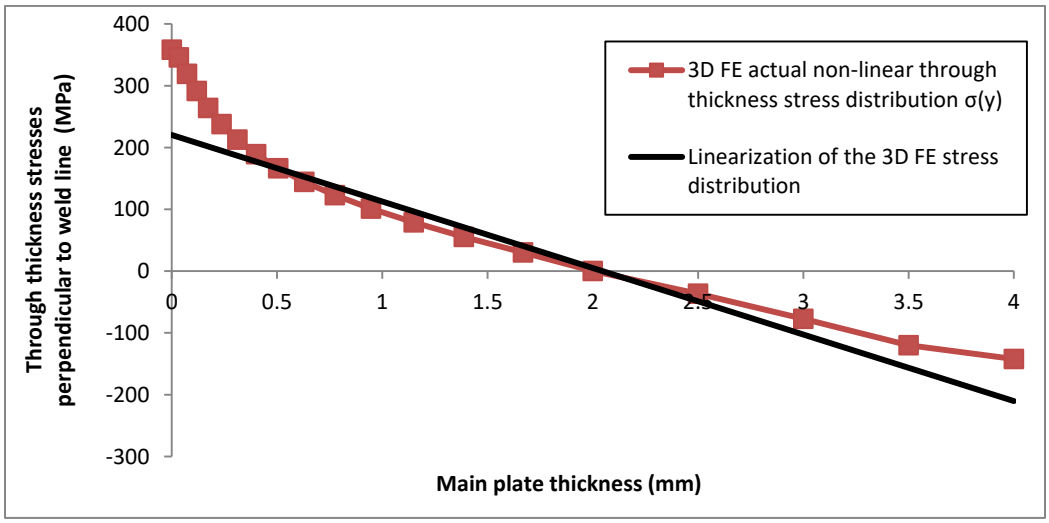

Figure 5-17: The 3D FE stress data, actual stress distribution, and the equivalent linearized stress distribution at the weld toe of the T-joint model subjected to in-plane bending loading

In Figure 5-17, the curve represents the actual non-linear stress distribution through the thickness of the weld toe cross section based on the 3D FE model. In the same figure, the solid line represents the linearization of the curve (actual non-linear stress distribution).

The stress results of both the shell and the 3D FE models (see Figure 5-14 and Figure 5-17) were compared after being normalized, as shown in Figure 5-18 and Figure 5-19. The normalization was done by dividing the shell and the 3D FE stress data by a load of F = 1000 N. The normalization was done so that the shell FE local reference stress data could be scaled later to the loads applied to the experiment specimens, which were based on loads of F = 1320 N and F = 2000 N.

Figure 5-18 shows a comparison between the actual non-linear through-thickness stress distribution σ(y) obtained from the 3D FE model and the non-linear through-thickness stress distribution $\sigma_{xx}(y)$ generated from the shell FE local reference stress data and the Monahan equation.

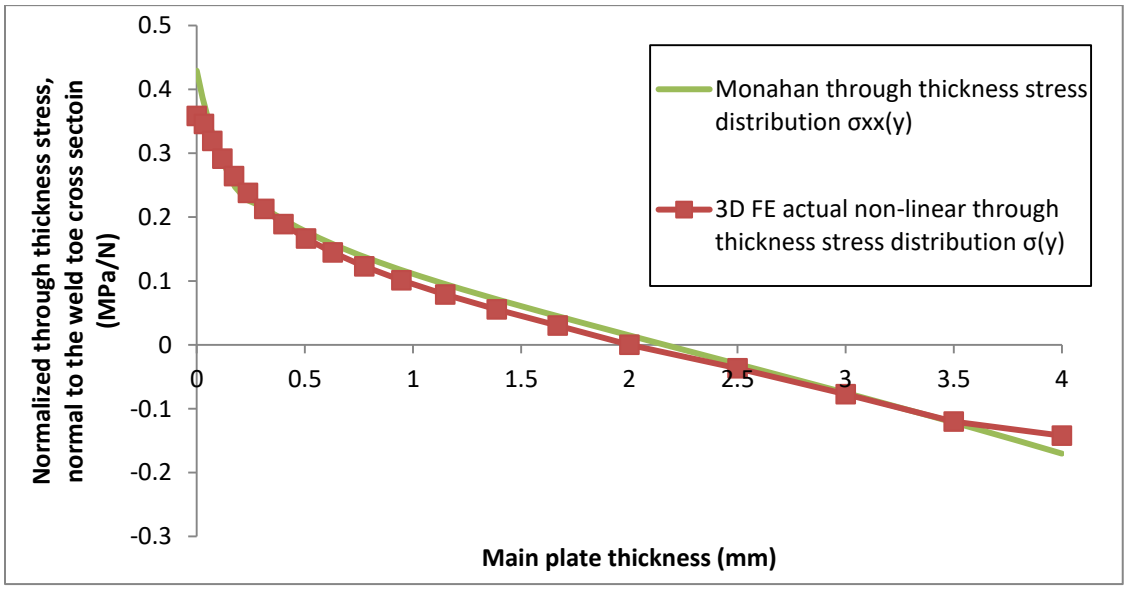

Figure 5-18: Comparison of the normalized actual stress distribution (3D FE model) and the normalized stress distribution (shell FE model and Monahan) through the main plate thickness of the T-joint

The difference between the actual peak stress based on 3D FE modelling (429.25 MPa) and the peak stress based on the shell FE local reference stress data (358.39 MPa) was approximately 20%. The compared stress distributions from both the shell and the 3D FE models showed good agreement. The 20% difference for the tensile part, which is the most important part because it is considered the location of the peak stress needed for the ε-N method.

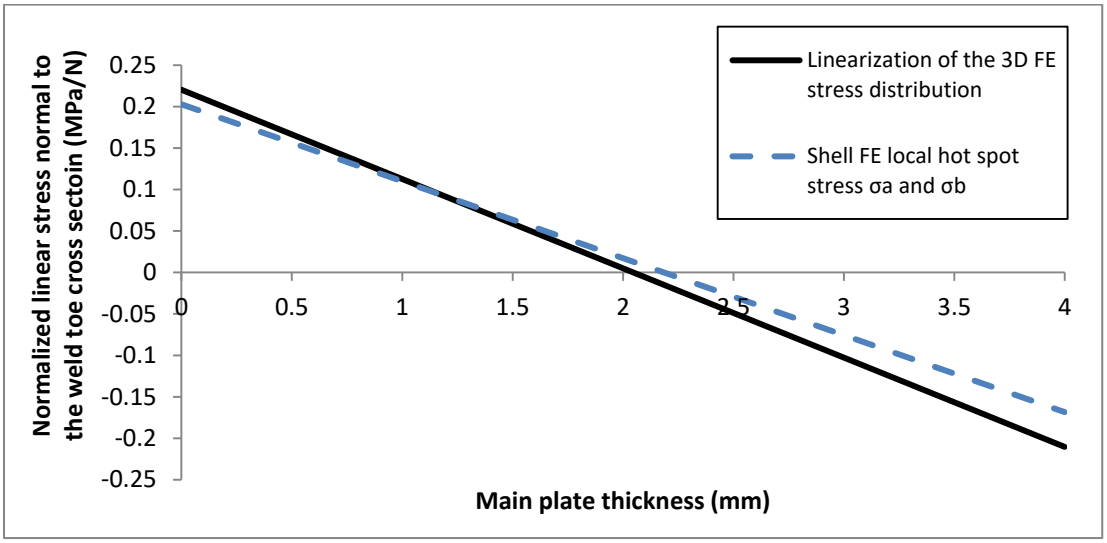

Figure 5-19: Comparison between the 3D FE and the shell FE linearized stress field across the weld toe cross section; T-joint subjected to in-plane cyclic loading

The linearized through-thickness stresses from the 3D FE model were higher than the shell FE local reference stresses in the bending and tensile parts of the base plate surfaces. The linearized stresses are compared to find out which stress part is causing the differences in the shell FE and the 3D FE stress data.

This validation is important because the peak stress based on the shell FE model will be used to determine the fatigue crack initiation life using the strain-life method. In addition, the through-thickness stress distribution based on the shell FE and Monahan equation (3.11) will be used to determine the stress intensity factor required to calculate the fatigue crack propagation life using the LEFM method.

The JD Company performed two series of fatigue tests to verify the predicted fatigue life for the T-joint subjected to in-plane cyclic loading. Both tests were conducted under fully reversed loading, but the first series of test specimens was subjected to F = ± 1320 N, whereas the second series was subjected to F = ± 2000 N. Therefore, the peak stress and the through-thickness distributions obtained from the shell FE modelling (the green curve in Figure 5-14) were scaled to the load levels applied to the experimental specimens (F = 1320 N and F = 2000 N), as shown in Figure 5-20 and Figure 5-21.

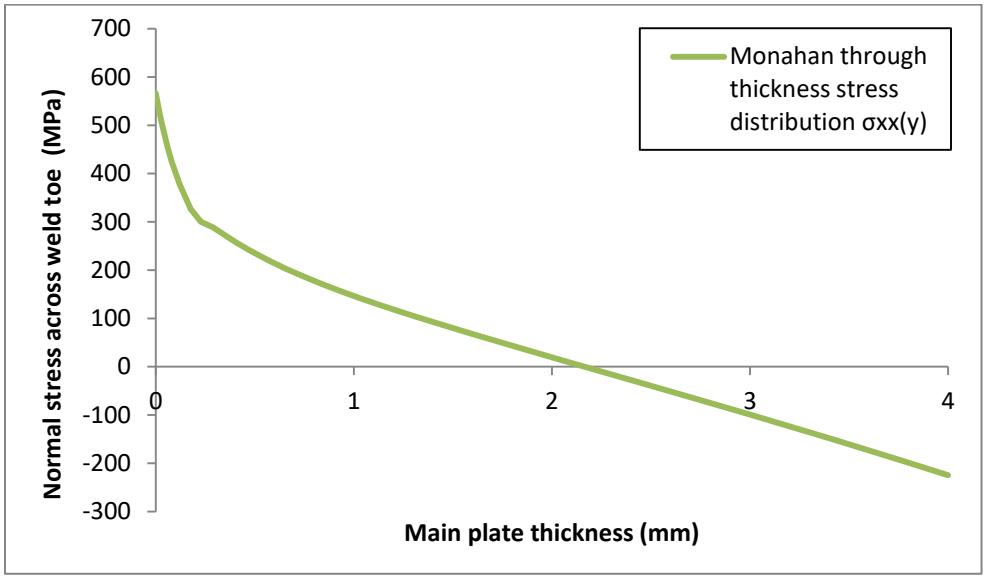

Figure 5-20: Scaled non-linear through-thickness stress distribution for a load of (F = 1320 N), based on the shell FE local reference stress data and Monahan equation

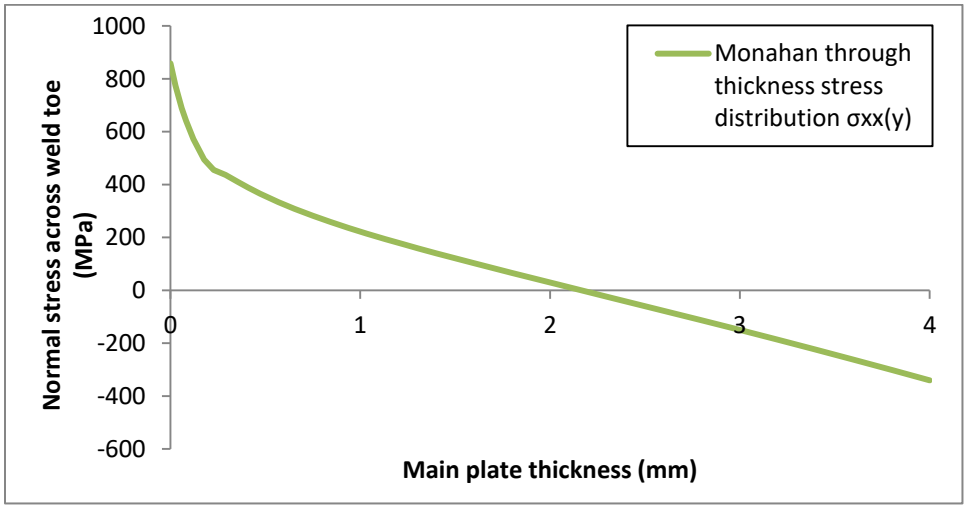

Figure 5-21: Scaled non-linear through-thickness stress distribution for a load of (F = 2000 N), based on the shell FE local reference stress data and Monahan equation

The fatigue life predictions were performed with and without the residual stresses. The residual stress was measured at the plate surface only (σ_r = 99 MPa), whereas the distribution was approximated by self-equilibrium of the linear field. The approximate residual stress distribution shown in Figure 5-22 was based on limited experimental data.

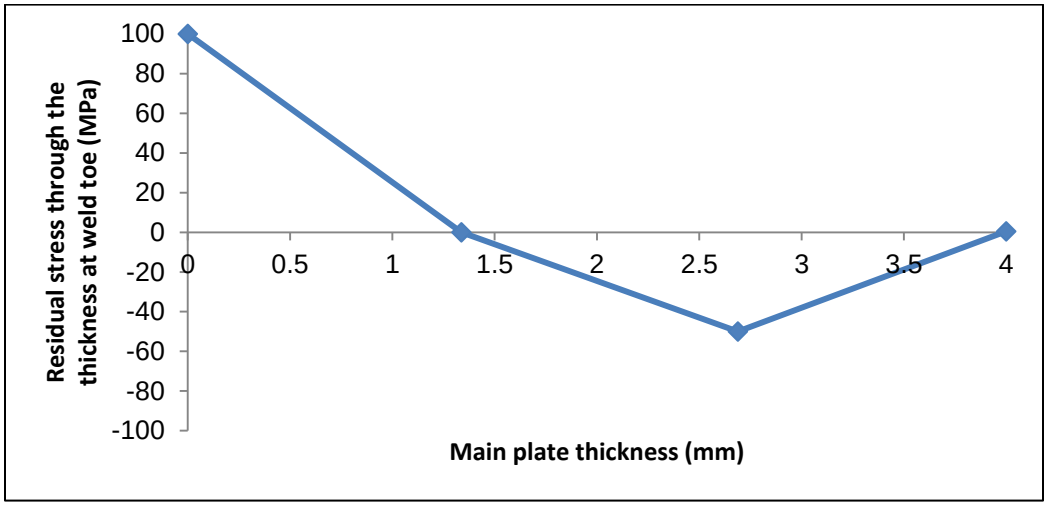

Figure 5-22: Approximation of the residual stress distribution through the attachment plate thickness of the T-joint subjected to in-plane bending load

5.3.4 Fatigue life prediction of a T-joint subjected to in-plane bending

The fatigue life is predicted by using the ε-N and the LEFM methods based on the shell FE local reference stress data. The ε-N method predicts the fatigue crack initiation life, whereas the LEFM method predicts the fatigue crack propagation life. Both methods, which are coded into the in-house FALIN and FALPR software packages, were used to find the total fatigue lives of the current case (T-joint subjected to in-plane cyclic loading). The total fatigue lives were determined by summing both the initiation and the propagation fatigue lives. Finally, the predicted total fatigue life was compared with the fatigue life of the experiment.

The first step is to determine the fatigue crack initiation life according to the procedure of the strain-life method described in Section (2.2). The material properties in Table 5-2 and Table 5-4 were input to the FALIN software to calculate the stresses and strains for each load cycle based on the Ramberg-Osgood fatigue stress-strain curve and the Neuber equation (see Figure 5-4 and Figure 2-12). The SWT equation (2.9) was then used to calculate the fatigue crack initiation life. The FALIN software simulates the stress-strain response and corresponding fatigue crack initiation life at the weld toe (output data). The fatigue crack initiation lives were predicted for the current case when subjected to load levels of F = 1320 N and F = 2000 N, without the effect of the residual stress, as shown in Figure 5-23 and

Figure 5-24. Figure 5-25 and Figure 5-26 show the fatigue crack initiation lives for the same load levels, including the residual stress effect.

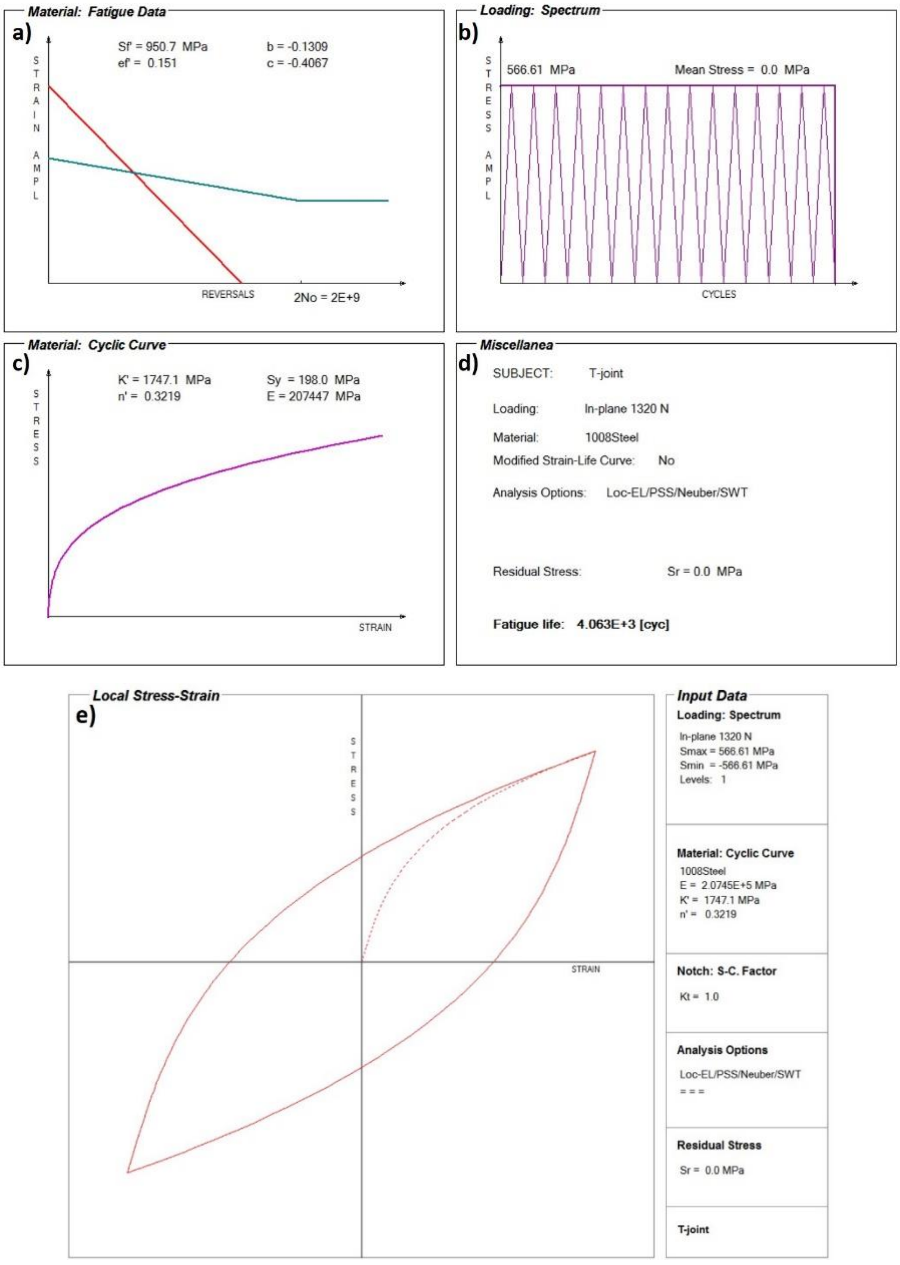

Figure 5-23: FALIN input and output data for the T-joint subjected to in-plane loading (F = 1320 N); a) Manson-Coffin curve, b) Stress loading history, c) Cyclic Ramberg-Osgood curve, d) the output data, e) Simulated stress-strain material response at the weld toe

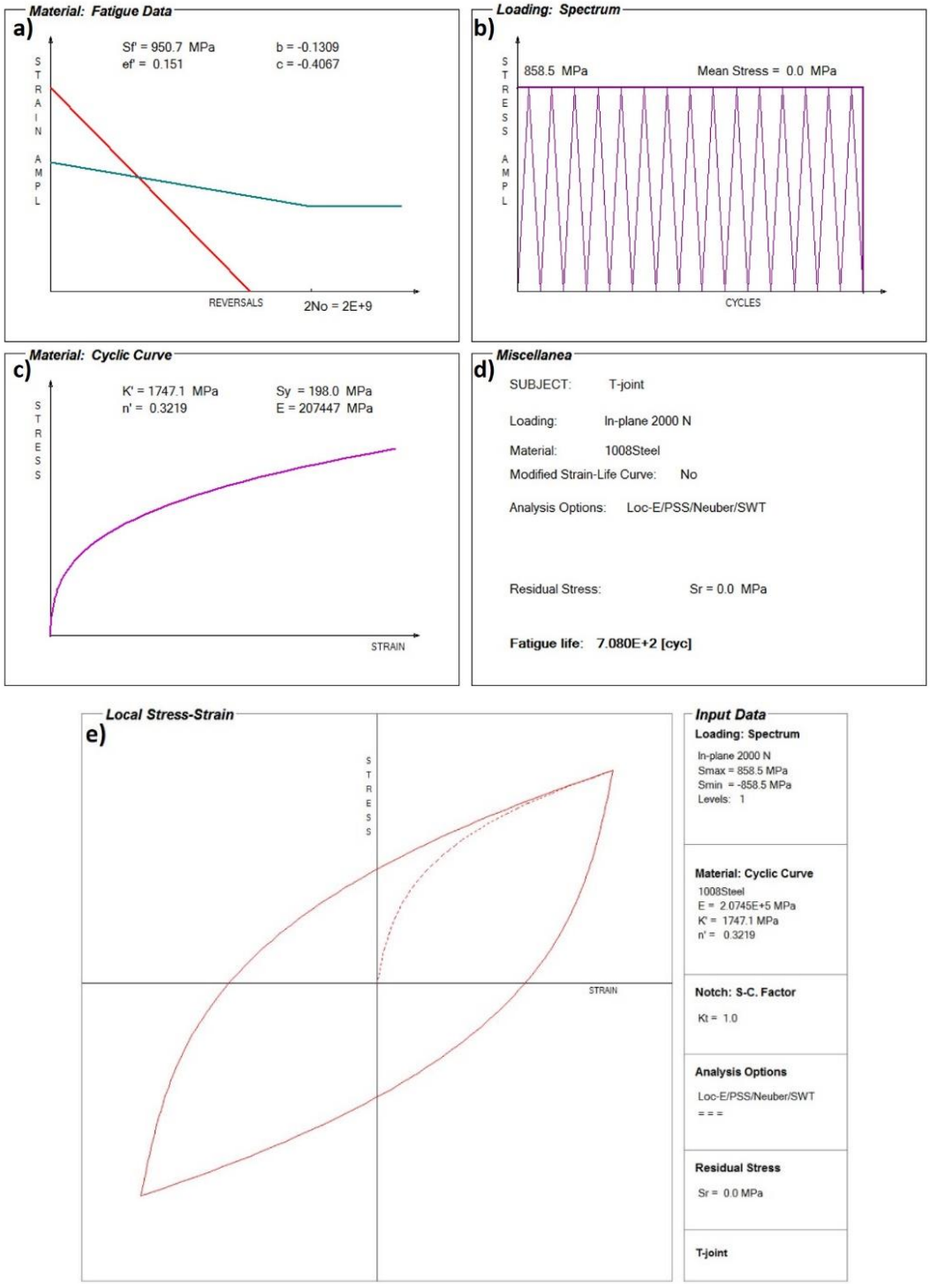

Figure 5-24: FALIN input and output data for the T-joint subjected to in-plane loading (F = 2000 N); a) Manson-Coffin curve, b) Peak stress loading, c) Ramberg-Osgood curve, d) Output data, e) Simulated stress-strain material response at the weld toe

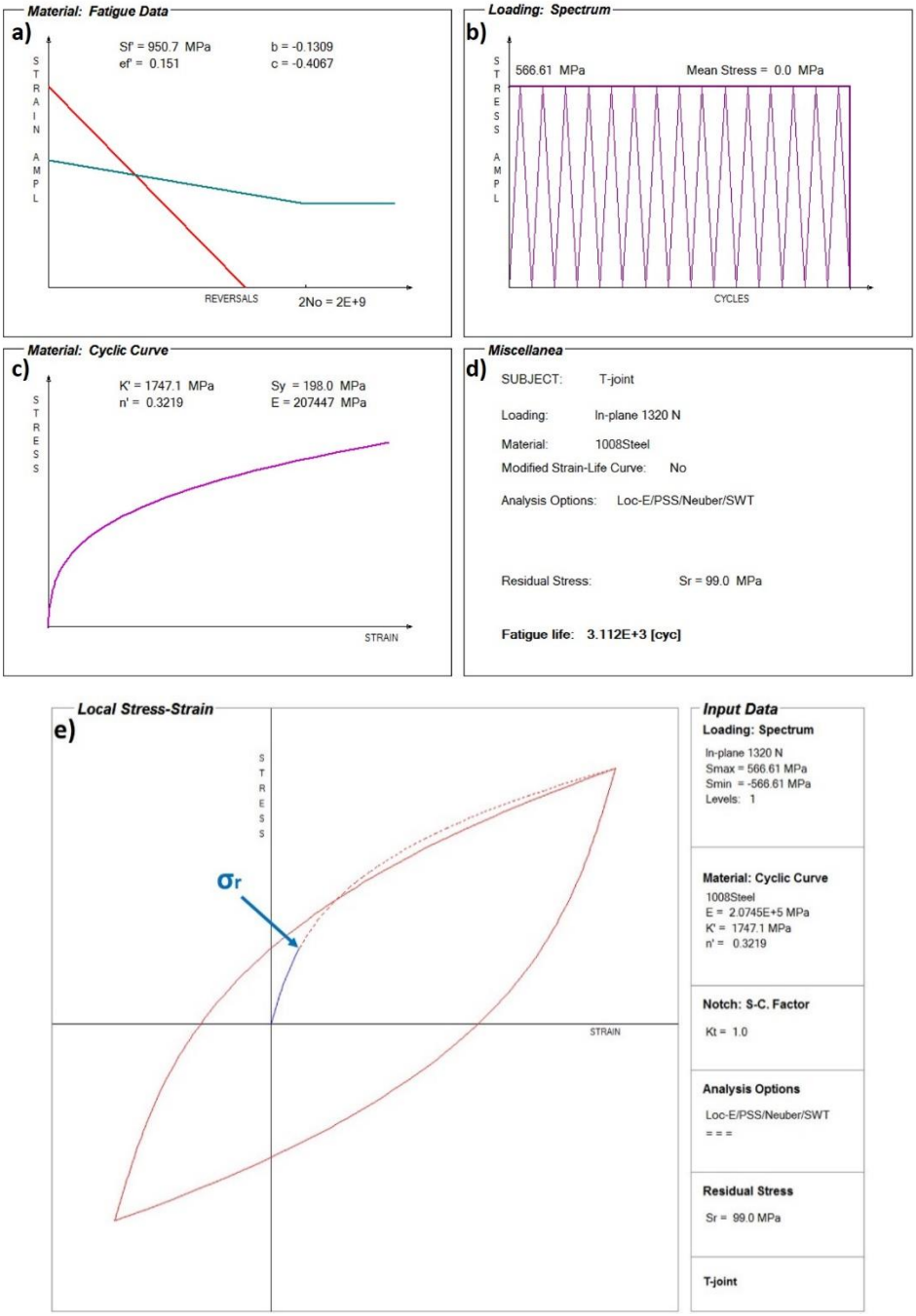

Figure 5-25: FALIN input and output data for the T-joint subjected to in-plane loading (F = 1320 N) in addition to the residual stress σ_r : a) Manson-Coffin curve, b) Peak stress loading, c) Ramberg-Osgood curve, d) Output data, e) Simulated stress-strain material response at the weld toe

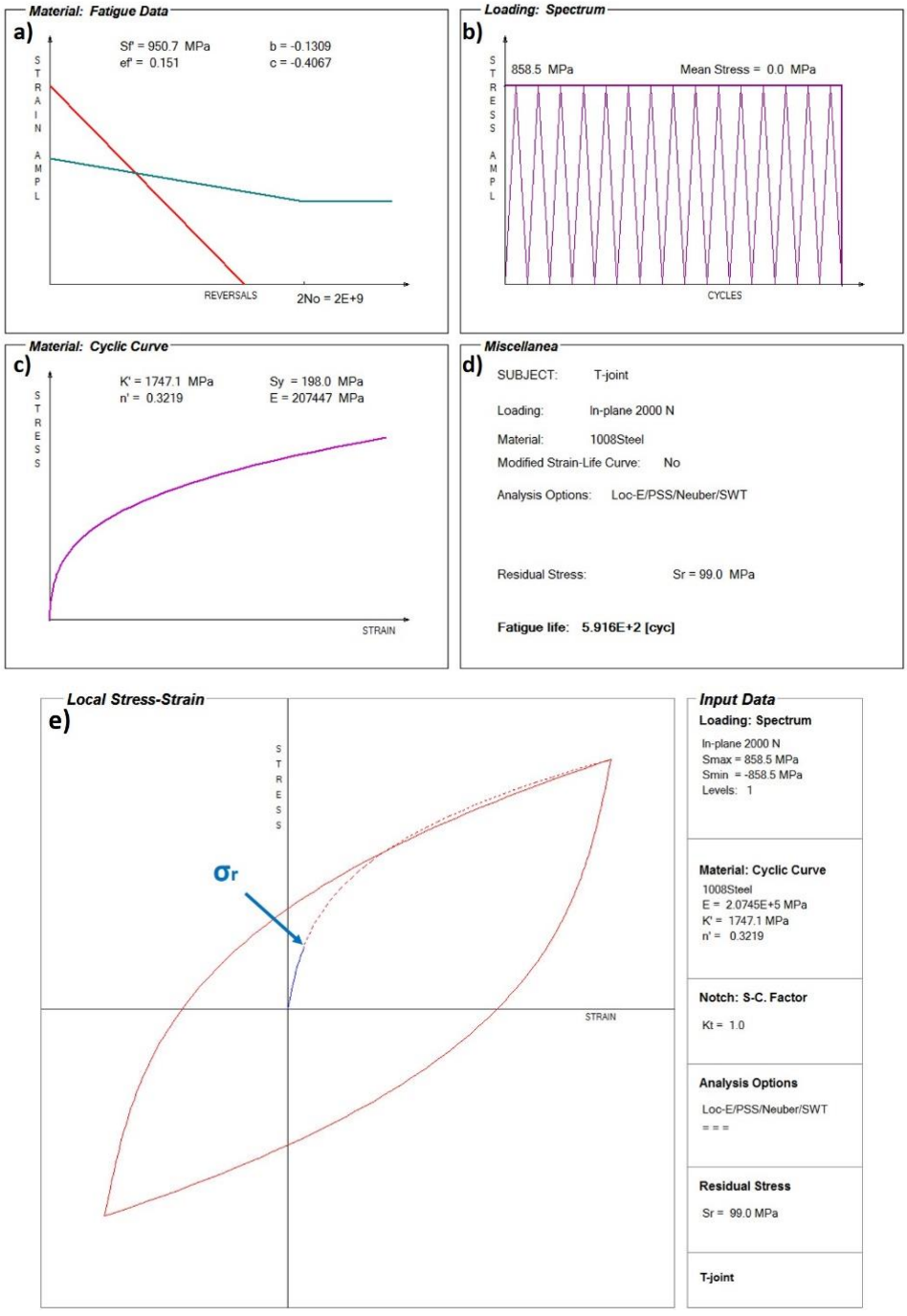

Figure 5-26: FALIN input and output data for the T-joint subjected to in-plane loading (F = 2000 N) in addition to the residual stress σ_r : a) Manson-Coffin curve, b) Peak stress loading, c) Ramberg-Osgood curve, d) Output data, e) Simulated stress-strain material response at the weld toe

The second step in the fatigue life analysis is the calculation of the fatigue crack propagation life using the LEFM method coded in the FALPR software. The observed cracks by the JD fatigue test experiments of the current case were found to be semi-elliptical in shape with a surface crack length of approximately 2c = 3.5 mm. Therefore, the initial crack size was assumed to be not greater than a_i = 0.5 mm in depth with an aspect ratio of (a/c = 0.286). Accordingly, the predictions of the fatigue crack propagation life were based on assuming a semi-elliptical planar crack in a finite thickness plate.

In the case of semi-elliptical cracks, two stress intensity factors at the depth and surface points are needed. Using the weight function method, with the through-thickness stress distribution $\sigma_{xx}(y)$ based on the shell FE modelling and Monahan equation, the stress intensity factors at the crack depth and surface (points A and B in Figure 3-13) can be determined. These two stress intensity factors are important for the determination of crack increments after each cycle for both surface and depth directions, as per equations (2.21 and 2.22). The crack increments due to the applied load cycles are calculated by using Paris' fatigue crack growth equation (2.20). To use the Paris equation, fatigue crack growth properties C and m are required for the material of the welded joint under investigation.

Fatigue crack growth properties for the material of the current case can be determined according to Section (2.3) by using Noroozi's [47] equations. For the determination the Paris equation constants C and m, the material properties in Table 5-2 and Table 5-4 were input to the FALIN software. Hence m = 3.720 and C = 1.95 x 10^{-12}, corresponding to R = 0 at N = 10^6 cycles.

The threshold stress intensity range and the critical stress intensity factor for the material of the current case at R = 0 were:

$\Delta K_{th} = 3.5\ \text{MPa}\sqrt{\text{m}}$, and $K_c = 80\ \text{MPa}\sqrt{\text{m}}$.

The through-thickness stress distribution based on the shell FE model and Monahan equation were input to FALPR to determine the stress intensity factors. It was found that the crack grew on the surface faster than the depth because of the high stress at the weld toe [62]. Therefore, the crack increments of the surface and deepest point have to be determined for each load cycle. Accordingly, the aspect ratio (a/c) has to be updated after each increment using Paris' fatigue crack growth. The fatigue crack propagation life has been predicted for the T-joint weld subjected to in-plane loadings of

(F = 1320 N, and F = 2000 N). The predictions of both load cases were carried out with and without the residual stress to investigate the effect of the residual stress.

Figure 5-27 through Figure 5-34 show the data input to FALPR, the predicted crack depth versus the number of cycles, the stress intensity factor versus the number of applied load cycles, the fatigue crack growth lives predictions, and the fatigue crack propagation lives of the weld joint under investigation when applying F = 1320 N and F = 2000 N, respectively, whereas Figure 5-31 through Figure 5-34 show the same results including the effect of the residual stress. Note that including the residual stress effect was done to study its effect on the fatigue life evaluation.

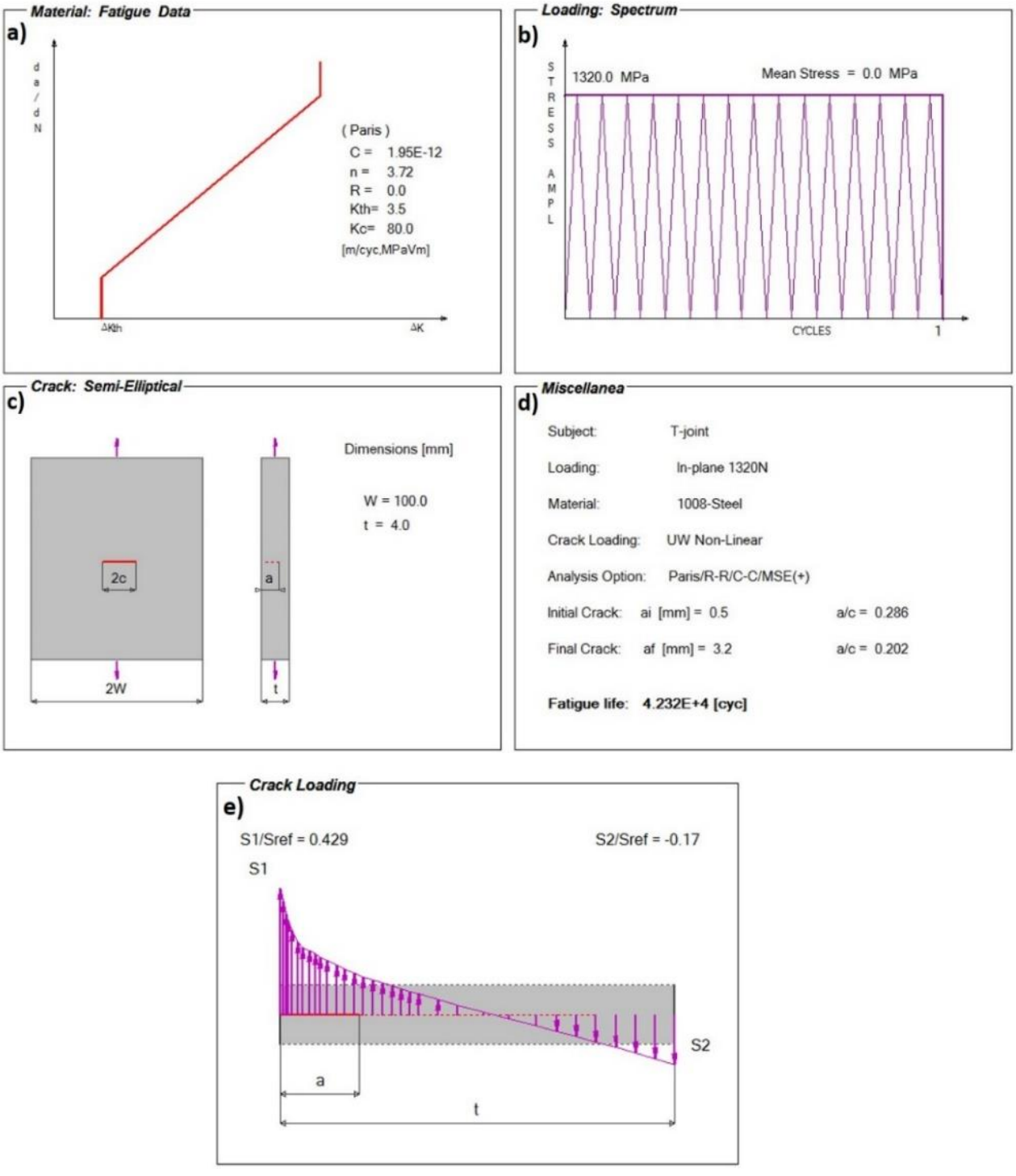

Figure 5-27: FALPR input data for fatigue crack propagation analysis of the T-joint the T-joint subjected to in-plane cyclic loading F = 1320 N (without residual stress): a) Paris fatigue crack growth curve, b) Loading history of the peak stress, c) Geometry of the crack, d) Fatigue life, e) The normalized through-thickness stress distribution

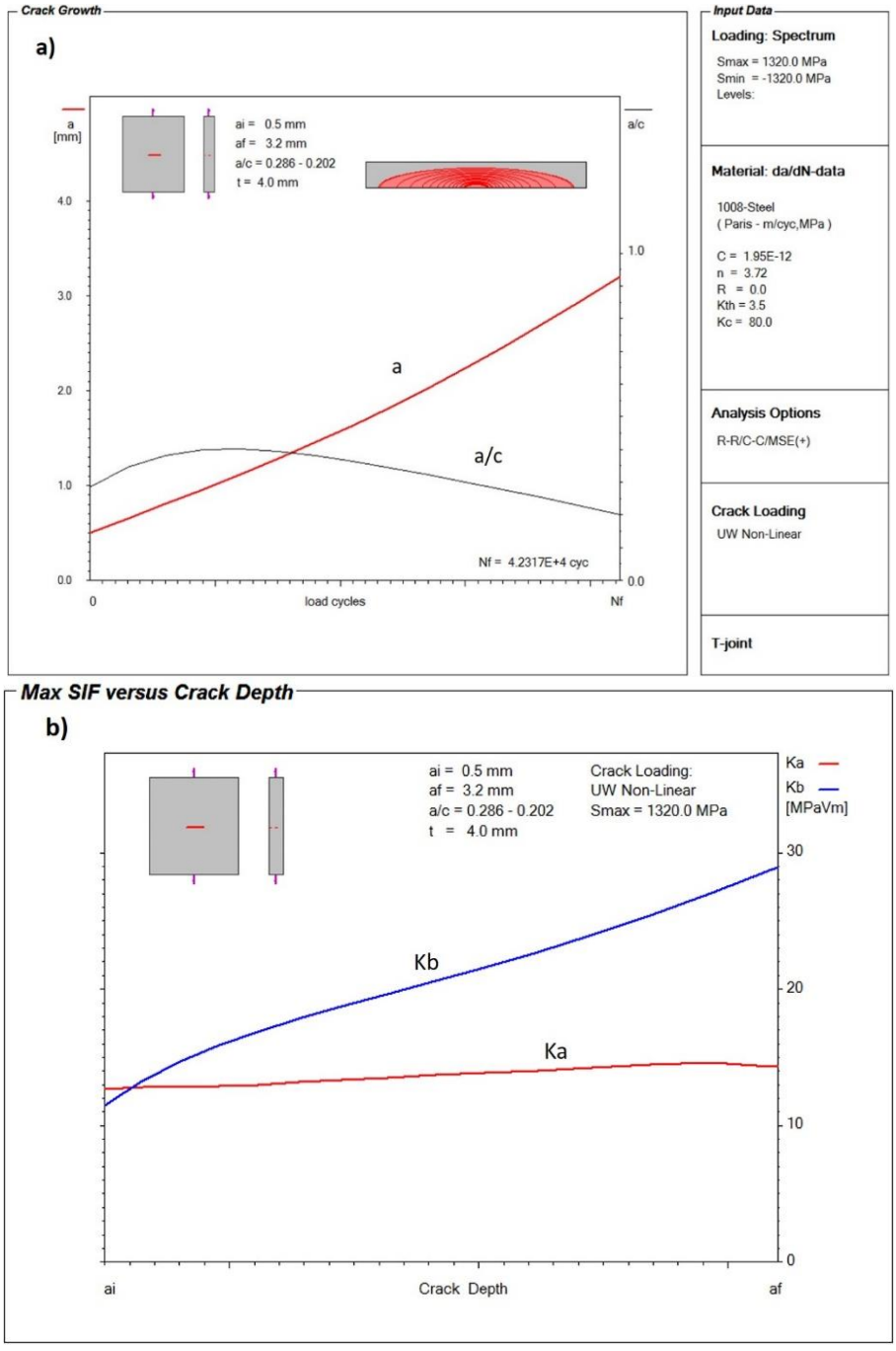

Figure 5-28: a) The crack depth versus the number of applied load cycles to failure (a-N diagram), b) The stress intensity factor values at the surface and depth points of the semi-elliptical crack versus the crack depth (K-a diagram); T-joint subjected to in-plane load F = 1320 N (without residual stress)

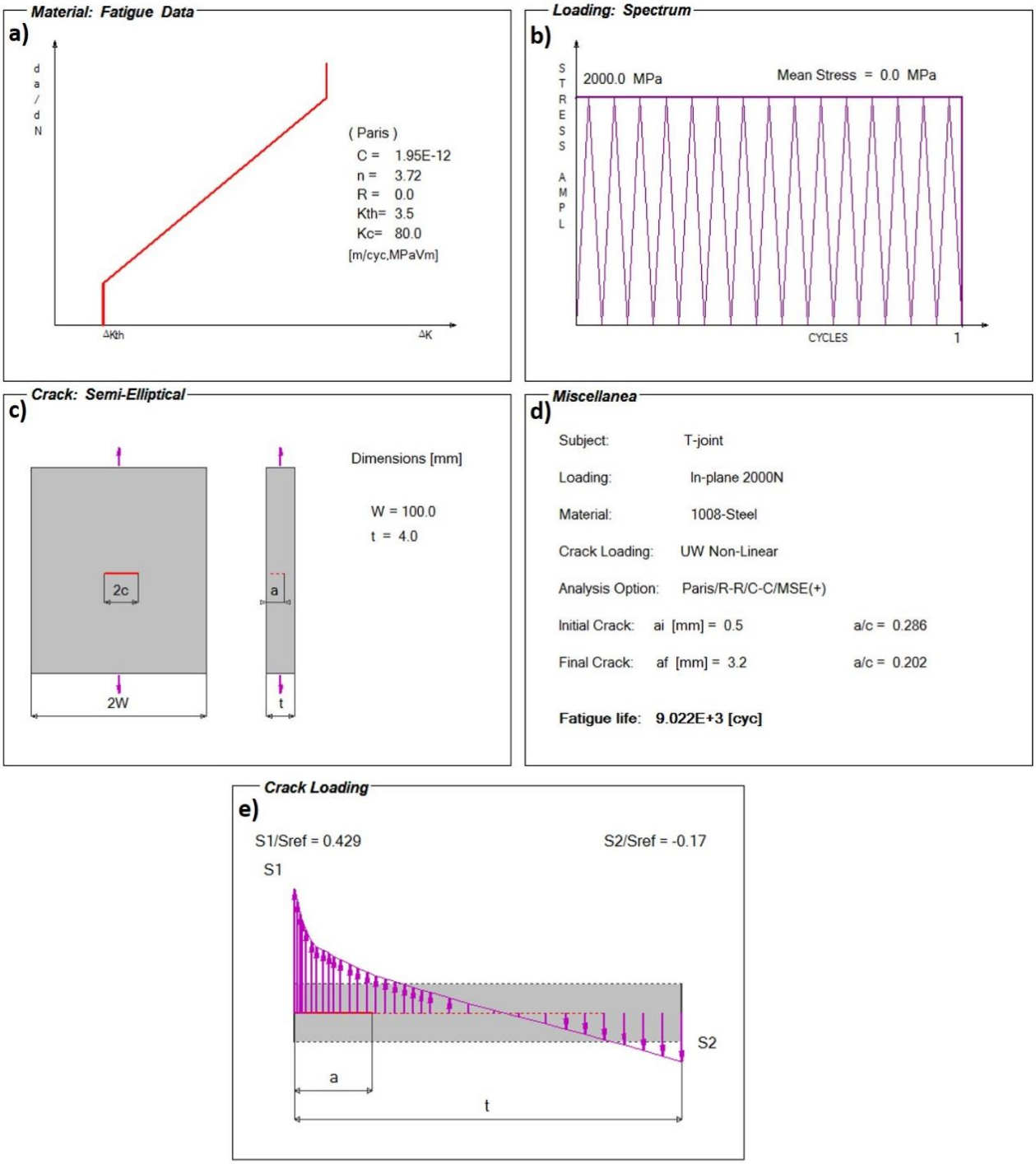

Figure 5-29: FALPR input data for fatigue crack propagation analysis of the T-joint subjected to in-plane loading F = 2000 N (without residual stress): a) Paris fatigue crack growth curve, b) Loading history of the peak stress, c) Geometry of the crack, d) Fatigue life, e) The normalized through-thickness stress distribution

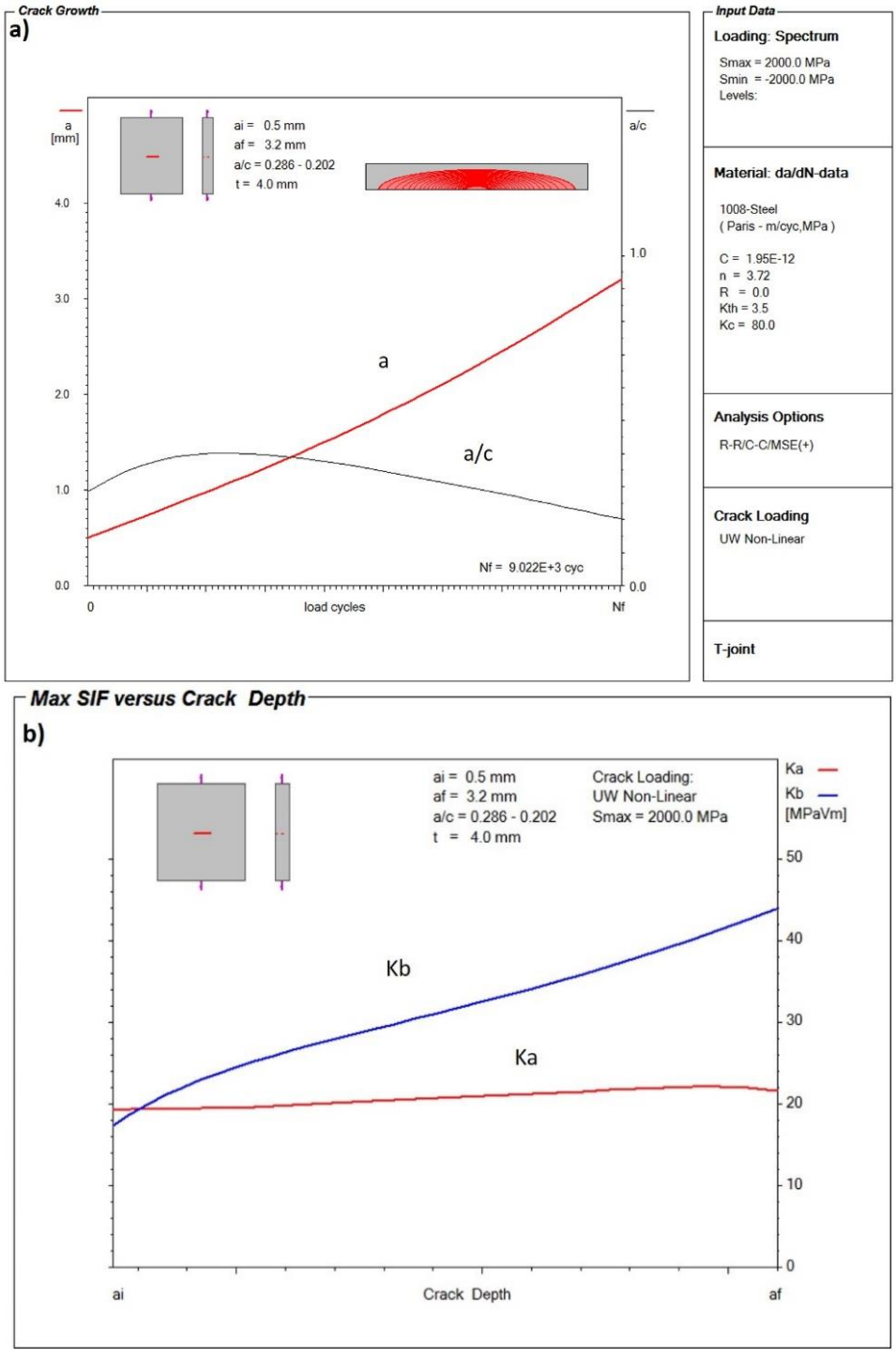

Figure 5-30: a) The crack depth versus the number of applied load cycles to failure: (a-N diagram), b) The stress intensity factor values at the surface and depth points of the semi-elliptical crack versus the crack depth (K-a diagram); T-joint subjected to in-plane load F = 2000 N (without residual stress)

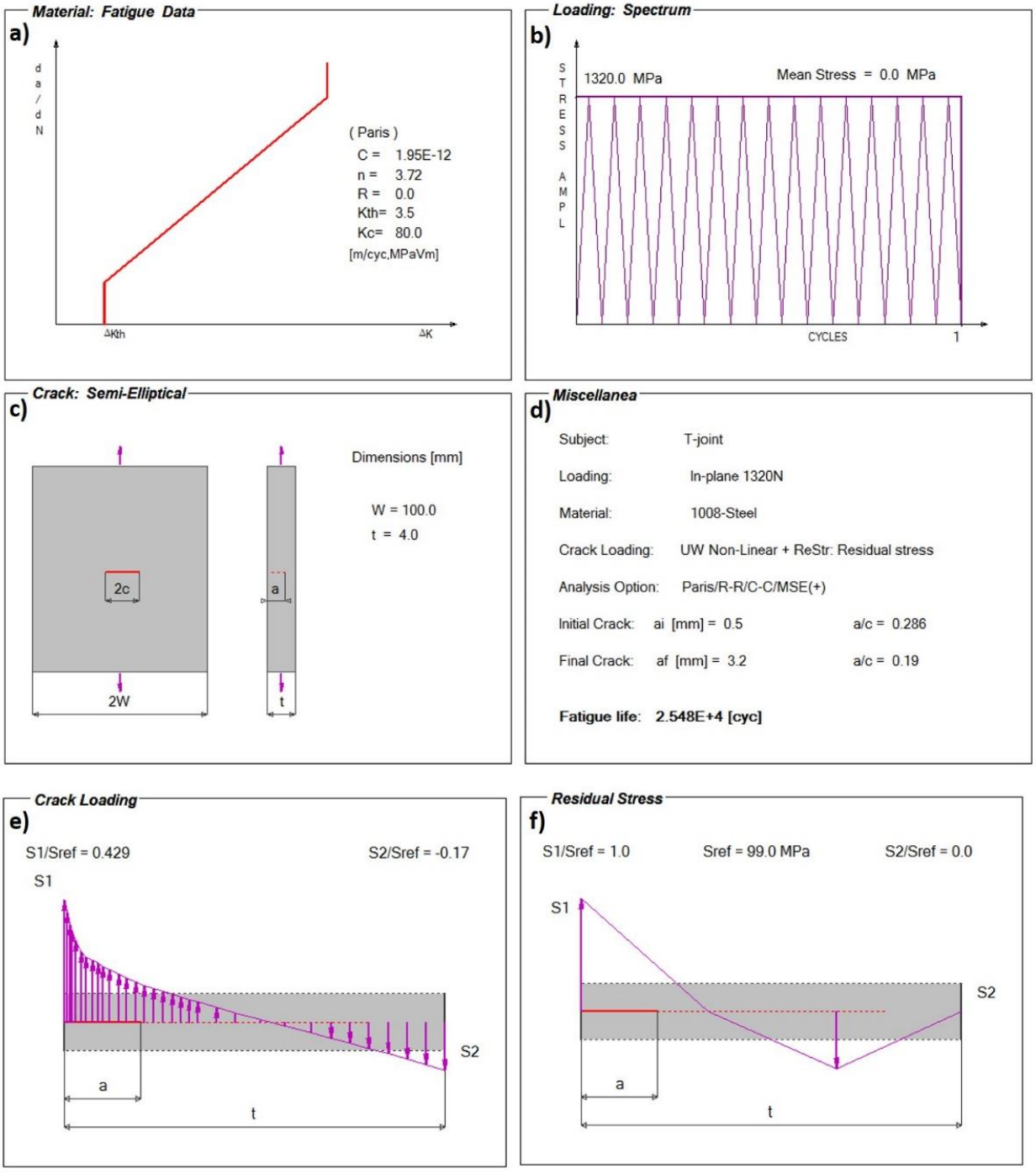

Figure 5-31: FALPR input data for fatigue crack propagation analysis of the T-joint subjected to in-plane loading F = 1320 N (with residual stress): a) Paris fatigue crack growth curve, b) Loading history of the peak stress, c) Geometry of the crack, d) Fatigue life, e) The normalized through-thickness stress distribution, f) Estimated residual stress distribution through the thickness of the weld toe cross section

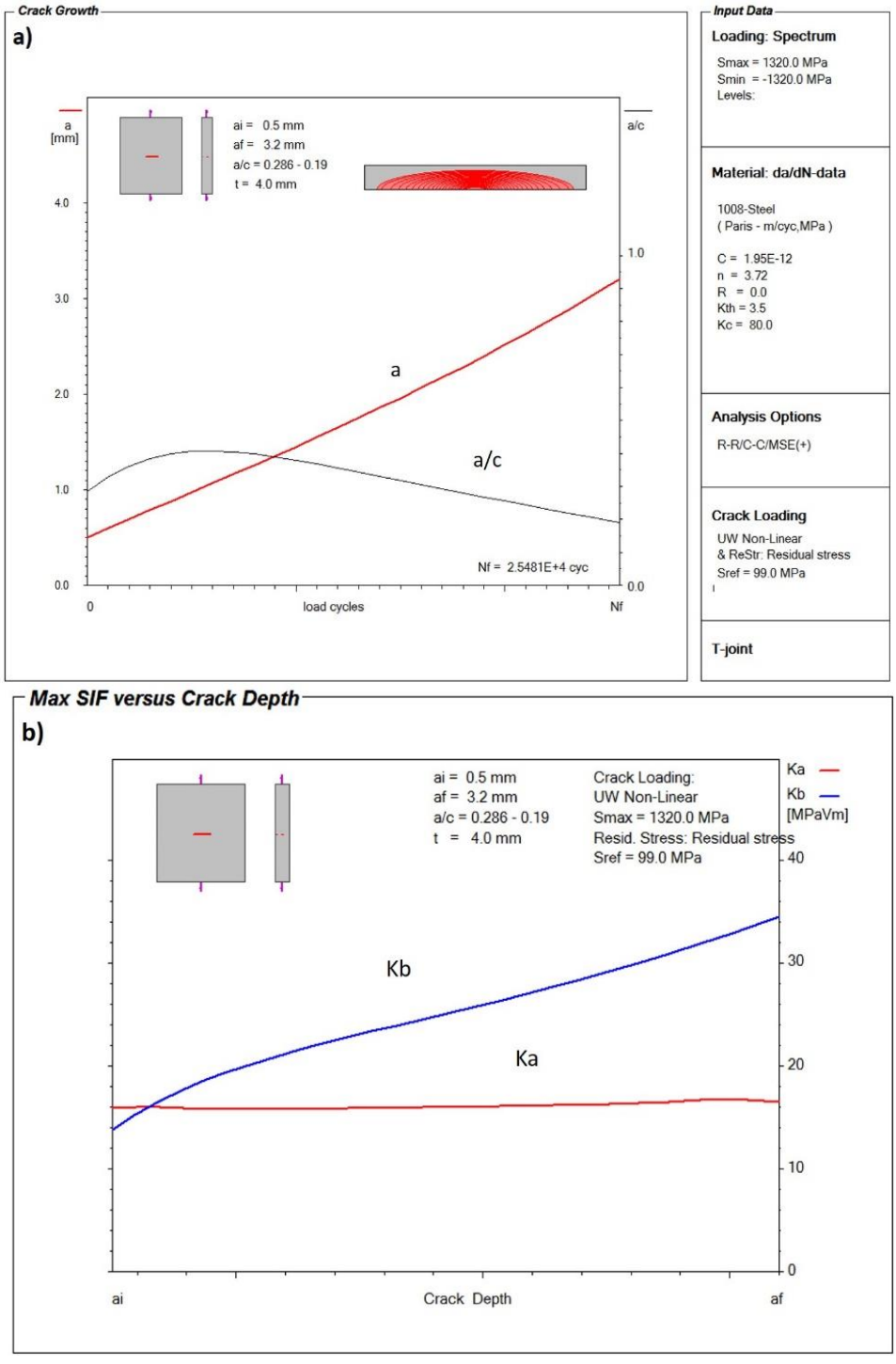

Figure 5-32: a) The crack depth versus the number of applied load cycles to failure (a-N diagram), b) The stress intensity factor values at the surface and depth points of the semi-elliptical crack versus the crack depth (K-a diagram); T-joint subjected to in-plane load F = 1320 N (with residual stress)

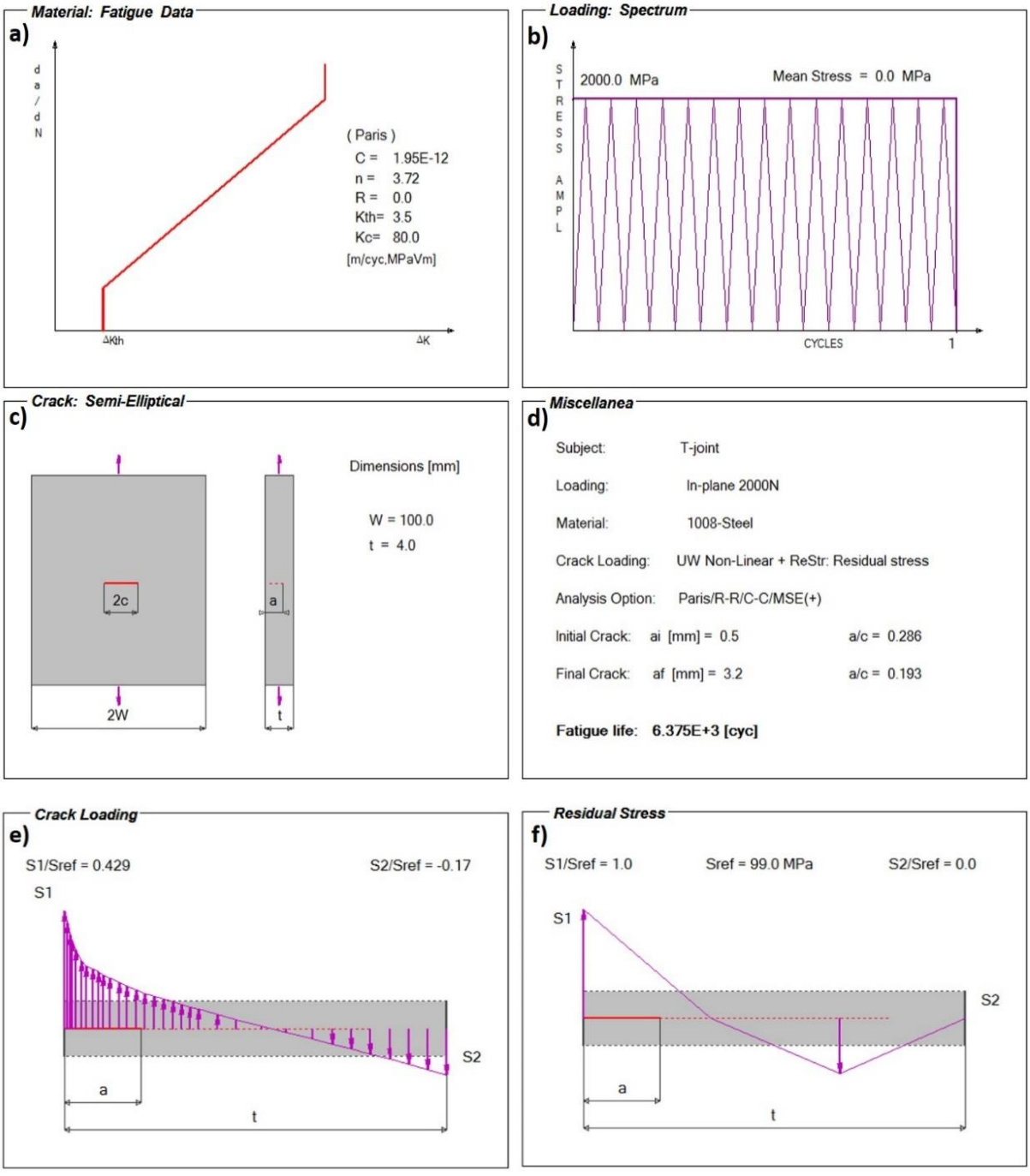

Figure 5-33: FALPR input data for fatigue crack propagation analysis of the T-joint subjected to in-plane loading F = 2000 N (with residual stress): a) Paris fatigue crack growth curve, b) Loading history of the peak stress, c) Geometry of the crack, d) Fatigue life, e) The normalized through-thickness stress distribution, f) Estimated residual stress distribution through the thickness of the weld toe cross section

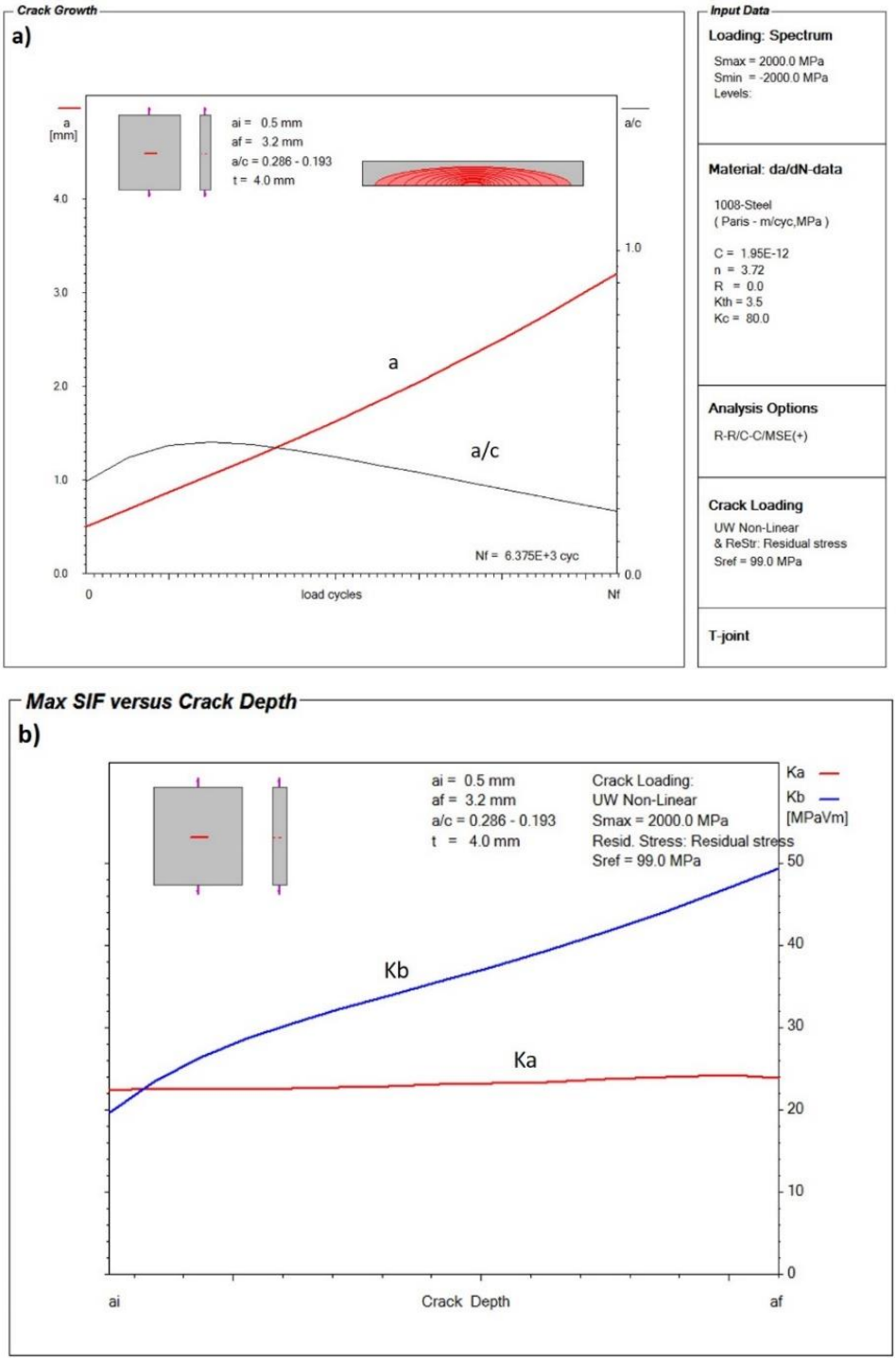

Figure 5-34: a) The crack depth versus the number of applied load cycles to failure (a-N diagram), b) The stress intensity factor values at the surface and depth points of the semi-elliptical crack versus the crack depth (K-a diagram); T-joint subjected to in-plane load F = 2000 N (with residual stress)

The fatigue analysis results are shown in Table 5-5 for the cases of the T-joint subjected to in-plane loading of F = 1320 N and F = 2000 N. The total fatigue life (N_f) was determined by summing the fatigue crack initiation life (N_i) and the fatigue crack propagation life (N_p). The ratios of the fatigue crack initiation life to fatigue crack propagation life and total fatigue life (N_i/N_p and N_i/N_f) are shown to determine which fatigue life was dominant for the total life.

Table 5-5: Summary of predicted fatigue lives for the T-joint subjected to in-plane cyclic loading

Case load	Residual Stress (MPa)	N_i (Cycle) a_i = 0.5 mm	N_p (Cycle) a_f = 3.2 mm	N_i/N_p	N_f (Cycle)	N_i/N_f
F= 1320 N	σ_r = 0	4036	42317	0.10	46353	0.09
	σ_r = 99	3112	25481	0.12	28593	0.11
F= 2000 N	σ_r = 0	708	9022	0.08	9730	0.07
	σ_r = 99	592	6375	0.09	6967	0.08

The small ratios of the fatigue crack initiation life (N_i) to the fatigue crack propagation life (N_p) and total fatigue life (N_f) indicate that most of the welded joint fatigue life was spent on propagating the crack from a_i = 0.5 mm to the final critical crack depth a_f = 3.2 mm.

The JD Company's laboratory tested eight samples of welded T-joints subjected to in-plane fully reversed cyclic loading for determining fatigue life. The test samples were subjected to an in-plane bending load of 1320 N, whereas the other two samples were subjected to an in-plane bending load of 2000 N. The experimental fatigue data for both load levels are shown in Table 5-6. The numbers of load cycles were obtained as a function of the measured surface crack length. Using the fatigue crack growth simulation data obtained from the FALPR program, the crack depth corresponding to the experimental surface crack length was estimated.

Table 5-6: JD Experimental fatigue crack propagation life data (2c-N) for the T-joint subjected to in-plane bending load

Sample #	Load (N)	Number of cycles (cycles)	Crack length 2c (mm)	Remarks
RE2	±1320	28777	5.5	First detected crack
RE3		46726	5.5	First detected crack
15		66774	7.0	First detected crack
		103825	8.5	-
		211631	10.0	-
16		464500	4.0	First detected crack
		1190502	6.0	-
17		117516	4.0	First detected crack
		230096	6.0	-
18		683500	6.5	First detected crack
		797116	13.4	-
11	± 2000	2196	4.5	First detected crack
		2500	10.0	-
		4600	16.0	-
19		4288	11.5	First detected crack
		8369	20.0	-

Unfortunately, there was a variation in the welding techniques used to construct the T-joint test samples, as shown in Figure 5-35. Some test samples had a continuous weld that was nicely wrapped around the gusset edges (Samples #16 and #18), whereas a few other test samples had welds deposited at the gusset edge using a tack weld option, which caused the weld to stop at the corners, resulting in higher SCF (Sample #15). In addition, test sample #RE3 did not have the weld deposit around the gusset edge. This variation in welding practices affects the experimental fatigue life data in Table 5-6. Test samples with welds that were nicely wrapped around the gusset edge had higher fatigue lives compared to the other test samples with improperly wrapped welds.

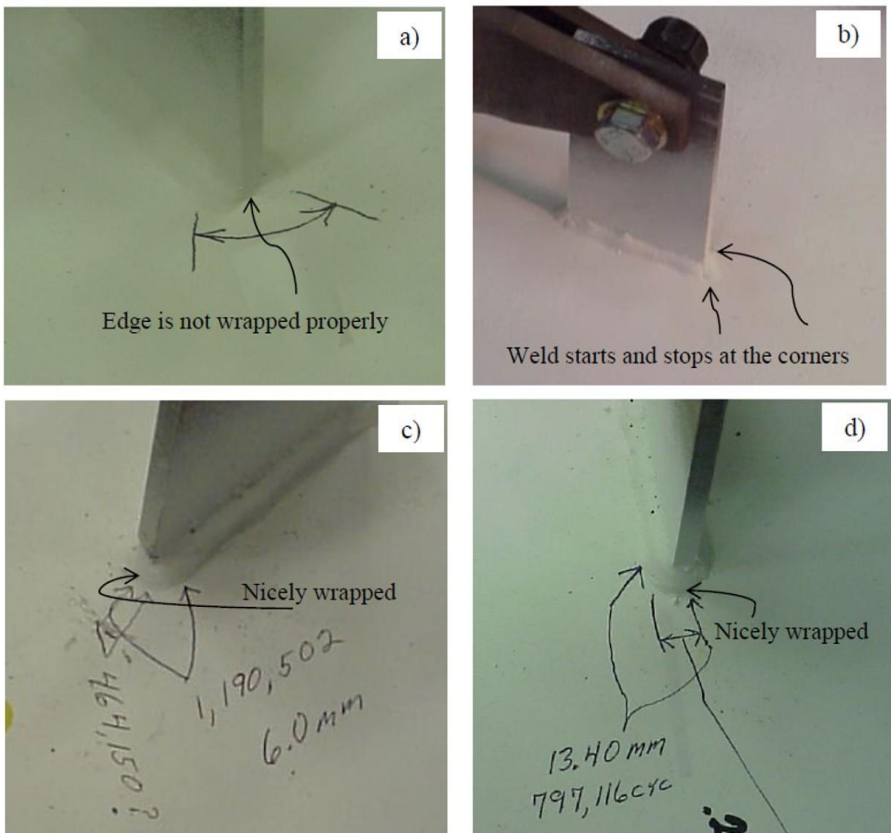

Figure 5-35: Variation in welded test samples: a) Missing weld deposit around the gusset edge (Sample # RE3), b) Weld starts and stops at the corners of the gusset edge (Sample #15), c) Nicely wrapped weld around the gusset edge (Sample #16), d) Another nicely wrapped weld (Sample #18) [65]

The fatigue life data in Table 5-5 and Table 5-6 are plotted as shown in Figure 5-36 and Figure 5-37 for both load levels. The fatigue life data are plotted in terms of the applied load cycles versus the surface crack length (2c) for comparison between the experimental and predicted fatigue life. The experimental fatigue data are plotted as a series of discrete points, whereas the predicted fatigue data are plotted as two curves. The hashed curve represents the fatigue life prediction without the effect of the residual stress (No-RS), and the solid curve represents the fatigue life prediction including the residual stress effect (with RS).

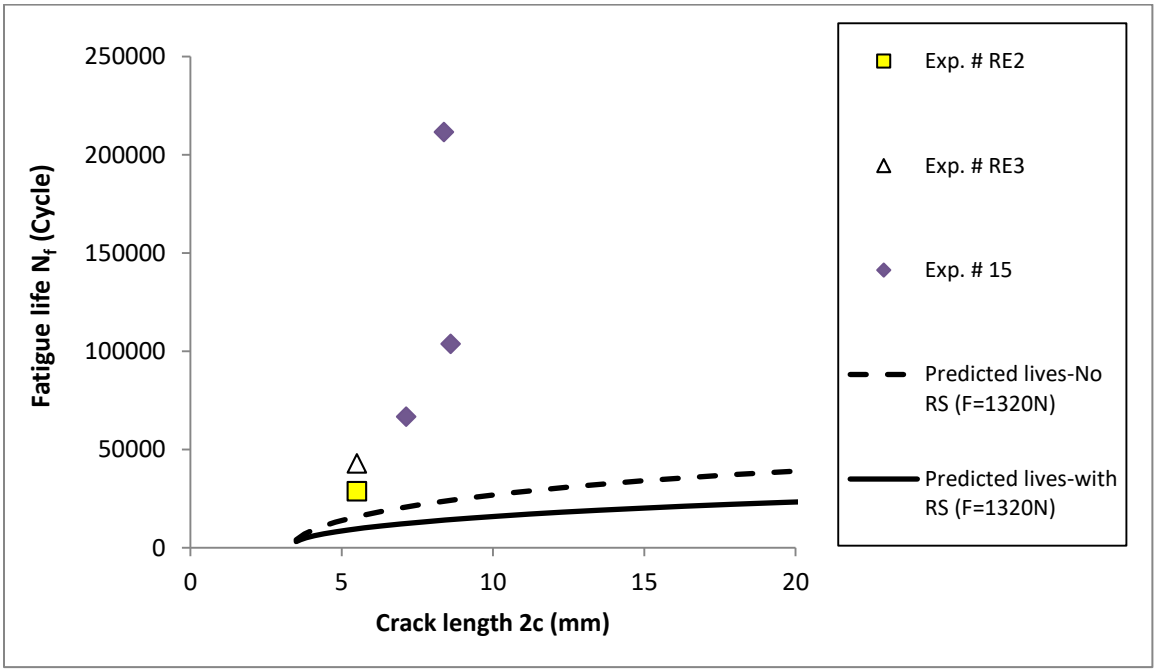

Figure 5-36: Comparison between experimental and predicted fatigue lives of the T-joint weld subjected to an in-plane bending load of (F = 1320 N)

Figure 5-36 shows that the predicted total fatigue lives based on the proposed shell FE method are more conservative (under prediction) than the experimental data. The difference between the experimental and predicted fatigue lives was approximately 1 to 5. This difference is due to assuming a planar crack model when calculating the fatigue crack propagation life (i.e., the initial crack grows to its final size in a direction normal to the weld toe). However, actual cracks in the experimental fatigue tests showed that the cracks were following the weld toe line (i.e., cracks started growing from the edge of the gusset weld and propagated later around the edge until they became parallel to the gusset plate). This occurred for most of the tested T-joints under 1320 N in-plane bending loading. Therefore, it is fair to say that the planar crack assumption is valid only for estimating crack growth up to the length of 2c = t (gusset thickness) because surface cracks with a size of 2c > t grow around the edge and not planar anymore. Accordingly, the fatigue life predictions in Figure 5-36 are comparable to the experimental data up to 2c = t or 4 mm. Unfortunately, the experimental fatigue lives were not recorded for cracks with 2c ≈ 4mm.

Another possible source of errors comes from over-estimating the initial crack size or the estimation of the semi-elliptical crack shape (planar crack model) in addition to the difference in the stress obtained from the local reference stress (see Figure 5-19). The total fatigue life predictions in

Figure 5-37 show better agreement with the experimental data for the higher load case of F= 2000 N ***because the high stress load level is less dependent on the accuracy of the assumed initial crack size.*** The results in both load levels (F=1320 N and F= 2000 N) indicated that it is important to include the residual stress distribution to the stress analysis of weldments.

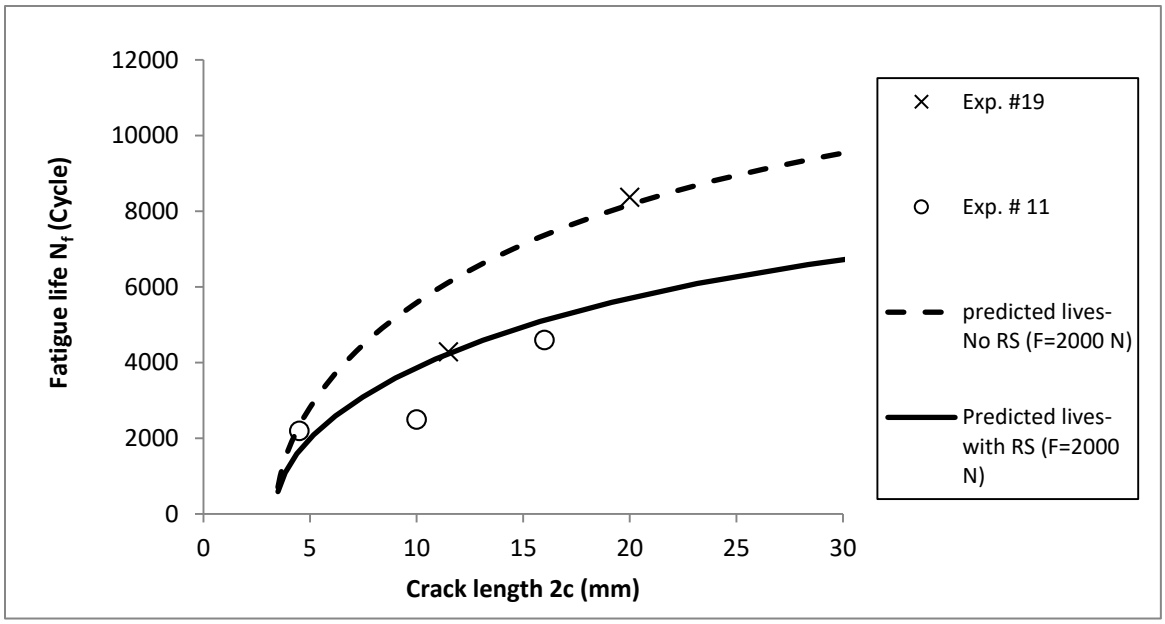

Figure 5-37: Comparison between experimental and predicted fatigue lives of the T-joint weld subjected to an in-plane bending load of (F = 2000 N)

In conclusion, the proposed method must be tested against more experimental data for more improvements, especially in the case of cracks at the gusset edge region with a low stress load level. However, the proposed method provides a valid way of predicting the total fatigue life of weldments using only shell FE local reference stress data. Finding the fatigue life based on shell FE with coarse mesh provided in this study is beneficial for complicated weld joints and full structures that are very difficult to model using the 3D FE. The contribution lies in finding a unique stress that can be used to supply all the necessary stress data required for the contemporary fatigue analysis methods by using only the shell FE model.

5.4 Fatigue analysis of a Tube-on-plate subjected to out of plane cyclic loading

Twelve samples of tube-on-plate welded joints were tested by the JD laboratories. The tube-on-plate joints was constructed by attaching a tube to a base plate. The welded samples were subjected to fully reversed cyclic loading of a force applied to the tube pinhole, as shown in Figure 5-38. The base plate or main plate dimensions were $500 \times 500 \times 4$ mm. The material of the tested samples was 1008 steel. The weldment was done using the Flux Core Arc Welding method. The dimensions of the weld were t = 4 mm, t_p = 7.25 mm, h = 4 mm, h_p = 4 mm, $\theta = 45°$, and ρ = 0.55 mm.

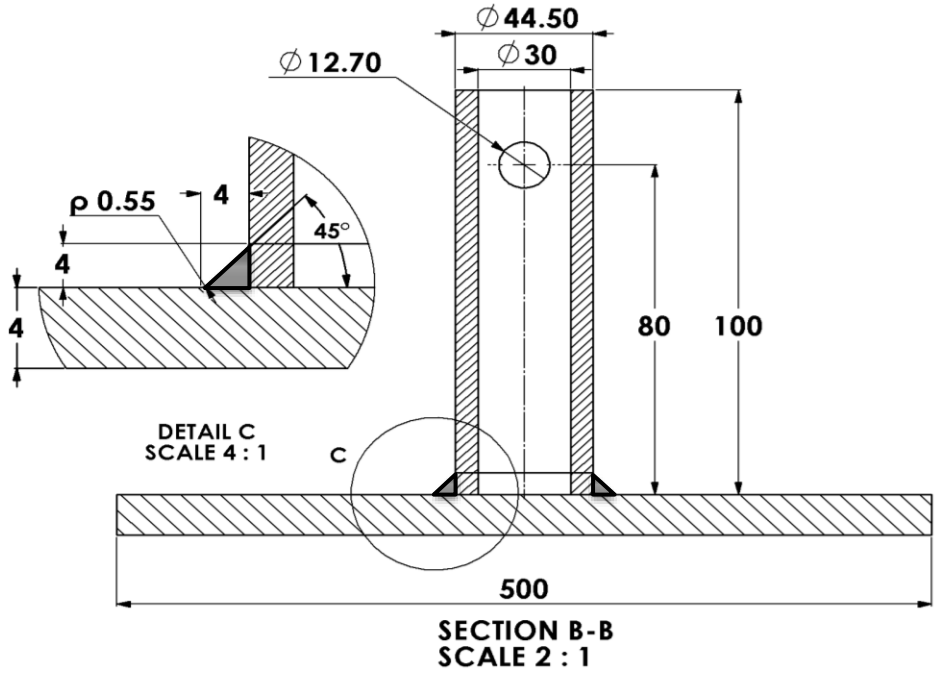

Figure 5-38: Dimensions and loading direction of tube-on-plate welded joint subjected to lateral loading

Six of the tested specimens were subjected to a load of F = ± 1000 N, while the rest of the test specimens were subjected to a load of F = ± 1225 N. The base plate of each specimen was fixed at all corners by a clamp with dimensions of 40×80 mm, whereas the pinhole of the attachment tube was subjected to lateral cyclic loading. One of the tested samples is seen in Figure 5-39. The highest stress is expected at the weld line perpendicular to the loading directions. Therefore, the stresses from the shell FE (σ_a and σ_b) must be evaluated in that region.

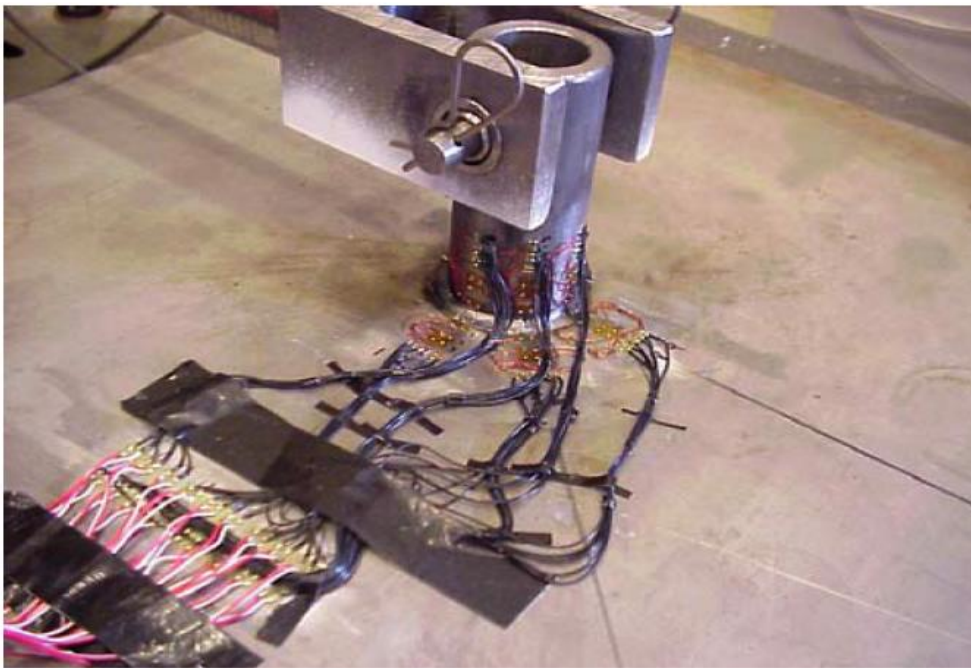

Figure 5-39: JD experiment for the tube-on-plate welded joint subjected to lateral loading (JD)

5.4.1 Material properties

The material properties of the welded joint under investigation are the same as Case #1. The chemical composition and mechanical properties are shown previously in Table 5-1 and Table 5-2, respectively. The fatigue test data for 1008 steel are shown in Table 5-3. The fatigue parameters based on UW analysis are shown in Table 5-4 for 1008 steel.

5.4.2 Shell FE modelling of a Tube-on-plate subjected to out of plane cyclic loading

The aim of this shell FE model is to determine the local reference stresses (σ_a and σ_b) and the resulting stress data. The membrane and bending hot spot stresses (σ_{hs}^{m} and σ_{hs}^{b}) are determined by using equations (3.12 and 3.13). Based on the micro-geometrical features of the welded joint, the membrane and bending SCFs (K_t^m and K_t^b) can be determined by using equations (3.15 and 3.16) in section 3.7. According to equation (3.11), this is the required stress information that will determine the peak stress σ_{peak} based on the shell FE local reference stresses. The same stress data (σ_{hs}^{m} ,σ_{hs}^{b}) and the proper SCFs (K_t^m and K_t^b) be used to determine the through-thickness stress distribution $\sigma_{xx}(y)$, as

per Monahan expression (3.11). The shell FE model must have the same geometry as the experimental specimen, whereas the stress data must be extracted at the weld's critical location.

Figure 5-39 shows the boundary conditions of the shell FE model for the welded joint under investigation. The plate corners were constrained for all displacement while a force of 1000 N was applied to the attachment plate's pinhole.

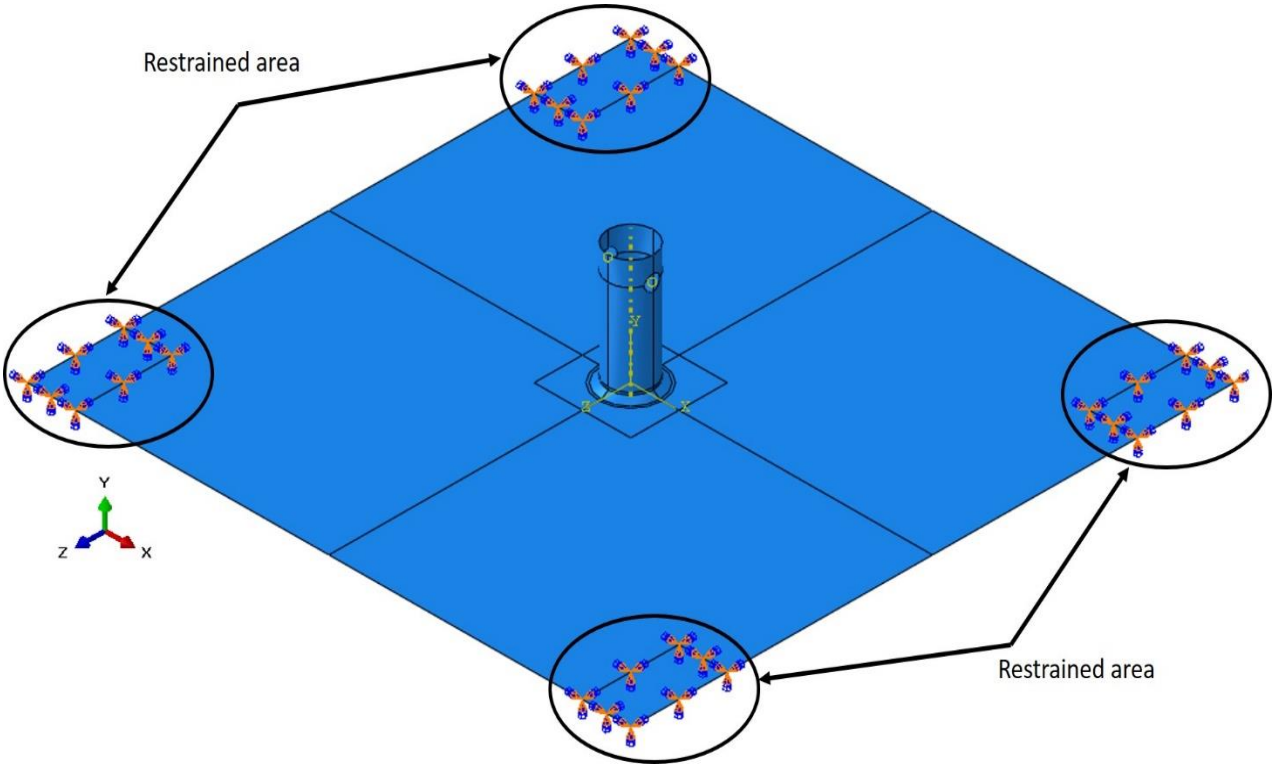

Figure 5-40: Shell FE modelling and boundary conditions for the tube-on-plate welded joint subjected to lateral loading (F = 1000 N)

The local reference stresses σ_a and σ_b were obtained from a reference point located at the lower weld toe of the attachment plate as shown in Figure 5-41. The reference point contains the local reference stresses, which represent surface and bottom stresses through the plate thickness. These stresses are used to determine the membrane and bending hot spot stresses that will be multiplied by the proper SCFs (see Section 3.7) to calculate the peak stress at the weld toe.

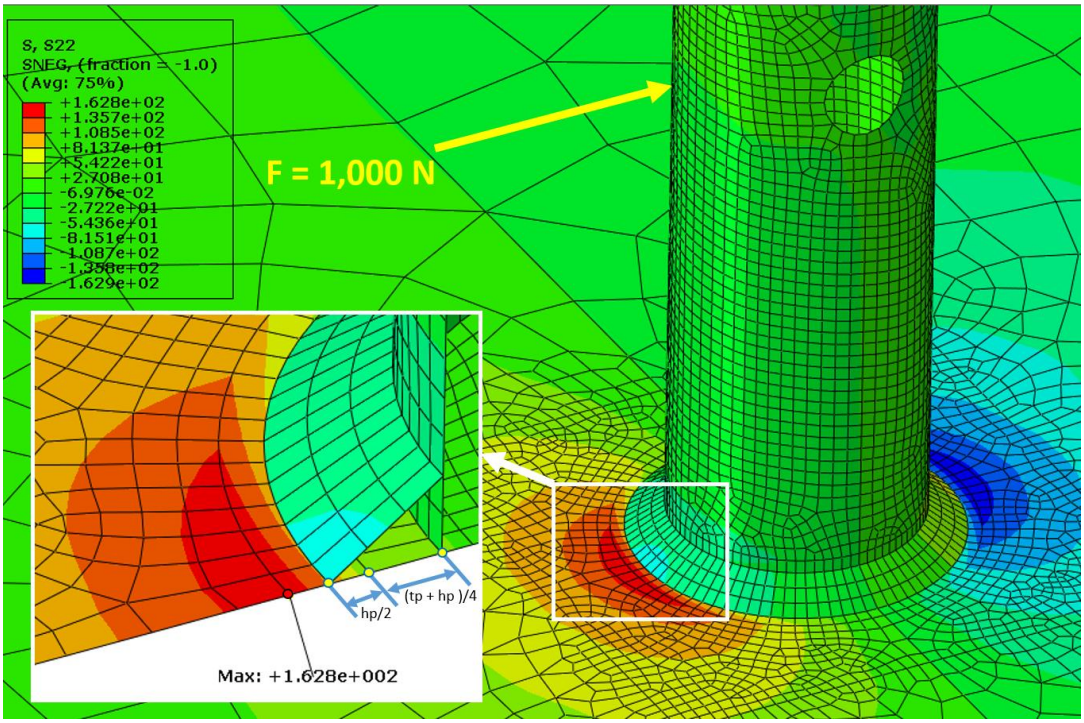

Figure 5-41: Shell FE contours of the maximum normal stress to the weld toe line; tube-on-plate welded joint subjected to a lateral loading (F = 1000 N).

According to the experiments, the maximum stress was expected to be at the upper weld toe of the attachment tube. Note that the reference points in the above shell FE model coincide with the actual location of the weld toe of the experimental specimen. Figure 5-41 indicates that the maximum stress is located at the lower weld toe, as expected. However, the required local reference stresses are to be extracted from a specific reference point and not at the maximum contour node. The distance of the reference points of the shell model was $h_p + (t_p / 2) = 7.625$ mm. At that specific reference point (lower weld toe), the local reference stresses σ_a and σ_b were extracted as they represent the stresses of the surface and bottom of the attachment tube. The local reference stresses through the attachment plate (σ_a and σ_b) were recorded as follows:

σ_a = 162.8 MPa

σ_b = -173.27 MPa

Therefore, the hot spot membrane and bending stresses σ_{hs}^{m} and σ_{hs}^{b}, per equations (3.12 and 3.13) were:

$$\sigma_{hs}^{m} = \frac{\sigma_a + \sigma_b}{2} = -5.234 \text{ MPa}$$

$$\sigma_{hs}^{b} = \frac{\sigma_a - \sigma_b}{2} = 168.04 \text{ MPa}$$

Using the weld geometrical features of the current case, the SCFs were calculated. However, according to available 3D FE data, the t_p parameter in equations (3.18 and 3.19) cannot be greater than 3t. Therefore, the attachment plate thickness t_p parameter was multiplied by a factor of 3 as an assumption for the SCFs at the edge of the gusset. This was based on the fact that the effect of the edge disappears at distances greater than 3t, and the SCF equations are not valid for large values of t_p:

$K_t^m = 1.581$

$K_t^b = 2.166$

As per equation (3.11), the peak stress at the weld toe induced by the applied load was:

$$\sigma_{peak} = \sigma_{hs}^{m}.K_t^m + \sigma_{hs}^{b}.K_t^b = 355.69 \text{ MPa}$$

Figure 5-42 shows two stress distributions through the base plate thickness in the direction normal to the weld toe. The linear stress distribution (hashed line) represents the local reference stresses (σ_a and σ_b). The non-linear stress distribution (solid curve) represents the Monahan equation $\sigma_{xx}(y)$.

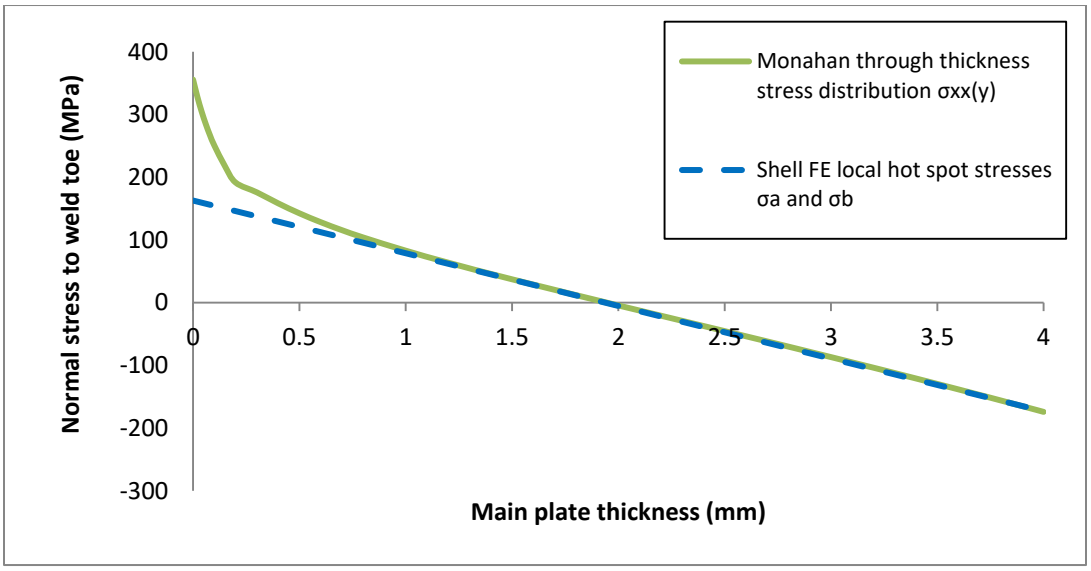

Figure 5-42: Tube-on-plate shell FE local reference stress (linear) and the Monahan non-linear through-thickness stress distribution at the weld toe

Figure 5-42 provides the stress data (σ_a, σ_b, $\sigma_{peak,}$ and $\sigma_{xx}(y)$) required for the fatigue analysis of the case under investigation. The stress data in Figure 5-42 are obtained from a shell FE model and must be validated against a detailed 3D FE model before proceeding with the fatigue analysis. A 3D FE model with the same geometry as the experiment is modelled in the following section to validate the shell FE local reference stress data.

5.4.3 Finite element 3D modelling of a Tube-on-plate subjected to out of plane cyclic loading

The 3D FE model should have the same geometry as the experimental specimen. Also, the stress data must be extracted from the weld's critical location in the same way as the shell FE model. For the case under investigation, the critical locations are expected at the weld toe (see Figure 5-41). According to the shell FE model, the maximum stress occurs at the lower weld toe on the compressive side. Therefore, it is expected the 3D FE model would have the peak stress at the same location. Figure 5-43 shows the 3D model boundary conditions. Due to the symmetry of the problem, only half of the component was modelled to reduce the computational time. The model was subjected to lateral force of 1000 N. The bottom corners of the base plate were constrained for all displacements, and the model elements were approximated by eight brick elements.

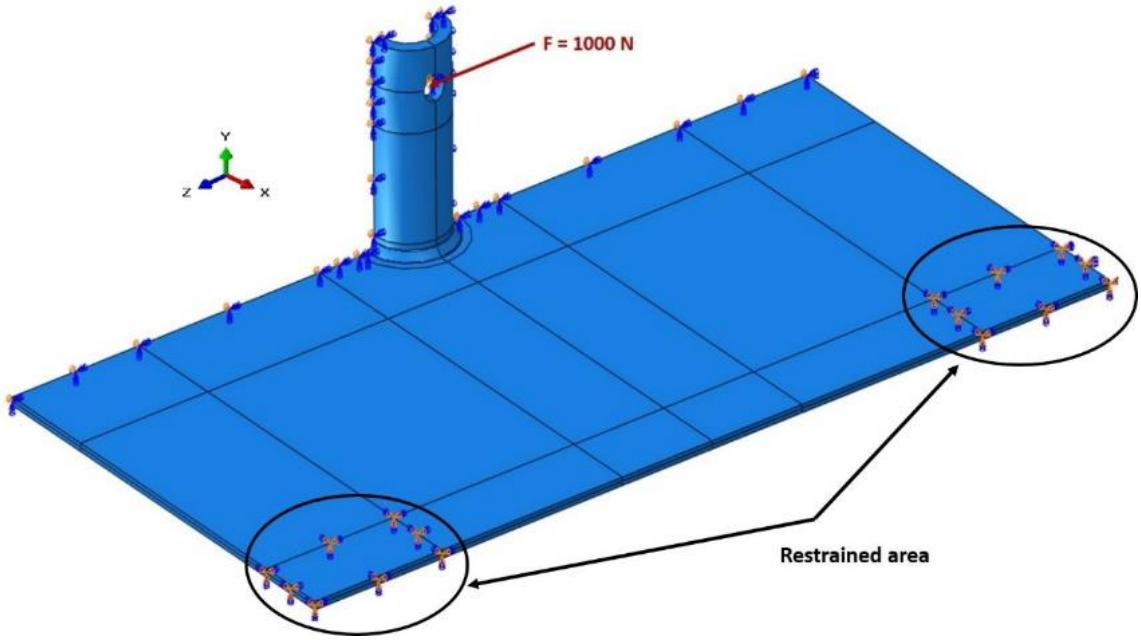

Figure 5-43: Boundary conditions of the 3D FE simulated tube-on-plate welded joint subjected to lateral load

The meshing was intensive at the critical area (lower weld toe), as shown in Figure 5-44. This area was expected to have the peak stress normal to the weld toe. The element size at the weld toe should be small enough to find a converged stress. The recommended element size is at least equal to a quarter of the weld toe radius [64].

The maximum stress (peak stress) normal to the weld toe in the 3D model was found at the expected location. Figure 5-44 shows the critical location of the 3D FE model where the stress data (the actual peak stress and the actual through-thickness stress distribution) are extracted.

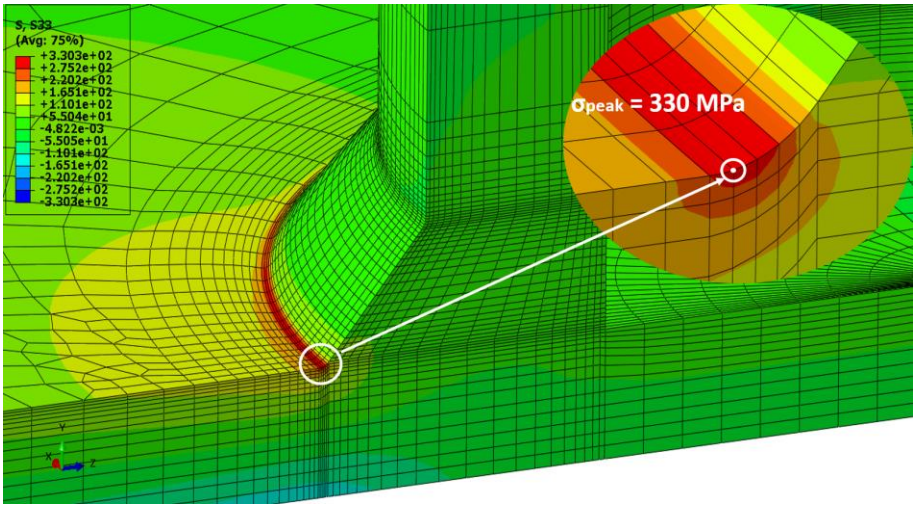

Figure 5-44: Intensive mesh at the weld toe of the tube-on-plate subjected to lateral loading (3D FE model)

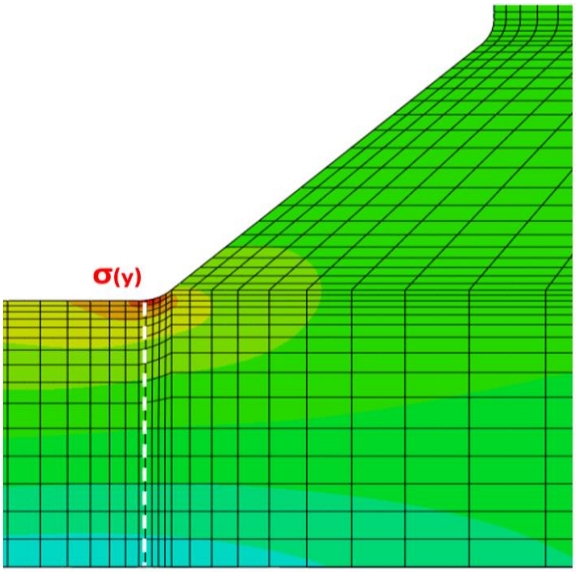

Figure 5-45: Through-thickness stress distribution path under the weld toe of the tube-on-plate 3D FE model)

Based on the 3D FE modelling, the actual peak stress obtained at the weld toe was 330 MPa, and the actual non-linear through-thickness stress distribution is shown in Figure 5-46. The latter stress distribution was processed according to section (4.1), while the membrane and bending hot spot stresses were found by linearization of the actual through-thickness stress distribution, as mentioned in equations (4.1 through 4.7):

$$\sigma_{hs}^{m} = 7.18 \text{ MPa}$$

$$\sigma_{hs}^{b} = 157.72 \text{ MPa}$$

Previous hot spot stresses result from linearizing the discrete non-linear through-thickness stresses σ(y) from the 3D FE model. Equations (4.6 and 4.7) were then used to find the linearized surface stresses as:

$$\sigma_{hs} = \sigma_n = \sigma_a = \sigma_{hs}^{m} + \sigma_{hs}^{b} = 164.9 \text{ MPa}$$

$$\sigma_b = \sigma_{hs}^{m} - \sigma_{hs}^{b} = -150.53 \text{ MPa}$$

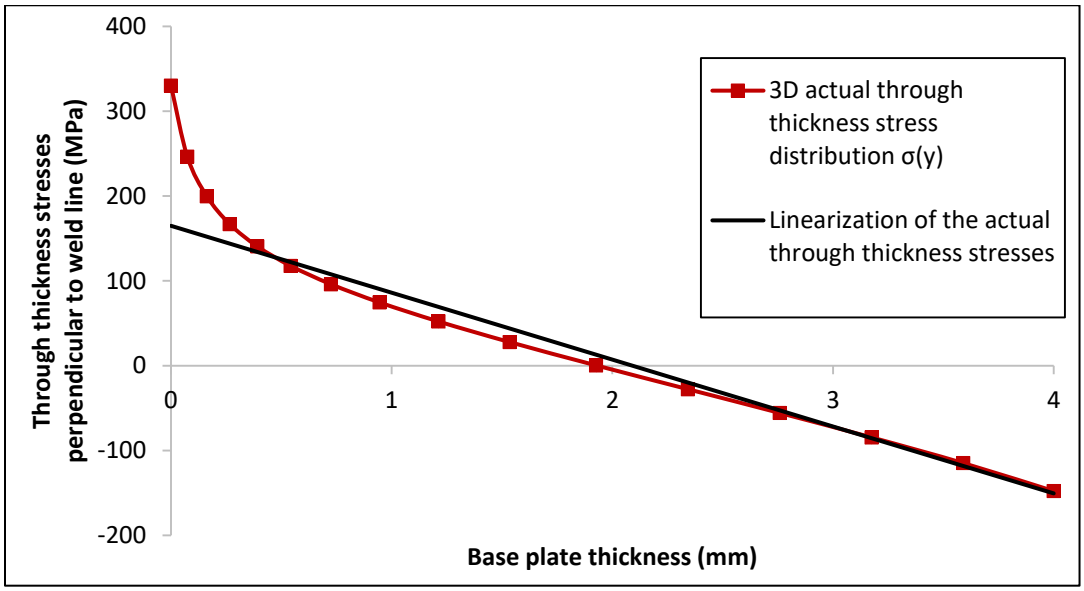

Figure 5-46: The 3D FE stress data, actual stress distribution, and equivalent linearized stress distribution at the weld toe of tube-on-plate welded joint (3D FE model stress data)

In Figure 5-46, the curve represents the actual non-linear stress distribution through the thickness of the weld toe cross section based on the 3D FE model. In the same figure, the solid line represents the linearization of the curve (actual non-linear stress distribution).

The stress results of both the shell and the 3D FE models (see Figure 5-42 and Figure 5-46) were compared after being normalized, as shown in Figure 5-18 and Figure 5-19. The normalization was done by dividing the shell and the 3D FE stress data by a load of F = 1000 N. The normalization was done so that the shell FE local reference stress data could be scaled later to the loads applied to the experiment specimens, which were based on loads of F = 1000 N and F = 1225 N.

Figure 5-47 shows a comparison between the actual non-linear through-thickness stress distribution σ(y) obtained from the 3D FE model and the non-linear through-thickness stress distribution $\sigma_{xx}(y)$ generated from the shell FE local reference stress data and the Monahan equation.

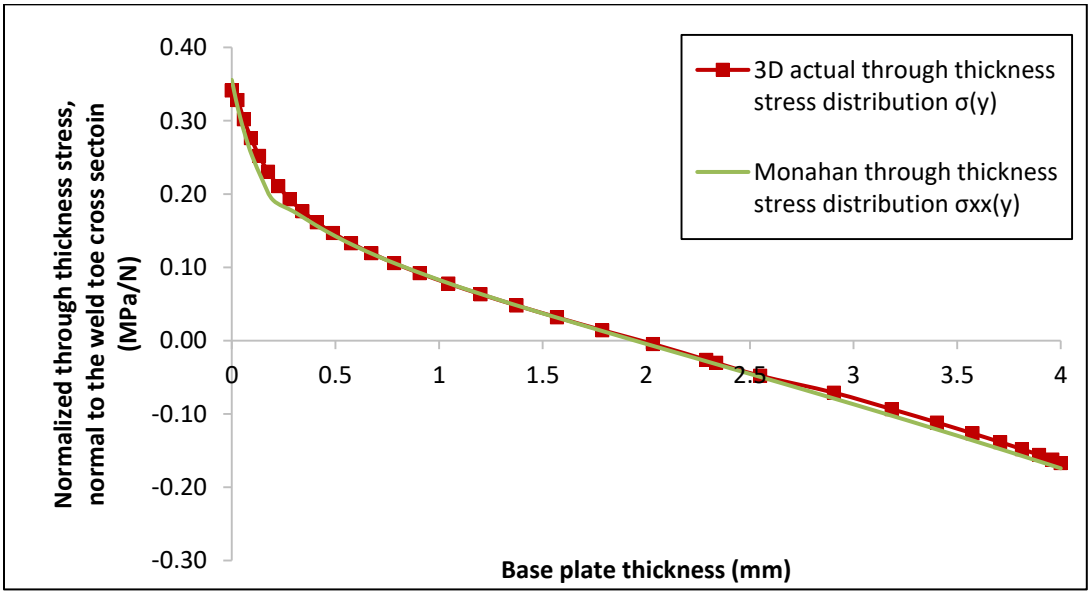

Figure 5-47: Comparison of the normalized actual stress distribution (3D FE model) and the normalized stress distribution (shell FE model and Monahan) through the main plate thickness of the tube-on-plate welded joint

The difference between the actual peak stress based on 3D FE modelling (330 MPa) and the peak stress based on shell FE local reference stress data (355 MPa) was approximately 8%. The compared stress distributions from both the shell and the 3D FE models showed good agreement.

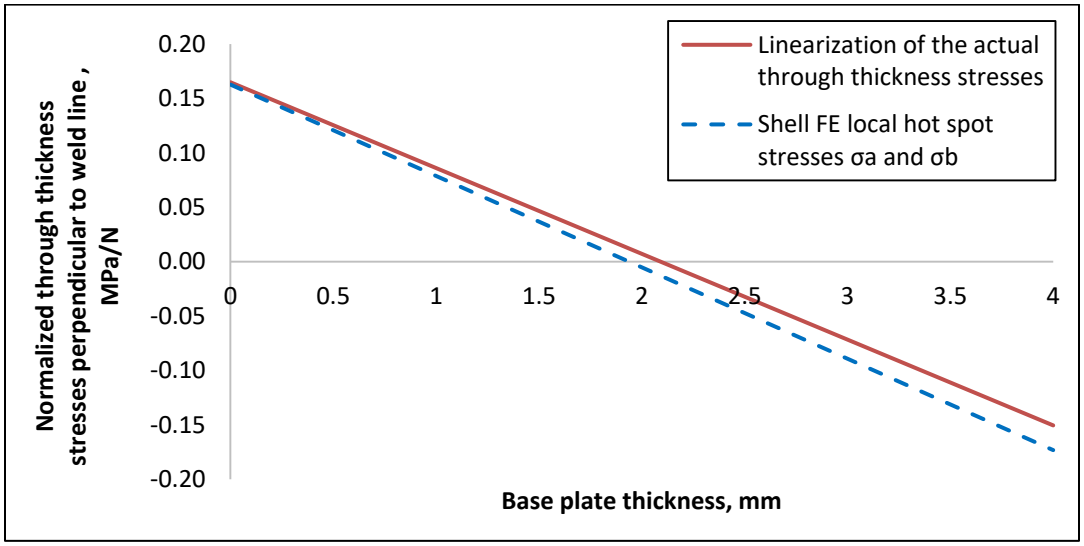

Figure 5-48: Comparison between linearized stresses based on the 3D FE model and shell FE model for the tube-on-plate welded subjected to lateral load

The linearized stress data based on the 3D FE model were higher than the shell FE local reference stresses in the tensile part and lower in the bending parts by (1% and 15%) respectively. Note that this difference does not affect the peak stress but rather the combination of the membrane and bending hot spot stresses does.

This validation is important because the peak stress based on the shell FE model will be used to determine the fatigue crack initiation life using the strain-life method. In addition, through-thickness stress distribution based on the shell FE and Monahan equation will be used to determine the stress intensity factor required to calculate the fatigue crack propagation life using the LEFM method.

The JD Company performed two series of fatigue tests to verify the predicted fatigue life for the tube-on-plate welded joint. Both tests were conducted under fully reversed loading, but the first series of test specimens was subjected to F = ± 1000 N, whereas the second series was subjected to F = ± 1225 N. Therefore, the peak stress and the through-thickness distributions obtained from the shell FE modelling (see the green curve in Figure 5-42) were scaled to the load levels applied to the experimental specimens (F = 1320 N and F = 2000 N), as shown in Figure 5-49 and Figure 5-50.

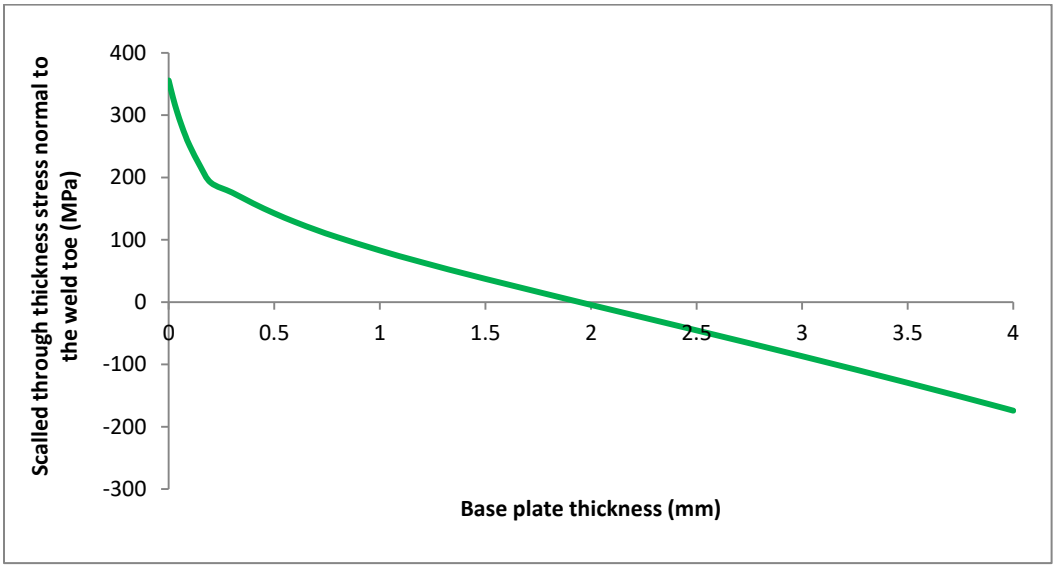

Figure 5-49: Scaled non-linear through-thickness stress distribution to load of (F = 1000 N), based on the shell FE stress data and Monahan equation

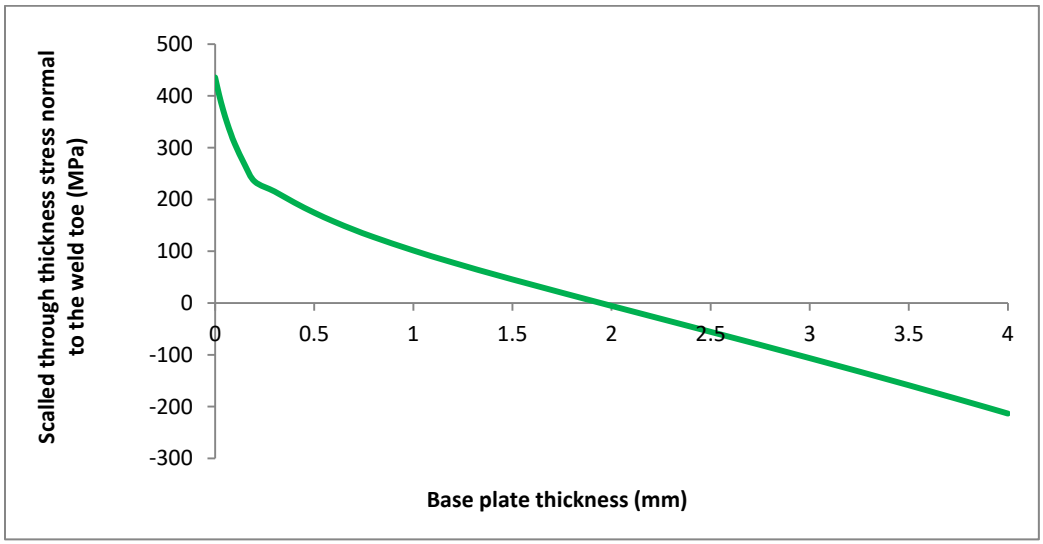

Figure 5-50: Scaled non-linear through-thickness stress distribution to load of (F = 1225 N), based on the shell FE local reference stress data and Monahan equation

The fatigue lives predictions were performed with and without the residual stresses. The residual stress distribution through the thickness at the weld toe provided by the JD Company's experimental data is shown in Figure 5-51.The residual stress was measured at the plate surface only hence the distribution was approximated by assuming self-equilibrated linear field. This was based on limited experimental data. The residual stress was assumed to be tensile and equal to the half of the material yield limit at the weld toe (σ_r = 99 MPa).

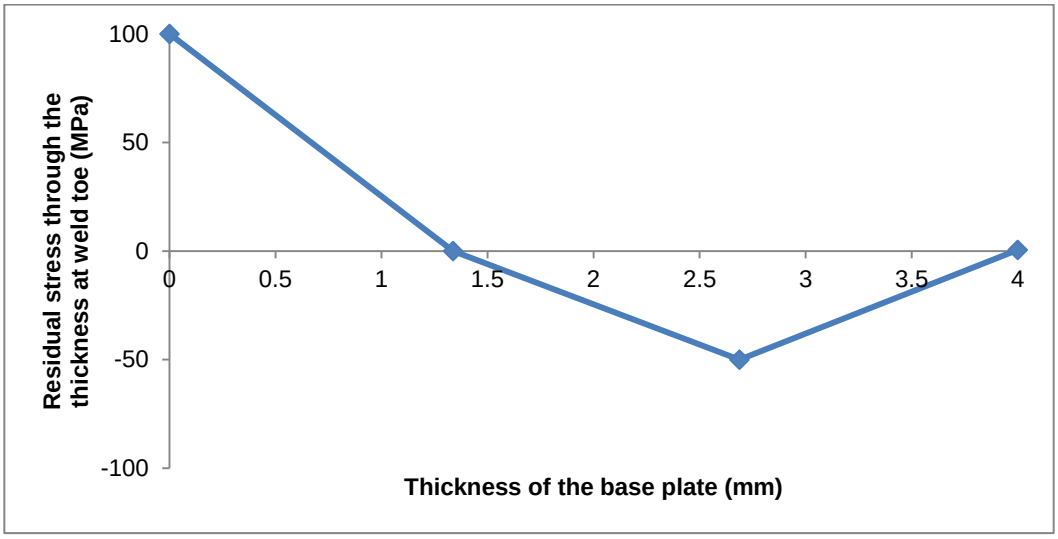

Figure 5-51: Approximation of the residual stress distribution through the base plate thickness under the weld toe for the tube-on-plate welded joint

5.4.4 Fatigue life prediction of a Tube-on-plate subjected to out of plane cyclic loading

The fatigue life is predicted by using the ε-N and the LEFM methods based on the shell FE local reference stress data. The ε-N method predicts the fatigue crack initiation life, whereas the LEFM method predicts the fatigue crack propagation life. Both methods, which are coded into the in-house FALIN and FALPR software packages, were used to find the total fatigue lives of the current case (t). The total fatigue lives were determined by summing both the initiation and the propagation fatigue lives. Finally, the predicted total fatigue life was compared with the fatigue life of the experiment.

The first step is to determine the fatigue crack initiation life according to the procedure of the strain-life method described in Section (2.2). The material properties in Table 5-2 and Table 5-4 were input to the FALIN software to calculate stresses and strains for each load cycle based on the Ramberg-Osgood fatigue stress-strain curve and the Neuber equation (see Figure 5-4 and Figure 2-12). The SWT equation (2.9) was then used to calculate the fatigue crack initiation life. The FALIN software simulates the stress-strain response and corresponding fatigue crack initiation life at the weld toe (output data). The fatigue crack initiation lives were predicted for the current case when subjected to load levels of F = 1000 N and F = 1225 N, without the effect of the residual stress, as shown in Figure 5-52 and Figure 5-53. Figure 5-54 and Figure 5-55 show the fatigue crack initiation lives for the same load levels, including the residual stress effect.

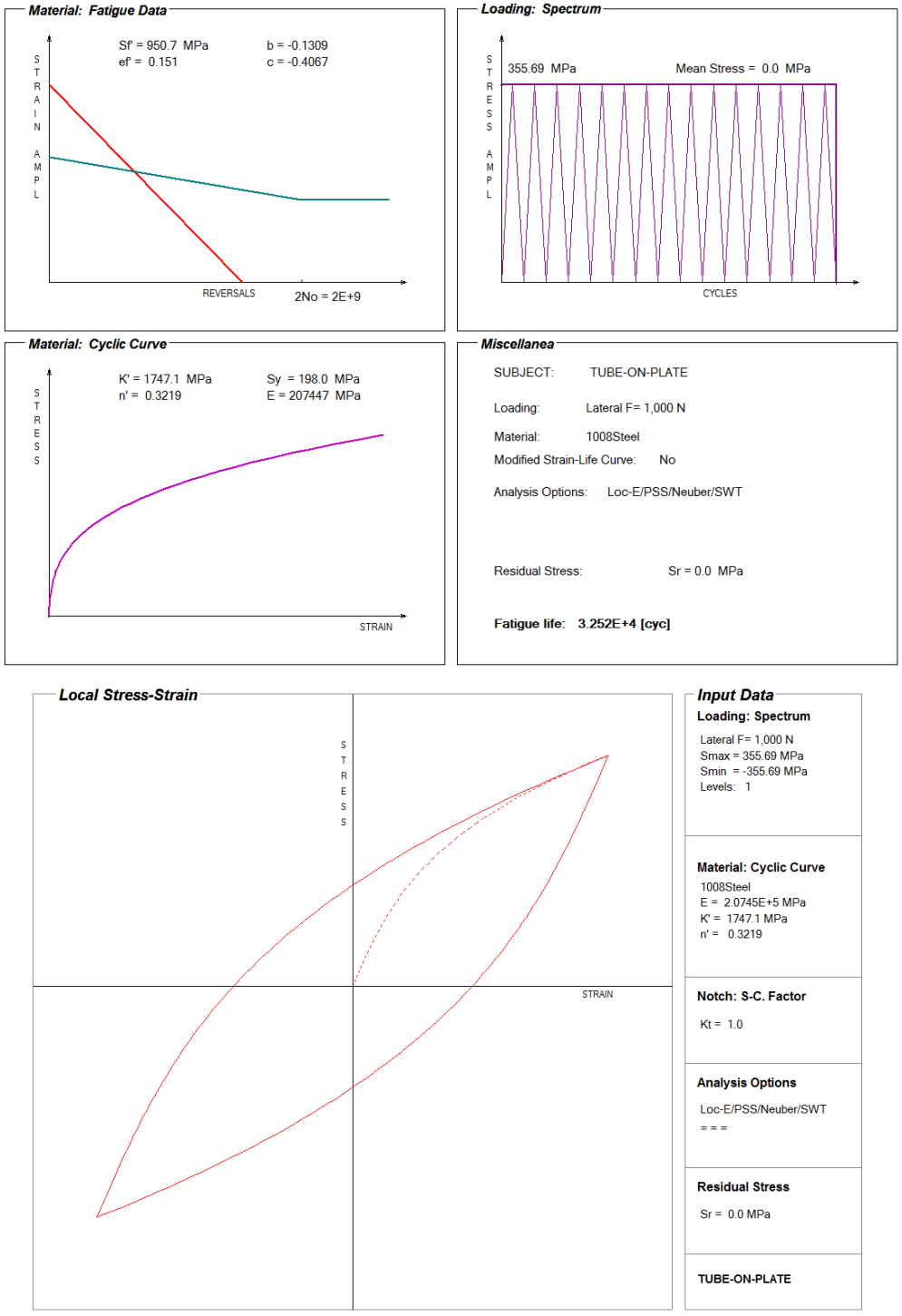

Figure 5-52: FALIN input and output data for the tube-on-plate welded joint (F = 1000 N); a) Manson-Coffin curve, b) Peak stress loading, c) Ramberg-Osgood curve, d) Output data, e) Simulated stress-strain material response at the weld toe

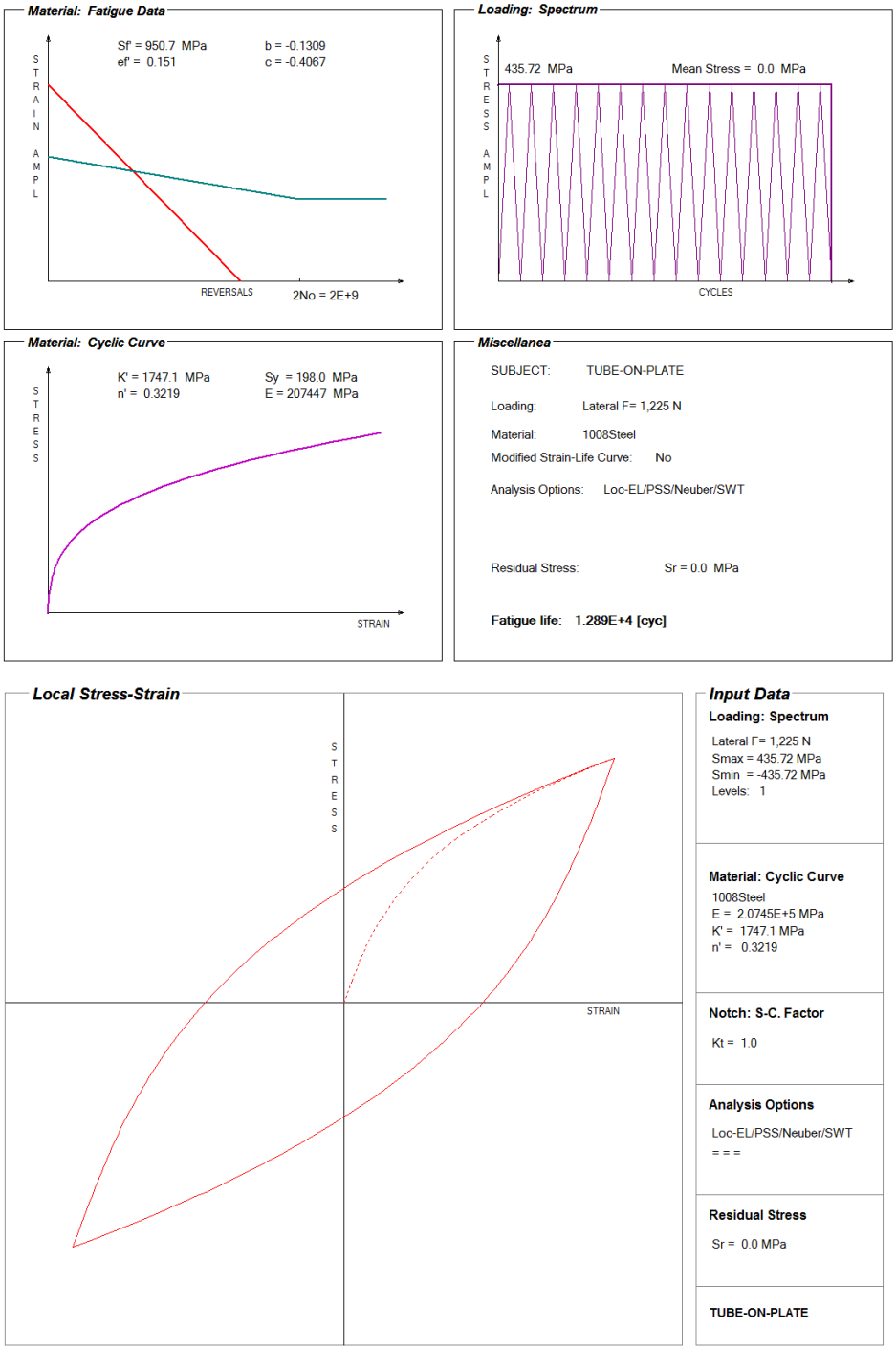

Figure 5-53: FALIN input and output data for the tube-on-plate welded joint (F = 1225 N); a) Manson-Coffin curve, b) Peak stress loading, c) Ramberg-Osgood curve, d) Output data, e) Simulated stress-strain material response at the weld toe

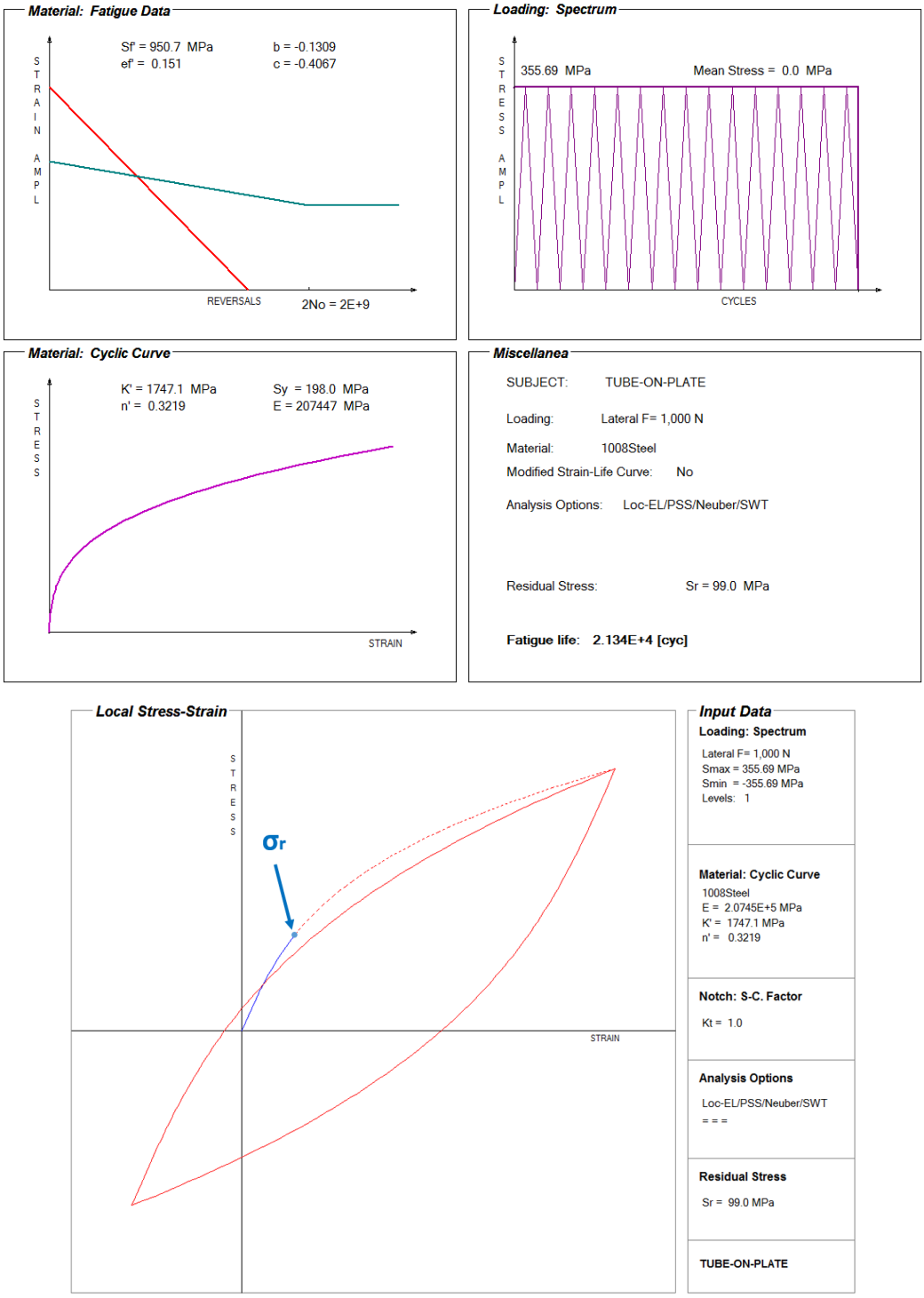

Figure 5-54: FALIN input and output data for the tube-on-plate welded joint (F = 1000 N) in addition to the residual stress σ_r : a) Manson-Coffin curve, b) Peak stress loading, c) Ramberg-Osgood curve, d) Output data, e) Simulated stress-strain material response at the weld toe

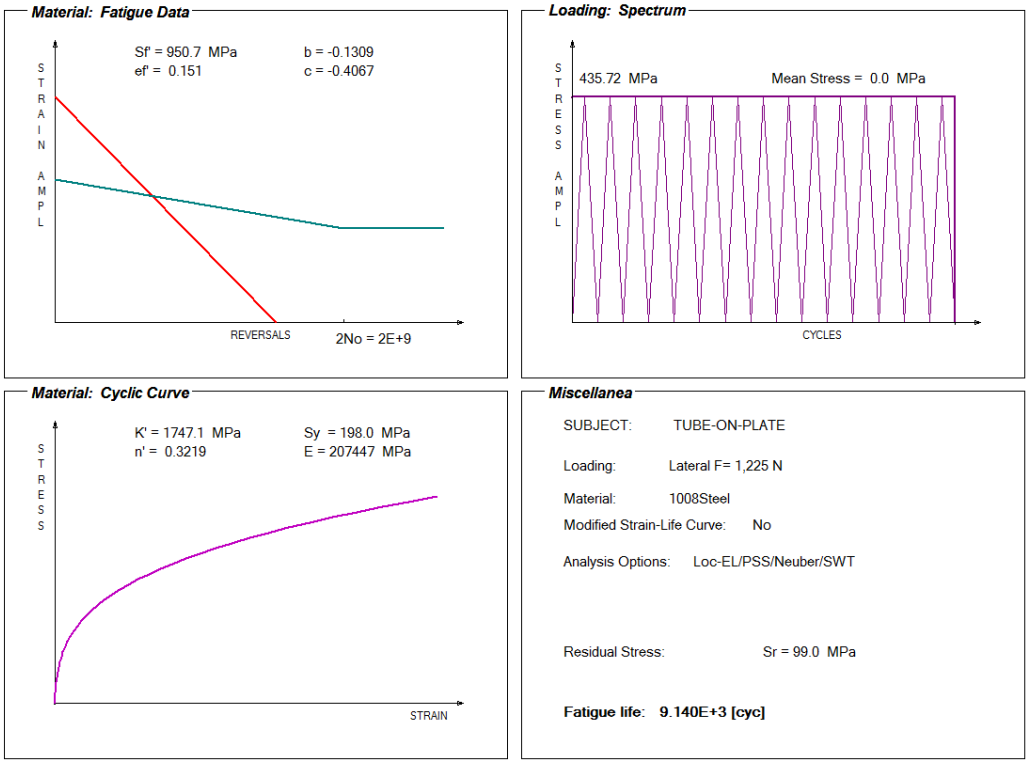

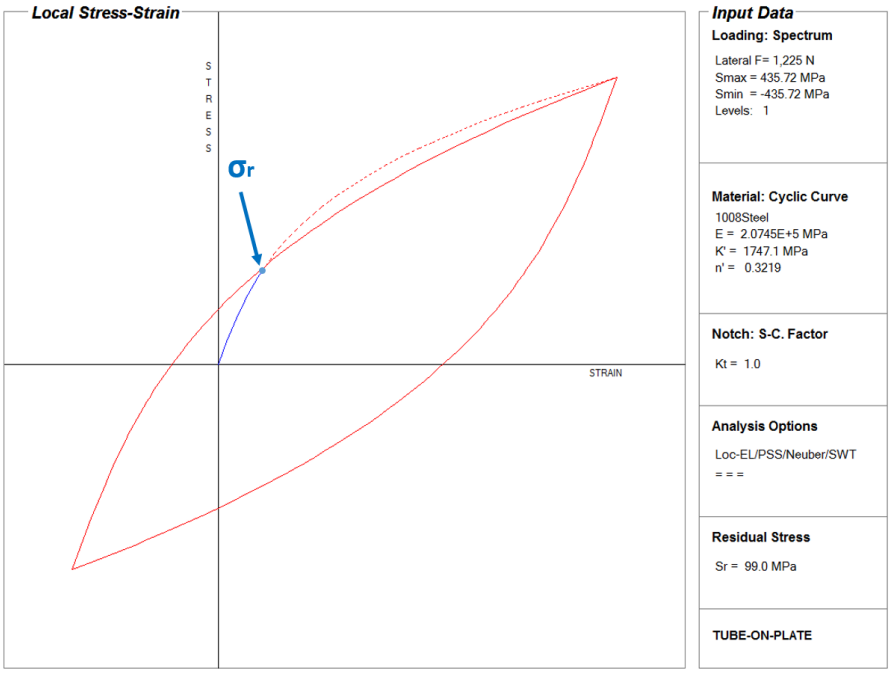

Figure 5-55: FALIN input and output data for the tube-on-plate welded joint (F = 1225 N) in addition to the residual stress σ_r : a) Manson-Coffin curve, b) Peak stress loading, c) Ramberg-Osgood curve, d) Output data, e) Simulated stress-strain material response at the weld toe

The second step in the fatigue life analysis is the calculation of the fatigue crack propagation life using the LEFM method coded in the FALPR software. The observed cracks for the JD fatigue test experiments for the current case were found to be semi-elliptical in shape with a surface crack length of approximately 2c = 3.5 mm. Therefore, the initial crack size was assumed to be not greater than a_i = 0.5 mm in depth with an aspect ratio of (a/c = 0.286). Accordingly, the predictions of the fatigue crack propagation life were based on assuming a semi-elliptical planar crack in a finite thickness plate.

In the case of semi-elliptical cracks, two stress intensity factors, at the depth and surface points, are needed. Using the weight function method, with the through-thickness stress distribution $\sigma_{xx}(y)$ based on the shell FE modelling and Monahan equation, the stress intensity factors at the crack depth and surface (points A and B in Figure 3-13) can be determined. These two stress intensity factors are important for the determination of crack increments after each cycle for both surface and depth directions, as per equations (2.21 and 2.22). The crack increments due to the applied load cycles are calculated by using Paris' fatigue crack growth equation (2.20). To use the Paris equation, fatigue crack growth properties C and m are required for the material of the welded joint under investigation. Fatigue crack growth properties for the material of the current case (T-joint subjected to out-of-plane cyclic loading) is the same as Case # 1 (see section 5.3.1).

The through-thickness stress distribution based on the shell FE model and Monahan equation were input to FALPR to determine the stress intensity factors. It was found that the crack was growing on the surface faster than the depth because of the high stress at the weld toe [62]. Therefore, the crack increments of the surface and deepest point have to be determined for each load cycle. Accordingly, the aspect ratio (a/c) has to be updated after each increment using Paris' fatigue crack growth. The fatigue crack propagation life has been predicted for the tube-on-plate welded joint subjected to lateral loadings of (F = 1000 N, and F = 1225 N). The predictions of both load cases were carried out with and without the residual stress to investigate the effect of the residual stress.

Figure 5-56 through Figure 5-59 show the input data to FALPR, the predicted crack depth versus the number of cycles, the stress intensity factor versus the number of applied load cycles, and the fatigue crack growth lives predictions, and the fatigue crack propagation lives of the weld joint under investigation when applying F = 308 N and F = 468 N, respectively, whereas Figure 5-60 through

Figure 5-63 show the same results, including the effect of the residual stress. Note that including the residual stress affect was done to study its effect on the fatigue life evaluation.

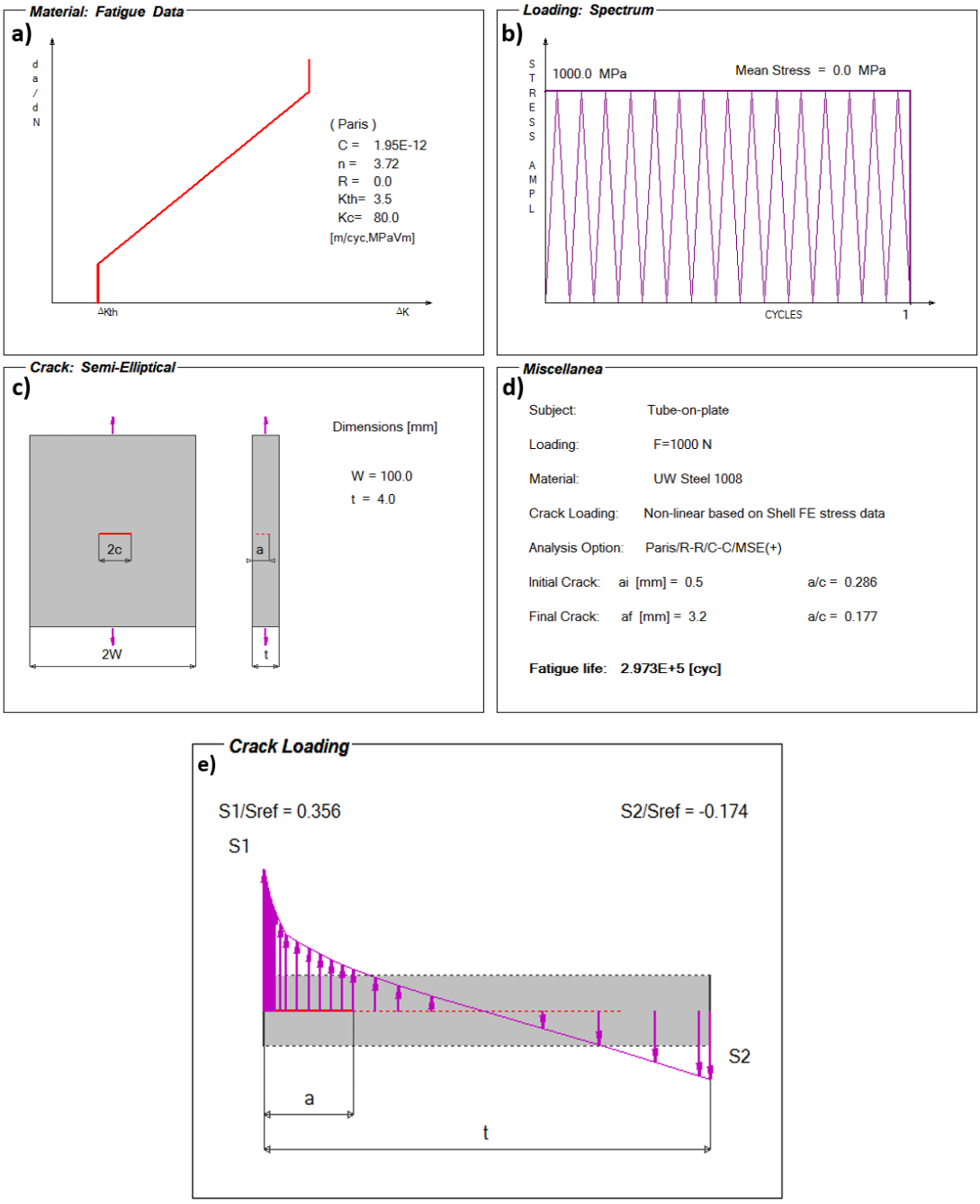

Figure 5-56: FALPR input data for fatigue crack propagation analysis of the tube-on-plate subjected to lateral loading F = 1000 N (without residual stress): a) Paris fatigue crack growth curve, b) Loading history of the peak stress, c) Geometry of the crack, d) Fatigue life, e) The normalized through-thickness stress distribution

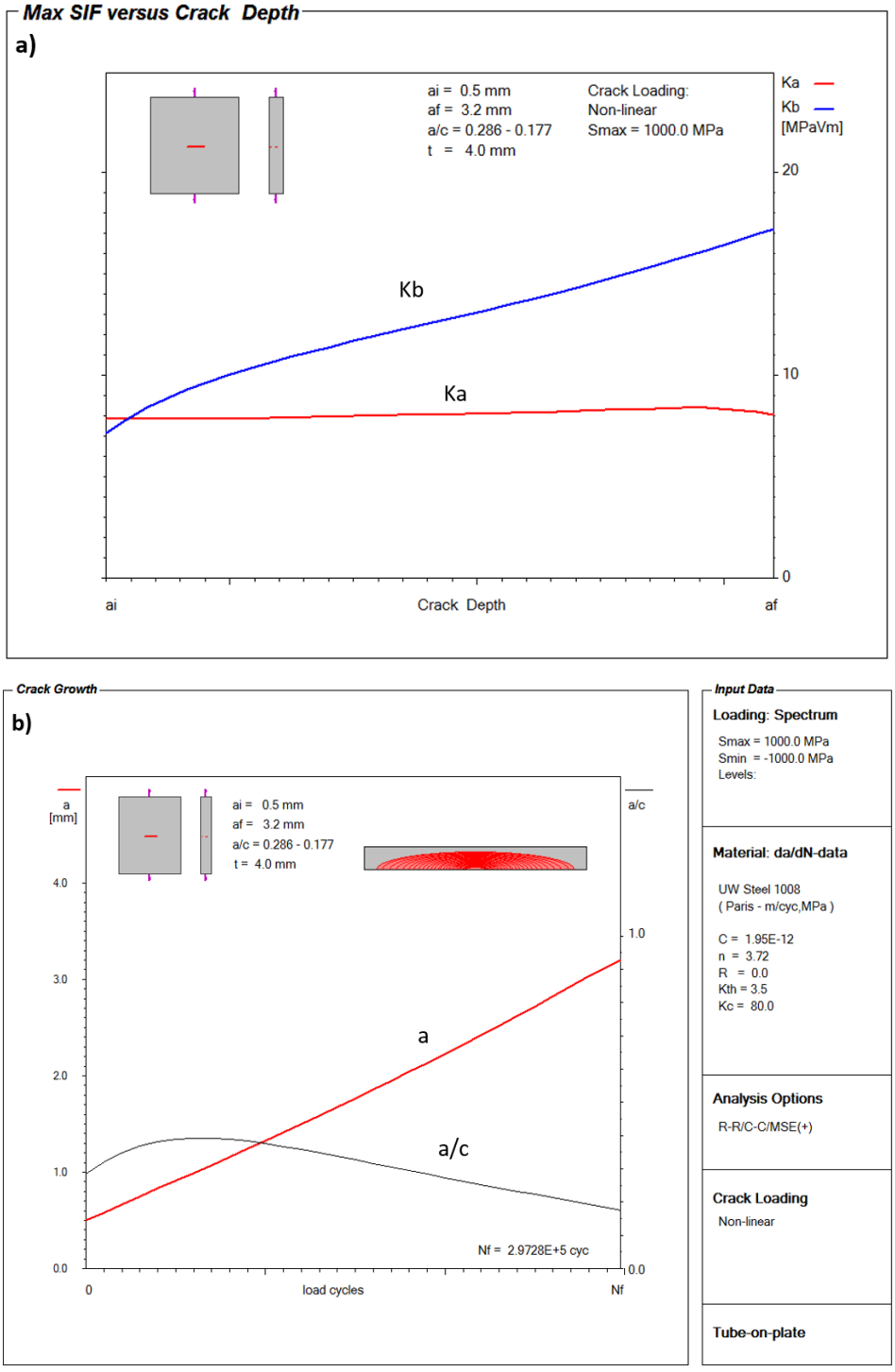

Figure 5-57: a)The crack depth versus the number of applied load cycles to failure (a-N diagram), b) The stress intensity factor values at the surface and depth points of the semi-elliptical crack versus the crack depth (K-a diagram); tube-on-plate subjected to lateral load F = 1000 N (without residual stress)

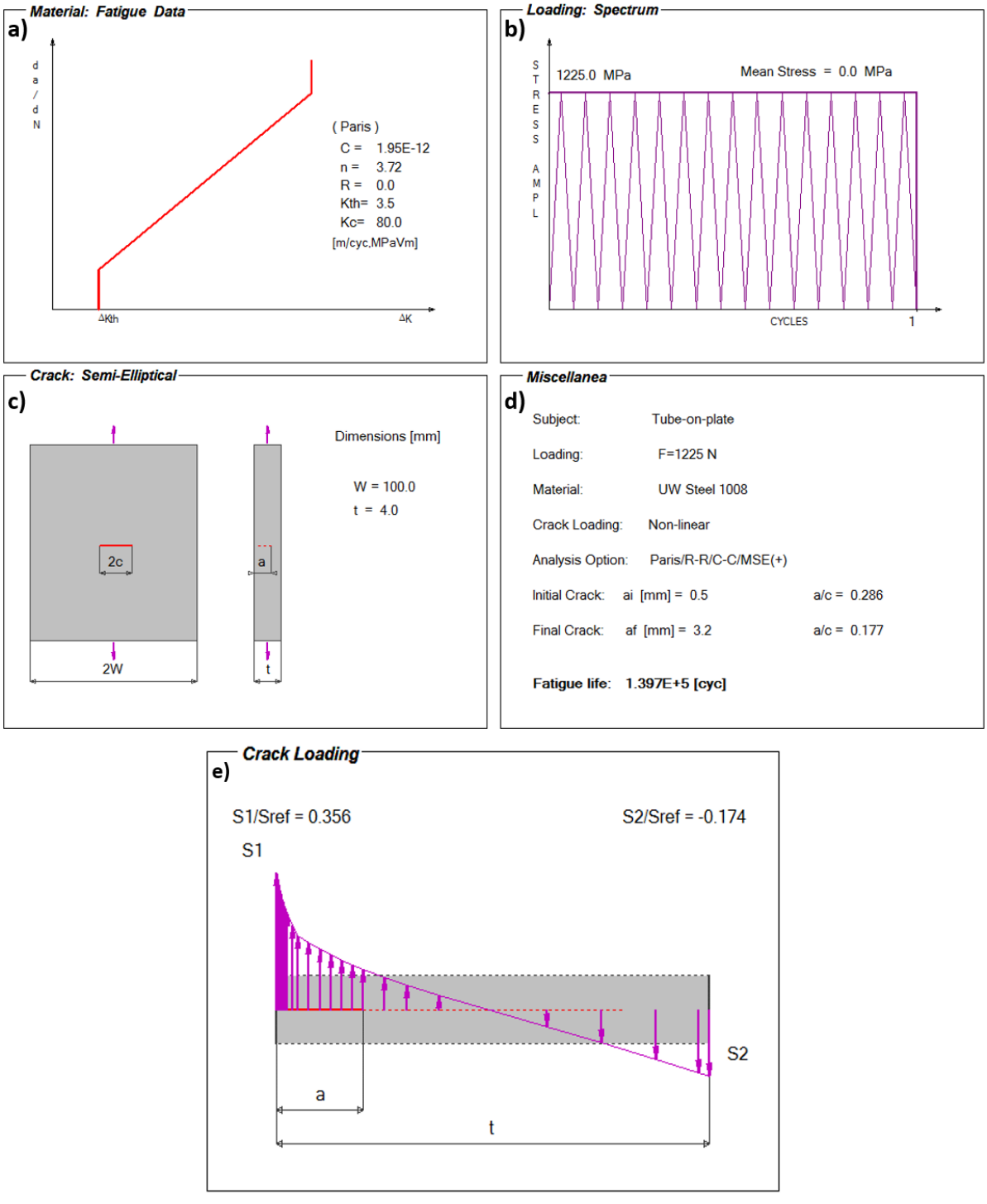

Figure 5-58: FALPR input data for fatigue crack propagation analysis of the tube-on-plate subjected to lateral loading F = 1225 N (without residual stress): a) Paris fatigue crack growth curve, b) Loading history of the peak stress, c) Geometry of the crack, d) Fatigue life, e) The normalized through-thickness stress distribution

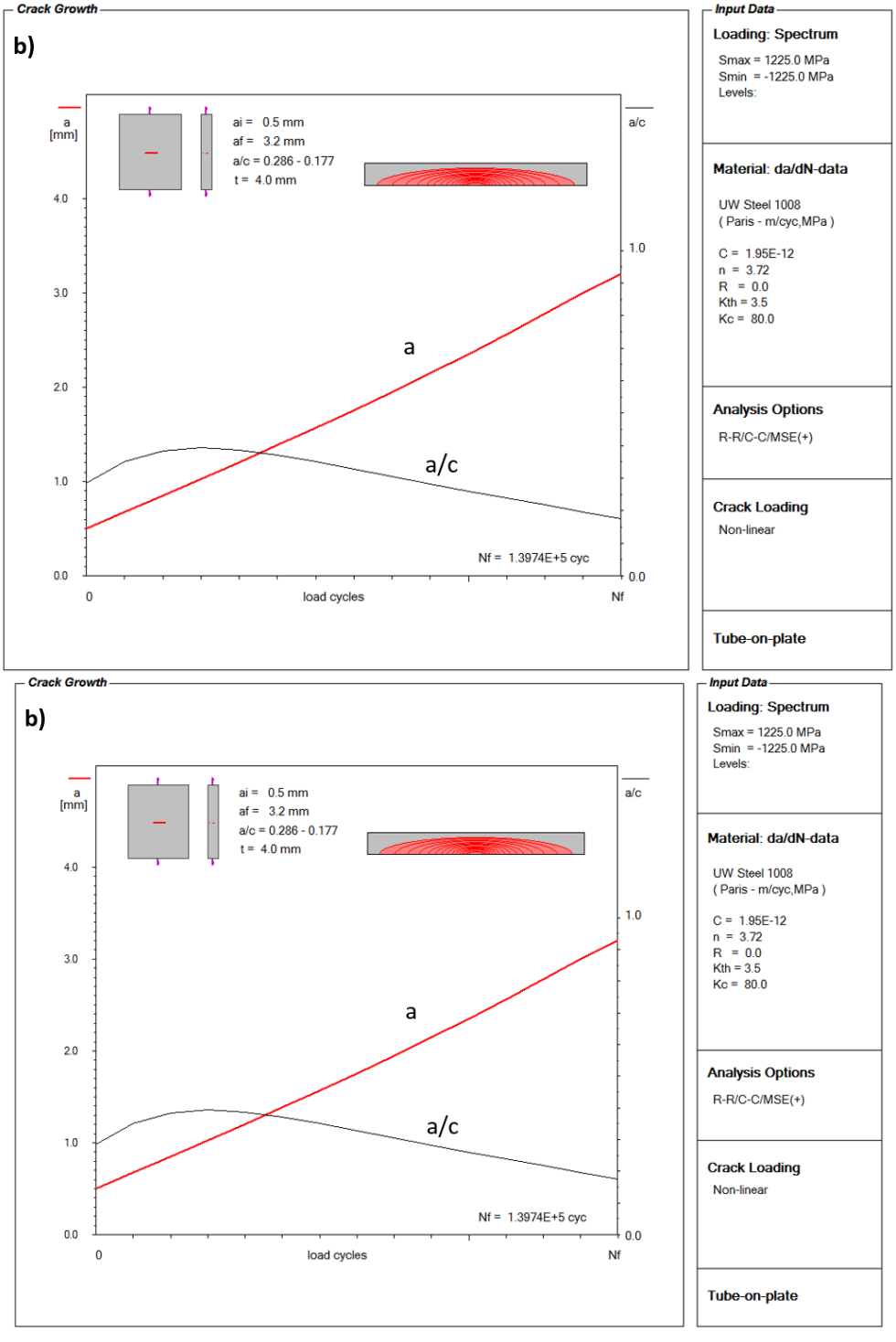

Figure 5-59: a)The crack depth versus the number of applied load cycles to failure (a-N diagram), b) The stress intensity factor values at the surface and depth points of the semi-elliptical crack versus the crack depth (K-a diagram); tube-on-plate subjected to lateral load F = 1225 N (without residual stress)

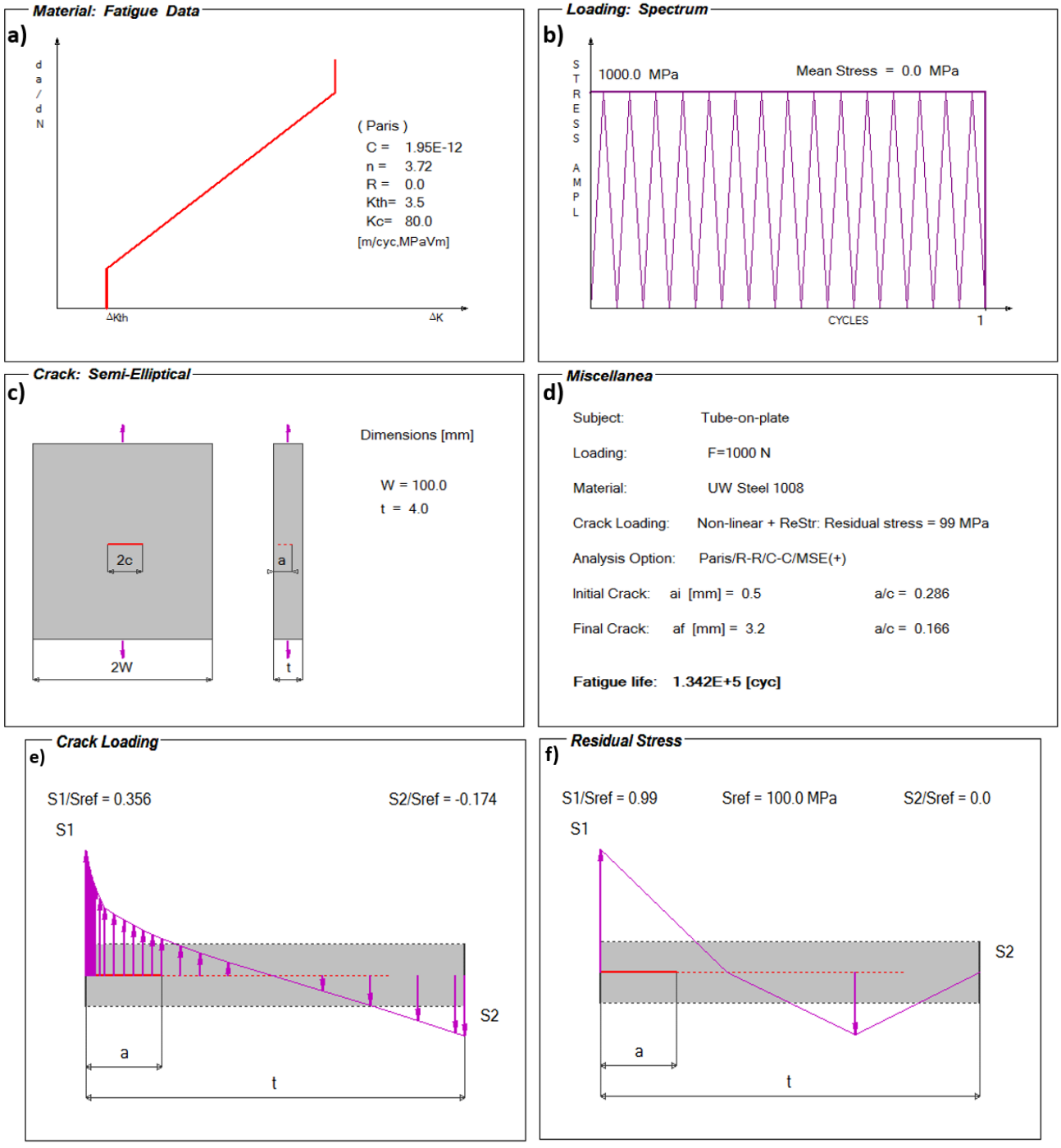

Figure 5-60: FALPR input data for fatigue crack propagation analysis of the tube-on-plate welded joint subjected to lateral loading F = 1000 N (with residual stress): a) Paris fatigue crack growth curve, b) Loading history of the peak stress, c) Geometry of the crack, d) Fatigue life, e) The normalized through-thickness stress distribution, f) Estimated residual stress distribution through the thickness of the weld toe cross section

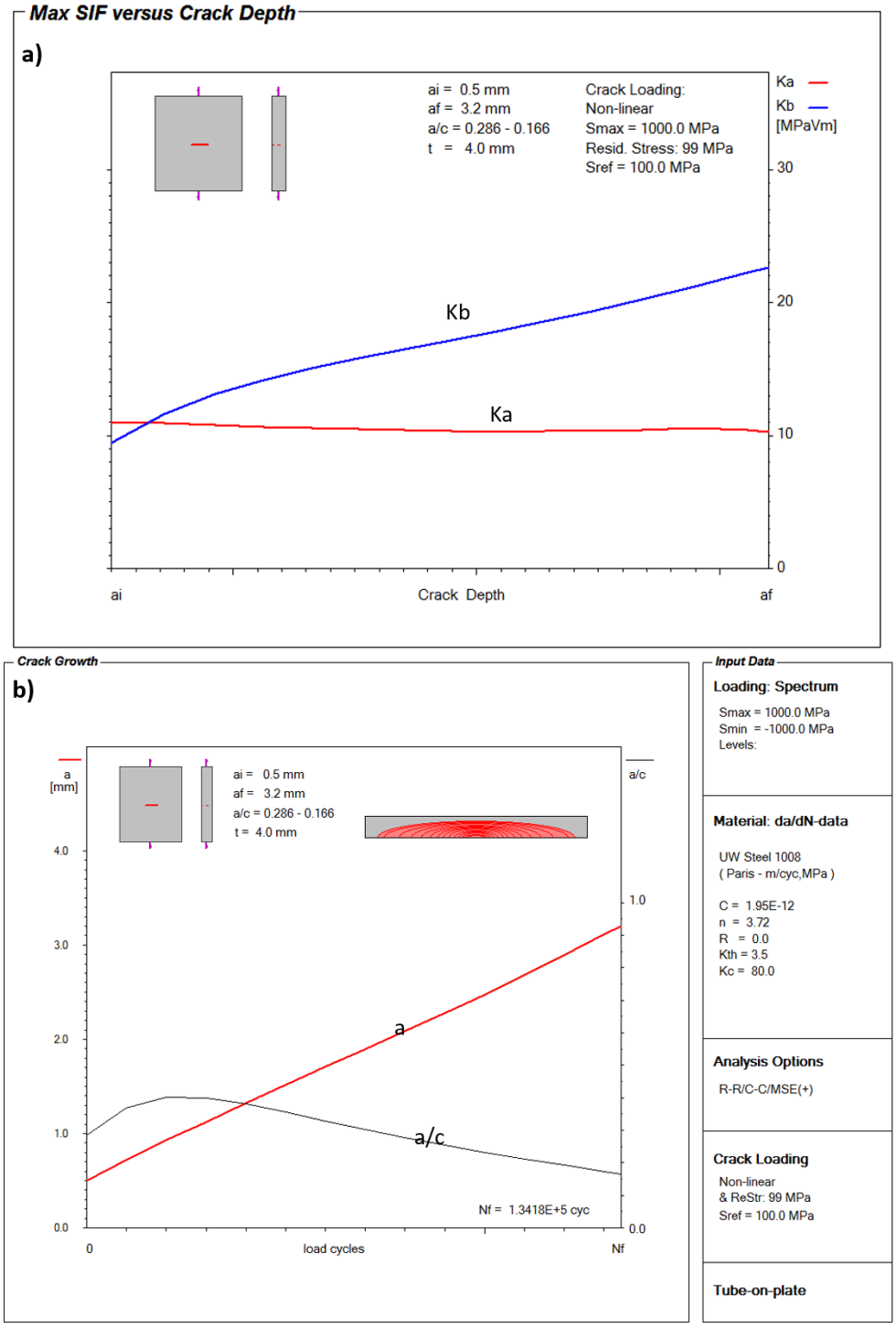

Figure 5-61: a) The crack depth versus the number of applied load cycles to failure (a-N diagram), b) The stress intensity factor values at the surface and depth points of the semi-elliptical crack versus the crack depth (K-a diagram); tube-on-plate welded joint subjected to lateral load F = 1000 N (with residual stress)

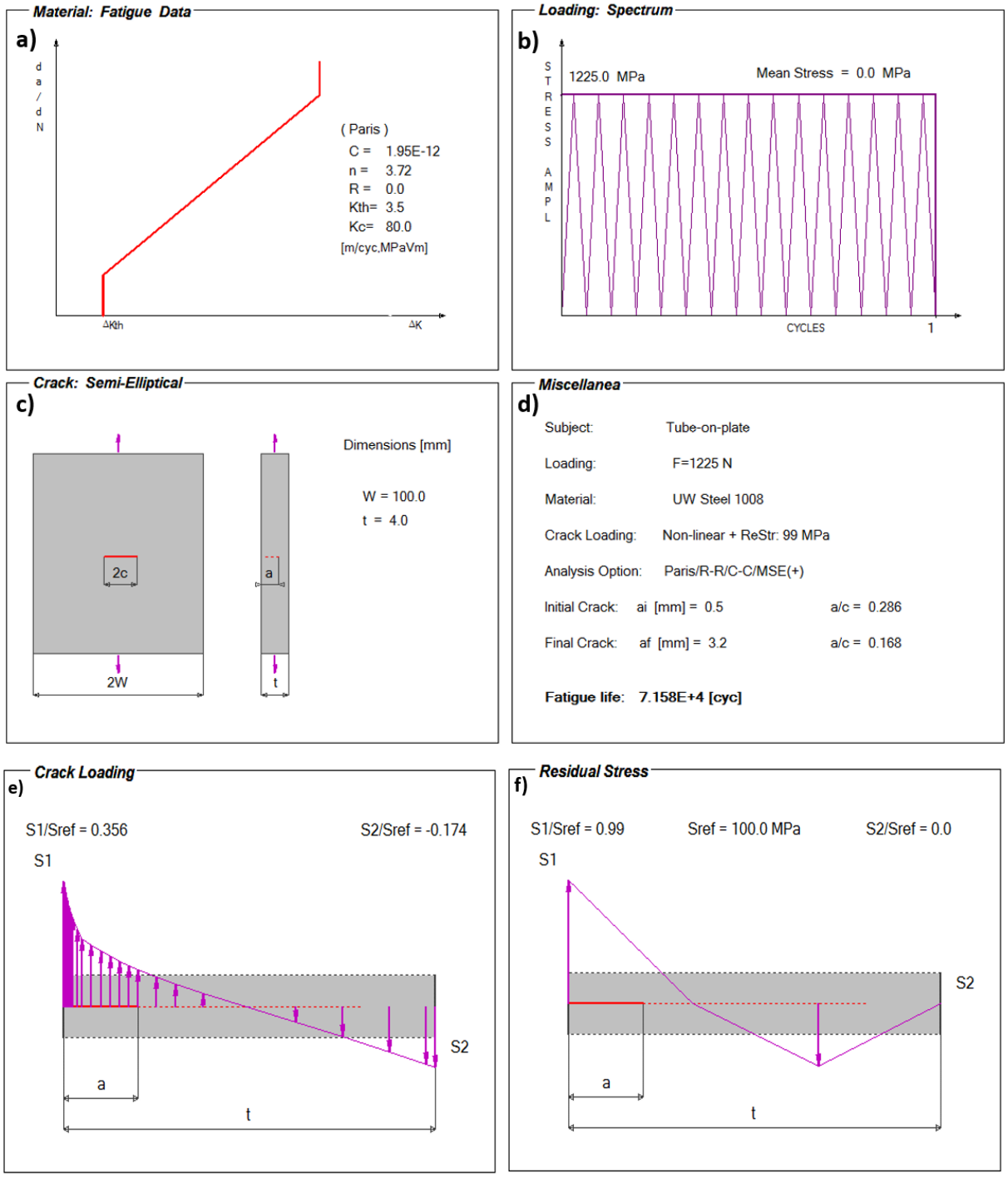

Figure 5-62: FALPR input data for fatigue crack propagation analysis of the tube-on-plate welded joint subjected to lateral loading F = 1225 N (with residual stress): a) Paris fatigue crack growth curve, b) Loading history of the peak stress, c) Geometry of the crack, d) Fatigue life, e) The normalized through-thickness stress distribution, f) Estimated residual stress distribution through the thickness of the weld toe cross section

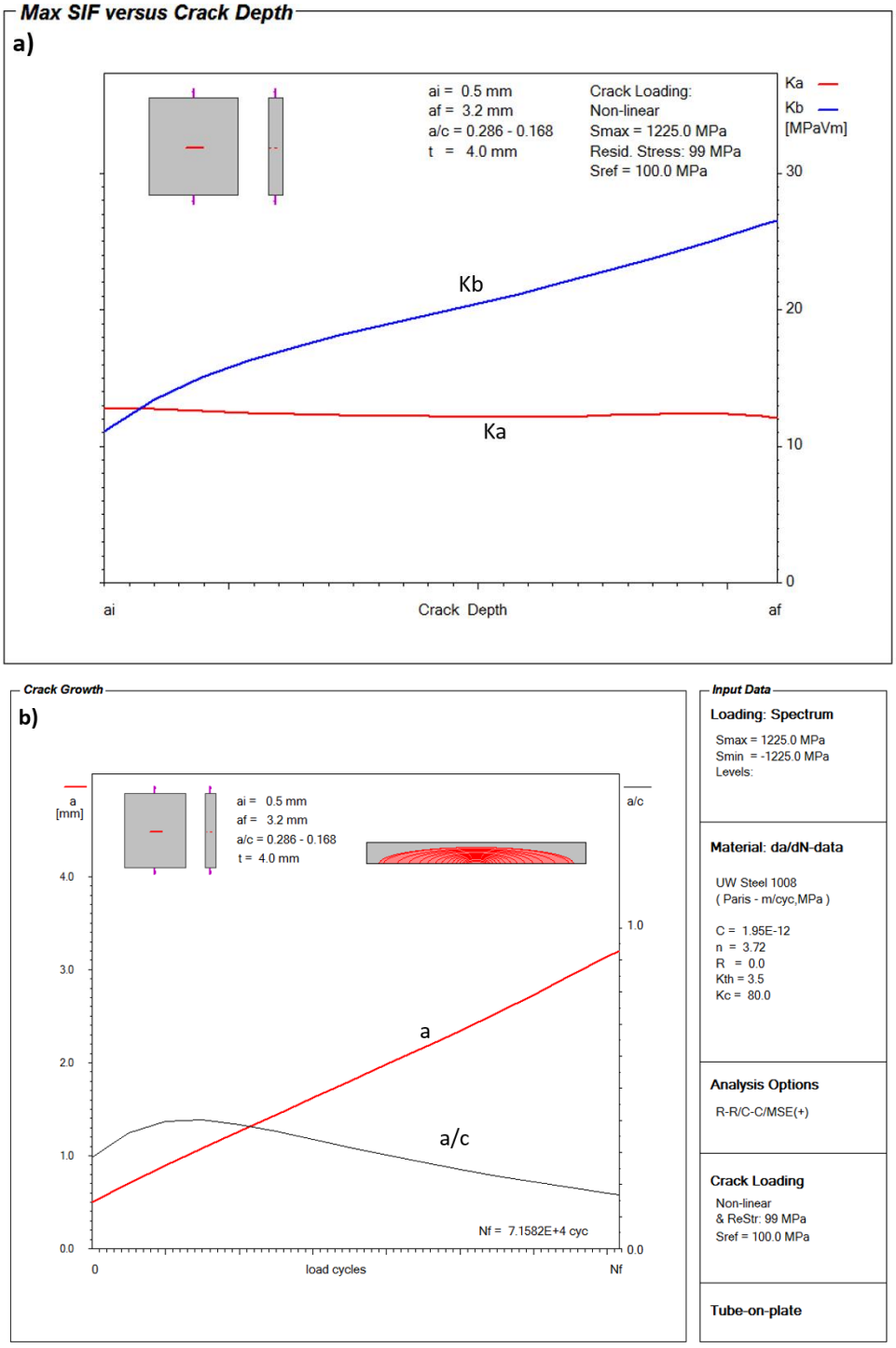

Figure 5-63: a) The crack depth versus the number of applied load cycles to failure (a-N diagram), b) The stress intensity factor values at the surface and depth points of the semi-elliptical crack versus the crack depth (K-a diagram); tube-on-plate welded joint subjected to lateral load F = 1225 N (with residual stress)

The fatigue analysis results are shown in Table 5-7 for the cases of the tube-on-plate welded joint subjected to lateral loading of F = 1000 N and F = 1225 N. The total fatigue life (N_f) was determined by summing the fatigue crack initiation life (N_i) and the fatigue crack propagation life (N_p). The ratios of the fatigue crack initiation life to the fatigue crack propagation life and the total fatigue life (N_i/N_p and N_i/N_f) are shown to determine which fatigue life was dominant to the total life.

Table 5-7: Summary of predicted fatigue lives for the tube-on-plate welded joint subjected to lateral loading

Case load	Residual Stress (MPa)	Ni (Cycle) ai = 0.5 mm	Np (Cycle) af = 3.2 mm	Ni /Np	Nf (Cycle)	Ni/Nf
F= 1000 N	$\sigma_r = 0$	32520	297283	0.109	329803	0.099
	$\sigma_r = 99$	21339	134180	0.159	155519	0.137
F= 1225 N	$\sigma_r = 0$	12889	139740	0.092	152629	0.084
	$\sigma_r = 99$	9140	71582	0.128	80722	0.113

The small ratios of the crack initiation life (N_i) to the crack growth life (N_p) and the total fatigue life (N_f) indicate that most of the welded joint fatigue life was spent on propagating the crack from a_i = 0.5 mm to the final critical crack depth a_f = 3.2 mm.

The JD Company's laboratory fatigue lives were calculated as the number of load cycles versus the measured length of the surface crack on the base plate. Using the fatigue crack growth simulation data obtained from the FALPR program, the crack depth corresponding to the measured crack length was estimated. The experimental data are shown in Table 5-8.

Table 5-8: JD Experimental fatigue crack propagation life data (2c-N) for the tube-on-plate welded joint subjected to lateral loading

Sample #	Load (N)	Number of cycles (cycles)	Crack length 2c (mm)	Remarks
3	1000	447463	53.8	Final crack
4		97892	53	
5		110160	13	
7		404729	17	
13		191213	43.63	
14		433000	49.28	
2	1225	52600	6.9	First detected crack
		70890	20.3	Final crack
8		24291	16.9	
9		274655	37.2	
10		149793	15.2	
11		72919	33.5	
12		306468	39.5	

The fatigue life data in Table 5-7 and Table 5-8 are plotted as shown in Figure 5-64 and Figure 5-65 for both load levels. The fatigue life data are plotted in terms of the applied load cycles versus the surface crack length (2c) for comparison between the experimental and predicted fatigue life. The experimental fatigue data are plotted as a series of discrete points, whereas the predicted fatigue data are plotted as two curves. The hashed curve represents the fatigue life prediction without the effect of the residual stress (No-RS), and the solid curve represents the fatigue life prediction, including the residual stress effect (with RS).

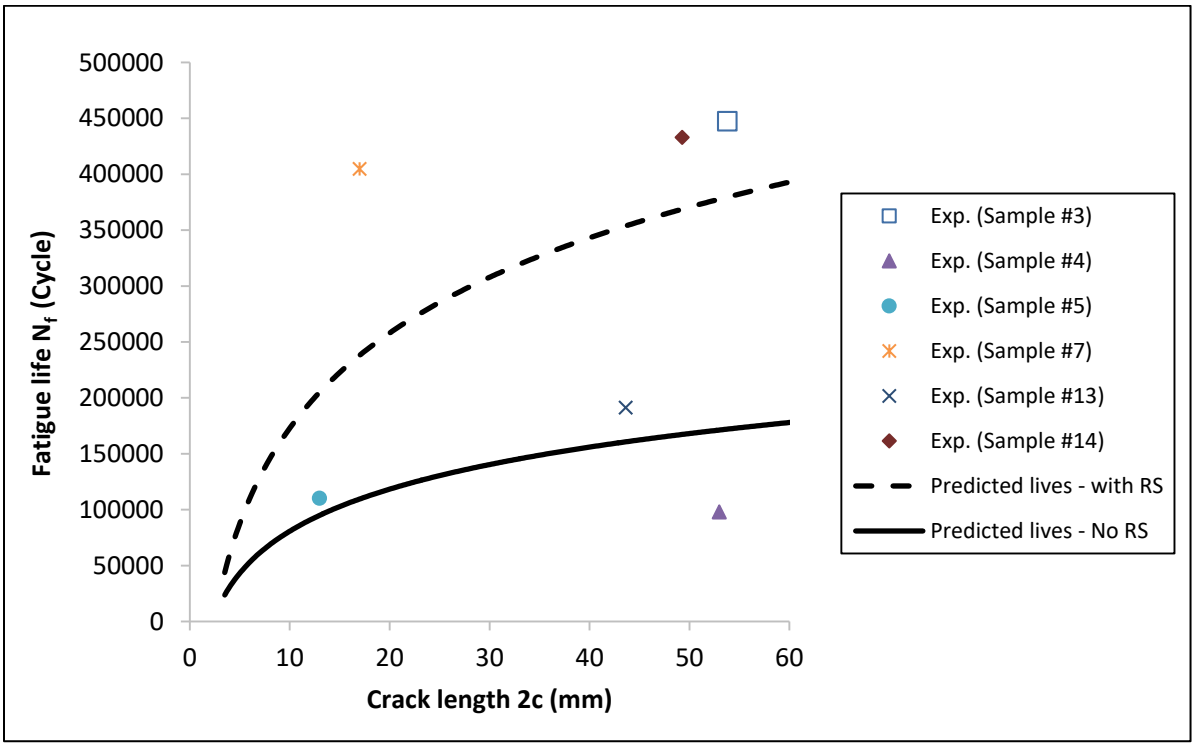

Figure 5-64: Comparison between experimental and predicted fatigue lives of the tube-on-plate welded joint subjected to lateral load (F = 1000 N)

Figure 5-64 shows the experimental and the predicted total fatigue lives for the tube-on-plate welded joint subjected to lateral load (F = 1000 N). According to the results shown in the above figure, the predicted fatigue life based on the proposed shell FE local reference stress method are overestimated compared to the experiments (#4, #5, and #13). Including the residual stress reduces the over estimation, significantly. This finding emphasizes the importance of including the residual stress effect when evaluating the fatigue life of welded joints.

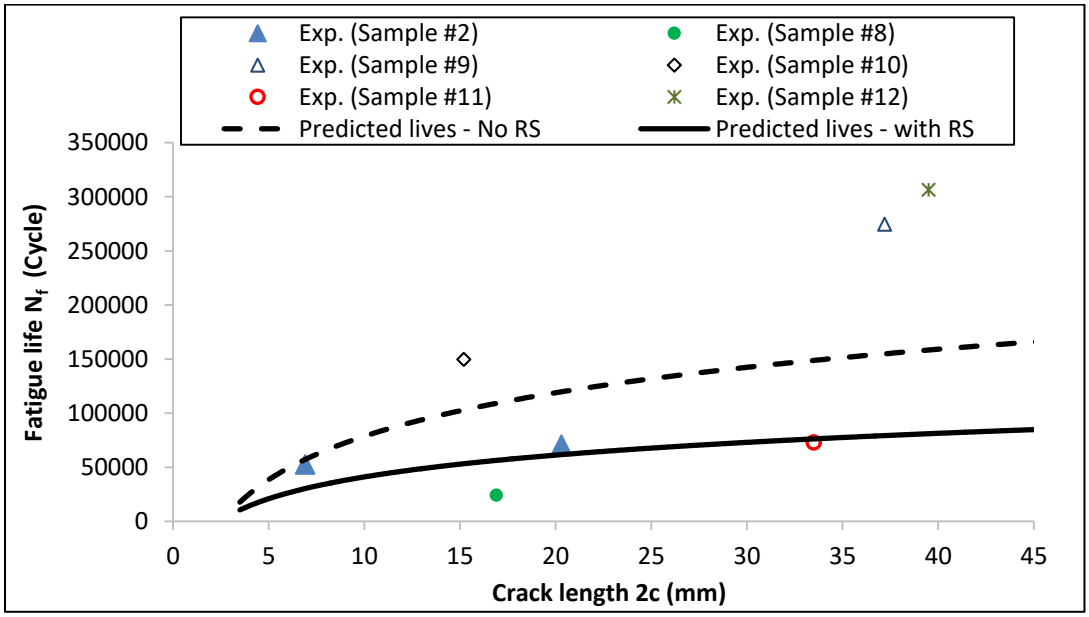

Figure 5-65: Comparison between experimental and predicted fatigue lives of the tube-on-plate welded joint subjected to lateral load (F = 1225 N)

Figure 5-65 shows the experimental and the predicted total fatigue lives for the tube-on-plate welded joint subjected to lateral load (F = 1225 N). According to the results shown in this figure, the predicted fatigue life based on the proposed shell FE method are overestimated compared to the experiments (#2, #8, and #11). Including the residual stress reduces the overestimation significantly. This finding emphasizes the importance of including the residual stress effect when evaluating the fatigue life of welded joints.

Generally, the total fatigue life predictions based on the proposed local reference stresses shows good agreement with the experimental data for both load levels (1000 N and 1225 N). The results in both cases (F = 1000 N and F = 1225 N) indicate that it is important to include the residual stress distribution to the stress analysis module when determining the fatigue life of weldments. The difference between the predicted fatigue lives and the experimental data could also be that some of the experimental welded joints are stress relieved. Assuming that it is obvious that experiment specimens number (3, 7, and 14) subjected to load F = ± 1000 N, in addition to experiment specimens number (9, 10, and 12) subjected to F = ± 1225 N, are stress-relieved. Based on this assumption, the difference in the results is fairly justified.

Chapter 6
Conclusion and future recommendations

The achievement of the general goal has been demonstrated through the development of a new stress reference that can provide all stresses required for the commonly used fatigue life methods under study. This objective was accomplished by improvements to the stress analysis step shown in Figure 1-1 .The stress data resulting from this enhanced step were then validated against detailed 3D FE modelling stress data for validation. The resulting stress data based on the shell FE local reference stress were used for the fatigue life prediction of five case studies. The findings revealed that the fatigue life results based on the proposed shell FE reference stress can be considered an adequate method for predicting the fatigue life of welded joints.

6.1 Summary and discussion of the stress data

The proposed method provides detailed stress information about weldments using relatively simple shell FE models of welded structures rather than 3D FE detailed fine mesh models. The shell FE local reference stress can successfully provide the peak stress at the critical point in a welded joint. The proposed simplified shell FE modelling can also produce a good estimate of the non-linear stress distribution through the thickness of the critical cross sections in a welded structure. The shell FE reference stress method is dependent on a meshing procedure introduced in this research in order to include in the analysis all important aspects of the geometry and load of a weld.

The proposed shell FE model proved to be able to simulate the stress fields in a variety of welded joints, such as T-joint (fillet joints), and square or circular tube on a plate. The shell FE local reference stress data were compared to the results obtained using detailed fine mesh 3D FE models. The accuracy of the stress data based on the shell FE models was under 15 % in all of the joints except for the gusset, which was around 20 %, as shown in Table 6-1, Table 6-2, and Table 6-3. The difference between the peak stress resulting from the shell FE local reference stress and the peak stress resulting from the 3D FE modelling was within 10 % for all the cases studied, with the exception of the first case, which was within 20 %, as shown in Table 6-2. With respect to the number of elements, the difference between the shell and 3D FE models was very large. The accuracy of the data produced by the proposed shell FE models matched that produced by the 3D fine mesh elements

but with 9 to 204 times fewer elements, as shown in Table 3-6. As a result, the proposed shell FE modelling method offers the advantage of simulating a full structure in a relatively short time and with fewer computational resources, as proven in the last case study involving the complex tubular joint. Such accurate stress data then enables fatigue life to be evaluated using the post-processed shell FE local reference stress data.

Table 6-1: Summary of stress data resulting from shell and 3D FE modelling

Case studies	Shell FE modelling (coarse mesh)					3D FE modelling (fine mesh)				
	Local reference stresses (MPa)		Post-processed stress data (MPa)			Actual peak stress (MPa)	Linearized stresses (MPa)			
	$\sigma_a = \sigma_n = \sigma_{hs}$	σ_b	σ_{hs}^m	σ_{hs}^b	σ_{peak}	σ_{peak}	σ_{hs}^m	σ_{hs}^b	σ_a	σ_b
(Case # 1) T-joint subjected to in-plane cyclic loading	202.82	-168.43	17.19	185.63	429.25	358.39	4.49	215.31	220.26	-210.37
(Case # 2) Tube-on-plate subjected to out of plane cyclic loading	162.8	-173.27	-5.234	168.04	355.69	330	7.18	157.72	164.9	-150.53
(Case # 3) T-joint subjected to out-of-plane cyclic loading	568.19	-568.187	0.0015	568.19	881.83	881	3.343	575.835	579.18	-572.94
(Case # 4) Square-tube-on-plate welded joint subjected to lateral cyclic loadings	79.77	12.70	46.28	33.50	161.66	179.42	43.69	36.38	80.07	7.31
(Case # 5) Complex tubular welded joint subjected to torsion and bending cyclic loading	8.87 psi	- 4.07 psi	2.4 psi	6.47 psi	18.535 psi	17.5 psi	2.59 psi	6.74 psi	9.33 psi	-4.16 psi

Table 6-2: Comparison between shell and 3D FE stress data

Case #	Difference (%)		
	Linearized stresses		Peak stress
1	7.92	19.94	-19.77
2	1.27	-15.11	-7.78
3	1.90	0.83	-0.09
4	0.37	-73.78	9.88
5	4.93	2.16	-5.91

Table 6-3: Comparison between number of elements for 3D and shell FE models

Case studies	Number of elements, δel		Difference (3D δel/shell δel)
	3D solid element model (3D δel)	Shell element model (shell δel)	
Case # 1) T-joint subjected to in-plane cyclic loading	474836	5427	87
Case # 2) Tube-on-plate subjected to out of plane cyclic loading	108760	6032	18
Case # 3) T-joint subjected to out-of-plane cyclic loading	56709	4543	12
Case # 4) Square-tube-on-plate welded joint subjected to lateral cyclic loadings	77499	8782	9
Case # 5) Complex tubular welded joint subjected to torsion and bending cyclic loading	1525849	7462	204

6.2 Summary and discussion of welded joint/case study fatigue analysis

With respect to the fatigue life predictions for the five case studies, according to the fatigue analysis of welded joints in the work presented in this thesis, the fatigue life to both crack initiation and propagation were calculated using the strain-life and LEFM method. The calculations were computed with and without the effect of the residual stress. It was found that for both crack initiation and propagation, the effect of residual stress on fatigue life is profound. The fatigue crack-growth lives in all of the cases studied were the same as or greater than the fatigue life to crack initiation. The following paragraphs discuss the experimental and the predicted fatigue life results based on a comparison of each experiment point to the predicted number of cycles to failure.

For the first case study (T-joint subjected to in-plane cyclic bending loading), the results were conservative for both the lower load level (F = 1320 N) and the higher load level (F = 2000 N), as shown in Figure 5-36 and Figure 5-37 In .the case of the T-joint subjected to in-plane cyclic loading of F = 1320, the predicted results were very conservative. The reason for the results obtained in this specific case study is that actual cracks in the experimental fatigue tests showed that the cracks were following the weld toe line: i.e., the cracks started growing from the edge of the gusset weld and later propagated around the edge until they became parallel to the gusset plate. This difference is due to the assumed planar crack model when the fatigue crack propagation life is calculated: i.e., the initial crack grows to its final size in a direction normal to the weld toe. It is therefore important to note that the fatigue life predictions are comparable to the experimental data up to 2c = t or 4 mm. Unfortunately, most of the experimental fatigue lives were not recorded for final cracks with 2c ≈ 4 mm; however, in experiments #16 and #17, the first crack size was 2c ≈ 4 mm. These results are

attributable to the variation in the welding techniques used for the experimental specimens. Another reason was the fact that the predictions were based on the assumption that the crack was planar whereas the actual cracks were growing around the gusset's weld line. Comparing the fatigue life of specimens with 4 mm cracks such as experiments # 16 and #17 is therefore reasonable. With respect to samples #16 and #18, the continuous weld that was nicely wrapped around the gusset edges resulting to longer fatigue lives. In sample #15, the welds were deposited at the gusset edge using a tack weld option, which caused the weld to stop at the corners, resulting in higher SCF-lower fatigue lives. Sample #RE3 did not involve a weld deposit around the gusset edge. The total fatigue life predictions for the T-joint subjected to in-plane cyclic loading of F= 2000 N were in better agreement, with a conservative factor of 5, compared with the experimental data because the high stress load level is less dependent on the accuracy of the assumed initial crack size.

For the second case study (tube-on-plate welded joint subjected to lateral cyclic loading), compared to case #1, the fatigue life predictions were better, for load levels of both 1000 N and 1225 N, as shown in Figure 5-64 and Figure 5-65. According to Figure 5-64, without the RS effect, the predicted fatigue lives are in better agreement than the experiments (#4, #5 and #13). The predicted fatigue lives with the RS effect underestimated the experiments (#4, #5 and #13) by an approximate factor of 2. The fatigue lives predicted using the local reference stress method can be considered reasonable, assuming that the test specimens (#4, #5, and #13) were stress relieved. According to the results shown in Figure 5-65 the ,fatigue lives predicted without the RS effect are in good agreement with the experiments (#2, #8, and #11), while the predictions that included the RS effect underestimated the fatigue lives compared to the experiments (#9, #10, and #12). The maximum fatigue life was underestimated by an approximate factor of 2. The predicted fatigue lives based on the local reference stress method are considered reasonable, assuming that the test specimens (#9, #10, and #12) were stress relieved.

For the third case study (T-joint weld subjected to out-of-plane cyclic loading), six specimens were tested in total, as detailed in Appendix A. This case study was conducted for two load levels, 304 N and 468 N, as illustrated in Figure A1- 28 and Figure A1- 29, respectively. The fatigue life predictions for the T-joint subjected to out-of-plane bending cyclic loading of F = 304 N (Figure A1-28) were more conservative (under-predicted) than the experimental data when the residual stress was not included in the calculation. However, for most of the specimen fatigue life span, the addition of

the RS improved the fatigue life prediction compared to experiment #6. In contrast, the other experimental specimens (#1 and #4) had only one fatigue life point, and both were marked as the first crack detected. This finding could mean that experiments #1 and #4 were interrupted or not observed as regularly as the specimen in experiment #6. The difference between the predicted life that included the residual stress and the experimental data could be attributed to several factors. Two possibilities could be overestimation of the initial crack size or the semi-elliptical crack shape.

The fatigue life predictions for the T-joint subjected to out-of-plane bending cyclic loading of F = 468 N (Figure A1- 29), were in good agreement with the experiments (#2, and #3). However, when the residual stress was not included in the calculation, the predictions overestimated the fatigue life by a factor of 2.5 when compared to experiment #5. It should be noted that experimental specimens #2 and #3 had only one fatigue life point, and both were marked as the first crack detected. This step could have been taken to check the crack initiation life and/or to check the crack shape and aspect ratio. Another explanation is that the experiments were interrupted or not observed as regularly as they should have been.

A total of eight specimens were tested for the fourth case study, as shown in Appendix A (square tube-on-plate welded joint subjected to a cyclic lateral loading). The experimental and predicted total fatigue lives for the square tube-on-plate welded joint subjected to lateral load levels of F = 21350 N, F = 13878 N, and F = 11565 N are as shown in Figure A2- 41, Figure A2- 40, and Figure A2- 39, respectively. For the first load level illustrated Figure A2- 41, only the fatigue data for sample #S4 Y were excluded from the comparison because the crack appeared at the lower weld toe. According to the rest of the results shown in Figure A2- 41, the predicted fatigue lives overestimated the fatigue life in general by a factor of 3 when the RS effect was not included. However, including the residual stress reduces the overestimation significantly. The addition of the RS effect in the fatigue life predictions for the square tube-on-plate welded joint led to the underestimation of the fatigue life compared to experiments #S2, and #S3 and to the overestimation of the fatigue life by factor of 1.6 to 2.3 compared to experiments #S5, #S6, #S7, and #S8. Therefore, it is reasonable to assume that the fatigue life prediction using the local reference stress is in good agreement with the experimental data.

For the second load level, illustrated by Figure A2- 40, eight specimens were tested in total, yet only in sample #S16 Y did the crack appear at the upper weld toe. The remainder of the experiments were thus not open to comparison. According to the results shown in this figure, the prediction of fatigue life without the effect of the RS overestimated the fatigue life. However, including the residual stress resulted in a more conservative fatigue life prediction by a factor of 2 compared to the number of cycles to failure in experiment #S16. In the third load level, illustrated in Figure A2- 39, only one specimen was tested (# S9 Y), and no crack was observed on the surface of the specimen. Comparing sample #S16 Y, subjected to F = 13878 N, to sample #S9 Y, subjected to F = 11565 N, indicates that the crack did not initiate because the load applied to the latter sample was too low. In conclusion, this case study demonstrated that the fatigue life predicted based on the proposed shell FE local reference stress data overestimated the fatigue life when the residual stress effect was not included. However, including the residual stress reduces the overestimation significantly and results in conservative fatigue life predictions.

A total of nine specimens were tested for the fifth case study, detailed in Appendix A (complex tubular welded joint subjected to torsion and bending cyclic loading). The experimental and predicted total fatigue lives for this case study were subjected to load levels of F = 3000 lb and F = 4000 lb, as shown in Figure A3-29 and Figure A3-30, respectively. Two specimens were tested for the 3000 lb load of and, according to the results shown in Figure A3-29, the fatigue life predictions were in good agreement with the experimental fatigue data when the residual stress effect was included in the calculations. Including the RS resulted in more conservative fatigue life predictions by factors of 2 and 3 compared to the experimental fatigue lives of specimens #3 and #9, respectively. Sample #13 seemed to have the crack growing around the weld after the crack size reached approximately 1in, which differs from the planar assumption used for the fatigue life predictions. On the other hand, seven specimens were tested with a load of F = 4000 lb, and the fatigue lives were used for a comparison, as shown in Figure A3-30. According to the results in this figure, the fatigue lives show good agreement with the experimental fatigue data when the residual stress was included. Including the residual stress proved to be important for evaluating the fatigue life of welded joints. Sample #11 seems to exhibit a different fatigue data trend than other experimental samples, which may have been stress-relieved, or the residual stress might not have formed as in the other specimens. The comparison is nonetheless reasonable up to a crack size of 1in since the cracks in the experimental

specimens grew around the weld toe line, which differs from the planar crack assumption used for the predicted fatigue lives. In conclusion, except in sample #11, adding the residual stress effect in the prediction calculations overestimated the fatigue life by an approximate factor of 2.

In summary, comparisons of the fatigue lives in most of the case studies revealed results that were conservative by an estimated average factor of 2 or less. The shell FE local reference stress method proved able to produce the consistent and accurate stress data required for the fatigue life analysis of welded joints. The work presented here can be improved in order to obtain more accurate stress data, but the general method of determining a reference stress that can supply accurate and consistent stress data for all of the three well-known fatigue analysis methods has been successfully validated.

It is recommended that the stress prediction be improved for the gusset or T-joint weldment type by enhancing the meshing technique near the gusset edges. To determine the stresses of a structure with different plates of varying thicknesses, the choice of weld shell thickness requires more study when the proposed method is used. The thickness of the shell element that simulates the weld is very important with the proposed method because it affects joint stiffness. The recommendation that accompanies the use of the proposed method is that the thickness of the weld shell element should be equal to the thinner of the welded plates or twice the thinner plate.

6.3 Recommendation for future work

Of the general steps in fatigue life evaluation, the proposed methodology is focused mainly on the stress analysis step, thus making accurate stress evaluation the key to improving the current work. One challenge with the current work is to establish the SCFs for the cases under investigation. The SCF equations are limited to specific welding geometries and could be improved to cover more practical cases and provide more accurate stress analysis. Another challenge could be the determination of the SIF if neither handbooks nor weight functions can provide the value of the SIF, as in case of a plate with a variable thickness. A very preliminary investigation was conducted with respect to both challenges in order to set the path for future work that can enhance the research presented here.

It is important to improve the SCF equations because of their geometry limitations and because even a small change in the SCF value can affect the fatigue life evaluation. The SCF affects the peak stress and the fatigue life to crack initiation accordingly. The SCF also affects the through-thickness

distribution based on Monahan equation and the fatigue crack growth consequently. Improving the SCF can be achieved by conducting a parametric study using FE technique. This will help to assess the accuracy of the fatigue life predictions of weldments when using the proposed shell FE local reference stress method.

Some investigation was done by the author to highlight the challenges of finding the SCFs. The FE technique was used to find the SCFs for a T-joint weld type subjected to tensile loading. The way that the SCF was determined can be used in the future to formulate new SCF expressions that can cover wider range of welding geometries.

It was expected from the existing SCF equations that the SCF curve versus the ratio of the weld toe radius ρ/T increases exponentially to infinity for the case of the very small $\rho/T \approx 0$. This is not entirely true, because the conducted FE results provided a curve that tends to stabilize at a certain value rather than going to infinity when the main plate thickness is large compared to the attachment plate width ratio ($L/T < 1.5$). In other words, the existing SCF equations provide reasonable results within their limitations only if the attachment width L/T is larger than 1.5 (for T-joints under tension). However, having a large SCF will cause a significant underestimation of the fatigue life-to-crack initiation due to an overestimation of the peak stress magnitude. It will also affect the fatigue life propagation of small cracks through an overestimation of the main plate through-thickness stress distribution. Therefore, few sets of FE models of T-joints, subjected to pure tensile loading, were conducted to evaluate the SCF when using different welding geometries. The considered geometrical features were the weld angle θ or α, the weld toe radius ρ, the attachment width L, and the main plate thickness T or t. Brennan's latest SCF formula for T-butt (T-joints) under tension was used to validate the FE modelling [67]. The SCF expressions to date were limited to certain geometries. The :s work'following weld geometries were the most general used in Brennan

- Weld angle: $30° \leq \theta \leq 60°$
- Attachment width ratio: $0.3 \leq L/T \leq 4.0$
- Weld toe radius ratio: $\frac{1}{100} \leq \rho/T \leq \frac{1}{15}$

The proposed sets of FE models had geometrical variation that went further than any previous work for T-joints under tension loading. The following weld geometries were used in the proposed work:

- Weld angle: $30° \leq \theta \leq 75°$
- Attachment width ratio: $0.3 \leq L/T \leq 36$
- Weld toe radius ratio: $0.01 \leq \rho/T \leq 1$

Some of the modelling was conducted with extreme geometrical values to verify some important notes. For example, the weld angle used was $\theta = 75°$, where the attachment width ratio L/T used was 0.08 and ρ went down to 0.001. The FE data and the resulting stress concentration factors provided interesting findings after being analyzed. It has been found that the reduction of the attachment width ratio L/T reduces the rapid increase expected from the small weld toe radius ratio $\rho/T \approx 0$ and large weld angle $\theta \approx 75°$ significantly. This phenomenon became more apparent when the FE sets were conducted and the results were validated against Brennan's FE results for T-joints under tension.

6.4 Stress concentration factor for a T-joint subjected to tensile loading

The FE software package ABAQUS was used to estimate the SCF of T-joints subjected to tensile load. Following Brennan's FE modelling, the models were conducted with a two-dimensional plane stress analysis with eight node shell elements. This was done so the resulting SCF would be valid for comparison with Brennan's SCF. One of the models and the applied boundary conditions is shown in Figure 6-1.

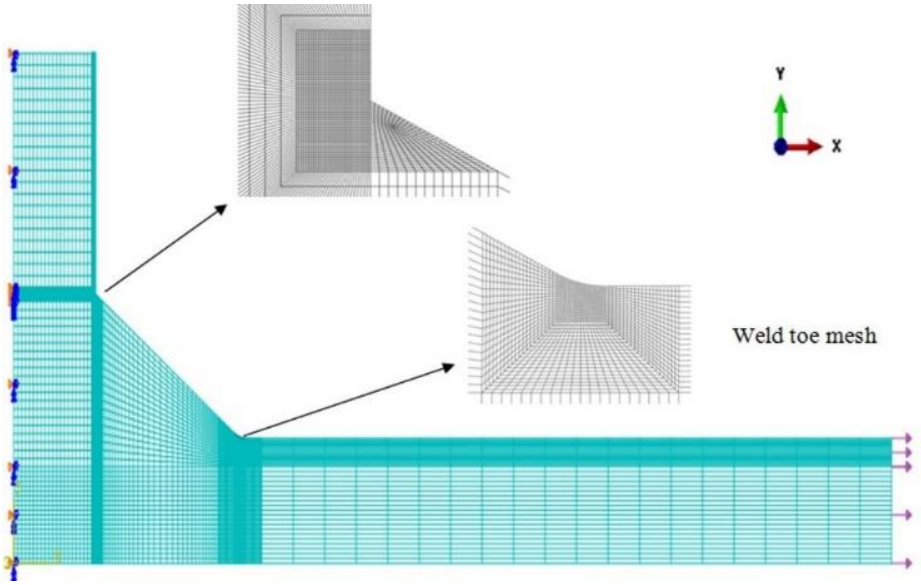

Figure 6-1: T-joint meshing pattern and boundary conditions (half model)

The left vertical edge of the model was the edge of symmetry, and it was restrained in the x-direction. The load was applied on the right edge in the x-direction. According to the International Institute of Welding (IIW) [17], the mesh size was chosen to be less than 1/6 of the weld toe radius ρ, as linear elements were used in the analysis to ensure convergence at critical areas where the maximum stress is expected to occur. The maximum stress is expected to occur at the weld toe surface, as shown in Figure 6-2, but the exact location varies at the weld toe area in each model. Sometimes, the SCF appeared in the root, which will be discussed later. The maximum principle stress was recorded at the weld toe surface and normalized by the applied stress to evaluate the SCF value since the principle stress is larger than the axial maximum stress. The stress contours and the maximum principal stress location are shown in Figure 6-2 for one of the FE models.

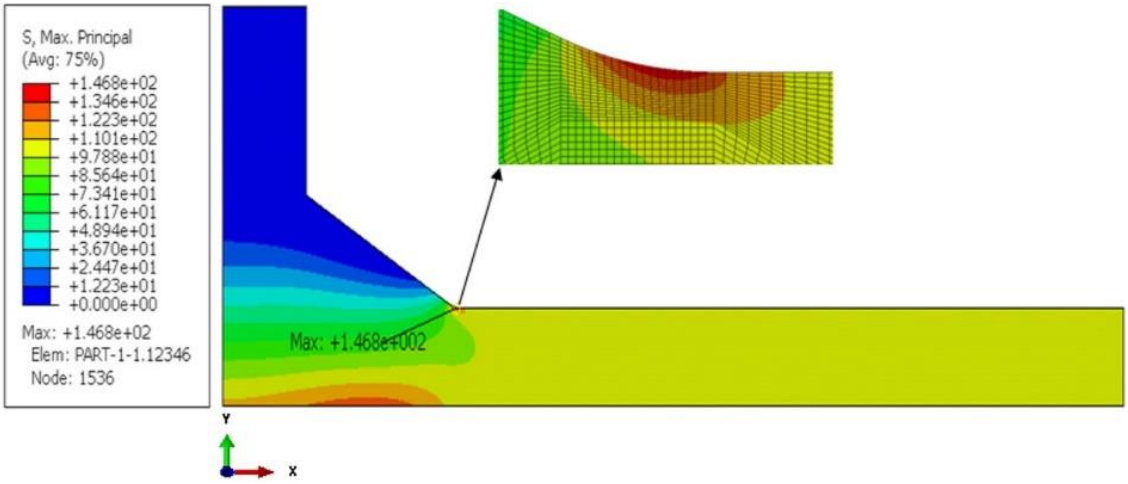

Figure 6-2: Stress contours of a T-joint under tension

The FE results are presented as the SCF versus the weld toe radius ratio ρ/T, as shown in Figure 6-3, to show the newly discovered curve that needs to be analyzed and fitted to come up with a new SCF formula.

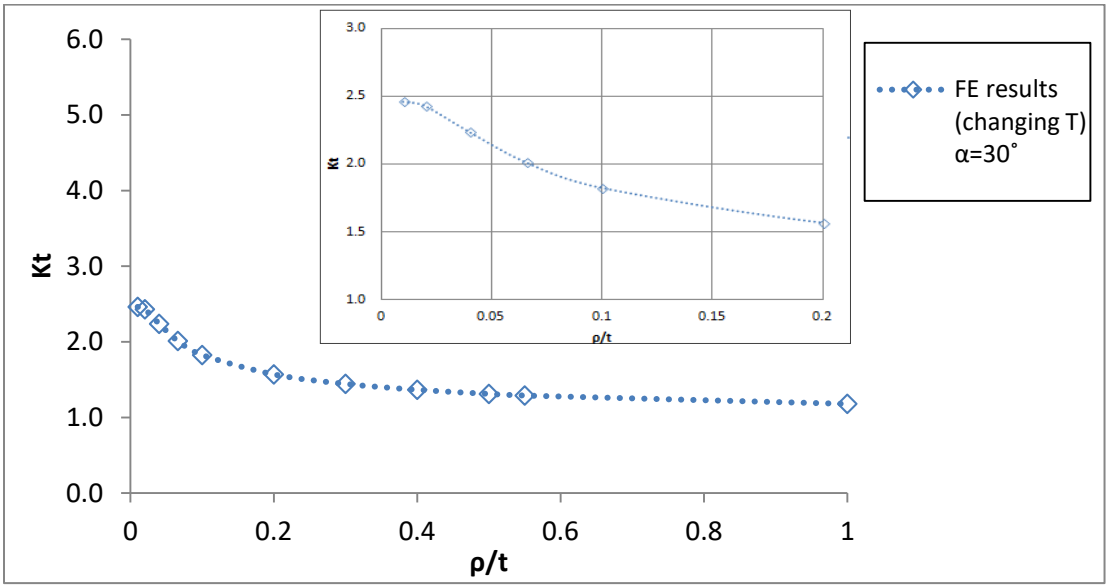

Figure 6-3: SCF results for a T-joint under tension with a weld angle θ = 30˚

The above results show that the SCF is reaching the value of 2.5 as ρ/T is reaching 0. All the FE T-joint model geometries were fixed except for the main plate thickness. This would change both ratios, ρ/T and L/T, simultaneously. However, previous SCF equations were formulated based on fixed L/T, and most have L/T >1.5 except for Brennan and Tsuji's equations. Knowing that, the modelling was done several times using different geometric variations to make sure that it is not a modelling error. Geometries of one of the FE modelling of a T-joint under tension load as an example of the geometric variation are shown in Table 6-4.

Table 6-4: Modelling geometries of the T-joint under tension load with the weld angle θ = 30˚

FE results (changing T) θ=30˚					
ρ (mm)	**L (mm)**	**T (mm)**	**ρ/T**	**L/T**	**FE SCF K_t**
1.32	**40.5**	**132**	**0.01**	**0.31**	**2.46**
		66	**0.02**	**0.61**	**2.43**
		33	**0.04**	**1.23**	**2.24**
		20	**0.066**	**2.02**	**2.01**
		13.2	**0.1**	**3.07**	**1.83**
	43.27	**6.6**	**0.2**	**6.56**	**1.57**
	45.07	**4.4**	**0.3**	**10.24**	**1.44**
	45.97	**3.3**	**0.4**	**13.93**	**1.37**
	46.50	**2.64**	**0.5**	**17.62**	**1.31**
	46.70	**2.4**	**0.55**	**19.46**	**1.29**
	47.58	**1.32**	**1**	**36.05**	**1.18**

The end results were compared to Brennan's equation since his equation, which was formulated based on FE models, accounted for the attachment width ratio, L/T, variation in addition to having a small L/T ratio less than 1.5. Figure 6-4 and

Figure 6-5 are from Brennan's work and validate the current work.

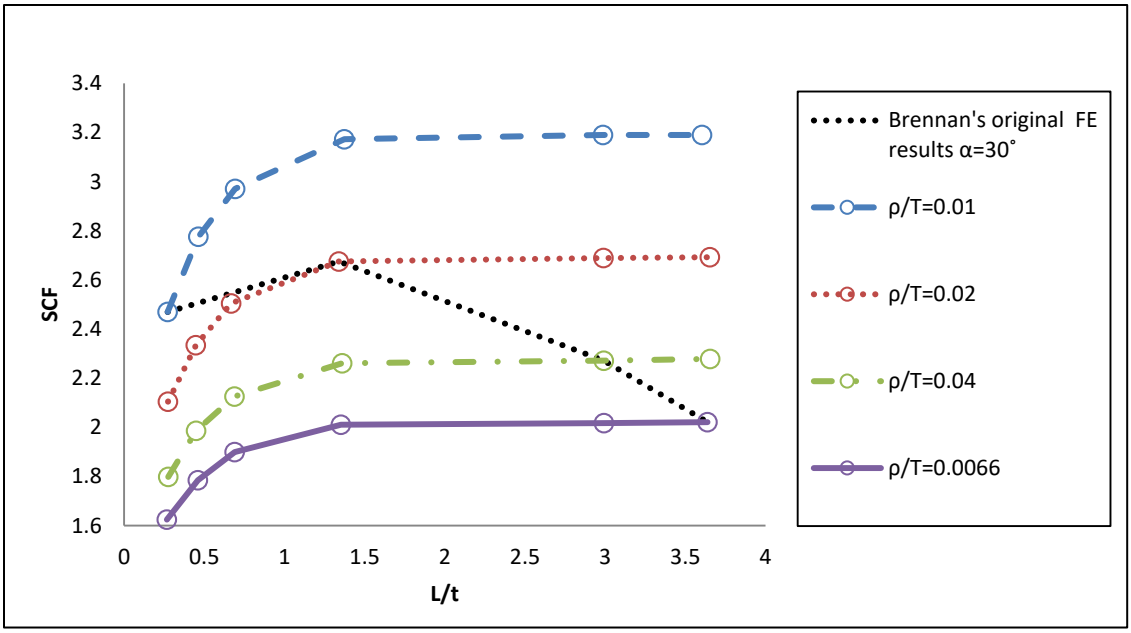

Figure 6-4: Digitized graph using Brennan's FE results for T-joints under tension load with θ = 30˚ [67]

Brennan modelled T-butt T-joints that had a weld angle of θ = 30˚ and varies the geometries of both ratio ρ/T and L/T. the trend of the proposed FE results shown earlier in Figure 6-3 is consistent with the black hashed line drawn into Brennan's FE modelling results as shown in Figure 6-4. To explain in more detail, both ratios, ρ/T and L/T, from Brennan's work should be compared to the proposed FE modelling, as shown in the figure below.

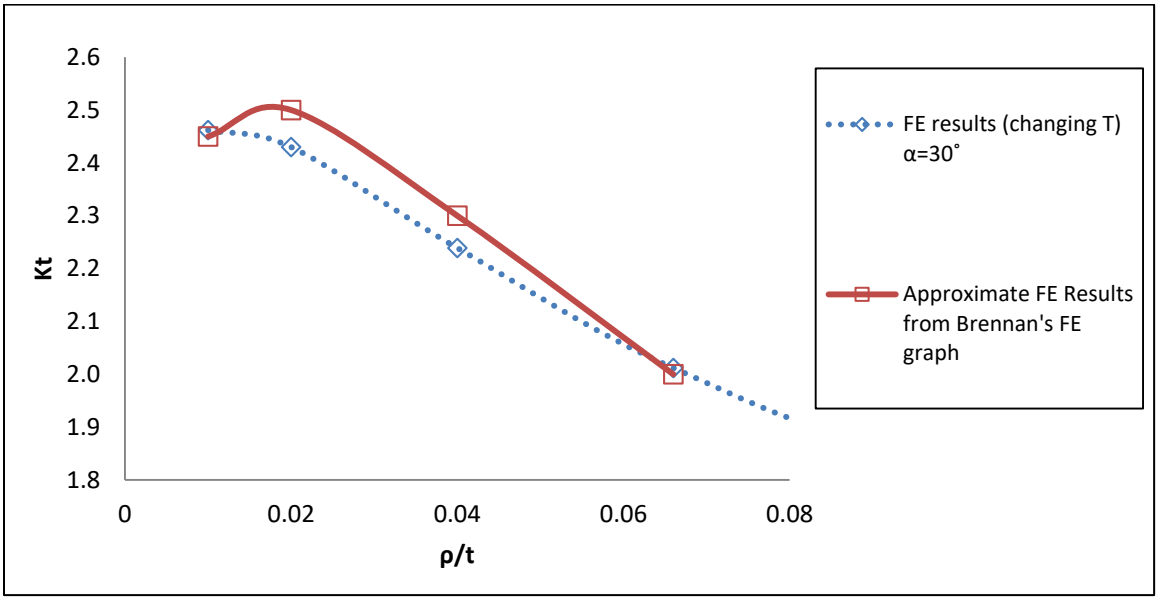

Figure 6-5: FE comparison between the proposed work and Brennan's SCF results for a T-joint subjected to tension with a weld angle θ = 30˚

The difference in the curves above is due to the way Brennan evaluated the SCF result based on the maximum normal stress in the direction of the load while the proposed FE modelling results were based on the principle stress rather than the maximum stress according to [68]. It is noted from Figure 6-6 that the reduction of the ratio L/T will affect the SCF despite the fact that ρ/T is becoming very small. In other, words the ratio L/T is a very important geometry factor in T-butt joint shapes, which has been considered only by Brennan and not by other SCF equations except for Tsuji [68] who included the effect of the attachment length ratio to the main plate thickness, L/T in his FE modelling but did not included it as a factor in his SCF formula. Therefore, after observing Brenan's results, it was confirmed that the FE results conducted by the author were genuine. However, if the SCF equations were formulated based on L/T being greater than 1.5, such as in Monahan and Ushirakawa, the curve would be exponential, which was confirmed by the trend of the red hashed line shown in Figure 6-6 as a result of the proposed FE modelling.

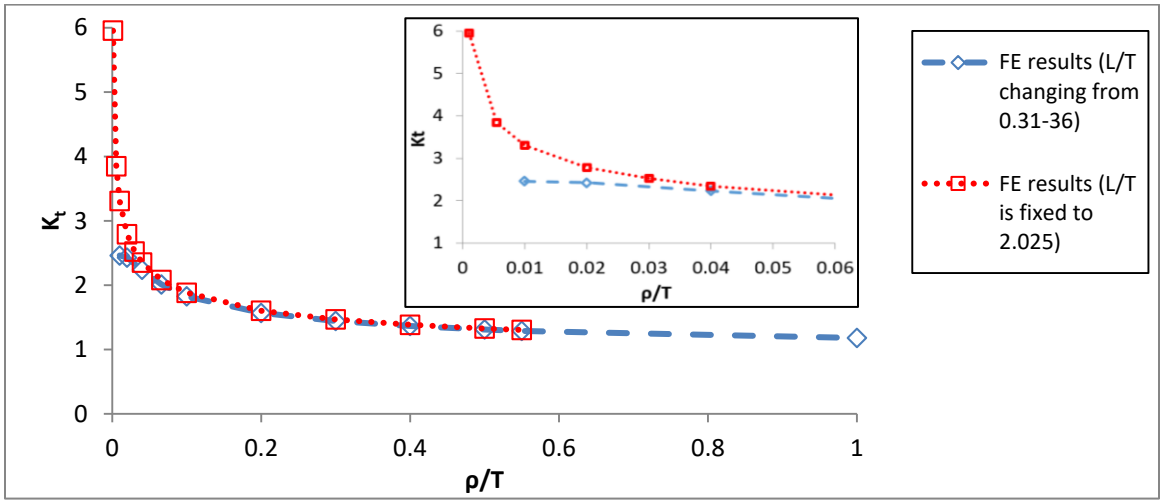

Figure 6-6: Comparison between FE results when changing the weld toe radii and main plate thickness

The red curve was the result of modelling the T-joint subjected to the tensile load with fixing L/T = 2.025 and changing the weld toe radius ρ to a very small number. It is evident that the relation is exponential in case the factor L/T is greater than 1.5. The blue hashed curve represents the SCF results when fixing the weld toe radius ρ and varying the main plate thickness T to a very large number which resulted in reducing the ratio L/T. As a result, the SCF curve stabilized rather than increasing exponentially. The geometry used for modelling the SCF curves in Figure 6-6 are shown in Table 6-5. K_t

Table 6-5: Geometries used for modelling the SCF of a T-joint subjected to tensile load

FE results					
Changing main plate thickness T (θ=30°)			Changing weld toe radius ρ (θ=30°)		
ρ/T	L/T	Kt	ρ/T	L/T	Kt
0.01	0.31	2.46	0.001	2.025	5.956
0.02	0.61	2.43	0.006	2.025	3.849
0.04	1.23	2.24	0.010	2.025	3.31
0.066	2.02	2.01	0.020	2.025	2.791
0.1	3.07	1.83	0.030	2.025	2.524
0.2	6.56	1.57	0.040	2.025	2.352
0.3	10.24	1.44	0.066	2.025	2.081
0.4	13.93	1.37	0.100	2.025	1.883
0.5	17.62	1.31	0.200	2.025	1.603
0.55	19.46	1.29	0.300	2.025	1.468
1	36.05	1.18	0.400	2.025	1.385
			0.500	2.025	1.327
			0.550	2.025	1.305

The problem found in the industry is which SCF value should be taken for the fatigue life calculations if such a case were to occur. The solution should mainly depend on the attachment width ratio L/T, whether it is more or less than 1.5. It can be said that, for a T-joint under a tensile load, the existing SCF equations give reasonable results only if L/T is larger than 1.5, despite the small range of geometric validity. If the ratio L/T is smaller than 1.5, then a new SCF should be established to account for the attachment width effect on K_t or the SCF value. In addition, it has been noticed that when ρ/T is less than 0.55, the maximum principal stress occurs in the weld root rather than the weld toe, as shown in

Figure 6-7. This would be one reason why most of the SCF equations are valid for $\rho/t \leq 0.4$. However, the maximum principal stress at the weld toe is very close to that at the weld root. Thus, more FE modelling should be done to investigate this case.

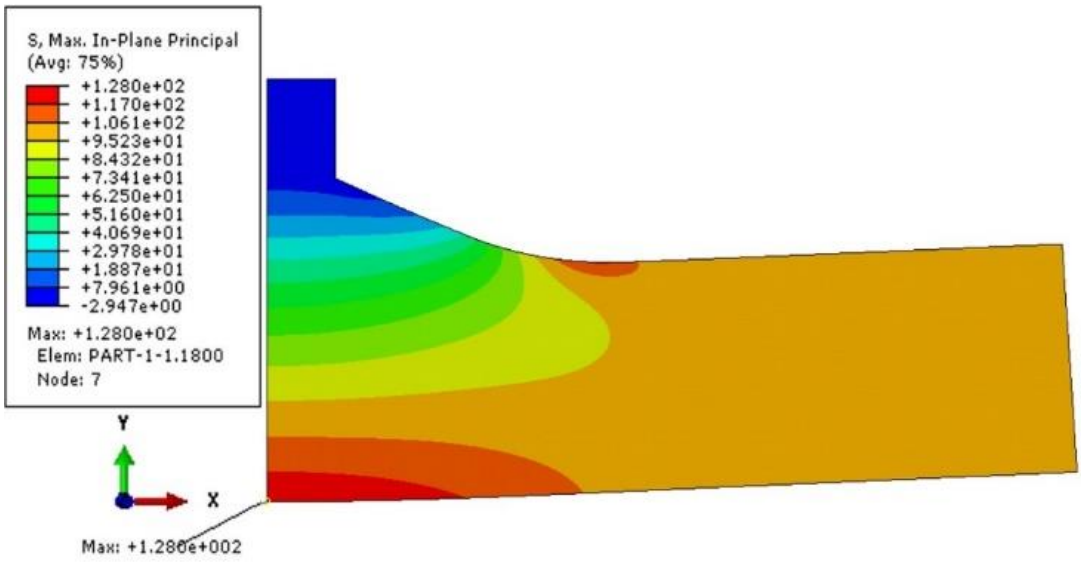

Figure 6-7: The maximum principal stress at the weld root.

As noted from studying the SCF equations up to date, the difference between two SCF curves for a T-butt weld under tension with weld angle θ=30° and θ=60° should be large and noticeable. The larger the weld angle θ, the larger the SCF. However, the conducted FE models showed that having L/T be less than 1.5 appeared to reduce not only the rapid increase caused by the small weld toe ratio ρ/T but also reduce the difference expected from a large weld angle. to confirm that the unexpected FE results are valid , the model geometries of two FE modelling sets (A and B) are compared to (C

and D) as shown in Table 6-6 and Figure 6-8, which show the calculated SCF using Brennan's simple equation for validation.

Table 6-6: FE model geometries

Curve A

FE Changing T α=30		
ρ/T	L/T	Kt
0.01	0.31	2.46
0.02	0.61	2.43
0.04	1.23	2.24
0.066	2.02	2.01
0.1	3.07	1.83
0.2	6.56	1.57
0.3	10.24	1.44
0.4	13.93	1.37
0.5	17.62	1.31
0.55	19.46	1.29
1	36.05	1.18

Curve C / Curve D

Changing ρ Brennan α=30°			Changing ρ Brennan α=75°		
ρ/T	L/T	Kt	ρ/T	L/T	Kt
0.010	3.91	3.66	0.010	3.39	4.15
0.020	3.87	2.93	0.020	2.51	3.16
0.040	3.91	2.40	0.040	3.39	2.66
0.066	3.91	2.11	0.066	3.39	2.32

Curve B

FE Changing ρ α=75		
ρ/T	L/T	Kt
0.01	0.08	2.60
0.01	0.16	2.61
0.02	0.32	2.59
0.04	0.65	2.45
0.07	1.07	2.22
0.10	1.62	1.97
0.20	4.64	1.64
0.30	8.33	1.49
0.40	12.01	1.41
0.55	17.54	1.32
1.00	34.13	1.27

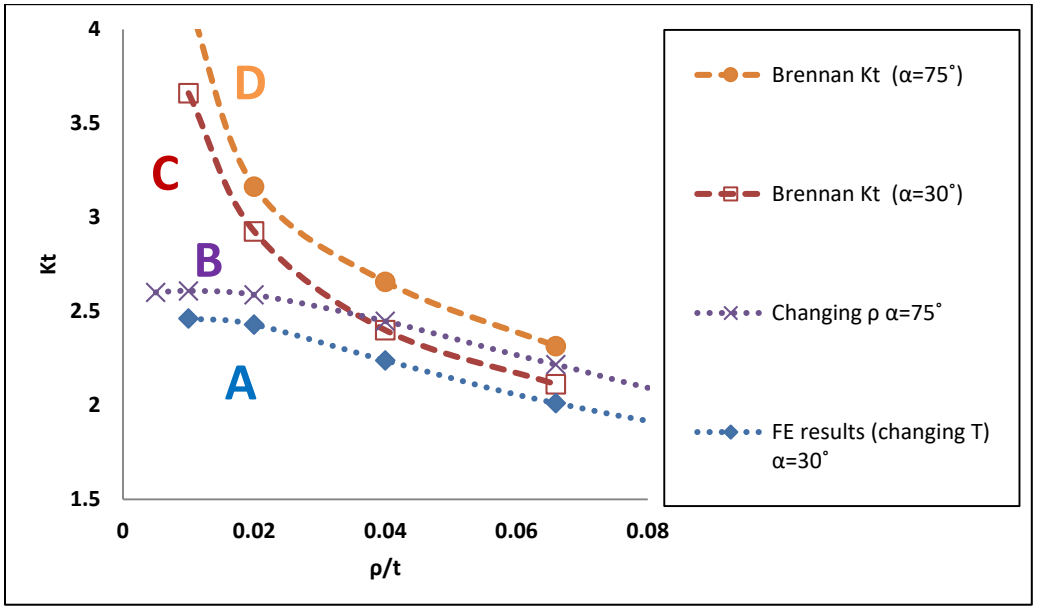

Figure 6-8: Comparison between FE and Brennan SCF equations for a T-butt under tension.

The difference shown in Figure 6-8 between curves A and B seems to be in agreement with the difference calculated using Brennan's simple equation in C and D. It is important to note that Curve B was for a weld angle of θ=75° and should be higher than C, which had θ=30°. It is evident that the ratio L/T affects not only the rapid increase expected from ρ/T but also reduces the increase expected from large weld angles.

To conclude the work to date, the following points are summarized:

- Brennan's formula accounts for the attachment size L/T and provides important information.
- It is only fair to compare FE results that have L/T > 1.5. Otherwise, the comparison is not valid, and this accounts for the differences in SCF equations.
- The SCF tends to decrease when L/T decreases to less than 1.5. In addition, the effect of L/T becomes stable when L/T is larger than 1.5, hence the exponential behavior.
- It is confirmed that the reduction of L/T ratio below 1.5 will reduce the SCF to a constant value despite the fact that ρ/T is getting smaller. Moreover, the same trend is expected for the bending load.
- The attachment width to main plate thickness ratio L/T is a major factor that affects both the weld angle θ and weld toe radius to the main plate thickness ratio ρ/T.
- A new SCF formula should be formulated to account for attachment size effect when L/T < 1.5 for T-joints subjected to tension and bending load.
- When modelling ρ/T greater than 0.55, the maximum principal stress in the direction of the tensile load no longer occurs at the weld toe but at the weld root instead.

6.5 Evaluating the stress intensity factor (SIF) for edge and central cracks with variable thickness using three-dimensional FEA

The available stress intensity factor solutions in handbooks are for constant thickness cases. Thus, the FE method will be used to assess several edge and central crack problems with variable thicknesses. The aim is to find a relationship that correlates the available well-known stress intensity factors based on constant thickness to the stress intensity factors based on variable thickness. This could assist in fatigue life predictions using the LEFM method.

The presented work in the following sections includes 3D-FE stress intensity factors (SIF/K-solutions) for different types of edge and central crack modelling with variable thickness. In addition, this section shows how to use the FE to model a 3D edge and central crack. Finally, the resulted 3D-FE SIF will be compared to FALPR results.

FALPR software was used along with the weight function to calculate the regular SIF. The weight function method can calculate the SIF regardless of the applied load. FALPR is able to produce accurate SIF results for two-dimensional (2D) edge and central cracks. One can put the load into FALPR and evaluate the corresponding SIF. However, FALPR is based on the assumption that the

crack thickness is constant. Therefore, the SIF from FALPR was found by scaling the applied load to account for the variable thickness. This was based on the fact that the different thickness has different load value over the area. The main focus was to relate the 2D weight function of a constant thickness edge crack to the 3D edge crack with variable thickness. This was also done for central cracks as well. Six sets of FE 3D modelling for the edge and central crack cases were conducted using the quadratic 3D element via ABAQUS software. The shape and geometries of the 3D FE modelling sets were as follows:

Table 6-7: 3D FE Models' geometries for cracked plates with variable thicknesses.

Model name	**Model shape**	
Tapered edge crack	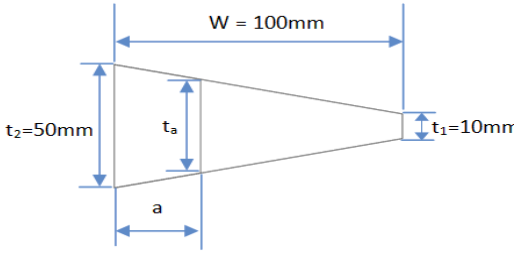 Thick to thin tapered edge crack (Tapered TKTN)	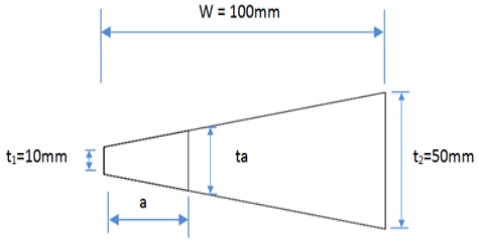 Thin to thick tapered edge crack (Tapered TNTK)
Central crack with trapezoidal section	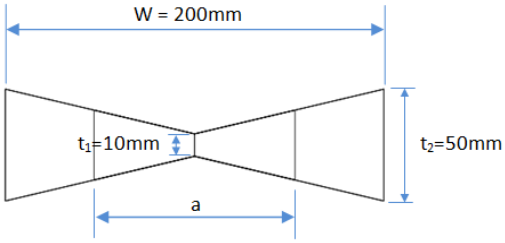 Thin to thick central crack (CCTK)	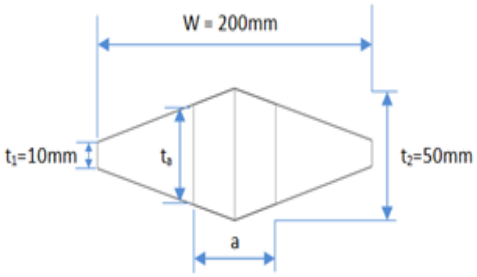 Thick to thin central crack (CCTN)

Edge crack with two different thicknesses	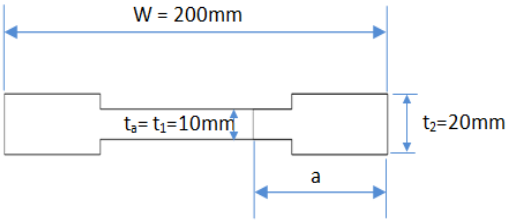 Thick to thin edge crack (Edge TKTN)	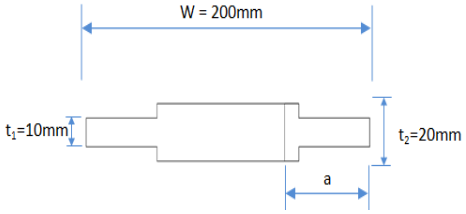 Thin to thick edge crack (Edge TNTK)

6.5.1 FE modelling of the tapered edge crack with variable thickness

The FE modelling sets were subjected to a tensile load on one side while fixing the other side. The symmetry advantage was taken for all the sets when suitable. An example of the thin to thick edge crack 3D model is shown in

Figure 6-9.

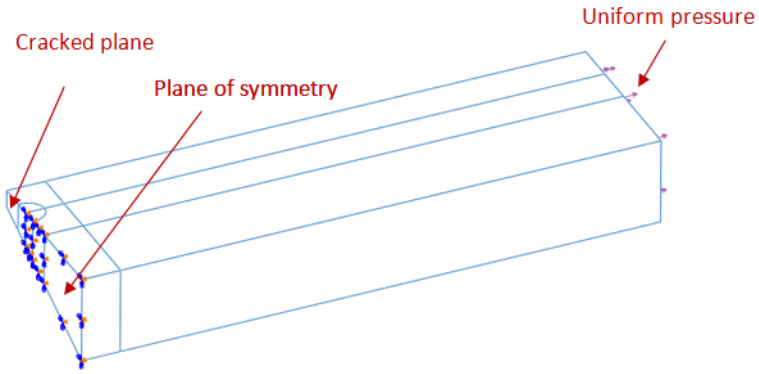

Figure 6-9: Edge crack with variable thickness

First, a 3D flat plate with an edge crack was modelled to verify the procedure of calculating the stress intensity factor. Then, the stress intensity factor from the FE software ABAQUS was compared to the well-known 2D edge crack in an infinite plate. The stress intensity factor was taken from ABAQUS within contours that are 0.15% to 3% the crack size. In other words, the distance from the crack tip or front to the last contour was 3% of the crack size. In addition, the triangular elements used in the first contours have an angular resolution for LEFM of 10˚ to resolve the angular

dependence of the strain field around the crack tip [64]. The following figure demonstrate the 3D FE meshing rules of the tapered edge crack with variable thickness.

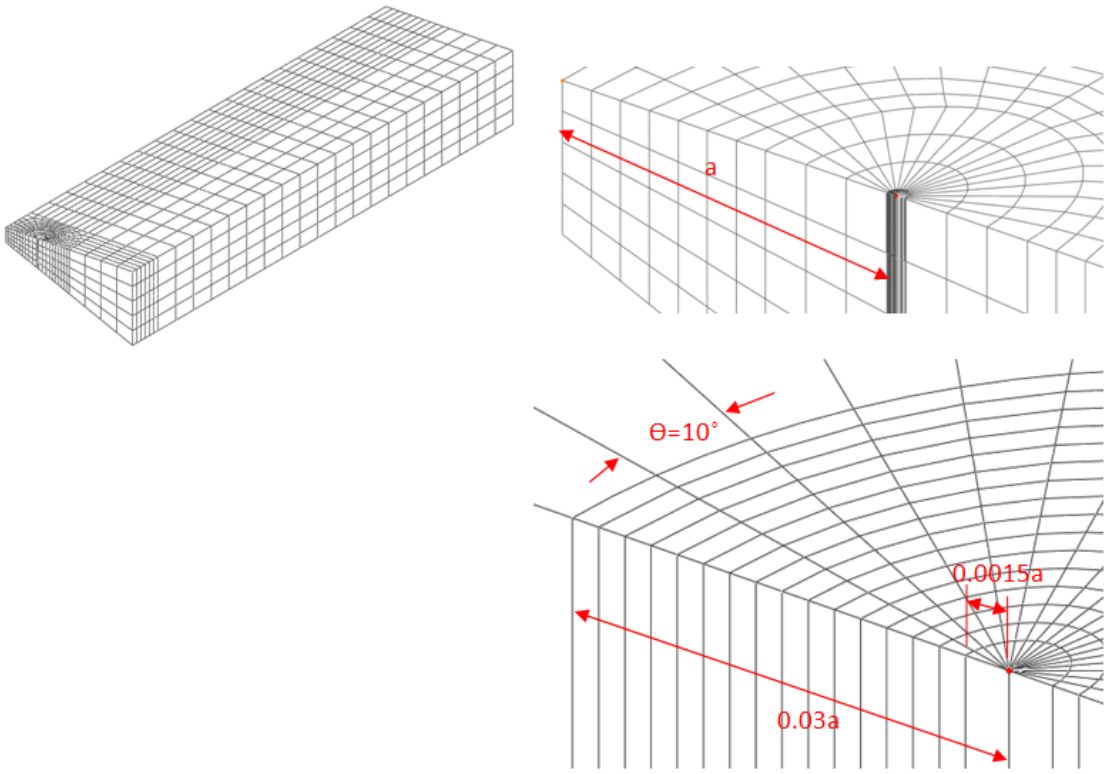

Figure 6-10: Tapered edge crack meshing rules

By observation and checking the ABAQUS manual, the stress intensity factor calculated by ABAQUS was for a plain strain case. This was done by comparing the stress intensity value K_I and J-integral at the same contours around the crack. The values of the SIF at the surfaces were neglected, and the results were taken from the middle of the thickness [64]. The location where the SIF values were recorded through the modelled edge crack thickness is shown in Figure 6-11. A comparison between the SIF of an edge crack (flat plate) with constant thickness and an edge crack with variable thickness is also shown in Figure 6-11.

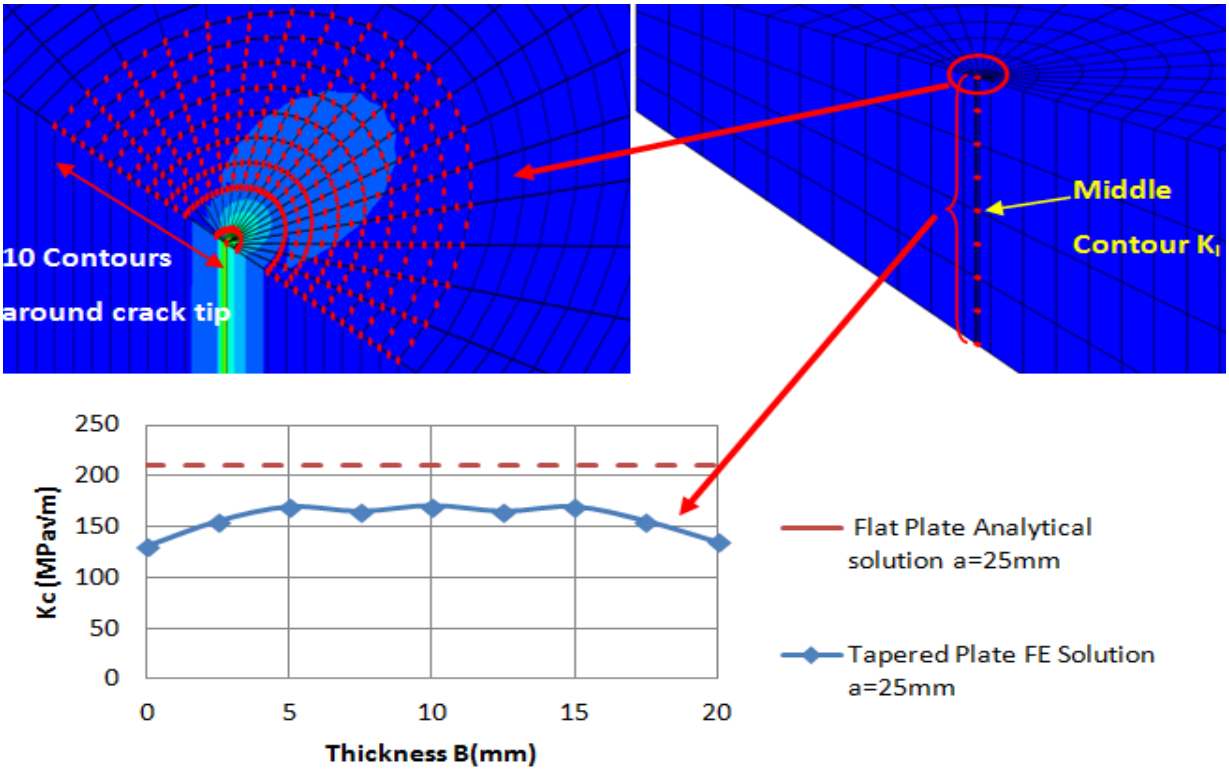

Figure 6-11: K_I values through the crack thickness

The thin to thick (TNTK) edge crack (Figure 6-9) is compared to the flat plat SIF solution. The FE results were less than the 2D solution as expected because the same load was applied over two different areas resulting in different stresses. After confirming the modelling and the boundary conditions, the SIF for the cases in Table 6-7 were conducted.

The SIF from FALPR was found by scaling the applied load to account for the change of thickness. In 2D crack problems, the weight function works fine regardless of the thickness since it is assumed to be constant. The applied load in FALPR over the cracked area was scaled according to the ratio of the crack edge thickness, t_a to the largest and smallest model thickness, t_1 and t_2, respectively. The results for each case are shown in the following sections.

6.5.2 Stress intensity factors of tapered edge crack with variable thickness

Two cases were modelled for the edge crack with trapezoidal sections. The first is called the thick to thin (TKTN) edge crack (see Figure 6-12) while the other is called thin to thick (TNTK) edge crack (see Figure 6-13). Comparison of both cases and the differences are shown in Table 6-8 and Table 6-

9. The applied load into FALPR SIF calculations was scaled based on the ratio of the crack edge thickness, t_a to the largest and smallest model thickness, t_1 and t_2, respectively. In other words, for the TKTN case the scaling factor was (SF=t2/ta) whereas (SF = t1/ta) for the TNTK case.

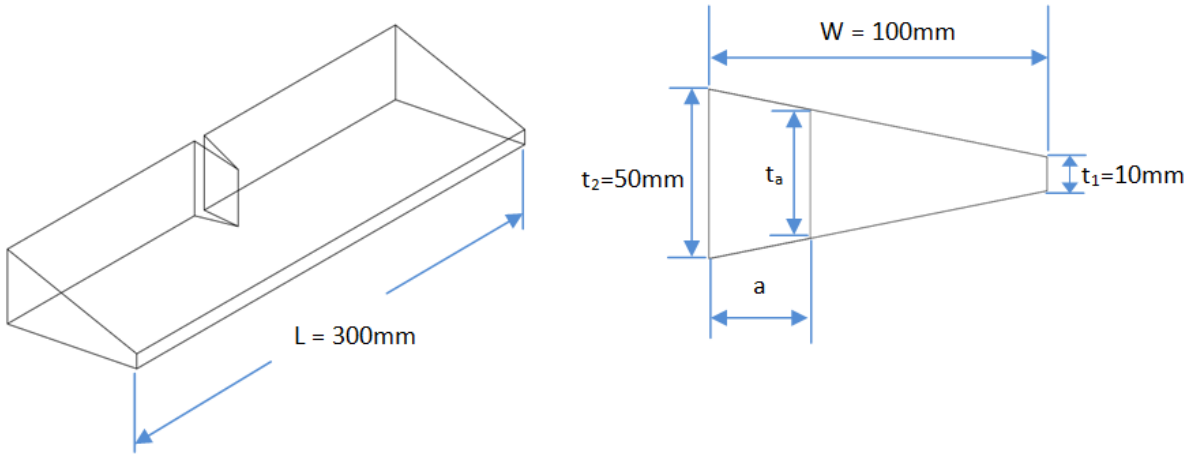

Figure 6-12: Thick to thin (TKTN) trapezoid edge crack geometry and annotations

Table 6-8: Comparison between the FE and FALPR stress intensity factors for the thick to thin (TKTN) trapezoid edge crack

Thick to Thin (TKTN)			
a (mm)	K_I (MPa$\sqrt{m}$)		
	FALPR- K_I (MPa$\sqrt{m}$)	FE- K_I (MPa$\sqrt{m}$)	Error%
20	187.46	216	-15.22
40	464.16	576	-24.10
60	1,359.08	1,831	-34.72
75	4,032.78	4,899	-21.48
AVG			-23.88

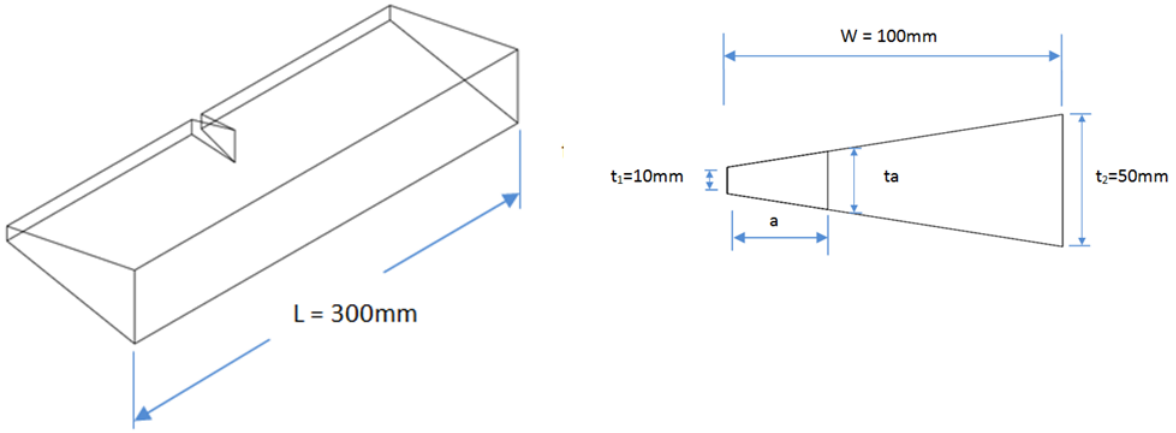

Figure 6-13: Thin to thick (TNTK) trapezoid edge crack geometry and annotations

Table 6-9: Comparison between the FE and FALPR stress intensity factors for the thin to thick (TNTK) trapezoid edge crack

Thin to Thick (TNTK)			
a (mm)	K_I (MPa$\sqrt{m}$)		
	FALPR- K_I (MPa$\sqrt{m}$)	FE- K_I (MPa$\sqrt{m}$)	Error%
10	94.84	93.14	1.79
25	163.87	160.3	2.18
40	259.94	254.71	2.01
60	538.04	545.82	-1.45
80	1649.18	1608	2.50
AVG			1.41

The average differences between the modelling and the proposed scaled SIF using FALPR were 15 to 24% for the case of TKTN and 2 to 2.5% for the case of TNTK as shown in Table 6-8 and Table 6-9, respectively. The scaled FALPR results underestimated the SIF for the TKTN case while overestimating the values in the case of TNTK when compared with the FE results. The FALPR SIFs are in a good agreement when the crack is from the thinner side (TNTK), whereas in the other case, the error is higher as shown by the red curve in Figure 6-14. It is believed that the error in the thick to thin case (TKTN) involves more bending force when the crack is deep (a > 40mm).

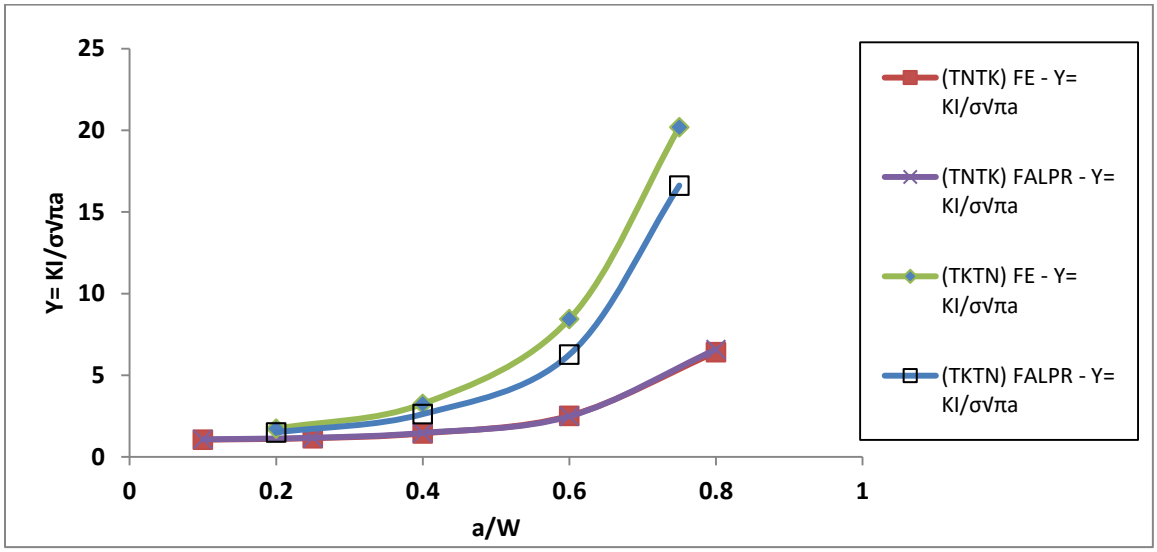

Figure 6-14: Comparison between FE and FALPR stress intensity values

The used method to scale the applied load to compensate for the difference or change of thickness works in the case of TNTK more than the TKTN. In conclusion, the proposed scaling method works fine for both cases of tapered edge crack only up to crack sized a = 40 mm as shown in Figure 6-14. It is obvious that applying the scaling method works for the case of TNTK up to a = 80 mm. Nevertheless, it is a start and could be modified with another scaling method that account for the bending moment expected to cause the increasing error for the TKTN.

6.5.3 Central crack with trapezoidal section

Two cases were modelled for the central crack with trapezoidal sections. The first is called the central crack with thinner center (CCTK) shown in Figure 6-15 while the other is called central crack with thinner center (CCTN) shown in Figure 6-16. Comparison of both cases and the differences are shown in Table 6-10 and Table 6-11. The applied load into FALPR SIF calculations was scaled based on the ratio of the crack edge thickness, t_a to the largest and smallest model thickness, t_1 and t_2, respectively.

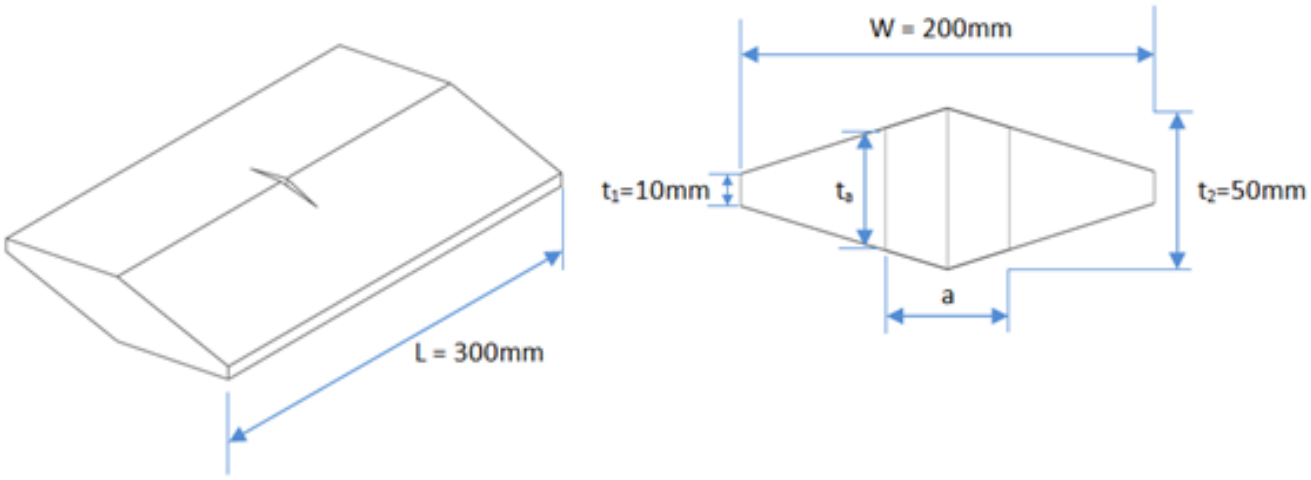

Figure 6-15: Central crack with variable thickness (CCTK) geometry and annotations

Table 6-10: Comparison between the FE and FALPR stress intensity factors for central crack with thicker center

Central Crack Thin To Thick (CCTK)			
a (mm)	**FALPR - KI (MPa√M)**	**FE- KI (MPa√M)**	**Error %**
20	**137.84**	**145**	**-5.19**
40	**233.57**	**263**	**-12.60**
60	**391.5**	**457**	**-16.73**
80	**808.4**	**935**	**-15.66**
AVG			**-12.55**

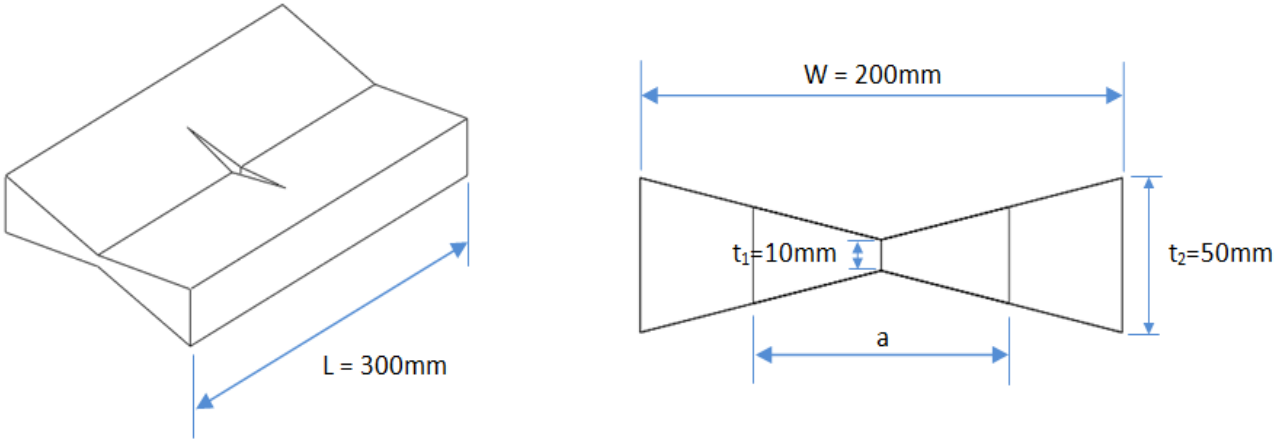

Figure 6-16: Central crack with variable thickness (CCTN) geometry and annotations

Table 6-11: Comparison between the FE and FALPR stress intensity factors for central crack with thinner center

Central Crack Thin To Thick (CCTN)			
a (mm)	FALPR - K_I (MPa$\sqrt{M}$)	FE - K_I (MPa$\sqrt{M}$)	Error%
20	107	114	-6.54
40	151	162.6	-7.68
60	202	223	-10.40
80	295.68	336.8	-13.91
AVG			-9.63

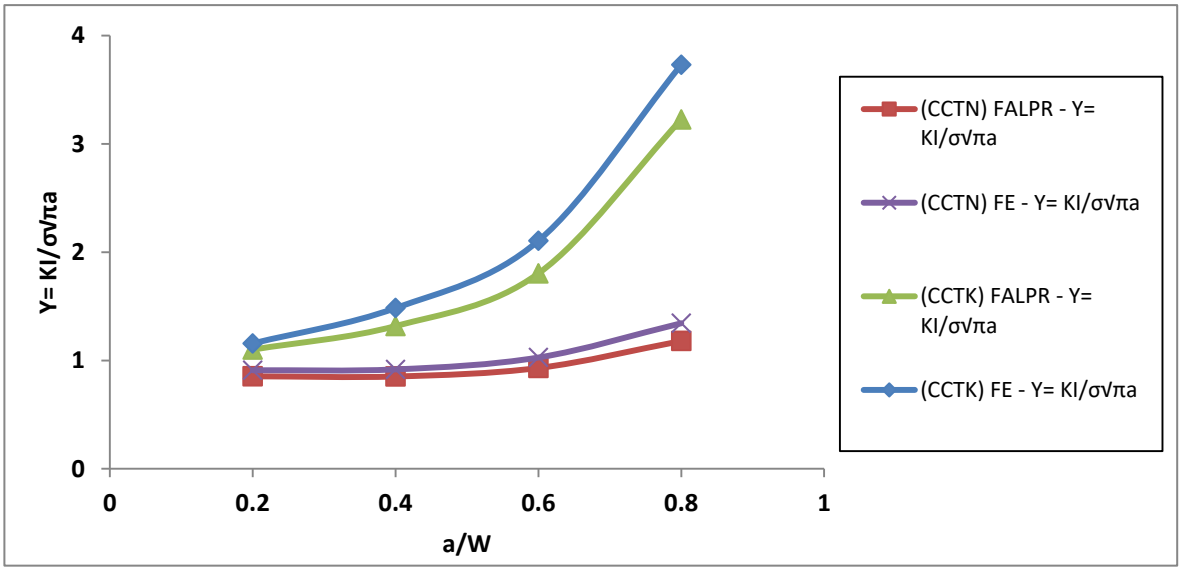

Figure 6-17: SIF results summary for the central crack with variable thickness

The FALPR software underestimated the stress intensity values in both the central crack cases above. The error is smaller in case of CCTN and is expected since the cracked area is smaller. The results in this section confirm that the moment is the cause of the over estimation in (TKTN) case from the previous section. In other words, the SIF of the CCTK case was not affected by the moments because they are balanced in the model unlike the TKTN edge crack case.

6.5.4 Edge crack with I-section

Two cases were modelled for the edge crack with I-section. I-section thick to thin edge crack (ITKTN) (Figure 6-18), while the other is called I-section thin to thick edge crack (ITNTK) (Figure 6-19). Comparison of both cases and the differences are shown in Table 6-12 and Table 6-13.

The applied load into FALPR SIF calculations was scaled based on the ratio of the crack edge thickness, t_a to the largest and smallest model thickness, t_1 and t_2, respectively.

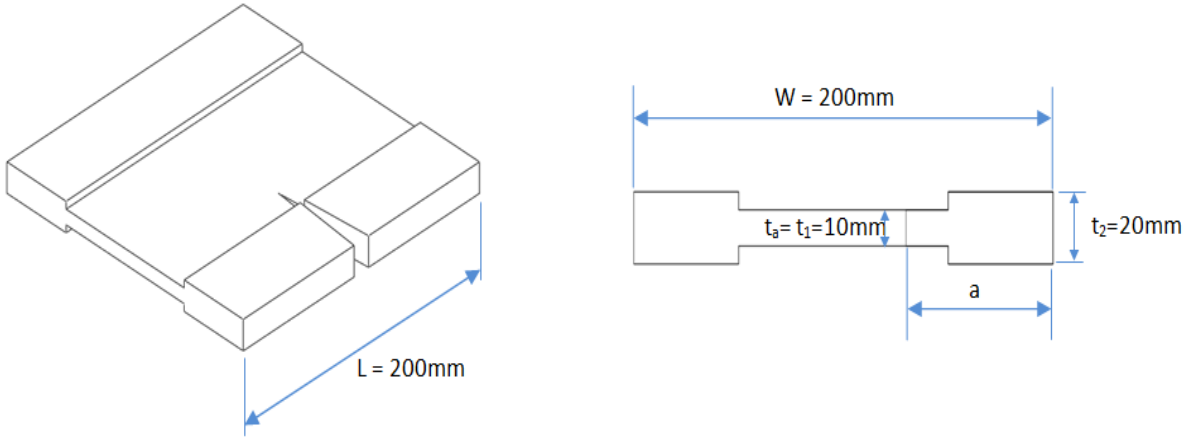

Figure 6-18: I-section thick to thin edge crack geometry

Table 6-12: Comparison between the FE and FALPR stress intensity factors for (ITKTN) edge crack.

I-Section Thick To Thin Edge Crack (ITKTN)			
a (mm)	**FALPR (MPa√M)**	**FE (MPa√M)**	**Error%**
20	**151.7**	**167.8**	**-10.61**
45	**353.5**	**367.4**	**-3.93**
55	**517.8**	**593.9**	**-14.70**
70	**652.4**	**720**	**-10.36**
AVG			**-9.90**

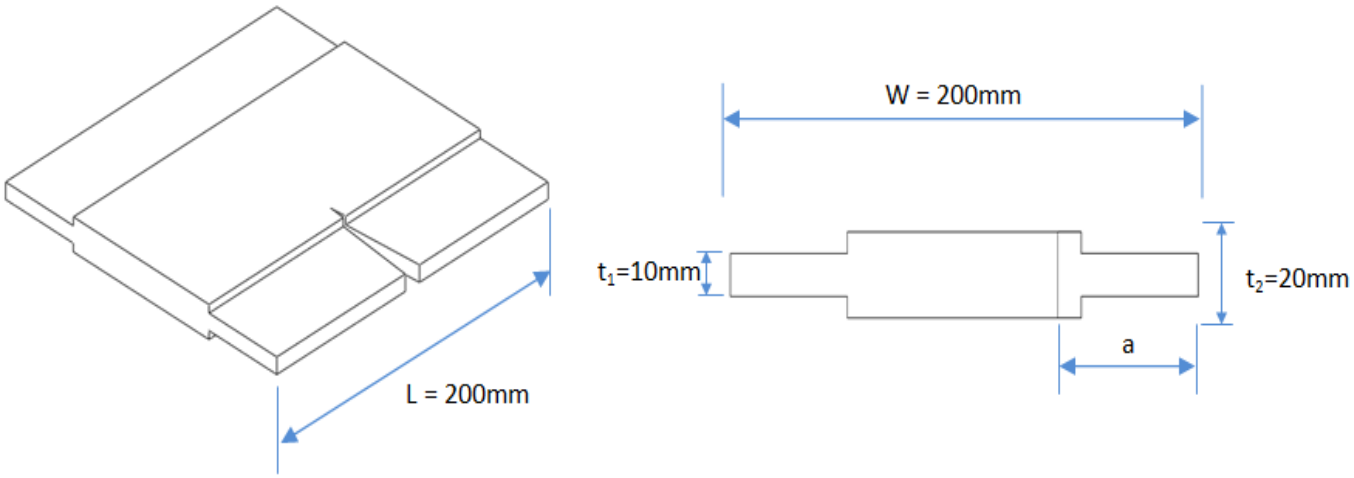

Figure 6-19: I-section thin to thick edge crack geometry

Table 6-13: Comparison between the FE and FALPR stress intensity factors for (ITNTK) edge crack

I-Section Thin To Thick Edge Crack (ITNTK)			
a (mm)	K_I FALPR (MPa$\sqrt{M}$)	K_I FE (MPa$\sqrt{M}$)	Error%
20	151.7	151.6	0.07
45	229.6	220.6	3.92
55	234.3	230.2	1.75
70	330.17	332	-0.55
AVG			1.30

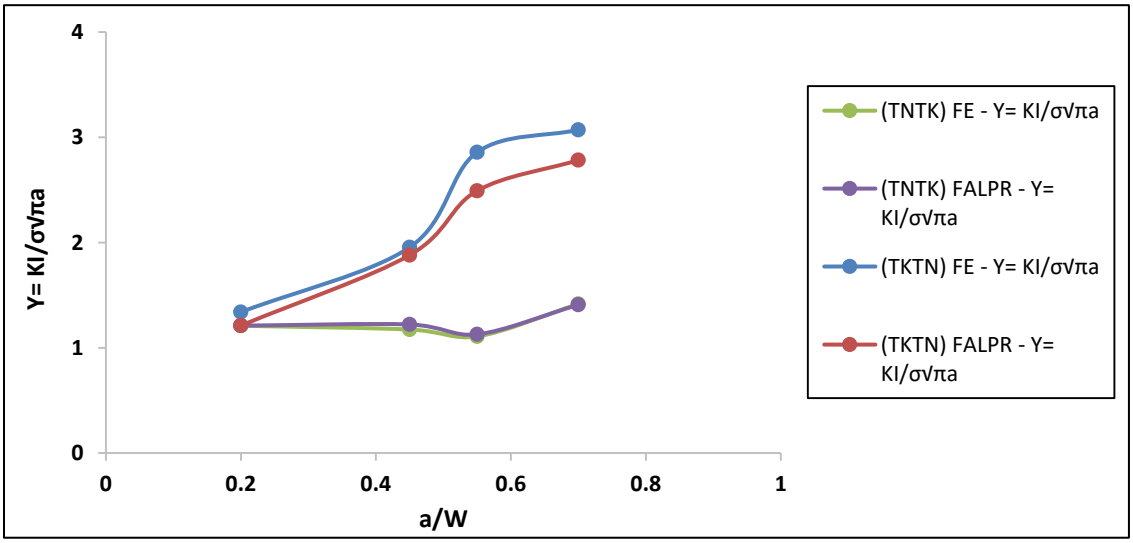

Figure 6-20: SIF results summary for the edge cracck with I-section

The K_I results from FALPR for the above cases show a good agreement with the FE results. The same trend is noticed for the thin to thick case. The ITKTN case underestimates the K_I values, whereas the other case slightly overestimates the results.

6.5.5 Results and conclusions

In conclusion, the FALPR weight function for the 2D edge and central crack could be modified for 3D cases with variable thickness with an acceptable error for small cracks in most of the cases investigated in this chapter. More investigation should be focused on the bending effect of the thick to thin cases in section 6.5.1. The geometrical scaling should work better if the bending effect is to be accounted for in future work. The conducted modelling was done for tensile loading only while bending could also be investigated to check the difference between the FALPR 2D weight function and the 3D FE SIF.

Bibliography

[1] ASTM E739-10(2015), Standard Practice for Statistical Analysis of Linear or Linearized Stress-Life (S-N) and Strain-Life (ε-N) Fatigue Data, ASTM International, West Conshohocken, PA, 2015, www.astm.org.

[2] Shigley, J. E., Mischke, C. R., & Budynas, R. G. (2004). *Mechanical engineering design*. New York, NY: McGraw-Hill.

[3] Glinka, G. (2014). *Lecture Notes* [PowerPoint slides]. Retrieved from University of Waterloo ME 627, Fatigue and Fracture Analysis of Engineering Material & Structures.

[4] Wöhler, A. (1860). Versuche über die Festigkeit der *Eisenbahnwagenachsen. Zeitschrift für Bauwesen*, 10, 160-161. (In German)

[5] Goodman, J. (1918). *Mechanics applied to engineering*. Longmans, Green.

[6] Basquin, O. H. (1910). The exponential law of endurance tests. In *proc. ASTM* (Vol. 10, No. Part II, p. 625).

[7] Palmgren, A. (1924). Die lebensdauer von kugellagern. *Zeitschrift des Vereins Deutscher Ingenieure*, *68*(14), 339-341.

[8] Miner, M. A. (1945). Cumulative fatigue damage. *Journal of applied mechanics*, *12*(3), A159-A164.

[9] Matsuishi, M., & Endo, T. (1968). Fatigue of metals subjected to varying stress. Japan Society of Mechanical Engineers, Fukuoka, Japan, 68(2), 37-40.

[10] Hobbacher, A. F. (2009). The new IIW recommendations for fatigue assessment of welded joints and components – A comprehensive code recently updated. *International Journal of Fatigue*, 31(1), 50-58.

[11] AWS, A. (1990). AWS D1. 1-90, Structural Welding Code–Steel.

[12] Niemi, E. (1999). Designer's Guide for Hot Spot Fatigue Analysis. IIW.

[13] Hobbacher, A. (2009). Recommendations for fatigue design of welded joints and components. New York: Welding Research Council.

[14] Huther, I., Gorski, S., Lieurade, H. P., Laborde, S., & Recho, N. (1999). Longitudinal non loaded welded joints-geometrical stress approach. *Welding in the World*, *43*(3), 20-26.

[15] Fricke, W. (2003). Fatigue analysis of welded joints: state of development. *Marine structures*, *16*(3), 185-200.

[16] Niemi, E., & Tanskanen, P. (2000). Hot spot stress determination for welded edge gussets. *Welding in the World*, *44*(5), 31-37.

[17] Fricke, W., & Bogdan, R. (2001). Determination of Hot Spot Stress in Structural Members with In-plane Notches Using Coarse Element Mesh. Paris: International Institute of Welding.

[18] Radaj, D., Sonsino, C. M., & Fricke, W. (2009). Recent developments in local concepts of fatigue assessment of welded joints. *International Journal of Fatigue*, *31*(1), 2-11.

[19] Betriebsfestigkeit, E. H. (2006). Verfahren und Daten zur Bauteilberechnung.

[20] Maddox, S. J. (2001, January). Recommended hot-spot stress design SN curves for fatigue assessment of FPSOs. In *The Eleventh International Offshore and Polar Engineering Conference*. International Society of Offshore and Polar Engineers.

[21] Maddox, S. J. (2002). Hot-spot stress design curves for fatigue assessment of welded structures. *International journal of offshore and Polar Engineering*, *12*(02).

[22] Niemi, E. (2001). Structural Stress Approach to Fatigue Analysis of Welded Components. Designer's Guide. International Institute of Welding, IIW-Document XIII-1819-00. XV-1090-01, XIII-WG3-06-99.

[23] Radaj, D. (1990). Design and analysis of fatigue resistant welded structures. Elsevier.

[24] Dong, P. (2001). A structural stress definition and numerical implementation for fatigue analysis of welded joints. *International Journal of Fatigue*, *23*(10), 865-876.

[25] Dong, P., Hong, J. K., & Cao, Z. (2001). A mesh-insensitive structural stress procedure for fatigue evaluation of welded structures. International Institute of Welding.

[26] Doerk, O., Fricke, W., & Weissenborn, C. (2003). Comparison of different calculation methods for structural stresses at welded joints. *International journal of fatigue*, *25*(5), 359-369.

[27] Xiao, Z. G., & Yamada, K. (2004). A method of determining geometric stress for fatigue strength evaluation of steel welded joints. *International Journal of Fatigue*, *26*(12), 1277-1293.

[28] Noh, B. W., Song, J. I., & Bae, S. I. (2006). Fatigue strength evaluation of the load-carrying cruciform fillet welded joints using hot-spot stress. In *Key Engineering Materials* (Vol. 324, pp. 1281-1284). Trans Tech Publications.

[29] Langer, B. F. (1937). Fatigue failure from stress cycles of varying amplitude. *Journal of Applied Mechanics*, *59*, A160-A162.

[30] Neuber, H. (1961). Theory of notch stresses: principles for exact calculation of strength with reference to structural form and material (Vol. 4547). USAEC Office of Technical Information.

[31] Coffin, L. F., & Tavernelli, J. F. (1962). Experimental support for generalized equation predicting low cycle fatigue. Transactions of the American Society of Mechanical Engineers (ASME), *Journal of Basic Engineering*, *84*, 533-537.

[32] Manson, S. S., & Hirschberg, M. H. (1964). Fatigue behavior in strain cycling in the low-and intermediate-cycle range.

[33] Smith, K. N., Watson, P., & Topper, T. H. (1970). A stress-strain function for the fatigue of metals (Stress-strain function for metal fatigue including mean stress effect). *Journal of materials*, *5*, 767-778.

[34] Topper, T. H., Sandor, B. I., & Morrow, J. D. (1967). *CUMULATIVE FATIGUE DAMAGE UNDER CYCLIC STRAIN CONTROL*. ILLINOIS UNIV URBANA DEPT OF THEORETICAL AND APPLIED MECHANICS.

[35] Neuber, H. (1961). Theory of stress concentration for shear-strained prismatical bodies with arbitrary nonlinear stress-strain law. *Journal of Applied Mechanics*, *28*(4), 544-550.

[36] ASTM, A. (2012). E606/E606M–12, Standard test method for strain-controlled fatigue testing. ASTM international, *West Conshohocken (PA USA): Book of Standards, 3.*

[37] Dowling, N. E. (2012). *Mechanical behavior of materials*. Pearson.

[38] Morrow, J. (1968). Fatigue design handbook. *Advances in engineering, 4*(3.2), 21-29.

[39] Kou, S. (2003). Welding Metallurgy, Hoboken.

[40] Irwin, G. R. (1997). Analysis of stresses and strains near the end of a crack traversing a plate. *Spie Milestone series MS, 137*(167-170), 16.

[41] Paris, P. C. (1962). *The growth of cracks due to variations in load* (Doctoral dissertation).

[42] Elber, W. (1997). Fatigue crack closure under cyclic tension.

[43] Paris, P. C. (1970). Testing for very slow growth of fatigue cracks. *MTS Closed Loop Magazine*, *2*(5), 177.

[44] Paris, P. C., & Schmidt, R. A. (1973). Threshold for fatigue crack propagation and the effects of load ratio and frequency. In *Progress in flaw growth and fracture toughness testing*. ASTM International.

[45] Paris, P. C., & Erdogan, F. (1963, December). A critical analysis of crack propagation laws. ASME.

[46] ASTM International. (2011). Standard test method for measurement of fatigue crack growth rates. ASTM International.

[47] Noroozi, A. H., Glinka, G., & Lambert, S. (2005). A two parameter driving force for fatigue crack growth analysis. *International Journal of Fatigue, 27*(10), 1277-1296.

[48] Mikheevskiy, S., & Glinka, G. (2009). Elastic–plastic fatigue crack growth analysis under variable amplitude loading spectra. *International Journal of Fatigue, 31*(11), 1828-1836.

[49] Handbook, S. I. F. (1987). Y. Murakami, ed. *Chief, Pergamon Books*.

[50] Glinka, G., Shen, G., (1991). Universal Features of Weight Functions for Cracks in Mode I. *Engineering Fracture Mechanics*, vol. 40, no. 6, pp. 1135-1146.

[51] Shen, G., & Glinka, G. (1991). Weight functions for a surface semi-elliptical crack in a finite thickness plate. *Theoretical and Applied Fracture Mechanics, 15*(3), 247-255.

[52] Glinka, G., & Burns, D. J. (1997). Weight functions for an external longitudinal semi-elliptical surface crack in a thick-walled cylinder. *Journal of pressure vessel technology, 119*, 75.

[53] Niemi, E. (1992). *Recommendations Concerning Stress Determination for Fatigue* Analysis of Welded Components. IIW Document IIW-1458-92. XV-797-92, International Institute of Welding.

[54] Fricke W, Von Stelle H. (1997). Form Factor Determination for Complex Shipbuilding Structural Details and Involvement in Fatigue Analyzes., In: Hobbacher A, editor. *Fortschritte beider Konstruktion und Berechnung geschwei Bter Bauteile*: Proceedings of the International Conference. Du'sseldorf: DVS 187, 59-64.

[55] Fayard, J. L., Bignonnet, A., & Van, K. D. (1996). Fatigue design criterion for welded structures. *Fatigue & Fracture of Engineering Materials & Structures, 19*(6), 723-729.

[56] Kyuba, H., & Dong, P. (2005). Equilibrium-equivalent structural stress approach to fatigue analysis of a rectangular hollow section joint. *International Journal of Fatigue, 27*(1), 85-94.

[57] Fricke, W. (2002). Recommended hot-spot analysis procedure for structural details of ships and FPSOs based on round-robin FE analyses. *International Journal of Offshore and Polar Engineering*, *12*(01).

[58] Monahan, C. C. (1995). Early fatigue crack growth at welds. *Computational mechanics*. Southampton, UK.

[59] Skolseg, E. (2002). The Transformation of Shell Finite Element Stress Analysis Data into Peak Stresses in Welded Structures (Doctoral dissertation, University of Waterloo).

[60] Niu, X., & Glinka, G. (1987). The weld profile effect on stress intensity factors in weldments. *International Journal of Fracture, 35*(1), 3-20.

[61] Ida, K., & Uemura, T. (1996). Stress concentration factor formulae widely used in Japan. *Fatigue & Fracture of Engineering Materials & Structures, 19*(6), 779-786.

[62] Yamada, K., & Hirt, M. A. (1982). Fatigue crack propagation from fillet weld toes. *Journal of the Structural Division, 108*(7), 1526-1540.

[63] Kurihara, M., Katoh, A., & Kawahara, M. (1986). Analysis on fatigue crack growth rates under a wide range of stress ratios. *Journal of pressure vessel technology, 108*, 209.

[64] Anderson, T. L., & Anderson, T. L. (2005). Fracture mechanics: fundamentals and applications. CRC press.

[65] Goyal, R. K. (2015). A stress analysis method for fatigue life prediction of welded structures.

[66] Malik, S. M. (2006). Fatigue life assessment of welded joints based on the decomposition of the structural hot spot stress. In *Masters Abstracts International* (Vol. 45, No. 04).

[67] Brennan, F. P., Peleties, P., & Hellier, A. K. (2000). Predicting weld toe stress concentration factors for T and skewed T-joint plate connections. *International Journal of Fatigue, 22*(7), 573-584.

[68] Tsuji, I. (1990). Estimation of stress concentration factor at weld toe of non-load carrying fillet welded joints. *Journal of the Society of Naval Architects of Japan, 80*, 241-251. (In Japanese).

[69] ABAQUS user's manual. (2013). ABAQUS 6.12-2, Dassault Systémes Simulia Corp., Providence, RI, USA.

Appendix A:
Additional Case Studies

A1.1 Fatigue analysis of a T-joint subjected to out-of-plane cyclic loading

This case study has the same material properties and weld geometry as Case # 1, but the direction of the applied load is different. In this case six T-joint specimens were tested at the JD laboratories by applying a fully reversed cyclic loading of a force perpendicular to the attachment plate length, as shown in Figure A1- 1. The base plate or main plate dimensions were $500 \times 500 \times 4$ mm, and the dimensions of the vertical attachment plate (gusset plate) located at the center of the main plate were $50 \times 100 \times 4$ mm. The material of the tested samples was 1008 steel. The weldment was done using the Flux Core Arc Welding method. The dimensions of the weld were t = 4 mm, t_p = 4 mm, h = 4 mm, h_p = 4 mm, $\theta = 45°$, and ρ = 0.55 mm.

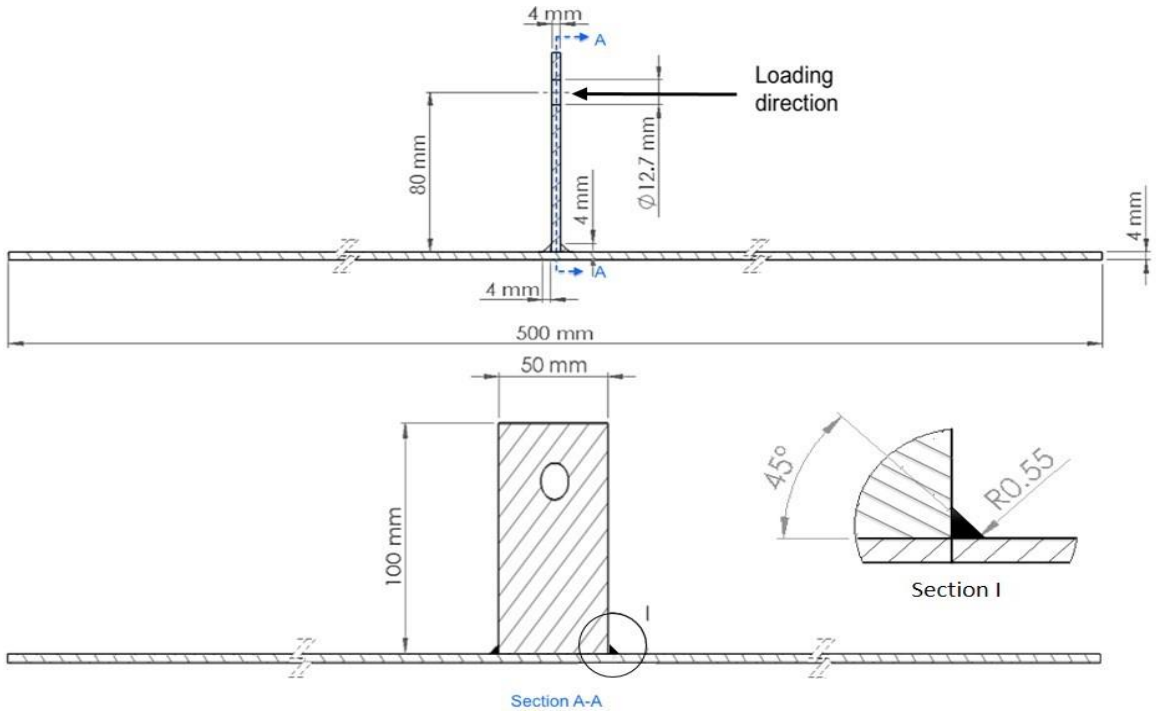

Figure A1- 1: Geometries of the T-joint specimen subjected to out of plane cyclic loading

Three of the test samples were subjected to an out of plane load of F = ± 308 N, while the rest of the test specimens were subjected to F = ± 684 N. The base plate of each specimen was fixed at all corners by a clamp with dimensions of 40×80 mm, whereas the pinhole of the gusset/attachment

plate was subjected to the out of plane cyclic loading. One of the tested samples is seen in Figure A1-2.

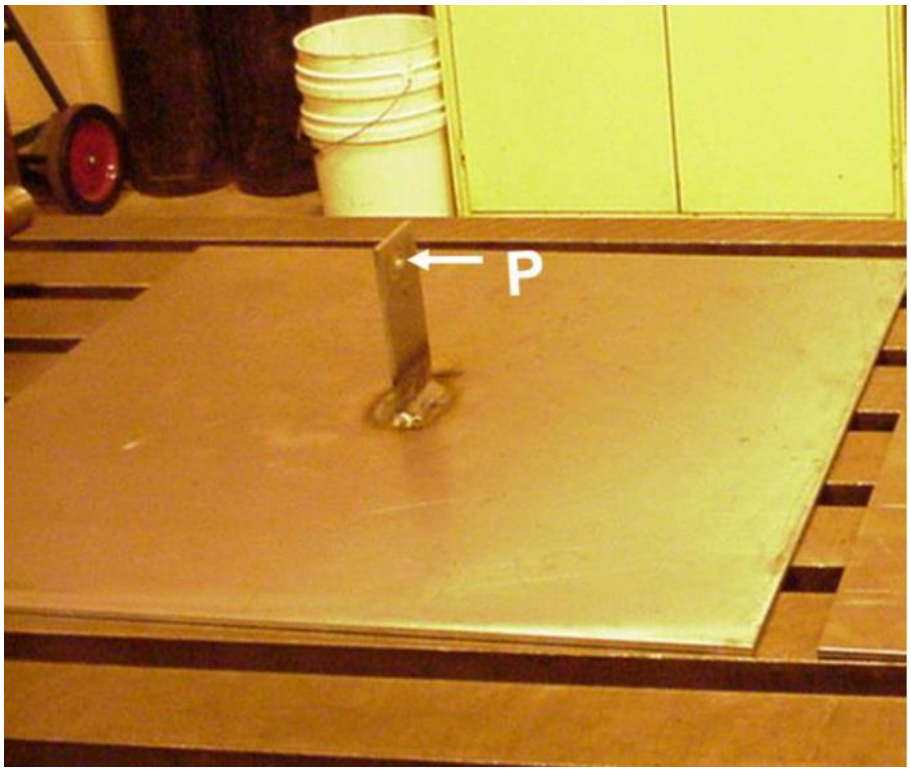

Figure A1- 2: Welded T-joint specimen subjected to out of plane bending loading (JD)

A1.1.1 Material properties

The material properties of the welded joint under investigation are the same as for Case #1. The chemical composition and mechanical properties are shown previously in Table 5-1 and Table 5-2, respectively. The fatigue test data for 1008 steel are shown in Table 5-3. The fatigue parameters based on UW analysis are shown in Table 5-4 for 1008 steel.

A1.1.2 Shell FE modelling of a T-joint subjected to out-of-plane cyclic loading

The aim of this shell FE model is to determine the local reference stresses (σ_a and σ_b) and the resulting stress data according to section 3.6. The membrane and bending hot spot stresses (σ_{hs}^{m} and σ_{hs}^{b}) are determined by using equations (3.12 and 3.13). Based on the micro-geometrical features of the welded joint, the membrane and bending SCFs (K_t^m and K_t^b) can be determined according to

section 3.7. According to equation (3.12), this is the required stress information that will determine the peak stress σ_{peak} based on the shell FE local references stresses. The same stress data (σ_{hs}^{m} , σ_{hs}^{b}) and the SCFs (K_t^m, K_t^b) can be used to determine the through-thickness stress distribution $\sigma_{xx}(y)$, as per the Monahan equation (3.11). The shell FE model must have the same geometry as the experimental specimen, whereas the stress data must be extracted at the weld's critical location.

The shell FE model and the boundary conditions for the welded joint under investigation is shown in Figure A1-3. The plate corners were constrained for all displacement while a force of 1000 N was applied to the attachment plate's pinhole.

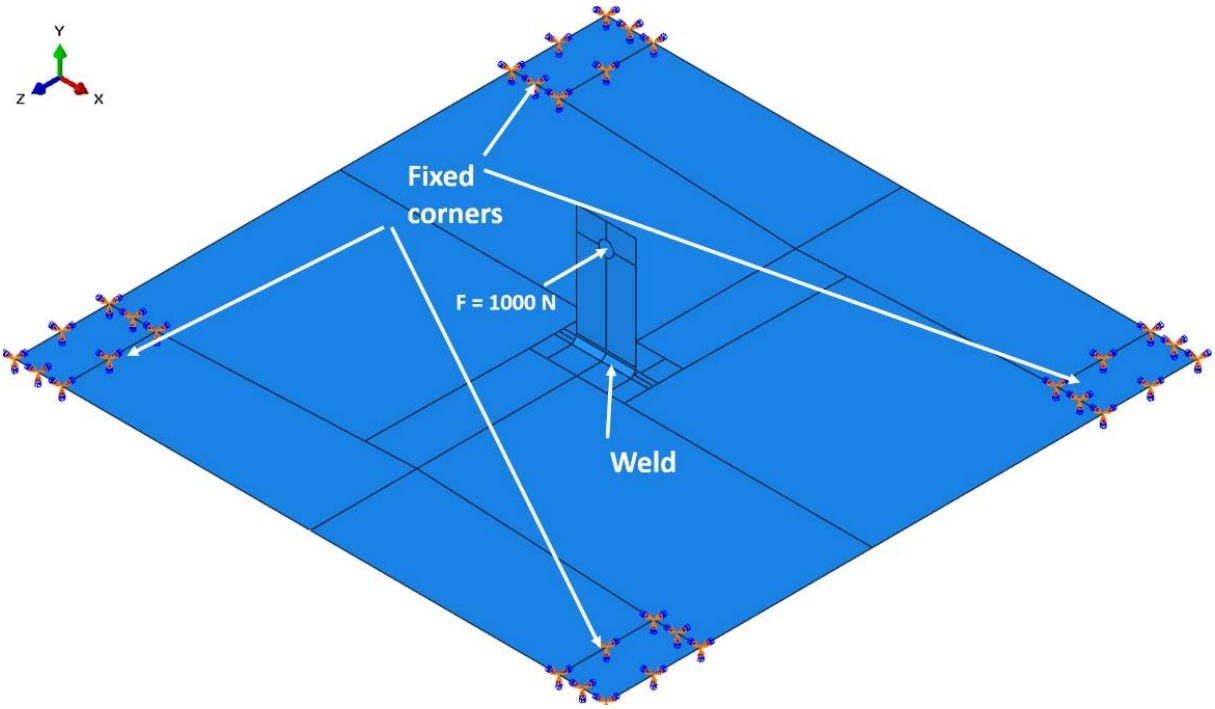

Figure A1-3: Shell FE modelling and boundary conditions for the T-joint subjected to out-of-plane cyclic loading (F = 1000 N)

The local reference stresses σ_a and σ_b were obtained from a reference point located at the upper weld toe of the attachment plate as shown in Figure A1- 4. The reference point contains the local reference stresses, which represent surface and bottom stresses through the plate thickness. These stresses are used to determine the membrane and bending hot spot stresses that will be multiplied by the proper SCFs to calculate the peak stress at the weld toe.

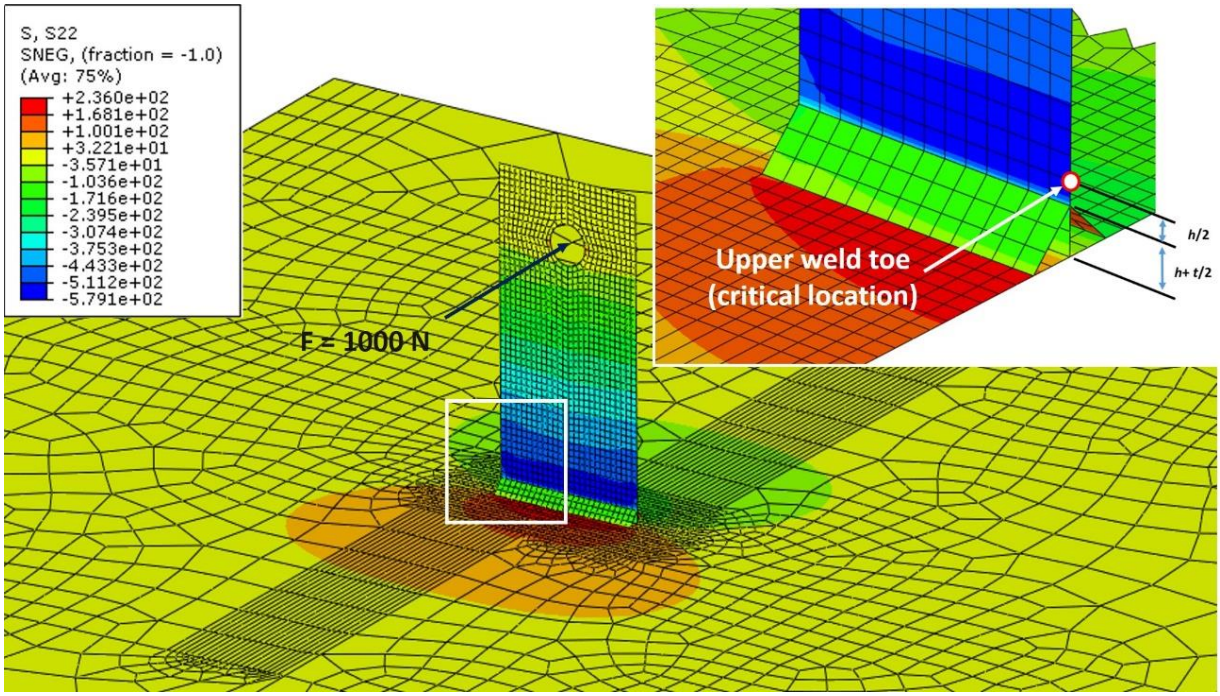

Figure A1- 4: Shell FE stress contours of the maximum stress normal to the weld toe line; T-joint subjected to out-of-plane cyclic loading (F = 1000 N)

According to the experiments, the maximum stress was expected to be at the upper weld toe of the attachment plate. Note that the reference points in the above shell FE model coincide with the actual location of the weld toe of the experimental specimen. The maximum stress was located at the middle of the upper weld toe line of the gusset, as expected. However, the required shell FE reference stresses are to be extracted from a specific reference point and not at the maximum contour node. The distance between the main plate surface and the upper weld toe reference points of the shell model was h+ (t /2) = 6 mm. At that specific reference point (middle of the upper weld line), the local reference stresses σ_a and σ_b were extracted as they represent the stresses of the surface sides of the attachment plate. The local reference stresses through the attachment plate (σ_a and σ_b) were recorded as follows:

σ_a = 568.19 MPa

σ_b = -568.187 MPa

Therefore, the hot spot membrane and bending stresses σ_{hs}^{m} and σ_{hs}^{b}, per equations (3.12 and 3.13) were:

$$\sigma_{hs}^{m} = \frac{\sigma_a + \sigma_b}{2} = 0.0015 \text{ MPa}$$

$$\sigma_{hs}^{b} = \frac{\sigma_a - \sigma_b}{2} = 568.19 \text{ MPa}$$

Using the weld geometrical features of the current case, the SCFs were calculated using equations (3.15 and 3.16):

$K_t^m = 2.082$

$K_t^b = 1.552$

As per equation (3.12), the peak stress at the weld toe induced by the applied load was:

$$\sigma_{peak} = \sigma_{hs}^{m}.K_t^m + \sigma_{hs}^{b}.K_t^b = 881.83 \text{ MPa}$$

Two stress distributions through the attachment plate thickness in the direction normal to the weld toe are shown in Figure A1- 5. The linear stress distribution (hashed line) represents the local reference stresses (σ_a and σ_b). The non-linear stress distribution (solid curve) represents Monahan equation $\sigma_{xx}(y)$. Note that the welded joint under investigation is considered a symmetric welded joint while Monahan equation is for non-symmetric welded joints. Therefore, the resulting through-thickness stress distribution in Figure A1- 5 is accurate only for half of the thickness y/t = 2 mm. In other words, the green nonlinear curve in Figure A1- 5 is correct through the half the attachment thickness or from 0 to 2 mm. However, there is a way to estimate the stress distribution for the remaining half of the attachment plate thickness (i.e., from 2 to 4 mm). The applied force to the attachment plate should result in a pure bending loading mode through the thickness of the attachment plate (maximum at the weld toe). Since the membrane hot spot stress is almost zero (0.0015 MPa), the current case can be considered as pure bending because the bending hot spot stress is the dominant through the thickness of the attachment plate. As a result of having a pure bending loading mode acting on the attachment plate, the stress through the thickness must be symmetrically distributed from the surface to the neutral axis (tensile stress) and from the neutral axis to the other surface of the plate (compression stress). Hence, the through-thickness stress distribution in Figure A1- 5 may be redrawn as shown in Figure A1- 6.

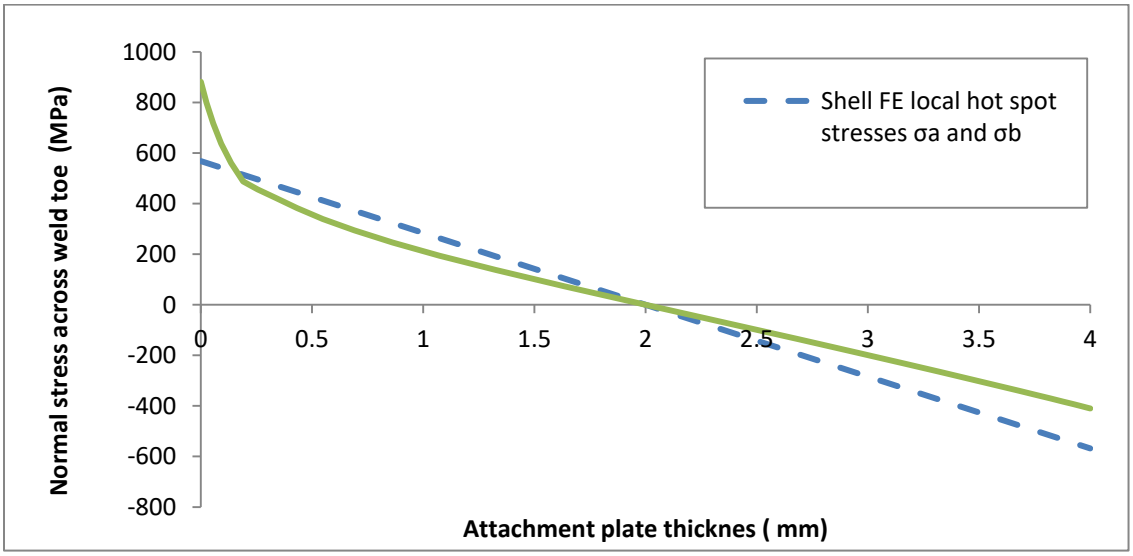

Figure A1- 5: The shell FE local reference stress data at the weld toe cross section of the T-joint under out of plane bending; linear distribution of the local reference stresses (σ_a and σ_b); and the Monahan non-linear through-thickness stress distribution

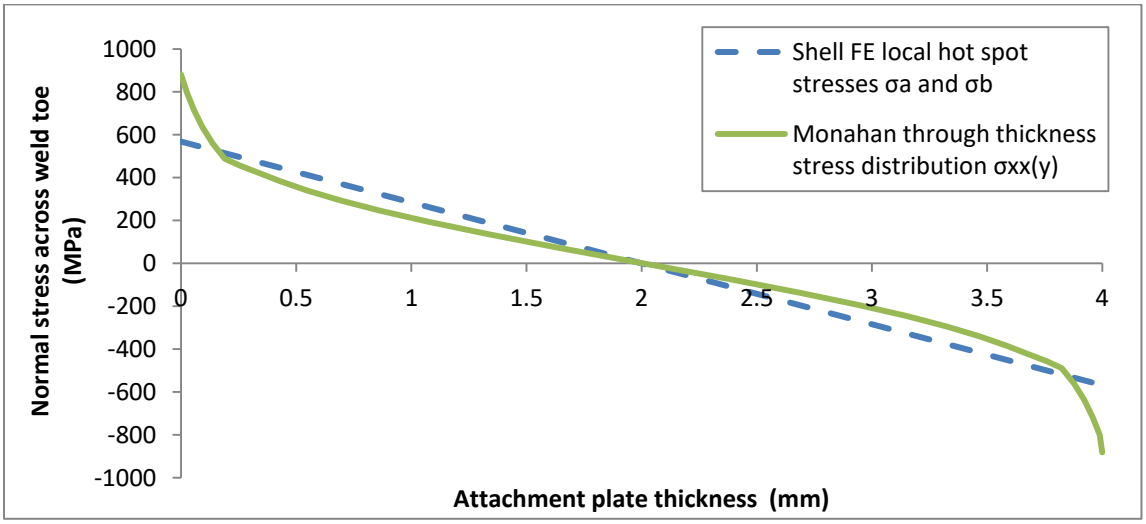

Figure A1- 6: Corrected non-linear through-thickness stress distribution at the weld toe and linear distribution of the local reference stresses (σ_a and σ_b) for case # 3 (T-joint under out of plane bending loading)

The stress data (σ_a, σ_b, $\sigma_{peak,}$ and $\sigma_{xx}(y)$) required for the fatigue analysis of the case under investigation are drawn in Figure A1- 6. The stress data in are obtained from a shell FE model and must be validated against a detailed 3D FE model, according to section 4.1, before proceeding with the fatigue analysis. A 3D FE model with the same geometry as the experiment is modelled in the following section to validate the shell FE local reference stress results.

A1.1.3 Finite element 3D modelling of a T-joint subjected to out-of-plane cyclic loading

The 3D FE model should have the same geometry as the experimental specimen and the stress data must be extracted from the weld's critical location in the same way as the shell FE model. For the case under investigation, the critical location is expected at middle of the upper weld toe of the attachment plate. According to the shell FE model, the maximum stress occurs at the upper weld toe of the attachment plate, as shown in Figure A1- 4. Therefore, it is expected that the 3D FE model would have the peak stress at the same location.

The boundary conditions of the 3D FE modelling for the T-joint subjected to out-of-plane cyclic loading are shown in Figure A1- 7. Because of the symmetry of the problem, only half of the component was modelled to reduce the computational time. The model was subjected to an out of plane force of F = 1000 N acting on the attachment pinhole. The bottom corners of the base plate were constrained for all displacements, and the model elements were approximated by eight brick elements.

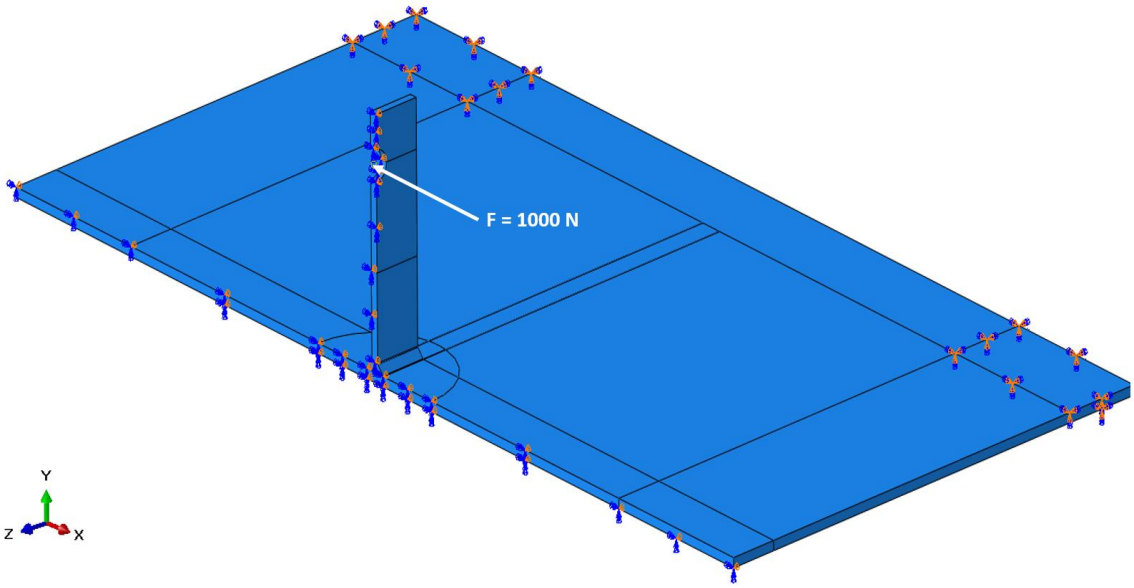

Figure A1- 7: Boundary conditions of the 3D FE simulated T-joint subjected to out-of-plane cyclic loading

The meshing was intensive at the critical areas (weld toes). These areas were expected to have the peak stress normal to the weld toe. The element size at the weld toe should be small enough to find a

converged stress. The recommended element size is at least equal to quarter of the weld toe radius [64]. The meshing of the weld toe is shown in Figure A1- 8.

The maximum stress (peak stress), normal to the weld toe line, in the 3D model was found at the middle of the attachment plate upper weld toe as shown in Figure A1- 8. The path where the actual non-linear through-thickness stress distribution, σ(y) was extracted is shown in Figure A1- 9.

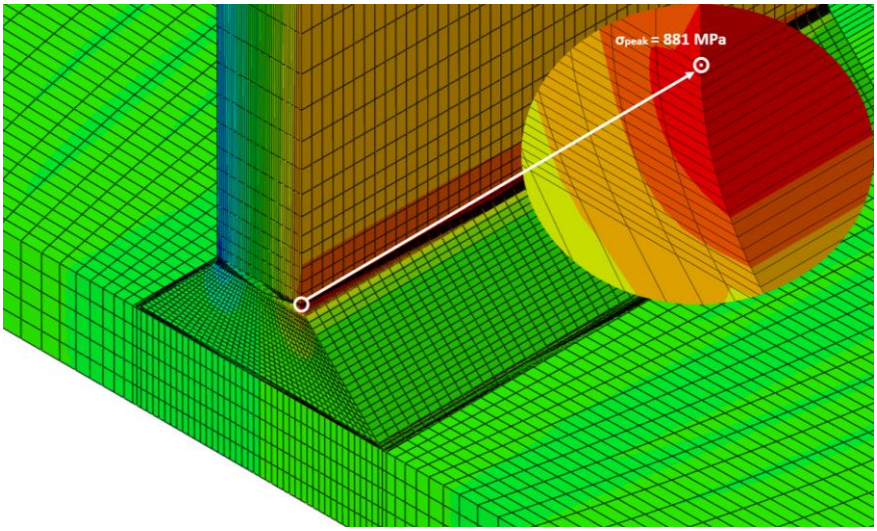

Figure A1- 8: Intensive mesh at the weld toe of the T-joint under out of plane bending (3D FE model)

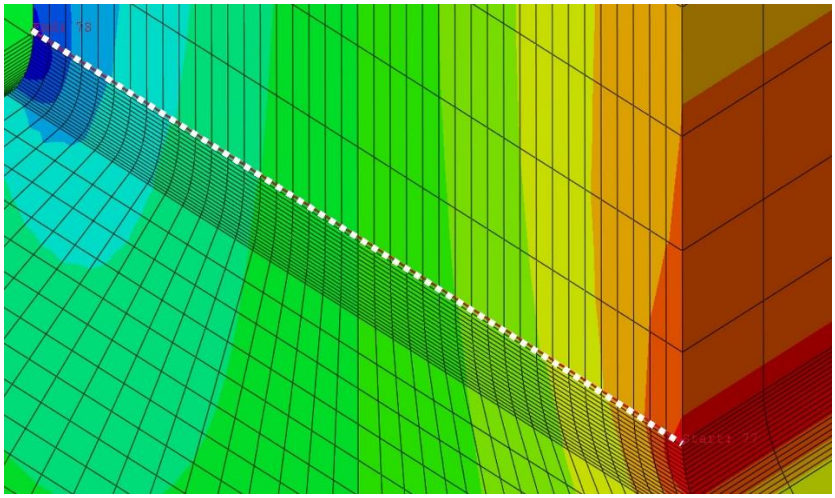

Figure A1- 9: Path of nodes at the middle of the weld toe line and through the thickness of the attachment plate (T-joint under out of plane bending)

Based on the 3D FE modelling, the actual peak stress obtained at the weld toe was 881 MPa. The actual non-linear through-thickness stress distribution, σ_{peak} (y) was processed according to Section

(4.1), while the membrane and bending hot spot stresses were found by linearization of the actual through-thickness stress distribution, as mentioned in equations (4.3 and 4.5):

$\sigma_{hs}^{m} = 3.343$ MPa

$\sigma_{hs}^{b} = 575.835$ MPa

Equations (4.6 and 4.7) were then used to find the linearized surface stresses as:

$\sigma_{hs} = \sigma_n = \sigma_a = \sigma_{hs}^{m} + \sigma_{hs}^{b} = 579.18$ MPa

$\sigma_b = \sigma_{hs}^{m} - \sigma_{hs}^{b} = -572.94$ MPa

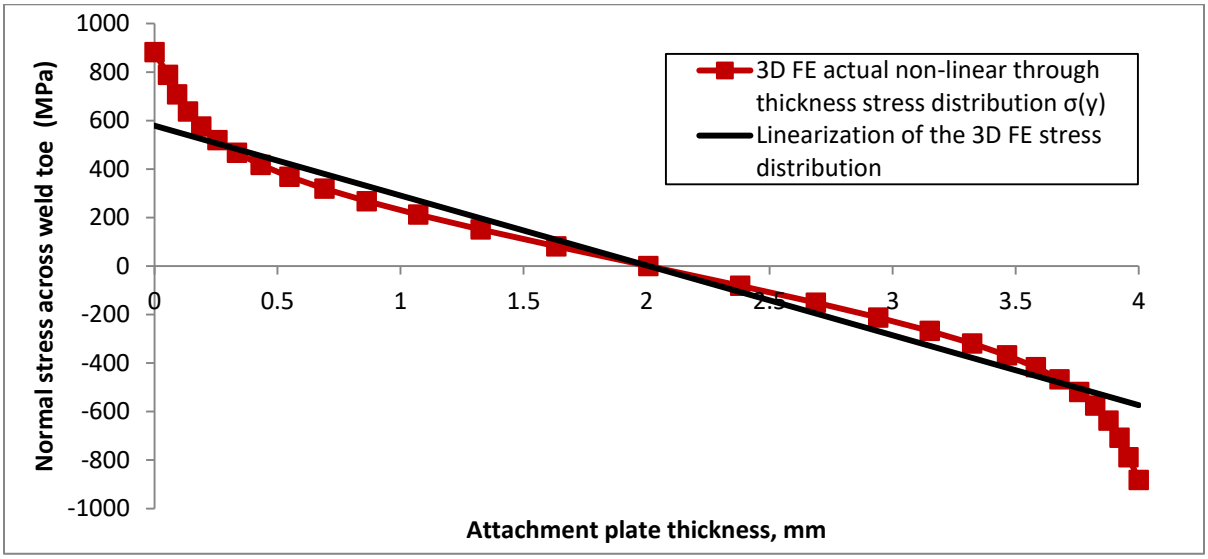

Figure A1- 10: The 3D FE stress data; actual stress distribution, and the equivalent linearized stress distribution at the weld toe of the T-joint model subjected to in-plane bending loading.

In the above figure the red curve represents the actual non-linear stress distribution through the thickness of the weld toe cross section based on the 3D FE model. In the same figure, the solid line represents the linearization of the curve (actual non-linear stress distribution).

The stress results of both the shell and the 3D FE models (see Figure A1- 6 and Figure A1- 10) were compared after being normalized, as shown in Figure A1- 11and Figure A1- 12. The normalization was done by dividing the shell and the 3D FE stress data by a load of F = 1000 N. The normalization was done so that the shell FE local reference stress data could be scaled later to the loads applied to the experiment specimens, which were based on loads of F = 308 N and F = 468 N.

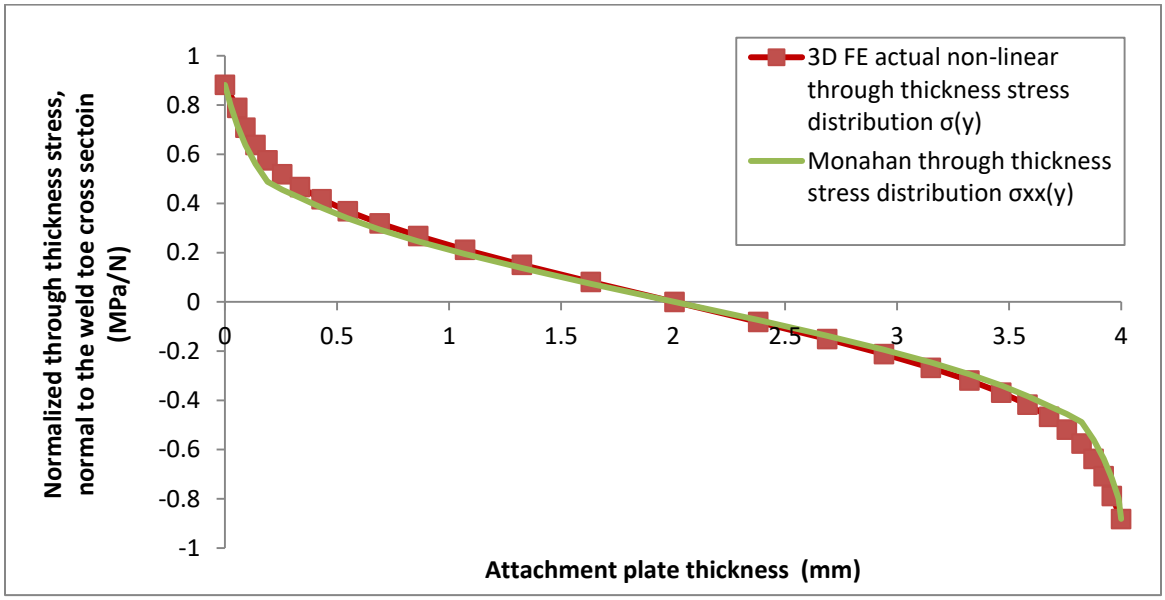

Figure A1- 11: Comparison of the normalized actual stress distribution (3D FE model) and the normalized stress distribution (shell FE model and Monahan) through the attachment plate thickness of the T-joint (out of plane bending)

The above figure shows a comparison between the actual non-linear through-thickness stress distribution σ(y) obtained from the 3D FE model and the non-linear through-thickness stress distribution $\sigma_{xx}(y)$ generated from the shell FE local reference stress data and the Monahan equation. It also shows that the value of the actual peak stress based on 3D FE modelling is close to value of the peak stress resulted from the shell FE modelling. The local reference stresses σ_a and σ_b acquired from the shell FE modelling were also compared to the linearized actual through-thickness stress distribution from the 3D FE modelling as shown in Figure A1- 12. As a result, the comparison of the 3D and shell FE stress data showed good agreement.

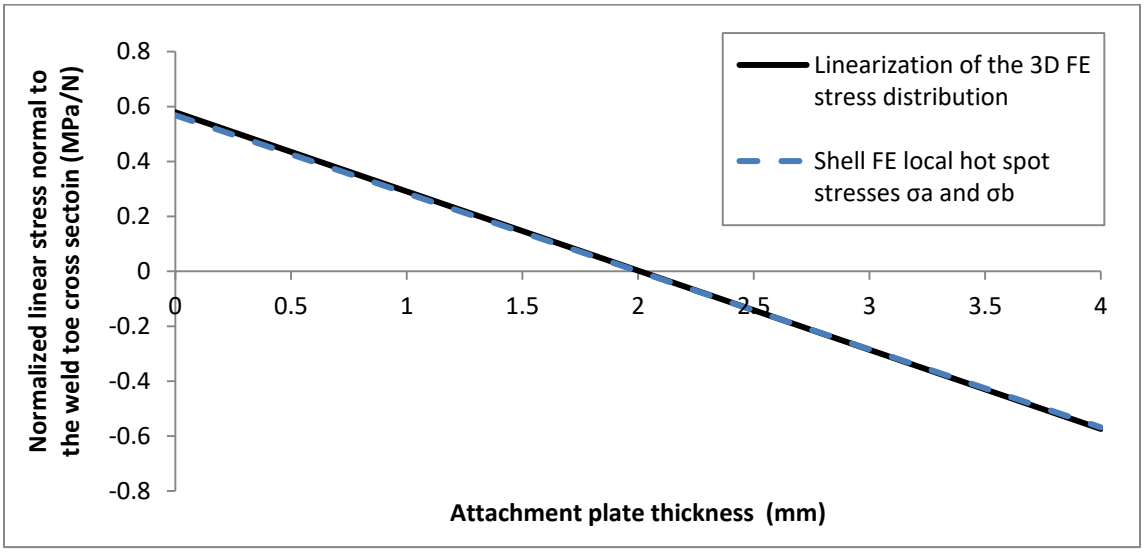

Figure A1- 12: Comparison between the 3D FE and the shell FE linearized stress field across the weld toe cross section; T-joint subjected to out-of-plane cyclic loading

The linearized through-thickness stress from the 3D FE model was almost the same as the one from the shell FE model. The linearized stresses based on the 3D FE model were higher than the shell FE local reference stresses in the bending and tensile parts by 1%.

This validation is important because the peak stress based on the shell FE model will be used to determine the fatigue crack initiation life using the strain-life method. In addition, the through-thickness stress distribution based on the shell FE and Monahan equation will be used to determine the stress intensity factor required to calculate the fatigue crack propagation life using the LEFM method.

The JD Company performed two series of fatigue tests to verify the predicted fatigue life for the T-joint subjected to out-of-plane cyclic loading. Both tests were conducted under fully reversed loading, but the first series of test specimens was subjected to F = ± 308 N, whereas the second series was subjected to F = ± 468 N. Therefore, the peak stress and the through-thickness distributions obtained from the shell FE modelling (the green curve in Figure A1- 11) were scaled to the load levels applied to the experimental specimens (F = 308 N and F = 468 N), as shown Figure A1- 13 and Figure A1- 14.

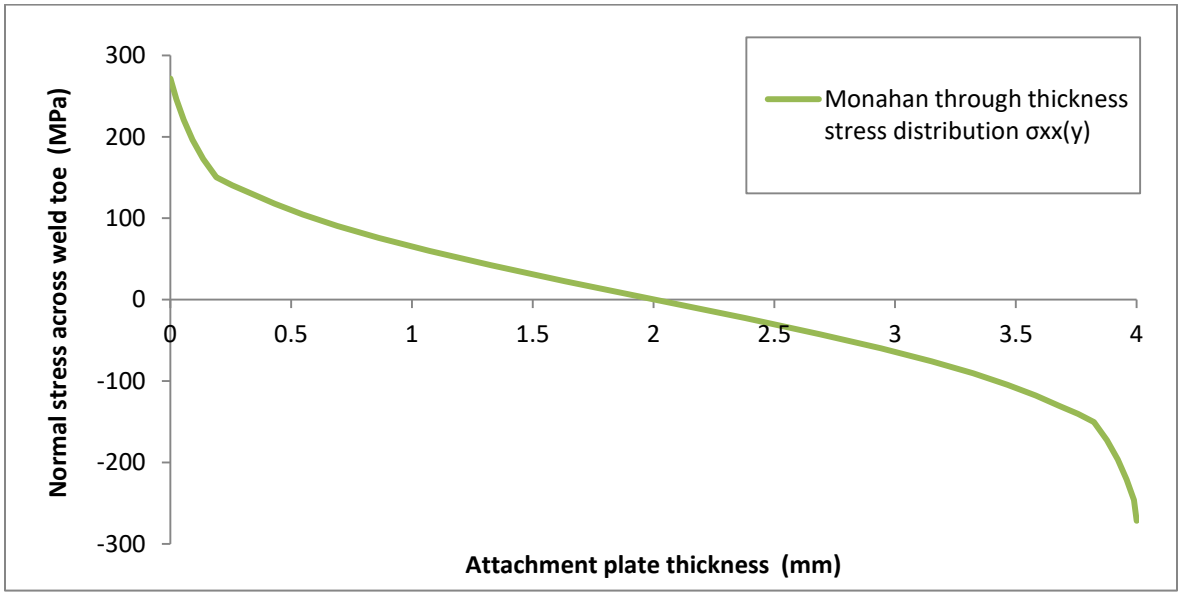

Figure A1- 13: Scaled non-linear through-thickness stress distribution for a load of (F = 308 N), based on the shell FE local reference stress data and Monahan equation

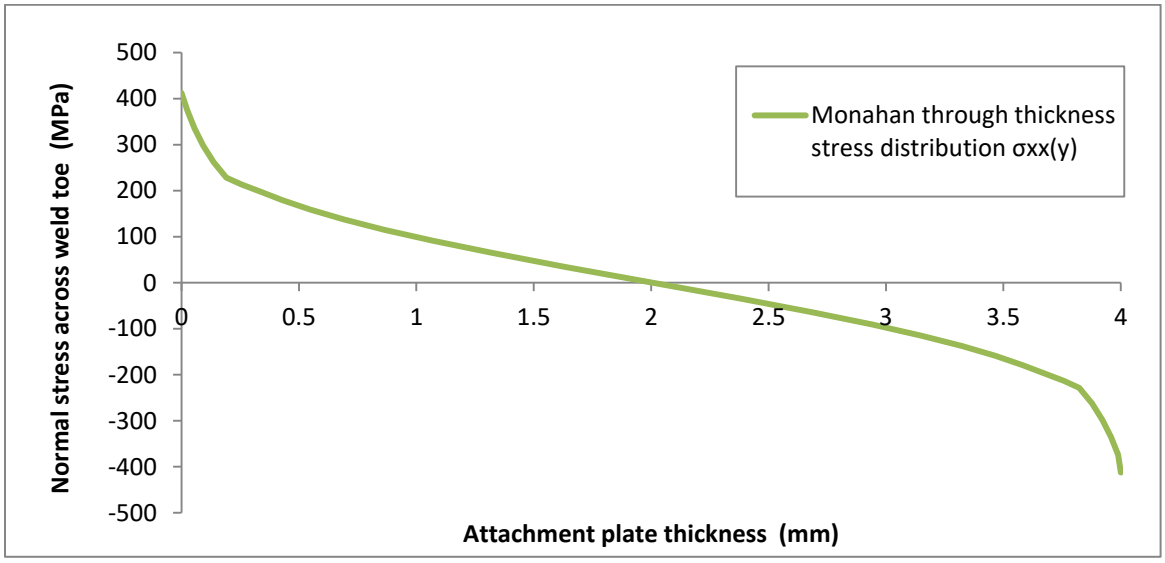

Figure A1- 14: Scaled non-linear through-thickness stress distribution to load of (F = 468 N), based on the shell FE local reference stress data and Monahan equation

The fatigue life predictions were performed with and without the residual stresses. The residual stress was measured at the plate surface only whereas the distribution was approximated by self-equilibrium of the linear field. The approximate residual stress distribution shown in Figure A1- 15 was based on limited experimental data.

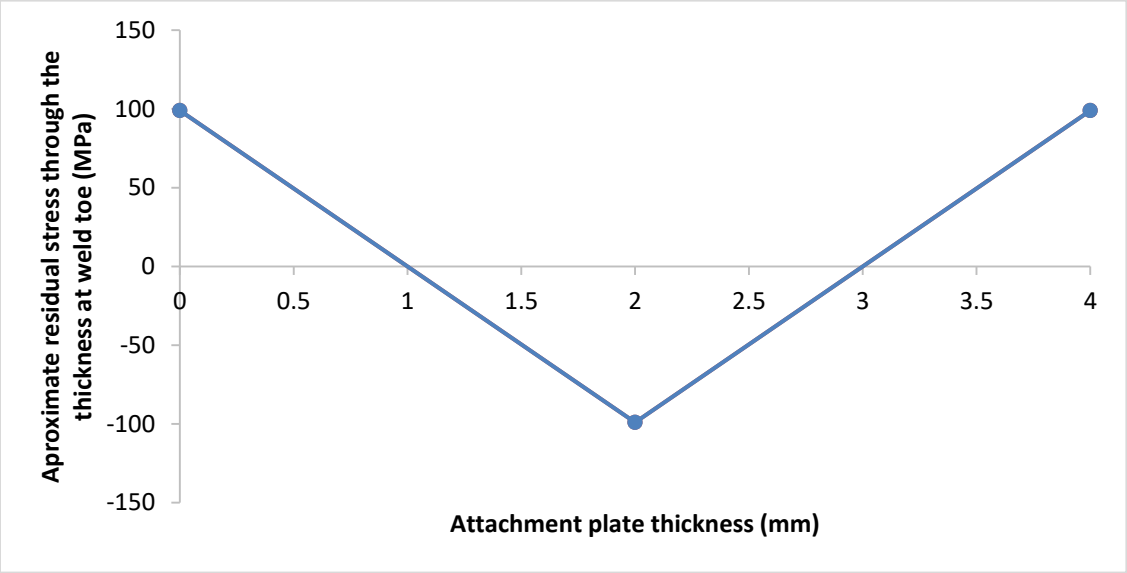

Figure A1- 15: Approximation of the residual stress distribution through the attachment plate thickness of the T-joint subjected to out-of-plane cyclic loading

A1.1.4 Fatigue life prediction of a T-joint subjected to out-of-plane cyclic loading

The fatigue life is predicted by using the ε-N and the LEFM methods based on the shell FE local reference stress data. The ε-N method predicts the fatigue crack initiation life, whereas the LEFM method predicts the fatigue crack propagation life. Both methods, which are coded into the in-house FALIN and FALPR software packages, were used to find the total fatigue lives of the current case (T-joint subjected to out-of-plane cyclic loading). The total fatigue lives were determined by summing both the initiation and the propagation fatigue lives. Finally, the predicted total fatigue life was compared with the fatigue life of the experiment.

The first step is to determine the fatigue crack initiation life according to the procedure of the strain-life method described in Section (2.2). The material properties in Table 5-2 and Table 5-4 were input to the FALIN software to calculate stresses and strains for each load cycle based on the Ramberg-Osgood fatigue stress-strain curve and the Neuber equation (see Figure 5-4 and Figure 2-12). The SWT equation (2.9) was then used to calculate the fatigue crack initiation life. The FALIN software simulates the stress-strain response and corresponding fatigue crack initiation life at the weld toe (output data). The fatigue crack initiation lives were predicted for the current case when subjected to load levels of F = 308 N and F = 468 N, without the effect of the residual stress, as

shown in Figure A1- 16 and Figure A1- 17. The fatigue crack initiation lives for the same load levels, including the residual stress effect are shown in Figure A1- 18 and Figure A1- 19.

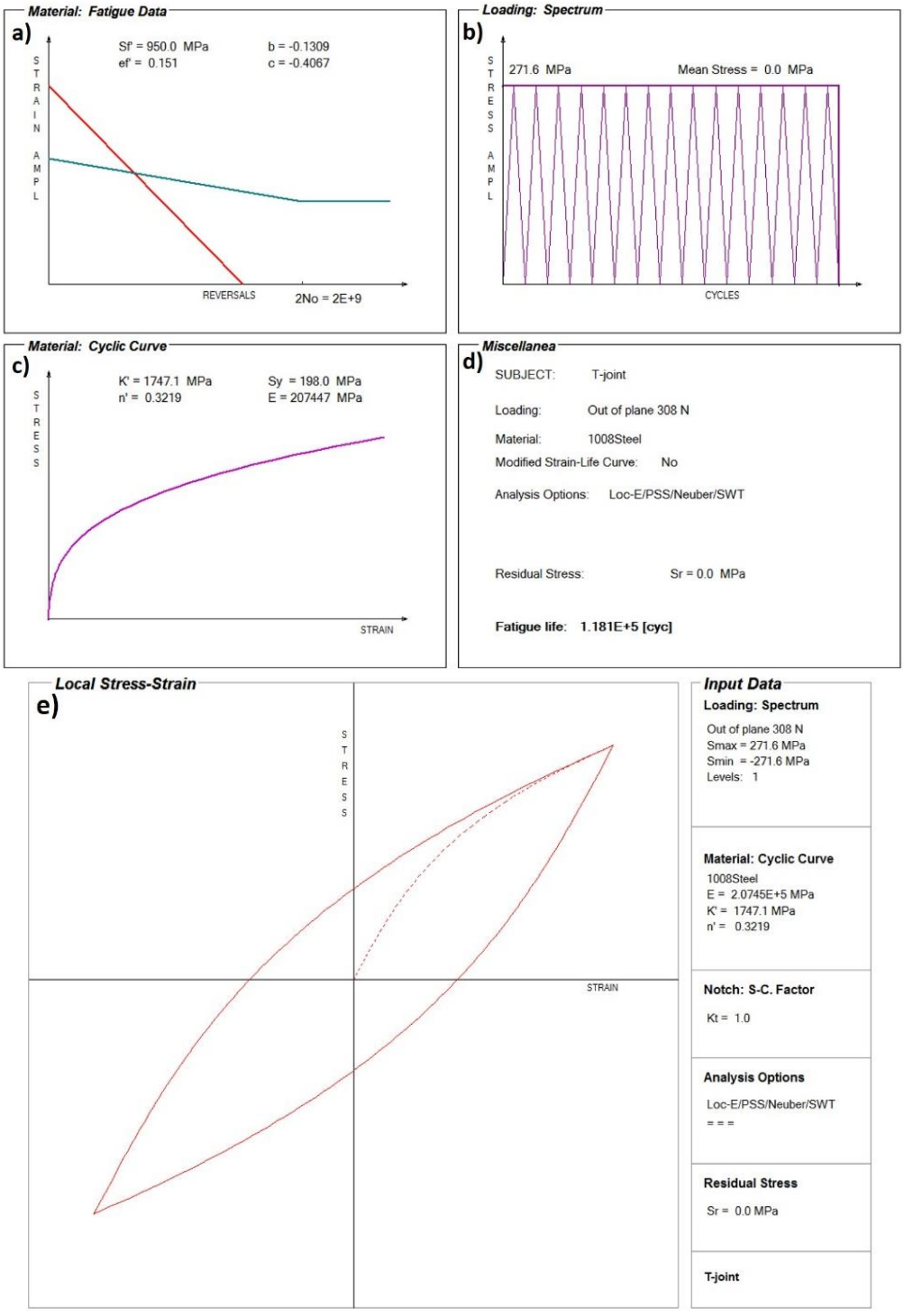

Figure A1- 16: FALIN input and output data for the T-joint subjected to out of plane loading of (F = 308 N); a) Manson-Coffin curve, b) Peak stress loading, c) Ramberg-Osgood curve, d) Output data, e) Simulated stress-strain material response at the weld toe

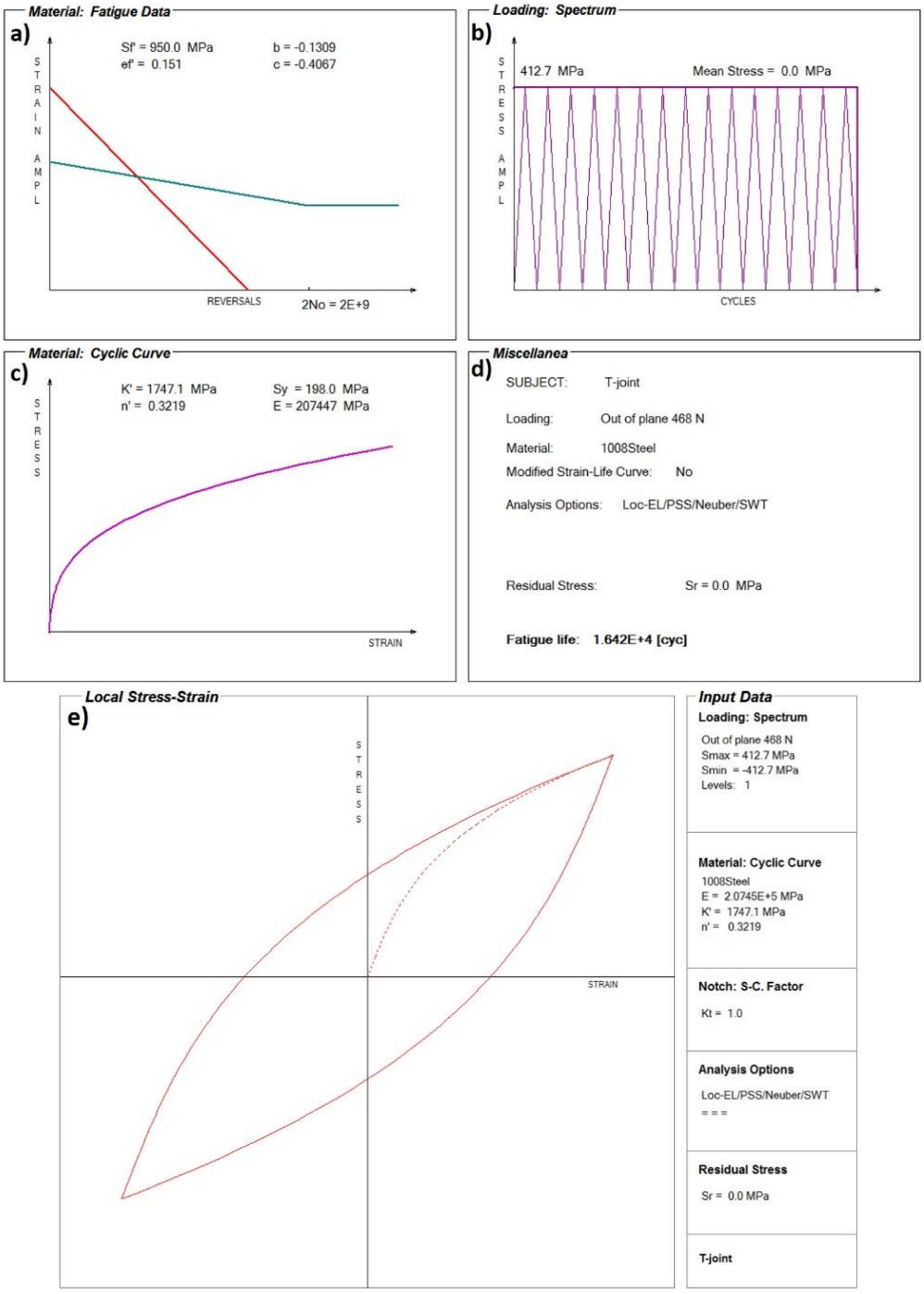

Figure A1- 17: FALIN input and output data for the T-joint subjected to out of plane loading of (F = 468 N); a) Manson-Coffin curve, b) Peak stress loading, c) Ramberg-Osgood curve, d) Output data, e) Simulated stress-strain material response at the weld toe

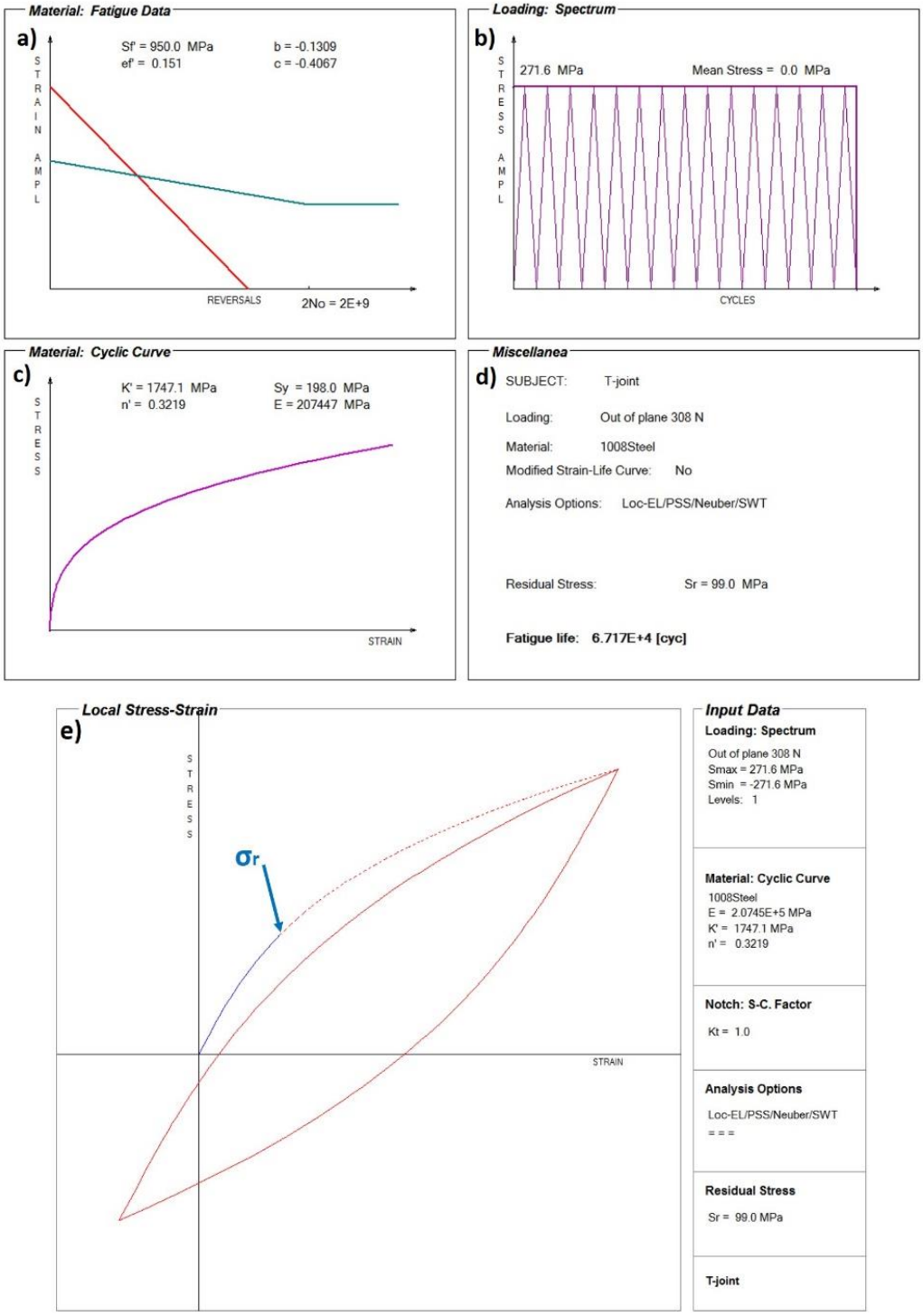

Figure A1- 18: FALIN input and output data for the T-joint subjected to out of plane loading of (F = 308 N) in addition to the residual stress σ_r : a) Manson-Coffin curve, b) Peak stress loading, c) Ramberg-Osgood curve, d) Output data, e) Simulated stress-strain material response at the weld toe

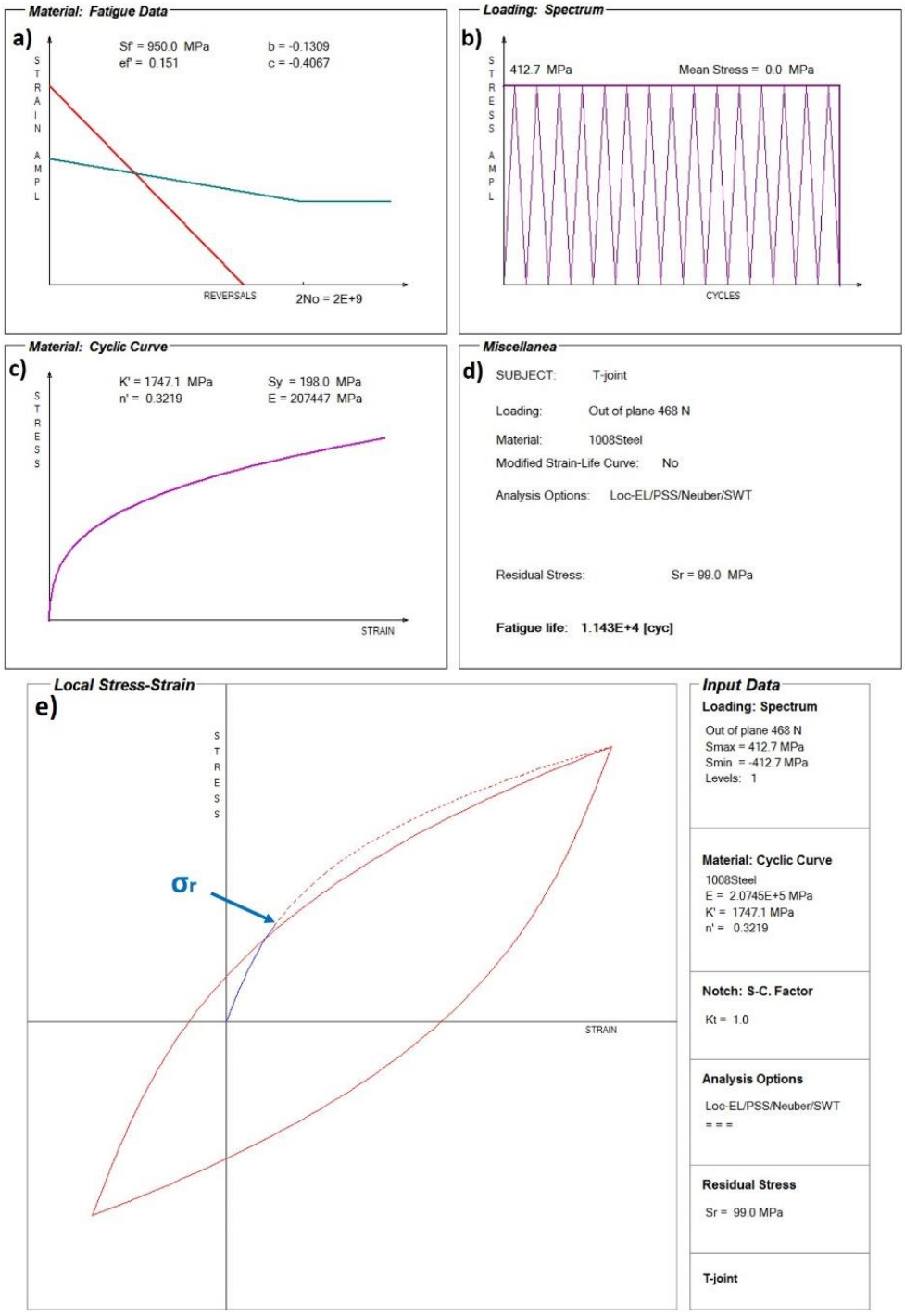

Figure A1- 19:FALIN input and output data for the T-joint subjected to out of plane load of (F = 468 N) in addition to the residual stress σ_r : a) Manson-Coffin curve, b) Peak stress loading, c) Ramberg-Osgood curve, d) Output data, e) Simulated stress-strain material response at the weld toe

The second step in the fatigue life analysis is the calculation of the fatigue crack propagation life using the LEFM method that is coded in the FALPR software. The observed cracks by the JD fatigue test experiments of the current case were found to be semi-elliptical in shape with a surface crack length of approximately 2c = 3.5 mm. Therefore, the initial crack size was assumed to be not greater than a_i = 0.5 mm in depth with an aspect ratio of (a/c = 0.286). Accordingly, the predictions of the fatigue crack propagation life were based on assuming a semi-elliptical planar crack in a finite thickness plate.

In the case of semi-elliptical cracks, two stress intensity factors, at the depth and surface points, are needed. Using the weight function method, with the through-thickness stress distribution $\sigma_{xx}(y)$ based on the shell FE modelling and Monahan equation, the stress intensity factors at the crack depth and surface (points A and B in Figure 3-13) can be determined. These two stress intensity factors are important for the determination of crack increments after each cycle for both surface and depth directions, as per equations (2.21 and 2.22). The crack increments due to the applied load cycles are calculated by using Paris' fatigue crack growth equation (2.20). To use the Paris equation, fatigue crack growth properties C and m are required for the material of the welded joint under investigation. Fatigue crack growth properties for the material of the current case (T-joint subjected to out-of-plane cyclic loading) is the same as Case # 1 (see section 5.3.1).

The through-thickness stress distribution based on the shell FE model and Monahan equation were input to FALPR to determine the stress intensity factors. It was found that the crack was growing on the surface faster than the depth because of the high stress at the weld toe [62]. Therefore, the crack increments of the surface and deepest point have to be determined for each load cycle. Accordingly, the aspect ratio (a/c) has to be updated after each increment using Paris' fatigue crack growth. The fatigue crack propagation life has been predicted for the T-joint weld subjected to out of plane bending loadings of (F = 308 N, and F = 468 N). The predictions of both load cases were carried out with and without the residual stress to investigate the effect of the residual stress.

The data input to FALPR, the predicted crack depth versus the number of cycles, the stress intensity factor versus the number of applied load cycles, and the fatigue crack growth lives predictions, and the fatigue crack propagation lives of the weld joint under investigation are shown in Figure A1- 20 through

Figure A1- 23 when applying F = 308 N and F = 468 N, respectively, whereas Figure A1- 24 through Figure A1- 27 show the same results, including the effect of the residual stress. Note that including the residual stress affect was done to study its effect on the fatigue life evaluation.

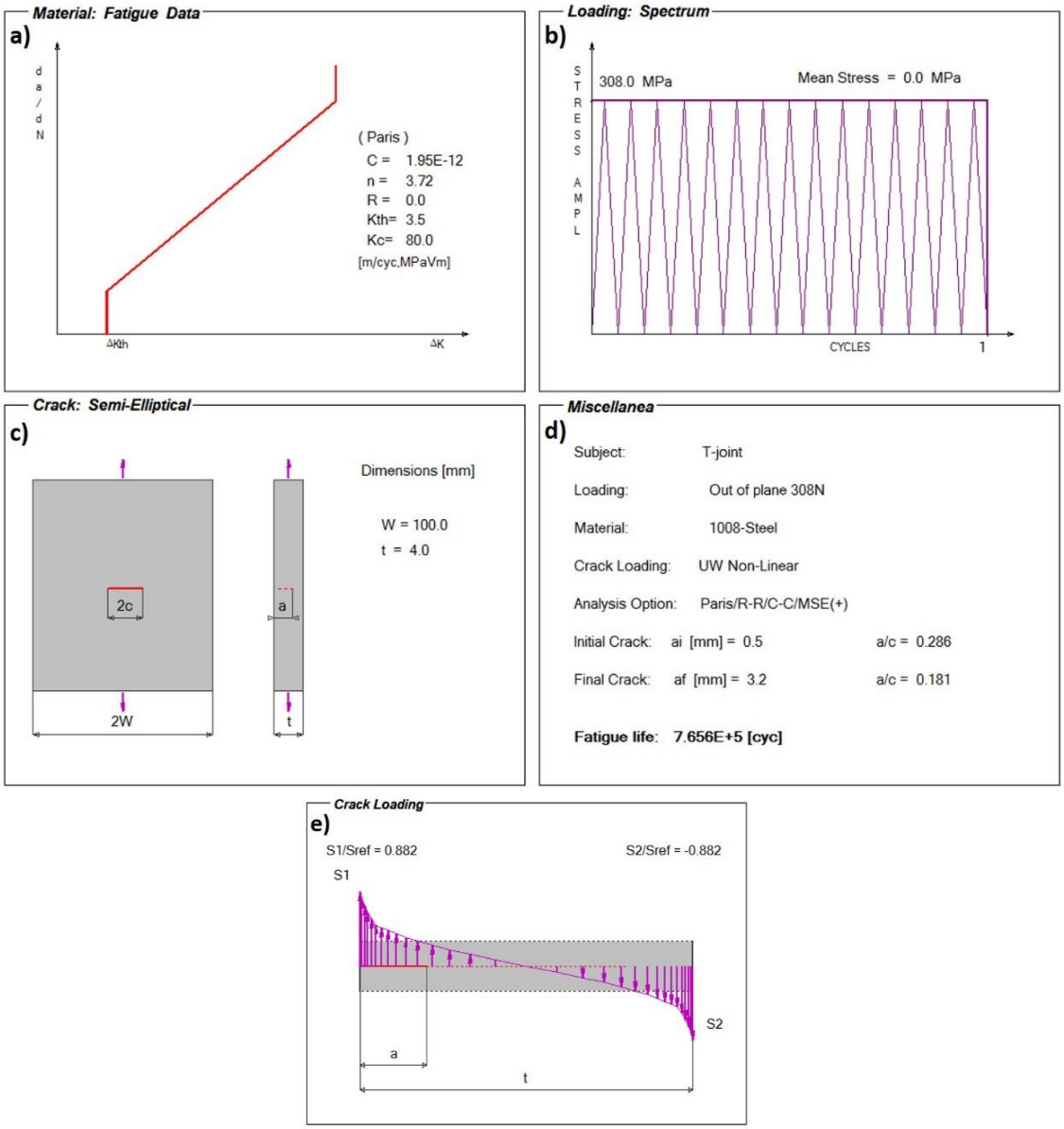

Figure A1- 20:FALPR input data for fatigue crack propagation analysis of the T-joint subjected to out-of-plane cyclic loading of F = 308 N (without residual stress): a) Paris fatigue crack growth curve, b) Loading history of the peak stress, c) Geometry of the crack, e) The normalized through-thickness stress distribution

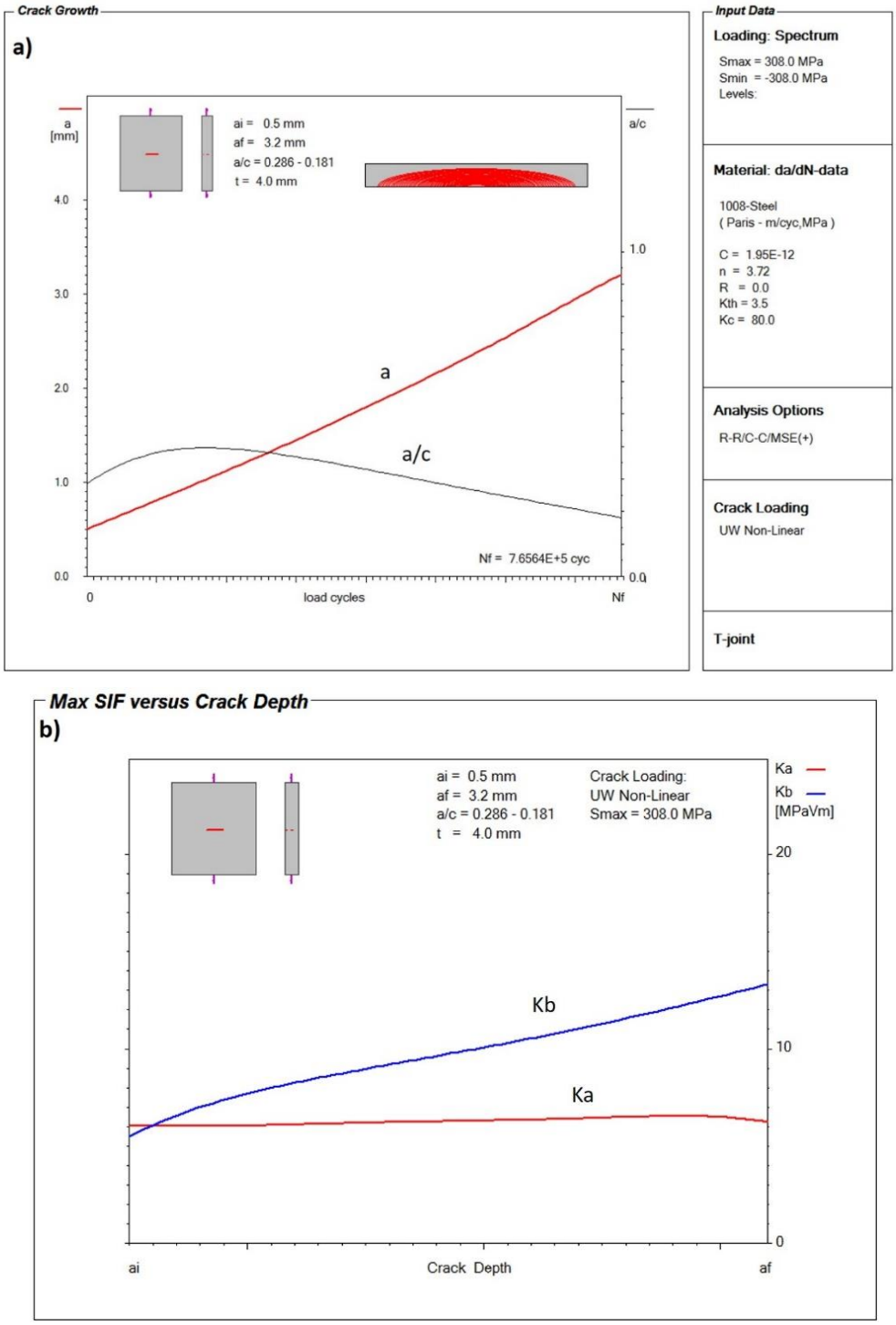

Figure A1- 21: a)The crack depth versus the number of applied load cycles to failure (a-N diagram), b) The stress intensity factor values at the surface and depth points of the semi-elliptical crack versus the crack depth (K-a diagram); T-joint subjected to out-of-plane cyclic loading of F = 308 N

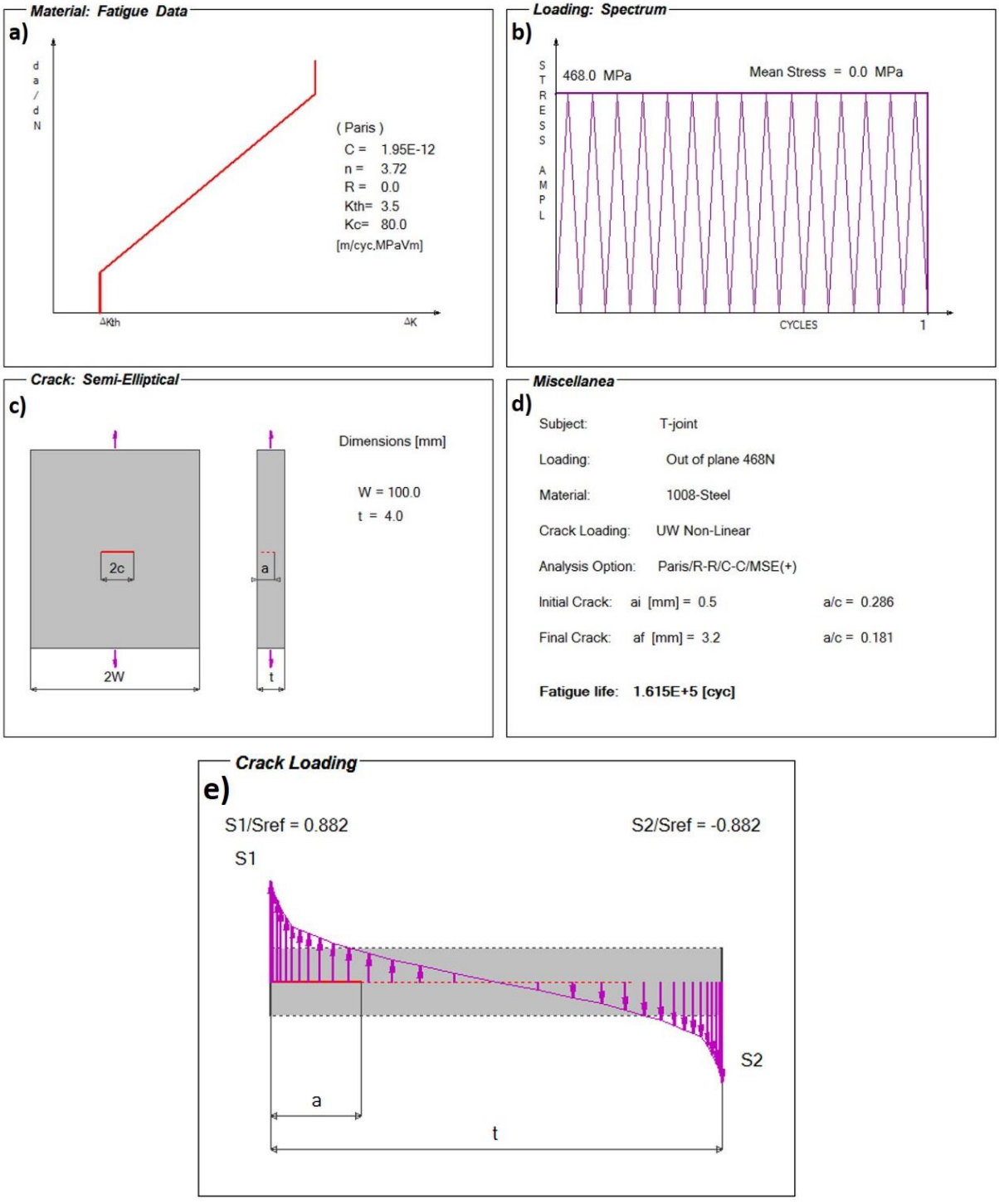

Figure A1- 22: FALPR input data for fatigue crack propagation analysis of the T-joint subjected to out-of-plane cyclic loading of F = 468 N (without residual stress): a) Paris fatigue crack growth curve, b) Loading history of the peak stress, c) Geometry of the crack, e) The normalized through-thickness stress distribution

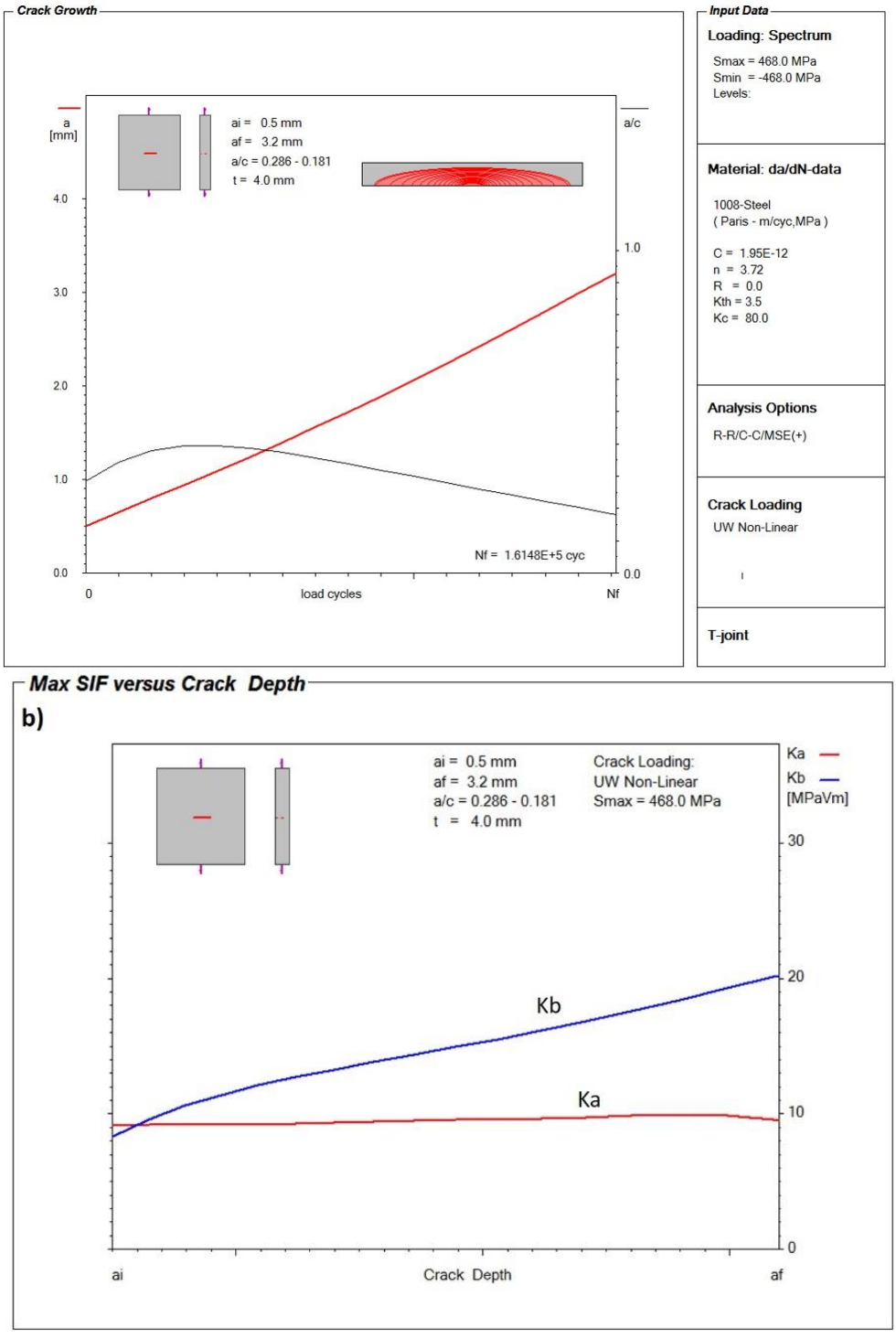

Figure A1- 23: a) The crack depth versus the number of applied load cycles to failure (a-N diagram), b) The stress intensity factor values at the surface and depth points of the semi-elliptical crack versus the crack depth (K-a diagram); T-joint subjected to out-of-plane cyclic loading of F = 468 N

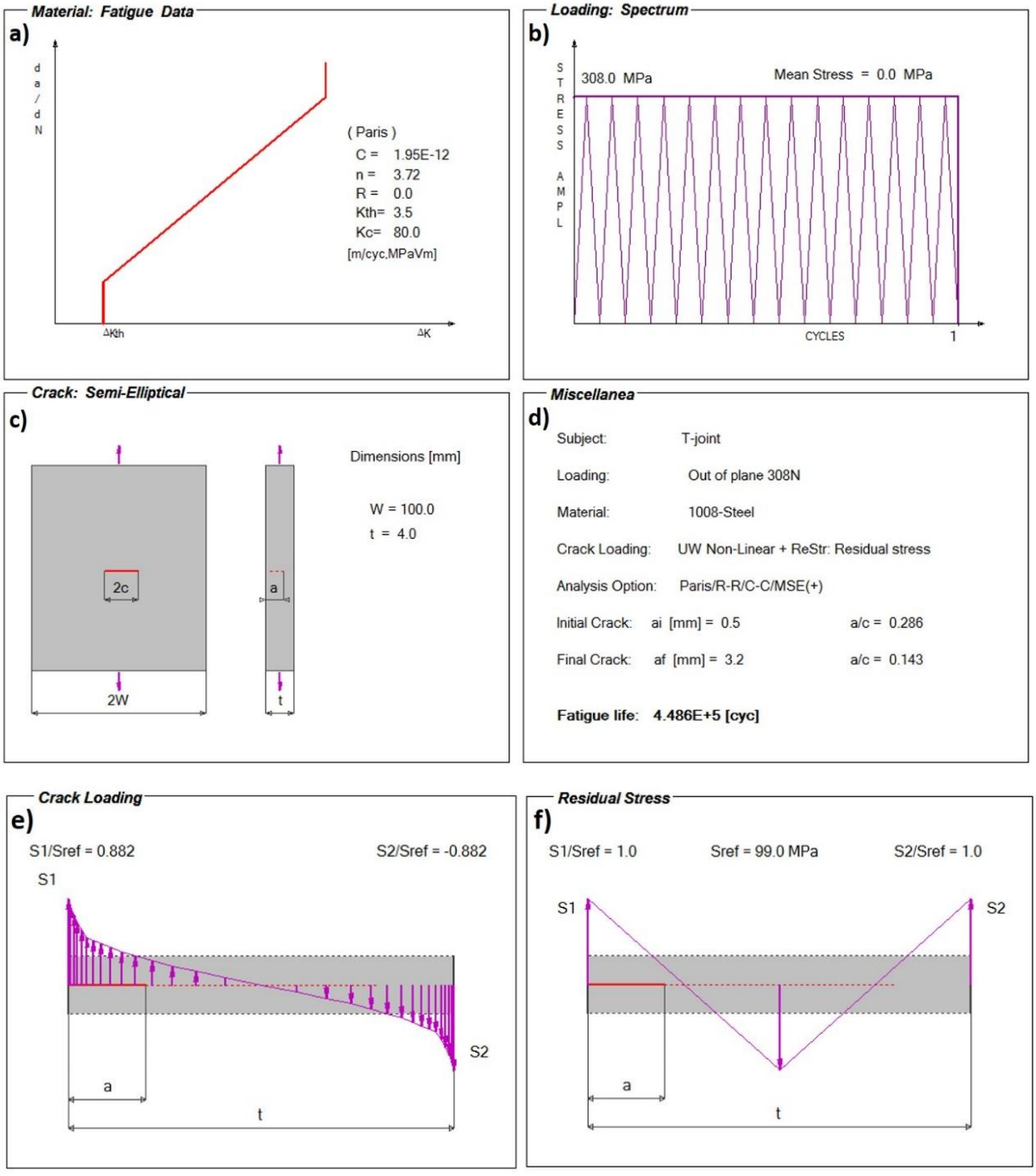

Figure A1- 24: FALPR input data for fatigue crack propagation analysis of the T-joint subjected to out-of-plane cyclic loading of F = 308 N (with residual stress): a) Paris fatigue crack growth curve, b) Loading history of the peak stress, c) Geometry of the crack, d) Fatigue life, e) The normalized through-thickness stress distribution, f) Estimated residual stress distribution through the thickness of the weld toe cross section

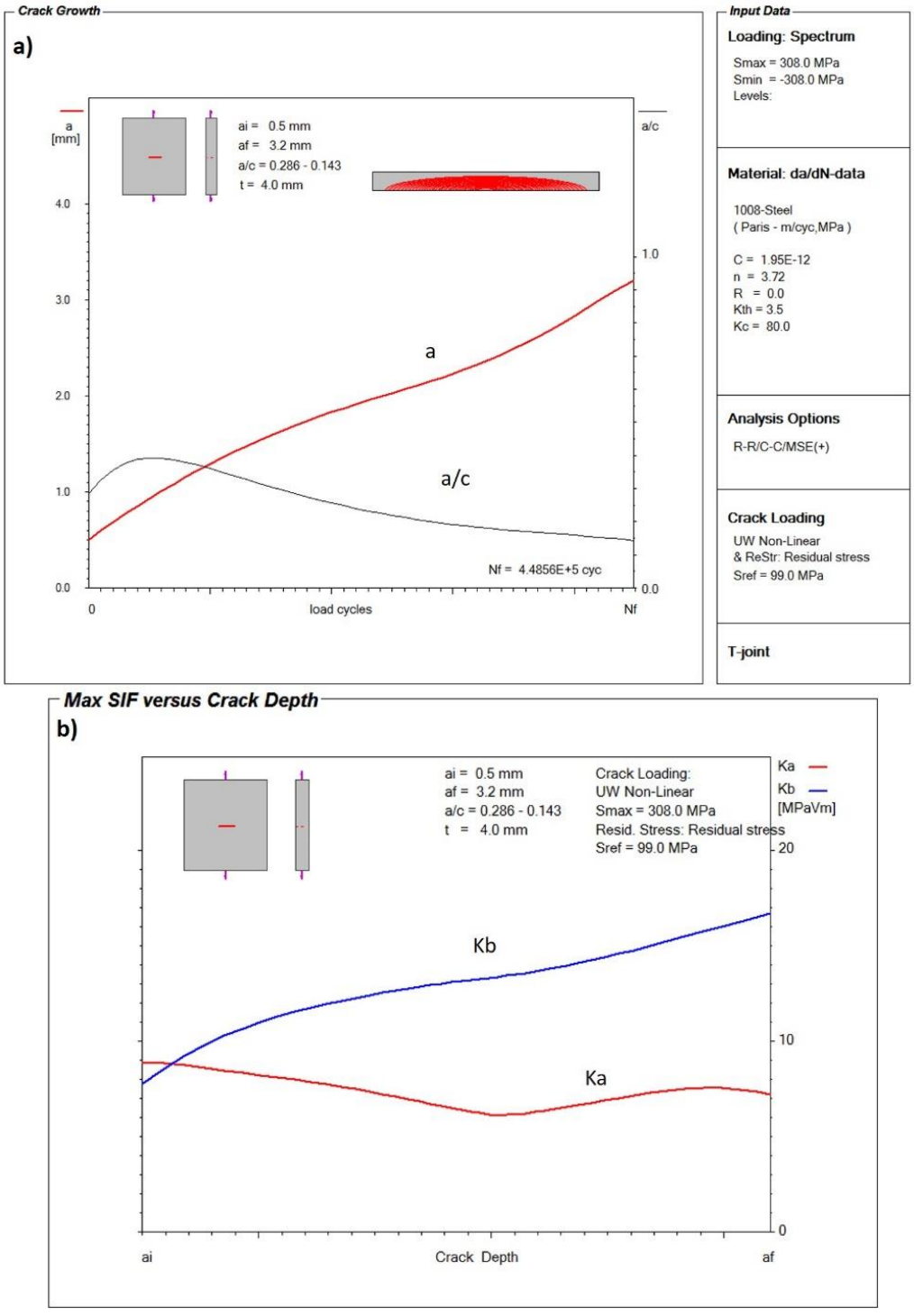

Figure A1- 25: a) The crack depth versus the number of applied load cycles to failure (a-N diagram), b) The stress intensity factor values at the surface and depth points of the semi-elliptical crack versus the crack depth (K-a diagram); T-joint subjected to out of plane load of F = 308 N (without residual stress)

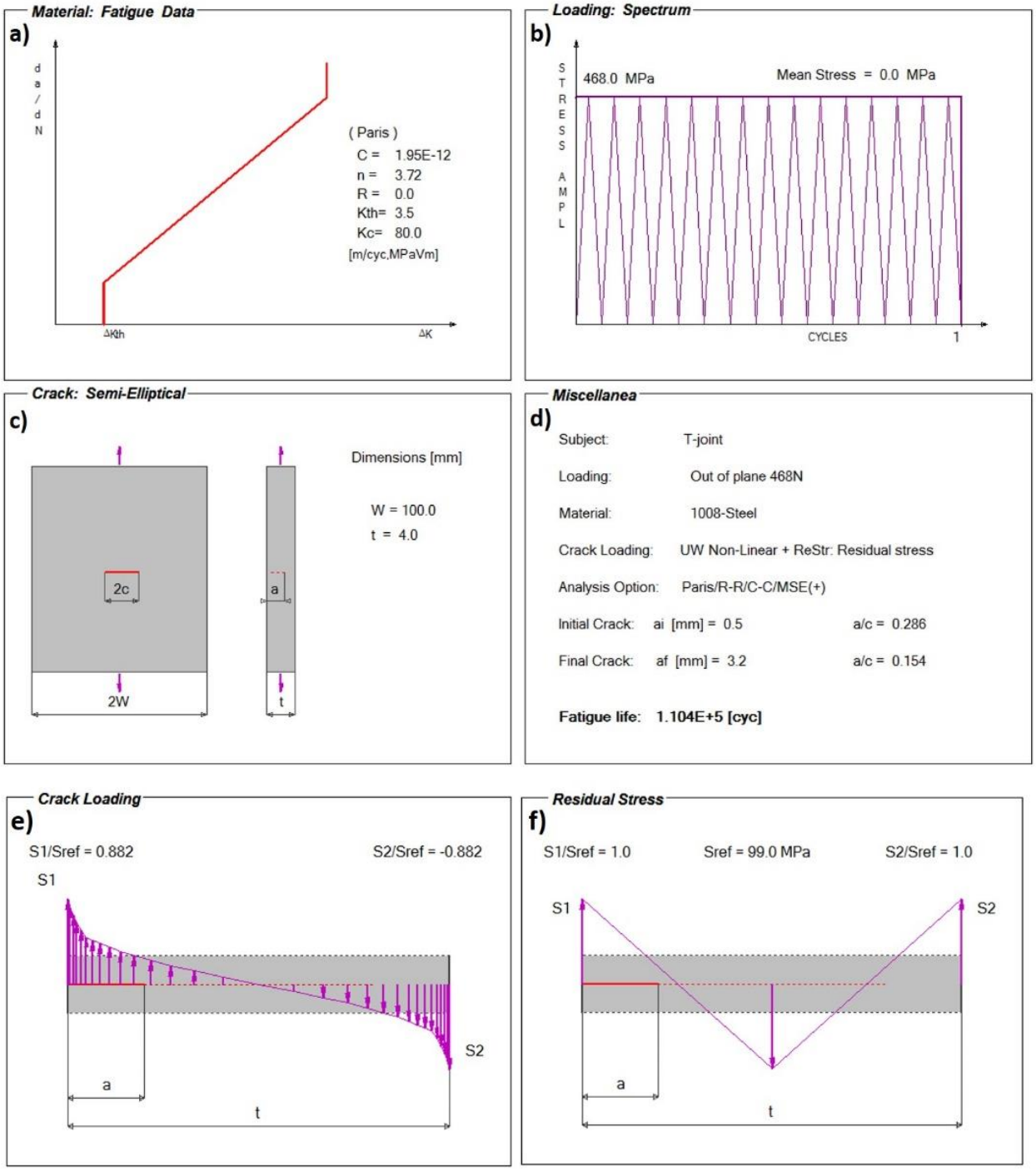

Figure A1- 26: FALPR input data for fatigue crack propagation analysis of the T-joint subjected to out-of-plane cyclic loading of F = 468 N (with residual stress): a) Paris fatigue crack growth curve, b) Loading history of the peak stress, c) Geometry of the crack, d) Fatigue life, e) The normalized through-thickness stress distribution

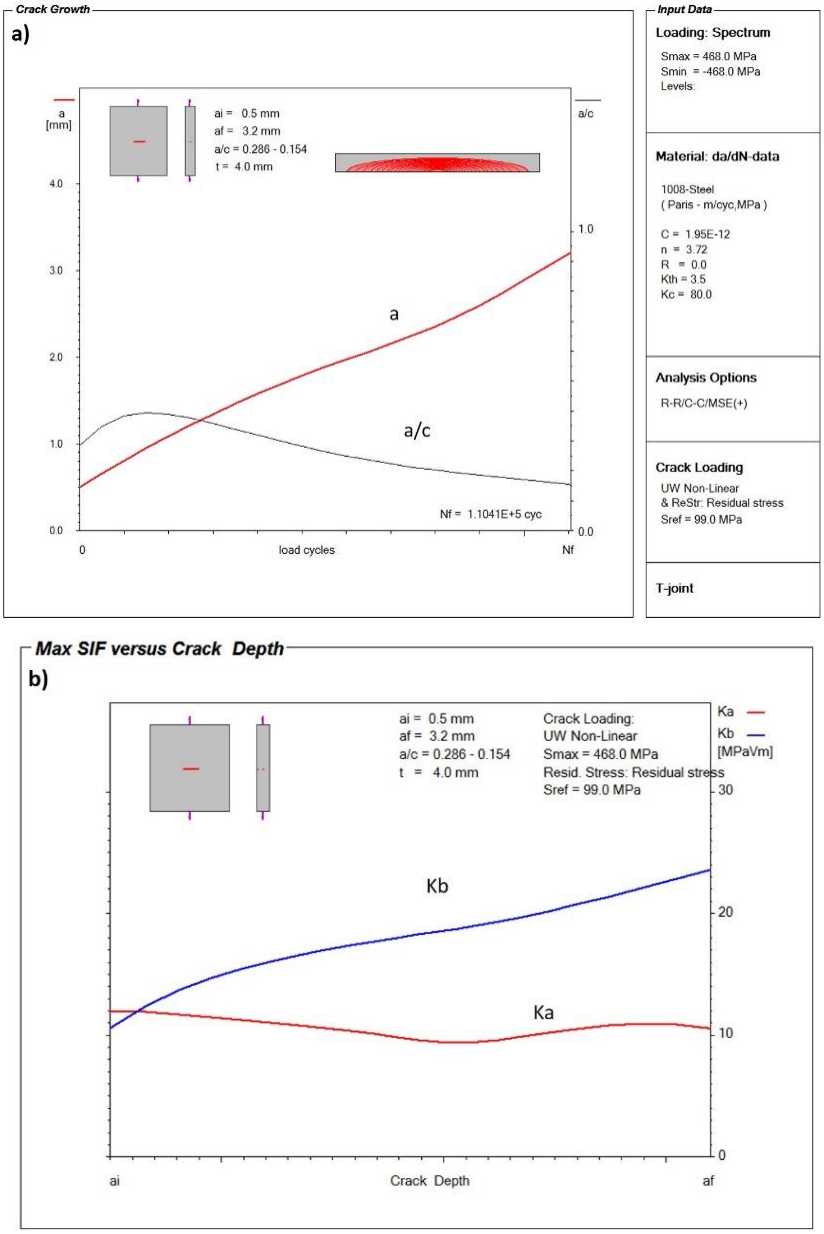

Figure A1- 27: a) The crack depth versus the number of applied load cycles to failure (a-N diagram), b) The stress intensity factor values at the surface and depth points of the semi-elliptical crack versus the crack depth (K-a diagram); T-joint subjected to out of plane load of F = 468 N (with residual stress)

The fatigue analysis results are shown in Table A- 1 for both cases of the T-joint subjected to out of plane loading of F = 308 N and F = 468 N. The total fatigue life (N_f) was determined by summing the fatigue crack initiation life (N_i) and the fatigue crack propagation life (N_p). The ratios of the

fatigue crack initiation life to the fatigue crack propagation life and the total fatigue life (N_i/N_p and N_i/N_f) are shown to determine which fatigue life was dominant to the total life.

Table A1- 1: Summary of predicted fatigue lives for the T-joint subjected to out-of-plane cyclic loading

Case load	Residual Stress (MPa)	N_i (Cycle) a_i = 0.5 mm	N_p (Cycle) a_f = 3.2 mm	N_i/N_p	N_f (Cycle)	N_i/N_f
F= 308 N	σ_r = 0	118117	765640	0.154	883757	0.134
	σ_r = 99	67165	448560	0.150	515725	0.130
F= 468 N	σ_r = 0	16420	161480	0.102	177900	0.092
	σ_r = 99	11430	110410	0.104	121840	0.094

The small ratios of the crack initiation life (N_i) to the crack growth life (N_p) and the total fatigue life (N_f) indicate that most of the welded joint fatigue life was spent on propagating the crack from a_i = 0.5 mm to the final critical crack depth a_f = 3.2 mm.

The JD Company's laboratory fatigue lives were calculated as the number of load cycles versus the measured length of the surface crack on the attachment plate. Using the fatigue crack growth simulation data obtained from the FALPR program, the crack depth corresponding to the measured crack length was estimated. The experimental data are shown in Table A1- 2.

Table A1- 2: JD Experimental fatigue crack propagation life data (2c-N) for the T-joint subjected to out-of-plane cyclic loading

Sample #	Load (N)	Number of cycles (cycles)	Crack length 2c (mm)
1	± 308	347000	3.5
4		533675	3.5
6		156200	3
		224560	5
		231802	6
		322650	6.5
		331054	7
		629456	8
2	± 468	15510	3.5
3		14131	3.5
5		13900	5
		17141	6
		18684	6.5
		30527	7
		40896	15
		53150	24.5
		57800	25
		64155	26
		72288	35

The fatigue life data in Table A1- 1 and Table A1- 2 are plotted as shown Figure A1- 28 and Figure A1- 29 in for both load levels. The fatigue life data are plotted in terms of the applied load cycles versus the surface crack length (2c) for comparison between the experimental and predicted fatigue life. The experimental fatigue data are plotted as a series of discrete points, whereas the predicted fatigue data are plotted as two curves. The hashed curve represents the fatigue life prediction without the effect of the residual stress (No-RS), and the solid curve represents the fatigue life prediction, including the residual stress effect (with RS).

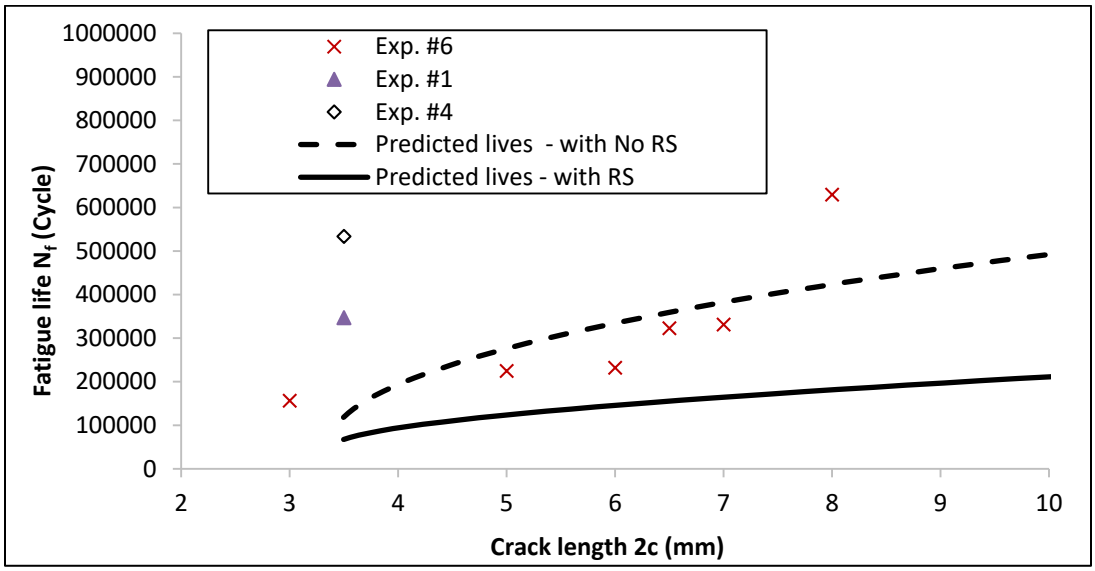

Figure A1- 28: Comparison between experimental and predicted fatigue lives of the T-joint weld subjected to out of plane bending load of (F = 308 N)

According to Figure A1- 28, the predicted total fatigue lives based on the proposed shell FE method are more conservative (under prediction) than the experimental data when the residual stress is not included in the calculation of the fatigue life. The predicted fatigue life using the proposed method showed good agreement with experiment number 6 for most of the specimen fatigue life span. In contrast, the other experiment specimens (Samples # 1 and 4) had only one fatigue life point, and both are marked as the first detected crack. This could mean that the experiments (Samples # 1 and 4) were interrupted or not observed as regular as specimen of experiment number 6. The difference between the predicted life including the residual stress (solid line in Figure A1- 28) and the experimental data could be because of several reasons. One reason could overestimating the initial crack size or the semi-elliptical crack shape. Further investigation is required.

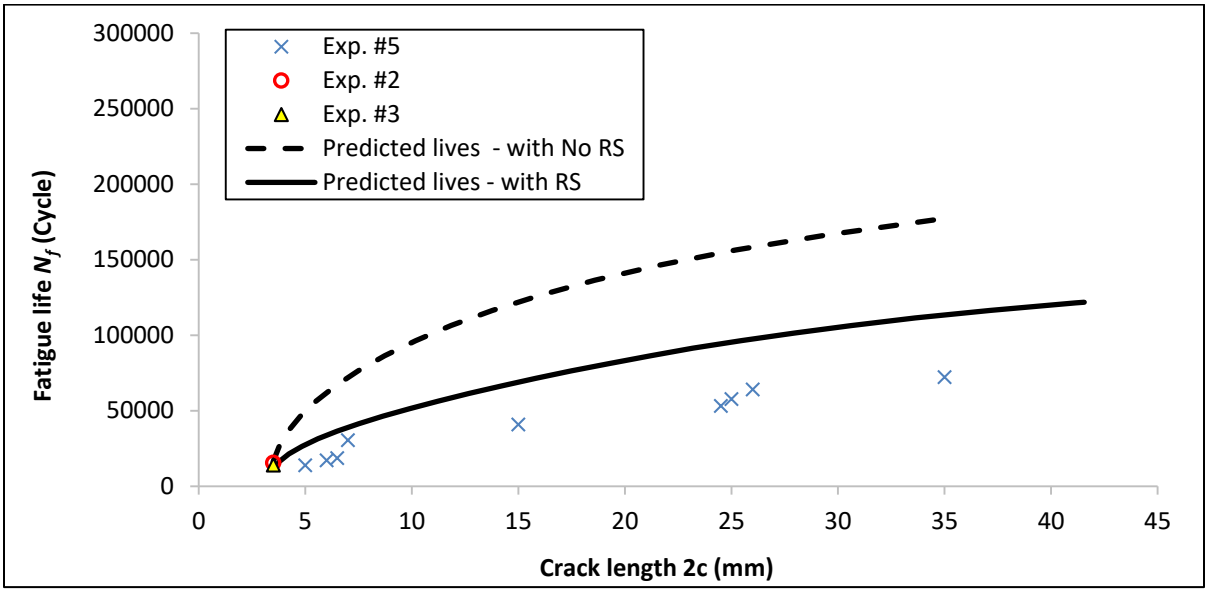

Figure A1- 29: Comparison between experimental and predicted fatigue lives of the T-joint weld subjected to out of plane bending load of (F = 468 N)

According to the results shown in Figure A1- 29, the predicted fatigue life based on the proposed shell FE method are overestimated compared to the experimental data. Including the residual stress reduces the over estimation which emphasizes the importance of including the residual stress effect when evaluating the fatigue life of welded joints.

The predicted fatigue life using the proposed method showed good agreement with experiment number 5 for all of the specimen fatigue life points. On the other hand, experiment specimens 2 and 3 had only one fatigue life point, and both are marked as the first detected crack. This could have been done to check the crack initiation life and/or to check crack shape and aspect ratio. It could also be the same as in the cases of experiments # 1 and 4, where the experiments were interrupted or not observed as regularly as they should be.

Generally, the total fatigue life predictions based on the proposed local reference stresses show good agreement with the experimental data. According to the experiment shown in Figure A1- 30, the crack initiated from the upper weld toe in the middle of the attachment plate just which agree with the results of the FE modellings. The results in both cases (F=308 N and F= 468 N) indicate that it is important to include the residual stress distribution in the stress analysis module when determining the fatigue life of weldments.

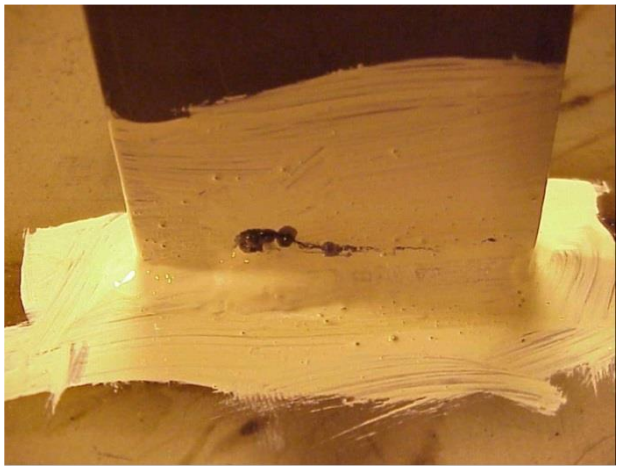

Figure A1- 30: Crack location in the attachment plate's upper weld toe of the T-joint subjected to out-of-plane cyclic loading

A2.1 Fatigue analysis of a Square-tube-on-plate welded joint subjected to lateral cyclic loadings

In this case, several welded joints connecting a square tube to a plate were tested at the JD laboratories by applying fatigue loading of a force lateral to the attachment tube length, as shown in Figure A2- 1. The welded joint is constructed of main or base plate of dimensions 304.8 × 304.8 × 25.4 mm, and attached square tube was located at the center of the base plate. The square tube thickness was 7.923 mm. The material of the tested components was A13C-RC5 steel. The weld geometries were t = 24.5 mm, t_p = 7.25 mm, h = 9 mm, h_p = 9 mm, θ= 45°, and ρ = 0.8 mm.

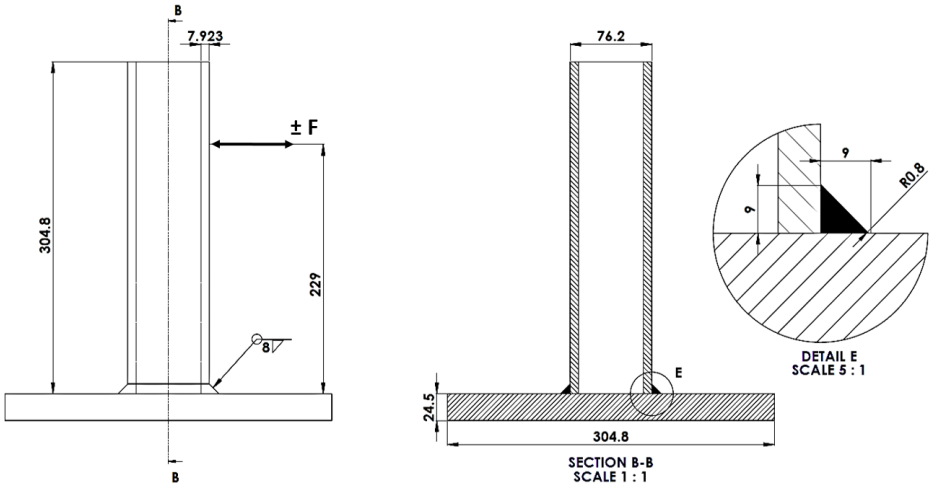

Figure A2- 1: Dimensions and loading direction of the Square-Tube-on-plate welded joint subjected to lateral loading (all dimensions in mm)

Seventeen specimens in total were tested by JD according to the ASTM standards [1]. Eight test specimens were subjected to a load of F = ± 21350 N, while the other eight test specimens were subjected to a load of F = ± 13878 N and one subjected to F = ± 11565 N. All forces were acting on the vertical attached square tube, as shown in Figure A2- 2. Each test specimen was fixed at all corners by a clamp. The highest stress is expected at the weld line perpendicular to the loading directions. Therefore, the stresses from the shell FE (σ_a and σ_b) must be evaluated in that region.

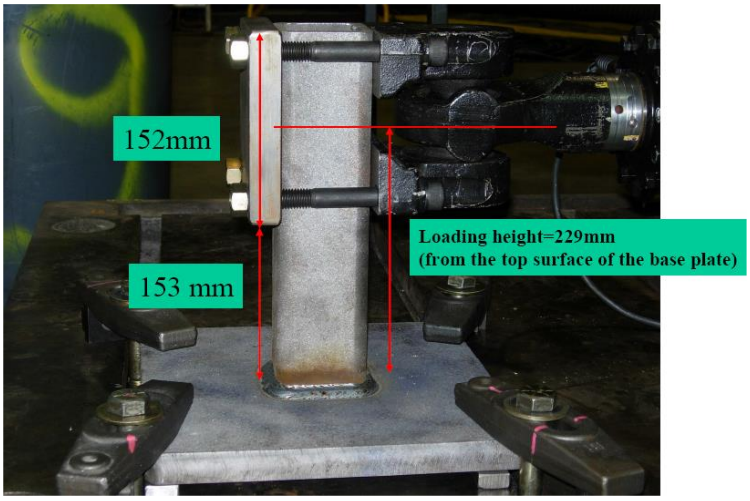

Figure A2- 2: JD experiment for the Square-Tube-on-plate welded joint subjected to lateral loading (JD)

A2.1.1 Material properties

The material properties of the welded joint under investigation (A13C-RC5 steel) were provided by the JD laboratories. The chemical composition and mechanical properties are shown in Table A2- 1 and Table A2- 2, respectively. The fatigue test data for the A13C-RC5 steel are shown in Table A2- 3.

Table A2- 1: Chemical composition of A13C-RC5 steel (weight %)

C	Si	P	S	Mn	Ni	Cr	Mo	Cu	Ca	Al
0.168	0.272	0.013	0.009	1.319	0.025	0.017	0.006	0.006	0.0032	0.0471
Sn	B	V	Zr	Co	Ce	Nb	Ta	Pb	Mg	
0.001	0.000227	0.054	0.003	0.005	0.0004	0.002	0.0069	0.00431	0.0005	

Table A2- 2: Mechanical properties of A13C-RC5 steel

Ultimate strength (Su)	Yield strength (Sy)	Elastic modulus (E)
622.0 (MPa)	386.54 (MPa)	206826 (MPa)

Using the experimental data obtained for a set of smooth specimens tested by the JD laboratory according to the ASTM standard [1], the fatigue properties of the A13C-RC5 steel were determined at the University of Waterloo (UW). The fatigue parameters were determined using the Ramberg-Osgood and the Manson-Coffin curves.

Table A2- 3: Fatigue test results for A13C-RC5 steel (JD material handbook data)

Experimental total strain amplitude	Stress amplitude σ_a (MPa)	Elastic strain amplitude	Plastic strain amplitude	Number of reversals (2Nf)
0.00980	526.7	0.00706	30	0.00274
0.00940	515.3	0.00688	2140	0.00252
0.00890	519.8	0.00639	3356	0.00251
0.00800	498.9	0.00556	4710	0.00244
0.00700	488.5	0.00463	6408	0.00237
0.00600	462.6	0.00370	9044	0.00230
0.00550	459.0	0.00326	10568	0.00224
0.00500	440.8	0.00285	13940	0.00215
0.00450	422.7	0.00240	21072	0.00210
0.00425	423.1	0.00219	21940	0.00206
0.00400	413.3	0.00199	21994	0.00201
0.00375	409.2	0.00180	27514	0.00195
0.00350	397.6	0.00158	42522	0.00192
0.00300	381.7	0.00115	52898	0.00185
0.00270	372.0	0.00090	95176	0.00180
0.00240	358.8	0.00067	169168	0.00173
0.00220	343.9	0.00053	300516	0.00167
0.00200	344.3	0.00034	245990	0.00166
0.00180	320.1	0.00024	1014950	0.00156
0.00175	328.4	0.00017	1224586	0.00158
0.00167	316.7	0.00015	10608604	0.00152
0.00160	305.9	0.00010	11839006	0.00150

The following figure represents the Ramberg-Osgood cyclic stress-strain curve based on the experimental data are shown Table A2- 3. Manson-Coffin equation (2.4) was used to determine the fatigue curves, as shown in Figure A2- 3 through Figure A2- 6.

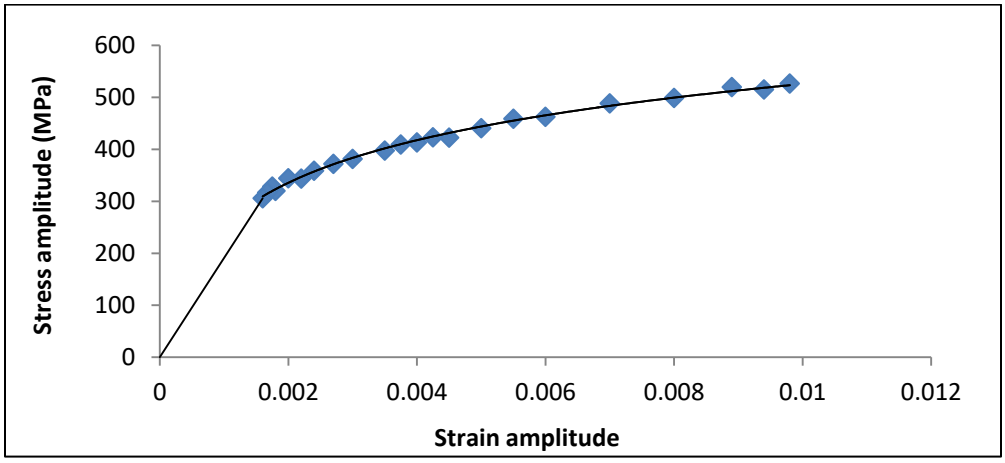

Figure A2- 3: Stress-strain curve of the A13C-RC5 steel

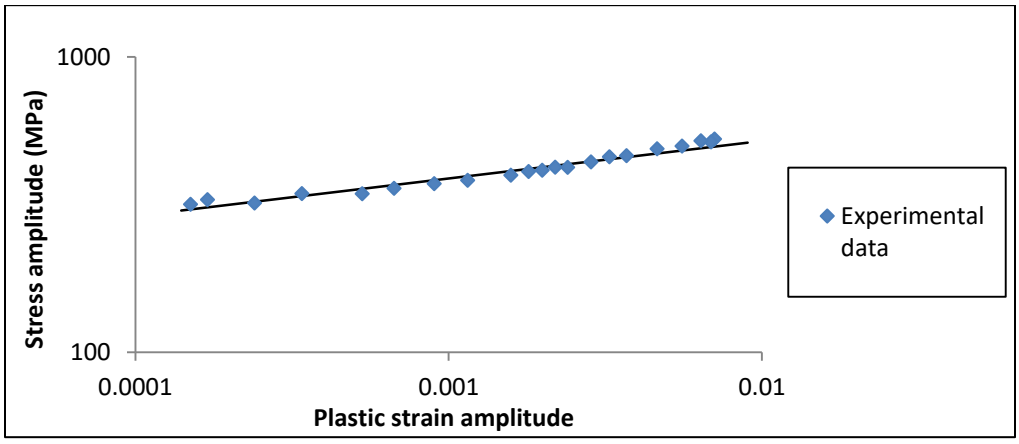

Figure A2- 4: Stress-plastic strain fatigue curve of the A13C-RC5 steel

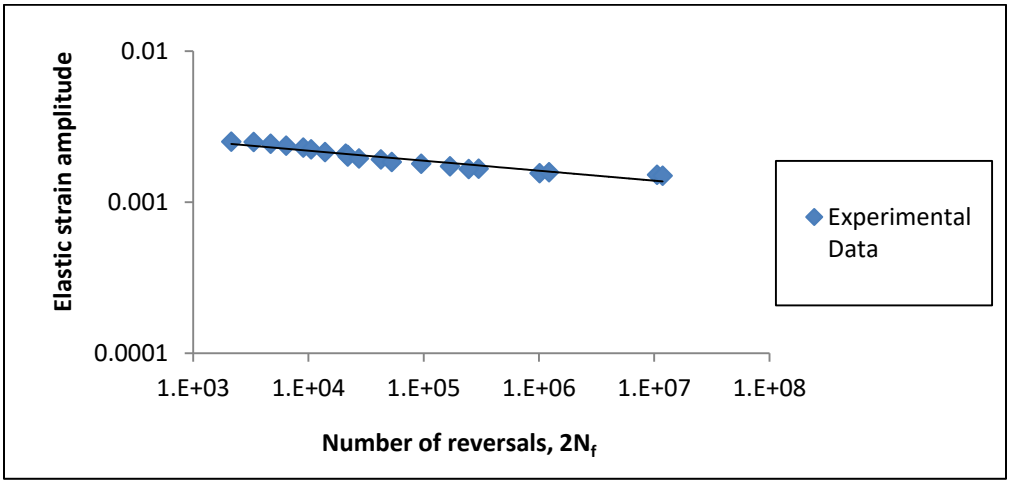

Figure A2- 5: The elastic strain amplitude-life ($\Delta\varepsilon_e/2$ - N_f) fatigue curves representing the JD experimental data and UW material data

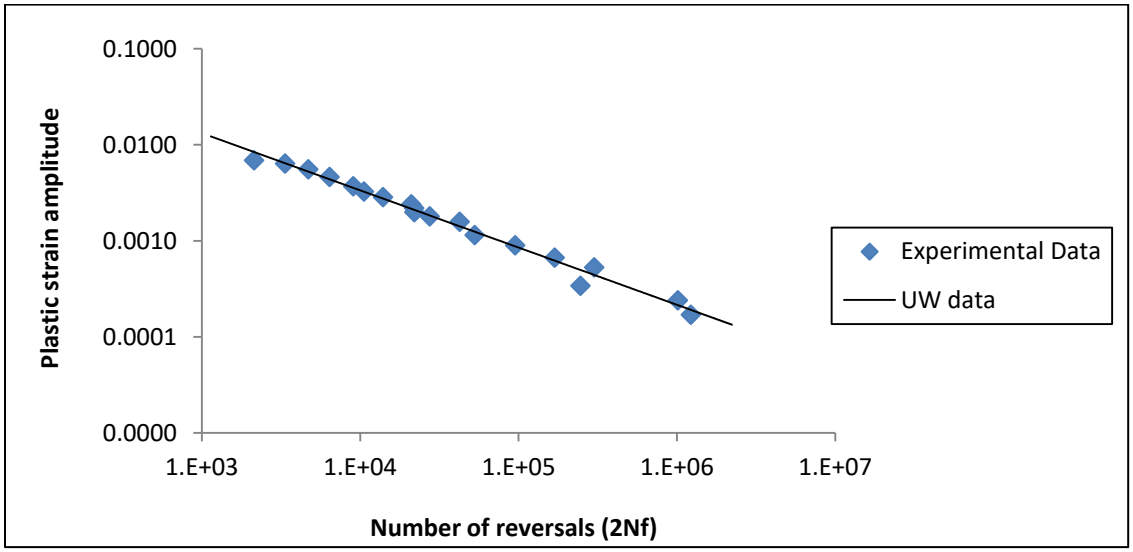

Figure A2- 6: The plastic strain amplitude-life fatigue curves representing JD experimental based on the UW analysis

The fatigue parameters that resulted from the UW analysis (curve fitting) are shown in Table A2-4 for the A13C-RC5 steel.

Table A2- 4: UW fatigue parameter for A13C-RC5 steel

Fatigue strength coefficient (σ_f')	**1080 (MPa)**
Fatigue strength exponent (b)	**-0.092**
Fatigue ductility coefficient (ε_f')	**1.0878**
Fatigue ductility exponent (c)	**-0.6236**
Cyclic strength coefficient (K′)	**931.8 (MPa)**
Cyclic strain hardening exponent (n′)	**0.127**

A2.1.2 Shell FE modelling of a Square-tube-on-plate welded joint subjected to lateral cyclic loadings

The shell FE model should have the same geometry as the experiment specimen. In addition, the stress data must be extracted from the weld's critical location. The expected critical locations are at the weld toe line perpendicular to the applied load direction. These two critical points A and B are shown in. The maximum stress that will initiate a crack could occur at either the upper weld toe (Point A) or the lower weld toe (Point B). The corresponding through-thickness stress distribution is either through (S - I or S – II) in Figure A2- 7.

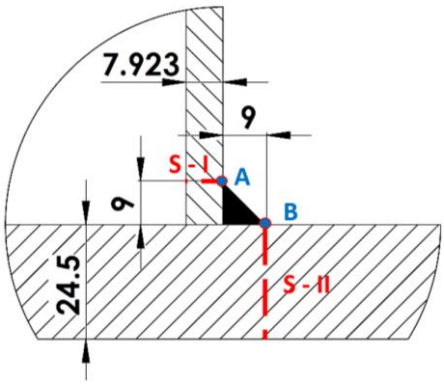

Figure A2- 7: Upper and lower weld toe and through-thickness cross-sections

The shell FE model's boundary conditions of the square-tube-on-plate welded joint under investigation. The base plate corners were constrained for all displacement while a force of F = 1 N was applied to the attachment tube pinhole.

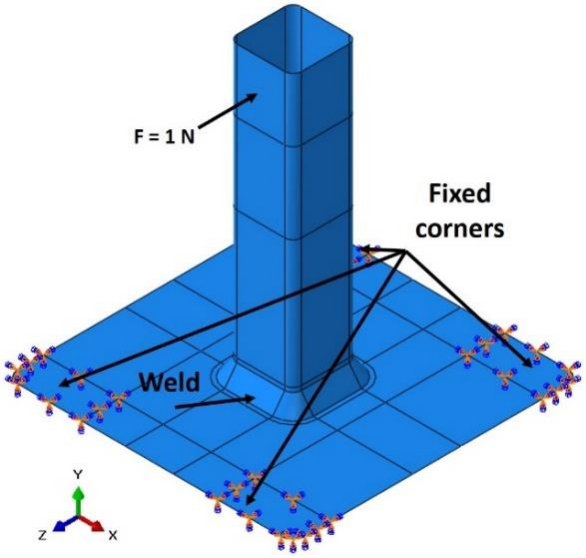

Figure A2- 8: Shell FE modelling and boundary conditions for the Square-Tube-on-plate welded joint subjected to lateral loading (F = 1 N)

The local reference stresses σ_a and σ_b were obtained from two critical points (A and B in Figure A2- 7). According to Figure A2- 8, it was found that the upper weld toe (reference point A) contains larger stresses than point B. The reference point contains the local reference stresses, which represent the stresses through the plate thickness. These stresses (local reference stresses) are used to determine the membrane and bending hot spot stresses that will be multiplied by the proper SCFs (see section 3.7) to calculate the peak stress at the weld toe.

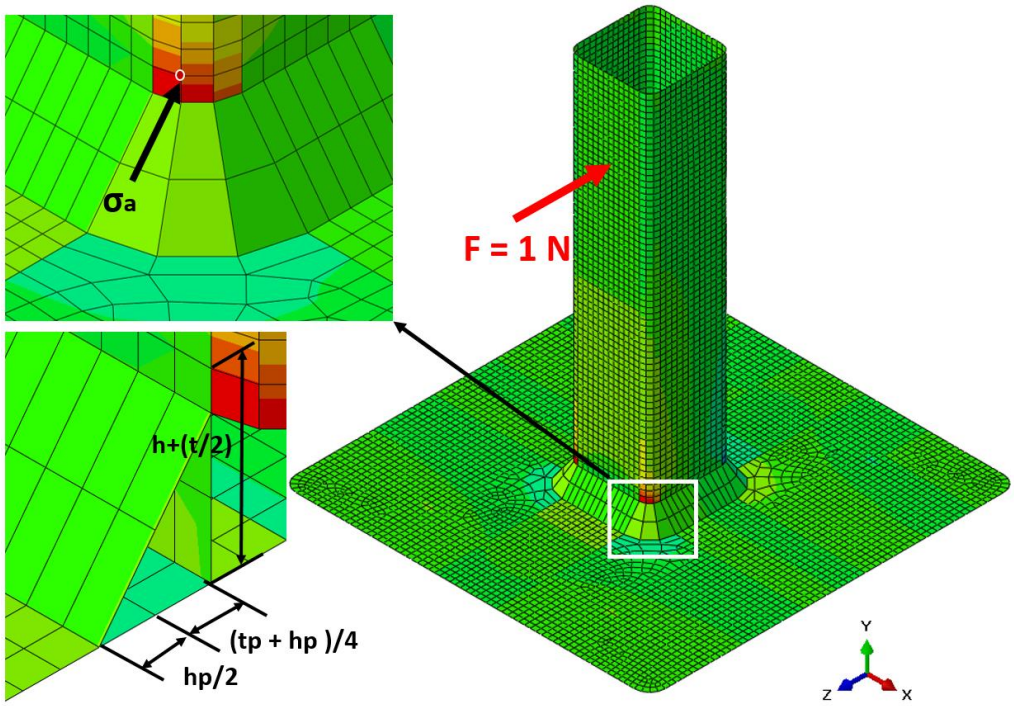

Figure A2- 9: Shell FE modelling and boundary conditions for the Square-Tube-on-plate welded joint subjected to lateral loading (F = 1 N)

Note that the reference points in the above shell FE model coincide with the actual location of the weld toe of the experimental specimen. The maximum stress is located at the weld toe, as shown in Figure A2- 9. However, the required shell FE reference stresses are to be extracted from a specific reference point and not at the maximum contour node. The distance between the main plate mid-plane and the reference point representing the upper weld toe was h + (t /2) = 21.7 mm. At that specific reference point, the local reference stresses σ_a and σ_b were extracted on the opposite surface sides of the attachment plate (two sides or surface points). The local reference stresses through the tube thickness at the critical point (σ_a and σ_b) were recorded as follows:

σ_a = 0.01055 MPa

σ_b = 0.00168 MPa

Therefore, the hot spot membrane and bending stresses σ_{hs}^{m} and σ_{hs}^{b}, per equations (3.12 and 3.13), were:

$$\sigma_{hs}^{m} = \frac{\sigma_a + \sigma_b}{2} = 0.00612 \text{ MPa}$$

$$\sigma_{hs}^{b} = \frac{\sigma_a - \sigma_b}{2} = 0.00443 \text{ MPa}$$

Using the weld geometrical features of the current case, the SCFs were calculated using equations (3.15 and 3.16):

$K_t^m = 1.72$

$K_t^b = 2.45$

As per equation (3.11), the peak stress at the weld toe induced by the applied load was:

$$\sigma_{peak} = \sigma_{hs}^{m}.K_t^m + \sigma_{hs}^{b}.K_t^b = 0.02138 \text{ MPa}$$

The stress data were found in the direction normal to the weld toe based on the shell FE model shown in Figure A2- 9. The linear stress distribution (hashed line) represents the local reference stresses σ_a and σ_b, while the non-linear stress distribution (solid curve) represents the Monahan equation $\sigma_{xx}(y)$ as shown in Figure A2- 10.

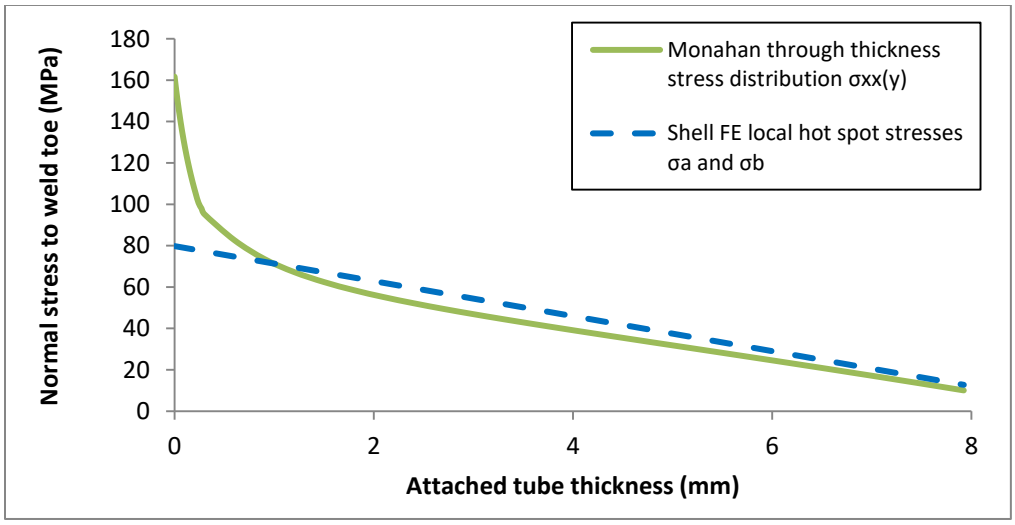

Figure A2- 10: Square-Tube-on-plate shell FE local reference stress (linear) and the Monahan non-linear through-thickness stress distribution at the weld toe

The stress data (σ_a, σ_b, $\sigma_{peak,}$ and $\sigma_{xx}(y)$) required for the fatigue analysis for the case under investigation are shown in Figure A2- 10. These stress data are obtained from a shell FE model and must be validated against a detailed 3D FE model before proceeding with the fatigue analysis. A 3D FE model with the same geometry as the experiment is modelled in the following section to validate the shell FE local reference stress data.

A2.1.3 Finite element 3D modelling of a tube-on-plate welded joint subjected to lateral loading

The 3D FE model should have the same geometry as the experimental specimen. Also, the stress data must be extracted from the weld's critical location in the same way as the shell FE model. For the case under investigation, the critical location is expected at corner of the upper weld toe of the attachment square tube. According to the shell FE model, the maximum stress occurs at the upper weld toe. Therefore, it is expected that the 3D FE model would have the peak stress at the same location. The boundary conditions of the 3D FE modelling for the square-tube-on-plate welded joint are shown in Figure A2- 11. Because of the symmetry of the problem, only half of the welded joint was modelled to reduce the computational time. The model was subjected to lateral force F = 7561.4 N acting on the attached tube. The corners of the base plate were constrained for all displacements, and the model elements were approximated by eight brick elements.

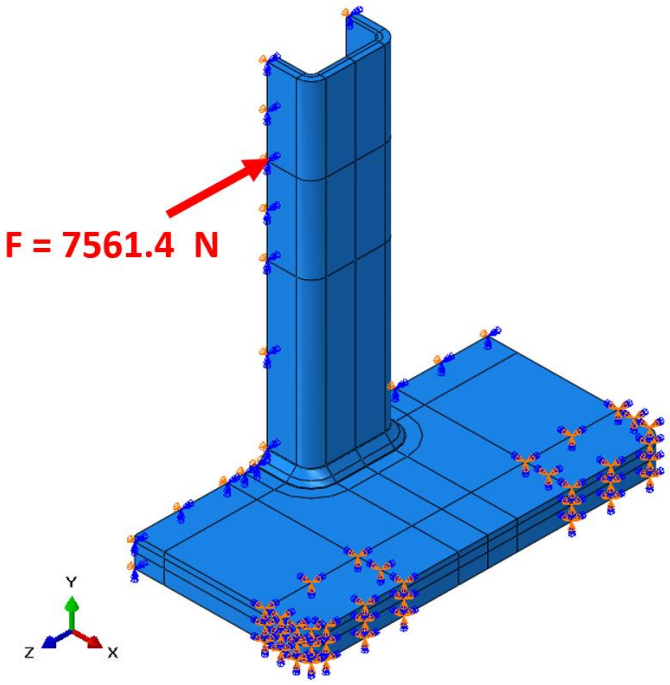

Figure A2- 11: Boundary conditions of the 3D FE simulated tube-on-plate welded joint subjected to lateral load

The meshing was intensive at the critical areas (weld toes). These areas were expected to have a peak stress normal to the weld toe. The element size at the weld toe should be small enough to find a

converged stress. The recommended element size is at least equal to quarter of the weld toe radius [64]. The meshing of the weld toe is shown in Figure A2- 12 and Figure A2- 13.

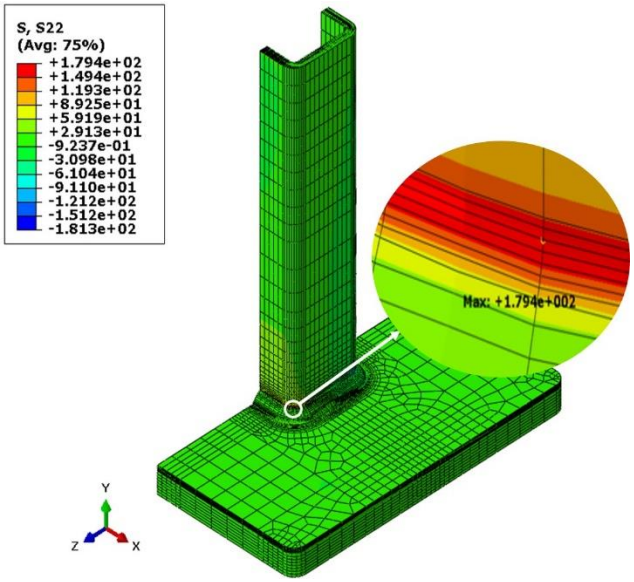

Figure A2- 12: Mesh and peak stress at the upper weld toe of the Square-Tube-on-plate joint (3D FE model)

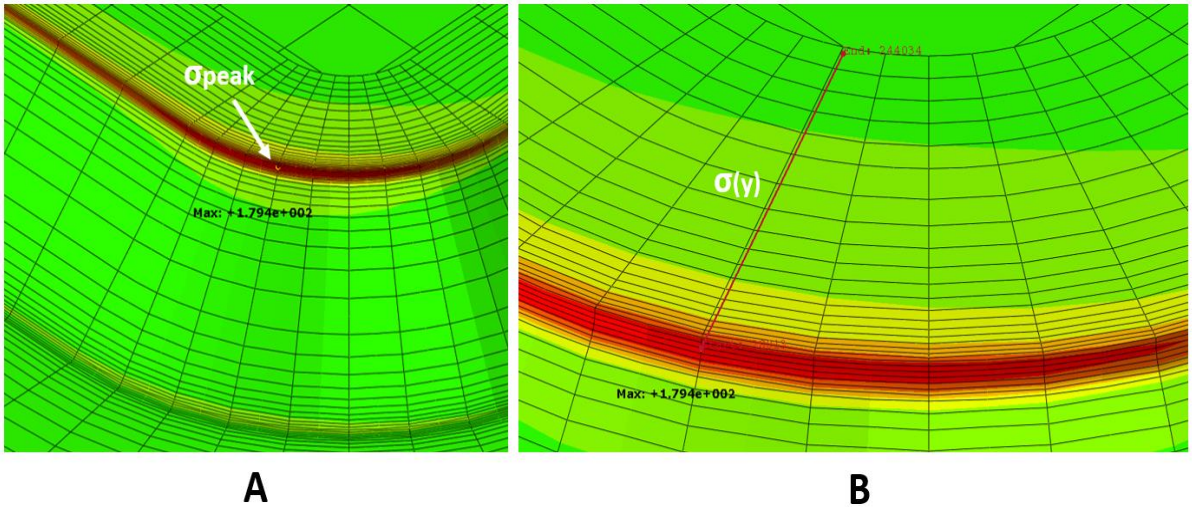

Figure A2- 13: A) The peak stress, B) The path of the through-thickness stress distribution along the upper weld toe of the Square-Tube-on-plate wall thickness

The maximum stress (peak stress) normal to the weld toe line in the 3D model was found at the upper weld toe. The location of the extracted peak stress is shown in Figure A2- 12, whereas Figure A2- 13 the path where the through-thickness stress was extracted.

Based on the 3D FE modelling, the actual peak stress obtained at the weld toe was 179 MPa (Figure A2- 12), and the actual non-linear through-thickness stress distribution is shown in Figure A2- 13 (A and B). The latter stress distribution was processed according to Section (4.1), while the membrane and bending hot spot stresses were found by linearization of the actual through-thickness stress distribution, as mentioned in equations (4.3 and 4.5):

$\sigma_{hs}^{m} = 43.69$ MPa

$\sigma_{hs}^{b} = 36.38$ MPa

Equations (4.6 and 4.7) were then used to find the linearized surface stresses as:

$\sigma_{hs} = \sigma_n = \sigma_a = \sigma_{hs}^{m} + \sigma_{hs}^{b} = 80.07$ MPa

$\sigma_b = \sigma_{hs}^{m} - \sigma_{hs}^{b} = 7.31$ MPa

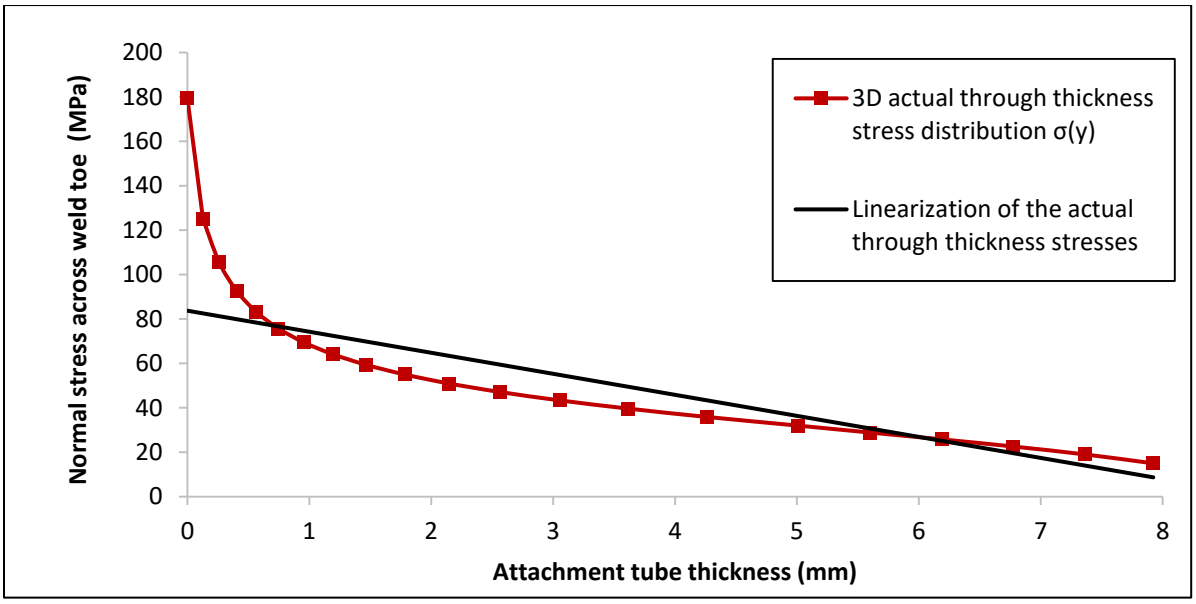

Figure A2- 14: The 3D FE stress data; actual stress distribution, and the equivalent linearized stress distribution at the weld toe of the square-tube-on-plate welded joint model subjected to lateral loading

The red curve in Figure A2- 14 represents the actual non-linear stress distribution through the thickness of the weld toe cross section based on the 3D FE model. In the same figure, the solid line represents the linearization of the red curve (linearized actual non-linear stress distribution).

The stress results of both the shell and the 3D FE models (see Figure A2- 14 and Figure A2- 10) were compared after being normalized, as shown in Figure A2- 15 and Figure A2- 16. The

normalization was done by dividing the shell and the 3D FE stress data by a load of F = 7561.4 N. The normalization was done so that the shell FE local reference stress data could be scaled later to the loads applied to the experiment specimens, which were based on loads of 21350 N, 13878 N, and 11565 N. A comparison between the actual non-linear through-thickness stress distribution σ(y) obtained from the 3D FE model and the non-linear through-thickness stress distribution $\sigma_{xx}(y)$ generated from the shell FE local reference stress data and the Monahan equation are shown in Figure A2- 15.

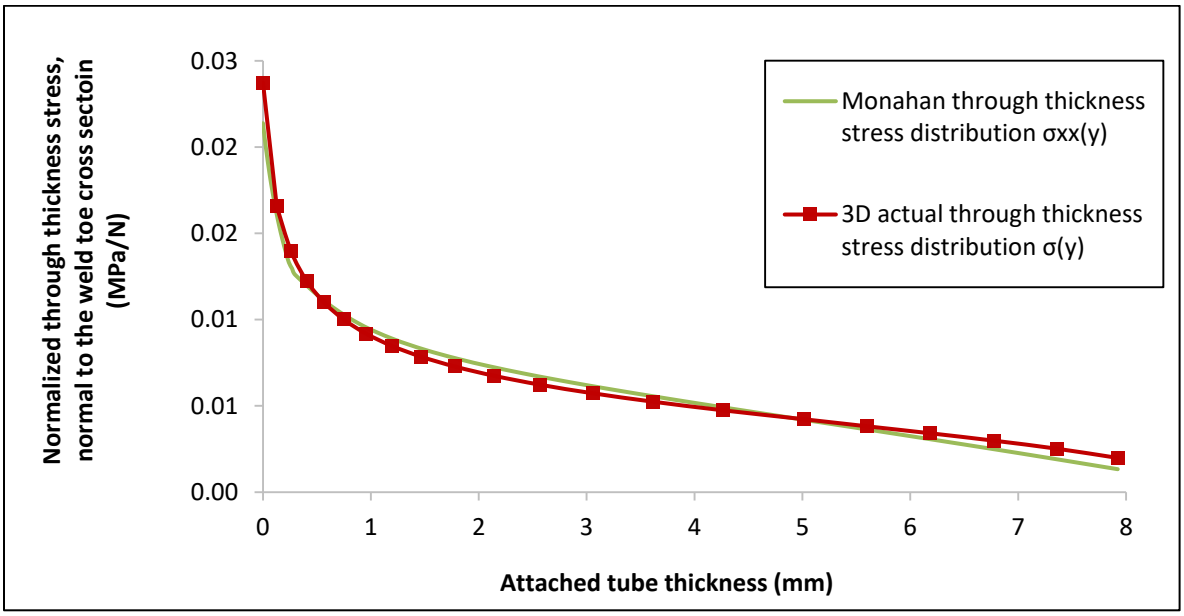

Figure A2- 15: Comparison between through-thickness stress distributions extracted from 3D FE model and shell FE model for the Square-Tube-on-plate welded joint subjected to a lateral load

The result the actual peak stress based on 3D FE modelling was almost the same as the peak stress based on the shell FE local reference stress. The comparison of the through-thickness stress distributions from the shell and the 3D FE models showed good agreement.

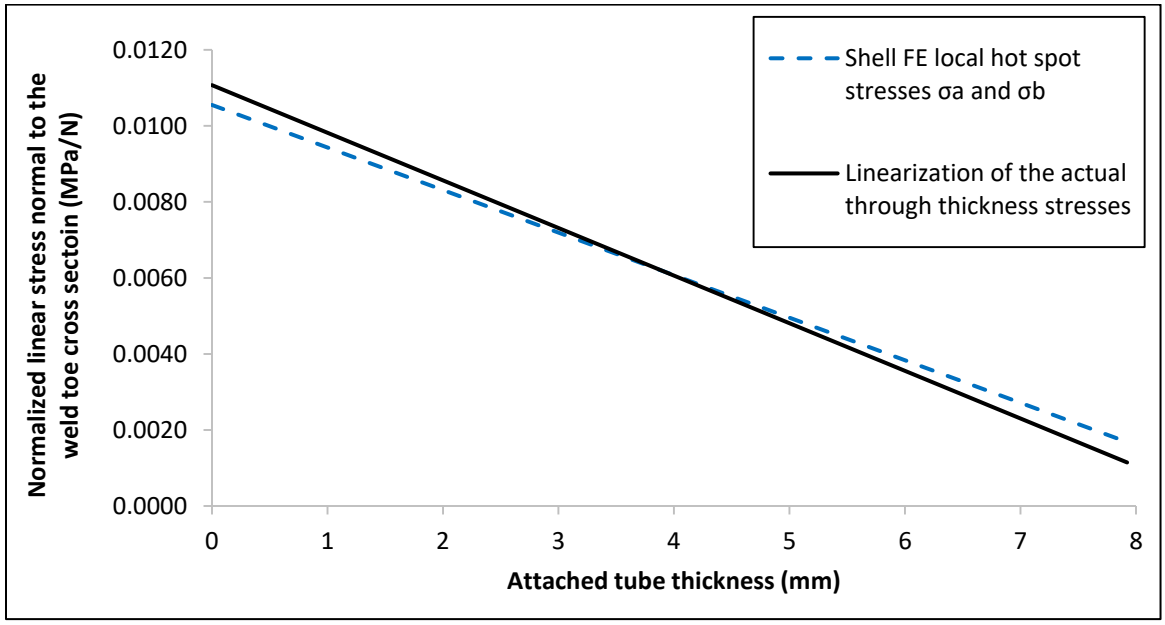

Figure A2- 16: Comparison between linearized stresses based on 3D FE model and shell FE model for the Square-Tube-on-plate welded joint subjected to a lateral load

The linearized stress data based on the 3D FE model are in good agreement with the shell FE local reference stresses in the tensile part. The shell FE was lower than the 3D FE stress in the bending parts. Note that this difference does not affect the peak stress, but the combination of the membrane and bending hot spot stresses does. The peak stress based on the 3D FE modelling was σ_{peak} = 179.42 MPa, whereas the peak stress based on the shell FE local reference stress analysis was σ_{peak} = 161.69 MPa. The difference was around 10 %. The peak stress is the important information, as it is the required stress for using the ε-N method.

This validation is important because the peak stress based on the shell FE model will be used to determine the fatigue crack initiation life using the strain-life method. In addition, the through-thickness stress distribution based on the shell FE and Monahan equation will be used to determine the stress intensity factor required to calculate the fatigue crack propagation life using the LEFM method.

The JD Company performed two series of fatigue tests to verify the predicted fatigue life for the Square-Tube-on-plate welded joint. Both tests were conducted under fully reversed loads, but the first series of test specimens was subjected to F = ± 21350 N, the second series was subjected to F = ± 13878 N, and the third was subjected to F = ± 11565 N. Therefore, the peak stress and the through-

thickness distributions obtained from the shell FE modelling (the green curve) were scaled to the experimental applied load (F= 21350 N, F = 13878 N, and F = 11565 N), as shown in Figure A2- 17, Figure A2- 18 and Figure A2- 19, respectively.

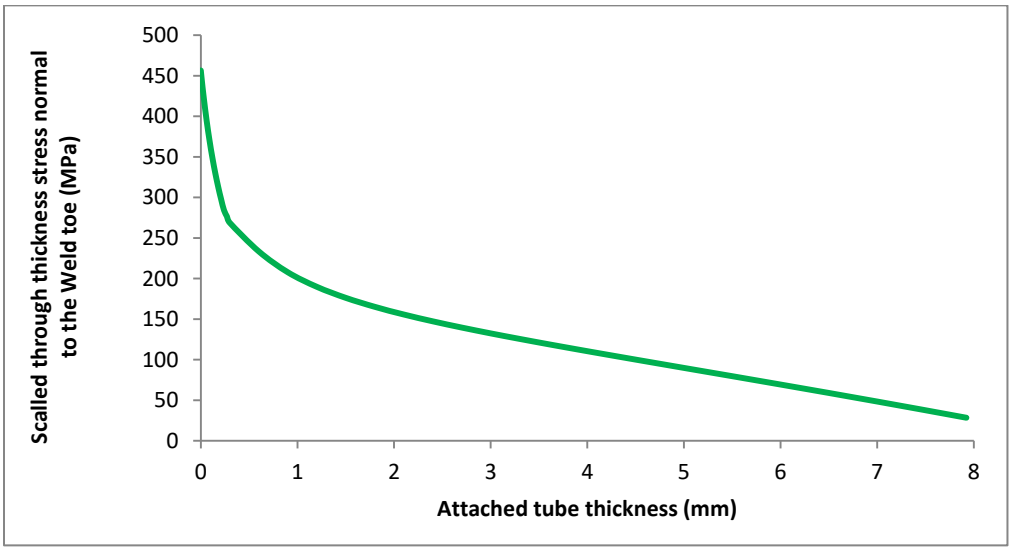

Figure A2- 17: Square-Tube-on-plate through-thickness stress distribution based on the local reference stresses and Monahan equation scaled to a load of F = 21350 N

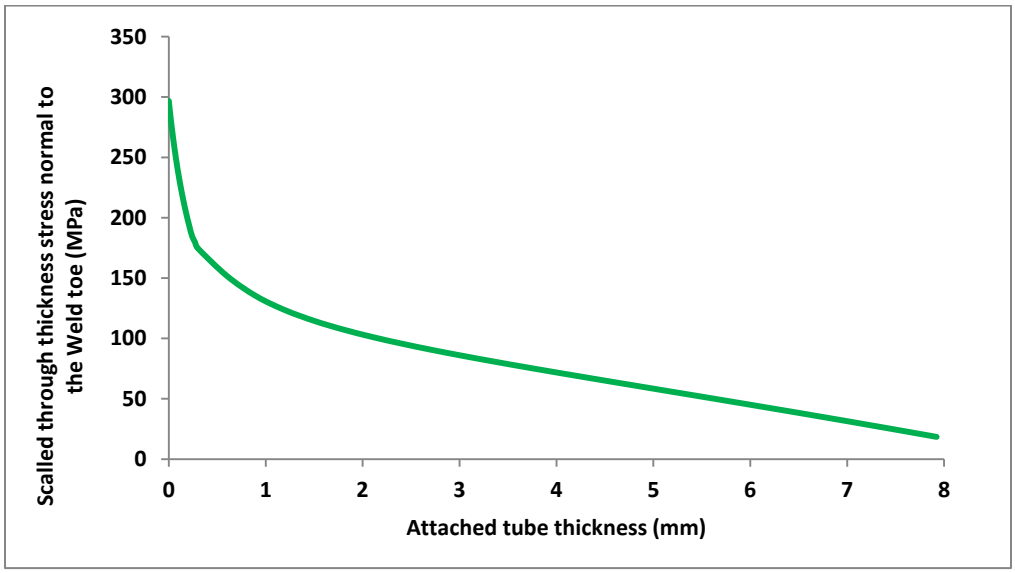

Figure A2- 18: Square-Tube-on-plate through-thickness stress distribution based on the local reference stresses and Monahan equation scaled to a load of F = 13878 N

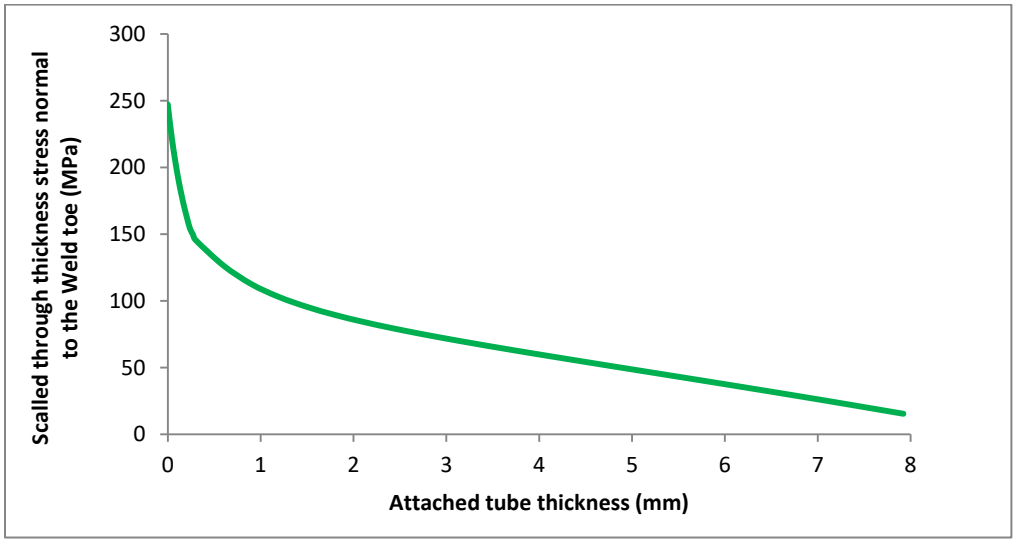

Figure A2- 19: Square-Tube-on-plate through-thickness stress distribution based on the local reference stresses and Monahan equation scaled to a load of F = 11565 N

The fatigue life predictions were performed with and without the residual stresses. The residual stress was measured at the plate surface only (σ_r = 193.27 MPa), whereas the distribution was approximated by self-equilibrium of the linear field. The approximate residual stress distribution, shown in Figure A2- 20, was based on limited experimental data.

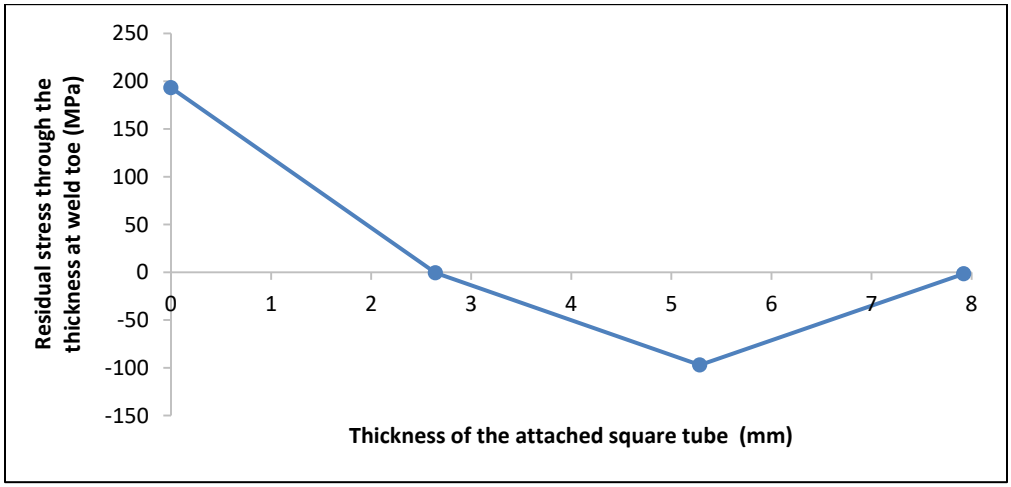

Figure A2- 20: Approximation of the residual stress distribution through the attached square tube thickness at the upper weld toe

A2.1.4 Fatigue life evaluation

The fatigue life is predicted by using the ε-N and the LEFM methods based on the shell FE local reference stress data. The ε-N method predicts the fatigue crack initiation life, whereas the LEFM

method predicts the fatigue crack propagation life. Both methods, which are coded into the in-house FALIN and FALPR software packages, were used to find the total fatigue lives of the current case (Square-Tube-on-plate subjected to lateral loading). The total fatigue lives were determined by summing both the initiation and the propagation fatigue lives. Finally, the predicted total fatigue life was compared with the fatigue life of the experiment.

The first step is to determine the fatigue crack initiation life according to the procedure of the strain-life method described in Section (2.2). The material properties in Table A2- 2 and Table A2- 4 were input to the FALIN software to calculate stresses and strains for each load cycle based on the Ramberg-Osgood fatigue stress-strain curve and the Neuber equation (see Figure 5-4 and Figure 2-12). The SWT equation (2.9) was then used to calculate the fatigue crack initiation life. The outputs from the FALIN software were the simulated stress-strain response and the fatigue crack initiation life at the weld toe. The fatigue crack initiation lives were predicted for the current case when subjected to load levels of F = 21350 N, F = 13878 N F = 11565 N, without the effect of the residual stress, as shown in Figure A2- 21 to Figure A2- 23. The fatigue crack initiation lives for the same load levels, including the residual stress effect are shown in Figure A2- 24 to Figure A2- 26.

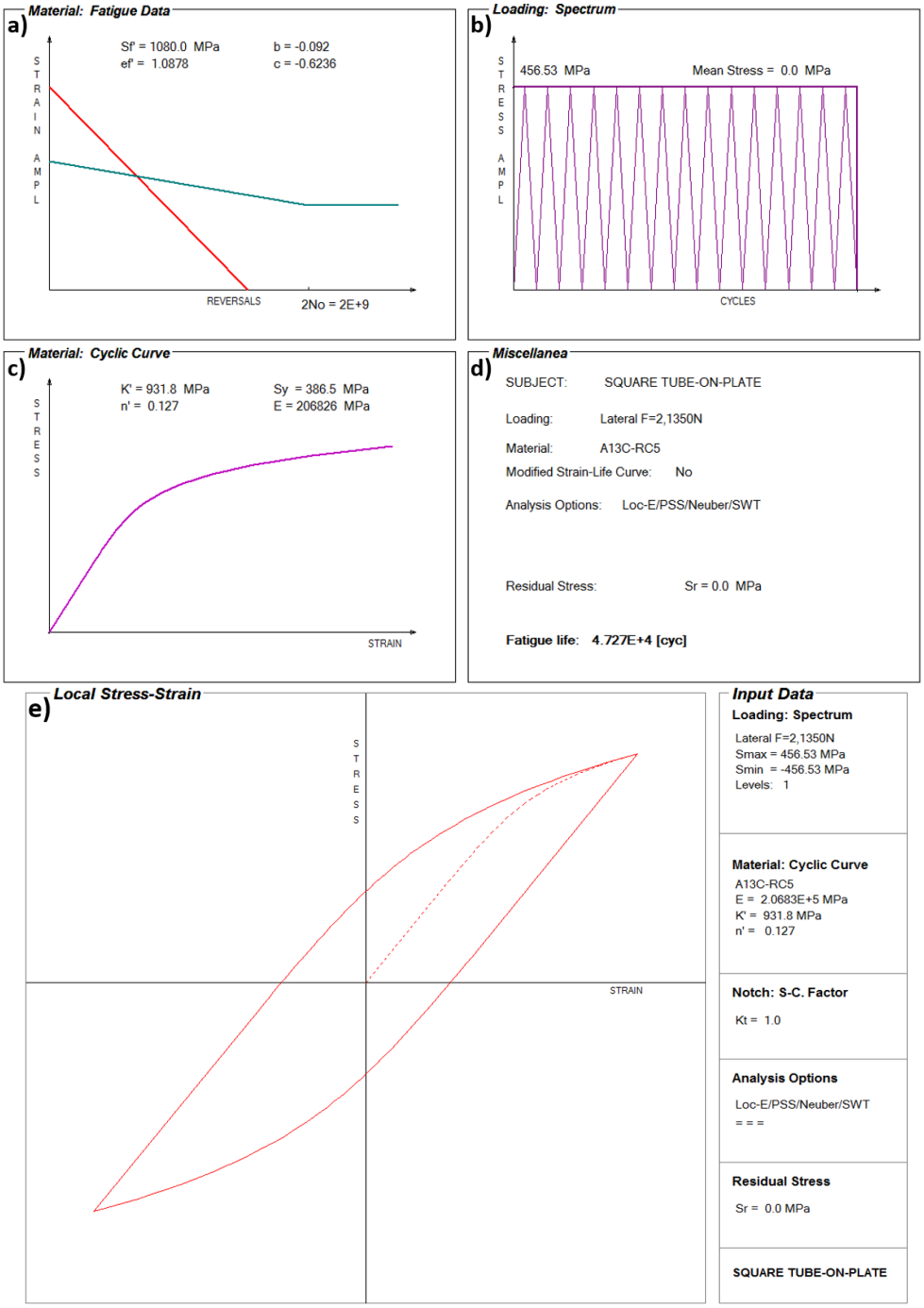

Figure A2- 21: FALIN input and output data for the Square-Tube-on-plate welded joint subjected to lateral load (F = 21350 N); a) Manson-Coffin curve, b) Peak stress loading, c) Ramberg-Osgood curve, d) Output data, e) Simulated stress-strain material response at the weld toe

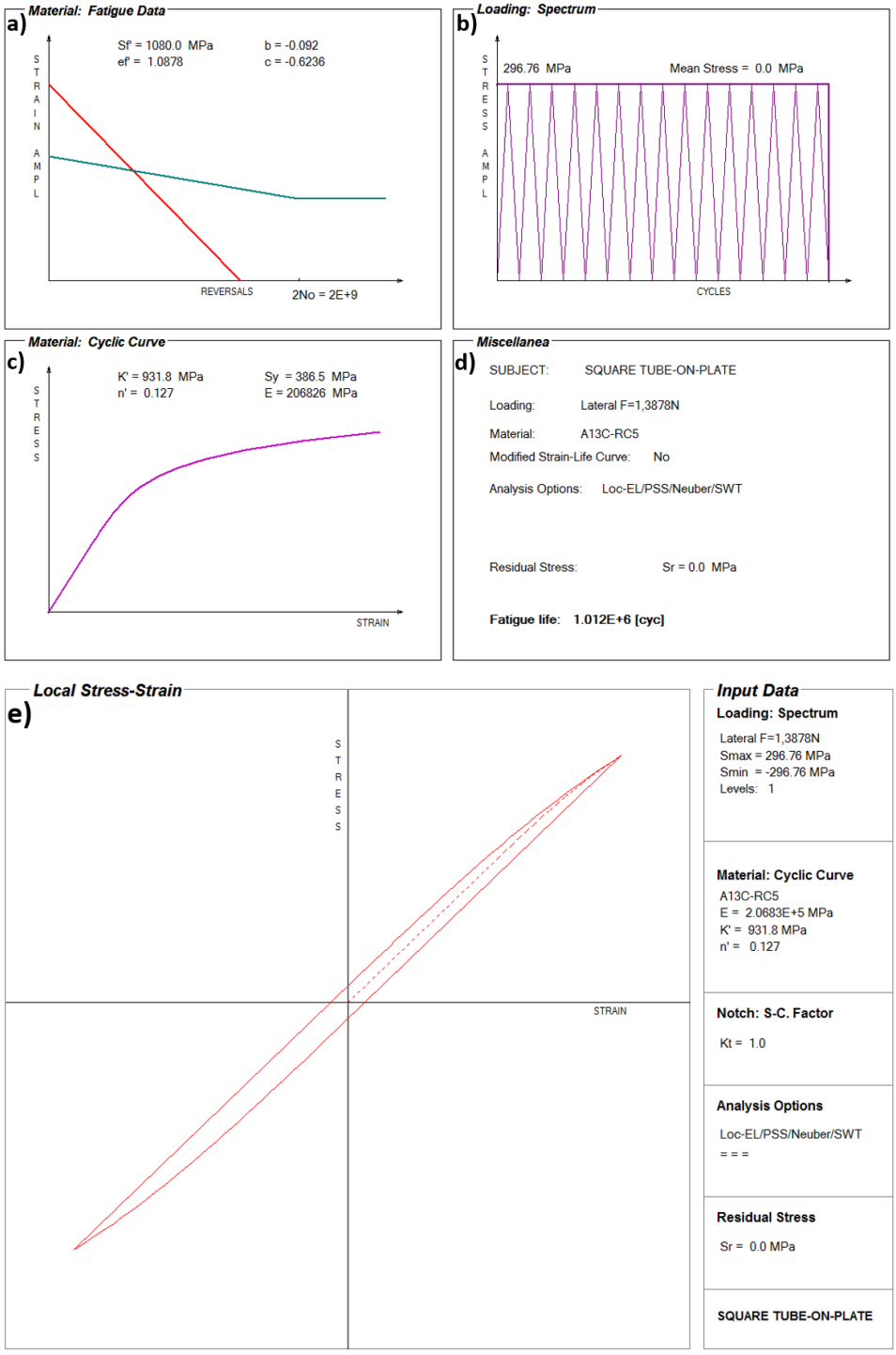

Figure A2- 22: FALIN input and output data for the Square-Tube-on-plate welded joint subjected to lateral load (F = 13878 N); a) Manson-Coffin curve, b) Peak stress loading, c) Ramberg-Osgood curve, d) Output data, e) Simulated stress-strain material response at the weld toe

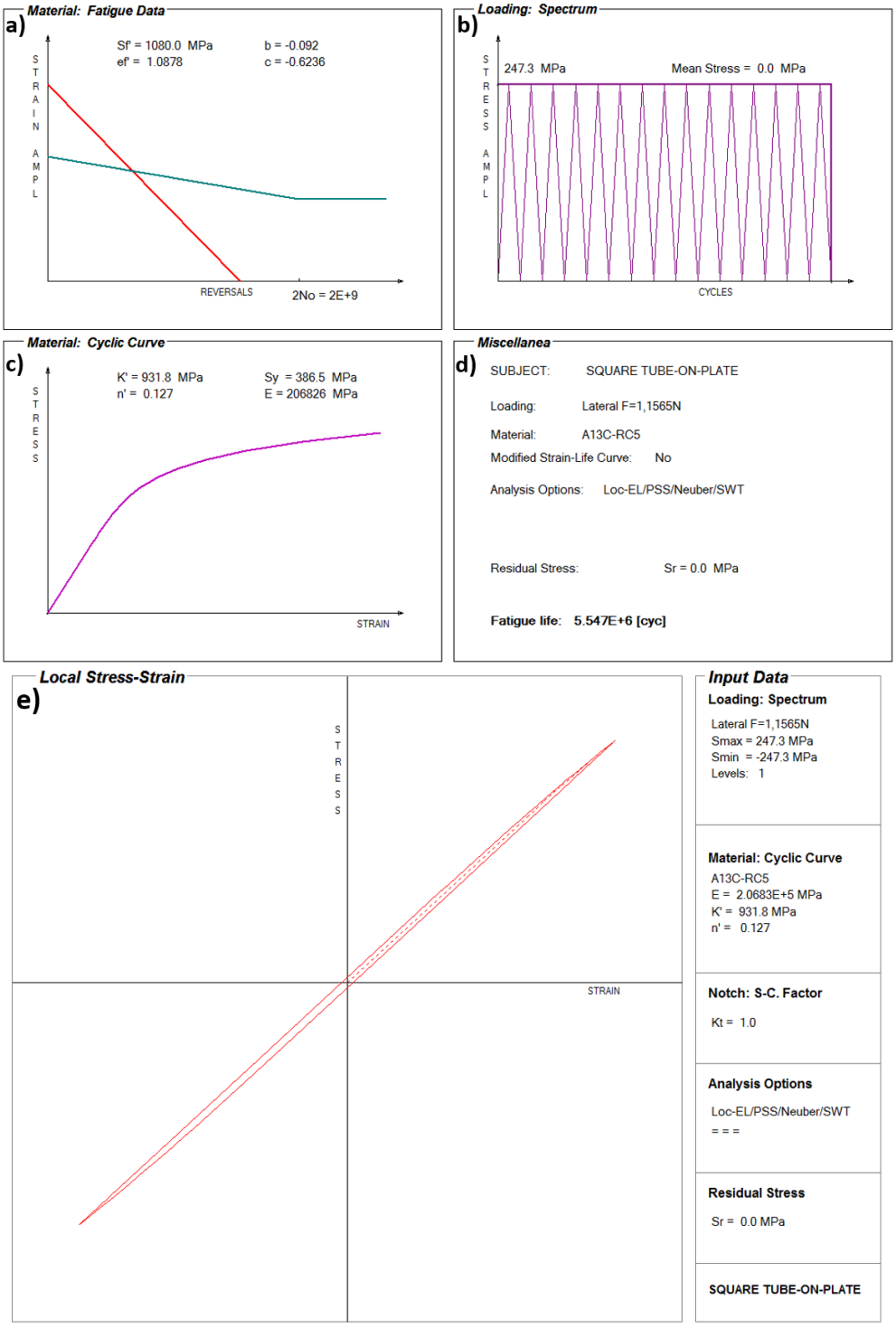

Figure A2- 23: FALIN input and output data for the Square-Tube-on-plate welded joint subjected to lateral load (F = 11565 N): a) Manson-Coffin curve, b) Peak stress loading, c) Ramberg-Osgood curve, d) Output data, e) Simulated stress-strain material response at the weld toe

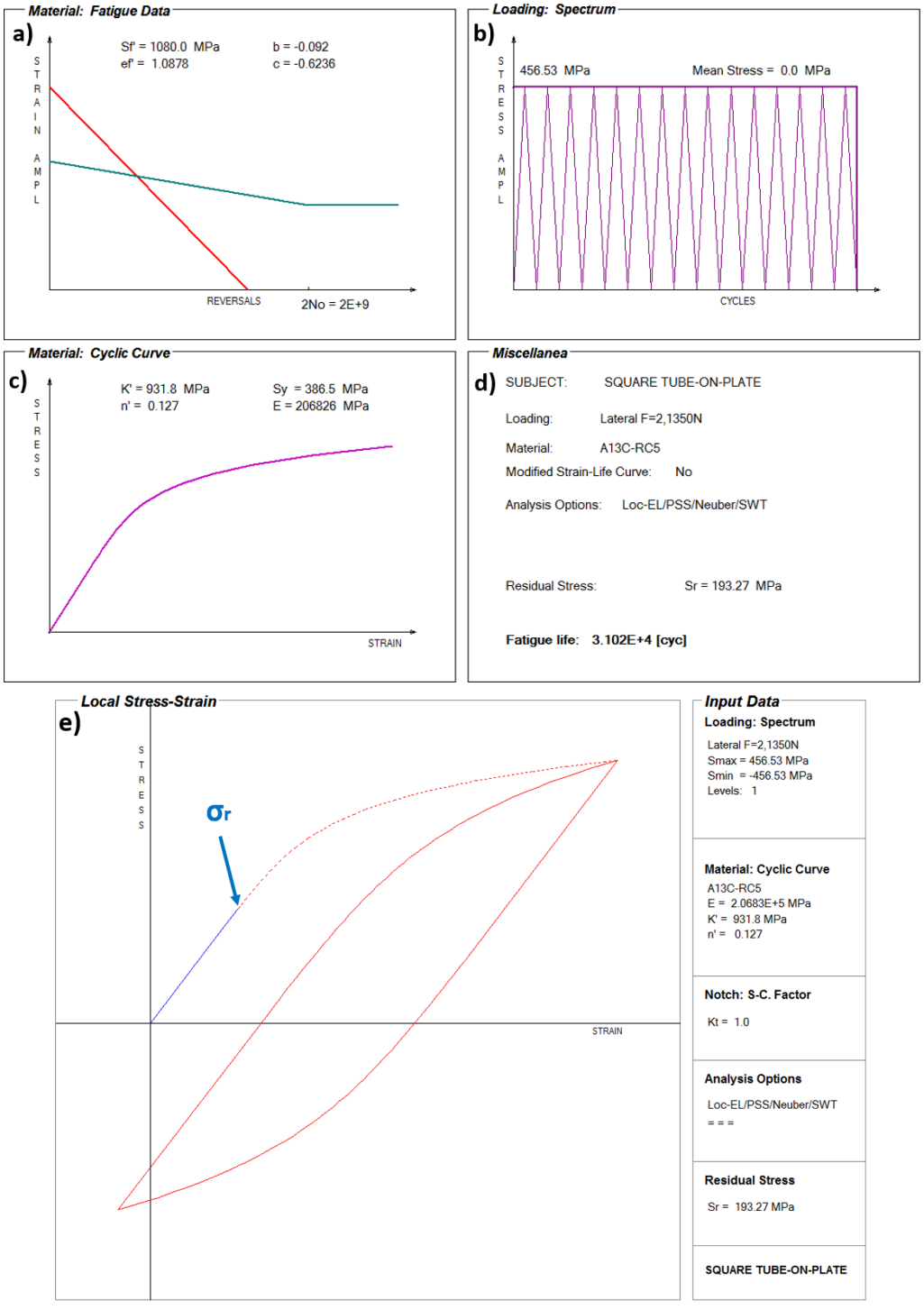

Figure A2- 24: FALIN input and output data for the Square-Tube-on-plate welded joint subjected to lateral load (F = 21350 N) in addition to the residual stress σ_r : a) Manson-Coffin curve, b) Peak stress loading, c) Ramberg-Osgood curve, d) Output data, e) Simulated stress-strain material response at the weld toe

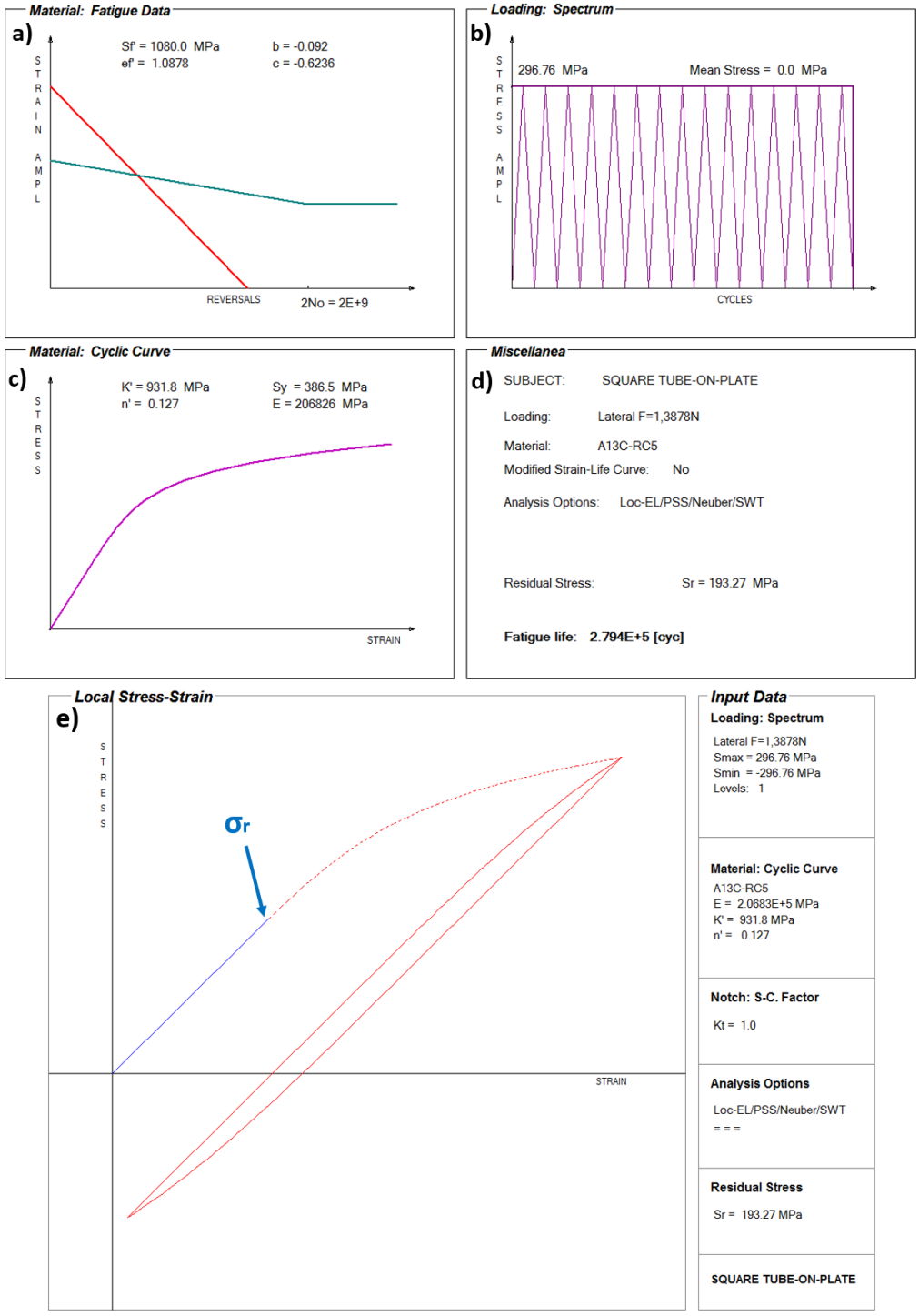

Figure A2- 25: FALIN input and output data for the Square-Tube-on-plate welded joint subjected to lateral load (F = 13878 N) in addition to the residual stress σ_r : a) Manson-Coffin curve, b) Peak stress loading, c) Ramberg-Osgood curve, d) Output data, e) Simulated stress-strain material response at the weld toe

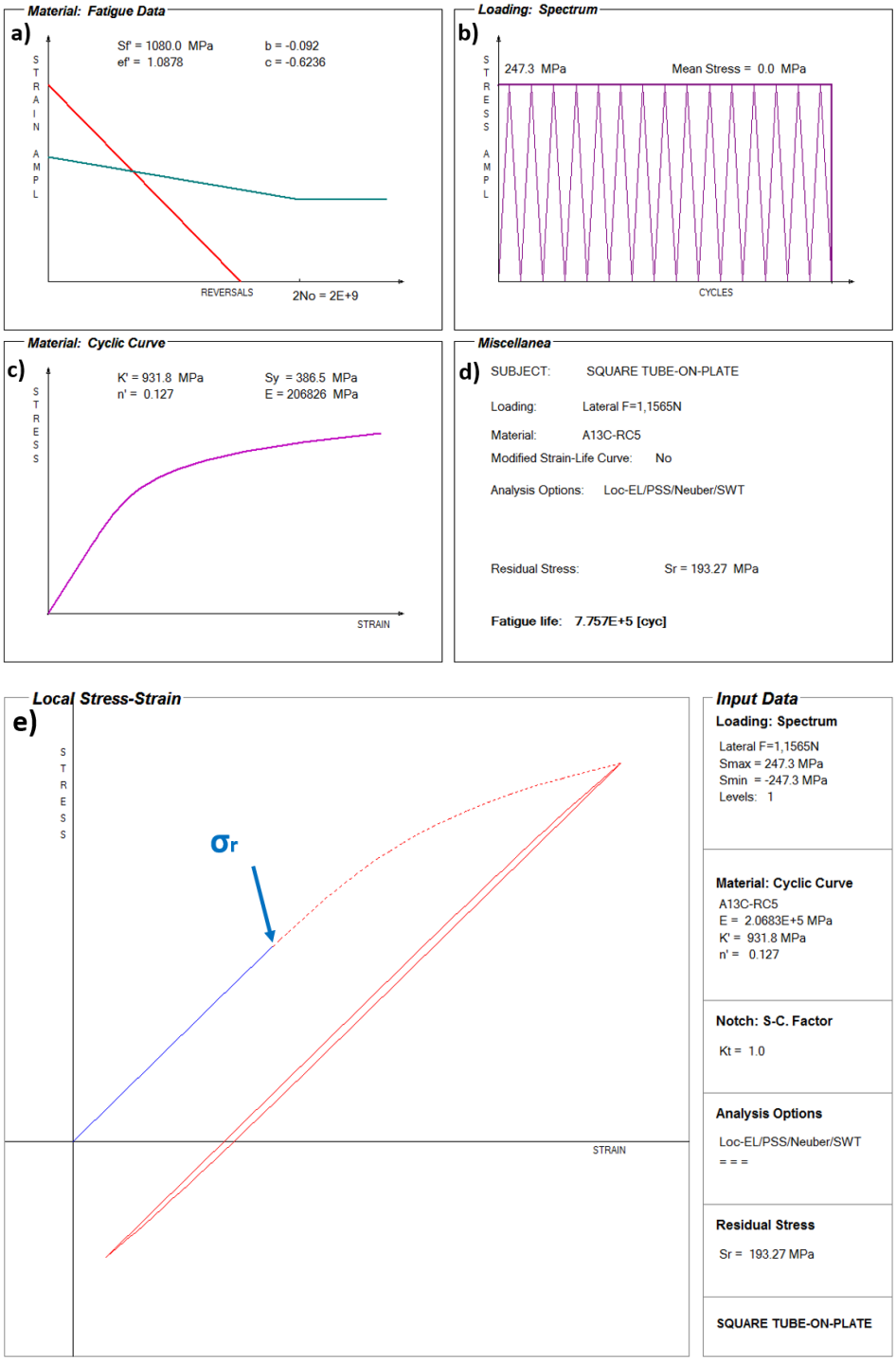

Figure A2- 26: FALIN input and output data for the Square-Tube-on-plate welded joint subjected to lateral load (F = 11565 N) in addition to the residual stress σ_r : a) Manson-Coffin curve, b) Peak stress loading, c) Ramberg-Osgood curve, d) Output data, e) Simulated stress-strain material response at the weld toe

The second step in the fatigue life analysis is the calculation of the fatigue crack propagation life using the LEFM method coded in the FALPR software. The observed cracks in the JD fatigue test experiments for the current case were found to be semi-elliptical in shape with a surface crack length of approximately 2c = 3.5 mm. Therefore, the predictions of the fatigue crack propagation life were based on assuming a semi-elliptical planar crack in a finite thickness plate. Accordingly, the initial crack size was assumed to be not greater than a_i = 0.5 mm in depth with an aspect ratio of (a/c = 0.286), whereas the final crack depth was assumed to be = 6.33 mm.

In the case of semi-elliptical cracks, two stress intensity factors, at the depth and surface points, are needed. Using the weight function method, with the through-thickness stress distribution $\sigma_{xx}(y)$ based on the shell FE modelling and Monahan equation, the stress intensity factors at the crack depth and surface (points A and B in Figure 3-13) can be determined. These two stress intensity factors are important for the determination of crack increments after each cycle for both surface and depth directions, as per equations (2.21 and 2.22). The crack increments due to the applied load cycles are calculated by using Paris' fatigue crack growth equation (2.20). To use the Paris equation, fatigue crack growth properties C and m are required for the material of the welded joint under investigation.

Fatigue crack growth properties for the material of the current case can be determined according to Section (2.3) by using Noroozi's [47] equations. For the determination the Paris equation constants C and m, the material properties in Table A2- 2 and Table A2- 4 were input to the FALIN software. Hence m = 2.795 and C = 1.232 x 10^{-11}, corresponding to R = 0 at N = 10^6 cycles.

The threshold stress intensity range and the critical stress intensity factor for the material of the current case at R = 0 were:

$\Delta K_{th} = 3.5\ \text{MPa}\sqrt{\text{m}}$, and $K_c = 80\ \text{MPa}\sqrt{\text{m}}$.

The through-thickness stress distribution based on the shell FE model and Monahan equation were input to FALPR to determine the stress intensity factors. It was found that the crack was growing on the surface faster than the depth because of the high stress at the weld toe [62]. Therefore, the crack increments of the surface and deepest point have to be determined for each load cycle. Accordingly, the aspect ratio (a/c) has to be updated after each increment using Paris' fatigue crack growth. The fatigue crack propagation life has been predicted for the Square-Tube-on-plate welded joint subjected to lateral loadings of (F = 21350 N, F = 13878 N, and F = 11565 N). The predictions for both load

cases were carried out with and without the residual stress to investigate the effect of the residual stress.

Figure A2- 27 through Figure A2- 32 show the input data to FALPR, the predicted crack depth versus the number of cycles, the stress intensity factor versus the number of applied load cycles, the fatigue crack growth lives predictions, and the fatigue crack propagation lives of the weld joint under investigation when applying F = 21350 N, F = 13878 N, and F = 11565 N, respectively, whereas Figure A2- 33 through Figure A2- 38 show the same results including the effect of the residual stress. Note that including the residual stress affect was done to study its effect on the fatigue life evaluation.

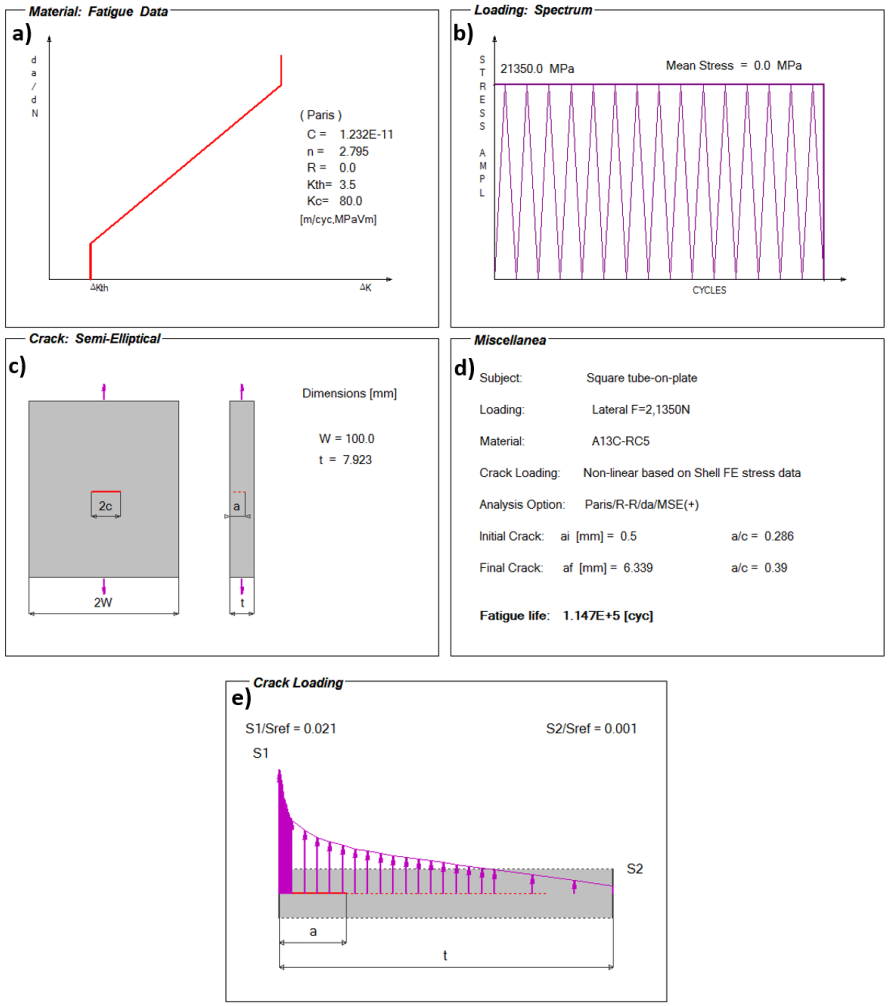

Figure A2- 27: FALPR input data for fatigue crack propagation analysis of the Square-Tube-on-plate subjected to lateral loading F = 21350 N (without residual stress): a) Paris fatigue crack growth curve, b) Loading history of the peak stress, c) Geometry of the crack, d) Fatigue life, e) The normalized through-thickness stress distribution

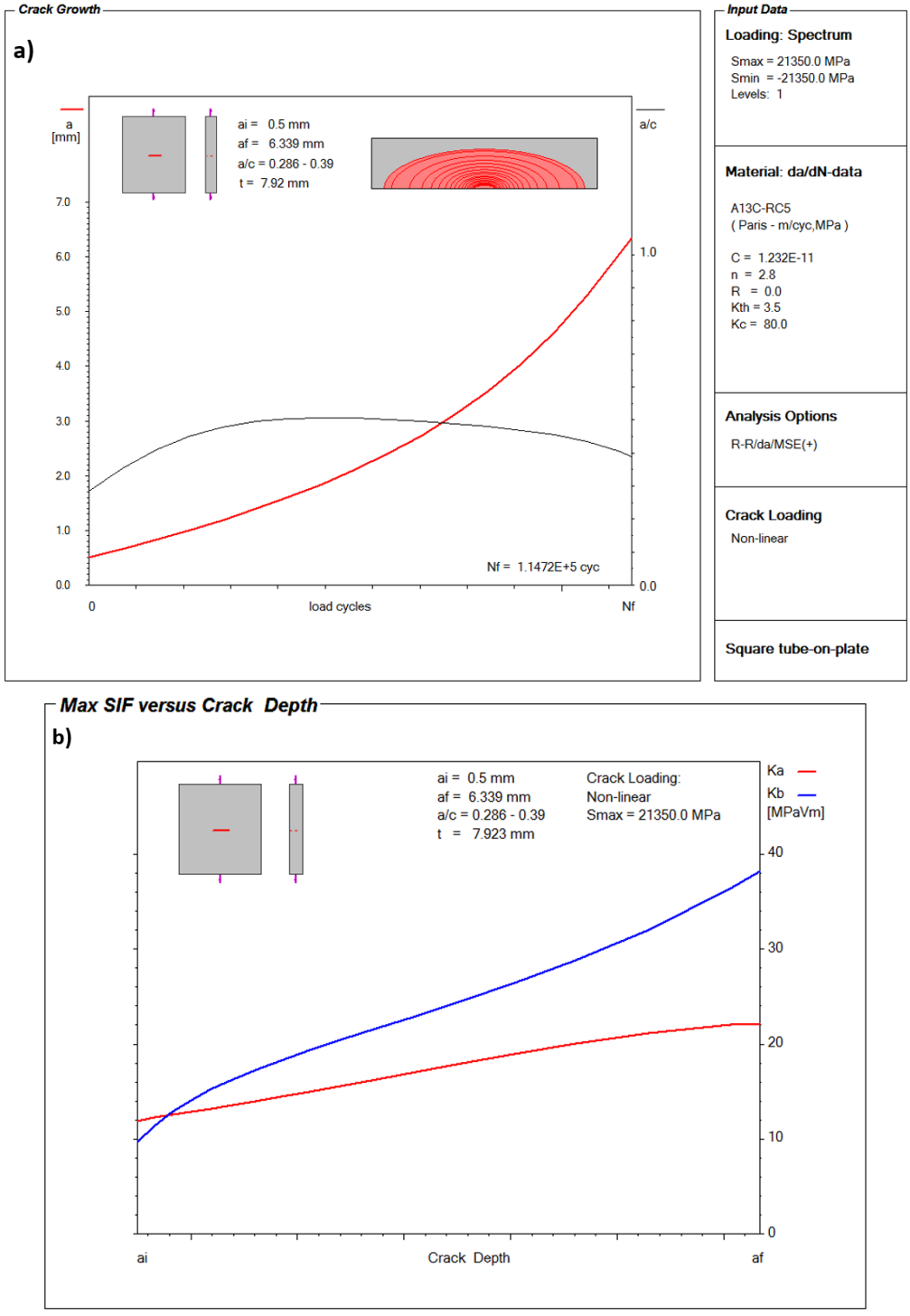

Figure A2- 28: a) The crack depth versus the number of applied load cycles to failure (a-N diagram), b) The stress intensity factor values at the surface and depth points of the semi-elliptical crack versus the crack depth (K-a diagram); tube-on-plate joint subjected to a lateral load of F = 21350 N (without residual stress)

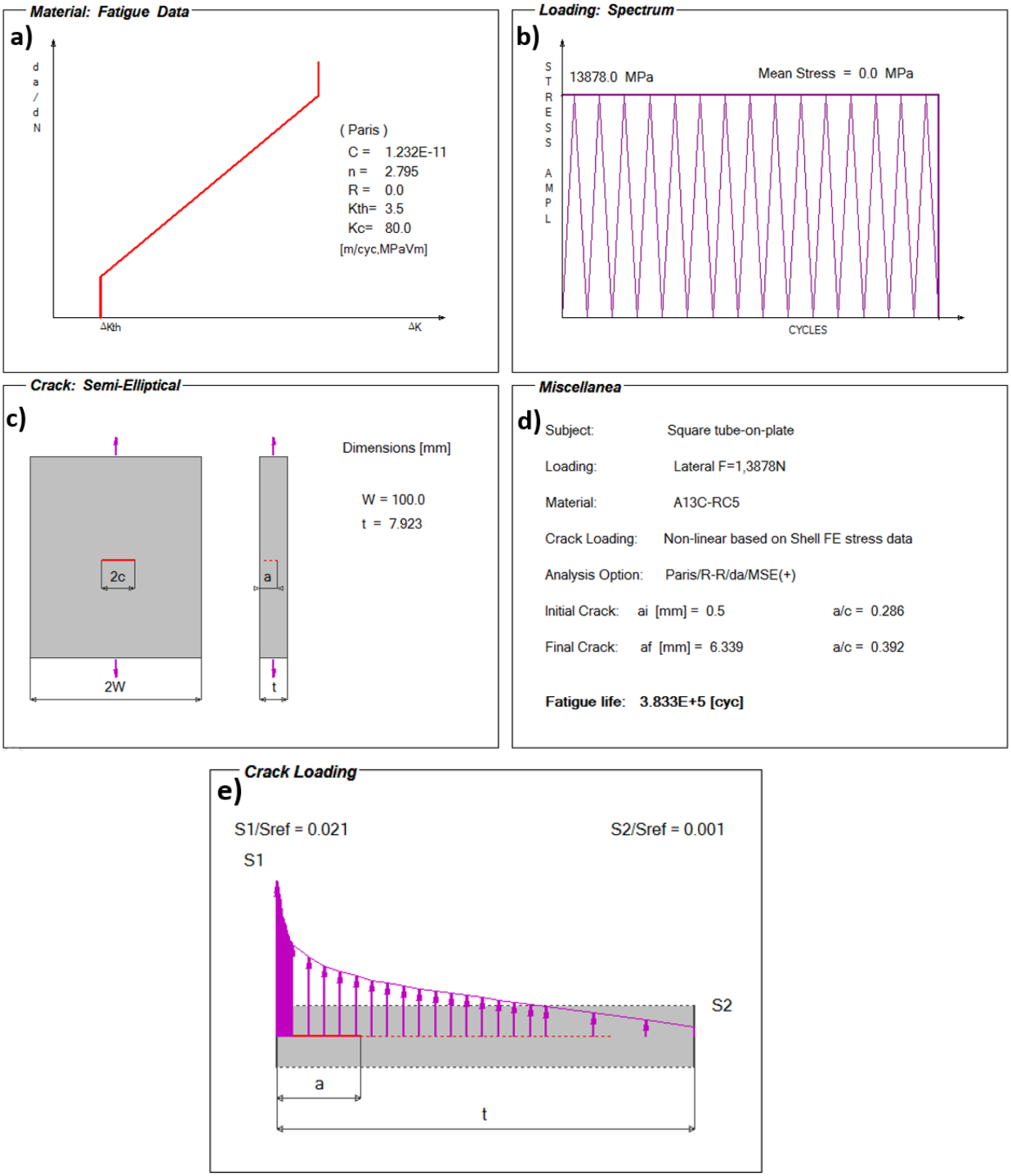

Figure A2- 29: FALPR input data for fatigue crack propagation analysis of the Square-Tube-on-plate subjected to lateral loading F = 13878 N (without residual stress): a) Paris fatigue crack growth curve, b) Loading history of the peak stress, c) Geometry of the crack, d) Fatigue life, e) The normalized through-thickness stress distribution

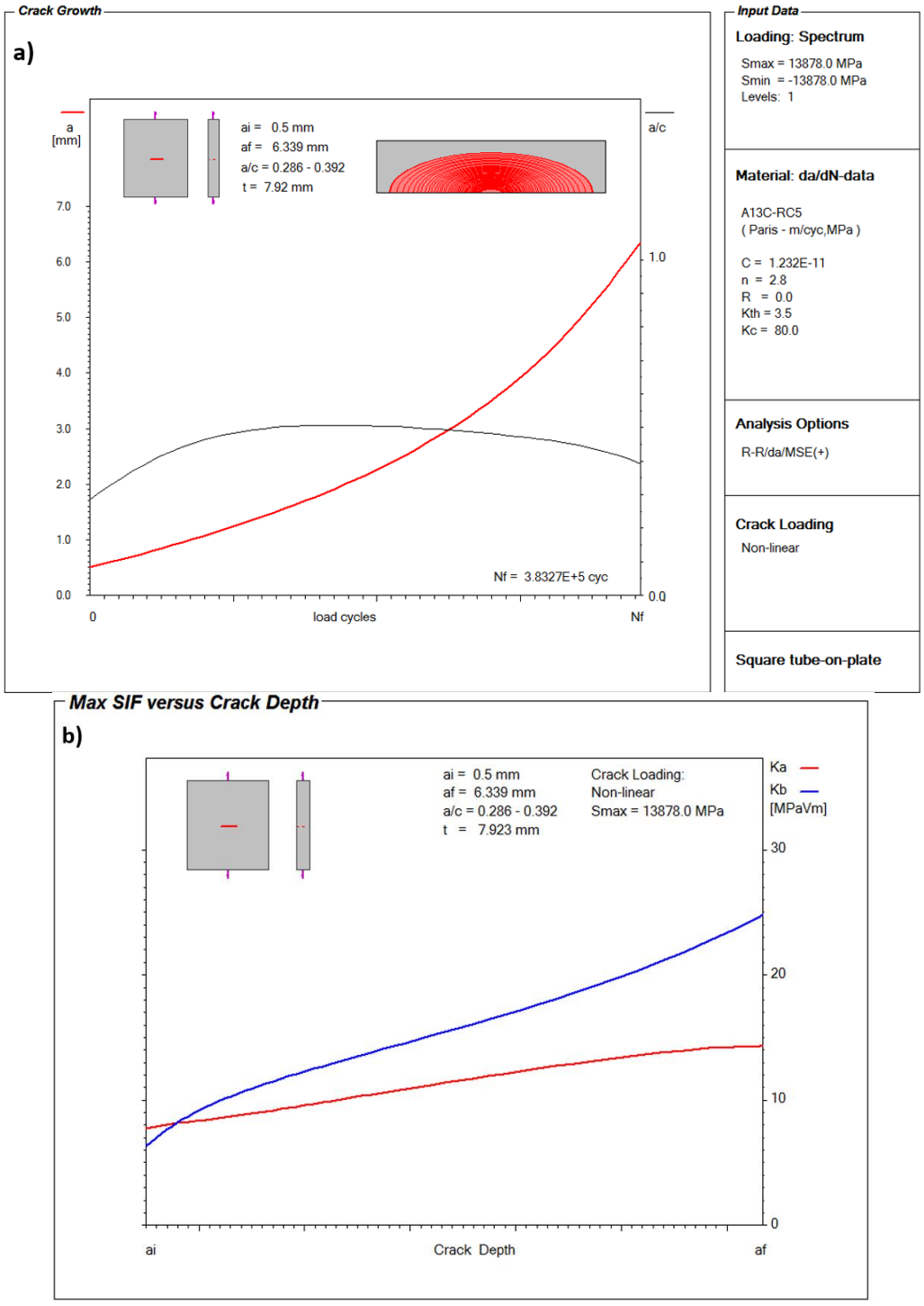

Figure A2- 30: a) The crack depth versus the number of applied load cycles to failure (a-N diagram), b) The stress intensity factor values at the surface and depth points of the semi-elliptical crack versus the crack depth (K-a diagram); tube-on-plate joint subjected to a lateral load of F = 13878 N (without residual stress)

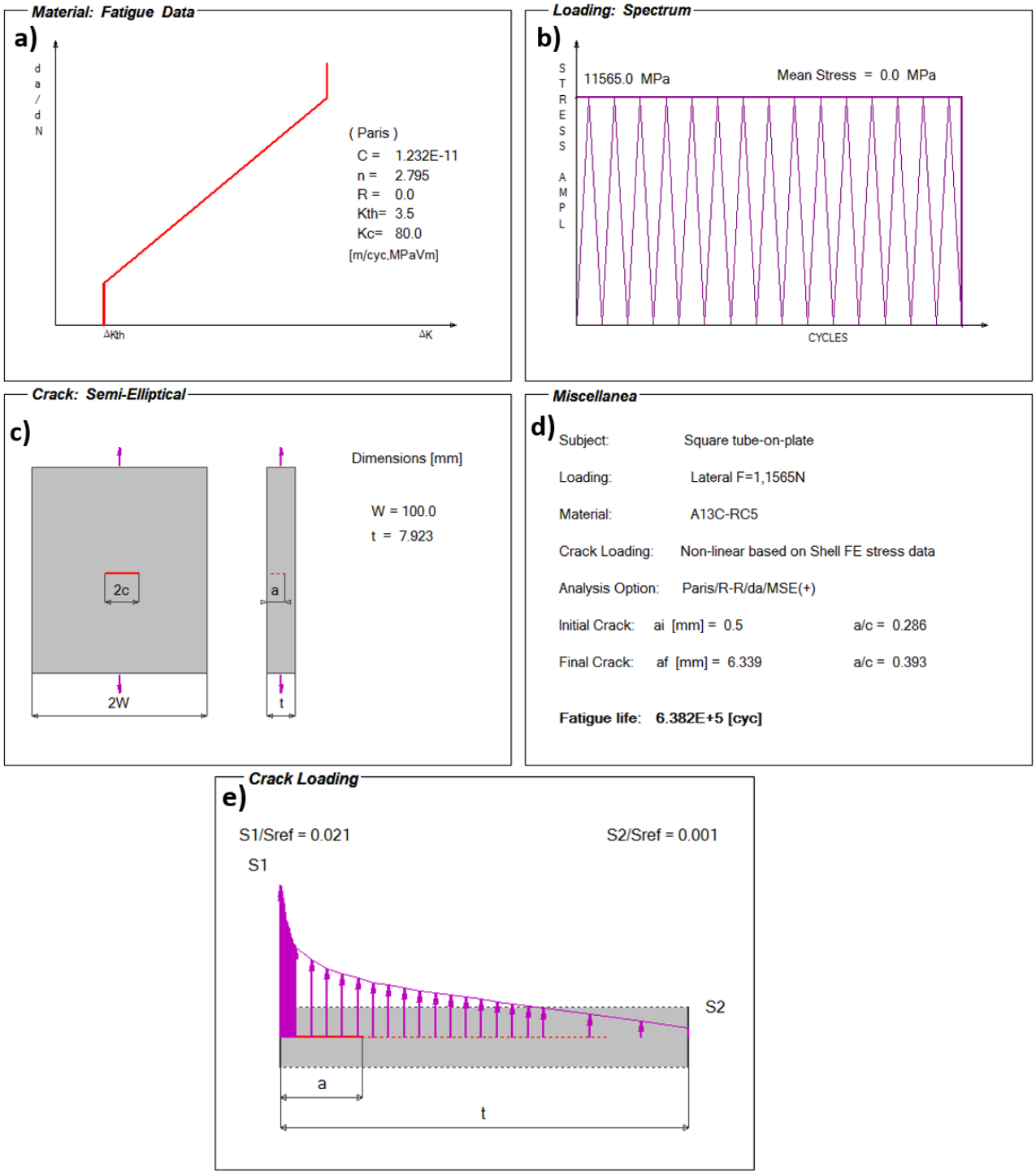

Figure A2- 31: FALPR input data for fatigue crack propagation analysis of the Square-Tube-on-plate subjected to lateral loading F = 11565 N (without residual stress): a) Paris fatigue crack growth curve, b) Loading history of the peak stress, c) Geometry of the crack, d) Fatigue life, e) The normalized through-thickness stress distribution

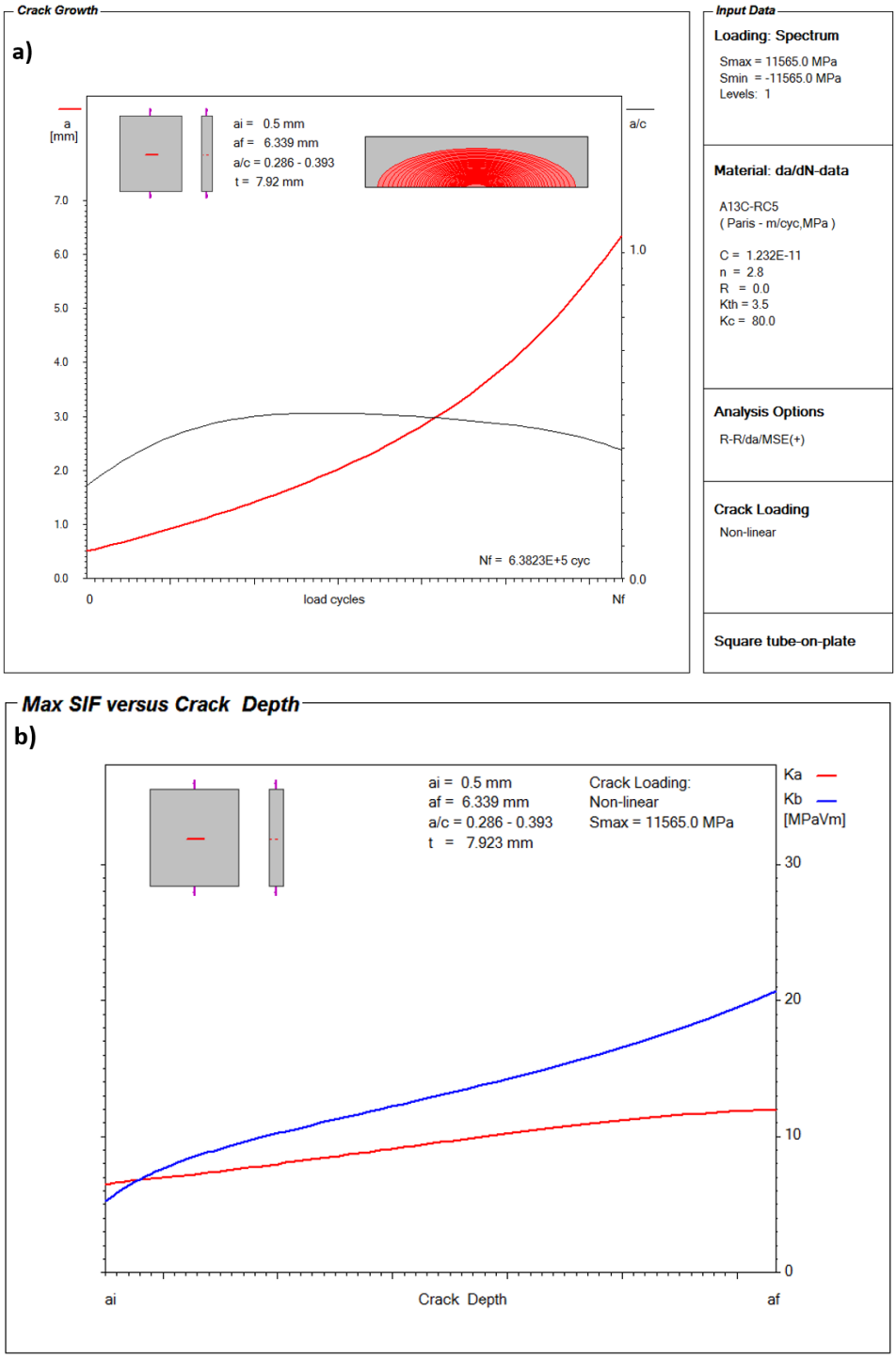

Figure A2- 32: a)The crack depth versus the number of applied load cycles to failure (a-N diagram), b) The stress intensity factor values at the surface and depth points of the semi-elliptical crack versus the crack depth (K-a diagram); tube-on-plate joint subjected to a lateral load of F = 11565 N (without residual stress)

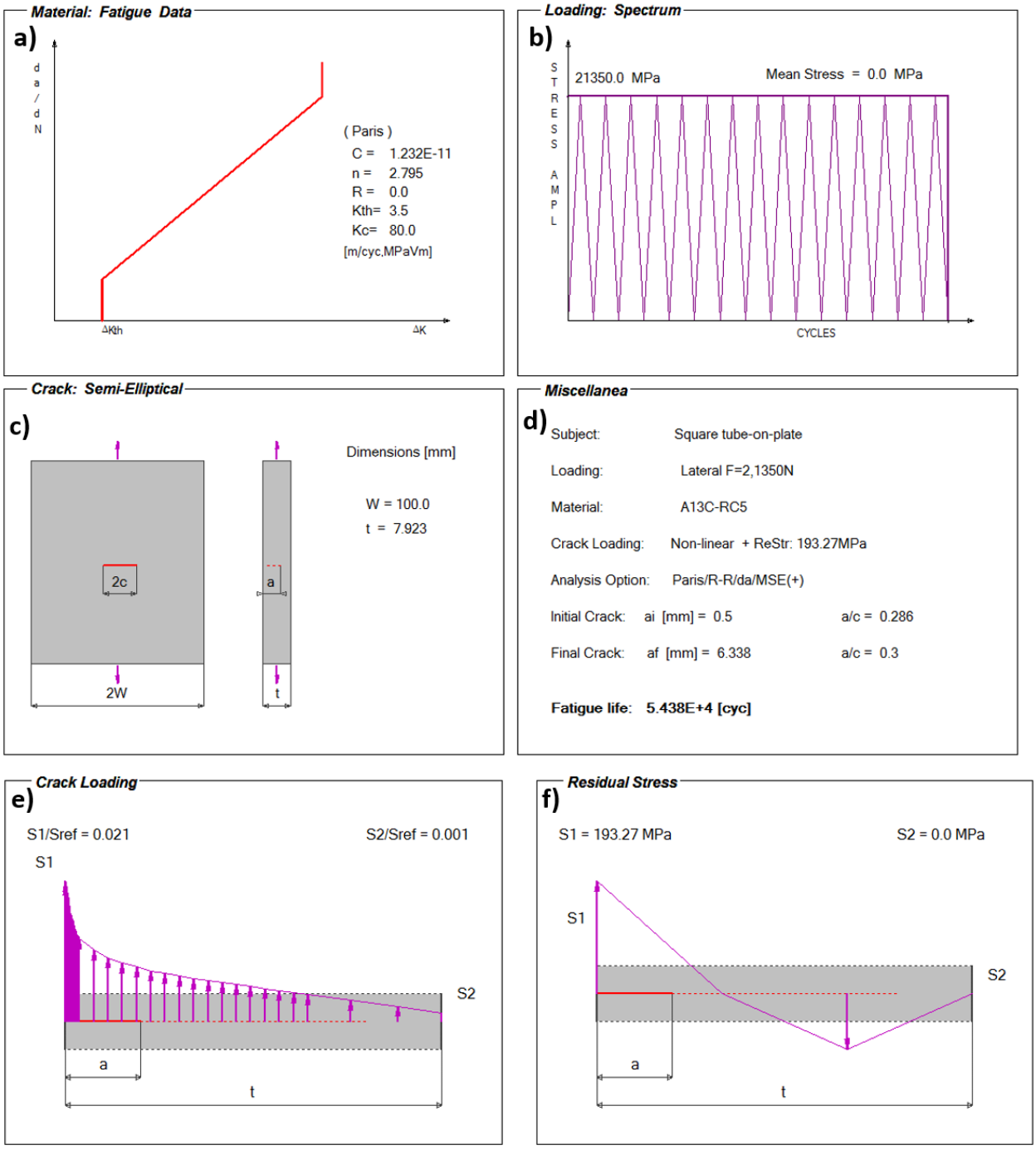

Figure A2- 33: FALPR input and output data for fatigue crack propagation analysis of the Square-Tube-on-plate welded joint subjected to a lateral load of F = 21350 N (with residual stress): a) Paris fatigue crack growth curve, b) Loading history of the peak stress, c) Geometry of the crack, d) Fatigue life, e) The normalized through-thickness stress distribution, f) Estimated residual stress distribution through the thickness of the weld toe cross-section

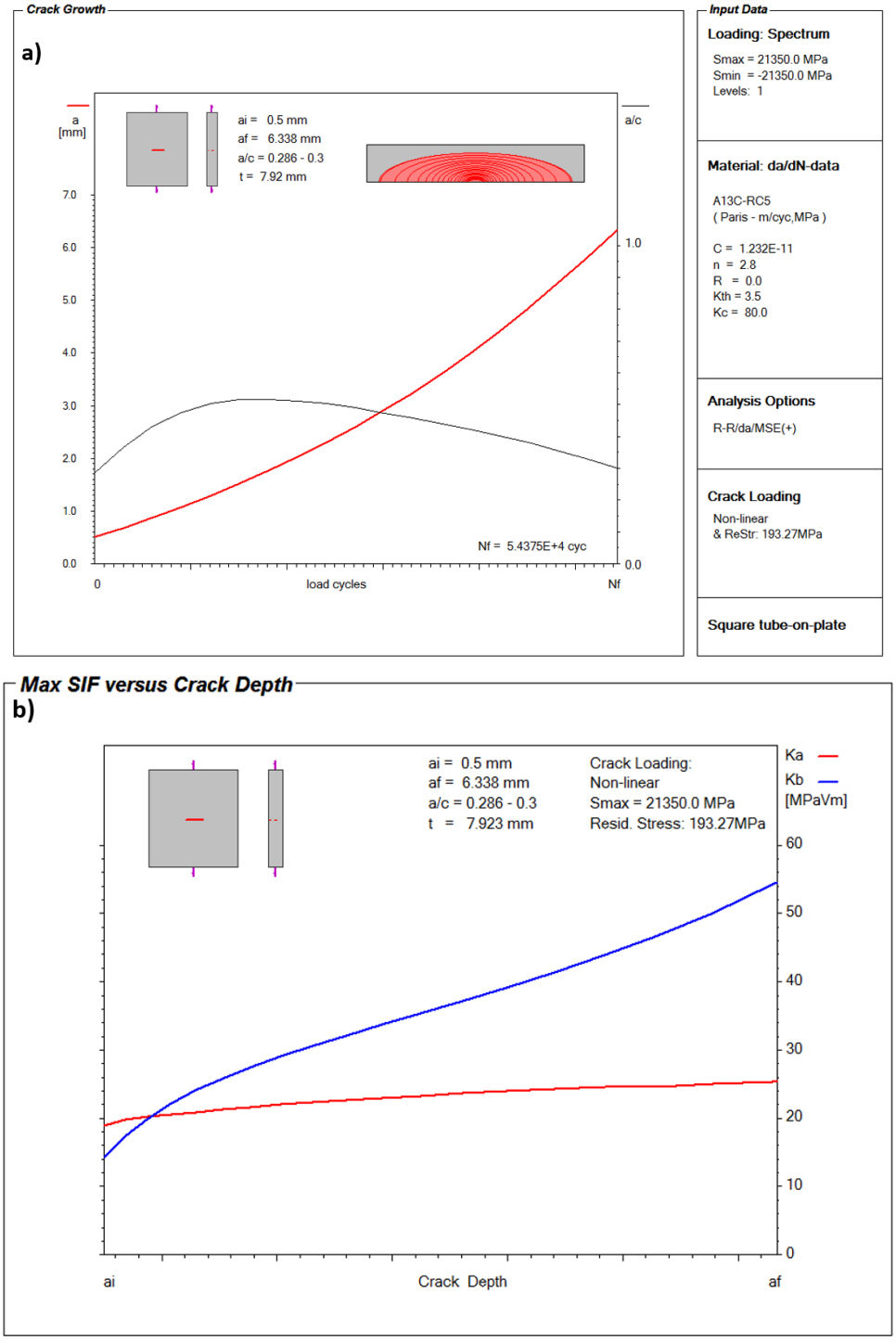

Figure A2- 34: a) The crack depth versus the number of applied load cycles to failure (a-N diagram), b) The stress intensity factor values at the surface and depth points of the semi-elliptical crack versus the crack depth (K-a diagram); Square-Tube-on-plate welded joint subjected to a lateral load of F = 21350 N (with residual stress)

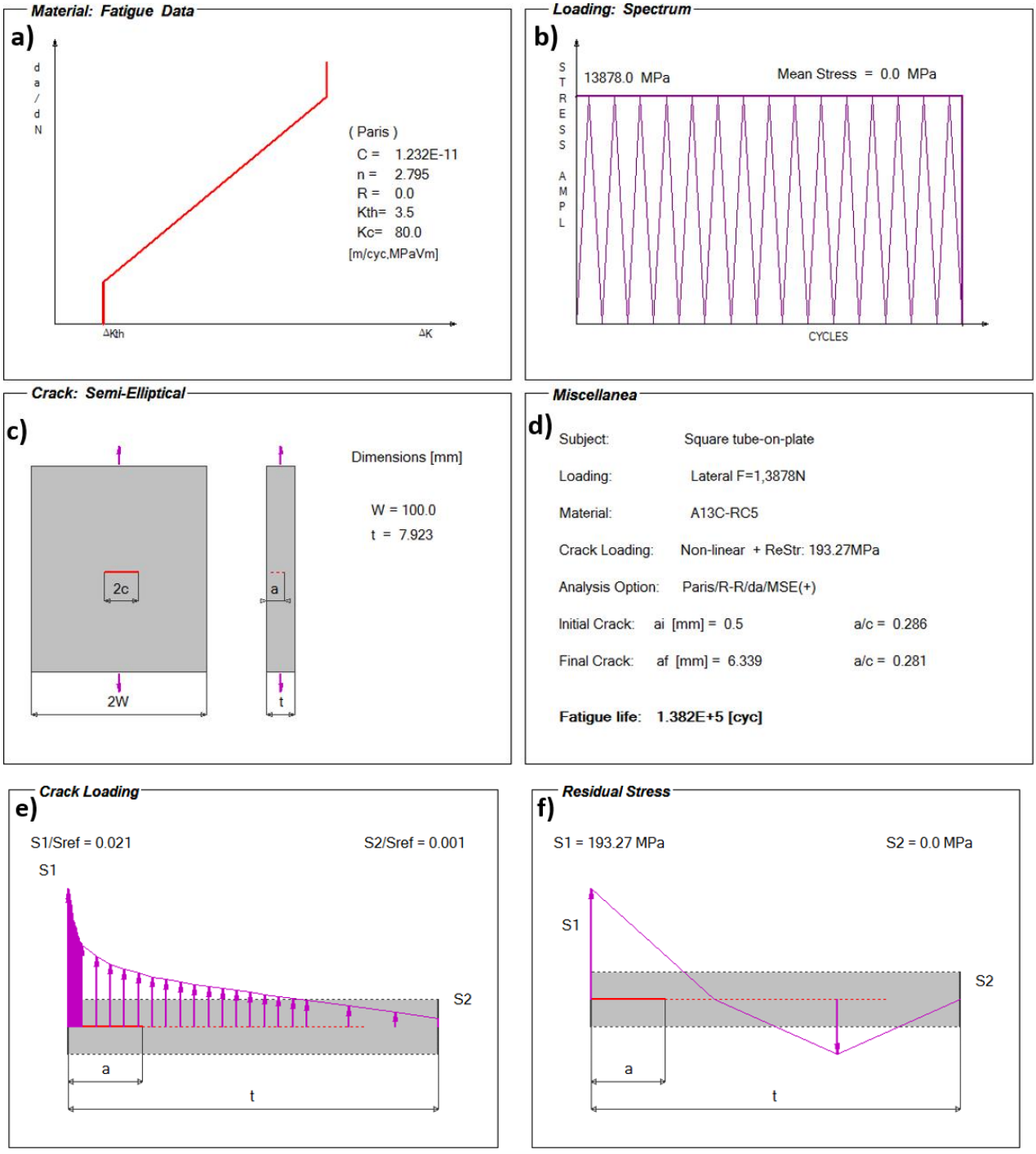

Figure A2- 35: FALPR input and output data for fatigue crack propagation analysis of the Square-Tube-on-plate welded joint subjected to a lateral load of F = 13878 N (with residual stress): a) Fatigue life, e) The normalized through-thickness stress distribution, f) Estimated residual stress distribution through the thickness of the weld toe cross-section

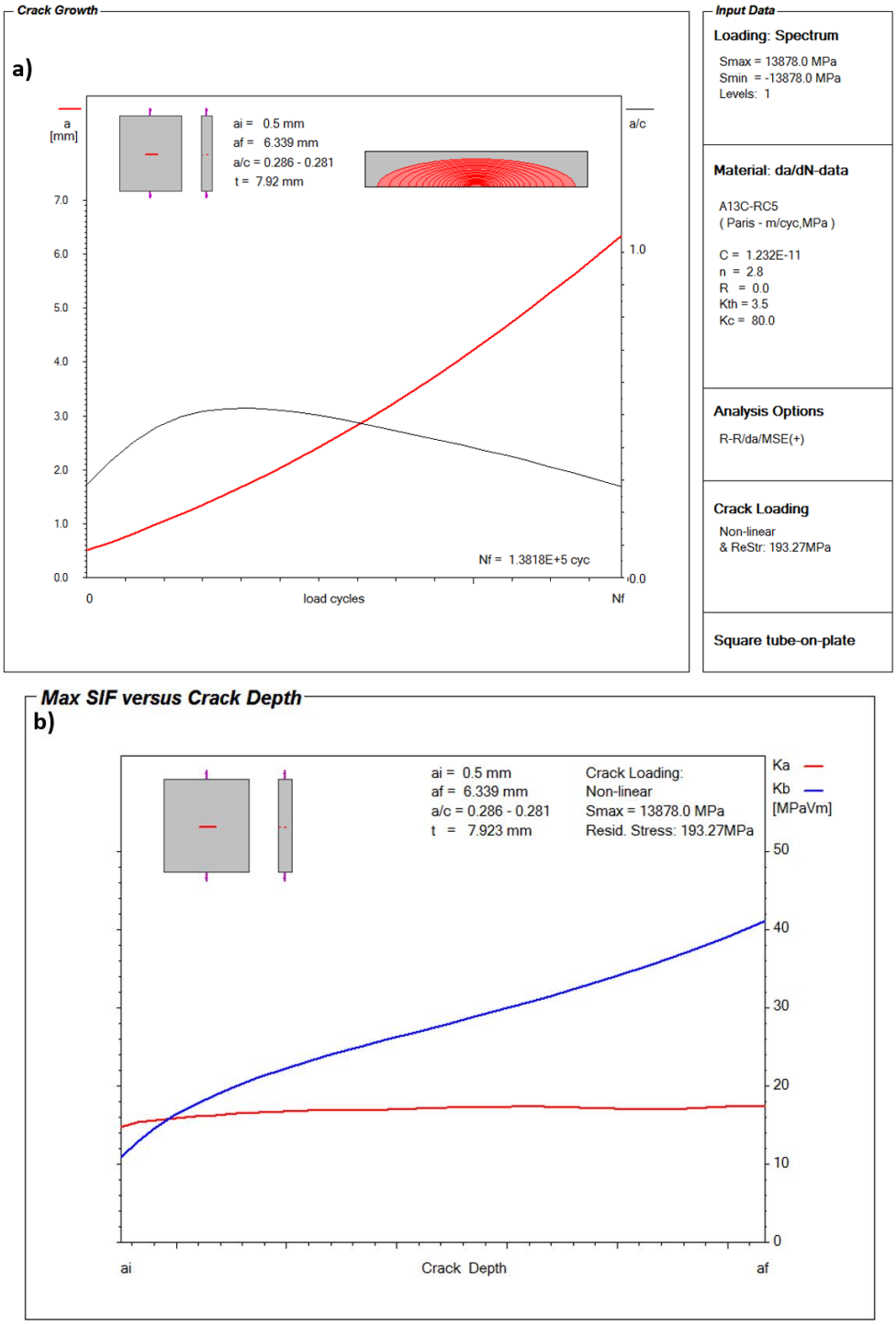

Figure A2- 36: a) The crack depth versus the number of applied load cycles to failure (a-N diagram), b) The stress intensity factor values at the surface and depth points of the semi-elliptical crack versus the crack depth (K-a diagram); Square-Tube-on-plate welded joint subjected to a lateral load of F = 13878 N (with residual stress)

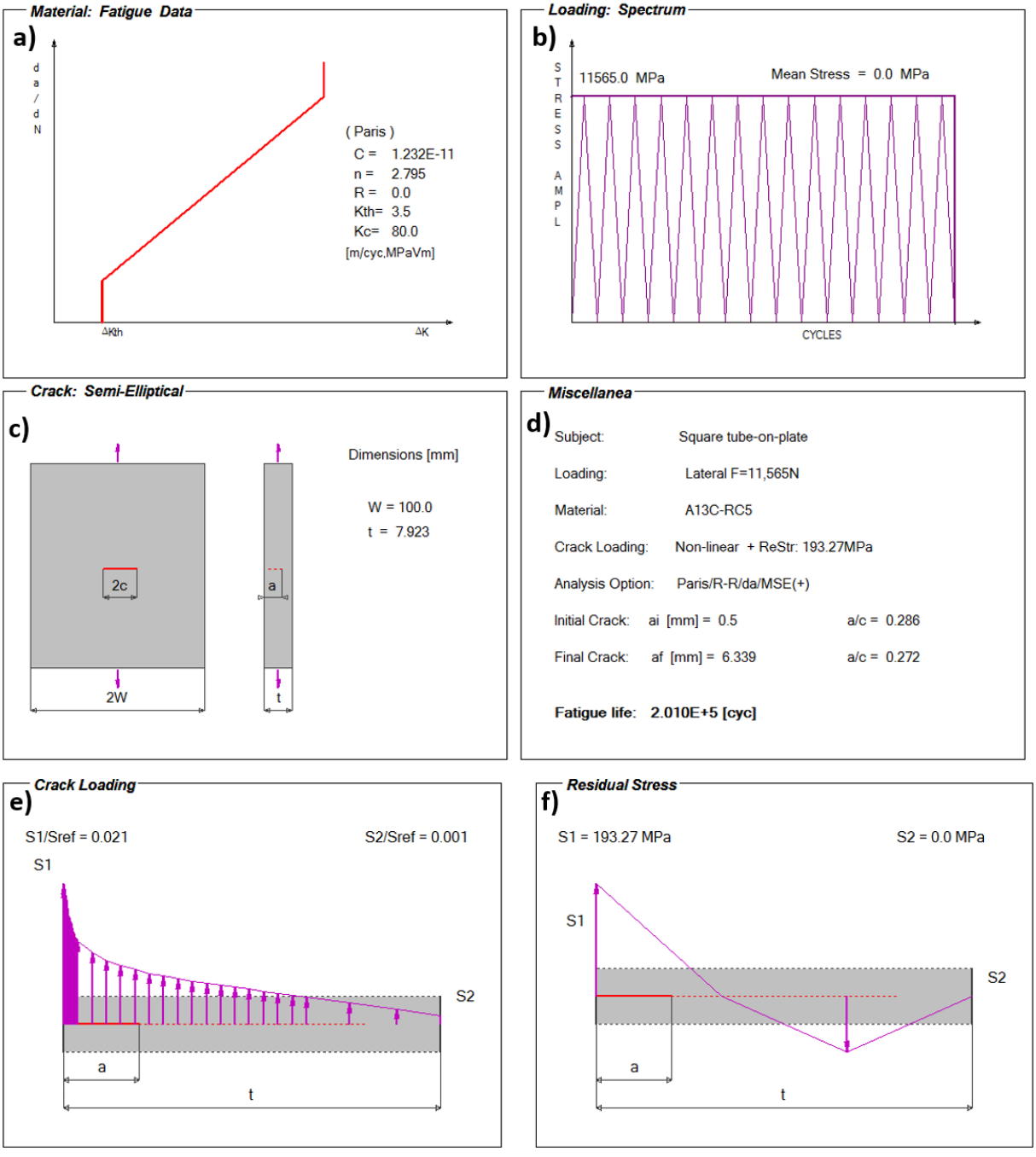

Figure A2- 37: FALPR input and output data for fatigue crack propagation analysis of the Square-Tube-on-plate welded joint subjected to a lateral load of F = 11565 N (with residual stress): a) Paris fatigue crack growth curve, b) Loading history of the peak stress, c) Geometry of the crack, d) Fatigue life, e) The normalized through-thickness stress distribution, f) Estimated residual stress distribution through the thickness of the weld toe cross-section

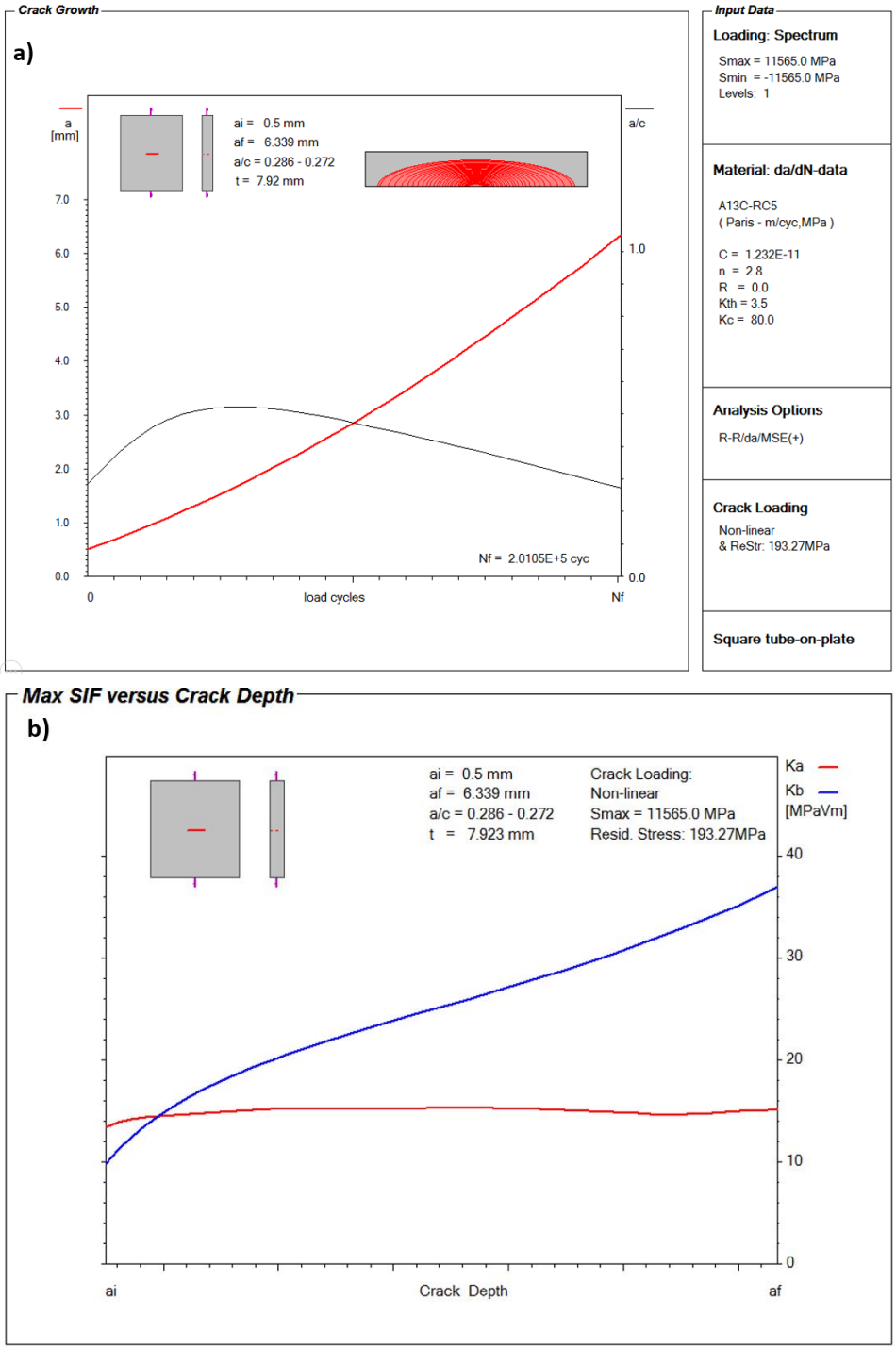

Figure A2- 38: a) The crack depth versus the number of applied load cycles to failure (a-N diagram), b) The stress intensity factor values at the surface and depth points of the semi-elliptical crack versus the crack depth (K-a diagram); Square-Tube-on-plate welded joint subjected to a lateral load of F = 11565 N (with residual stress)

The fatigue analysis results are shown in Table A2- 5, Table A2- 6, and Table A2- 7 for the Square-Tube-on-plate welded joint subjected to lateral load levels of F = 21350 N, F = 13878 N, and F = 11565 N, respectively. The total fatigue life (N_f) was determined by summing the fatigue crack initiation life (N_i) and the fatigue crack propagation life (N_p). The ratios of the fatigue crack initiation life to the fatigue crack propagation life and the total fatigue life (N_i/N_p and N_i/N_f) are shown to determine which fatigue life was dominant to the total life.

Table A2- 5: Summary of predicted fatigue lives for the Square-Tube-on-plate welded joint subjected to a lateral load of F = 21350 N

Residual Stress (MPa)	N_i (Cycle) a_i = 0.5 mm	N_p (Cycle) a_f = 3.2 mm	N_i/N_p	N_f (Cycle)	N_i/N_f
σ_r = 0	47300	115000	0.412	162000	0.292
σ_r = 193.27	31000	54400	0.571	85400	0.363

The small ratios of the crack initiation life to the crack growth life (N_i/N_f = 0.292 and 0.363) indicate that most of the welded joint fatigue life, in the case of a high load, was spent on propagating the crack from a_i = 0.5 mm to the final critical crack depth of a_f = 6.338 mm.

Table A2- 6: Summary of predicted fatigue lives for the Square-Tube-on-plate welded joint subjected to a lateral load of F = 13878 N

Residual Stress (MPa)	N_i (Cycle) a_i = 0.5 mm	N_p (Cycle) a_f = 3.2 mm	N_i/N_p	N_f (Cycle)	N_i/N_f
σ_r = 0	1010000	383000	2.64	1400000	0.725
σ_r = 193.27	279000	138000	2.022	418000	0.669

Table A2- 7: Summary of predicted fatigue lives for the Square-Tube-on-plate welded joint subjected to a lateral load of F = 11565 N

Residual Stress (MPa)	N_i (Cycle) a_i = 0.5 mm	N_p (Cycle) a_f = 3.2 mm	N_i/N_p	N_f (Cycle)	N_i/N_f
σ_r = 0	5550000	638000	8.69	6180000	0.897
σ_r = 193.27	776000	138180	5.613	914000	0.849

The high ratios of the crack initiation life to the total fatigue life (N_i/N_f = 0.725, 0.669, 0.897, and 0.849) in Table A2- 6, and Table A2- 7 indicate that most of the welded joint fatigue lives for lower loads of (F = 13878 N and F = 11565 N) were spent on crack initiation to a_i = 0.5 mm.

The JD Company's laboratory fatigue lives were calculated as the number of load cycles versus the measured length of the surface crack on the attachment square tube. Using the fatigue crack growth simulation data obtained from the FALPR program, the crack depth corresponding to the measured crack length was estimated. The experimental data are shown in Table A2- 8.

Table A2- 8: JD Experimental fatigue crack propagation life data (2c-N) for the Square-tube-on-plate welded joint subjected to lateral loading

Sample #	Load (N)	Number of cycles (Cycles)	Crack length 2c (mm)	Remarks
S1 N	21350	35	98900	top toe
S4 N		20	117029	bottom toe
S6 N		8	32000	top toe
S8 N		6	20000	top toe
S2 Y		20	84864	top toe
S3 Y		25	97045	top toe
S5 Y		9	21298	top toe
S7 Y		4	21000	top toe
S10 N	13878	11	600000	root crack
S12 N		12	550000	root crack
S14 N		14	530000	root crack
S16 N		5	480000	top toe **
S11 Y		12	1550000	root crack
S13 Y		6	3160000	bottom toe
S15 Y		17	625000	bottom toe
S17 Y		11	450000	bottom toe
S9 Y	11565	-	5200000	no crack

The fatigue life data in Table A2- 5, Table A2- 6, and Table A2- 7 are plotted as shown in Figure A2- 39, Figure A2- 40, and Figure A2- 41 for all load levels applied to the Square-Tube-on-plate welded joint. The fatigue life data are plotted in terms of the applied load cycles versus the surface crack length (2c) for comparison between the experimental and predicted fatigue life. The experimental fatigue data are plotted as a series of discrete points, whereas the predicted fatigue data are plotted as two curves. The hashed curve represents the fatigue life prediction without the effect of the residual stress, and the solid curve represents the fatigue life prediction, including the residual stress effect.

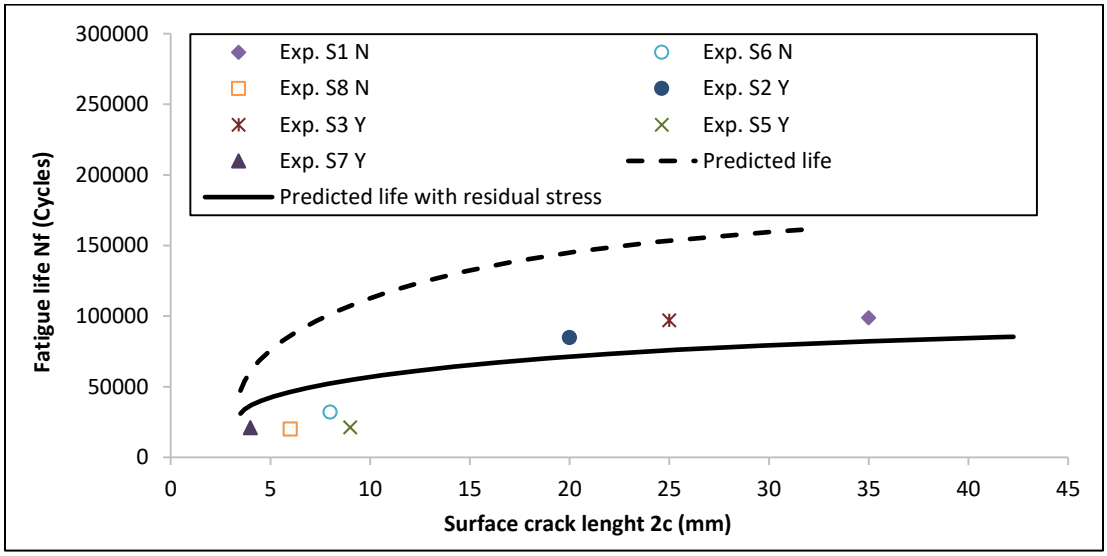

Figure A2- 39: Comparison between experimental and predicted fatigue lives of the Square-Tube-on-plate welded joint subjected to a lateral load of F = 21350 N

Figure A2- 39 shows the experimental and predicted total fatigue lives for the Square-Tube-on-plate welded joint subjected to a lateral load of F = 21350 N. Eight specimens were tested in total. Only the sample # (S4 Y) fatigue data were excluded from the comparison because the crack appeared at the lower weld toe. According to the results shown in the above figure, the predicted fatigue life, based on the proposed shell FE method, overestimated the fatigue life. However, including the residual stress reduces the overestimation significantly. This finding emphasizes the importance of including the residual stress effect when evaluating the fatigue life of welded joints.

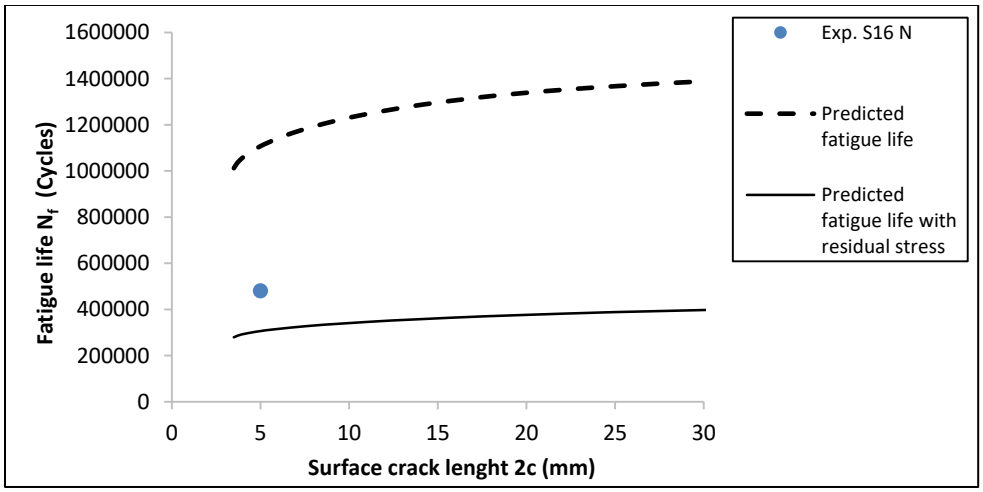

Figure A2- 40: Comparison between the experimental and predicted fatigue lives of the Square-Tube-on-plate welded joint subjected to a lateral load of F = 13878 N

Figure A2- 40 shows the experimental and the predicted total fatigue lives for the Square-Tube-on-plate welded joint subjected to a lateral load of F = 13878 N. Eight specimens were tested in total, yet only sample # (S16 Y) had the crack appear at the upper weld toe. Thus, the rest of the experiments were not comparable. According to the results shown in the above figure, the predicted fatigue life, based on the proposed shell FE method, overestimated the fatigue life. However, including the residual stress reduces the overestimation significantly. This finding emphasizes the importance of including the residual stress effect when evaluating the fatigue life of welded joints.

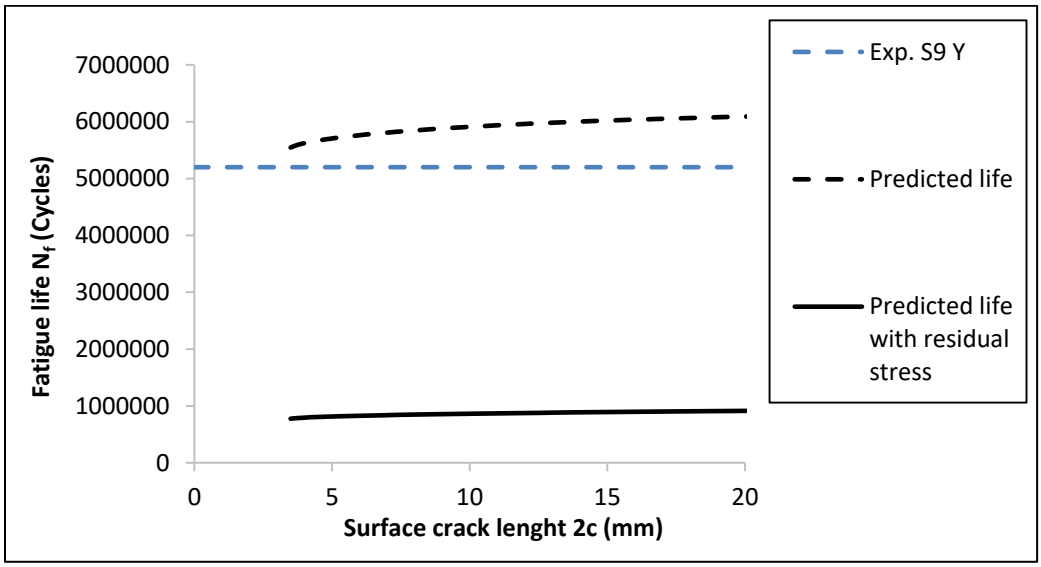

Figure A2- 41: Comparison between experimental and predicted fatigue lives of the Square-Tube-on-plate welded joint subjected to a lateral load of F = 11565 N

Figure A2- 41 shows the experimental and predicted total fatigue lives for the Square-Tube-on-plate welded joint subjected to a lateral load of F = 11565 N. Only one specimen was tested (sample # S9 Y), and no crack was observed on the surface of the specimen. Comparing sample # S16 Y, subjected to F = 13878 N, to sample # S9 Y subjected to F = 11565 N, may be indicative that the crack did not initiate because the load applied to the later sample was too low. According to the results shown in the above figure, the predicted fatigue life, based on the proposed shell FE method, overestimated the fatigue life. However, including the residual stress reduces the overestimation significantly. This finding emphasizes the importance of including the residual stress effect when evaluating the fatigue life of welded joints.

Generally, the total fatigue life predictions based on the proposed local reference stresses resulted in reasonably good fatigue life estimations at the highest load level, and the fatigue life predictions were less accurate for low load levels. The results also indicate that it is important to include the residual stress distribution to the stress analysis module when determining the fatigue life of weldments. The difference between the predicted fatigue lives and the experimental data could be that some of the experimental specimens are stress-relieved. The fatigue crack propagation period was relatively less significant at low loads and more significant at high loads.

A3.1 Fatigue analysis of a Complex tubular welded joint subjected to torsion and bending cyclic loading

In this case, several tubular welded joints connecting two tubes to each other with plates were tested at the JD laboratories, as shown in Table A3 - 1. The welded joint is constructed of a long tube with dimensions of 4 × 4 × 23.625 in, and another, shorter tube with dimensions of 2 × 6 × 14.313 in. The thickness of both tubes was 0.312 in. Each tube was connected to the base plate by plates with a thickness of 0.1875in. The material for the tested tubes was A22-H steel. The weld geometries were t = 0.312 in, t_p = 0.312 in, h = 0.312 in, h_p = 0.312 in, $\theta = 45°$, and ρ = 0.312 in.

Nine specimens in total were tested by JD. Two specimens were subjected to a load of F = ± 3000lb, whereas the rest were subjected to a load of F = ± 4000lb. All forces were applied as fully-reversed cyclic loading to the attached plate connected to one side of the longer tubes. The force direction, as shown in Figure 6-21, produces torsion and bending loading on the component. Each tube of the component was attached to a plate that is fixed on the main base plate. The main base plate of each test component was fixed via eight holes using M8 bolts.

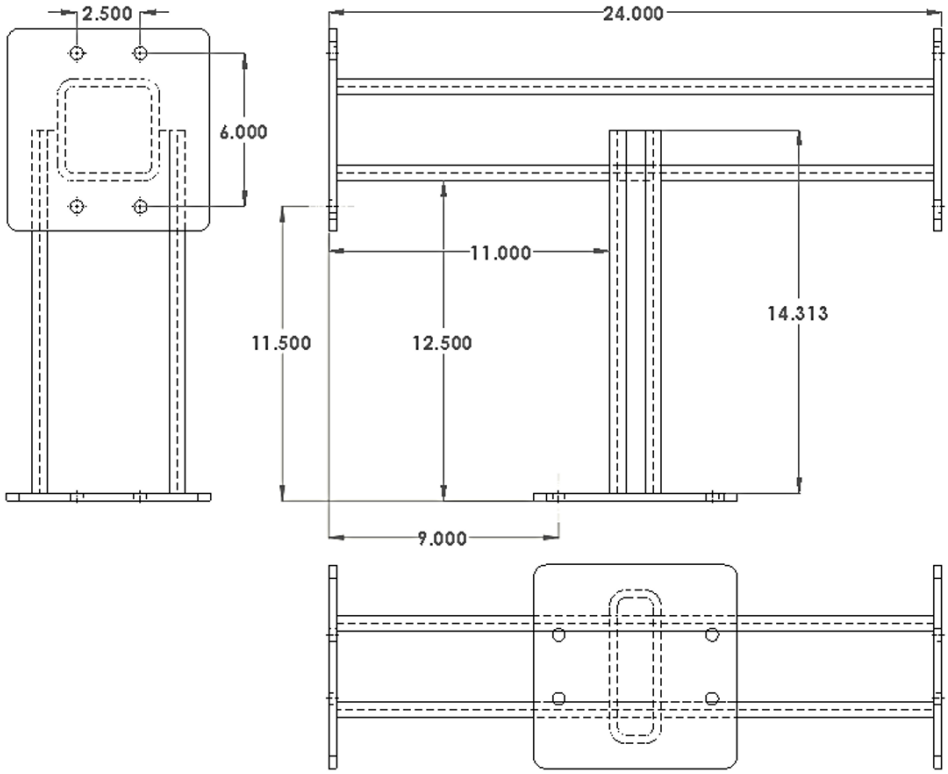

Figure A3- 1: Dimensions of the Complex tubular welded joint subjected to torsion and bending cyclic loading (all dimensions are in inches)

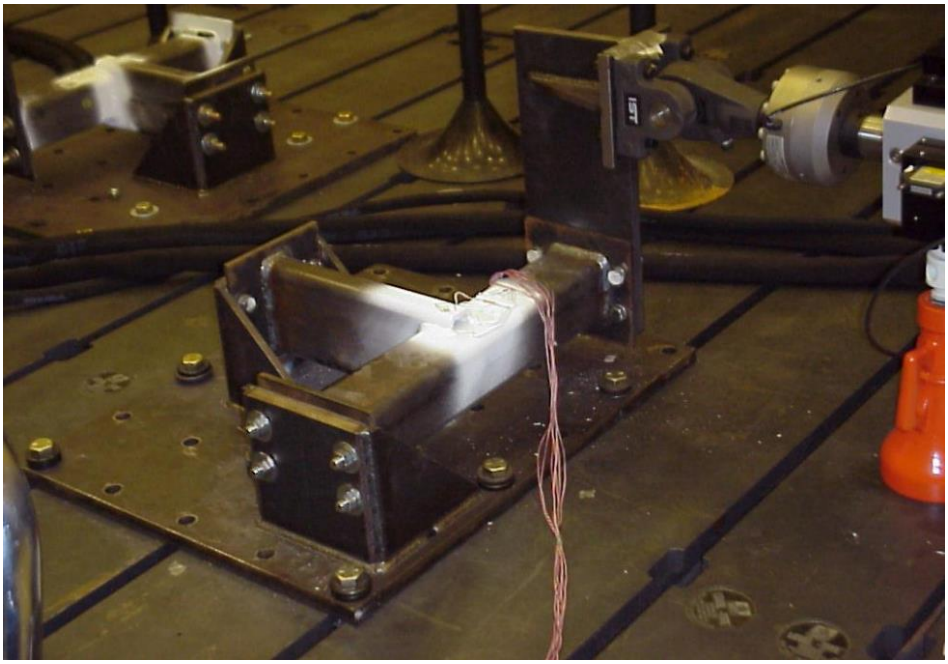

Figure A3- 2: JD fatigue test of the tubular welded joint subjected to torsion and bending loading (JD)

A3.1.1 Material properties

The material properties of the welded joint under investigation (A22-H steel) were provided by the JD laboratories. The mechanical properties are shown in Table A3 - 1, whereas the Ramberg-Osgood stress-strain curve provided by JD for A22-H steel, is shown in Figure A3- 3. The strain-life curves were provided by JD for A22-H steel, as shown in Figure A3- 4. The cyclic and fatigue properties are shown in Table A3 - 2.

Table A3 - 1: Mechanical properties of A22-H steel

Ultimate strength (Su)	Yield strength (Sy)	Elastic modulus (E)
79.0 (Ksi)	68.89 (Ksi)	29938 (Ksi)

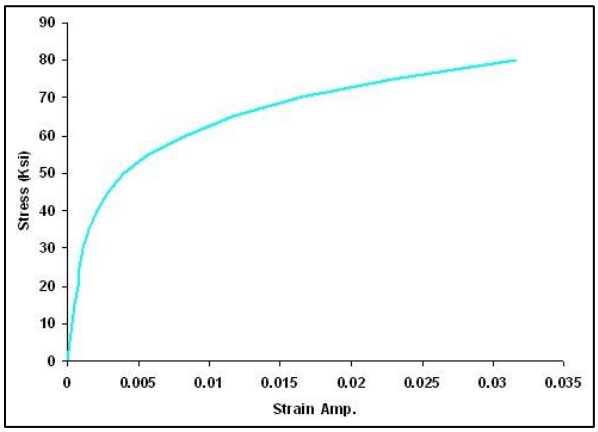

Figure A3- 3: The Ramberg-Osgood stress-strain curve for A22-H steel (JD)

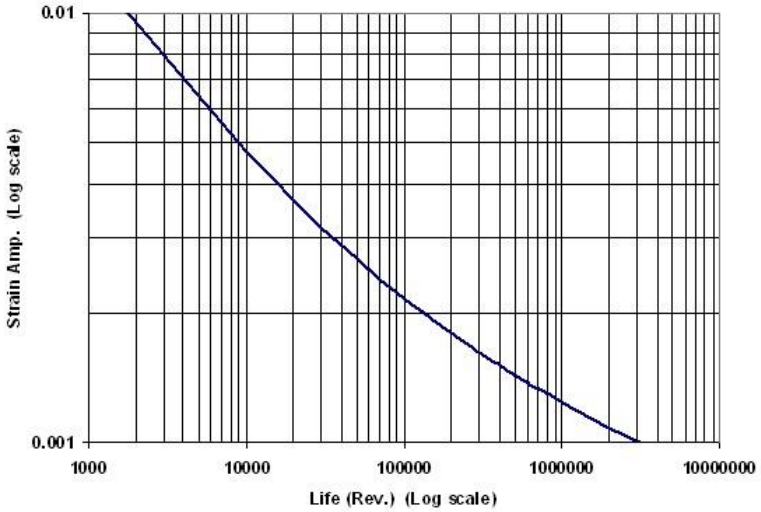

Figure A3- 4: The strain-life fatigue curve for A22-H steel (JD)

Table A3 - 2: JD fatigue parameters for A22-H steel

Fatigue strength coefficient (σ'_f)	**169.98 (Ksi)**
Fatigue strength exponent (b)	**-0.12**
Fatigue ductility coefficient (ε'_f)	**0.648**
Fatigue ductility exponent (c)	**-0.543**
Cyclic strength coefficient (K′)	**931.8 (Ksi)**
Cyclic strain hardening exponent (n′)	**0.187**

A3.1.2 Shell FE modelling of a Complex tubular welded joint subjected to torsion and bending cyclic loading

The shell FE model's boundary conditions for the Complex tubular welded joint under investigation is shown in Figure A3- 5. The shell FE model should have the same geometry as the experiment specimen. In addition, the stress data must be extracted from the weld's critical location. The base plate was constrained for all displacement, while a lateral force of 1 lb was applied to the vertical plate attached to one side of the longer tube.

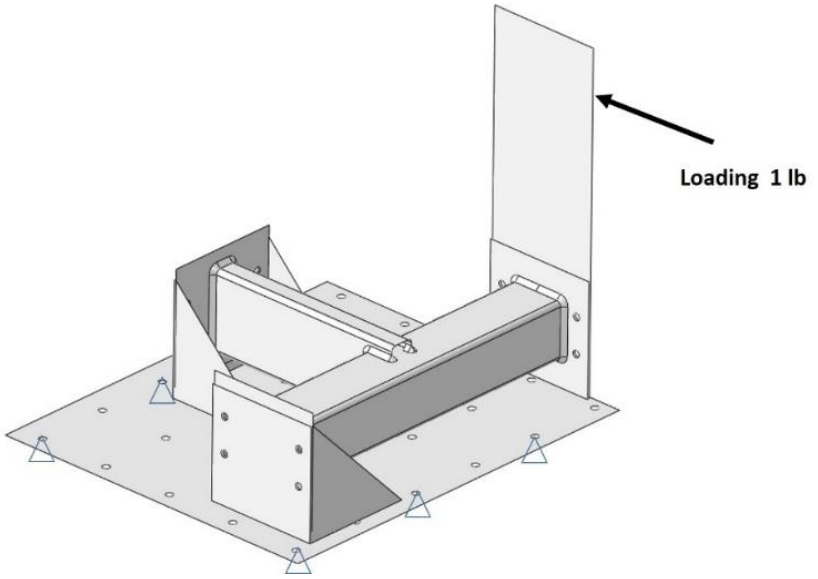

Figure A3- 5: Shell FE modelling and boundary conditions for the Complex tubular welded joint subjected to torsion and bending cyclic loading (F = 1 lb)

The local reference stresses σ_a and σ_b were obtained from a reference point located at the weld toe of the shorter tube, as shown in Figure A3- 6. The reference point contains the local reference stresses, which represent the surface and bottom stresses through the tube thickness. These stresses are used to determine the membrane and bending hot spot stresses that will be multiplied by the proper SCFs (see Section 3.7) to calculate the peak stress at the weld toe.

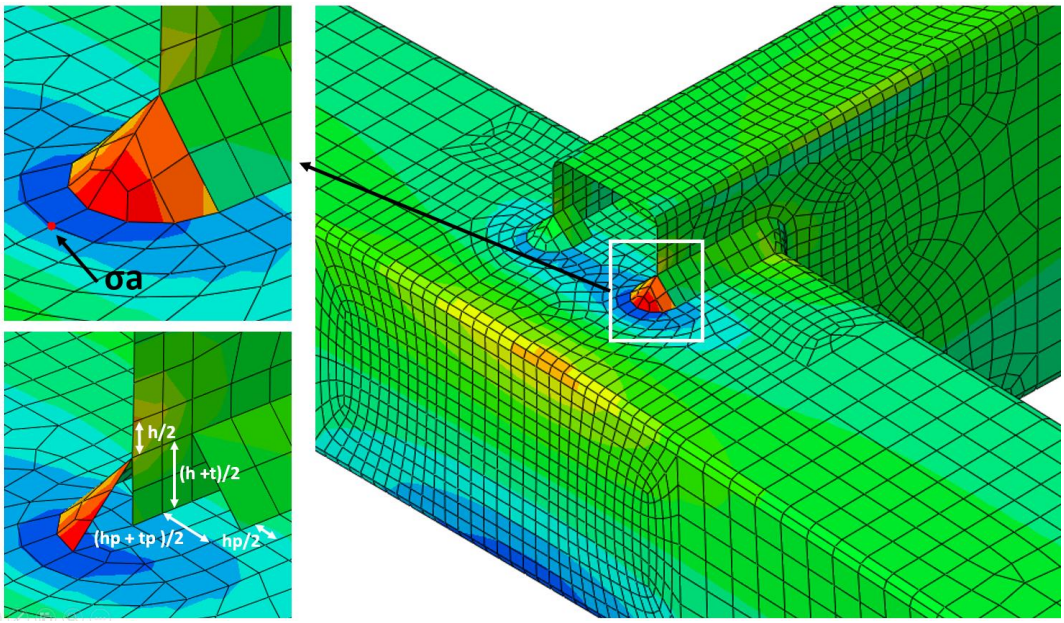

Figure A3- 6: Shell FE contours of the maximum normal stress to the weld toe line; Complex tubular welded joint

According to the experiments, the maximum stress was expected to be at the weld toe of the gusset edge. Note that the reference points in the above shell FE model coincide with the actual location of the weld toe of the experimental specimen. The maximum stress is located at the weld toe, as expected (see Figure A3- 6). However, the required shell FE reference stresses are to be extracted from a specific reference point and not at the maximum contour node. The distance between the attachment side and the weld toe reference point of the shell model was $h_p + (t_p/2) = 1.468$ in. At that specific reference point (at the critical location [weld toe]), the local reference stresses σ_a and σ_b were extracted from the longer tube thickness (top and bottom). The local reference stresses through the base plate (σ_a and σ_b) were recorded as follows:

$\sigma_a = 8.87$ psi

$\sigma_b = -4.07$ psi

Hence, the hot spot stresses were:

$$\sigma_{hs}^{m} = \frac{\sigma_a + \sigma_b}{2} = 2.4 \text{ psi}$$

$$\sigma_{hs}^{b} = \frac{\sigma_a - \sigma_b}{2} = 6.47 \text{ psi}$$

Using the weld geometrical features of the current case, the SCFs were calculated. However, according to the 3D FE data, the t_p parameter in equations (3.18–3.19) cannot be greater than 3t. Therefore, the attachment plate thickness t_p parameter was multiplied by a factor of 3 as an assumption for the SCFs at the edge of the gusset. This was based on the fact that the effect of the edge disappears at distances greater than 3t, and the SCF equations are not valid for large values of t_p. The thickness of the tube t_p was assumed to be t_p = 0.936 in, and the SCFs are:

$K_t^m = 1.784$

$K_t^b = 2.203$

As per equation (3.11), the peak stress at the weld toe induced by the applied load was:

$$\sigma_{peak} = \sigma_{hs}^m . K_t^m + \sigma_{hs}^b . K_t^b = 18.535 \text{ psi}$$

Two stress distributions through the base plate thickness in the direction normal to the weld toe are shown in Figure A3- 7. The linear stress distribution (hashed line) represents the local reference stresses (σ_a and σ_b). The non-linear stress distribution (solid curve) represents the Monahan equation $\sigma_{xx}(y)$.

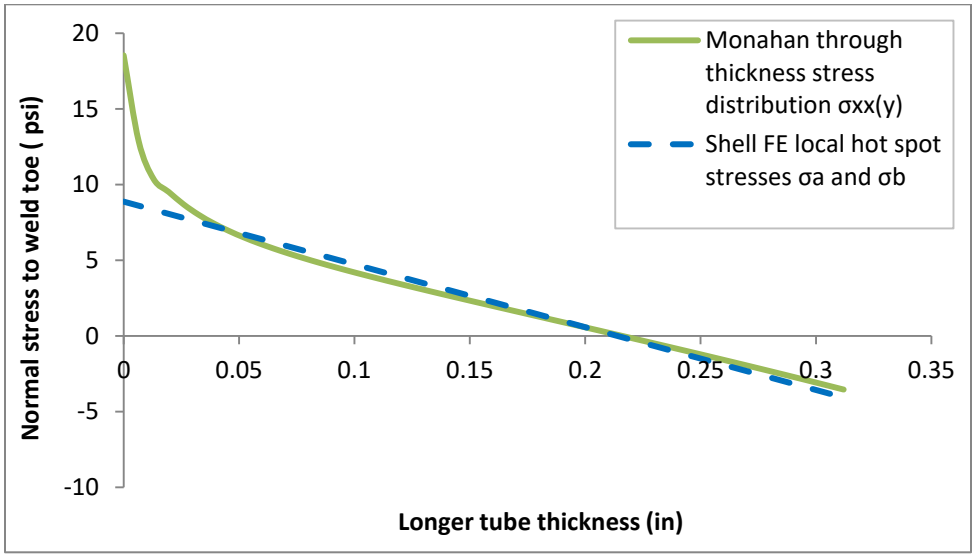

Figure A3- 7: Shell FE local stresses (linear) and the Monahan non-linear through-thickness stress distribution at the weld toe of the Complex tubular welded joint

The above figure provides the stress data (σ_a, σ_b, $\sigma_{peak,}$ and $\sigma_{xx}(y)$) required for the fatigue analysis of the case under investigation. The stress data in the above figure are obtained from a shell FE model

and must be validated against a detailed 3D FE model before proceeding with the fatigue analysis. A 3D FE model with the same geometry as the experiment is modelled in the following section to validate the shell FE local reference stress data.

A3.1.3 Finite element 3D modelling of a Complex tubular welded joint subjected to torsion and bending cyclic loading

The 3D FE model should have the same geometry as the experimental specimen. Also, the stress data must be extracted from the weld's critical location in the same way as the shell FE model. According to the shell FE model, the maximum stress occurs at the lower weld toe (see Figure A3- 6); therefore, it is expected that the 3D FE model would have the peak stress at the same location. The 3D model boundary conditions is shown in

Figure A3- 8 whereas Figure A3- 9 shows the fine mesh at the expected critical weld toe [65]. The 3D modelling of this case was done by JD and the stress data was digitized from [65]. Because of the symmetry of the problem, only half of the component was modelled to reduce the computational time. The model was subjected to lateral loading of 1 lb in order to apply bending and torsion stresses at the weld. The bottom corners of the base plate were constrained for all displacements, and the model elements were approximated by eight brick elements.

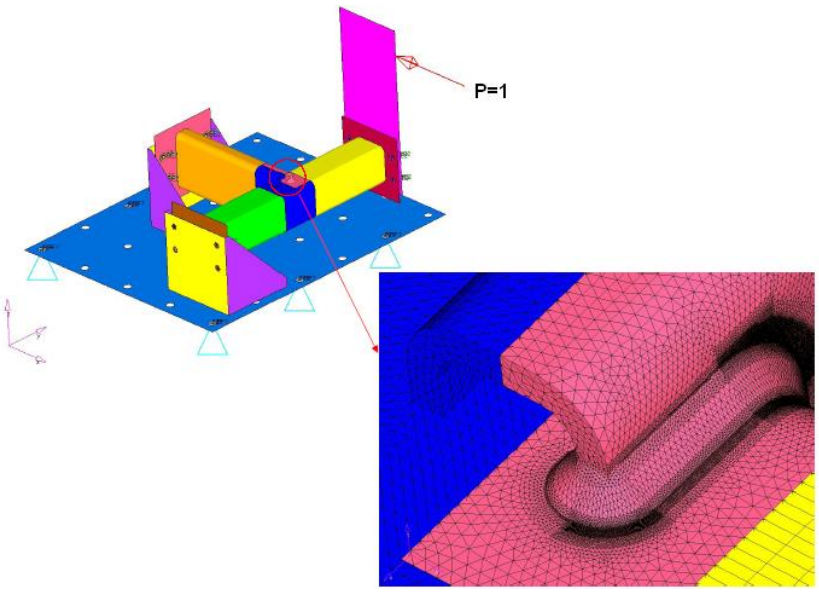

Figure A3- 8: Boundary conditions of the 3D FE simulated Complex tubular subjected to torsion and bending loading [65]

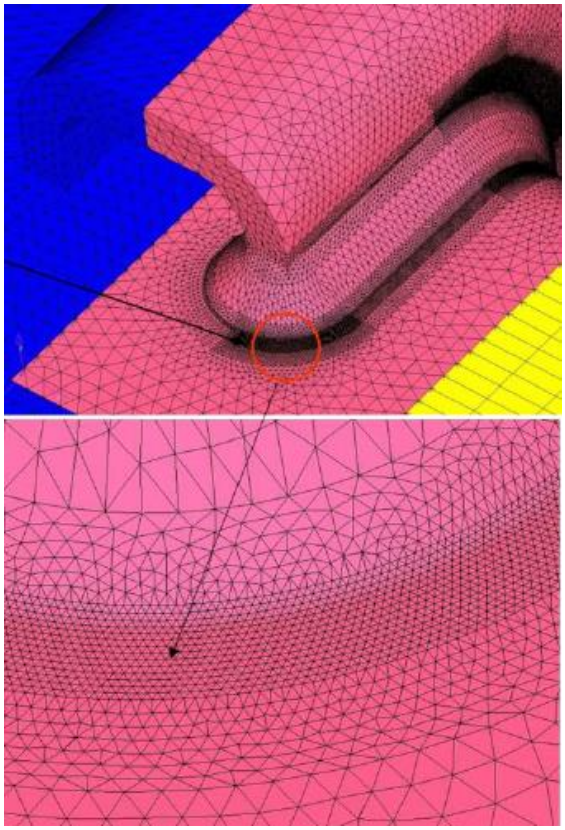

Figure A3- 9: Intensive mesh at the weld toe of the Complex tubular subjected to torsion and bending loading (3D FE model) [65]

Based on the 3D FE modelling, the actual peak stress obtained at the weld toe was 17.5 psi, whereas the actual non-linear through-thickness stress distribution is shown in Figure A3- 10. The latter stress distribution was processed according to Section (4.1), while the membrane and bending hot spot stresses were found by linearization of the actual through-thickness stress distribution, as mentioned in equations (4.3 and 4.5):

$\sigma_{hs}^{m} = 2.59$ psi

$\sigma_{hs}^{b} = 6.74$ psi

Equations (4.6 and 4.7) were then used to find the linearized surface stresses as:

$\sigma_a = \sigma_{hs}^{m} + \sigma_{hs}^{b} = 9.33$ psi

$\sigma_b = \sigma_{hs}^{m} - \sigma_{hs}^{b} = -4.16$ psi

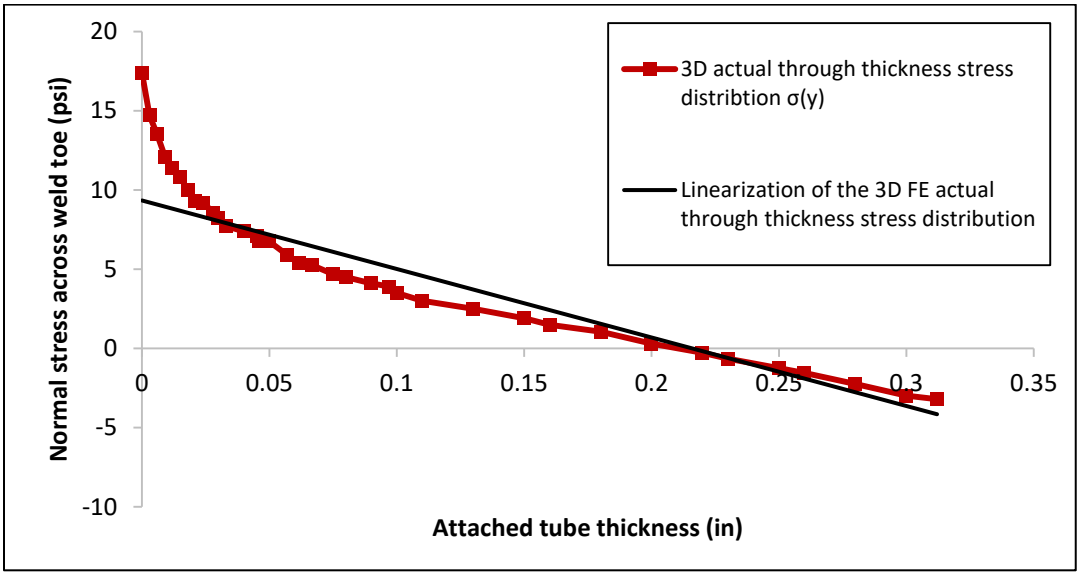

Figure A3- 10: The actual through-thickness stress distribution and its equivalent linearization stress at the weld toe of the Complex tubular welded joint 3D FE model [65]

In the above figure, the red curve represents the actual non-linear stress distribution through the thickness of the weld toe cross section based on the 3D FE model. In the same figure, the solid line represents the linearization of the curve (actual non-linear stress distribution). The stress results of the shell and the 3D FE models were compared as shown in Figure A3- 11 and Figure A3- 12, respectively. A comparison between the actual non-linear through-thickness stress distribution σ(y) obtained from the 3D FE model and the non-linear through-thickness stress distribution $\sigma_{xx}(y)$ generated from the shell FE local reference stress data and the Monahan equation as shown in Figure A3- 11. The shell FE local reference stresses are compared with the 3D FE modelling linearized stresses in Figure A3- 12.

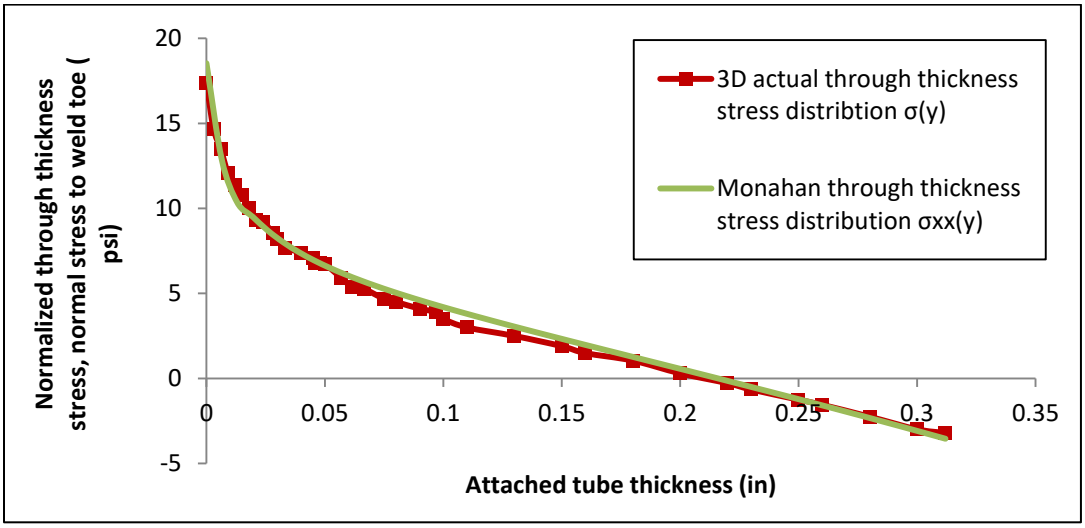

Figure A3- 11: Comparison of the actual stress distribution (3D FE model) and the stress distribution (shell FE model and Monahan) through the longer tube thickness of the Complex tubular weld joint subjected to torsion and bending load [65]

The difference between the actual peak stress based on 3D FE modelling (17.5 psi) and the peak stress based on shell FE local reference stress data (18.535) was approximately 6%. The compared stress distributions from the shell and 3D FE models result in a 5% difference for the tensile part, which is the most important part because it is considered the location of the peak stress needed for the ε-N method.

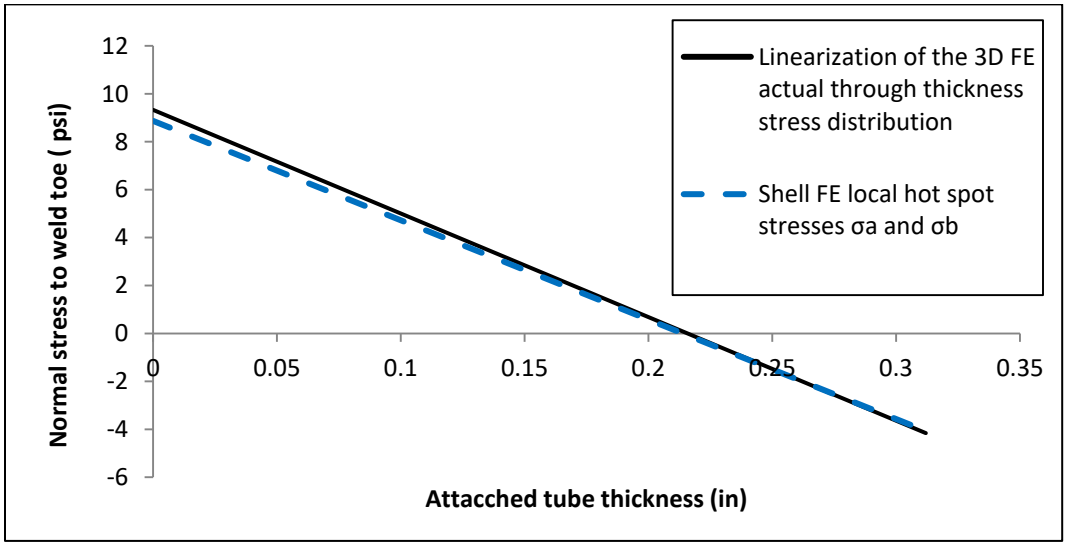

Figure A3- 12: Comparison between linearized stresses based on the 3D FE model and shell FE model for the Complex tubular weld joint subjected to torsion and bending load

The linearized through-thickness stresses from the 3D FE model were higher than the shell FE local reference stresses in the bending and tensile parts of the base plate surfaces.

This validation is important because the peak stress based on the shell FE model will be used to determine the fatigue crack initiation life using the strain-life method. In addition, the through-thickness stress distribution based on the shell FE and Monahan equation will be used to determine the stress intensity factor required to calculate the fatigue crack propagation life using the LEFM method.

The JD Company performed two series of fatigue tests to verify the predicted fatigue life for the Complex tubular weld joint subjected to torsion and bending loading. Both tests were conducted under fully reversed loading, but the first series of test specimens was subjected to F = ± 3000 lb, whereas the second series was subjected to F = ± 4000 lb. Therefore, the peak stress and the through-thickness distributions obtained from the shell FE modelling (the green curve in Figure A3- 13 and Figure A3- 14) were scaled to the load levels applied to the experimental specimens (F = 3000lb and F = 4000 lb).

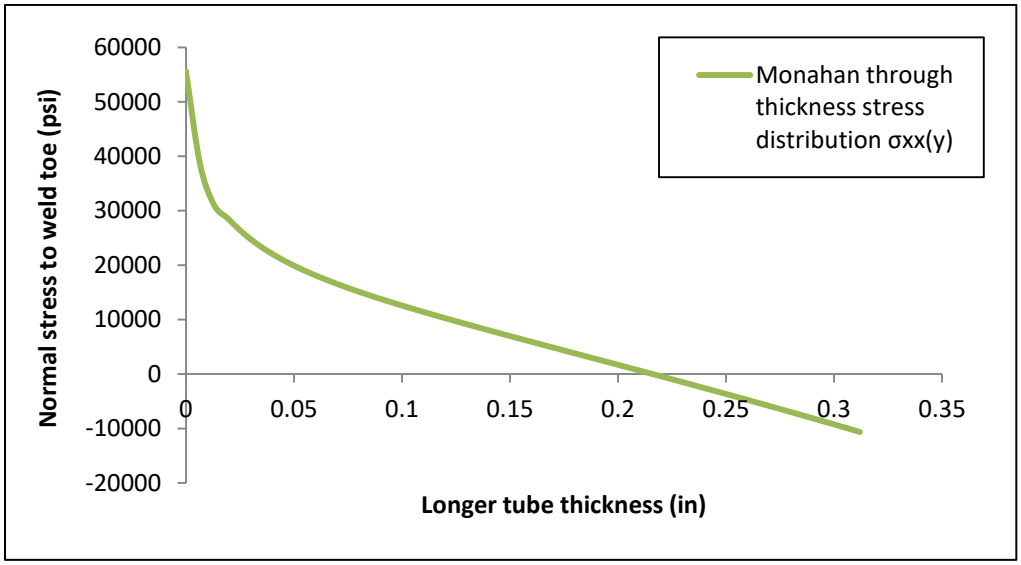

Figure A3- 13: Scaled non-linear through-thickness stress distribution to a load of 3000 lb, based on the shell FE local reference stress data and Monahan equation

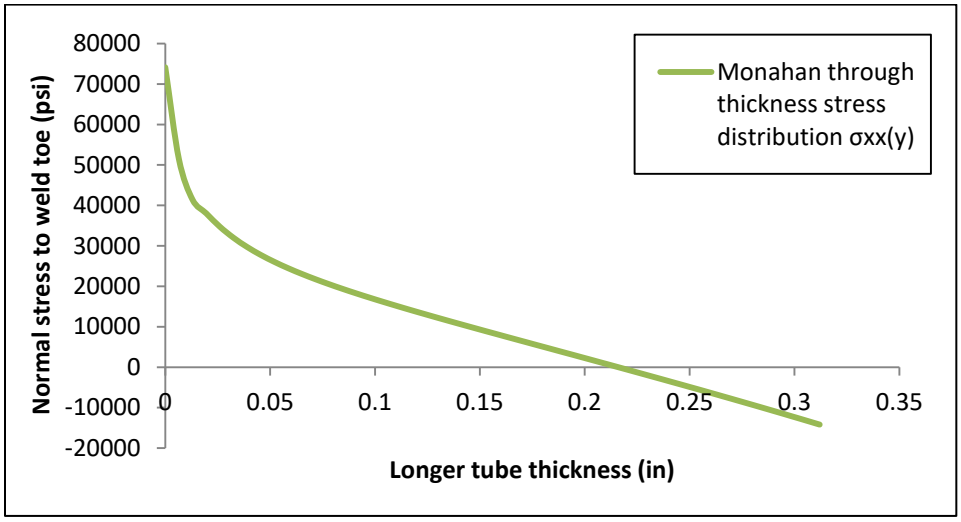

Figure A3- 14: Scaled non-linear through-thickness stress distribution for a load of 4000 lb, based on the shell FE local reference stress data and Monahan equation

The fatigue life predictions were performed with and without the residual stresses. The residual stress at the weld toe was measured by the JD Company, as shown in Figure A3- 15. Unfortunately, the residual stress measurements were for the tube surface only; therefore, the distribution was approximated through the tube thickness by assuming a self-equilibrated linear field. The residual stress distribution is shown in Figure A3- 16.

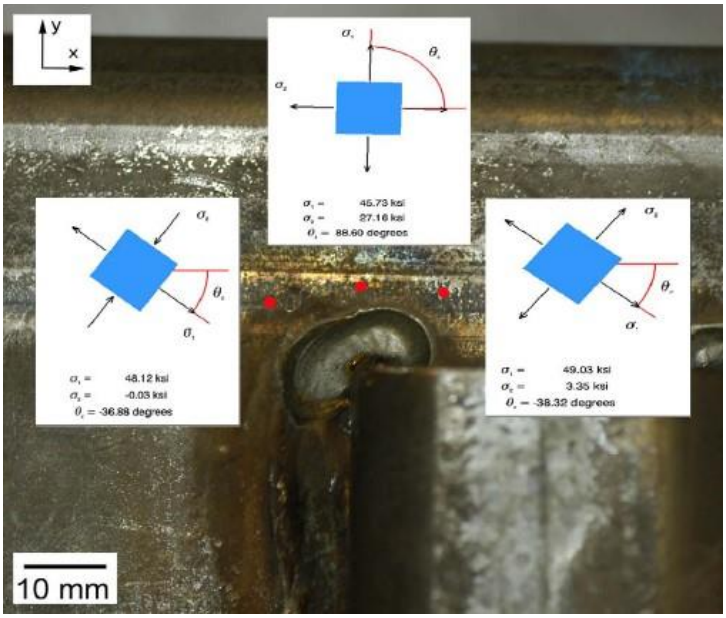

Figure A3- 15: The residual stress measurements near the weld toe surface for a Complex tubular welded joint under torsional and bending loads [65]

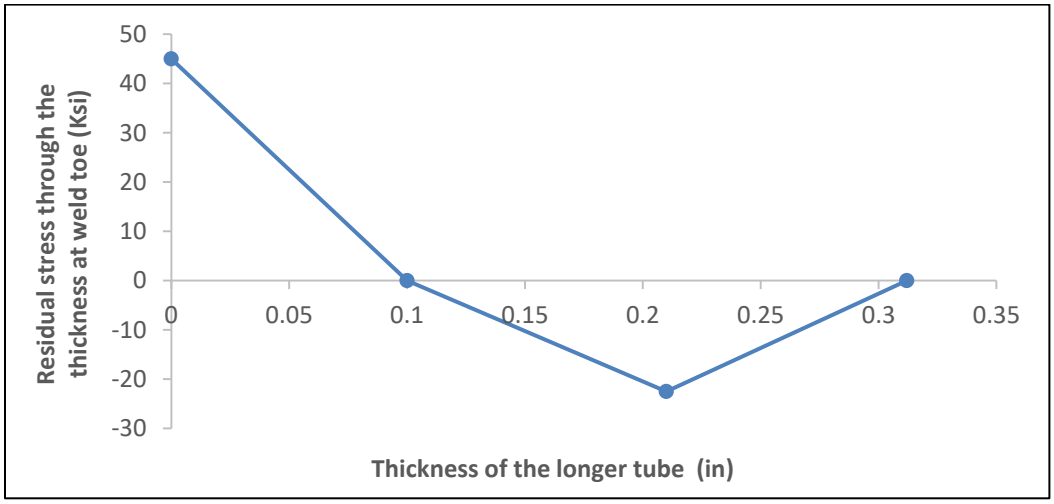

Figure A3- 16: Approximation of the residual stress distribution through the thickness of the longer tube for the Complex tubular weld joint

A3.1.4 Fatigue life evaluation

The fatigue life is predicted by using the ε-N and the LEFM methods based on the shell FE local reference stress data. The ε-N method predicts the fatigue crack initiation life, whereas the LEFM method predicts the fatigue crack propagation life. Both methods, which are coded into the in-house FALIN and FALPR software packages, were used to find the total fatigue lives of the current case (Complex tubular weld joint subjected to torsion and bending loading). The total fatigue lives were determined by summing both the initiation and the propagation fatigue lives. Finally, the predicted total fatigue life was compared with the fatigue life of the experiment.

The first step is to determine the fatigue crack initiation life according to the procedure for the strain-life method described in Section (2.2). The material properties in Table A3 - 1 and Table A3 - 2 were input to the FALIN software to calculate the stresses and strains for each load cycle based on the Ramberg-Osgood fatigue stress-strain curve and the Neuber equation (see Figure A3- 3 and Figure A3- 4). The SWT equation (2.9) was then used to calculate the fatigue crack initiation life. The outputs from the FALIN software were the simulated stress-strain response and the fatigue crack initiation life at the weld toe. The fatigue crack initiation lives were predicted for the current case when subjected to load levels of 3000 lb and 4000 lb without the effect of the residual stress, as shown in Figure A3- 17 and Figure A3- 18. The fatigue crack initiation lives for the same load levels, including the residual stress effect are shown in Figure A3- 19 and Figure A3- 20.

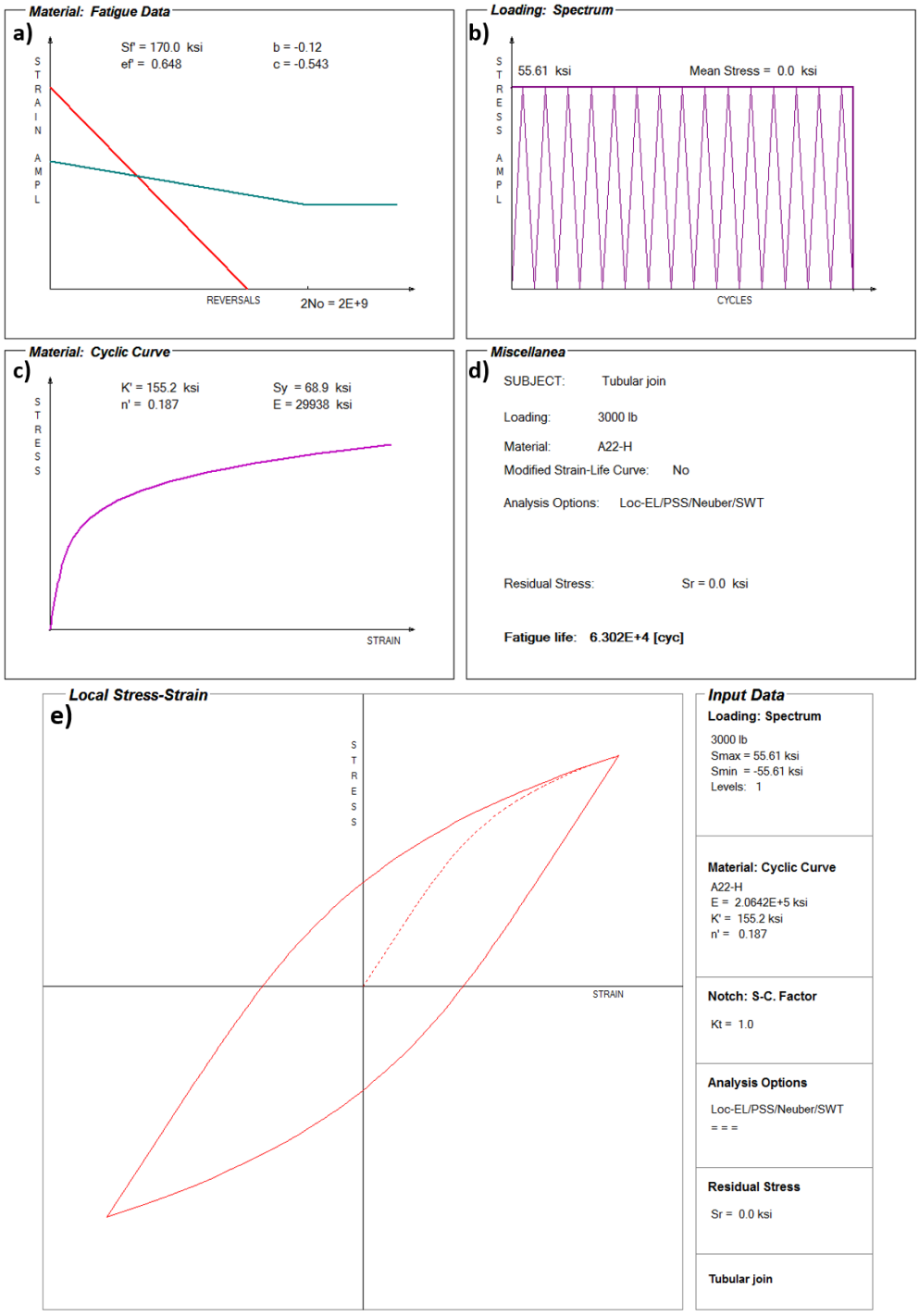

Figure A3- 17: FALIN input and output data for the Complex tubular welded joint subjected to a load of F = 3000 lb; a) Manson-Coffin curve, b) Peak stress loading, c) Ramberg-Osgood curve, d) Output data, e) Simulated stress-strain material response at the weld toe

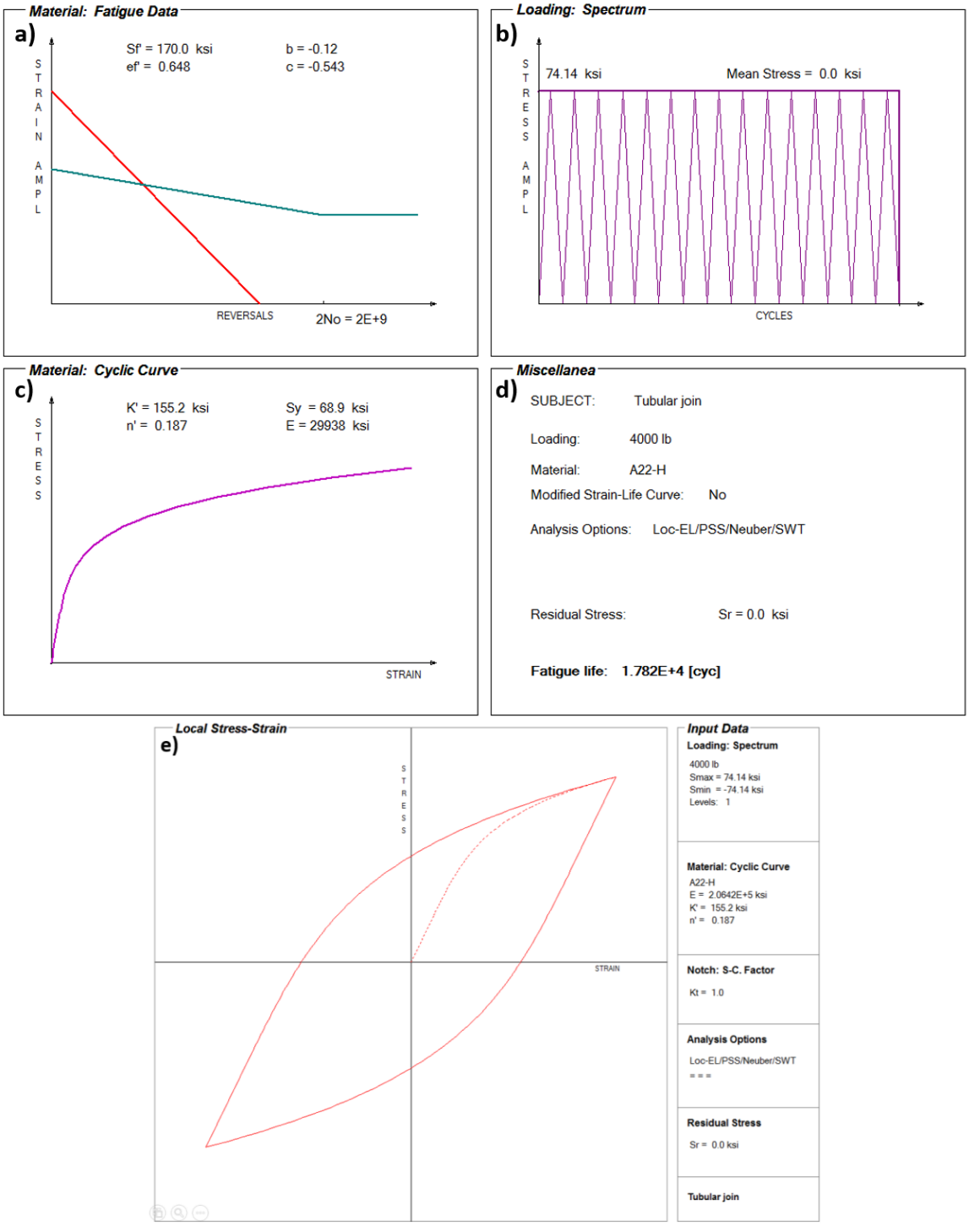

Figure A3- 18: FALIN input and output data for the Complex tubular welded joint subjected to a load of F = 4000 lb; a) Manson-Coffin curve, b) Peak stress loading, c) Ramberg-Osgood curve, d) Output data, e) Simulated stress-strain material response at the weld toe

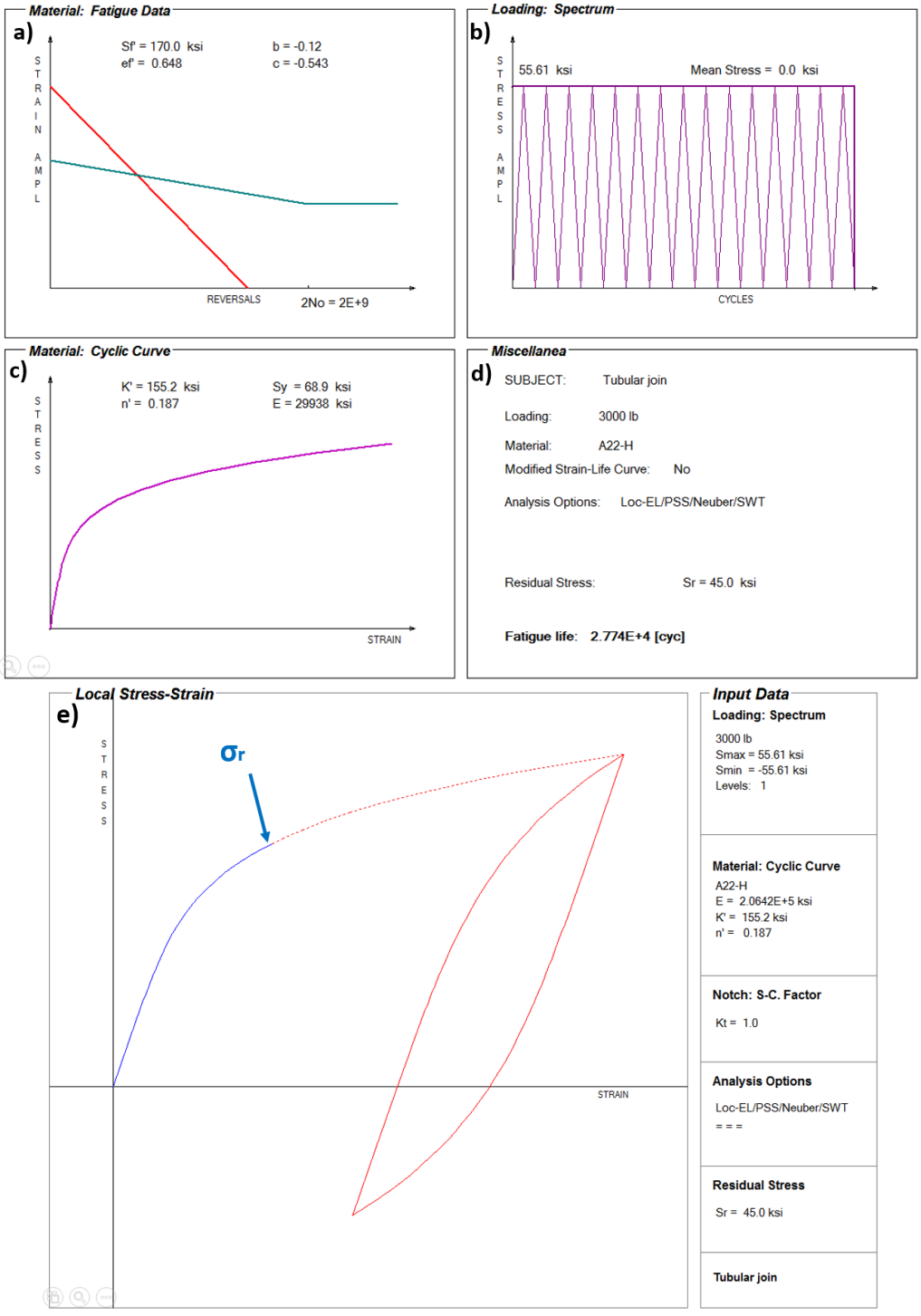

Figure A3- 19: FALIN input and output data for the Complex tubular welded joint subjected to a load of F = 3000 lb in addition to the residual stress σ_r ; a) Manson-Coffin curve, b) Peak stress loading, c) Ramberg-Osgood curve, d) Output data, e) Simulated stress-strain material response at the weld toe

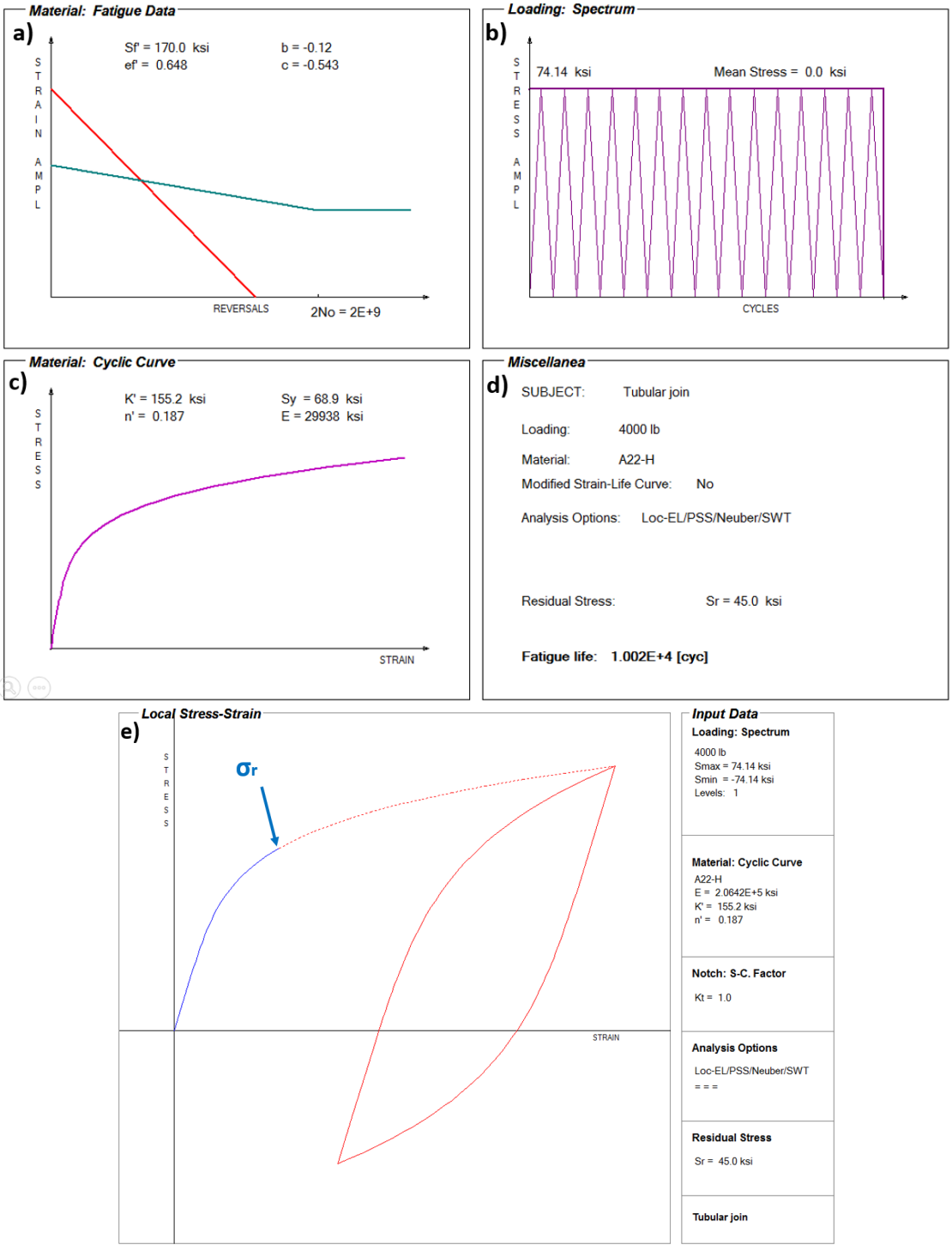

Figure A3- 20: FALIN input and output data for the Complex tubular welded joint subjected to a load of F = 4000 lb in addition to the residual stress σ_r ; a) Manson-Coffin curve, b) Peak stress loading, c) Ramberg-Osgood curve, d) Output data, e) Simulated stress-strain material response at the weld toe

The second step in the fatigue life analysis is the calculation of the fatigue crack propagation life using the LEFM method coded in the FALPR software. The observed cracks in the JD fatigue test experiments for the current case were found to be semi-elliptical in shape with a surface crack length of approximately 0.14 in. Therefore, the initial crack size was assumed to be not greater than $a_i = 0.02$ in depth with an aspect ratio of (a/c = 0.286). Accordingly, the predictions of the fatigue crack propagation life were based on assuming a semi-elliptical planar crack in a finite thickness plate.

In case of semi-elliptical cracks, two stress intensity factors at the depth and surface points are needed. Using the weight function method, with the through-thickness stress distribution $\sigma_{xx}(y)$ based on the shell FE modelling and Monahan equation, the stress intensity factors at the crack depth and surface (points A and B in Figure 3-13) can be determined. These two stress intensity factors are important for the determination of crack increments after each cycle for both surface and depth directions, as per equations (2.21 and 2.22). The crack increments due to the applied load cycles are calculated by using Paris' fatigue crack growth equation (2.20). To use the Paris equation, fatigue crack growth properties C and m are required for the material of the welded joint under investigation.

Fatigue crack growth properties for the material of the current case can be determined according to Section (2.3) by using Noroozi's [47] equations. For the determination the Paris equation constants C and m, the material properties in Table A3 - 1 and Table A3 - 2 were input to FALIN software. Hence m = 3.02 and C = 2.97364 x 10^{-10}, corresponding to R = 0 at N = 10^6 cycles.

The threshold stress intensity range and the critical stress intensity factor for the material of the current case at R = 0 were:

$\Delta K_{th} = 3.19\ \text{ksi}\sqrt{\text{in}}$, and $K_c = 72.81\ \text{ksi}\sqrt{\text{in}}$.

The through-thickness stress distribution based on the shell FE model and Monahan equation were input to FALPR to determine the stress intensity factors. It was found that the crack was growing on the surface faster than the depth because of the high stress at the weld toe [62]. Therefore, the crack increments of the surface and deepest point have to be determined for each load cycle. Accordingly, the aspect ratio (a/c) has to be updated after each increment using Paris' fatigue crack growth. The fatigue crack propagation life has been predicted for the Complex tubular welded joint subjected to torsion and bending cyclic loadings of F = 3000 lb and F = 4000 lb. The predictions for both load

cases were carried out with and without the residual stress to investigate the effect of the residual stress.

The input data to FALPR, the predicted crack depth versus the number of cycles, the stress intensity factor versus the number of applied load cycles, the fatigue crack growth life predictions, and the fatigue crack propagation lives of the weld joint under investigation when applying loads of F = 3000 lb and F = 4000 lb are shown in Figure A3- 21 through Figure A3- 24, whereas Figure A3- 25 through Figure A3- 28 show the same results including the effect of the residual stress. Note that including the residual stress effect was done to study its effect on the fatigue life evaluation.

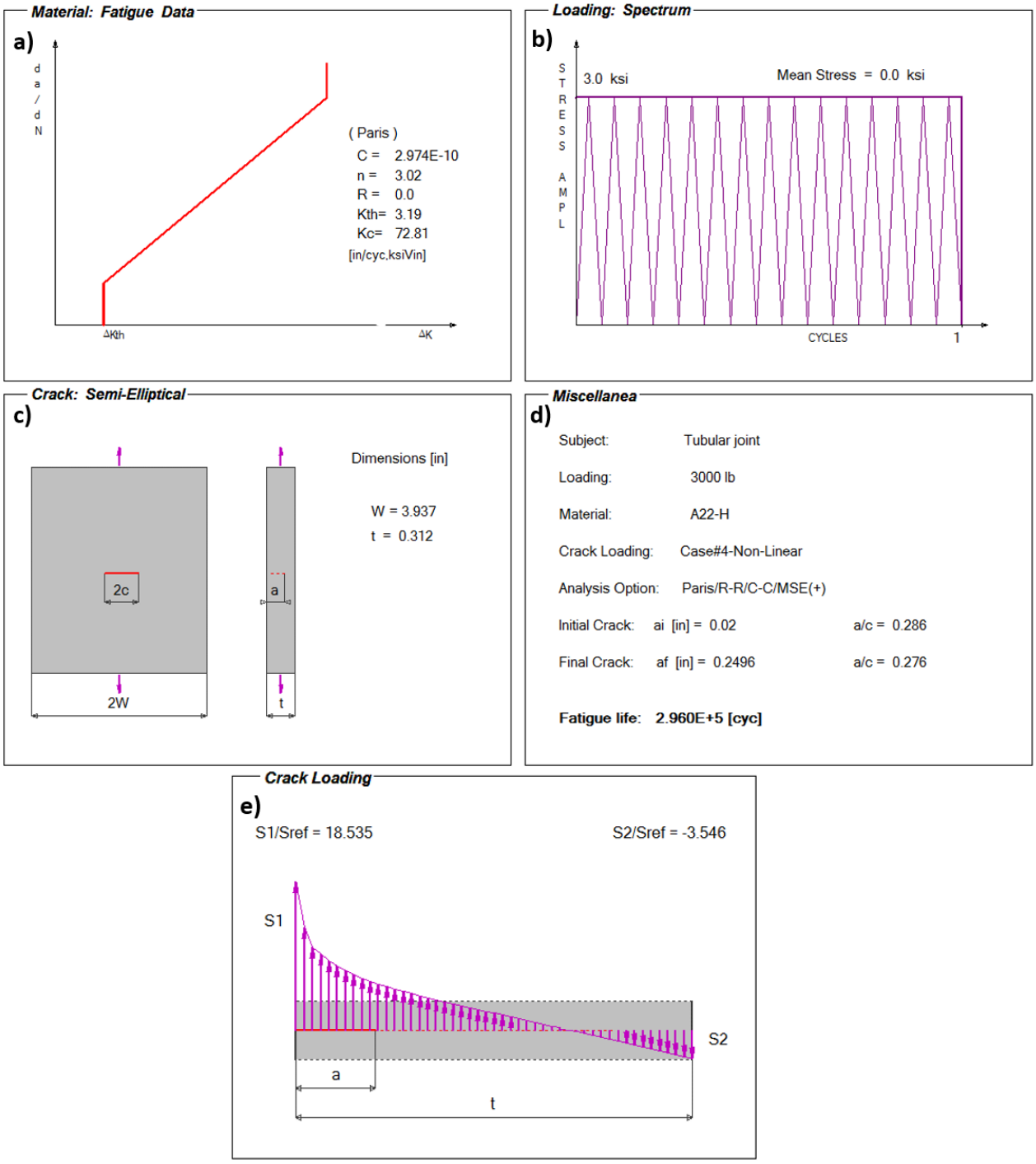

Figure A3- 21: FALPR input and output data for fatigue crack propagation analysis of the Complex tubular welded joint subjected to torsional and bending loading of F = 3000 lb (without residual stress): a) Paris fatigue crack growth curve, b) Loading history of the peak stress, c) Geometry of the crack, d) Fatigue life, e) The normalized through-thickness stress distribution

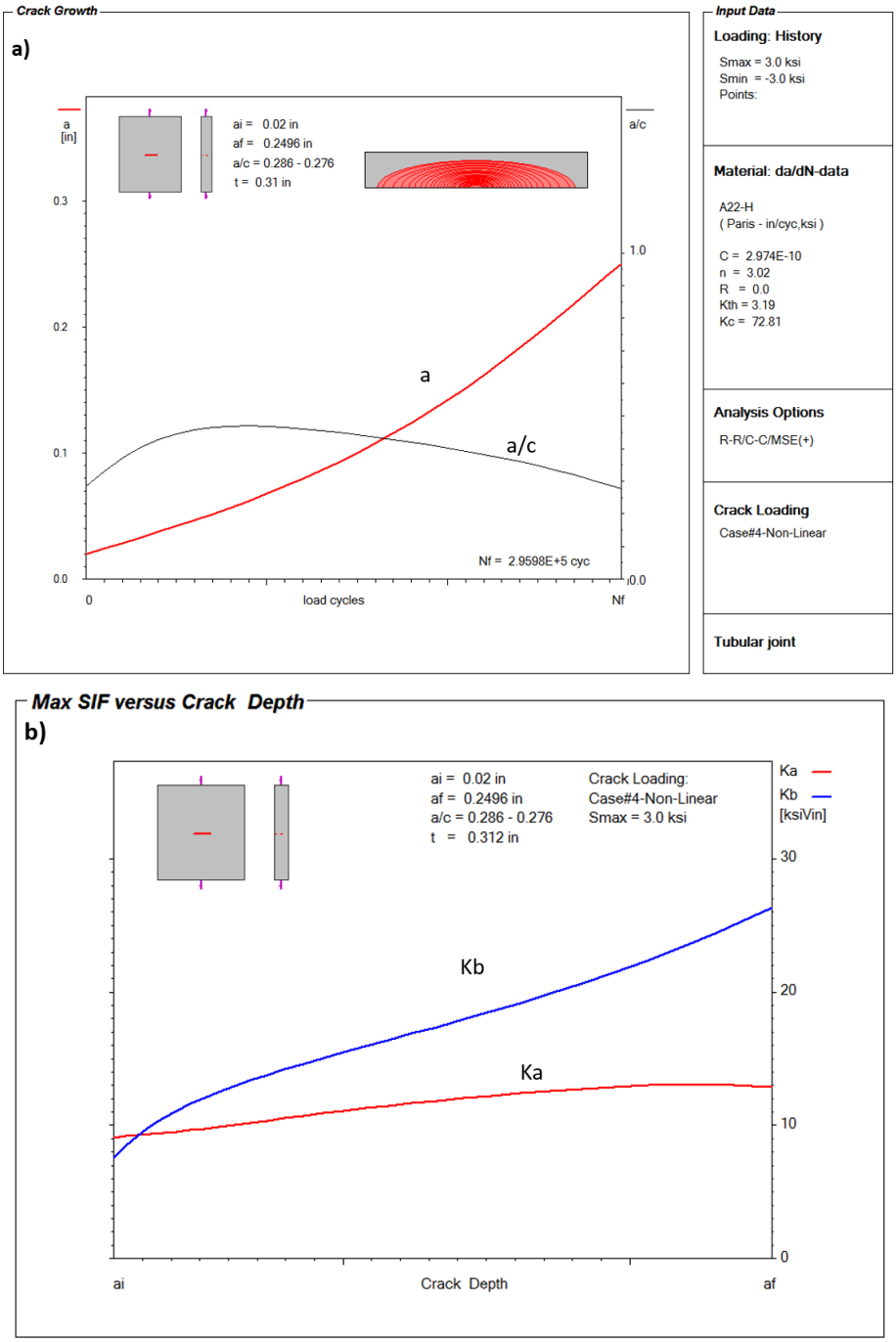

Figure A3- 22: a) The crack depth versus the number of applied load cycles to failure (a-N diagram), b) The stress intensity factor values at the surface and depth points of the semi-elliptical crack versus the crack depth (K-a diagram); Complex tubular welded joint subjected to torsional and bending loading of F = 3000 lb (without residual stress)

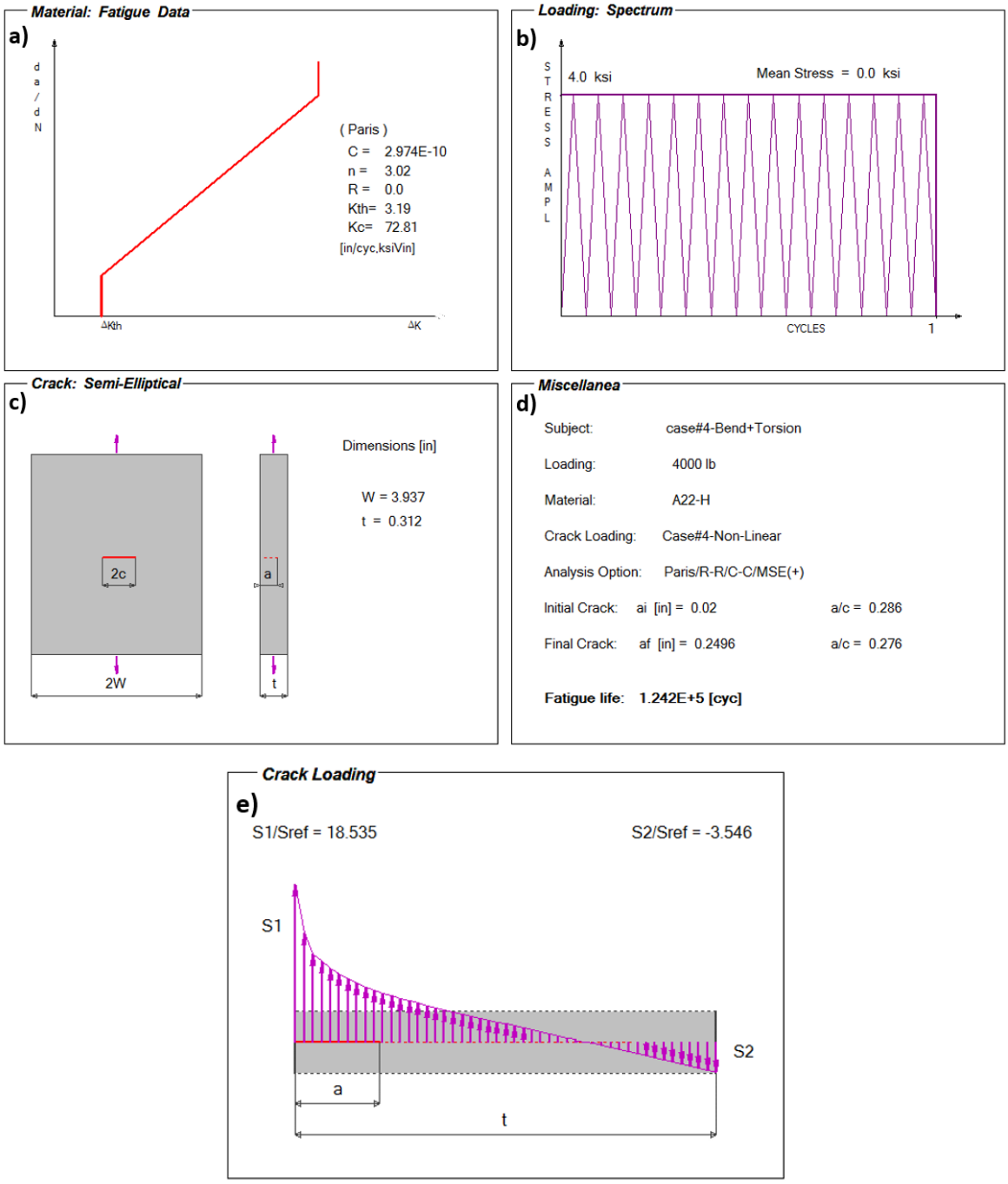

Figure A3- 23: FALPR input and output data for fatigue crack propagation analysis of the Complex tubular welded joint subjected to torsional and bending loading of F = 4000 lb (without residual stress): a) Paris fatigue crack growth curve, b) Loading history of the peak stress, c) Geometry of the crack, d) Fatigue life, e) The normalized through-thickness stress distribution

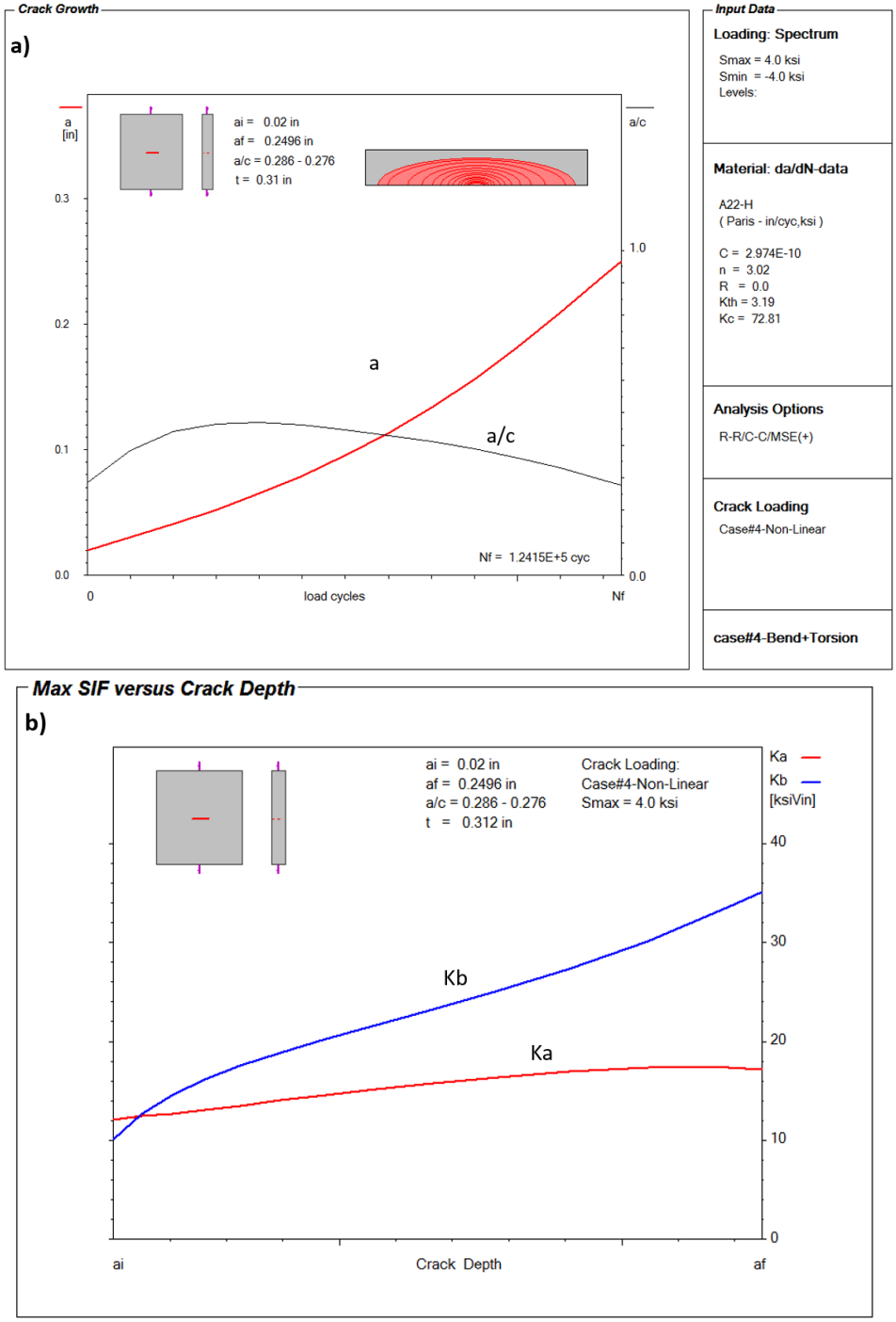

Figure A3- 24: a) The crack depth versus the number of applied load cycles to failure (a-N diagram), b) The stress intensity factor values at the surface and depth points of the semi-elliptical crack versus the crack depth (K-a diagram); Complex tubular welded joint subjected to torsional and bending loading of F = 4000 lb (without residual stress)

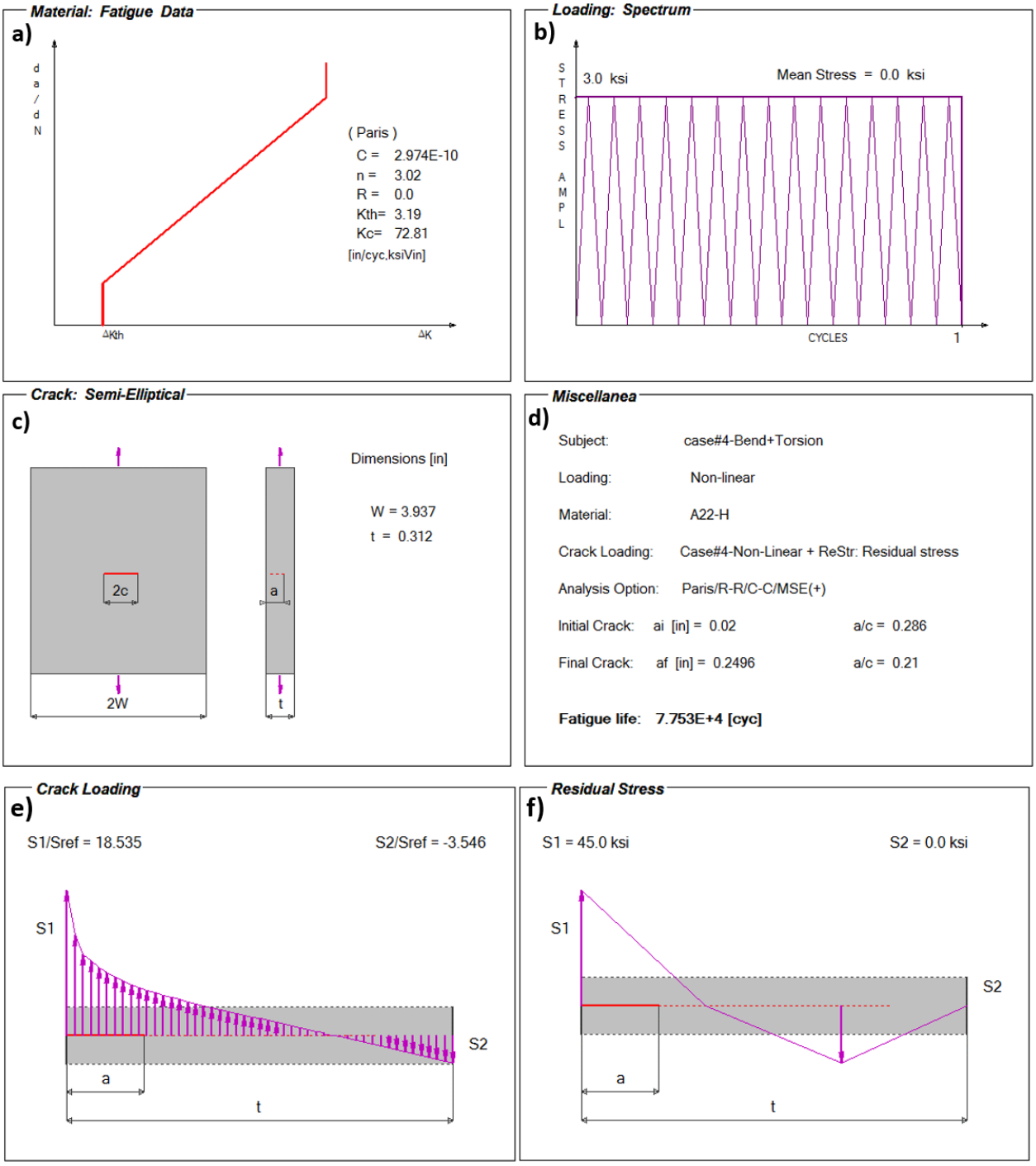

Figure A3- 25: FALPR input data for fatigue crack propagation analysis of the Complex tubular welded joint subjected to torsional and bending loading of F = 3000 lb (with residual stress): a) Paris fatigue crack growth curve, b) Loading history of the peak stress, c) Geometry of the crack, d) Fatigue life, e) The normalized through-thickness stress distribution, f) Estimated residual stress distribution through the thickness of the weld toe cross-section

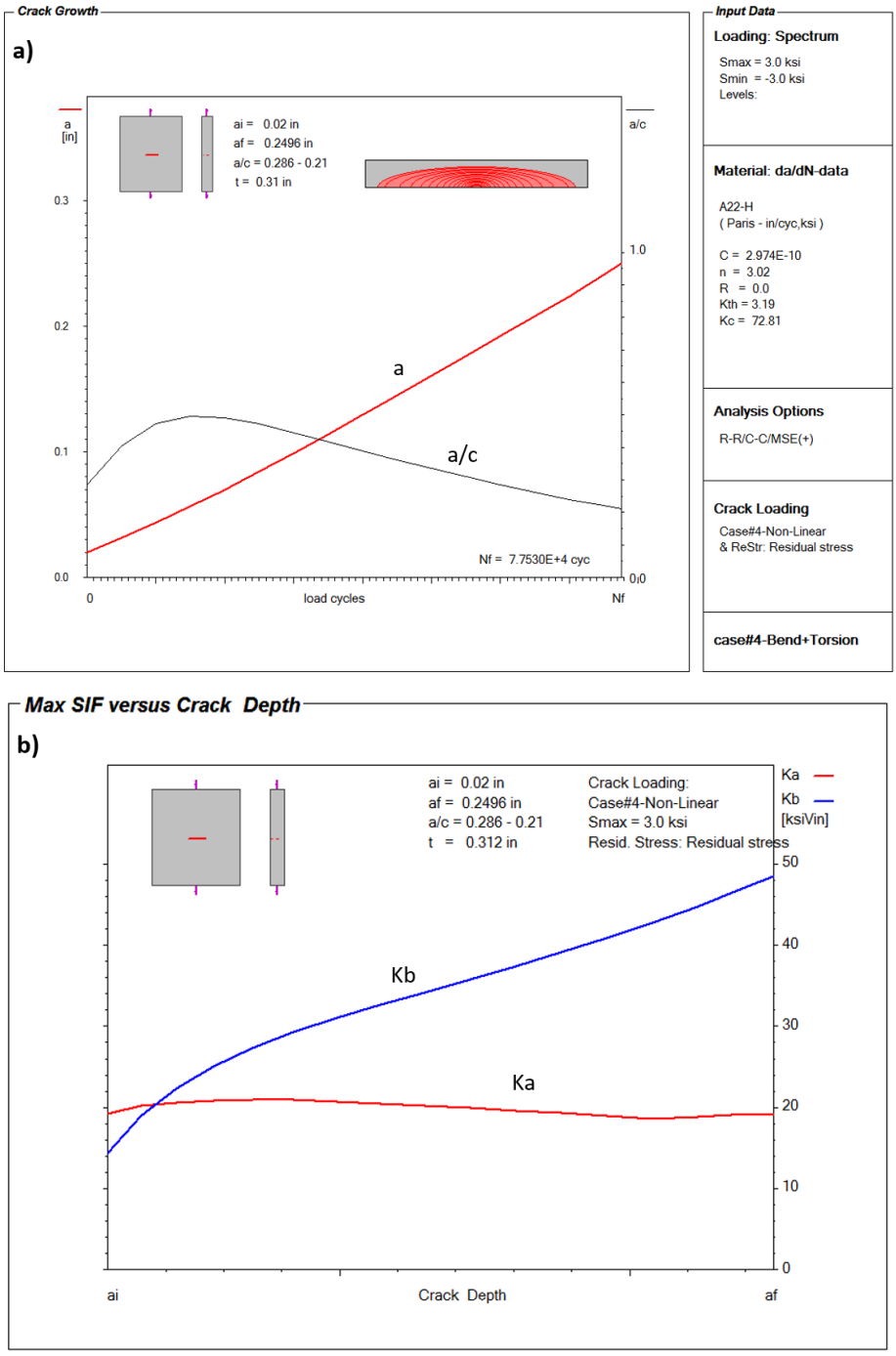

Figure A3- 26: a) The crack depth versus the number of applied load cycles to failure (a-N diagram), b) The stress intensity factor values at the surface and depth points of the semi-elliptical crack versus the crack depth (K-a diagram); Complex tubular welded joint subjected to torsional and bending loading of F = 3000 lb (with residual stress)

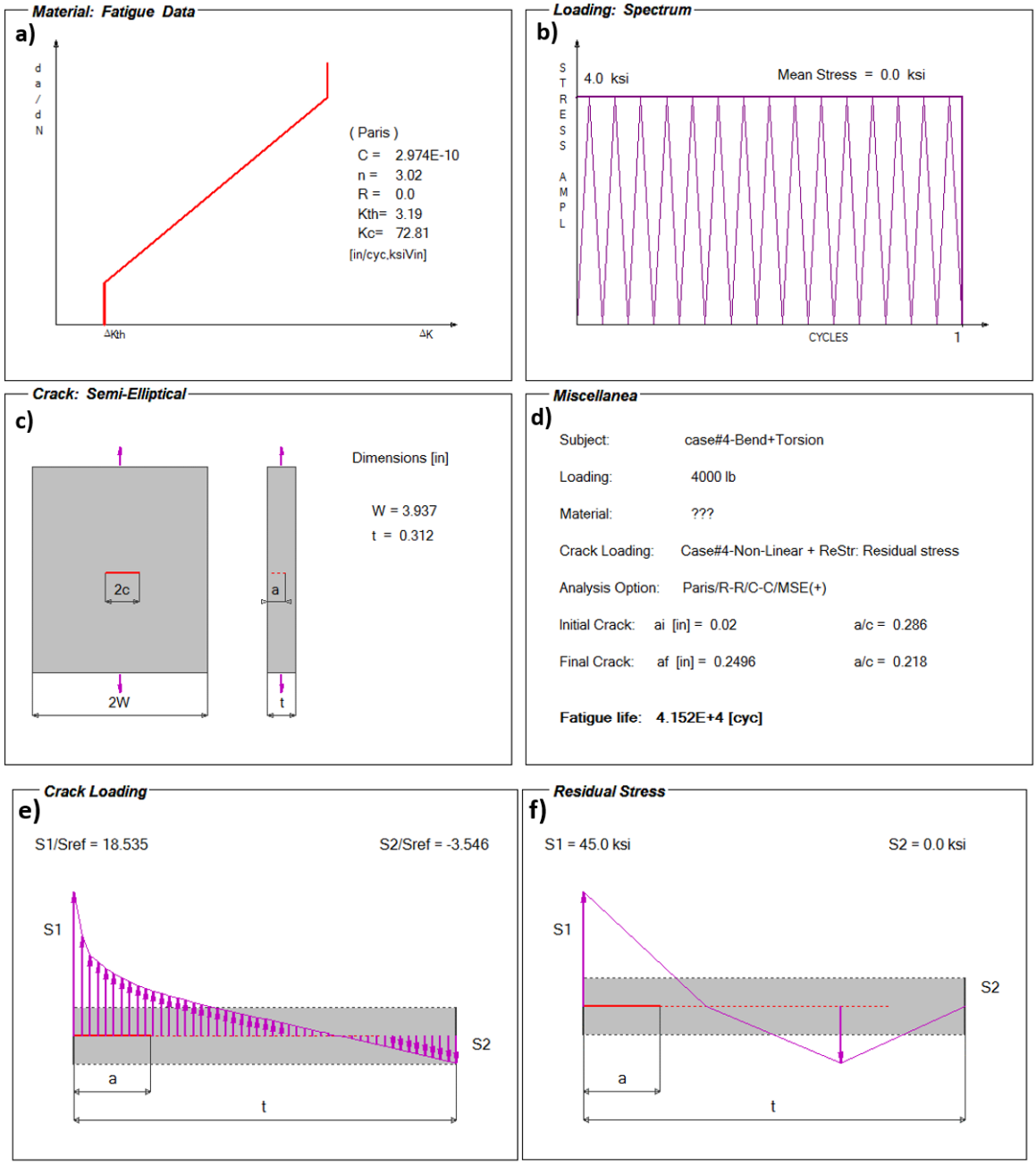

Figure A3- 27: FALPR input data for fatigue crack propagation analysis of the Complex tubular welded joint subjected to torsional and bending loading of F = 4000 lb (with residual stress): a) Paris fatigue crack growth curve, b) Loading history of the peak stress, c) Geometry of the crack, d) Fatigue life, e) The normalized through-thickness stress distribution, f) Estimated residual stress distribution through the thickness of the weld toe cross-section

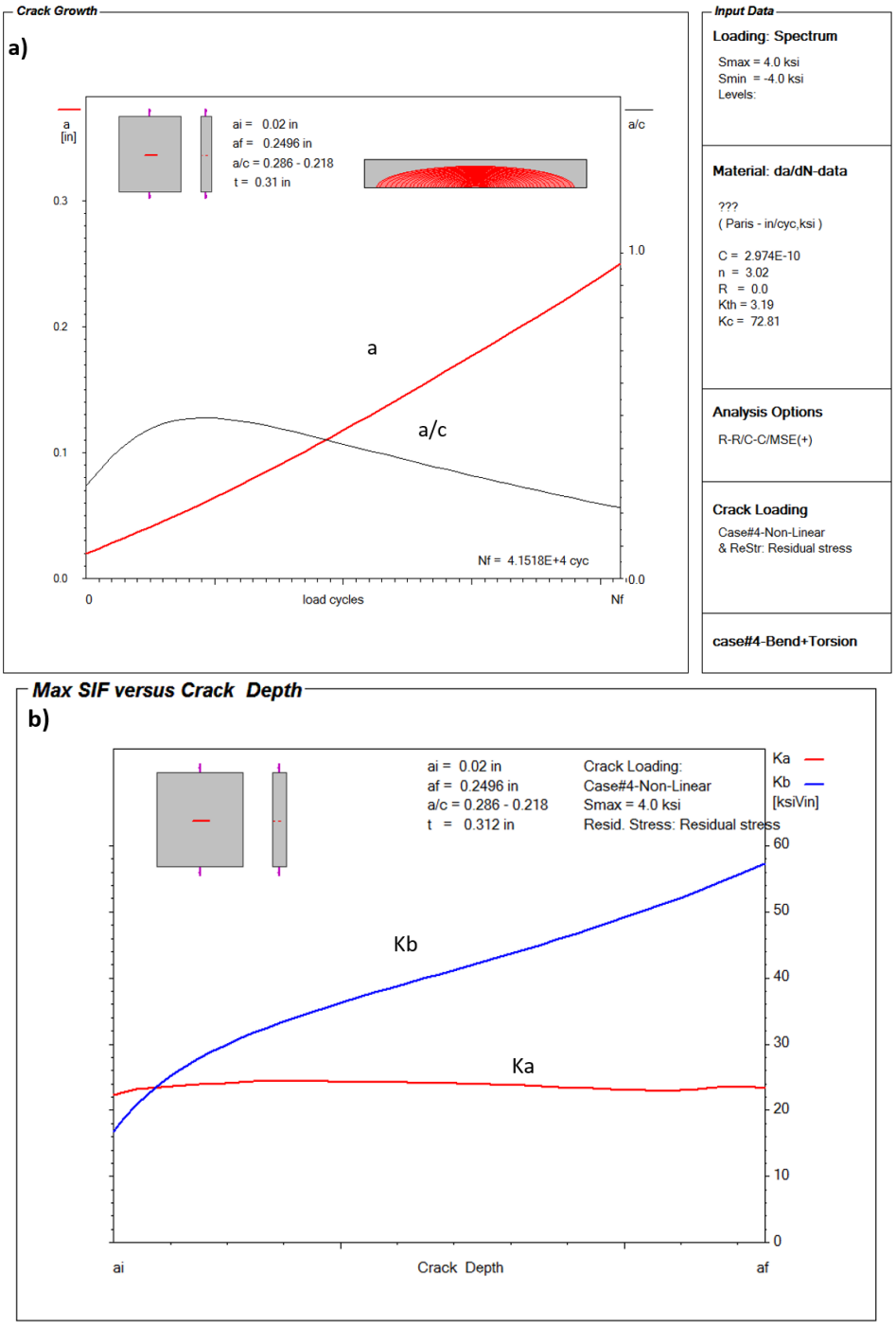

Figure A3- 28: a) The crack depth versus the number of applied load cycles to failure (a-N diagram), b) The stress intensity factor values at the surface and depth points of the semi-elliptical crack versus the crack depth (K-a diagram); Complex tubular welded joint subjected to torsional and bending loading of F = 4000 lb (with residual stress)

The fatigue analysis results are shown in Table A3 - 3 and Table A3 - 4 for the two cases of the T-joint subjected to in-plane loading levels of F = 3000 lb and F = 4000 lb, respectively. The total fatigue life (N_f) was determined by summing the fatigue crack initiation life (N_i) and the fatigue crack propagation life (N_p). The ratios of the fatigue crack initiation life to the fatigue crack propagation life and the total fatigue life (N_i/N_p and N_i/N_f) are shown to determine which fatigue life was dominant to the total life.

Table A3 - 3: Summary of predicted fatigue lives for the Complex tubular welded joint subjected to torsion and bending cyclic loading with F = 3000 lb

Residual Stress (Ksi)	N_i (Cycle) a_i = 0.02 in	Np (Cycle) a_f = 0.14 in	N_i/Np	N_f (Cycle)	N_i/N_f
σ_r = 0	63007	295980	0.213	358987	0.176
σ_r = 45	27737	77530	0.358	105267	0.263

Table A3 - 4: Summary of predicted fatigue lives for the Complex tubular welded joint subjected to torsion and bending cyclic loading with F = 4000 lb

Residual Stress (Ksi)	N_i (Cycle) a_i = 0.02 in	Np (Cycle) a_f = 0.14 in	N_i/N_p	N_f (Cycle)	N_i/N_f
σ_r = 0	17822	124150	0.144	141972	0.126
σ_r = 45	10017	41518	0.241	51535	0.194

The ratios of the fatigue crack initiation life to the fatigue crack propagation life and the total fatigue life (e.g., $N_i/N_p \leq 0.358$ and $N_i/N_f \leq 0.241$) indicate that most of the welded joint fatigue life was spent in propagating the crack from a_i = 0.02 in to the final critical crack depth a_f = 0.14 in.

The JD Company's laboratory tested nine samples of a Complex tubular welded joint subjected to lateral fully reversed cyclic loading to determine the fatigue life. The test samples were subjected to torsion and bending of ±3000 lb, whereas the other seven samples were subjected to loading of ± 4000 lb. The experimental fatigue data for both load levels are shown in Table A3 - 5. The numbers of load cycles were obtained as a function of the measured surface crack length. Using the fatigue crack growth simulation data obtained from the FALPR program, the crack depth corresponding to the experimental surface crack length was estimated.

Table A3 - 5: Experimental fatigue crack propagation life data (2c-N) for the Complex tubular welded joints subjected to torsion and bending loading

Sample #	Load (N)	Number of cycles (cycles)	Crack length 2c (in)
9	3000	267000	1.5
13		72525	0.75
		84844	1
		96670	1.25
		175235	1.5
11	4000	21000	0.25
		59529	0.63
		166218	0.74
		316205	1.25
12		28000	0.75
		48131	1
		134907	3
14		22000	0.75
		60000	1.06
15		10691	0.44
		26149	0.84
		31611	1.5
16		10292	0.75
		30793	1
		35100	1.3
		40893	1.5
17		12085	0.75
		14853	1
		37507	1.5
18		9550	0.25
		12195	0.38
		18332	0.44
		19354	0.62
		26537	1.5

The predicted fatigue life data in Table A3 - 3 and Table A3 - 4 as well as the experimental fatigue life data from Table A3 - 6, are plotted as shown in Figure A3- 29 and Figure A3- 30 for both load levels. The fatigue life data are plotted in terms of the applied load cycles versus the surface crack length (2c) for comparison between the experimental and predicted fatigue life. The experimental fatigue data are plotted as a series of discrete points, whereas the predicted fatigue data are plotted as two curves. The hashed curve represents the fatigue life prediction without the effect of the residual stress, and the solid curve represents the fatigue life prediction including the residual stress effect.

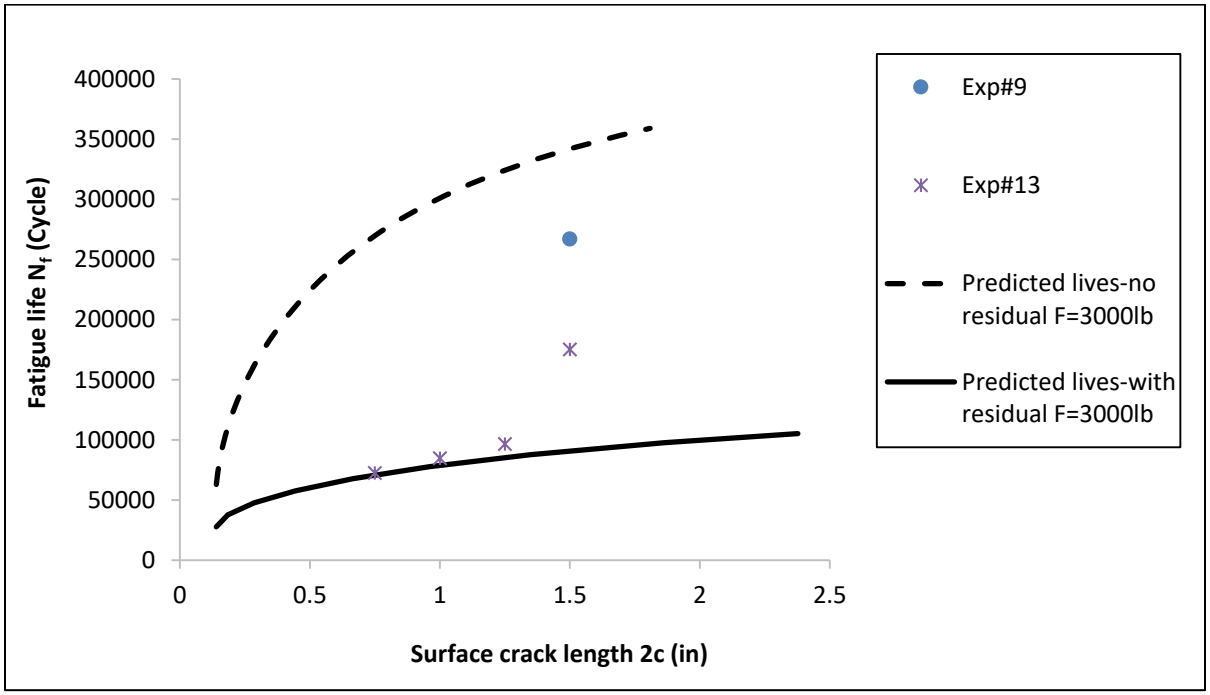

Figure A3- 29: Comparison between the experimental and predicted fatigue lives of the Complex tubular welded joint subjected to torsion and bending cyclic loading with F = ± 3000 lb

Two specimens were tested with a load of F= 3000 lb, and the fatigue lives were used for comparison. According to the results shown in Figure A3- 29, the predicted fatigue life based on the proposed shell FE method underestimated the fatigue life compared to the experimental data when the residual stress effect was not included. Including the residual stress effect resulted in overestimation of the fatigue life predictions by factors 2 to 3 compared to the experimental fatigue lives of specimens (#3 and #9) respectively. Sample #13 seems to have the crack growing around the weld after the crack size reaches approximately 1in which is different from the planar assumption used for the fatigue life predictions. Including the residual stress proved to be important when evaluating the fatigue life of welded joints. This finding emphasizes the importance of including the residual stress effect when evaluating the fatigue life of welded joints.

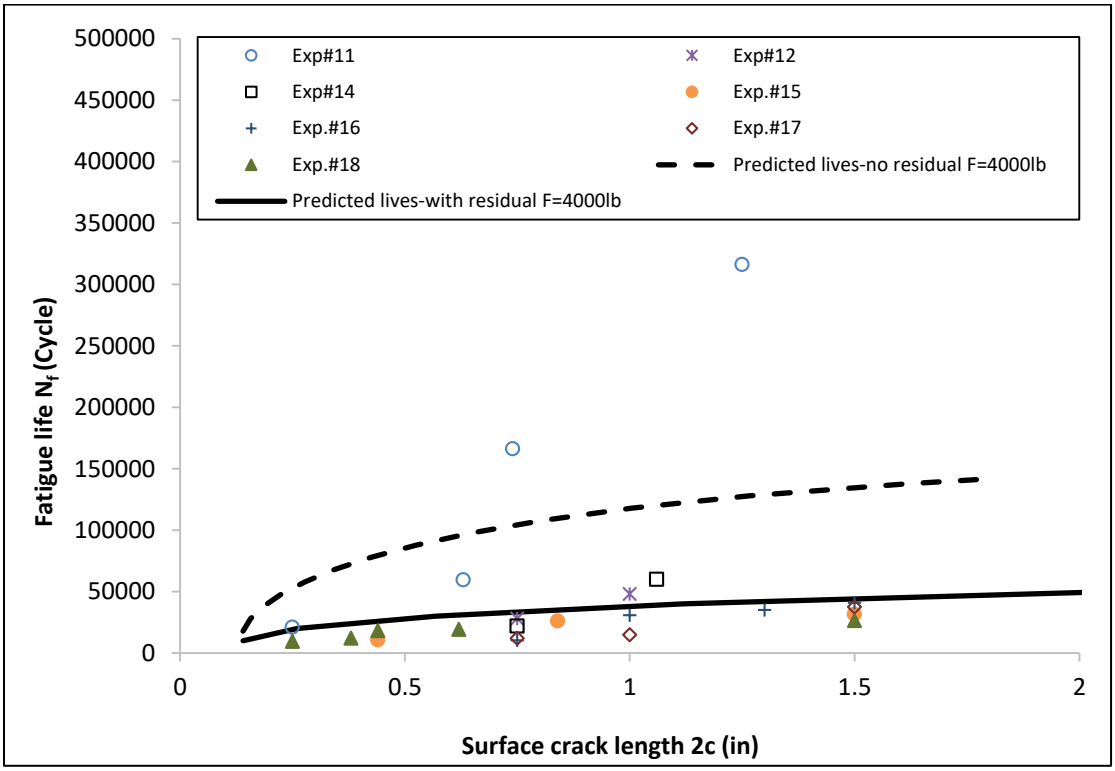

Figure A3- 30: Comparison between the experimental and predicted fatigue lives of the Complex tubular welded joint subjected to torsion and bending cyclic loadings with F = ± 4000 lb

Seven specimens were tested with a load of F= 4000 lb, and the fatigue lives were used for comparison. According to the results in the above figure, the fatigue life predictions based on the proposed method show good agreement with the experimental fatigue data when the residual stress was not included. Including the residual stress proved to be important when evaluating the fatigue life of welded joints. This finding emphasizes the importance of including the residual stress effect when evaluating the fatigue life of welded joints. The difference between the predicted fatigue lives and the experimental data could be because of the residual stress distribution estimation. Based on this, the difference in the results is fairly justified.

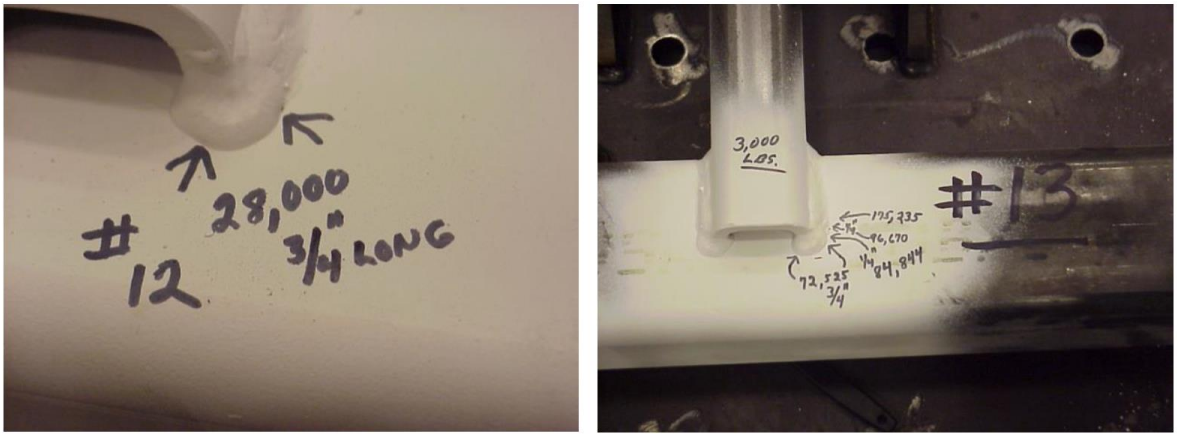

Figure A3- 31: Fatigue crack at the weld toe of the Complex tubular welded joint (Sample # 12 and 13) (JD)

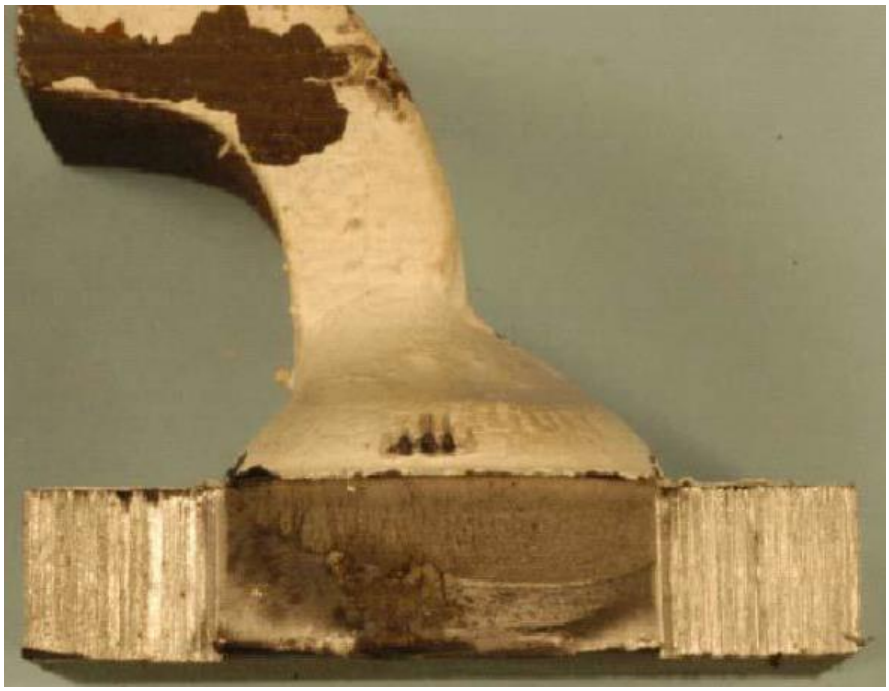

Figure A3- 32: Crack profile in one of the experimental Complex tubular subjected to torsion and bending loading (JD)

Sample # 11 seems to have a different fatigue data trend than other experimental samples. This particular specimen (Sample # 11) may have been stress-relieved, or the residual stress was not formed as in the other specimens. Few experimental specimens and the location of the critical cracks are shown in Figure A3- 31 and Figure A3- 32. The actual fatigue crack tends toward a semi-elliptical shape while growing through the tube thickness across the weld toe thickness.